University of Newcastle upon Tyne
Department of Civil Engineering

ROCK BEHAVIOUR UNDER MULTIAXIAL COMPRESSION

A Thesis Submitted for the Degree of
Doctor of Philosophy

By

Mahmoud Ibrahim Alsayed
BEng, MSc

July 1996

To

my parents

ACKNOWLEDGEMENTS

Whenever I was asked how it was going, I often described it like climbing a series of mountains. On completion, there is naturally a feeling of achievement and relief, but equally, there is much appreciation and gratitude to those who made the journey possible.

I would like first to express my deepest thanks to Dr E. K. S. Passaris for his continual guidance and unlimited support. His consideration, advice and encouragement have been invaluable to this work and beyond.

I would also like to gratefully acknowledge the support and encouragement received from a number of academic staff, particularly Professor C. J. F. P. Jones.

The experimental work has been carried out with the assistance of dedicated technical staff whose skills, cooperation and friendliness have been indispensable. In particular, I would like to profoundly thank J. Moore, L. Moore, F. Beadle, M. McKenna, J. Allan, C. Hunt and T. Edmonds. Maybe one day we will hit the jackpot! Thanks also go to the computing, library and secretarial staff at both Newcastle and Glasgow.

Many friends and colleagues deserve my thanks for their support and encouragement, in particular: I. E. White, J. Butterfield, N. & J. Alderson, W. J. Miller, S. El-Masri, W. Hu, Y. Alexiou, Susana & Colin, R. Wilson, K. Fortin, C. Deshayes, A. Schander, E. Kelly, G. Richardson, Elaine & Jimmy, J. Singh, Chris & Saff, B. Stewart and B. MacLeod.

I am specially grateful to Dunja and to R. & G. Stenzel for their warm support, inspiration and constant encouragement. Thanks to Dafi as well.

Finally, my eternal gratitude and admiration go to my parents, brothers and sisters for their understanding, patience and never ending inspiration and support.

July 1996

M. I. Alsayed

ABSTRACT

An experimental study has been carried out to investigate the behaviour of rock under multiaxial compression and assess the influence of both the stress conditions and test configuration on the apparent characteristics of this behaviour. Over three hundred specimens of Springwell sandstone, of various forms, have been tested using different loading techniques and most encountered stress fields. Cubes and thick-walled hollow cylinders have been subjected to uniaxial, biaxial, triaxial and polyaxial compression, and solid cylinders have been subjected to standard uniaxial and triaxial compression.

Extensive work has initially been put into designing and developing the testing facilities required. A new multiaxial hollow cylinder test apparatus has been devised using a Hoek triaxial cell and specially designed system for the application of internal pressure, major modifications have been made to an existing multiaxial cubical test apparatus, and appropriate testing arrangements and procedures have been developed.

Prior to initiating the experimental programme, characterisation tests have been conducted to determine the fundamental properties of the rock, and non-destructive ultrasonic wave velocity tests have been utilised together with statistical methods to examine any inherent variations in the specimens used. A remarkable agreement has emerged between the rock static and dynamic Young's moduli and the results have confirmed that the Springwell sandstone can practically be regarded as linear elastic, homogeneous and isotropic.

The concept of the multiple failure state triaxial test has been utilised and extended to conduct multiple failure state polyaxial tests. While the concept remains useful, strain results obtained beyond the first failure state are likely to be inconsistent.

Results of cube tests have been found to be highly influenced by the boundary conditions. Although the use of PTFE sheets can reduce the effect of friction between the specimen and the loading platens, it may equally have a weakening effect on the test specimen.

The theory of elasticity has been found adequate to calculate the stresses in the hollow cylinders but remains inexact when deviation from linear behaviour occurs prior to failure. When the outer and inner surfaces of the cylinder are not perfectly concentric, the effect on the test results has proved negligible. Hollow cylinders have been found to provide an alternative means for measuring the rock indirect tensile strength.

Results of biaxial and polyaxial tests on both cubes and hollow cylinders have confirmed the marked influence of the intermediate principal stress on the apparent strength of rock.

Comparison of results from multiaxial tests on cubes, hollow and solid cylinders have shown that the apparent strength, deformability and failure characteristics of the rock are remarkably influenced by the stress conditions imposed as well as the test configuration used. Available failure criteria have advantages and disadvantages, but none of them can explain the diversity of the results obtained. On the whole, the results appear to cast doubt on common conceptions of rock failure and ultimately pose the question of how realistic current testing techniques are in their prediction of the actual behaviour of rock.

CONTENTS

Notation xi

Conventions xiii

Chapter 1, Introduction *1*

1.1 Problem Statement 2

1.2 Scope of the Thesis 5

Chapter 2, Review of Previous Multiaxial Testing Studies *7*

2.1 Introduction 8

2.2 Typical Means and Objectives of Previous Studies 9

2.3 Studies Based on Direct Multiaxial Loading 11

2.4 Studies Based on Indirect Multiaxial Loading 23

Chapter 3, Design and Description of the Testing Facilities *35*

3.1 Introduction 36

3.2 The Multiaxial Cubical Test Apparatus 37

3.2.1 Brief History 37

3.2.2 General Description and Features 37

3.2.3 Previous Polyaxial Testing Set-up 39

3.2.4 Pilot Tests and Problems Encountered 39

3.2.5 Inspection of the Testing Facilities 41

3.2.6 Modification and Enhancement of the Testing Facilities 42

3.3 The Design of the Hollow Cylinder Test Apparatus 48

3.3.1 Inadequacy of Existing Testing Apparatus 48

3.3.2 Fundamental Design Considerations 48
3.3.3 The Design Approach 50
3.3.4 Construction and Configuration 51
3.4 The Servo-Controlled Loading System 58
3.4.1 Soft, Stiff and Servo-Controlled Testing Machines 58
3.4.2 Description of the Servo-Controlled Loading Facilities 58
3.5 The Pressure Intensifier System 61
3.6 The Data Acquisition System 62

Chapter 4, Rock Characterisation and Specimen Preparation *64*

4.1 Introduction 65
4.2 Petrographic Description of the Rock 66
4.3 Physical and Mechanical Properties of the Rock 68
4.3.1 Determination of Moisture Content, Porosity and Density 68
4.3.2 Uniaxial Compression and Deformability Tests 69
4.3.3 Uniaxial Indirect Tensile Strength Tests 73
4.4 Specimen Preparation 76
4.4.1 Categorisation of the Test Specimens 76
4.4.2 Rock Sampling and Specimen Production 76
4.5 An Investigation into Inherent Specimen Variations and other Properties of Springwell Sandstone 78
4.5.1 The Question of Inherent Specimen Variations 78
4.5.2 Non-Destructive Ultrasonic Wave Velocity Tests 78
4.5.3 Determination of the Directional Values of the Dynamic Young's Modulus 79
4.5.4 Statistical Analysis of the Results 80
4.5.5 Discussion of the Results 80
4.5.6 Inference of the Rock Isotropy 81
4.5.7 Further Analysis for the Determination of the Overall Dynamic Young's Modulus of the Rock 85

4.5.8 Comparison between the Static and Dynamic Young's Moduli of the Rock 90

Chapter 5, Multiaxial Compression of Cubical Specimens ***93***

5.1 Introduction 94

5.2 General Testing Configuration and Procedure 95

5.3 Polyaxial Compression Tests - First Series 100

5.3.1 Outline of the Tests 100

5.3.2 The Experimental Results 100

5.3.3 Discussion of the Results 104

5.4 Polyaxial Compression Tests - Second Series 107

5.4.1 Outline of the Tests 107

5.4.2 The Experimental Results 108

5.4.3 Discussion of the Results 114

5.5 Polyaxial Compression Tests - Third Series 120

5.5.1 Outline of the Tests 120

5.5.2 The Experimental Results 121

5.5.3 Discussion of the Results 123

5.6 Polyaxial Compression Tests - Fourth Series, Multiple Failure State Polyaxial Tests 125

5.6.1 Outline of the Tests 125

5.6.2 The Experimental Results 126

5.6.3 Discussion of the Results 128

5.7 Triaxial Compression Tests 130

5.7.1 Outline of the Tests 130

5.7.2 The Experimental Results 130

5.7.3 Discussion of the Results 135

5.8 Biaxial Compression Tests 137

5.8.1 Outline of the Tests 137

5.8.2 The Experimental Results 138

5.8.3 Discussion of the Results 142

5.9 Uniaxial Compression Tests 144
5.9.1 Outline of the Tests 144
5.9.2 The Experimental Results 145
5.9.3 Discussion of the Results 148

Chapter 6, Multiaxial Compression of Thick-Walled Hollow Cylinders ***150***

6.1 Introduction 151
6.2 Fundamental Considerations 153
6.2.1 Stresses in a Hollow Cylinder 153
6.2.2 Effect of Eccentricity 156
6.2.3 Strains in the Cylinder 157
6.2.4 Employed Procedure for Calculating the Principal Strains 157
6.3 General Testing Configuration and Procedure 159
6.4 Polyaxial Compression Tests - First Series 168
6.4.1 Outline of the Tests 168
6.4.2 The Experimental Results 168
6.4.3 Discussion of the Results 179
6.5 Polyaxial Compression Tests - Second Series 182
6.5.1 Outline of the Tests 182
6.5.2 The Experimental Results 182
6.5.3 Discussion of the Results 194
6.6 Triaxial Compression Tests 195
6.6.1 Outline of the Tests 195
6.6.2 The Experimental Results 195
6.6.3 Discussion of the Results 200
6.7 Biaxial Compression Tests - First Series 201
6.7.1 Outline of the Tests 201
6.7.2 The Experimental Results 201
6.7.3 Discussion of the Results 207
6.8 Biaxial Compression Tests - Second Series 209

6.8.1 Outline of the Tests 209
6.8.2 The Experimental Results 209
6.8.3 Discussion of the Results 216
6.9 Biaxial Compression Tests - Effect of Eccentricity 218
6.9.1 Outline of the Tests 218
6.9.2 The Experimental Results 218
6.9.3 Discussion of the Results 219
6.10 Uniaxial Compression Tests - First Series 221
6.10.1 Outline of the Tests 221
6.10.2 The Experimental Results 221
6.10.3 Discussion of the Results 222
6.11 Uniaxial Compression Tests - Second Series 225
6.11.1 Outline of the Tests 225
6.11.2 The Experimental Results 226
6.11.3 Discussion of the Results 229
6.12 Tensile Strength Tests 230
6.12.1 Outline of the Tests 230
6.12.2 The Experimental Results 230
6.12.3 Discussion of the Results 231

Chapter 7, Triaxial Compression of Solid Cylinders ***234***

7.1 Introduction 235
7.2 Testing Configuration and Procedure 237
7.3 Outline of the Tests 240
7.4 The Experimental Results 243
7.5 Discussion of the Results 247

Chapter 8, General Discussion and Comparison of Results ***249***

8.1 Introduction 250
8.2 Results of Polyaxial Compression 251
8.3 Results of Triaxial Compression 260

8.4 Results of Biaxial Compression 265
8.5 Results of Uniaxial Compression 269
8.6 Applicability of Available Failure Criteria 276

Chapter 9, Conclusions and Recommendations ***279***

9.1 Introduction 280
9.2 Previous Multiaxial Studies 281
9.3 Testing Facilities, Design and Developments 281
9.4 Testing Configurations and Procedures 282
9.5 Rock Characterisation 283
9.6 Rock Strength in Multiaxial Compression 284
9.7 Rock Deformability 287
9.8 Rock Failure Characteristics 290
9.9 Failure Criteria 293
9.10 Suggestions for Further Research 293

References ***295***

NOTATION

Most symbols in this thesis are defined every time they occur, but the following are more commonly used.

D	Diameter
e	Eccentricity
E or E_s	Young's modulus (static)
E_d	Dynamic Young's modulus
$E_{d(x)}$, $E_{d(y)}$, $E_{d(z)}$	Directional dynamic Young's moduli
F	Force or load
L	Length
n	Porosity
n	Number of items in a sample
P_i, P_o	Internal and external pressures
r	Radial distance
r, θ, z	Cylindrical polar coordinates
R_i, R_o	Inner and outer radii of hollow cylinder
S_d	Standard deviation
t	Thickness
t	Statistic (Students' t distribution)
u_z, u_r	Axial and radial displacement components
V	Volume
V_p	Velocity of compression wave
ΔV	Volume change
ΔV_h	Volumetric change of the hole
w	Water or moisture content
$\bar{x}$	Average or mean of a sample
X, Y, Z	Cartesian or rectangular coordinates
α	Probability of error or significance level

β	Bipolar coordinate
γ	Bulk density
γ_d	Dry density
$\varepsilon_1, \varepsilon_2, \varepsilon_3$	Major, intermediate and minor principal strains
$\varepsilon_z, \varepsilon_\theta, \varepsilon_r$	Axial, tangential and radial principal strains
ε_v	Volumetric strain
ε_{vh}	Volumetric strain of the hole
μ	Mean of the population
ν or ν_s	Poisson's ratio (static)
ν_d	Dynamic Poisson's ratio
$\sigma_1, \sigma_2, \sigma_3$	Major, intermediate and minor principal stresses
$\sigma_z, \sigma_\theta, \sigma_r$	Axial, tangential and radial principal stresses
σ_u	Uniaxial compressive strength
σ_t	Indirect tensile strength

CONVENTIONS

Throughout this thesis test results are expressed conforming whenever possible to the suggestions of the International Society for Rock Mechanics, ISRM, and except in some figures drawn from other sources or studies, the units used follow the metric units of the Système International, SI.

Stresses are reckoned positive when they are compressive and negative when they are tensile. Likewise, strains are regarded positive when they are contractile and negative when they are extensile.

The term 'strength' or 'peak strength' is sometimes used to refer to the maximum stress that the material can sustain under given loading conditions. This stress corresponds in all multiaxial compression tests to the maximum level of the major principal stress, σ_1, recorded at failure.

The term 'multiaxial' is used to generally describe stress conditions that are not limited to standard uniaxial and triaxial compression. In terms of the major, intermediate and minor principal stresses, σ_1, σ_2, σ_3, respectively, the following states of stress are defined:

Uniaxial compression	$\sigma_1 > \sigma_2 = \sigma_3 = 0$
Biaxial compression	$\sigma_1 > \sigma_2 > \sigma_3 = 0$
Triaxial compression	$\sigma_1 > \sigma_2 = \sigma_3 > 0$
Polyaxial compression	$\sigma_1 > \sigma_2 > \sigma_3 > 0$
Hydrostatic or isotropic compression	$\sigma_1 = \sigma_2 = \sigma_3 > 0$

Chapter

1

Introduction

1.1 Problem Statement

The behaviour of rock and other engineering materials are often assessed on the basis of simplistic tests and inadequate constitutive relations. If σ_1, σ_2 and σ_3 are the major, intermediate and minor principal stresses, respectively, most experimental studies of the compressive strength and deformability of rock utilise standard axisymmetric tests in which specimens in the form of solid cylinders are subjected to a state of uniaxial compression, $\sigma_1 > \sigma_2 = \sigma_3 = 0$, or more frequently triaxial compression, $\sigma_1 > \sigma_2 = \sigma_3 > 0$. While these tests have the advantage of requiring simple equipment and being easy to conduct, their greatest disadvantage lies in the fact that they are rarely of direct relevance to what elements of rock or soil may experience in nature or around engineering works.

Stress conditions encountered in practice are seldom axisymmetric and no two of the three principal stresses can in general be equal at failure. In the majority of cases, such as around underground structures or in the walls of supported openings, all three principal stresses are independent and the state of stress is truly three-dimensional or polyaxial compression, $\sigma_1 > \sigma_2 > \sigma_3 > 0$. In special cases, such as in the free face of a rock slope or in the walls of unsupported excavations, one of the three principal stresses vanishes and the state of stress is reduced to two-dimensional or biaxial compression, $\sigma_1 > \sigma_2 > \sigma_3 = 0$. These conditions are very real and can neither be simulated nor assessed by standard testing configurations.

The limitations of conventional tests are generally matched by those of commonly used constitutive models and failure criteria. Most classical models for rock behaviour have been guided by results from standard uniaxial and triaxial compression tests, and have hardly proved successful in providing realistic solutions when faced with more complex stress conditions. Similarly, available failure criteria suffer from various disadvantages and have repeatedly been found unable to adequately predict failure under diverse loading conditions. Moreover, in line with conventional tests, many of these criteria do not account for the independence of all three principal stresses and ignore the often acknowledged effect of the intermediate principal stress, σ_2, on failure.

With the inadequacy of conventional experimental and theoretical approaches, different multiaxial testing techniques have been used to study the behaviour of rock under true stress conditions and acquire better knowledge for the development of more realistic constitutive models and failure criteria. These techniques are generally of two main types: one involves direct loading of specimens in the form of rectangular prisms or more often cubes, and the other involves indirect loading of thick-walled hollow cylinders. Both techniques are versatile and enable the simulation of a wide range of stress paths with three independently varying principal stresses. Nevertheless, different advantages and disadvantages are associated with each technique, and depending on the nature of the investigation, one technique may sometimes be more suitable than the other.

Multiaxial loading of prisms or cubes is achieved by direct application of predetermined principal stresses to the opposite faces of the test specimen. One of the main advantages of this technique is that the principal stresses are known as they are applied, and generally, the principal strains can also be directly measured. On the other hand, the three principal stress directions are fixed and forced to coincide with those of the principal strains. However, the major problem associated with such tests is that of ensuring uniform distribution of stresses over the specimen faces by minimising the effect of friction between the specimen and the loading platens. In this regard, a number of solutions have been suggested ranging from using soft materials or lubricants with solid platens to the application of loads through brush bearing platens or flexible membranes.

In the case of thick-walled hollow cylinders, predetermined axial, tangential and radial principal stresses are induced in the cylinders by a combination of axial load and external and internal pressures. The major disadvantage of this technique is that the tangential and radial stresses are not directly applied but calculated from the applied pressures using elastic, plastic or elastic-plastic solutions which may not lead to accurate results. In addition, the stresses in the cylinder are not homogeneous and high stress gradient exists at the cylinder inner surface which could also influence the test results. One more problem with hollow cylinder tests is that of acquiring direct and independent measurements of the tangential and radial strains. On the advantageous side, hollow cylinders have an ideal geometry for simulating stress conditions around underground openings such as shafts,

boreholes and tunnels where stress gradients are also present. Furthermore, the principal stress directions are not necessarily fixed in the test, and with the application of torsion, the stresses can have any angle with the cylinder axis and rotate continuously or intermittently during the test.

Despite their versatility, both multiaxial testing techniques remain relatively far from being widely utilised due to the considerable complications and difficulties involved. In addition, unlike conventional equipment, multiaxial testing facilities are seldom available in laboratories nor are they standardised or readily obtainable. Therefore, researchers have often been involved in the lengthy process of design and development of suitable facilities. With the absence of established multiaxial testing procedures, tests have generally been conducted in the light of conventional methods and available suggestions.

A thorough review of literature has shown that the majority of previous multiaxial testing studies have been limited to either polyaxial or more often biaxial compression tests. Moreover, these tests have generally been carried out by either direct loading of cubes or indirect loading of hollow cylinders. Despite their valuable contribution towards a better understanding of the behaviour of engineering materials, most previous studies may be criticised for being biased in favour of one technique or the other. While some researchers such as Amadei *et al.* (1984) have opted for cube tests and perceived hollow cylinders being associated with insurmountable disadvantages, others such as Bažant (1983) have highlighted the versatility of hollow cylinders and deemed cube tests to have serious limitations. It is to the best of the author's knowledge that no study has ever attempted to experimentally draw a constructive comparison between the two testing techniques.

In view of the limitations of conventional tests and the contrasting approaches to multiaxial testing, this study has aimed to simultaneously utilise both multiaxial testing techniques as well as conventional methods in order to first, thoroughly examine the behaviour of rock under most encountered stress fields, and second, assess the effect of the test configuration on the apparent characteristics of this behaviour.

In order to achieve the aims of this study, extensive work has initially been put into designing and developing the testing facilities required. In this regard, a new multiaxial

hollow cylinder test apparatus has been devised, major modifications have been made to an existing multiaxial cubical test apparatus, a pressure intensifier system has been acquired and incorporated into the testing set-up, an existing data acquisition system has been upgraded and the operating software has been revised, and appropriate testing arrangements and procedures have been developed.

Subsequently, well over three hundred specimens of Springwell sandstone, of various shapes, have been used to cover the wide scope of this study. Prior to initiating the multiaxial testing programme, characterisation tests have been carried out to re-assess the fundamental properties of the rock and obtain results specific to the samples used in this study. Furthermore, in order to examine the uniformity of the test specimens, non-destructive ultrasonic wave velocity tests have been performed and statistical methods have been used to analyse the results.

A variety of stress conditions have been simulated in the multiaxial testing programme utilising three types of specimens. Cubes and thick-walled hollow cylinders have been involved in series of tests carried out under a range of comparable stress fields corresponding to uniaxial, biaxial, triaxial and polyaxial compression. In addition, solid cylinders have been involved in standard uniaxial and triaxial compression tests.

It is hoped that the results of this study will shed some more light on the actual behaviour of rock under different stress conditions, improve current approach to rock testing and contribute to the development of more adequate constitutive models and failure criteria.

1.2 Scope of the Thesis

Following this introduction, Chapter 2 provides a thorough review of previous multiaxial testing studies which generally involved biaxial or polyaxial compression tests. Since researchers utilised either direct or indirect loading techniques, the reviewed studies have been grouped on this basis and presented separately.

Chapter 3 introduces the main testing facilities employed in this study together with an account of the modifications made to the cubical apparatus, the design and construction of

the hollow cylinder apparatus, and other developments in experimental techniques and equipment made prior to testing.

Chapter 4 begins with a petrographic description of the Springwell sandstone and then presents characterisation tests performed to determine the physical and mechanical properties of the rock. This is followed by a categorisation of all specimens used and a brief account of their production. The final part presents the results of an investigation into inherent specimen variations and other properties of the rock carried out using non-destructive ultrasonic wave velocity tests and statistical methods.

Chapter 5 presents multiaxial compression tests conducted on cubes. The general testing configuration and procedure is described at the beginning and then the tests are introduced in series according to the type of stress field imposed on the specimens. Each series of tests is first outlined and then the results are presented and specifically discussed.

Chapter 6 presents multiaxial compression tests on thick-walled hollow cylinders. The chapter begins with an overview of the theory of hollow cylinders and the solutions for calculating the stresses and strains. Then, the chapter proceeds following the same format as in Chapter 5.

Chapter 7 presents multiple failure state triaxial compression tests on solid cylinders. Uniaxial compression tests on solid cylinders are presented in Chapter 4 as part of characterisation tests.

Chapter 8 provides general discussions and comparisons of all multiaxial test results and assesses the effect of both the stress conditions and test configuration on the apparent behaviour of rock.

Finally, Chapter 9 recapitulates on the main aspects of this study, summarises major findings and conclusions reached and provides recommendations for further research.

Chapter

2

Review of Previous Multiaxial Testing Studies

2.1 Introduction

Conventional tests such as uniaxial and triaxial compression of solid cylinders have long been realised as being limited and inappropriate to assess in-situ loading conditions in which the rock is under biaxial or polyaxial compression. Over the years, many researchers have addressed this problem and attempted to develop more versatile testing techniques capable of simulating a wide range of true stress fields. Different approaches and means have been employed in efforts to give a better understanding of the behaviour of engineering materials and improve contemporary constitutive models and design criteria. However, in comparison with conventional tests, the task of conducting biaxial or polyaxial tests has proved to be more complicated, costly and associated with enormous experimental difficulties. These factors are well recognised and have often been perceived by some researchers as barriers to initiating such non-conventional tests.

This chapter provides a comprehensive review of multiaxial testing studies conducted over the years in the field of rock mechanics that are relevant to the present work. Studies that have mainly been confined to conventional testing are not reviewed, and most of the work presented herein involves biaxial or polyaxial tests.

Literature has shown that the ongoing development in multiaxial testing on rock has often interacted with similar ones on other engineering materials such as soil and concrete, and there has equally been extensive work on both materials. Although an account of such work is clearly beyond the scope of this review, an effort has been made to incorporate several studies which are of direct relevance.

Since researchers have generally conducted their investigations by either direct loading of rectangular specimens or indirect loading of hollow cylinders, the reported studies have been grouped on this basis and presented separately. A brief description of each study is given together with highlights of the most relevant and significant outcome. Prior to the review, the chapter presents an overview of common means used and general objectives intended in most previous multiaxial studies.

2.2 Typical Means and Objectives of Previous Studies

The majority of previous multiaxial testing studies have been limited to either polyaxial compression tests or more often biaxial compression tests. These tests have generally been conducted by either direct loading of cubes, prisms or plates; or indirect loading of hollow cylinders. Very few attempts have been made to test hollow cylinders with holes other than circular or to drill openings in blocks of rocks to resemble different shapes of underground excavations. With the lack of conventional multiaxial testing facilities, researchers have frequently been involved in designing and developing appropriate apparatus to conduct their investigations. As a result, a number of studies have largely focused on construction and design. In addition, due to the absence of standard multiaxial test procedures, tests have generally been conducted in the light of established methods and conventions.

A wide variety of issues related to engineering concepts and practice have been investigated by previous multiaxial testing studies. Numerous researchers have realised the limitations of conventional uniaxial and triaxial compression tests, and have therefore conducted biaxial or polyaxial tests to study the behaviour of rock and other engineering materials under more realistic stress conditions. Besides, many studies have attempted to simulate stress paths encountered in the field and reproduce loading conditions around underground openings and other engineering structures.

With most commonly used constitutive models and failure criteria being based on results from conventional test, researchers have often questioned the validity of these relations and sought better knowledge for the development of more realistic ones.

In questioning the validity of conventional tests and theoretical approaches, researchers have frequently addressed a number of unresolved issues. One such issue repeatedly investigated in previous studies has been the effect of the intermediate principal stress, σ_2, on the apparent strength of the test material. Conventional tests and failure criteria

generally ignore such effect, but many of the studies reviewed herein have suggested that the effect is rather considerable.

In addition to issues related to conventional tests, attention has also been directed towards problems associated with multiaxial testing techniques. An outstanding problem in direct loading tests has been of reducing the effect of friction between the specimen and the bearing platens. A number of studies have focused on this issue and utilised different solutions in efforts to achieve uniform distribution of stresses over the faces of the test specimen. A widely used solution has been the insertion of a form of friction reducer such as PTFE sheets or lubricants between the specimen and the loading platens. However, the dissatisfaction of some researchers with the effectiveness of this solution has prompted the development of other techniques such the application of loads through brush bearing platens or flexible membranes.

A commonly explored issue in most hollow cylinder tests has been the initiation of failure. A number of researchers have recognised the versatility of the specimen geometry and utilised it to study the development of failure around underground openings.

2.3 Studies Based on Direct Multiaxial Loading

As earlier described, direct biaxial and polyaxial compression tests involve the application of predetermined levels of principal stresses to the opposite faces of rectangular prisms, plates or more often cubes. Among early work of such nature was that of Hobbs (1962) and that of Pomeroy and Hobbs (1962). Both works investigated the strength of various types of British coal in the form of cubes under biaxial compression. Such a stress field is often experienced in mining practice at the coal face. The results of these tests suggested that the strength of coal is considerably influenced by the magnitude of the intermediate principal stress, σ_2, and its direction relative to the bedding planes. As Figure 2.1 shows, the fracture stress was observed to increase with increasing σ_2 up to a point, after which it started to fall. The only failure criterion that appeared to satisfy the experimental observations was the Mises - Hencky constant elastic strain energy of distortion criterion, derived from von Mises (1913) and Hencky (1924).

Mogi (1967) attempted to examine the influence of the intermediate principal stress on rock failure. Cylindrical and prismatic specimens of various rocks were tested under different loading conditions. The experimental results were found remarkably influenced by the intermediate principal stress, σ_2. The strength at failure increased with σ_2 by an amount proportional to, but smaller than, the amount of the minor principal stress, σ_3. This effect of σ_2 appeared to be much more pronounced for brittle materials than for ductile. However, for both materials, the angle between fracture surfaces and the direction of the major principal stress, σ_1, was observed to markedly decrease as σ_2 was increased. Failure criteria such as those of Mohr, Griffith, and Von-Mises in their various forms were found either inapplicable or unable to correlate the results of all tests. Hence, a new form of an empirical failure criterion was proposed.

A significant and regular effect of the intermediate principal stress, σ_2, on the compressive strength of rock was reported in Figure 2.2 by Hojem and Cook (1968) who designed a polyaxial cell and subsequently conducted polyaxial tests on rectangular prisms of Karroo dolerite. Failure in these tests was observed to result in two roughly

plane fractures lying in the direction of the intermediate principal stress and inclined at a narrow angle to the direction of the major principal stress.

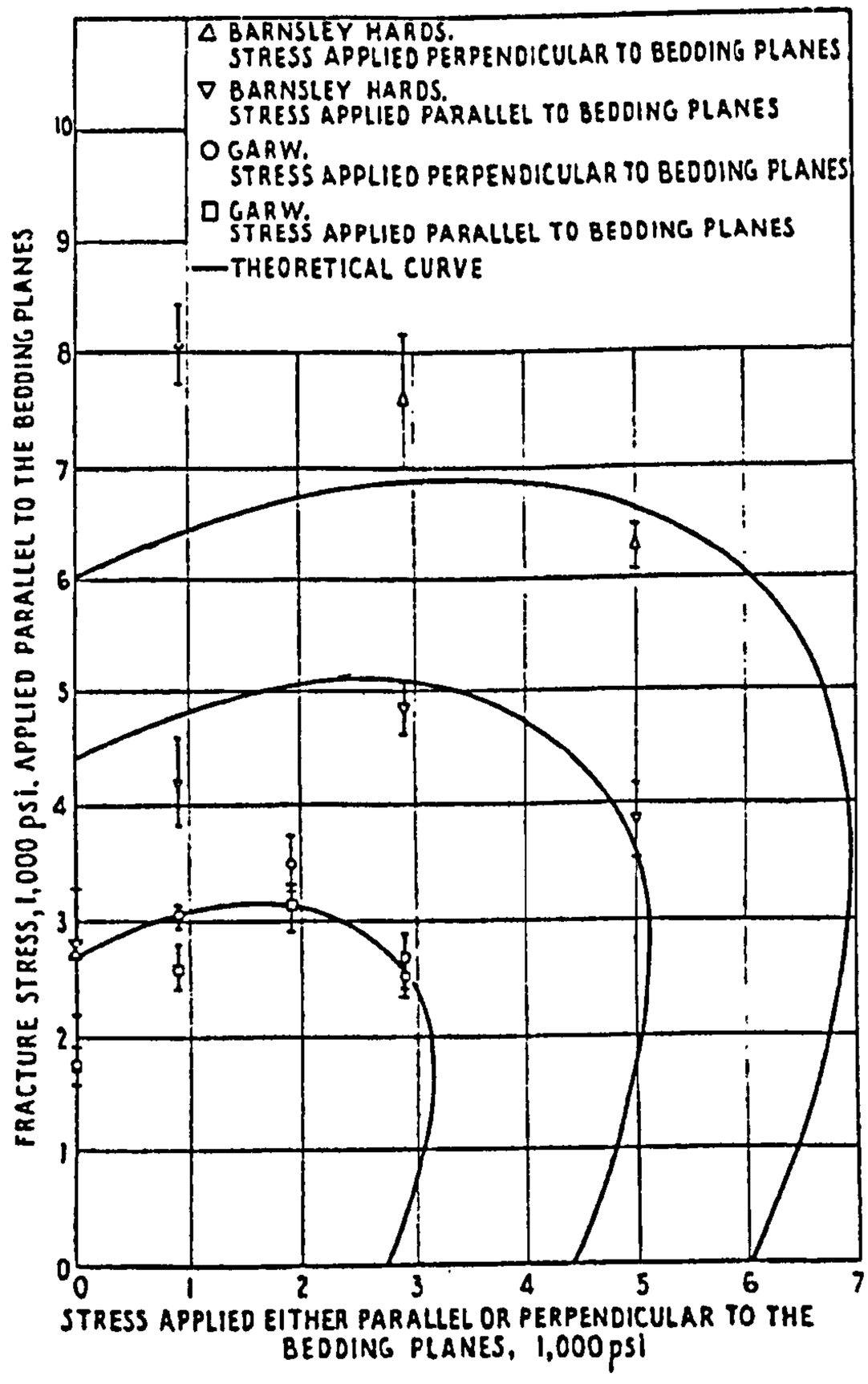

Figure 2.1 Results of biaxial experiments on cubes of coal (after Hobbs, 1962)

Stavropoulou (1982) tested rectangular prisms of Karoo sandstone under biaxial compression, $\sigma_3 = 0$, in plane-strain loading conditions, $\varepsilon_2 = 0$. There appeared to be a dramatic increase of the strength of sandstone by as much as 49% in comparison to the uniaxial compressive strength. This effect was ascribed to the presence of the intermediate principal stress, σ_2. Elastic constants appeared to decrease in comparison to corresponding uniaxial values. Moreover, dilatancy was also reduced while the pre-failure brittleness of the rock increased.

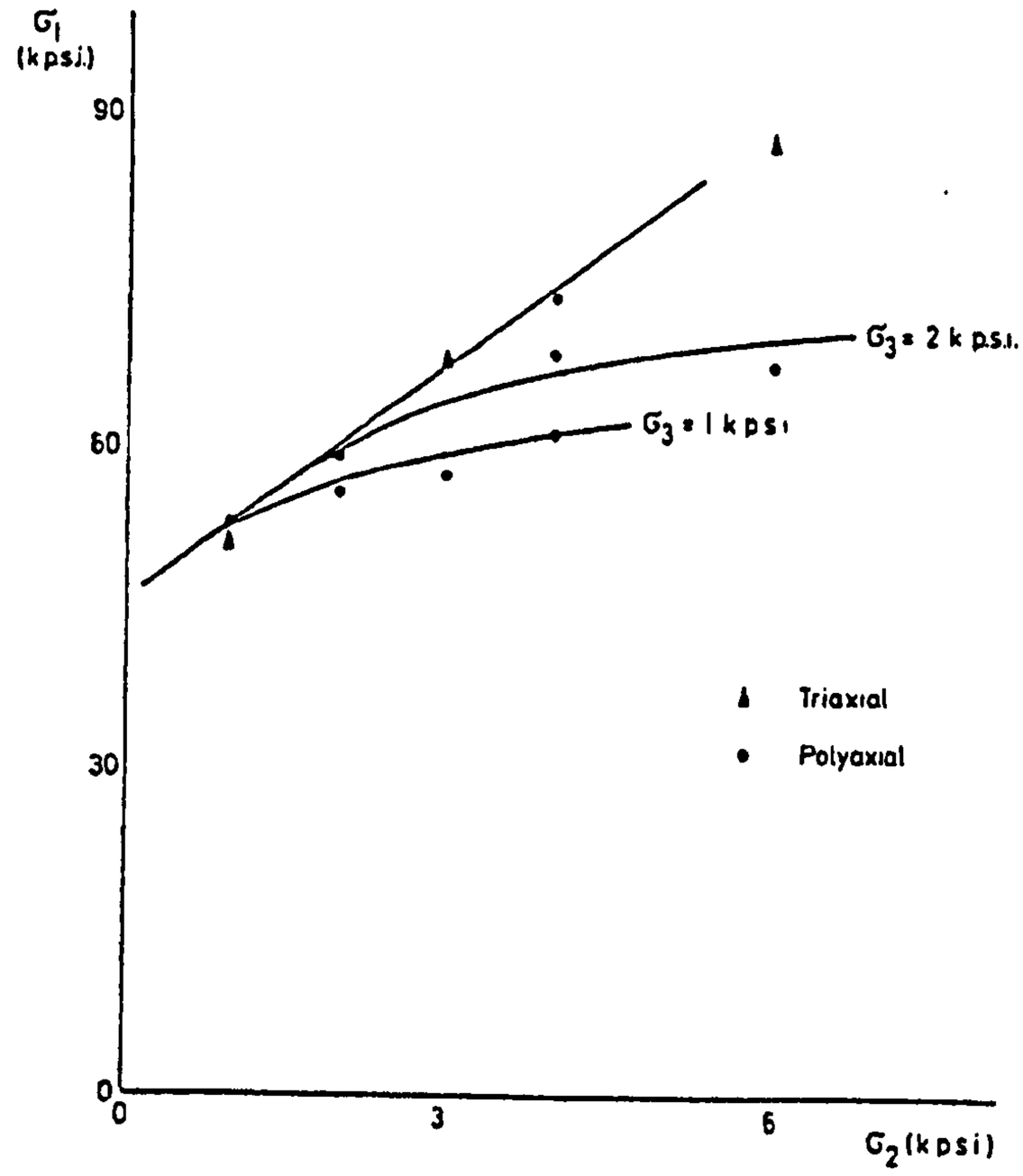

Figure 2.2 Effect of intermediate principal stress, σ_2, on the strength of Karroo dolerite (after Hojem and Cook, 1968)

The effect of the intermediate principal stress on rock behaviour was confirmed by Michelis (1985) from results of polyaxial tests on prismatic specimens of granular dense marble. As illustrated in Figure 2.3, under a constant value of the minor principal stress, σ_3, the strength observed to increase considerably with increasing the intermediate principal stress, σ_2, up to a point after which yield started to take place. During yielding the specimen weakened (work-softening in contrast with work-hardening behaviour under standard triaxial conditions) and the peak strength decreased with increasing the intermediate stress. The minor principal strain, ε_3, increased substantially with increasing σ_2 while the intermediate principal strain, ε_2, decreased. The permanent axial strain prior to peak strength decreased with increasing σ_2 and increased simultaneously with σ_3.

The effect of the intermediate principal stress, σ_2, has also been reported in work on engineering materials other than rock. Wang *et al.* (1987) carried out multiaxial tests on cubes of concrete. The level of σ_2 appeared to have a significant effect on the failure

strength of concrete. The major principal stress, σ_1, at failure was observed to increase with increasing ratio of σ_2 / σ_1 up to a point after which it started to decrease.

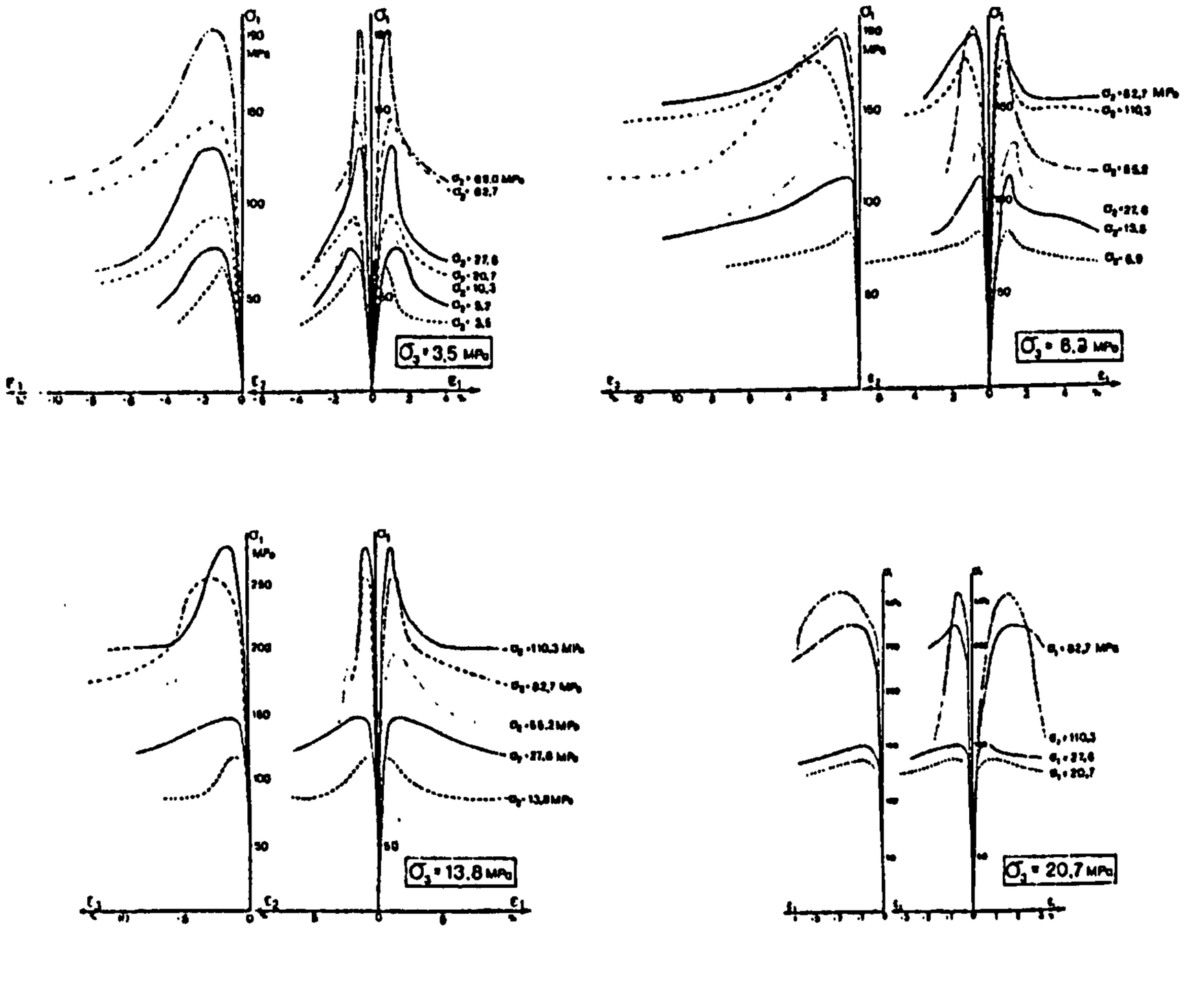

Figure 2.3 Results of polyaxial tests grouped according to the level of minor principal stress (after Michelis, 1985)

Brown (1974) placed emphasis on the effect of boundary conditions and the importance of applying uniformly distributed stresses in direct multiaxial tests. He carried out biaxial compression tests on plates of Wombeyan marble using brush bearing platens, an approach developed by Hilsdorf (1965). Tests with solid platens were also performed for comparison. As shown in Figure 2.4, results of both tests were scattered but the scatter was less with solid platens than with brush platens. The uniaxial compressive strength for the material found to be the same for both brush and solid platens. However, under biaxial conditions the strength increased over its uniaxial compressive value, but the rate of increase observed to be higher with solid platens than with brush platens. Nevertheless, it was pointed out that, in extremely brittle material, decreases in biaxial strength might accompany increases in the intermediate principal stress. Generally, failure occurred by

extension in the direction of the minor principal stress, $\sigma_3 = 0$. A variety of failure criteria were discussed, but the experimental results seemed explicable in terms of failure criteria based on effective tensile stress or maximum extensional strain concepts.

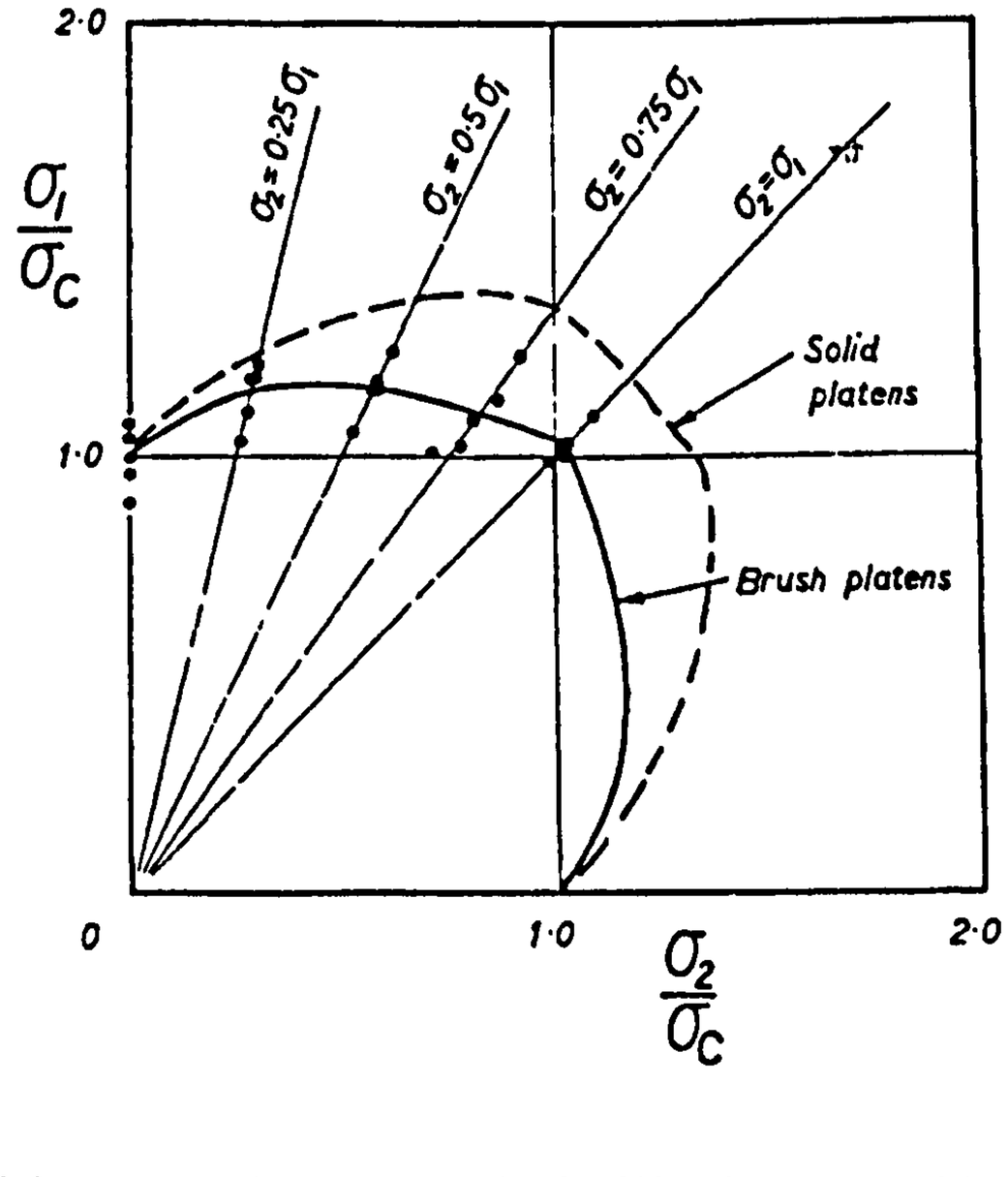

Figure 2.4 Biaxial compression test results for Wombeyan marble (after Brown, 1974)

The importance of achieving a uniform loading at the specimen boundaries was highly heeded by Maso and Lerau (1980) in their biaxial compression tests on prisms of Darney sandstone. The loading machinery used was aimed to apply stresses free from any extraneous flexion torque. In addition, loading plates with short broad pins were employed in order to eliminate friction at specimen ends and avoid differences of local strains. Different ratios of σ_1 / σ_2 were applied, and the three principal strains were systematically monitored up to failure. Failure was explosive and, most of the time, fracture took place along the central plane of the specimen. A picture of a typical fracture pattern, Figure 2.5, suggests that failure was of the extension type with the main fracture surface being almost perpendicular to the direction of the minor principal stress. The strength results obtained indicated a slight anisotropy of the material. More important, the intermediate principal stress appeared to have an appreciable influence on the failure conditions. It was believed that a failure criterion expressed in terms of stress is unable to

explain the results of these tests, and that the appropriate criterion should be the maximum extensional strain criterion expressed in terms of ε_3, except near the zone $\sigma_1 = \sigma_2$.

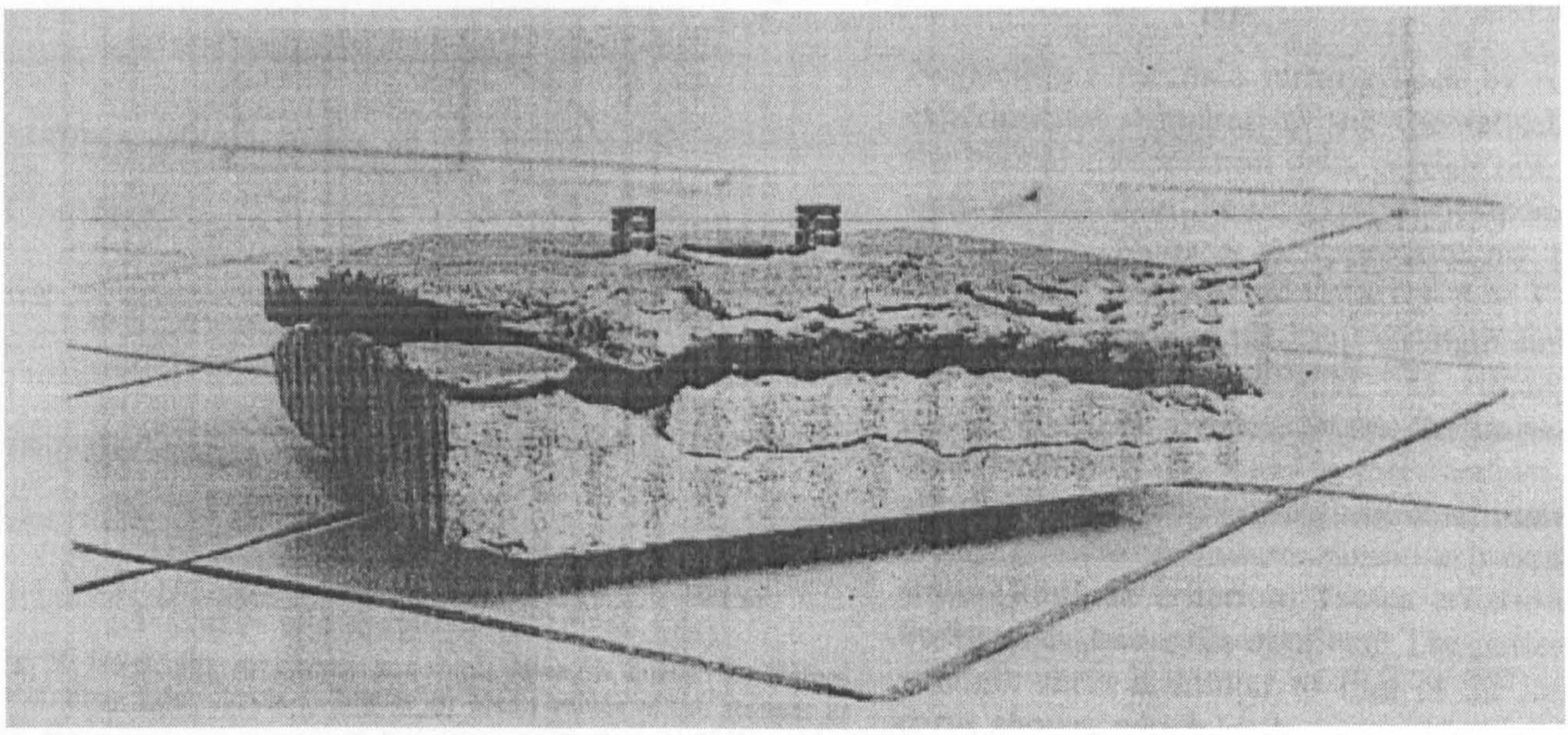

Figure 2.5 Typical fracture pattern observed in biaxial compression tests on prisms of Darney sandstone (after Maso and Lerau, 1980)

Another approach to overcome the boundary effects was employed by Amadei *et al.* (1984) in a series of multiaxial tests. Cubical specimens of Indiana limestone were tested under uniaxial compression and tension, biaxial compression, and combined biaxial compression-tension. Compressive loads were applied through hydraulically pressured flexible fluid cushions, while brush bearing platens were used for tensile loading. The test results indicated that rock strength is influenced by the relative magnitude of the intermediate principal stress. The strength of the limestone in biaxial compression was evidently higher than in uniaxial compression and appeared dependent on the value of the stress ratio σ_1 / σ_2. However, under biaxial compression-tension, the tensile strength seemed to decrease when the applied compressive stress was close to the uniaxial compressive strength. The observed fracture planes in most of these biaxial tests suggested that failure was of the extension type. Thus, the experimental observations discredited any failure criterion that neglects the effect of the intermediate principal stress. Furthermore, it was suggested that failure criteria based on maximum tensile stress or

maximum tensile strain would be more appropriate to model the strength of the tested rock than those based on shear failure.

Following the previous work, Amadei and Robison (1986) presented results from further tests on cubes of Indiana limestone incorporating multiaxial loading conditions. The apparent dependency of the strength on the intermediate principal stress in biaxial compression seemed less pronounced under true triaxial compression, $\sigma_1 > \sigma_2 > \sigma_3$. Contrary to what reported by other workers using solid or brush platens, Brown (1974), the equibiaxial compressive strength was found to be 20-25% lower than the uniaxial compressive strength. This lower strength was attributed to the boundary conditions imposed by the fluid cushions. Results of biaxial tension-compression tests suggested a decrease in the tensile strength with increasing compression. Results of conventional triaxial, triaxial extension, and simple shear tests indicated a decrease in the stress path effect on the strength as the level of the hydrostatic loading increased. The prediction of failure was assessed in terms of three failure criteria: Mohr-Coulomb, Hoek and Brown (1980b), and the three parameter criterion proposed by Kim and Lade (1984). Although all three failure criteria appeared to have advantages and disadvantages with regard to prediction accuracy, Figure 2.6, none of them fitted the results of all tests conducted.

Gau *et al.* (1983) conducted polyaxial compression tests on cubes of red sandstone. Two different boundary conditions, termed as rigid and flexible contact, were employed using PTFE sheets and emulsified rubber bags filled with Vaseline quartz sand mixture, respectively. The strength results were evidently influenced by the intermediate principal stress. In addition, the results of the flexible contact tests appeared to provide better reflection of the intrinsic mechanical properties of the rock tested.

Protopsaltis (1986) carried out polyaxial tests on cubes of Springwell sandstone using Teflon (PTFE) strips as a friction reducer at specimen-platen contacts. Failure appeared to occur by tensile splitting along the direction of the minor principal stress, σ_3, with the failure planes being parallel or slightly inclined to the direction of the intermediate principal stress, σ_2. The effect of σ_2 was found to be small yet measurable on the values of both σ_1 and ε_1, but considerable on the value of ε_3. However, an investigation carried

out in Chapter 5 has revealed that the failure mechanism in these experiments was highly influenced by having the PTFE strips overlapped.

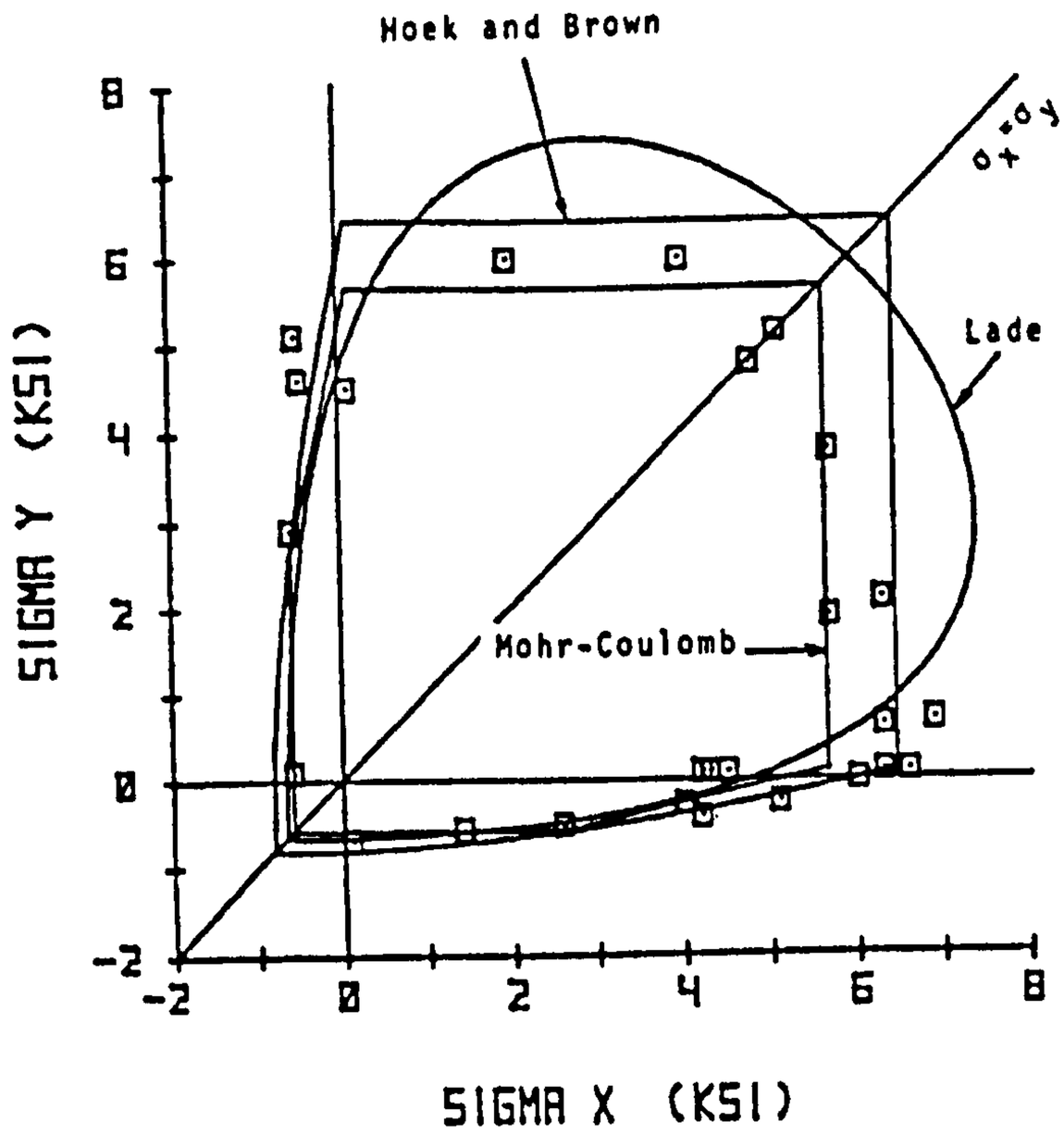

Figure 2.6 Failure envelopes for three failure criteria in the biaxial plane (after Amadei and Robison, 1986)

Akai and Mori (1970) presented results of multiaxial compression tests on cubes of sandstone. The effect of friction at specimen - platen contacts was reported to have been substantially reduced by using thin sheets of rubber wetted with silicon oil. While failure occurred by axial splitting or slicing under both uniaxial and biaxial compression, inclined shear fractures appeared to characterise failure under triaxial and polyaxial conditions, particularly at high levels of minor and intermediate principal stresses. Typical failure patterns observed are shown in Figure 2.7. As in other investigations, the test results appeared to confirm the effect of the intermediate principal stress, σ_2, on the levels of σ_1 recorded at failure.

Hunsche and Albrecht (1990) conducted multiaxial strength tests on cubes of different types of rock salt. Paraffin wax was found to be an effective friction reducer at room temperature, while graphite was found effective at elevated temperatures. Rock strength

appeared to be independent of the effect of specimen size. However, the measured strength was found considerably influenced by the ratio of the edge length of the specimen to that of the platens. Both mean stress and stress path emerged to be the main factors that influence the fracture strength of rock salt.

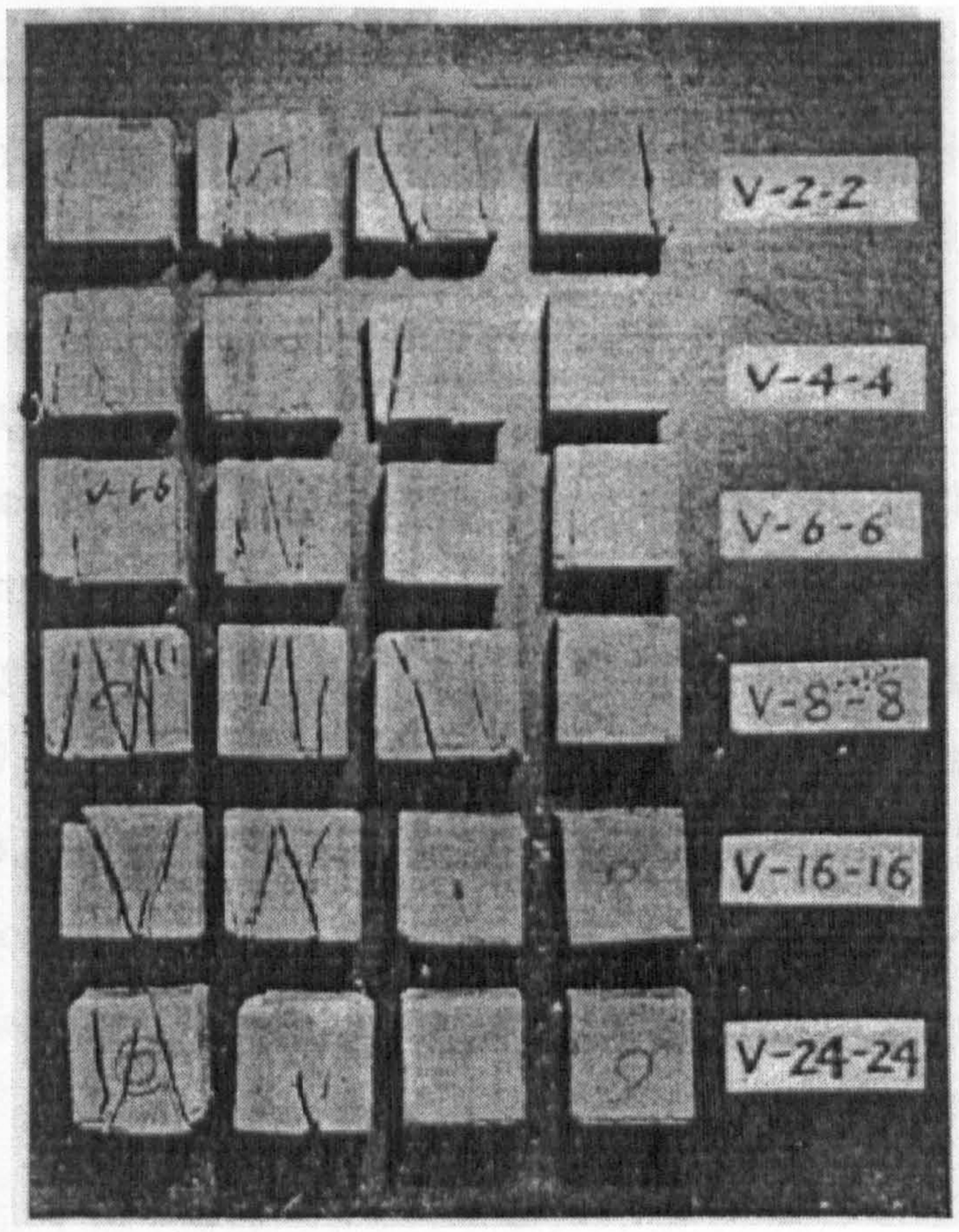

Figure 2.7 Failure pattern of specimens in triaxial compression test (after Akai and Mori, 1970)

The effect of various boundary conditions in direct multiaxial testing on the apparent material properties was exclusively investigated by Gerstle *et al.* (1980) on plain concrete. Cubes as well as cylinders and plates of the same concrete were tested in a joint laboratory programme under loading systems differing fundamentally in the specimen boundary conditions. Despite the numerous techniques employed, the tests can be grouped as constrained boundary tests and unconstrained boundary tests. These tests involved biaxial compressive loading with different stress ratios of σ_2 / σ_1, and triaxial loading incorporating three stress paths: triaxial compression, constant intermediate principal stress, and triaxial extension. Strain measurements were obtained utilising also different

monitoring approaches. There appeared to be a considerable scatter in the stress-strain results regardless of the test method used, but the scatter was much greater in the results of tests with constrained boundaries than in those with frictionless boundaries. Moreover, boundary constraint found to inhibit transverse specimen deformations, and therefore, are likely to result in erroneous material parameters.

Another investigation into the effect of boundary conditions in multiaxial tests was carried out by van Mier (1987). Cubes of concrete were subjected to multiaxial compression, while prisms of the same cross-sectional area and different heights were loaded in uniaxial compression. The post-peak stress-strain response of the prisms appeared to vary with the prism height, and fracture in uniaxial compression appeared to be a localised phenomenon. Failure occurred by shear, and the inclination of the shear plane seemed to decrease as the friction between the loading platen and the specimen was reduced by changing the boundary conditions. This observation appeared to agree with that of Kotsovos (1983) who suggested that the slope of the shear plane is not an intrinsic material property, but rather a direct result of the boundary shear between the loading platen and the specimen. Results of the multiaxial compression tests on cubes also indicated that fracture is a localised phenomenon as long as the brittle-ductile transition is not exceeded.

Demiris (1987) investigated the boundary friction effects in polyaxial tests by loading cubes of marble with different combinations of friction reducers. The test results suggested that a combination of three thin Teflon sheets lubricated with silicon grease could virtually eliminate side friction effects. Under triaxial conditions, $\sigma_1 > \sigma_2 = \sigma_3 > 0$, the specimen deformation appeared to progress by formation of a cone and propagation of cracks surrounding it, while under polyaxial conditions, $\sigma_1 > \sigma_2 > \sigma_3 > 0$, the cone is transferred into wedges and the specimen deforms by sliding along the fracture planes.

Guangzhi *et al.* (1988) attempted to examine the effect of stress path on the strength of rock. Rectangular specimens of sandstone and limestone were tested under three distinct stress paths. It was experienced that failure of rock could be caused not only by increasing the maximum principal stress, σ_1, but also by decreasing the intermediate and minimum

principal stresses, σ_2 and σ_3, respectively. Furthermore, the strength of the rocks tested appeared to be dependant on the stress path employed.

The effect of stress path was evident in results of compression tests conducted by Kawamoto *et al.* (1970) on cubical specimens of cement mortar simulating rock-like materials. Teflon sheets wetted with silicon grease were placed between the specimen faces and the loading plates in an effort to reduce the effect of friction. The experimental results showed that the moduli of deformation are considerably influenced by the hydrostatic and deviatoric stress components as well as the stress path. In addition, there appeared to be a transformation in behaviour from brittle to ductile with increasing the octahedral normal stress. Although the test material was believed to be homogeneous and isotropic in macroscale, anisotropy in deformation was observed under high deviatoric stresses.

A remarkable influence of the stress path on the strength and stress-strain relations was reported by Sargand *et al.* (1987) in multiaxial tests on cubical specimens of compacted shales conducted under various loading conditions. In a set of simple shear tests, in which σ_2 was held constant while σ_1 and σ_3 were increased and decreased respectively by the same amount, it was observed that as the intermediate stress increased, the intermediate strain moved from extension to compression.

In addition to prominent factors reported in the foregoing studies to influence the results of direct multiaxial compression tests, a number of other factors have been acknowledged by various researchers. Wichter (1979) tested cubical and cylindrical specimens of Jurassic clay shale under biaxial and triaxial loading conditions, respectively. The test results were found significantly influenced by the orientation of the bedding planes, specimen size, and strain rate.

Angeli Radovani (1986) discussed results of multiaxial compression tests on cubes of concrete. The level of lateral confinement presented by σ_2 and σ_3 appeared to have a great influence on the deformational behaviour of concrete. High levels of σ_2 and σ_3 were found to increase concrete strength and reduce crack formation and propagation. In addition, while splitting type of failure was found associated with low levels of lateral

stresses, crushing with a complete disintegration of concrete inner structure seemed to accompany near hydrostatic state of compressive stresses.

Angeli Radovani (1990) presented results of further multiaxial compression tests on cubes of concrete. As in previous tests, loads were applied through steel brush bearing platens to reduce friction and ensure uniform stress and strain at the specimen boundaries. However, the obtained stress-strain curves showed exaggerated deformation and nonlinear behaviour at the beginning of the tests. This phenomenon was attributed to the *nonideal* interface between the brush platens and the test specimen. Once more, the results of these tests confirmed the influence of the applied levels of σ_2 and σ_3 on the concrete behaviour and failure mode.

2.4 Studies Based on Indirect Multiaxial Loading

Indirect multiaxial compression of rock has often been achieved by subjecting specimens, in the form of thick-walled hollow cylinders, to various combinations of internal and external hydrostatic pressures in addition to axial load. The loading conditions are usually governed by the nature of stress field intended to be induced in the cylinder, and most researchers have used the theory of elasticity to determine the corresponding levels of principal stresses at the specimen inner walls.

The use of hollow cylinders in rock testing appears to date back to early this century when it was conjectured by some that underground openings at a depth of about six miles would close in and collapse due to the existence of great pressure at such level. Adams (1912) quoted a comment made by C. A. Parsons saying:

"It would however be interesting to subject a cylinder of granite or quartz rock carefully fitted into a steel mould and having a small hole bored through its centre to a pressure of say 100 tons to the square inch and see what shrinkage in the hole would result."

Adams (1912) took the initiative to carry out an experimental investigation on the depth of the flow zone in the earth's crust. Cylinders of Solenhofen limestone and Westerly granite with small axial and transverse holes were constrained laterally and subjected to different values of axial compression and temperature. The holes were inspected upon completion of tests for any closure that might have taken place. Signs of structural damage in the holes such as spalling were detected under loading conditions representing depths in the earth's crust much greater than had been suggested. The results of these experiments were analysed mathematically by King (1912) who also discussed the systems of fracture that might develop in hollow cylinders of rock under various states of stress.

The work of Adams was later repeated by Bridgman (1918) under different loading conditions. Hollow cylinders of rocks and crystals were crushed under external hydrostatic pressure. The obtained stress at failure was found considerably lower than that

of Adams. Failure of the cylinders appeared to initiate by the spalling, *shooting-off* or *flaking-off*, of minute fragments from the walls of the hole.

Since the date of Adams' pioneering work on hollow cylinders of rock, many researchers have utilised hollow specimens to investigate various aspects in the field of rock mechanics.

Robertson (1955) examined the strength of several rocks using hollow cylinders with closed ends of different sizes and a range of ratios between their outer and inner diameters. The cylinders were subjected only to increasing hydrostatic pressure applied to their outer surfaces. Results from tests on cylinders of Solenhofen limestone, Figure 2.8, exhibited a notable effect of size as well as wall thickness on the rupture strength. However, the evidence that the small cylinders were stronger was attributed to either unrecognised differences in processing the cylinders or to fewer imperfections of gross dimension. Specimens with radius ratios less than 3 appeared to fail directly by total collapse, while those with ratios greater than 3 failed by spalling at the inside surface. The failure by spalling was found accompanied by plastic deformation in a middle layer and elastic strain in the outer part of the cylinder. A single plane of weakness in hollow cylinders was found not to have any significant effect on the cylinder strength and failure mode. Temperatures much higher than 20° C appeared to increase both rupture strength and the rate of plastic deformation up to a point where rapid plastic flow occurred.

The biaxial work of Hobbs (1962) and that of Pomeroy and Hobbs (1962) on cubes of coal were accompanied by tests on thick-walled hollow cylinders. The cylinders were fractured in one of two ways: either under an increasing external hydrostatic pressure only, or under a predetermined constant external hydrostatic pressure and an additional increasing axial load. The observed fracture surfaces appeared to generally follow the maximum shear stress surfaces. Once again, the effect of the intermediate principal stress on the fracture stress was confirmed and appeared more pronounced than in the case of the cube tests. In addition, the results endorsed the inadequacy of the available failure criteria.

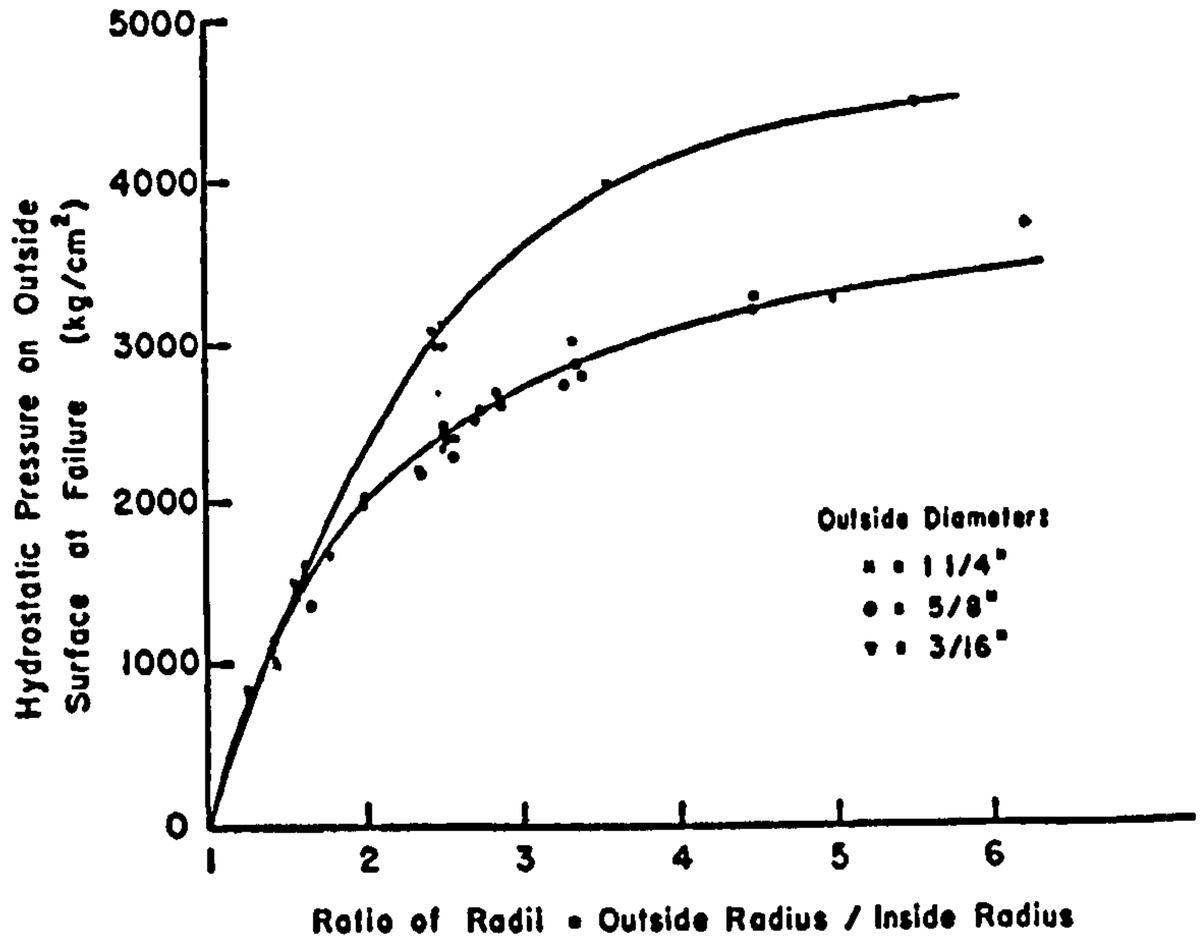

Figure 2.8 Hydrostatic pressure at failure vs. ratio of radii for three sizes of hollow cylinders of Solenhofen limestone (after Robertson, 1955)

The numerous attempts made by researchers using cubical specimens to evaluate the effect of the intermediate principal stress, σ_2, on the apparent strength of rock have been matched by similar attempts utilising specimens in the form of hollow cylinders. One such attempt was made by Mazanti and Sowers (1966) who initiated a testing programme in which hollow cylinders of rock were subjected to different combinations of internal and external pressures together with axial loads. The effect of the intermediate principal stress, σ_2, on the strength of rock was illustrated by results from tests in which the minor principal stress, $\sigma_3 = \sigma_r$, was held constant while the intermediate stress, $\sigma_2 = \sigma_\theta$, was increased with the major principal stress, $\sigma_1 = \sigma_z$, at a constant ratio until failure occurred. As demonstrated by Figure 2.9, there appeared to be an increase in the level of σ_1 with increasing σ_2 / σ_1 ratio up to a point, after which σ_1 decreased. An investigation into the onset of failure under the conditions $\sigma_1 = \sigma_z > \sigma_2 = \sigma_\theta > \sigma_3 = \sigma_r$ appeared to substantiate the premise that failure initiates by spalling at the inner surface of the cylinders, as pictured in Figure 2.10.

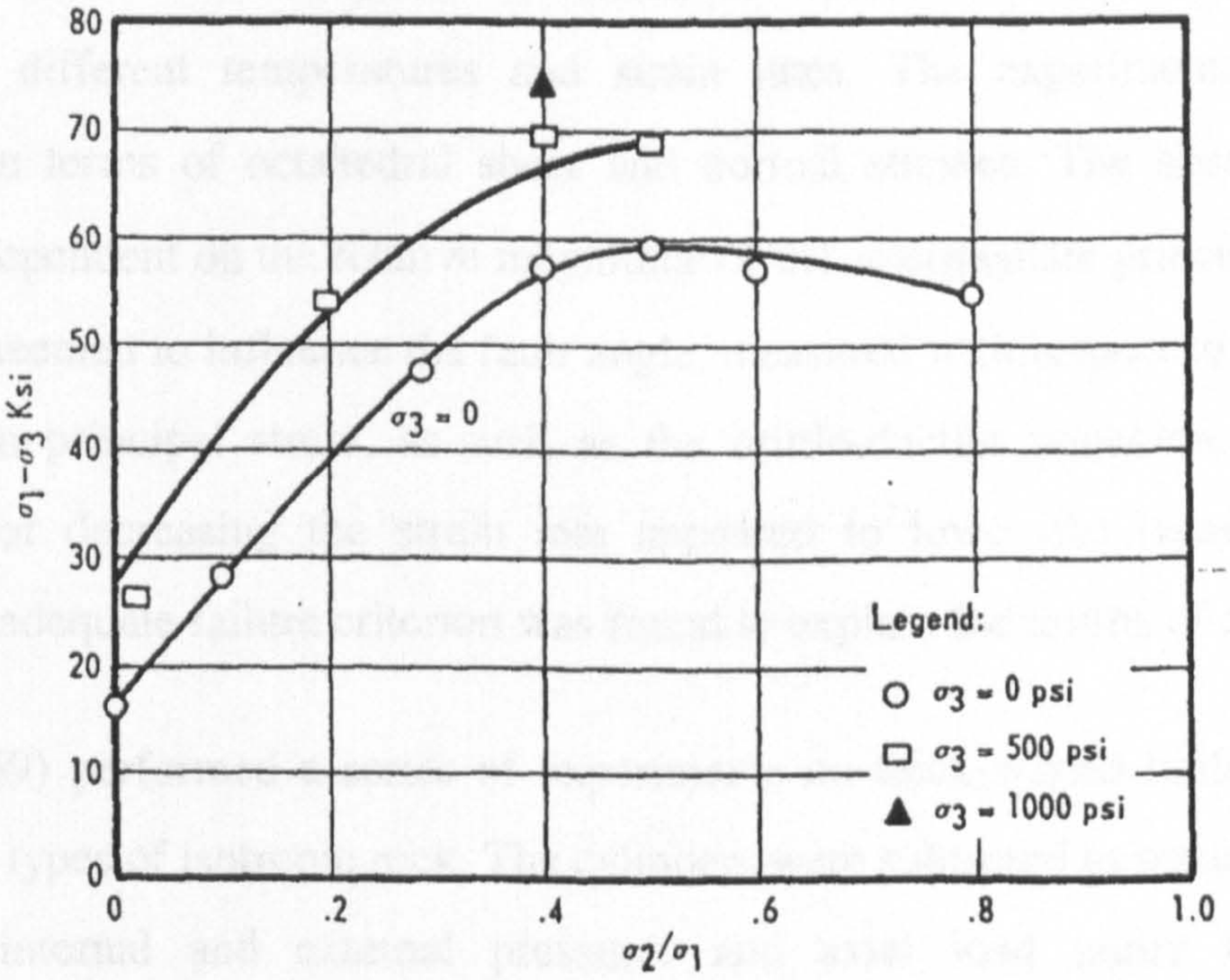

Figure 2.9 Variation of principal stress difference with σ_2 / σ_1 ratio for granite hollow cylinders (after Mazanti and Sowers, 1966)

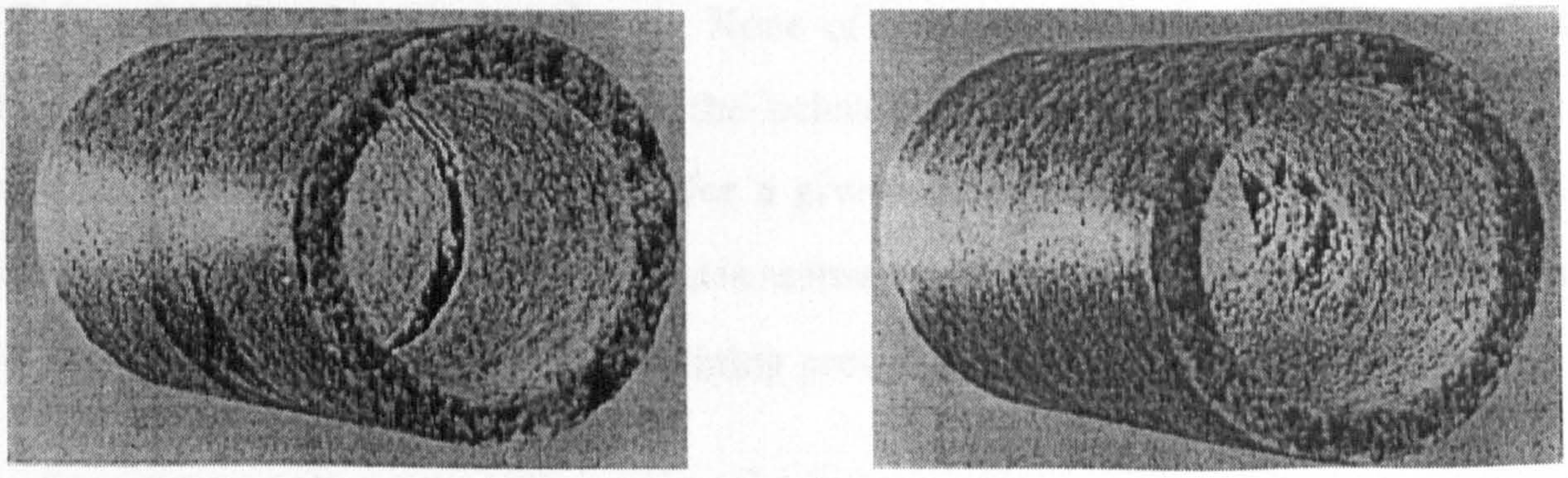

View 1 *View 2*

Figure 2.10 Spalling inside granite hollow cylinder unloaded prior to fracture $\sigma_3 = 0$ and with $\sigma_2 / \sigma_1 = 0.88$ (after Mazanti and Sowers, 1966)

Another attempt to assess the effect of the intermediate principal stress on rock failure was made by Handin *et al.* (1967). Solid and hollow cylinders of Solenhofen limestone and Blair dolomite were subjected to combined torsion and triaxial compression or extension at different temperatures and strain rates. The experimental results were represented in terms of octahedral shear and normal stresses. The shear strength was found to be dependent on the relative magnitude of the intermediate principal stress σ_2. In addition, σ_2 seemed to influence the fault angle, measured with respect to the direction of the maximum principal stress, as well as the brittle-ductile transition. Increasing the temperature or decreasing the strain rate appeared to lower the transition confining pressure. No adequate failure criterion was found to explain the results of all tests.

Hoskins (1969) performed a series of experiments on thick-walled hollow cylinders of five different types of isotropic rock. The cylinders were subjected to separately controlled and varied internal and external pressures and axial load under which different arrangements of principal stresses at failure were attained. Various types of fractures were observed, and there appeared to be a smooth transition from tensile failure to compressive or shear failure under combined polyaxial stress conditions. While stress gradients achieved in the tests seemed to have little effect on rock strength in compression, the magnitude of the intermediate principal stress emerged to have a marked and regular effect on the strength of the rocks tested. Some of the experimental results are presented in Figure 2.11 for three types of rock. None of the commonly used failure criteria for brittle materials adequately predicted the behaviour of these rocks. Nevertheless, the proposal to generate a failure surface for a given material by rotating triaxial test data about the $\sigma_1 = \sigma_2 = \sigma_3$ principal stress axis seemed reasonably substantiated by the results of these experiments at least at low confining pressures when $\sigma_z > \sigma_\theta > \sigma_r$.

Bandis *et al.* (1987) investigated the state of stress and failure modes around circular openings excavated in polyaxially stressed blocks of rock-like material. Shear failure was dominant and the intermediate principal stress (axial in the experiments) appeared to have a significant stabilising effect.

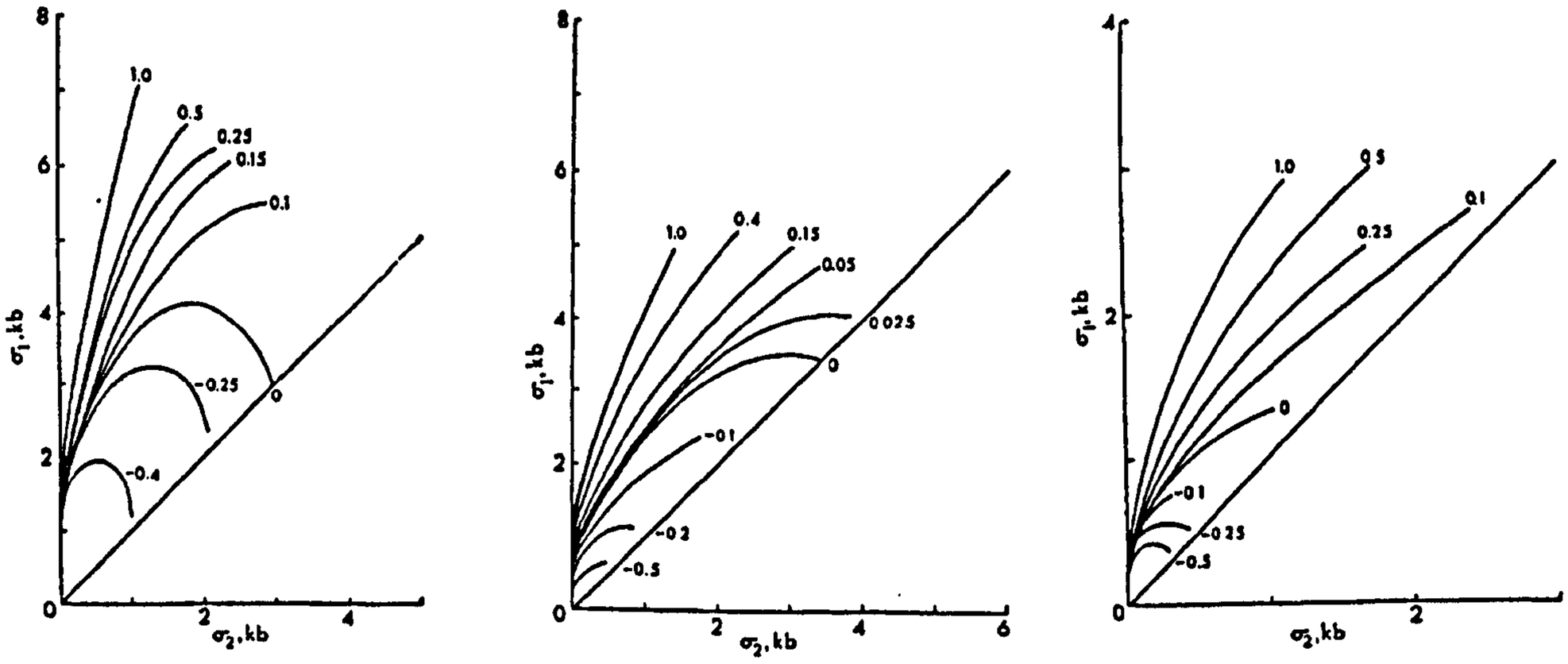

Trachyte *Marble* *Sandstone*

Figure 2.11 Results of hollow cylinder experiments on different types of rock σ_1 vs. σ_2 for various ratios of σ_3 / σ_2 (after Hoskins, 1969)

Alsayed (1988) subjected thick-walled hollow cylinders of four types of rock to constant levels of external hydrostatic pressure and increasing axial loads, thus inducing at the cylinder inner walls a biaxial stress field in which $\sigma_1 = \sigma_z > \sigma_2 = \sigma_\theta > \sigma_3 = \sigma_r = 0$. The test results appeared to confirm the marked influence of the intermediate principal stress, σ_2, on the behaviour of rock. A substantial increase in the level of σ_1 at failure was recorded with increasing the level of σ_2. This phenomenon appeared to hold within the range of external pressure applied. As a result, any failure criterion that does not account for σ_2 effect was discredited and deemed inapplicable to the experimental results.

Senseny *et al.* (1989) performed polyaxial and triaxial compression creep tests on hollow and solid cylinders, respectively, of natural rock salt. The levels of principal stresses imposed were selected to maintain the same levels of mean and octahedral shear stresses for both types of tests. A comparison between the test results showed differences in the behaviour of the two types of specimens, and suggested that approximating polyaxial

conditions to triaxial conditions may lead to inaccurate prediction of salt behaviour around underground openings.

While most researchers have advocated that rock strength is influenced by the magnitude of the intermediate principal stress, converse opinions have occasionally been voiced. One such opinion was that of Obert and Stephenson (1965) who fractured thick-walled hollow cylinders of different rocks under increasing external pressure and predefined levels of axial stress. The attained values of external pressure at fracture were found to be for practical purposes independent of the level of axial stress applied. This observation appeared to substantiate the postulate of Mohr's theory that failure is independent of the intermediate principal stress.

An area where hollow cylinders have been favoured and extensively used has been in the study of underground structures and related issues. Many researchers have recognised the versatility of the specimen geometry and potential loading arrangements to simulate a wide range of in-situ stress conditions.

Daemen and Fairhurst (1971) used hollow cylinders of Indiana limestone and concrete to study the influence of failed rock properties on tunnel stability. The cylinders were subjected to external hydrostatic pressure with the axial stress in the specimen being determined by the end conditions. These conditions were such that the axial stress for the limestone specimens was close to a value determined by plane strain conditions, and close to the hydrostatic stress for the concrete specimens. Failure around the opening appeared to initiate by the loosening of fine dust particles from the opening walls. As the applied pressure was increased, slabbing started to take place. The applied pressure reached a value representing a tangential compressive stress of at least 4 times the uniaxial compressive strength of the material before there was any indication of failure. A complete collapse occurred at a relative value of tangential stress of 5 to 6 times the uniaxial compressive strength.

Gay (1973) attempted to resemble different shapes of underground mining excavations by using thick-walled cylinders of sandstone and quartzite with circular, elliptical and rectangular holes. The cylinders were subjected to an equal axial and outer lateral

hydrostatic pressure. Most of the specimens were not taken to failure in order to study the growth of fractures around their openings. The obtained measurements of hole volume closure during loading showed that at low applied pressure the openings deformed in an elastic manner with a relatively large volumetric strain. However, at higher values of applied pressure yielding appeared to take place accompanied by rapid closure, but the onset of this stage and the behaviour thereafter seemed to vary with the opening shape as well as the rock type. The observed initial fracture patterns around all the openings tested were fundamentally the same and suggested similar failure origin and mechanism. As shown in Figure 2.12, failure appeared to initiate by shearing at two diametrically opposite points and progress by spalling at these loci. Extension cracks parallel to the maximum principal stress were also likely to form but mainly under high values of applied hydrostatic pressure. Bedding planes appeared to influence the failure mode and act as preferential planes of fracturing.

Gay (1976) extended his previous work to study the fracture growth around circular and rectangular openings in blocks of the same rocks. There appeared to be a good agreement between the results of both works.

Another study of the deformation and fracture around underground openings through experiments on thick-walled hollow cylinders of rock was carried out by Ewy *et al.* (1988). The experiments incorporated the following features: plane strain loading condition with the specimens being constrained in the axial direction, the ability to impose different stress paths on the rock using independent internal and external pressures, and freezing of the fracture geometry under load using a metal injection technique. Measurements of the elastic volume deformations of the hole, i.e. volumetric change, due to internal and external pressures were made and then used, assuming homogeneity and isotropy, with the equation for plane strain deformation of a finite hollow cylinder to calculate the two elastic moduli, namely Young's modulus and Poisson's ratio. Results from preliminary tests on Berea sandstone suggested that deformations, strengths and failure processes in hollow cylinder tests are not necessarily the same as in solid cylinder tests. The measured deformations yielded different elastic moduli than those reported from uniaxial compression tests. The unconfined strength of

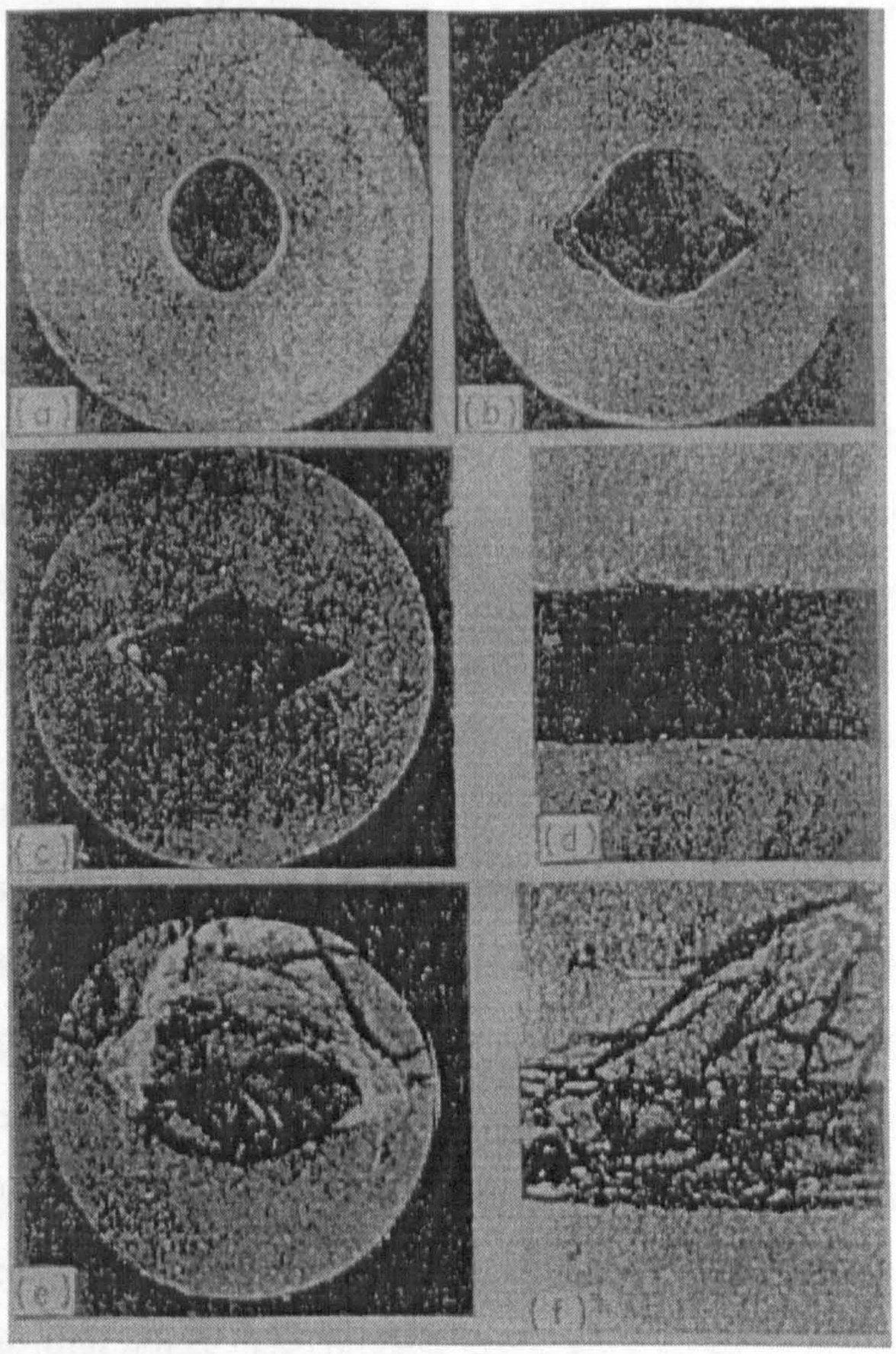

Figure 2.12 Polished sections of deformed sandstone cylinders containing circular holes after different levels of post-yield volume strain, ε_v
(a) specimen S4 at ε_v = 1%; (b) S5 at 2.5%; (c,d) S6 at 4.4%; (e,f) S2 at 14.5%
(after Gay, 1973)

the rock surrounding the hole was two to three times the typical uniaxial strength. This high strength thought to be due to a combination of size effect, the presence of an intermediate (axial) principal stress, stress gradients, and other geometric effects such as the restriction of dilation to only one curved surface. A confining (radial) stress in the hole found to strengthen the rock as does the confining pressure in solid cylinder tests. Under constant external pressure and decreasing internal pressure, or increasing external pressure with zero internal pressure, brittle spalling appeared to control the failure process. Although the load was axisymmetric, there was a preferred direction of failure.

The observed failure characteristics believed to raise doubts about the applicability of continuum theories describing the formation of a strain - softened or plastic zone.

Along the lines of the previous work, Ewy and Cook (1990a) & (1990b) carried out further tests on thick-walled hollow cylinders of Berea sandstone and Indiana limestone. In addition to the previous features, the tests incorporated transference of the external pressure from a finite radius to infinity by surrounding the specimen by a steel jacket of a correct thickness so that its stiffness would match that of an infinite extent of surrounding rock. Only two samples were fitted with steel jackets on the outer diameter; the rest of the samples were rubber-jacketed. Measurements of the hole deformations due to internal pressure were found to be controlled by overall moduli different from those controlling hole deformations due to external pressure. These moduli appeared to be determined by the different stress paths caused by the two loading sequences. A radially anisotropic moduli model was found to successfully explain the observed deformational behaviour. The failure process appeared to be accompanied by substantial radial dilation in the failing material especially for unsupported holes, and no existing model could adequately predict the resulting hole closures. In addition, the failure process was found to be time-dependent, notably in the absence of support. Microscopic observations indicated that fracture is initiated by the growth of small, opening-mode, splitting cracks oriented parallel to the tangential stress. The process starts very close to the hole and progresses deeper in the rock with increasing stress. A support pressure in the hole seemed to prevent the formation of macroscopic splitting fractures and the consequent spalling. However, with high enough stress, features of localized damage were evident, but the failed rock maintained significant cohesion and the damage features appeared to be bands of shear localisation. Failure of the cylinders occurred on the two opposite sides of the opening where the tangential stress was parallel to the bedding planes. The size of the failed zones seemed to be influenced not only by the final stress state but also by the stress path, strain rate and test boundary conditions. Transferring the external pressure to infinity appeared to reduce hole deformations and cause failure to progress in a more stable manner.

The development of macroscopic failure in thick-walled hollow cylinders was investigated by Santarelli and Brown (1989). Hollow cylinders of three sedimentary rocks were tested under increasing linearly with time external hydrostatic pressure. In addition,

solid cylinders of the same rocks were tested in standard triaxial compression. The test results indicated that, qualitatively, an element of rock at the inner wall of the cylinder hole goes through the same deformation process as a specimen of the same rock tested in uniaxial compression. This deformation process which was summarized by Paterson (1978) consists of plastic pore and crack closure followed by a phase of almost elastic deformation and then a phase of microcrack development. A model of crack propagation in heterogeneous media developed by Zaitsev (1985) appeared to be able to explain qualitatively the failure patterns observed for all three rocks in hollow cylinder tests as well as in uniaxial compression tests. Consequently, the test results appeared to cast doubt on the quantitive prediction of failure development around circular underground excavations using conventional approaches.

The nature of failure in thick-walled hollow cylinders has always been a primary issue for experimental investigations. Périé and Goodman (1988) tested thick-walled cylinders of rock-like material, made of gypsum cement, under axial load and external confining pressure. The use of artificial rock was aimed to make the experiment more easily reproducible and eliminate the influence of unknown stress history on the failure characteristics. Failure was achieved by increasing the axial load while maintaining the external confining pressure constant at a predefined level. The specimen underwent two loading stages and was unloaded in between for visual inspection. The first loading stage was often marked by audio cracking while the second stage was ended by the specimen failure. The axial stress at failure was found to be closer to the value of the uniaxial compressive strength than to the strength of a confined cylindrical specimen. Hence, it was suggested that a rock fails at a smaller stress when loaded axially than when loaded radially in a thick cylinder configuration. The visual inspection during and after the test revealed *evidence of new failure patterns in a thick- walled cylinder experiment*. As illustrated in Figure 2.13, three long axial cracks were observed at the inner wall extending along the specimen longitudinal axis, and round failure regions appearing as rings regularly spaced along the wall of the specimen hole. Spalling seemed to have taken place in these round regions The axial cracks were interpreted as splitting in the direction of the maximum compressive stress, while the ring-like cracks were regarded as shear failures. The equal spacing of these shear rings was found to be explicable by the theory.

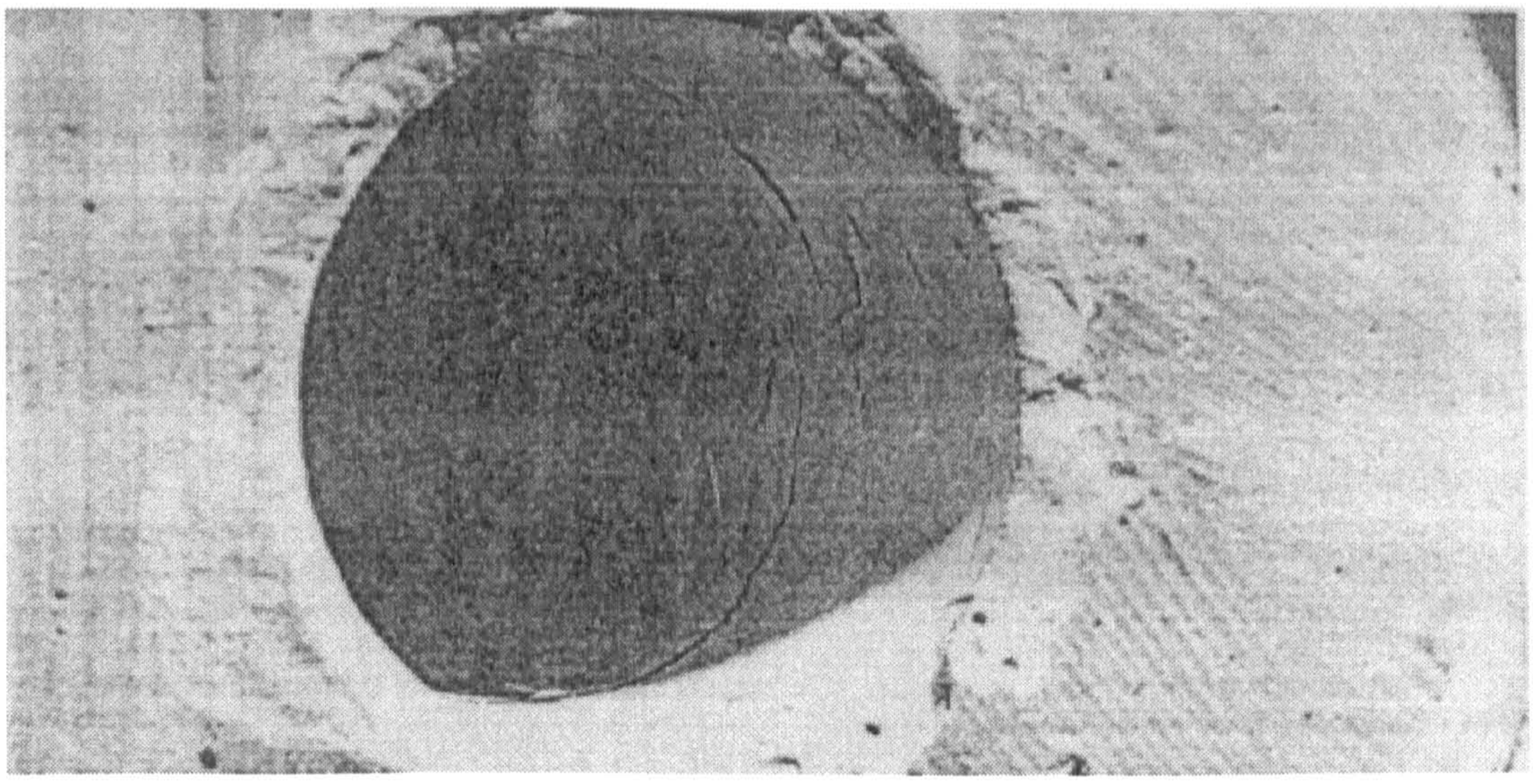

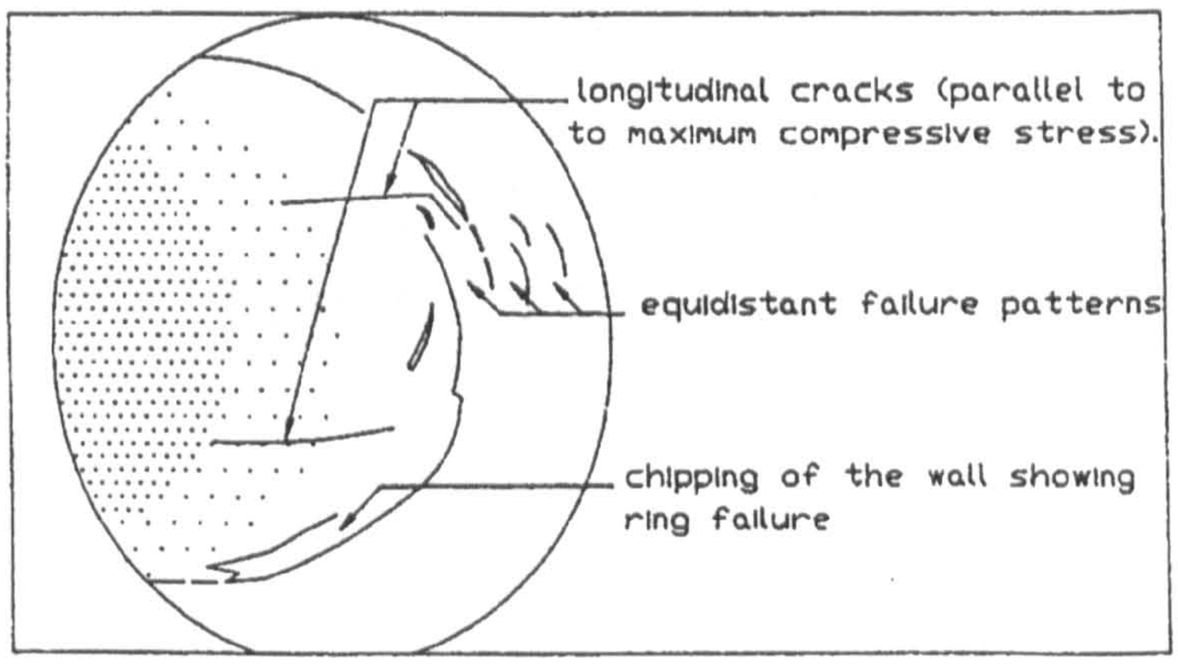

Figure 2.13 A view of the hole after the experiment and an illustration of this view (after Périé and Goodman,1988)

Chapter

3

Design and Description of the Testing Facilities

3.1 Introduction

The Rock Mechanics Laboratory at the University of Newcastle upon Tyne, where the experimental work was conducted, is well equipped with comprehensive facilities for rock testing and monitoring. However, the undertaking of a non-conventional testing programme incorporating polyaxial loading of cubical and hollow cylindrical specimens has involved the design and acquisition of new testing facilities, in addition to modification of existing equipment and improvement of testing configuration. In this respect, a new apparatus has been devised for testing thick-walled hollow cylinders of rock under internal and external lateral hydrostatic pressures together with axial load. An existing multiaxial cubical test apparatus used for loading cubes of rock has been thoroughly scrutinised and undergone major modifications. A pressure intensifier system has been acquired and introduced into the testing configuration where an accurate control over the confining pressure and monitoring of the specimen volumetric deformation are essential for effective testing. In order to eliminate the effect of the testing machine stiffness on the failure process of the test specimen and have a better control over the test course, all multiaxial tests have been conducted using the Laboratory servo-controlled loading system. An existing data acquisition system has been enhanced by a new personal computer, and the operating program has been revised for compatibility with the new hardware as well as the operating system and data processing software.

This chapter introduces the main testing facilities employed in the present work, and provides a short account of the developments in experimental techniques and equipment made to accomplish the testing programme.

3.2 The Multiaxial Cubical Test Apparatus

3.2.1 Brief History

The multiaxial cubical test apparatus, also called the polyaxial rig, has been available in the Rock Mechanics Laboratory for sometime. It was constructed at Newcastle University around 1972 for laboratory testing of evaporite rocks. Thereafter, the apparatus was used by Protopsaltis (1982) and Canli (1983) to investigate the effect of the intermediate principal stress on the level of the major principal stress at failure. Protopsaltis (1986) conducted further investigations in which he made some modifications to the apparatus aimed to improve its rigidity and efficiency. Subsequently, Laderian (1987) used the apparatus along the same lines.

3.2.2 General Description and Features

Pictured in Figures 3.1 to 3.3 after it has been modified in the present study, the multiaxial cubical test apparatus is basically formed by a rigid steel frame with four welded rectangular walls which define the apparatus body and accommodate its main components. These components comprise two load cells, two single-acting hollow plunger hydraulic cylinders, and loading platens. The load cells are bolted to the apparatus walls with each cell facing one of the hydraulic cylinders mounted on the opposite wall. The hydraulic cylinders, often referred to as hydraulic rams, are of a maximum capacity of 60 tons and an effective area of 8800 mm^2. The cylinders are equipped with standard collar threads and a carrying handle for readily threading into mounting. Push-fit bearing platens are inserted into the hollow piston of the hydraulic cylinders to force the specimen against the load cells upon application of pressure. Each bearing platen is fastened to a rod housed inside the hollow cylinder and travels through as the platen moves. The deformation of the specimen along the platen path is traced by a transducer clamped at the back of the hydraulic cylinder with its armature resting on a small disc attached to the free end of the platen rod. Naturally, these bearing platens are often called the moving platens, but to avoid confusion, they are going to be referred to as the hydraulic ram platens. In

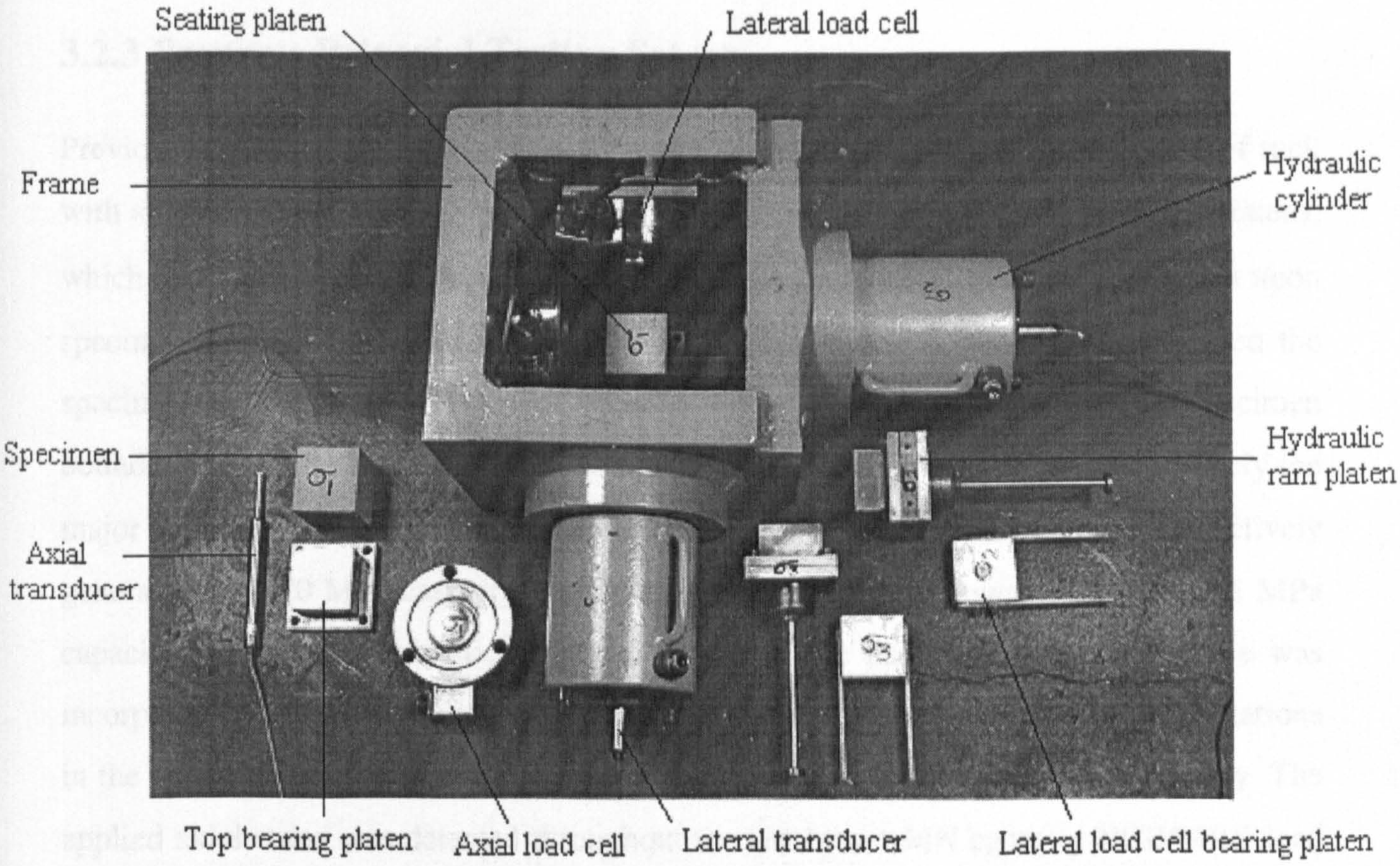

Figure 3.1 A view of the multiaxial cubical test apparatus showing its main components after it has been modified in the present study.

addition to its movement with the piston along the cylinder axis, the platen can be rotated around this axis and is slightly adjustable in the plane normal to this direction so that proper alignment and contact with the specimen can be ensured.

When a specimen is placed inside the apparatus, it rests on a square prismatic steel platen located in the middle of the frame and tied by four steel plates. For three-dimensional loading, a bearing platen is laid on top of the specimen facing the seating platen, and a third load cell and a transducer are incorporated in this direction. Generally in a polyaxial test, the minor and intermediate principal stresses are applied laterally through the hydraulic cylinders using hydraulic pumps to provide the required pressures. The major principal stress is applied axially by a loading machine. The applied loads or stresses are sensed by the load cells, and the corresponding deformations of the test specimen along the three principal directions are tracked by the transducers. The output of these units are acquired by means of a data acquisition system.

3.2.3 Previous Polyaxial Testing Set-up

Previous employment of the cubical apparatus in polyaxial testing involved cubes of rock with side length of 72 mm. The specimen size was chosen to prevent the bearing platens, which have a square cross section of 70×70 mm, from coming together into contact upon specimen loading and subsequent deformation. Teflon sheets were placed between the specimen and the bearing platens in order to reduce the effect of friction at the specimen boundaries. A soft or non-stiff 5 MN AVERY loading machine was utilised to apply the major principal stress. The intermediate and minor principal stresses were respectively generated by a 70 MPa capacity FARNELL mobile hydraulic power pack and a 35 MPa capacity ENERPAC hydraulic hand pump. Along the hand pump, a relief valve was incorporated in order to have a better control over the applied pressure. Due to limitations in the loading machine, tests were carried out under a constant axial stress rate only. The applied axial stress was detected throughout the test by a 1 MN capacity NCB/MRE load cell, while each of the mounted load cells in the lateral directions had a capacity of 500 kN. One of these mounted load cells was attached to a bearing platen and the other was in direct contact with the specimen. The seating platen was secured inside the cubical apparatus by four tying steel plates, of which one plate was bolted to the apparatus frame while the others were resting firmly against the walls. These plates were arranged to permanently stabilise the seating platen and enable it a degree of self-adjustment upon application of axial stress. The specimen deformations in the principal directions were measured by a set of three Linear Variable Differential Transformers, LVDT's. An INTERCOLE SPECTRA-ms logging system was used along with a non-IBM compatible SIRIUS micro-computer for monitoring and recording the output of the measuring devices.

3.2.4 Pilot Tests and Problems Encountered

Based on the previous set-up, pilot tests on cubes of Springwell sandstone were attempted to review the experimental technique and verify some of the results reported in antecedent polyaxial work using the same set-up. Enormous difficulties were experienced while

conducting these tests, and the data obtained did not conform neither to the reported results nor to the basic properties of the rock tested.

One of the main problems encountered was the difficulty in managing the testing equipment to achieve an accurate loading of the test specimen. The intended loading procedure was to initially increase all principal stresses simultaneously. Then, upon reaching their designated values successively, the minor and intermediate principal stresses would be maintained constant while the major principal stress would continually increase until the specimen fails. However, it was encountered that as soon as the axial load was applied, the top bearing platen slid along the Teflon sheet at the specimen interface. This problem was somewhat minimised by holding the bearing platen firmly by hand and applying very slowly the initial load. In addition, the seating platen was observed to tilt upon applying the axial load, resulting in an imperfect contact with the bottom platen of the testing machine. While the axial load was set to increase systematically by the testing machine at a specified loading rate, manual control of other loading components was necessary throughout the test. Both the hydraulic power pack and the hand pump were unable to maintain constant levels of stress generated, and continuous adjustment was needed to attain the designated levels of intermediate and minor principal stresses. Controlling these stresses became more difficult as the axial stress increased and the specimen approached failure. At this stage, any attempt to adjust the level of the intermediate stress through the power pack could easily result in a considerable imbalance. The problem along the minor principal direction was even worse since at this stage the stress increased ceaselessly. The relief valve mounted in line with the hand pump was ineffective, and even a complete release of pressure did not immediately succeed in bringing down the minor stress level.

Throughout the tests, the digital output of the load cells and that of the LVDT's were displayed on the computer screen in terms of stress and strain, respectively, and these values were the main reference for monitoring the test progress. The pressure devices were equipped with gauges of low resolution, and therefore, it was not possible to rely on these gauges for accurate loading of the test specimen. Furthermore, there were considerable discrepancies between the stress levels corresponding to the pressure readings indicated by the gauges and the levels of stresses suggested by the output of the

load cells. Regarding the output of the LVDT's, the strain measurements appeared to present an improper picture of the specimen deformational behaviour. All strains were remarkably excessive and indicated contraction in the test specimen along the three principal directions, with the intermediate principal strain being often the greatest. These problems were combined with an unreliable micro-computer which often froze during the test leaving no option but to terminate the test and restart the experimental procedure. Nevertheless, a number of tests were completed. Failure of the test specimen was often explosive and resulted in irregular fractures and patterns.

3.2.5 Inspection of the Testing Facilities

The pilot tests incited the view that the testing facilities were suffering from some major defects and ought to be closely inspected. Concentrating first on the cubical test apparatus, initial observations and basic measurements revealed significant levels of eccentricity along the three principal loading directions. The seating platen was found misplaced inside the frame, leaving it noticeably out of alignment with the platens of the hydraulic rams. The four plates tying the seating platen, Figure 3.2, were in tight contact with the apparatus walls and could not allow any adjustment to the platen location. In addition, the platen was excessively high with reference to the hydraulic ram platens, causing further imperfect loading conditions. The platen tendency to tilt upon the application of axial load, as observed during the tests, appeared to be caused by the tying plate that was bolted to the apparatus body. This plate was found not properly levelled and did not have at its bolted end the freedom to accommodate any vertical movements in the seating platen. All bearing platens appeared to have suffered some wear and tear, and their contact surfaces with the specimen were neither smooth nor even.

Having established some serious imperfections in the apparatus structure, all parts were dismantled, and the next step was to examine the reliability of the monitoring devices, namely the load cells and the LVDT's. Re-calibration of these units showed that they all lacked sensitivity and were unable to function properly over their entire working ranges. Moreover, the calibration results indicated that these units were no longer linear in their response.

The defects in the multiaxial cubical apparatus were evidently combined with other defects and problems related to the rest of the testing facilities. An inspection of the 5 MN AVERY loading machine revealed that the machine was liable to induce eccentric loading due to an offset centre of gravity of its upper platen. This seemed to explain the tendency of the top bearing platen to slide as soon as the axial load was applied. It was also believed that the specimen failure was influenced by such a malfunction in the loading machine in addition to the effect of the machine softness or lack of stiffness. Manual control of the machine appeared to be inevitable, and the loading rate could not be displacement or strain controlled, hence only stress rate controlled tests could be carried out.

Malfunctions and limitations in the pressure devices were easily recognised. The FARNELL hydraulic power pack was a weight loaded type in which the generated pressure is counter balanced by loading weights. As a result, a required level of pressure could not be achieved accurately. Moreover, it was evident that the power pack was unstable and proved unable to maintain a steady level of pressure. The hand pump was equally unstable, and the relief valve proved inefficient to control the minor principal stress. As earlier mentioned, these devices were all equipped by gauges of low resolution and could not provide accurate readings of the pressure applied.

The SIRIUS micro-computer was an early generation computer, non-IBM compatible, which used MS-DOS version 1.25a as an operating system. Thus, besides its unreliability, the computer was out of date and incompatible with most present software and hardware alike.

3.2.6 Modification and Enhancement of the Testing Facilities

In the light of the aforementioned findings, it was clear that the testing facilities were virtually unusable and that proper testing could not be initiated unless all defects were rectified. Concerning the cubical apparatus and its components in the first instance, it was found that both the LVDT's and the load cells could not be repaired, and that new units had to be acquired. Consequently, the LVDT's were replaced by three APEK MPE

transducers, type HS 25B, which have a working spindle displacement range of ±25.9mm. Similarly, three RDP SENSOTEC *pancake* shaped load cells, model 43-compression only design, were chosen to supersede the existing ones. One of the new load cells has a capacity of 1 MN and was intended to be used along the axial direction, while the other two load cells have a capacity of 700 kN and were intended to be mounted in the cubical apparatus along the lateral directions. It should be noted that all three load cells are granted a 50% overload factor of safety. Among various considerations for deciding on these load cells was the convenience of their low profile for a proper integration into the apparatus as well as overcoming some major drawbacks in the previous configuration. It was intended to first, ensure an unencumbered access to all the components inside the apparatus, and second, accommodate a bearing platen between the specimen and each of the load cells mounted, thus unifying the loading boundaries of the test specimen. While mounting the load cells, extreme care was taken to secure a perfect alignment between the spherically shaped loading surface of the cell and the axis of the hydraulic ram on the opposite side. It is worth noting that prior to mounting, both the load cells and the transducers were calibrated and their linear response was confirmed.

Upon mounting the load cells, Figure 3.2, the seating platen was to be installed. First, it was necessary to reduce its height and alter the tying plates to suit the new position of the platen. Thereafter, the platen was located inside the apparatus, perfectly aligned and levelled in both lateral directions, and then permanently secured to the apparatus frame. It should to be noted here that the new height of the platen has been designed for cubical specimens with a side length of 74 mm instead of 72 mm as used in previous work. This was intended to strengthen the specimen edges and ensure that the bearing platens surrounding the specimen could not come into contact upon loading.

Having installed the seating platen, it was possible to determine the exact thickness of the bearing platens intended to be placed between the specimen and the lateral load cells. Subsequently, using the appropriate thickness, two 70 × 70 mm platens were constructed with adjustable legs for accurate positioning of the platens. In order to distinguish these platens from others, they are referred to as the load cell platens, Figure 3.1.

On completing the aforementioned tasks, the platens of the hydraulic rams together with the top bearing platen were ground and polished. As shown in Chapter 5 in Figure 5.1, two spirit levels were introduced into the system to enable accurate setting of the specimen and all the platens involved.

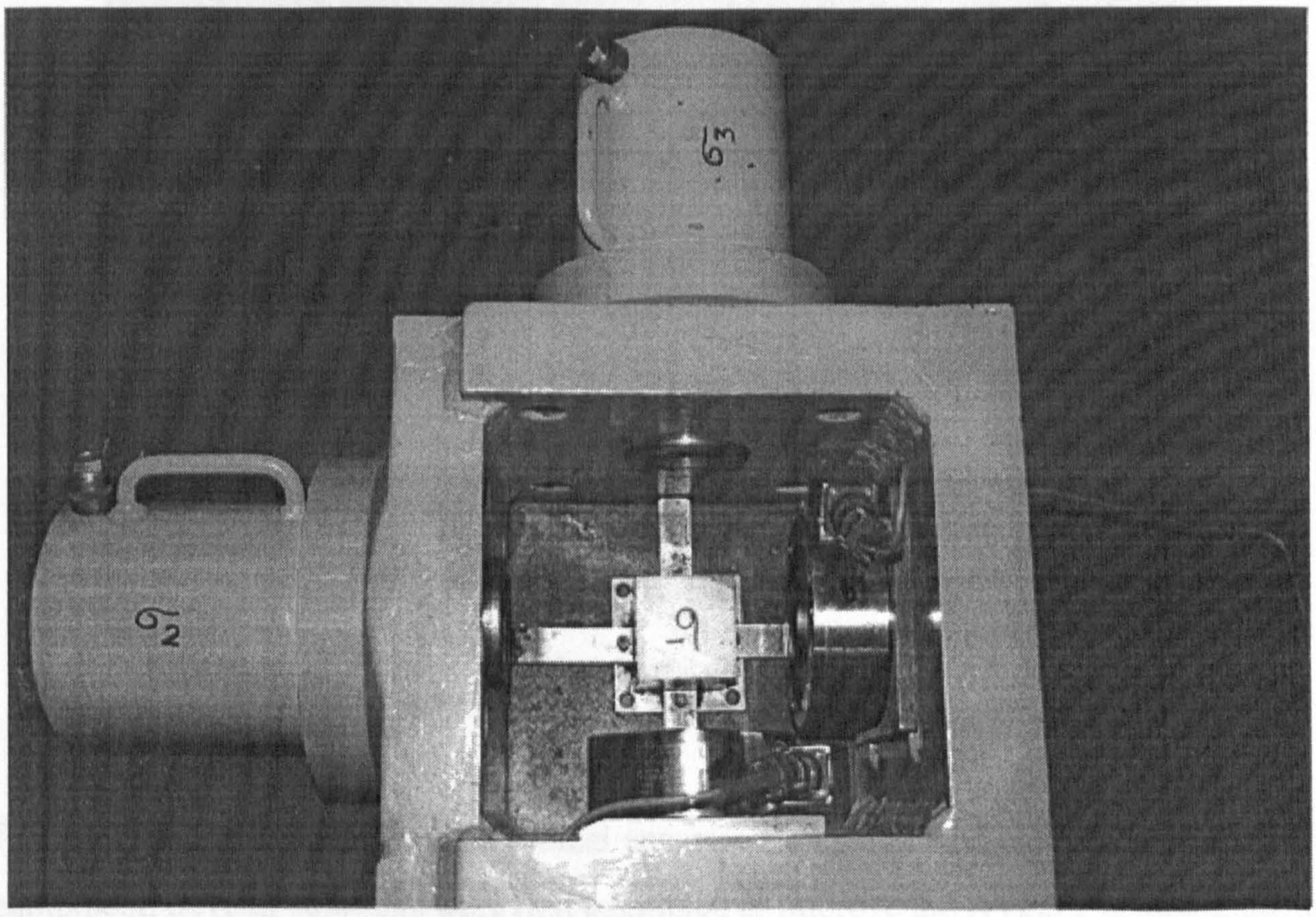

Figure 3.2 Inside view of the multiaxial cubical test apparatus showing the bottom seating platen with the tying plates, and the newly fitted lateral load cells.

In order to enable measurements of the specimen lateral deformation to be made when one or two faces of the specimen are free from any contact, as in biaxial or uniaxial compression tests, two clamping platens were designed to set up the transducers inside the apparatus and rest their armatures directly against the specimen, as illustrated in Chapter 5 in Figures 5.26 and 5.33.

It ought to be mentioned that prior to re-assembling the cubical apparatus, its frame together with the hydraulic cylinders were cleaned and painted for protection against

corrosion. Figure 3.3 shows the apparatus assembled in its present form with a test specimen inside prior to mounting the loading arrangement in the vertical direction.

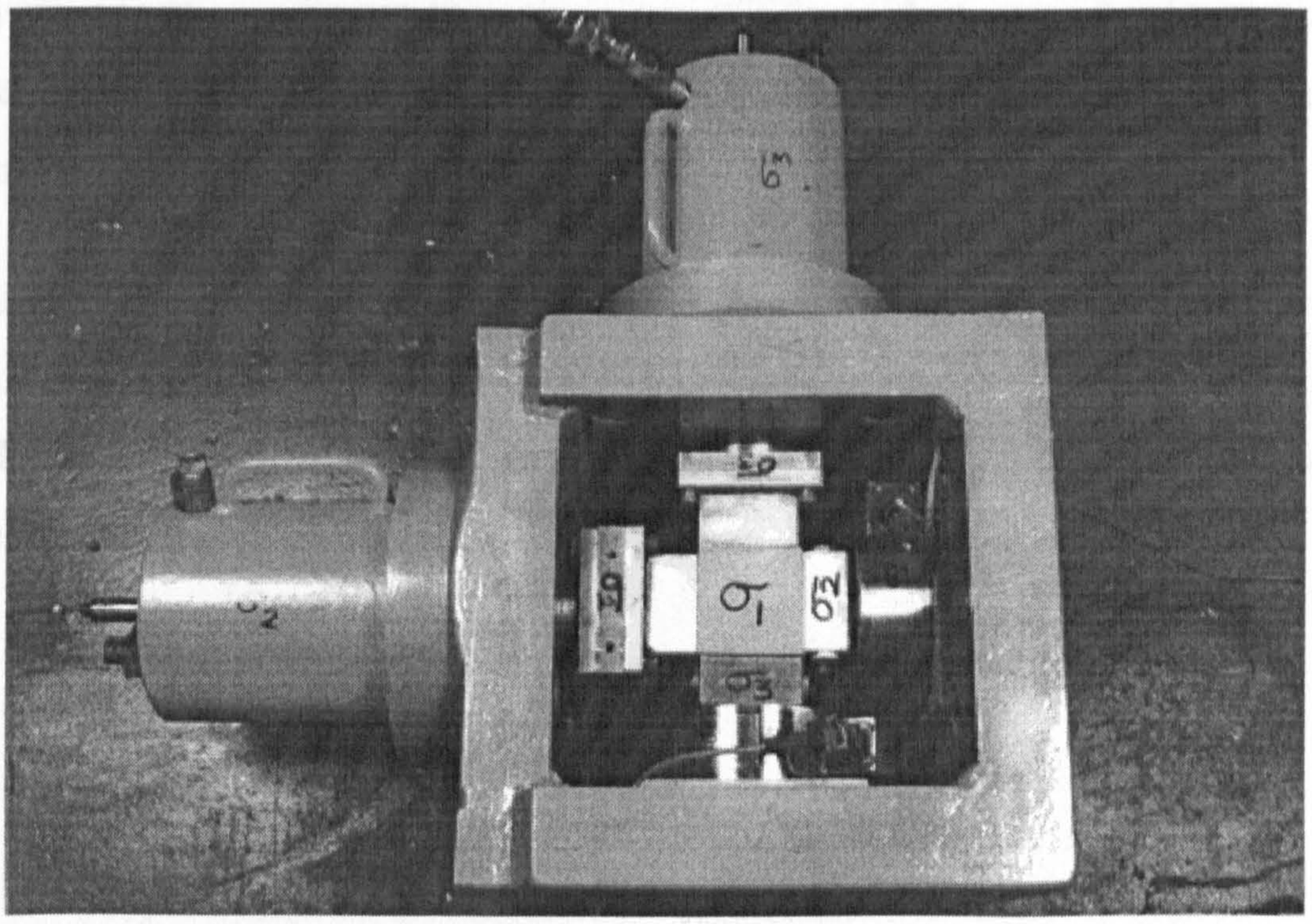

Figure 3.3 A view of the multiaxial cubical test apparatus in its present form assembled with a test specimen inside.

Following the rectification of the cubical apparatus, attention was directed to the loading equipment. Several solutions were first attempted to improve the AVERY testing machine and overcome the problem of eccentric loading. But failing to do so, together with the intention to conduct strain controlled tests and overcome the effect of the machine stiffness on the specimen failure, resulted in considering the use of an alternative machine. Consequently, it was decided to employ the 5 MN servo-controlled loading system for the application of the axial stress. Similarly, new arrangements were made along the lateral directions. Aiming for an optimum control over the minor principal stress, the newly acquired pressure intensifier system was to be utilised along this direction. The intermediate principal stress direction was equipped with a more efficient mobile hydraulic power pack, made by ELE, along with a relief valve. Being spring loaded and fitted with a regulating valve, the hydraulic power pack enables a fair control over the application of pressure up to 70 MPa.

Finally, in order to enhance the data acquisition system and facilitate processing and presentation of the test results, the SIRIUS micro-computer was replaced by a new IBM compatible AMSTRAD personal computer. This involved a revision of the data acquisition operating program to ensure compatibility with the new hardware as well as the operating system and the data processing software. A general view of the testing configuration and facilities involved is shown in Figure 3.4.

It should be noted that the foregoing process of inspection and subsequent modification of the cubical apparatus and enhancement of associated equipment did not take place at once. It was a lengthy process involving extensive experimental investigations and technical consultations.

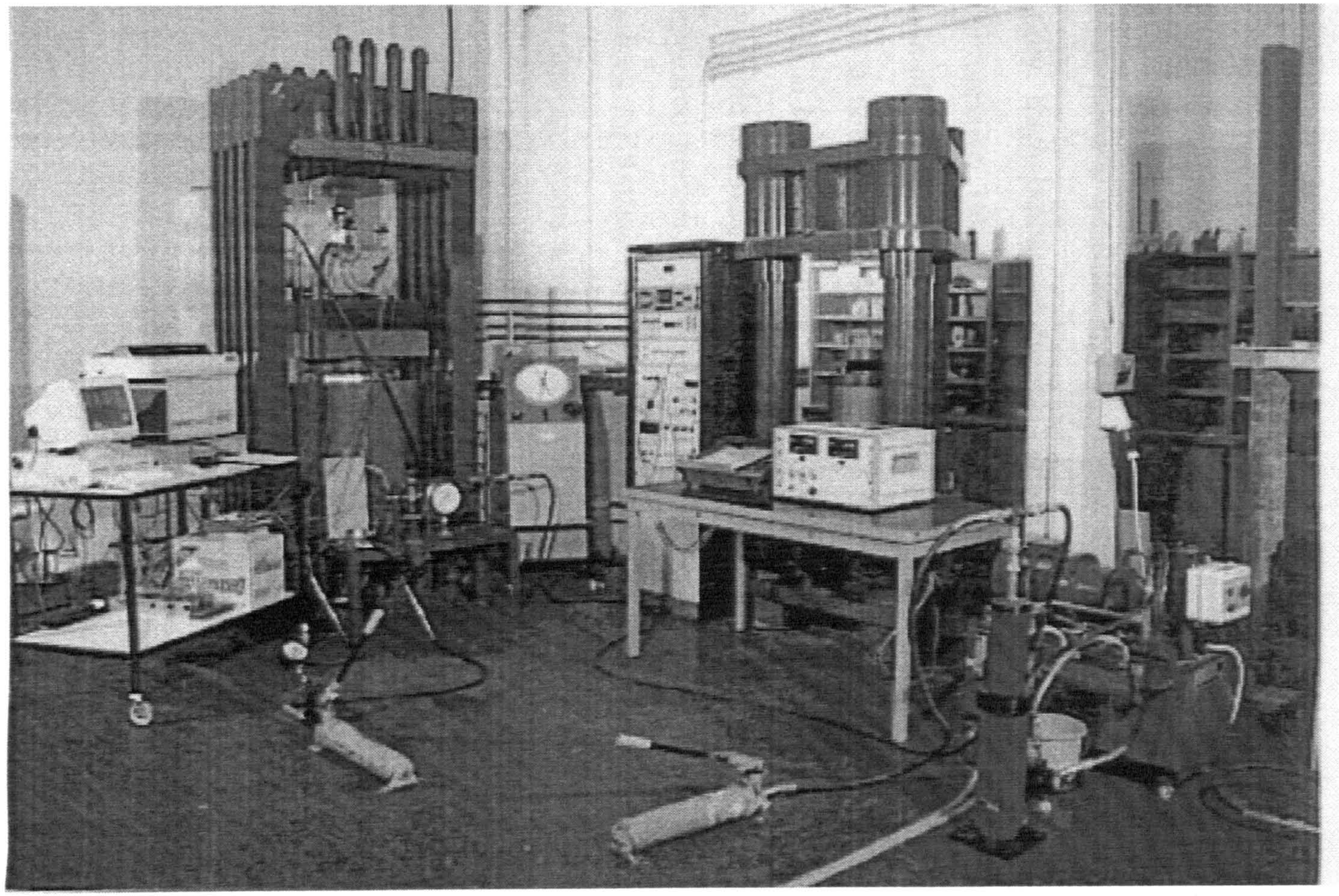

Figure 3.4 A general view of the multiaxial cubical testing configuration

3.3 The Design of the Hollow Cylinder Test Apparatus

3.3.1 Inadequacy of Existing Testing Apparatus

The latest experimental work on thick-walled hollow cylinders of rock in the Rock Mechanics Laboratory at the University was carried out by Alsayed (1988) using an in house built hollow cylinder cell, Figure 3.5. Due to the inability of the cell to accommodate internal pressure, the specimens were tested under axial load and external pressure only. Such limitations in the loading conditions mean that only uniaxial and biaxial compressive stress fields can be induced in the test cylinders. Polyaxial compression of thick-walled hollow cylinders can not be achieved unless the cylinders are subjected to a combination of internal and external pressures together with axial load. Since polyaxial testing was intended to be a major part of the present study, it was clear that the available cell was inadequate. An immediate consideration was to modify the cell, but this appeared neither feasible nor desirable for a number of reasons. As polyaxial testing devices for hollow cylindrical specimens are not available commercially, it was clear that a new apparatus was to be devised.

3.3.2 Fundamental Design Considerations

Several features were considered essential to be incorporated in the design. A leading feature was obviously the ability of the apparatus to accommodate lateral internal and external hydrostatic pressures together with axial load. This ability was to be combined with a reliable as well as manageable system of sealing both the inner and outer surfaces of the test hollow cylinder. Such a sealing system would have to sustain the maximum level of pressure that could be generated by the available pressure devices, up to 70 MPa, with no leakage or intrusion. In order to cut down specimen preparation and testing cost, and increase productivity in both operations, the apparatus size was to be minimised to a degree that would enable easy handling. However, the apparatus would have to accommodate rock hollow cylinders of a reasonable size and wall thickness which would

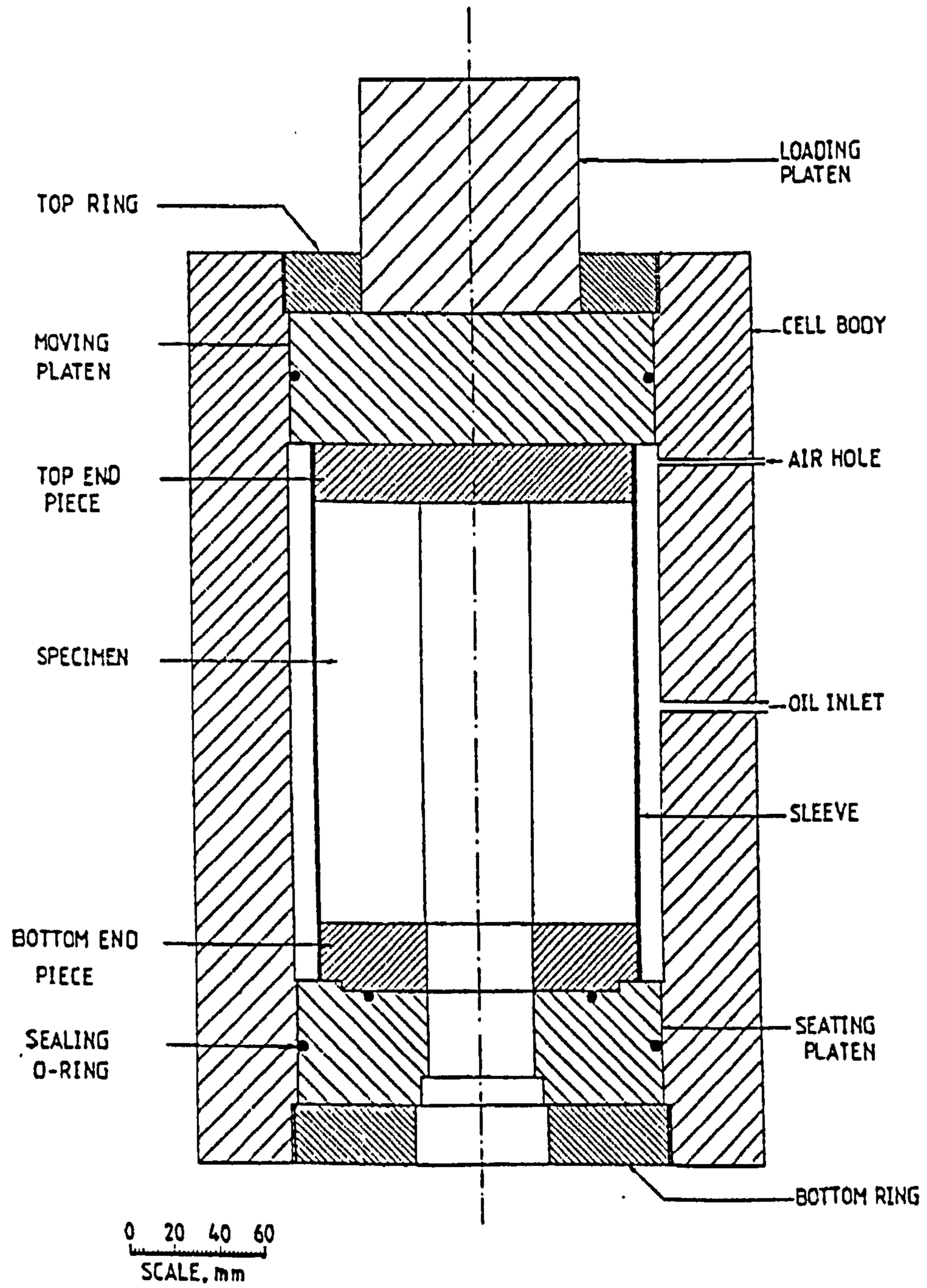

Figure 3.5 An illustration of hollow cylinder test apparatus used in a previous study but found inadequate for the present one (after Alsayed, 1988)

approach a thick-walled condition. these fundamental features were to be embodied in a foolproof apparatus to be devised and constructed at as less cost and time as possible. In addition, the apparatus was to be integrated into an adequate testing configuration which would enable a wide range of axial load, internal and external pressures to be independently applied and effectively controlled. Measurements of the load and pressures

applied would have to be continuously monitored and acquired together with the corresponding deformations of the test specimen.

3.3.3 The Design Approach

On the basis of the above considerations, a number of plans were explored in efforts to produce a satisfactory design for a hollow cylinder test apparatus. The design brief was that the apparatus would be a triaxial test cell with the ability to accommodate internal pressure. In this regard, a particular attention was paid to the structure of the well-known Hoek triaxial cell, developed by Hoek and Franklin (1968), due to its proven efficiency and remarkable practicality. One of the most significant features of the cell, Figure 3.6, is

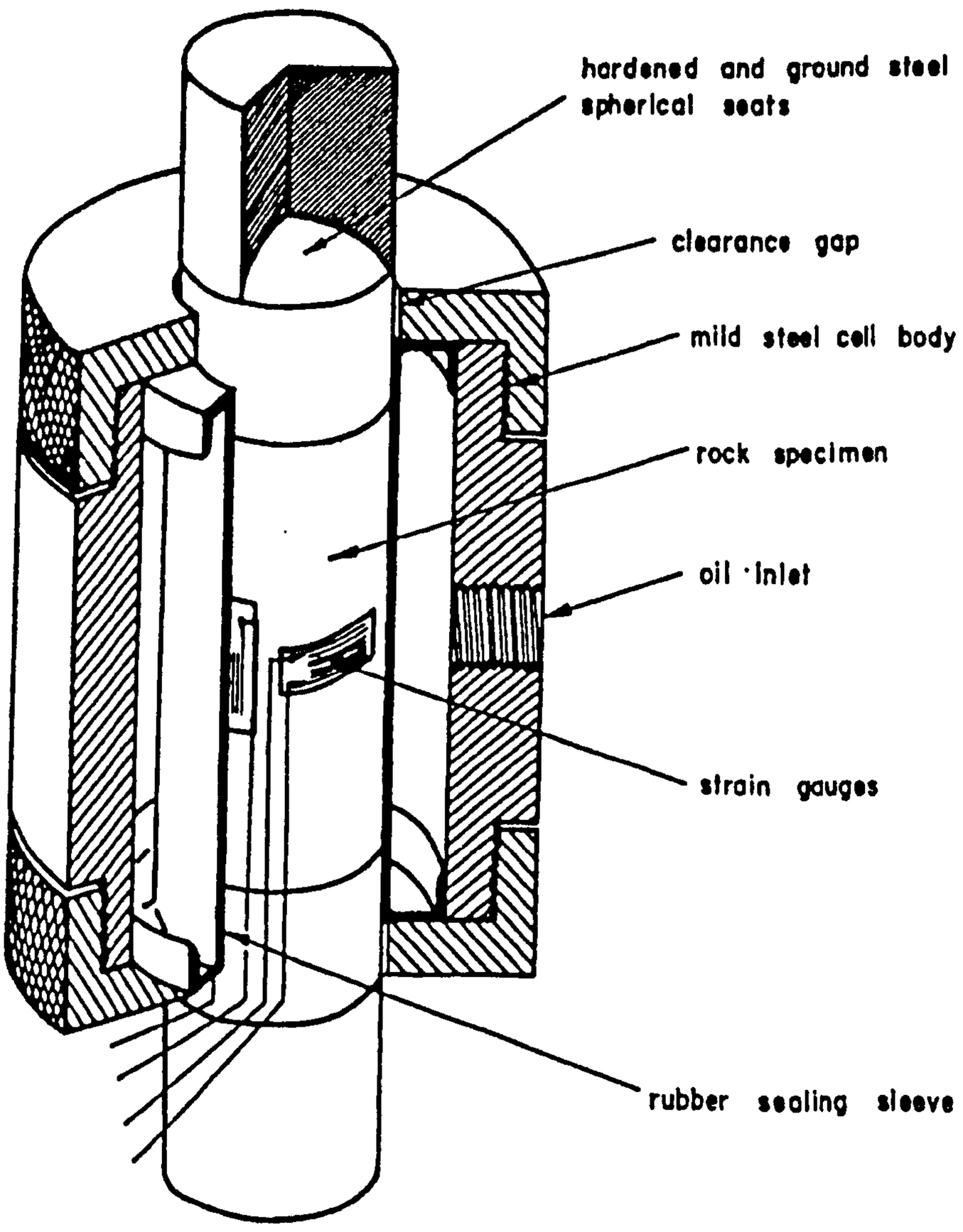

Figure 3.6 Cut-way view of Hoek triaxial cell (after Hoek and Franklin, 1968)

that the confinement hydraulic oil is retained inside the cell and sealed by a durable synthetic rubber sleeve, making it possible to test and remove the specimen without breaking the seal. Attempts to incorporate such an advantageous feature in the design of the testing apparatus drew the attention to a feasible employment of a Hoek triaxial cell in the apparatus configuration. It was conceived that employment of the cell would mainly involve the replacement of the cell spherical seating platens by new sets of platens which would enable the application of internal confining pressure. This approach appeared to meet most of the design fundamental considerations, and consequently, was adopted. The required platens were to be designed and constructed accordingly.

3.3.4 Construction and Configuration

Having decided on the design approach, a Hoek triaxial cell, Figure 3.9, was acquired to house cylindrical specimens of 150 mm length and 75 mm diameter. Governed by the thick-walled condition and the availability of a proper size of a coring barrel as well as inner sleeve materials, the test hollow cylinders were to have an inner diameter of 27 mm, yielding a wall thickness of 24 mm. An appropriate rubber tube was selected for sleeving the inner hole of the cylinder.

Two identical sets of cylindrical platens were designed as illustrated in Figure 3.7 to be used in conjunction with the acquired Hoek cell for testing thick-walled hollow cylinders of the selected size. The platens were constructed from EN8 steel and then hardened prior to grinding and lapping. Shown in Figures 3.8 to 3.10, each set of platens consists of the following parts:

- A hollow end platen with a tapered hole to be placed at the specimen end. A rubber O-ring is fitted to one side of the platen to be forced against the central part to ensure a positive sealing of the internal confining oil.

- The central part is a platen designed to provide the internal confining oil and seal the specimen inner hole. It contains the oil inlet and is constructed with a tapered spigot to

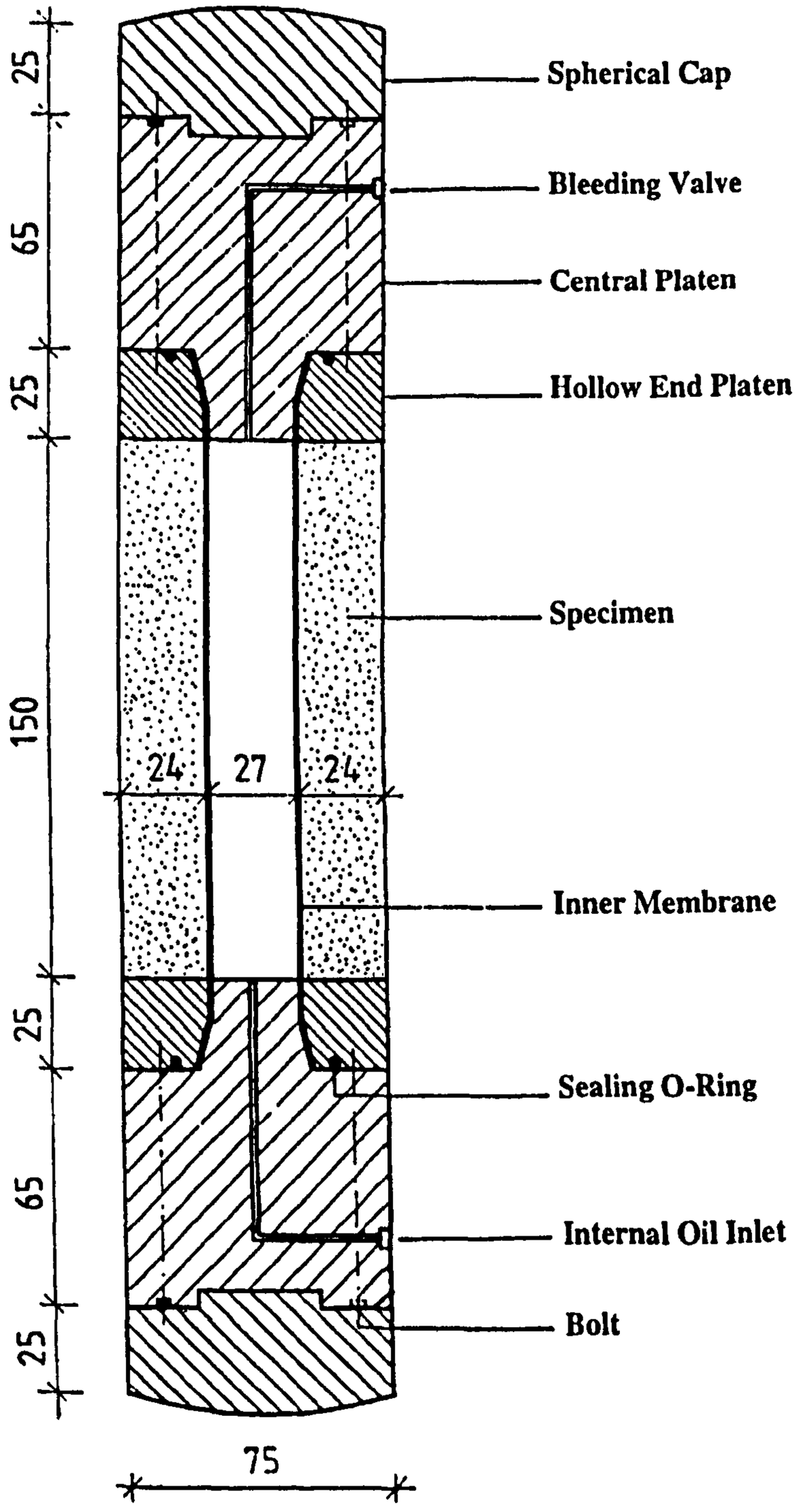

Figure 3.7 Designed Internal pressure configuration for the hollow cylinder test apparatus.
A corresponding actual view after the design was implemented
can be seen in Figure 3.10

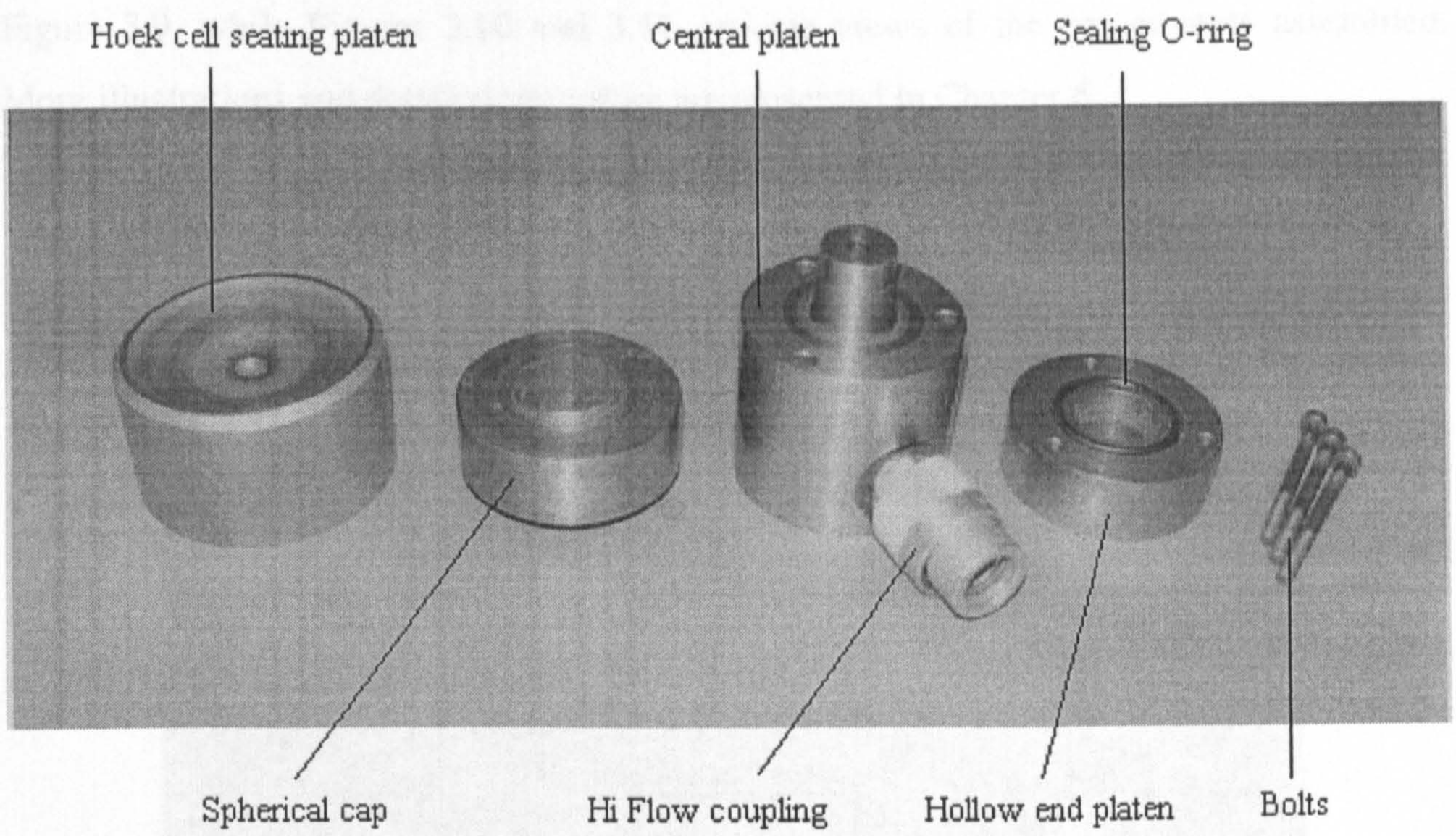

Figure 3.8 One set of the constructed platens for the internal pressure configuration

mate the hole of the end platen. Sealing of the specimen inner hole is achieved by pinching the inner sleeve between the spigot and the inner surface of the end platen. A perfect coupling and sealing between the central platen and the hollow end platen is accomplished by means of three bolts forcing the rubber O-ring to actuate between the two parts. One central platen is fitted with a self sealing Hi Flow coupling for connection to the internal pressure device, and intended to be placed at the lower end of the cell, while the other central platen at the upper end of the cell is fitted with a bleeding valve to free the internal confinement from any trapped air.

- The top part is a spherical cap machined to be fitted onto the central part and match the seating platen supplied with the acquired Hoek cell.

Upon their assemblage, Figure 3.10, the test specimen and the platens are inserted in the Hoek cell and properly positioned so that the specimen lies centrally inside the cell. A sufficient amount of external pressure is pumped up to hold the assembly firm prior to transference to the testing machine.

A view of the main components of the devised hollow cylinder test apparatus is shown in Figure 3.9, while Figures 3.10 and 3.11 provide views of the components assembled. More illustrations and detailed procedure are presented in Chapter 6.

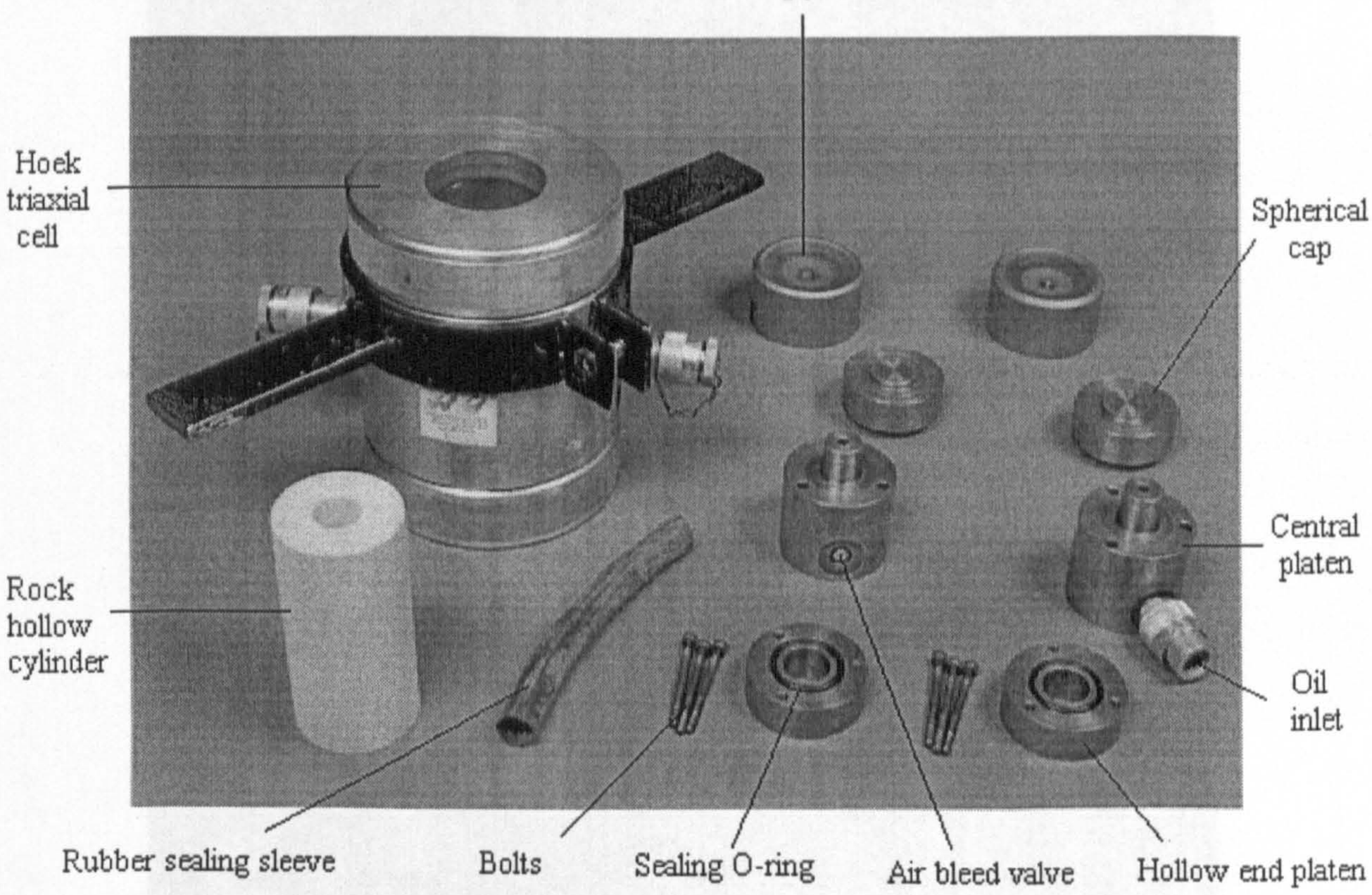

Figure 3.9 A view of the devised hollow cylinder test apparatus showing its main components.

In line with the cubical test enhanced configuration, tests were to be carried out using the 5 MN servo-controlled testing machine for the application of the axial load. An RDP SENSOTEC 1 MN load cell, model 43, was incorporated in the axial direction for measuring the applied load, and the specimen axial deformation was acquired via an APEK MPE transducer. Regarding the pressure devices, the external pressure was generated by the ELE hydraulic power pack, while the pressure intensifier system was dedicated for managing the internal pressure. A pressure gauge was incorporated along the ELE hydraulic power pack and connected to the data acquisition system in order to obtain measurement of the external pressure applied. Measurements of the internal

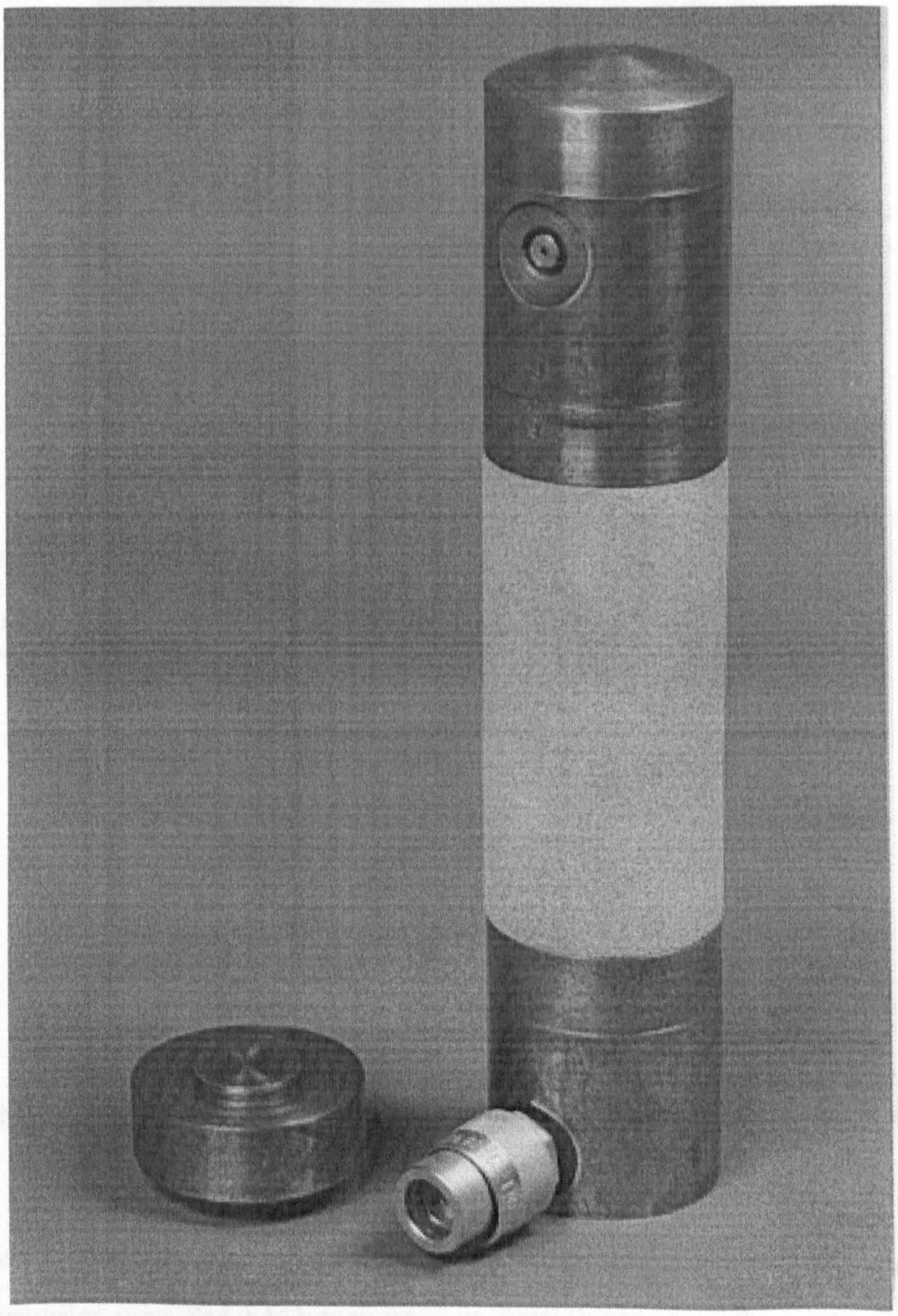

Figure 3.10 A view of the test specimen assembled with the internal pressure platens prior to insertion in the Hoek cell

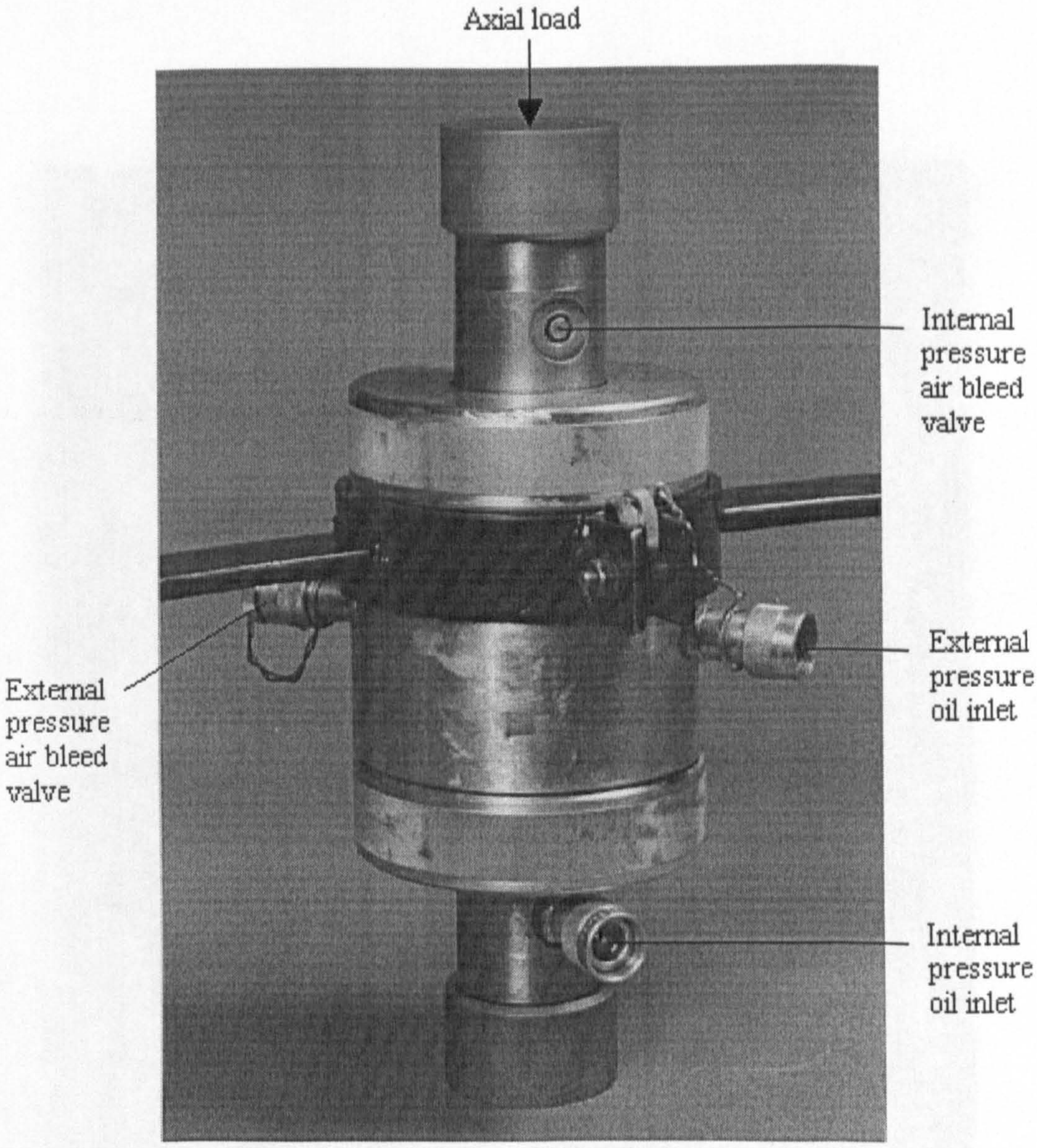

Figure 3.11 The hollow cylinder test apparatus with a specimen inside ready to be transferred to the loading machine.

pressure were recorded directly from the pressure intensifier, and a PHILIPS multipurpose A4 X-Y recorder type PM 8141 was used in conjunction with the pressure intensifier system to trace the volumetric deformation of the specimen hole. The INTERCOLE SPECTRA-ms data acquisition system along with the AMSTRAD PC were employed for monitoring and acquiring the test data. A general view of the hollow cylinder testing arrangement and facilities used is pictured in Figure 3.12.

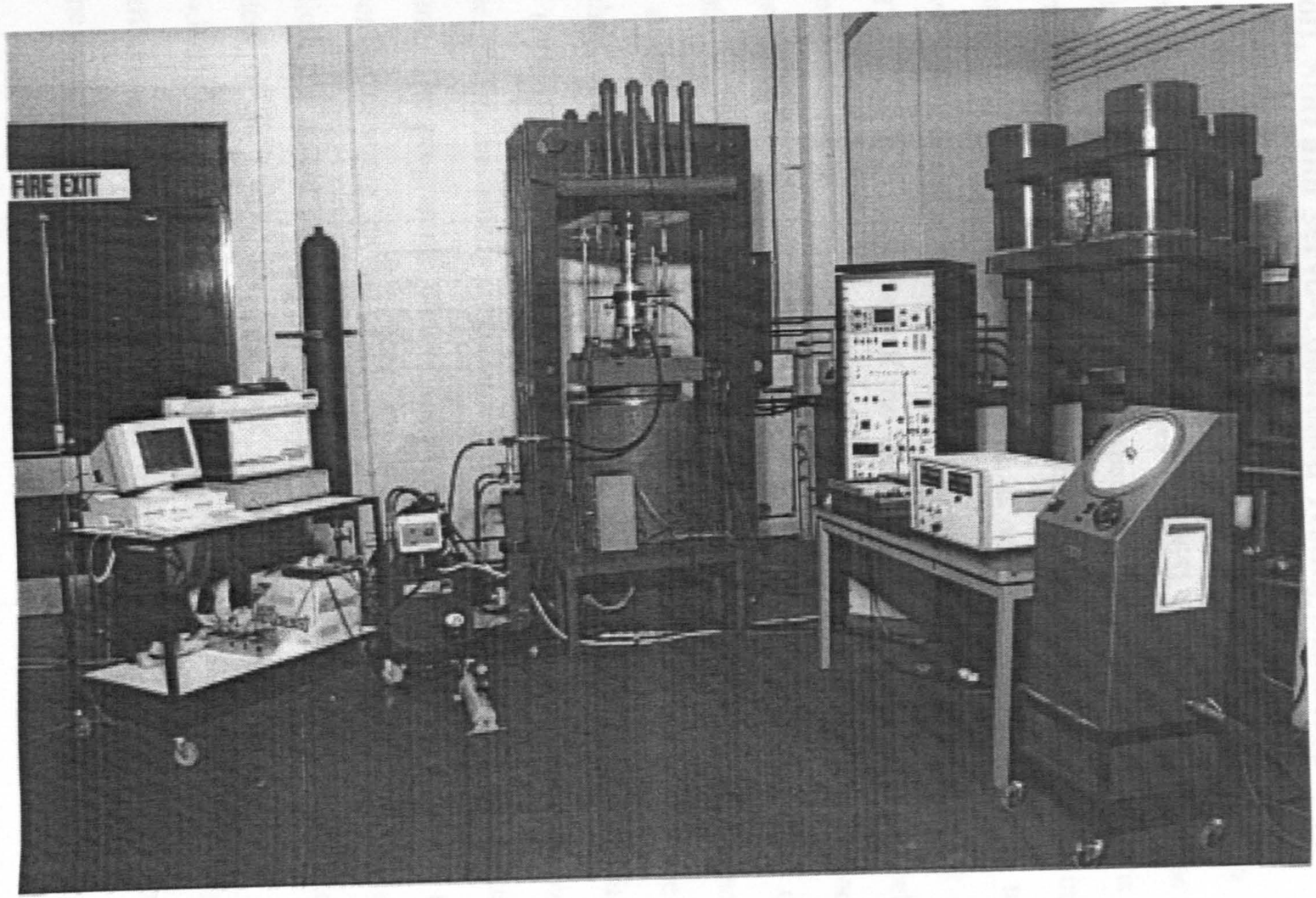

Figure 3.12 A general view of the hollow cylinder testing arrangement

3.4 The Servo-Controlled Loading System

3.4.1 Soft, Stiff and Servo-Controlled Testing Machines

Failure of test specimens of brittle materials was long recognised by a number of researchers, such as Whitney (1943) and Cook (1965), to be influenced by the stiffness of the loading machine relative to that of the specimen. When a rock specimen is loaded in a testing machine, a large amount of elastic energy is stored in both the specimen and the testing machine. If the machine is *soft*, such as one with hydraulic loading, uncontrolled explosive failure of the specimen occurs at or, shortly after, the peak of the stress-strain curve. The violent disintegration of the specimen is attributed to a rapid release of the machine stored energy into the specimen at or near maximum load. Since rock failure in nature is rarely that catastrophic, and in order to study the rock post-failure or post-peak behaviour, tests may be conducted in a rigid or *stiff* testing machine. A machine of this type is designed to enable a complete stress-strain curve of the loaded specimen to be established. An alternative approach of controlling the specimen failure without relying on the stiffness of the machine is the use of a closed-loop *servo-controlled* testing machine. Such a machine is programmed to follow a prescribed loading sequence varying with time. The programme controlling parameter is generally a constant rate of axial displacement or strain, or that of load or stress. If the test, for example, is displacement controlled, the actual displacement of the test specimen is continually measured by a transducer or an LVDT and fed back to the servo-controller where it is compared electronically with the value provided by the preset loading ramp history. Whenever there is a difference between the two values, a servo valve adjusts the pressure within the machine actuator to eliminate the difference.

3.4.2 Description of the Servo-Controlled Loading Facilities

Seen in Figures 3.4 and 3.12, the servo-controlled system used in the present experimental work was described by Price (1980). It was constructed in *kit form* by local firms and installed in 1973 in the Rock Mechanics Laboratory in St. Thomas' street, University of

Newcastle upon Tyne. In 1975, the Laboratory was moved to the Drummond Building and the system was dismantled and reassembled on its present site. Since then, the system has been used in a number of experimental investigations.

Briefly, the system at present comprises the following main parts:

- Two adjacent loading frames of different sizes, each of which is equipped with a double acting hydraulic actuator and a servo-valve. The hydraulic actuator on the larger frame is capable of applying a maximum compressive force of 5 MN, Figure 3.13, while the actuator on the other frame offers a maximum compressive force of 1 MN. Both actuators are connected to the same hydraulic power system and operated via the same control console, and therefore only one loading machine can be used at a time.

- A hydraulic power pack which provides a maximum operating pressure of 25 MPa. The pack is installed near the loading frames in a sound-proofed container and equipped with a heat exchanger cooled by a tap water and controlled by a thermostat to maintain the hydraulic oil at a constant temperature.

- A control console which houses the electronic control units and is mounted in a cabinet on sub-chassis sited between the two loading frames. Externally, the control console is connected to the following units:

  - The hydraulic power system.
  - The servo-valve in use.
  - An RDP LVDT type D5/2000A for monitoring the axial deformation of the test specimen.
  - Either a departmentally built 5 MN load cell, or an NCB/MRE 1 MN load cell type 440 for monitoring the applied load.
  - A PHILIPS multipurpose A4 X-Y recorder type PM 8141 for plotting the load-displacement curve during loading.
  - A data acquisition system may also be connected to acquire the load-displacement measurements.

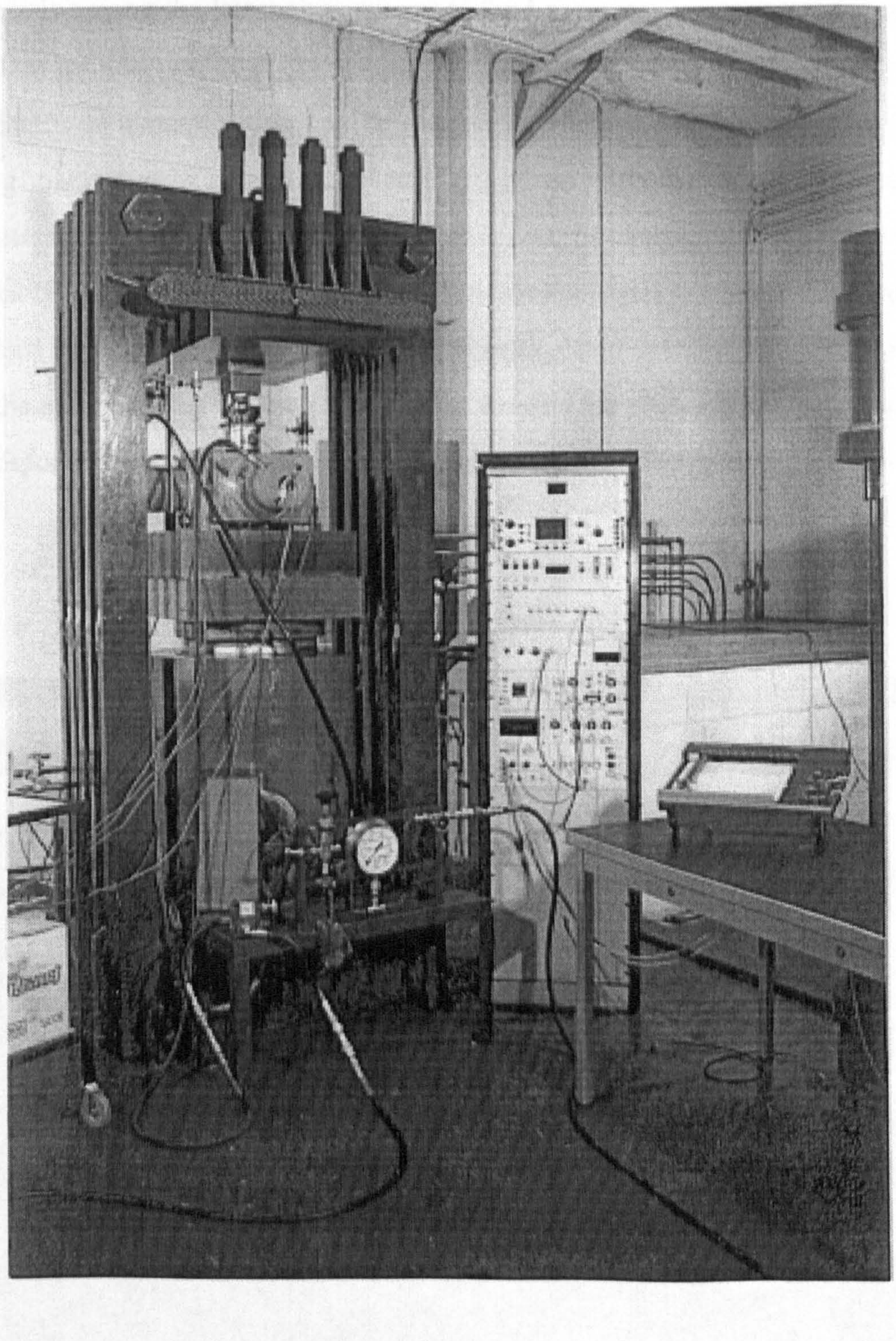

Figure 3.13 The 5 MN servo-controlled loading system shown with the control console and the multiaxial cubical test apparatus.

3.5 The Pressure Intensifier System

This system is among the latest acquisitions of the Laboratory, and is intended to provide and maintain an accurate control over the confining pressure of triaxial cells or similar devices. Static or dynamic tests can be carried out with pressure or volume being the controlling parameter. Pictured in Figure 3.14, the system consists of three main components: a pressure intensifier type PI 80S, a control console, and a mobile hydraulic power pack type M5/40. These components work in conjunction and are all manufactured and supplied by RDP - Howden Ltd. Full description and detailed specifications can be found in the manufacturer's operating manuals. Briefly, the pressure intensifier is basically a high response servo-hydraulic unit controlled by an electro-hydraulic servo valve

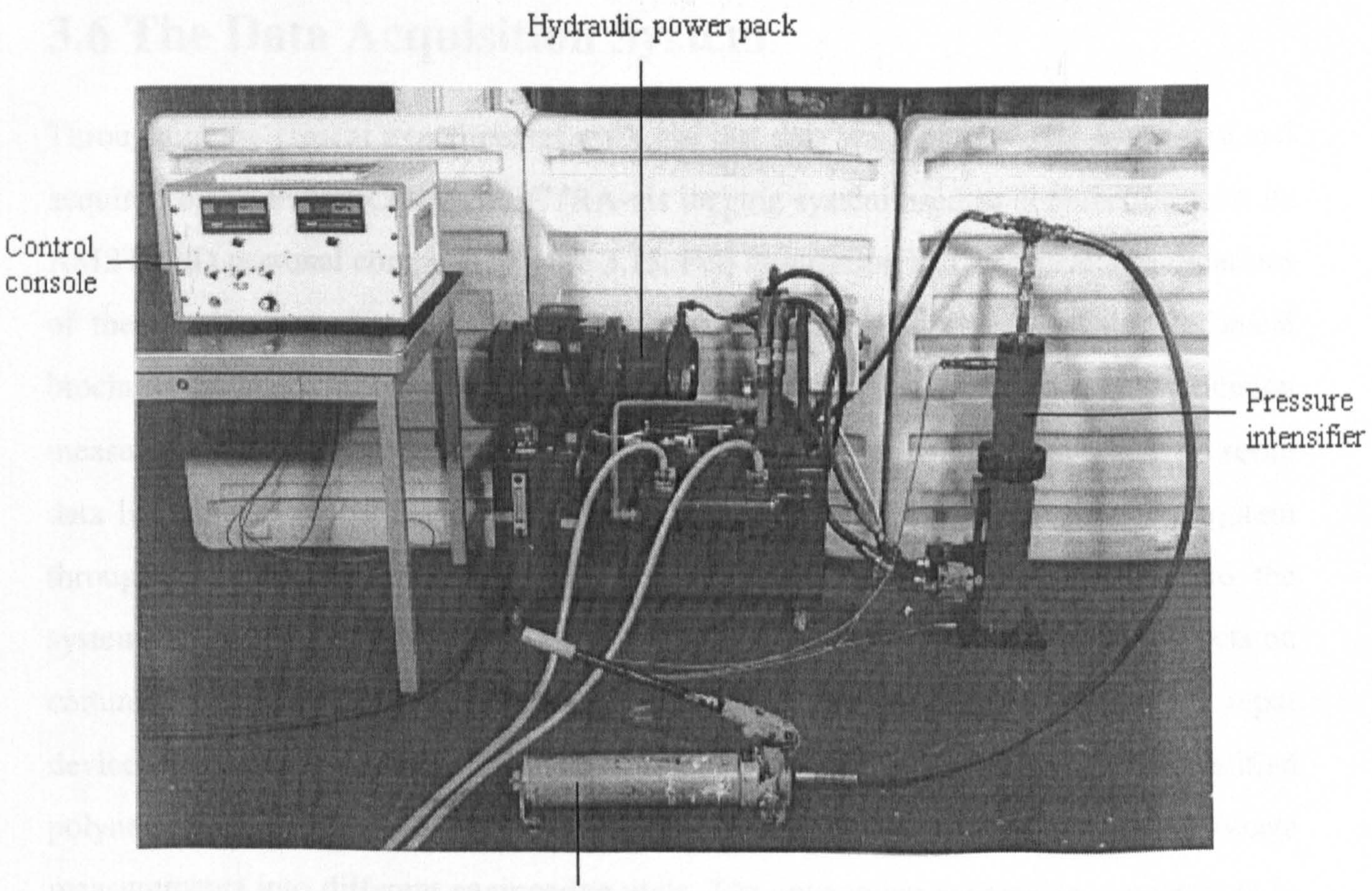

Figure 3.14 The pressure intensifier system

operating under closed-loop control. A precision strain gauged transducer senses the output pressure, and an internal displacement transducer (LVDT) produces a signal proportional to volume change. The control console houses all electronic control and monitoring modules. A servo-amplifier provides the drive signal for the controlling servo-valve and incorporates facilities to change control modes. A dual amplifier / digital monitor unit provides signal conditioning for the transducers together with a simultaneous display of test pressure and volume change in MPa and cm^3 units to a resolution of 0.1 units. The hydraulic power pack provides a maximum operating pressure of 30 MPa, which enables the pressure intensifier to operate at a pressure up to 70 MPa over a 120 cm^3 volume change. In order to retain a sufficient level of operating volume, a filling pump is used to inject oil into the pressure intensifier. For this task, an ENERPAC hydraulic hand pump was employed.

3.6 The Data Acquisition System

Throughout the present experimental work, the test data was continuously monitored and acquired by an INTERCOLE SPECTRA-ms logging system used in conjunction with an AMSTRAD personal computer, Figure 3.15. Full description and technical specifications of the logging system can be found in the manufacturer's user manual and technical brochure. In brief, the SPECTRA-ms system is a microprocessor controlled, precision measurement and control module which communicates with the host computer via a serial data link. Input devices such as transducers and load cells are connected to the system through individual channels provided by a remote connection module linked to the system. The SPECTRA measurement system operates from the host computer and acts on commands of a special program written in BASIC. The physical response of an input device is repeatedly acquired in volts and supplied to the host computer. A user specified polynomial expression may be held in the system to convert the acquired voltage measurements into different engineering units. The conversion expression can have up to five terms and is of the form:

$$Y = a + b\,X + c\,X^2 + d\,X^3 + e / X$$

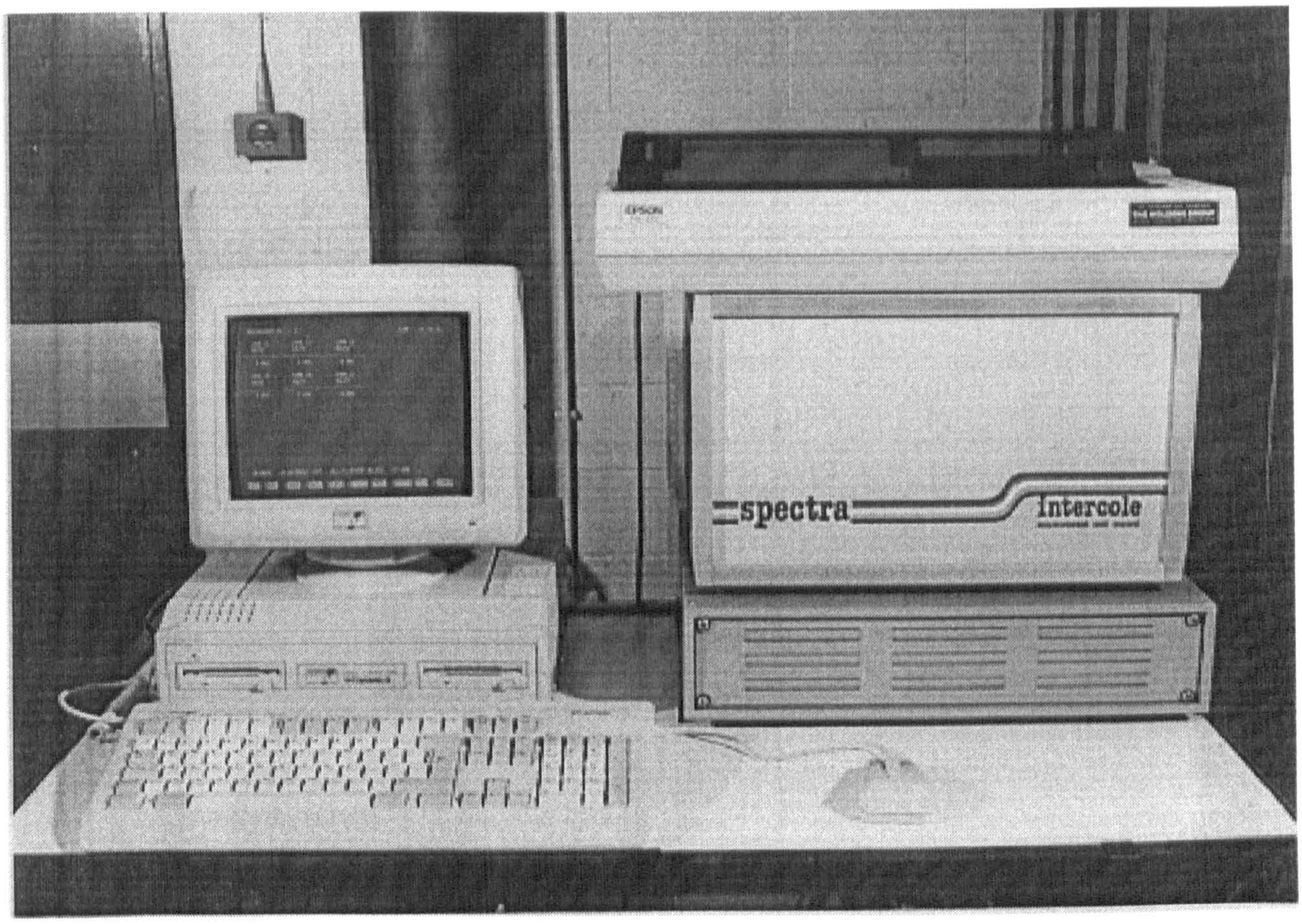

Figure 3.15 The data acquisition system

where *a, b, c, d, e* are user specified coefficients, *Y* is the output result, and *X* is the measured value in volts.

In the present work, a cubic polynomial expression of four terms was selected for all transducers and load cells involved. Prior to connection to the SPECTRA system, these units were calibrated and the coefficients *a, b, c, d* of each unit were defined corresponding to transducer output in mm and load cell output in kN. For convenience, the polynomial coefficients were converted with respect to the dimensions of the test specimen so that the output measurements of the transducers and the load cells correspond to strain % and stress in MPa, respectively. Throughout the test, the output measurements were acquired at predefined time intervals, displayed on the PC screen and written to a data file.

Chapter

4

Rock Characterisation and Specimen Preparation

4.1 Introduction

The rock material selected for the present experimental study is known as Springwell sandstone. It is extracted from the Springwell Quarry at Gateshead, Tyne & Wear, and supplied by Natural Stone Products Limited. Amongst the prime considerations for this selection was that the rock is abundantly obtainable indigenously and well documented in a number of previous investigations. Besides, it was used in the preceding cubical polyaxial studies at the University by Protopsaltis (1986) and Laderian (1987).

As far as the rock properties are concerned, the Springwell sandstone is commonly described as well sorted, medium strong, linear elastic, homogeneous and isotropic in terms of both its strength and elastic properties with no preferred orientations of minerals. Nevertheless, in order to obtain results specific to the samples used in this study, most of the fundamental characteristics of the rock have been re-assessed in accordance with the ISRM suggested methods reported by Brown (1981).

The comprehensive nature of the present study has involved a large number of specimens of different sizes and shapes including cubes, hollow cylinders, solid cylinders and disc-shaped specimens. Using conventional rock cutting and specimen preparation facilities, all specimens have been produced in the laboratory from rock samples collected from the Springwell Quarry in the form of blocks.

In order to account for any inherent variations in the specimens produced, and equally, ascertain other properties of the rock, non-destructive ultrasonic wave velocity tests have been performed on all cubical specimens and solid cylinders prior to their respective loading. Statistical methods have been employed to analyse the results of these tests and evaluate their significance with regard to the rock characteristics.

This chapter begins with a petrographic description of the rock, and then gives details of its most significant physical and mechanical properties as determined in this study. This is followed by a description of the various types of specimens used in the testing

programme, together with a brief account of the techniques employed to produce these specimens. Finally, the non-destructive tests are presented with highlights of their significance and in-depth analysis and discussion of other rock properties inferred from the test results.

4.2 Petrographic Description of the Rock

The Springwell sandstone belongs to the Middle Coal Measures, Upper Carboniferous - Westphalian C. This pale brownish-yellow rock is uniformly fine-grained and well sorted with clay and muscovite partings. The rock mineral composition and texture have been ascertained from a micro-petrographic examination of two thin sections of the rock carried out in the Laboratory by Tountas (1991) using a polarising microscope. As illustrated in Figure 4.1, the modal analysis indicated that quartz composes 69% by volume, clay 17%, muscovite 1%, feldspars 0.5%, rock fragments (mainly quartz) 5%, and voids 7.5%. A photomicrograph of the rock is shown in Figure 4.2.

The rock fabric closely resembles that of lithic arenites. To a first approximation, the Springwell sandstone can be modelled as a rock with a competent framework of quartz grains in a weaker matrix of clay with precipitated quartz fragments. Most of the quartz grains are fine, sub-rounded to sub-angular, and do not show any preferred orientations.

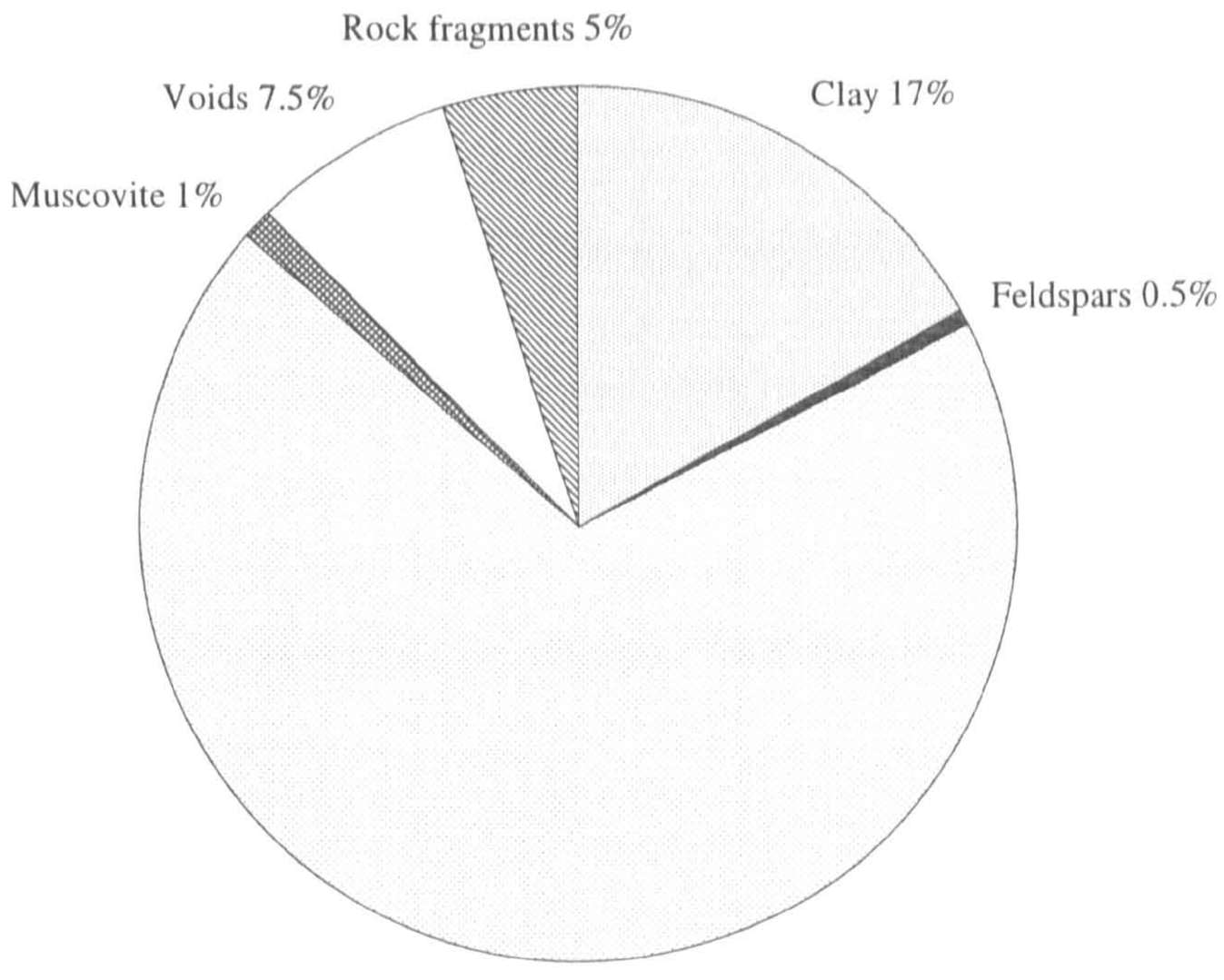

Figure 4.1 Mineral composition of Springwell sandstone

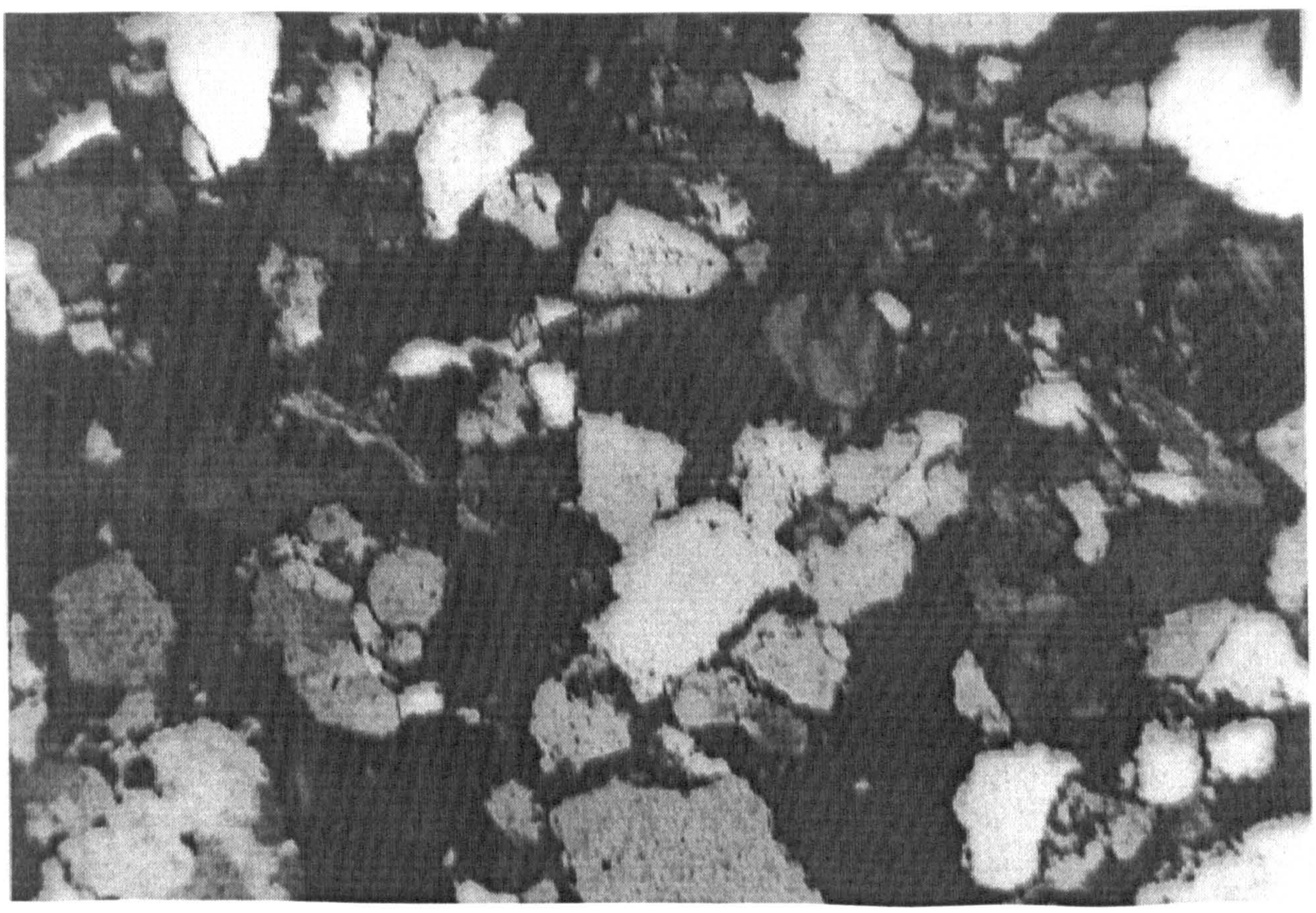

Figure 4.2 Photomicrograph of Springwell sandstone, magnification x125

4.3 Physical and Mechanical Properties of the Rock

4.3.1 Determination of Moisture Content, Porosity and Density

Following the ISRM suggested method, Brown (1981), ten representative specimens of Springwell sandstone in the form of lumps were used for the determination of the rock water or moisture content, w. An average value of w = 0.57% was obtained with a standard deviation, S_d, of approximately 0.06%. Individual results for all specimens involved are given in Table 4.1.

Table 4.1 Moisture content test results.

Specimen No.	Moisture Content w, %
LMC1	0.57
LMC2	0.56
LMC3	0.69
LMC4	0.61
LMC5	0.60
LMC6	0.59
LMC7	0.59
LMC8	0.54
LMC9	0.50
LMC10	0.48
Average w	0.57
Standard deviation, S_d	0.06

The porosity, n, and dry density, γ_d, of the rock were determined using the saturation and caliper techniques suggested by ISRM. The test involved six disc-shaped specimens of 25 mm nominal thickness and 75 mm diameter prepared from a representative cylindrical sample. The results of the test yielded an average value for porosity of n = 10.7% with a standard deviation of 0.07%, and an average value for dry density of γ_d = 2226 kg/m^3 with

a standard deviation of S_d = 3 kg/m^3. Individual results for all specimens are given in Table 4.2.

Table 4.2 Porosity and dry density test results.

Specimen No.	Porosity n, %	Dry Density γ_d, kg/m^3
DPO1	10.9	2223
DPO2	10.7	2232
DPO3	10.7	2229
DPO4	10.7	2225
DPO5	10.8	2225
DPO6	10.7	2224
Average	10.7	2226
S_d	0.07	3

The bulk density, γ, of the material was determined by averaging the individual bulk densities of all the specimens involved in the testing programme. That included the aforementioned porosity and dry density test specimens, Brazilian disc test specimens, solid cylinders used in uniaxial compression and triaxial compression tests, cubical specimens used in multiaxial compression tests, and thick-walled hollow cylinder test specimens. Prior to testing, each specimen was weighed for its bulk mass, its bulk volume was calculated from an average of several vernier measurements for each dimension, and consequently the specimen bulk density was determined. Considering all the specimens involved, an average value of γ = 2235 kg/m^3 was obtained with a standard deviation of S_d = 29 kg/m^3.

4.3.2 Uniaxial Compression and Deformability Tests

Ten air-dried cylindrical specimens of 75 mm diameter and 150 mm height were loaded to failure under standard uniaxial compression, $\sigma_1 > \sigma_2 = \sigma_3 = 0$, in order to determine the uniaxial compressive strength and the elastic constants, namely Young's modulus and

Poisson's ratio. The tests were conducted using the 1 MN capacity servo-controlled loading system with the feedback signal being an axial displacement increase rate of 0.25% / min. Measurements of the applied axial load were monitored by a 1 MN capacity load cell, and the specimen axial deformation due to loading was monitored by a transducer measuring between the loading platens. The diametric or lateral deformation was monitored by three transducers mounted on a steel ring specially designed to enable the radially oriented transducers to be positioned at the specimen mid-height with 120° circumferential spacing. The output of the monitoring devices was acquired via the SPECTRA-ms data acquisition system and stored in a PC data file. In addition, an X-Y recorder was employed for direct plotting of the axial load-axial deformation curve during the test.

Failure of the test specimen was generally marked by audible cracking accompanied by a sharp fall in the level of the axial stress. As pictured in Figure 4.3, different failure patterns were observed ranging from axial splitting to inclined shear fractures and evidence of developing shear cones.

The uniaxial compressive strength, Young's modulus and Poisson's ratio have been determined on the basis of the following considerations:

- The axial compressive stress, $\sigma_{ax} = \sigma_1$, in the test specimen was calculated by dividing the measured axial load by the original cross-sectional area of the specimen. Regarding the maximum load carried by the specimens, an average value of 44.113 MPa was obtained for the rock uniaxial compressive strength, σ_u, with a standard deviation level of S_d = 1.53 MPa.

- The axial strain, $\varepsilon_{ax} = \varepsilon_1$, was calculated by dividing the measured axial displacement, regarded positive for a decrease in length or contraction, by the original height of the specimen.

- The radial or lateral strain, $\varepsilon_{lat} = \varepsilon_2 = \varepsilon_3$, was calculated by dividing the mean of the measured lateral displacements, regarded negative for an increase in diameter or extension, by the original radius of the specimen.

- The volumetric strain of the test specimen, defined by $\varepsilon_v = \Delta V / V$, where ΔV is the change in the specimen volume during compression and V is the original volume of the specimen., was calculated as the sum of the three principal strains using the following equation:

$$\varepsilon_v = \Delta V / V = \varepsilon_1 + \varepsilon_2 + \varepsilon_3 = \varepsilon_{ax} + 2\,\varepsilon_{lat} \qquad (4.1)$$

Typical curves of the axial stress versus axial, lateral and volumetric strains are illustrated in Figure 4.4.

- Young's modulus, E, defined as:

$$E = \delta\,\sigma_{ax} \,/\, \delta\,\varepsilon_{ax} \qquad (4.2)$$

was determined from the slope of a straight line fitted to the more-or-less linear portion of the axial stress-axial strain curve. Regarding all specimens tested, an average value of $E = 7.527$ GPa was obtained with a standard deviation of 0.949 GPa.

- Poisson's ratio, ν, was calculated from the equation:

$$\nu = -\,E \,/\, \text{slope of axial stress-lateral strain curve} \qquad (4.3)$$

where the slope of the axial stress-lateral strain curve was determined in the same manner employed for the determination of Young's modulus. Regarding all specimens tested, an average value of $\nu = 0.261$ was obtained with a standard deviation of 0.041.

The Uniaxial compressive strength, σ_u, Young's modulus, E, and Poisson's ratio, ν, for each specimen tested are presented in Table 4.3 together with the average results.

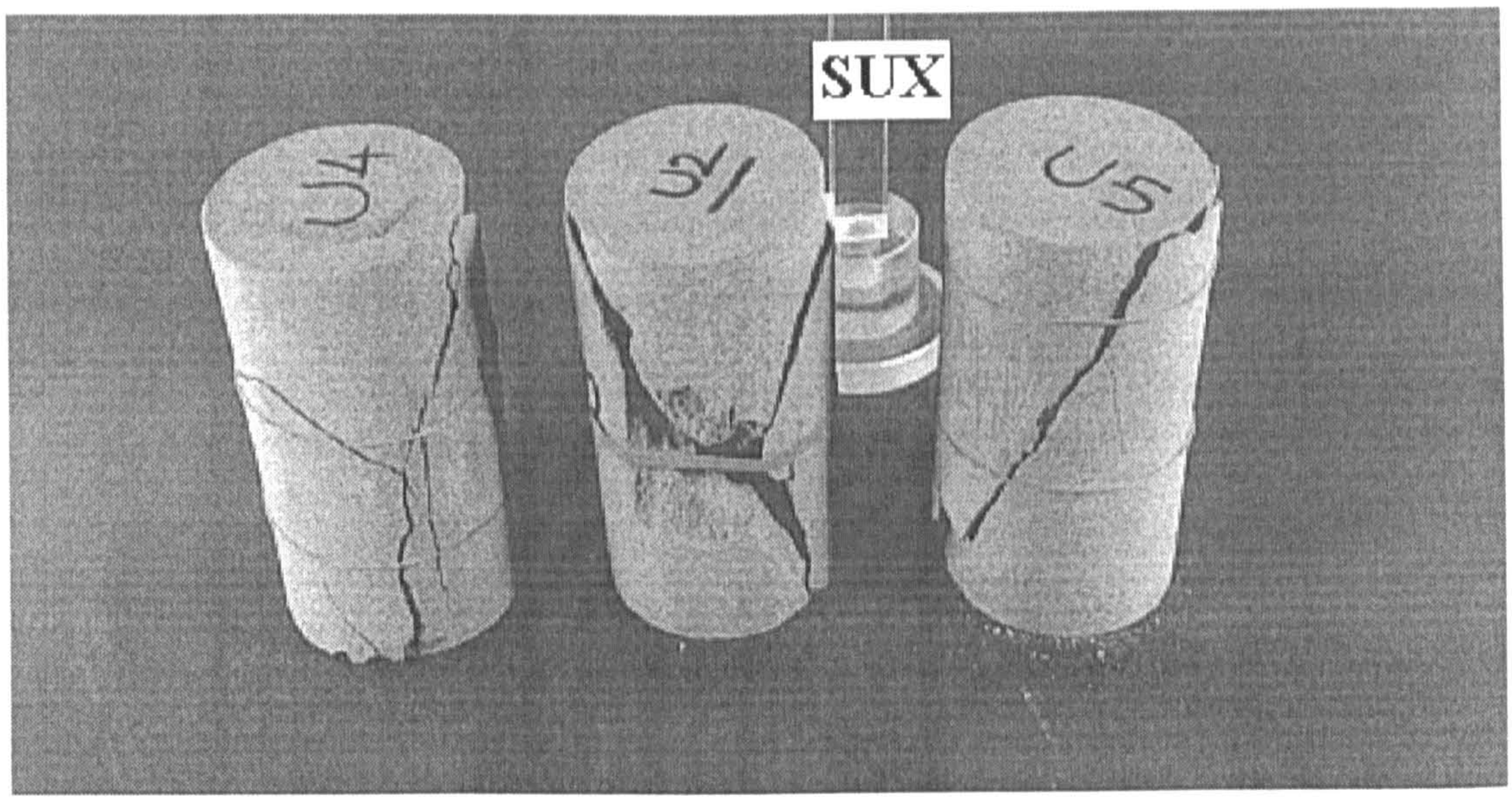

Figure 4.3 Typical failure modes observed in standard uniaxial compression tests on solid cylinders of Springwell sandstone.

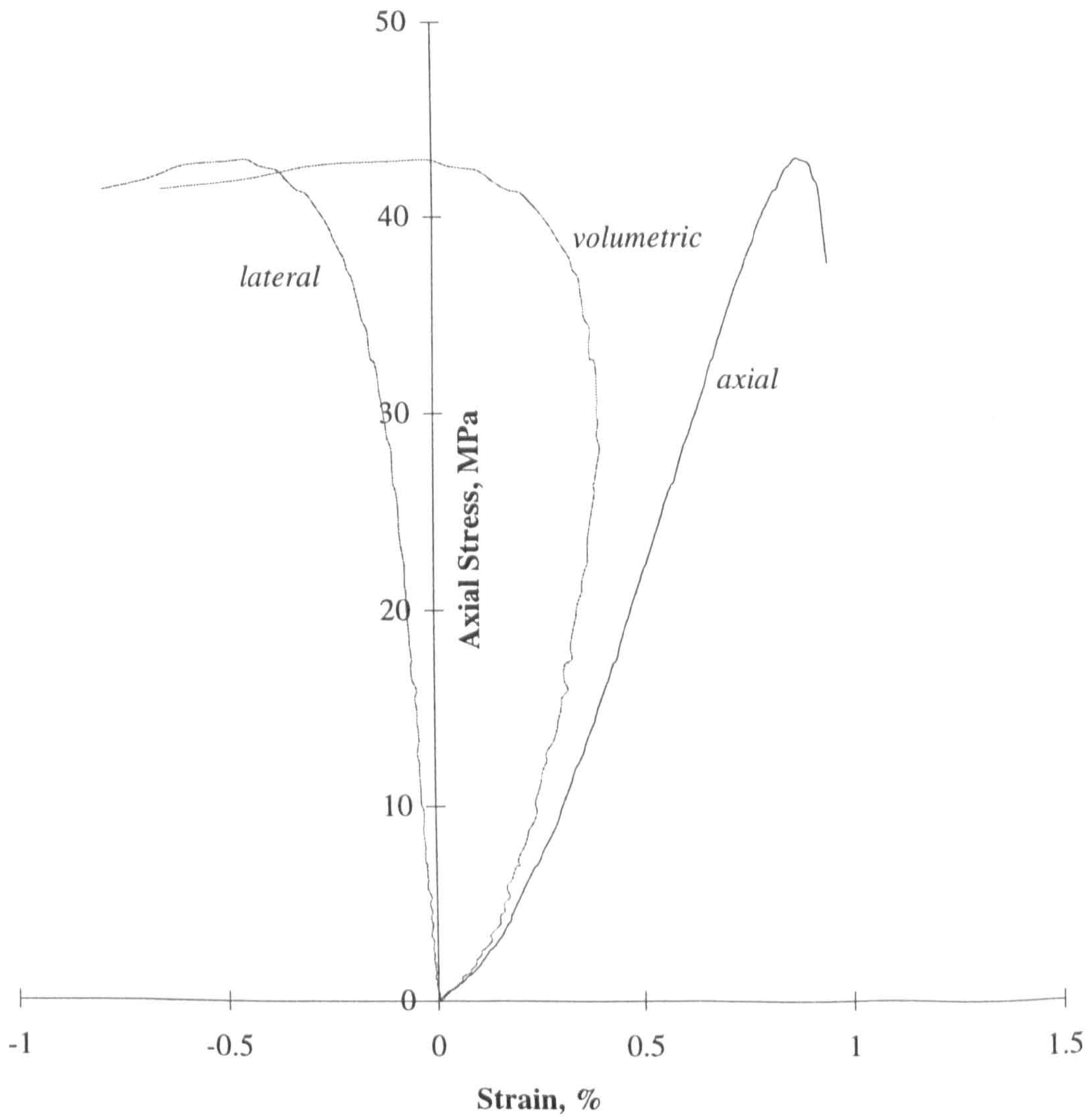

Figure 4.4 Typical curves of axial stress versus axial, lateral and volumetric strains obtained from standard uniaxial compression tests on solid cylinders of Springwell sandstone.

Table 4.3 Results of uniaxial compression and deformability tests.

Specimen No.	Compressive Strength σ_u, MPa	Young's Modulus E, GPa	Poisson's Ratio ν
SUX1	41.963	6.473	0.250
SUX2	47.148	7.880	0.325
SUX3	44.940	6.971	0.212
SUX4	42.899	6.250	0.207
SUX5	44.702	8.239	0.273
SUX6	46.149	7.250	0.280
SUX7	43.374	6.713	0.222
SUX8	42.756	7.713	0.298
SUX9	43.637	8.239	0.227
SUX10	43.561	9.539	0.316
Average	44.113	7.527	0.261
S_d	01.530	0.949	0.041

4.3.3 Uniaxial Indirect Tensile Strength Tests

A total of nineteen air-dried specimens of 75 mm diameter and 37.5 mm thickness were failed in Brazilian disc tests in order to measure the uniaxial tensile strength of the Springwell sandstone. The specimens were cut from the same cores from which the uniaxial compression test specimens were prepared. The tests were conducted using an in-house constructed Brazilian test apparatus. An AVERY 250 kN capacity testing machine was employed for applying and measuring compressive loads to the test specimen at a stress increase rate of 0.2 MPa / min. Prior to testing, the specimen periphery was wrapped with a layer of adhesive paper tape, conforming to the ISRM suggested methods.

The tensile strength of the specimen was calculated using the following formula:

$$\sigma_t = 0.636\, F / D\, t \qquad (4.4)$$

where σ_t is the tensile strength measured in MPa,

F the load at failure in N,

D the specimen diameter in mm, and

t the specimen thickness in mm.

An average value of σ_t = 3.725 MPa was obtained with a standard deviation of 0.214. The tensile strength for each specimen tested is given in Table 4.4.

Table 4.4 Uniaxial indirect tensile strength measurements from Brazilian disc tests.

Specimen No.	Tensile Strength σ_t, MPa
DBR1	3.819
DBR2	4.032
DBR3	3.778
DBR4	3.842
DBR5	3.829
DBR6	3.329
DBR7	3.852
DBR8	3.538
DBR9	3.605
DBR10	3.276
DBR11	3.747
DBR12	3.849
DBR13	3.641
DBR14	3.460
DBR15	3.505
DBR16	3.957
DBR17	3.957
DBR18	3.980
DBR19	3.776
Average	3.725
S_d	0.214

Table 4.5 summarises the physical and mechanical properties of the rock as measured from the above tests. Also shown the level of standard deviation, S_d, for the results of each property.

Table 4.5 Summary of measured physical and mechanical properties of Springwell sandstone

Property Measured	Symbol	Value	Unit	S_d
Moisture Content	w	0.57	%	0.06
Porosity	n	10.74	%	0.07
Dry Density	γ_d	2226	kg/m^3	3
Bulk Density	γ	2235	kg/m^3	29
Uniaxial Compressive Strength	σ_u	44.113	MPa	1.530
Young's Modulus	E	7.527	GPa	0.949
Poisson's Ratio	ν	0.261	-	0.041
Indirect Tensile Strength	σ_t	3.725	MPa	0.214

4.4 Specimen Preparation

4.4.1 Categorisation of the Test Specimens

Well over three hundred specimens of Springwell sandstone have been required to accomplish all the investigations undertaken in the present study. Governed by the nature of the tests involved, these specimens were of various shapes and sizes, and may be categorised as follows:

- Thin sections especially prepared for micro-petrographic examination of the rock mineral composition and texture.
- Lumps used for the determination of the rock moisture content, w.
- Disc-shaped specimens of 75 mm diameter and different thickness used to determine the rock porosity, n, dry density, γ_d, and uniaxial tensile strength, σ_t.
- Solid cylinders of 75 mm diameter and 150 mm height used in standard uniaxial and triaxial compression tests.
- Cubes measuring 74 × 74 × 74 mm used in direct multiaxial compression tests involving different stress fields.
- Thick-walled hollow cylinders of 75 mm outer diameter, 27 mm inner diameter, and 150 mm height, used in indirect multiaxial tests involving different stress fields.
- Determination of the rock bulk density, γ, involved all the disc-shaped specimens, the solid cylinders, the cubical specimens and the thick-walled hollow cylinders.
- Non-destructive ultrasonic wave velocity tests have been conducted on all cubes and solid cylinders.

4.4.2 Rock Sampling and Specimen Production

All specimens were sampled and produced in the Rock Cutting Workshop using appropriate machine tools and following conventional procedures. No particular sampling procedure was followed in the field, and the sandstone was brought to the Laboratory

from the Springwell Quarry in blocks. Visibly, the blocks were largely structureless and uniform in texture, and did not present any significant signs of impurity or pronounced bedding planes. Nevertheless, very subtle mineralic segregations could be observed which helped to define the "way upness" of the rock. In order to evade the influence of any potential anisotropy in the rock, each block was marked with reference to an *X*, *Y*, *Z* co-ordinate system oriented with the *Z* coordinate being normal to the bedding direction. Using a diamond-edge saw, the quarried blocks were cut up perpendicular to the *X*, *Y*, *Z* directions into slabs of an approximate thickness of 180 mm in the *Z* direction. Subsequently, the test specimens were produced from these slabs and marked accordingly with respect to the coordinate system directions.

Both solid and hollow cylinders were cored along the *Z* direction using a radial arm drilling machine equipped with diamond-tipped core barrels. Water was admitted through a swivel in order to clear the drill cuttings and cool the bits. The specimen ends were trimmed and then ground flat and perpendicular to the longitudinal axis, in accordance with ISRM specifications, to the final height of 150 mm.

The disc-shaped specimens were produced from solid cores and their ends were prepared as suggested by ISRM.

For the production of the cubical specimens, rectangular prisms of an approximate cross sectional area of 80 × 80 mm were cut from the slabs perpendicular to the *X*, *Y*, *Z* coordinate system. Then, each prism was ground square to a cross sectional area of 74 × 74 mm and then sliced at approximate intervals of 80 mm. This length was then reduced to 74 mm by grinding the sliced faces flat and square.

Since water was used during production, all specimens were air-dried for a period of 48 hours after which their masses and dimensions were measured.

4.5 An Investigation into Inherent Specimen Variations and other Properties of Springwell Sandstone

4.5.1 The Question of Inherent Specimen Variations

As mentioned earlier, no particular sampling procedure was followed in the field and the rock samples were collected from the Quarry in the form of blocks. Due to the comprehensive nature of the experimental programme, many blocks were required for the production of all test specimens. Since the sufficient quantity of rock could not be estimated beforehand, the specimens were produced in batches and several visits to the Quarry were necessary. Consequently, it was not possible to obtain all blocks from the same parent rock mass.

Rocks in nature are generally neither isotropic nor homogeneous, and their properties may well vary from one location to another or from sample to sample. Variations can also be expected to occur even among specimens prepared from the same sample. In rock testing, when assessing any property of the material, it is often experienced that the experimental results are scattered. Therefore, it is of prime importance to verify whether the scatter in the results is caused by experimental errors or it is related to variations in the intrinsic properties of the rock specimens.

Thus, in order to account for any inherent variations in the specimens used in the present study, non-destructive ultrasonic wave velocity tests have been performed on all cubes and solid cylinders prior to their prospective loading. The thick-walled hollow cylinders have not been involved in the investigation due to their peculiar geometry. Statistical methods have been employed to analyse the test results and evaluate the rock isotropy and dynamic Young's modulus.

4.5.2 Non-Destructive Ultrasonic Wave Velocity Tests

The employed testing technique involved measuring the propagation velocity of the longitudinal or compressional wave, V_p, in the rock specimens using a portable apparatus

known as PUNDIT, which derives its name from the initial letters of the title " Portable Ultrasonic Non-destructive Digital Tester". The apparatus generates low frequency ultrasonic pulses and indicates in micro-seconds the time of their travel from a transmitting transducer coupled at one end of the test specimen to a receiving transducer at the other end. By determining the travel time of the pulses and measuring the travel distance between the two transducers, then the pulse velocity can be calculated by using the equation:

$$\text{Pulse velocity} = \text{travel distance} / \text{travel time} \qquad (4.5)$$

In the present investigation, measurements of the travel time of the compressional wave in the cubical specimens were taken along the three principal directions of the cube. As earlier explained, these directions corresponded to an *X, Y, Z* coordinate system along which the specimens were produced. For the solid cylindrical specimens, measurements of the travel time of the compressional wave were taken along the specimen longitudinal axis only, which is the *Z* direction along which the specimens were cored. In both cases, the transmitter and receiver were greased by a thin film of liquid soap and then manually pressed to the centre of the specimen surfaces normal to the direction of wave propagation.

4.5.3 Determination of the Directional Values of the Dynamic Young's Modulus

For a more adequate interpretation of the results of the ultrasonic wave velocity tests, obtained values of the compressional wave propagation velocity have been used to determine the corresponding values of the so-called dynamic Young's modulus of the rock. From the theory of elastic wave propagation, it can be shown that:

$$E_d = \frac{\gamma V_p^2 (1+\nu_d)(1-2\nu_d)}{(1-\nu_d)} \qquad (4.6)$$

where E_d is the dynamic Young's modulus,

γ is the density of the rock,

V_p is the velocity of compressional wave, and

v_d is the dynamic Poisson's ratio of the rock.

Thus, using equation (4.6), and regarding the co-ordinate directions *X, Y, Z* along which the travel times of the compressional wave were measured in the specimens, the respective directional dynamic Young's moduli identified as $E_{d(x)}$, $E_{d(y)}$, $E_{d(z)}$ have been calculated. Note that the dynamic Poisson's ratio, v_d, in equation (4.6) was assumed equal to the Poisson's ratio determined in section 4.3.2 from the uniaxial compression and deformability tests.

4.5.4 Statistical Analysis of the Results

Statistical methods have been employed in order to analyse the obtained values of the dynamic Young's moduli and assess their variability. The results of the analysis are presented in terms of common statistical descriptive measures and graphs. Table 4.6 presents a summary of statistics determined for the values of each of the moduli $E_{d(x)}$, $E_{d(y)}$, $E_{d(z)}$. Figures 4.5 to 4.8 illustrate plots of the normal distribution curve superimposed on frequency histogram for the values of each modulus. Plots of the relative frequency polygons for all moduli are illustrated in Figure 4.9. Detailed descriptions of statistical terminology, concepts and techniques can be found in a number of relevant text books, notably, Kennedy and Neville (1986), Volk (1980), Leeming (1969), Beyer (1981).

4.5.5 Discussion of the Results

In view of the results of the statistical analysis, it is clear that all moduli are slightly skewed, either positively or negatively, or asymmetrically distributed about their central values. Comparing the values of the arithmetic mean or average, median, mode and geometric mean stated in Table 4.6, the central tendency of the values of each modulus may efficiently be measured by the average value. Moreover, all moduli seem to differ little from each other in their central tendency. The levels of variance, standard deviation and some other measures given in Table 4.6 indicate that values of the $E_{d(x)}$, $E_{d(y)}$, $E_{d(z)}$ of the cubical specimens are more or less equally dispersed. In the case of the solid cylinders, the dispersion of the values of $E_{d(z)}$ is noticeably less than that of the cubes.

Besides the fact that rock, by its very nature, is non-homogenous material, the dispersion of the results is likely to have been amplified by equipment and procedural errors. The PUNDIT apparatus used in the investigation proved to be inconsistent sometimes, and measurements of the travel times of the pulse propagation are likely to have been influenced by variations in the level of the manually applied pressure to the test specimens. The relatively less pronounced scatter of the results of the cylindrical specimens may be attributed to minimum equipment and procedural errors. This is related to the fact that while the cylinders underwent the non-destructive test successively, the cubical specimens were tested in groups over a long period of time following the cubical multiaxial testing programme.

Discrepancies between the results of the two types of specimens might also have been caused by variations in the sandstone blocks from which the specimens were produced. All the solid cylinders were produced in one batch from two blocks of Springwell sandstone obtained from the same location at the Quarry. By contrast, the cubical specimens were produced in batches from several groups of blocks collected from different locations over a period of time.

4.5.6 Inference of the Rock Isotropy

One of the most significant outcome of the preceding analysis lies in the evidence that the moduli $E_{d(x)}$, $E_{d(y)}$, $E_{d(z)}$ are, overall, of a very similar nature with respect to their dispersion and central tendency. If these moduli are to be represented by their average values, then it may be stated that the dynamic Young's modulus of the Springwell sandstone is the same in all three directions. Such a property is a clear indication of the isotropy of the rock.

Table 4.6 Descriptive statistical measures for each of the directional dynamic Young's moduli $E_{d(x)}$, $E_{d(y)}$, $E_{d(z)}$. Modulus values and related statistics are expressed in GPa.

Statistics	Cubical Specimens			Solid Cylinders
	$E_{d(x)}$	$E_{d(y)}$	$E_{d(z)}$	$E_{d(z)}$
Sample Size, No.	74	74	74	29
Average	7.323	7.414	7.254	7.531
Median	7.080	7.159	7.253	7.492
Mode	7.078	7.138	7.642	7.492
Geometric Mean	7.234	7.326	7.194	7.524
Variance	1.315	1.350	0.842	0.115
Standard Deviation	1.147	1.162	0.918	0.340
Standard Error	0.133	0.135	0.107	0.063
Variation Coefficient, %	15.66	15.67	12.66	4.51
Minimum	5.081	5.295	4.775	6.895
Maximum	9.497	9.954	9.078	8.100
Range	4.416	4.658	4.302	1.205
Lower Quartile	6.437	6.524	6.643	7.274
Upper Quartile	8.329	8.430	7.924	7.817
Interquartile Range	1.892	1.905	1.281	0.543
Skewness	0.092	0.351	-0.352	-0.034
Kurtosis	-0.839	-0.769	-0.163	-0.979

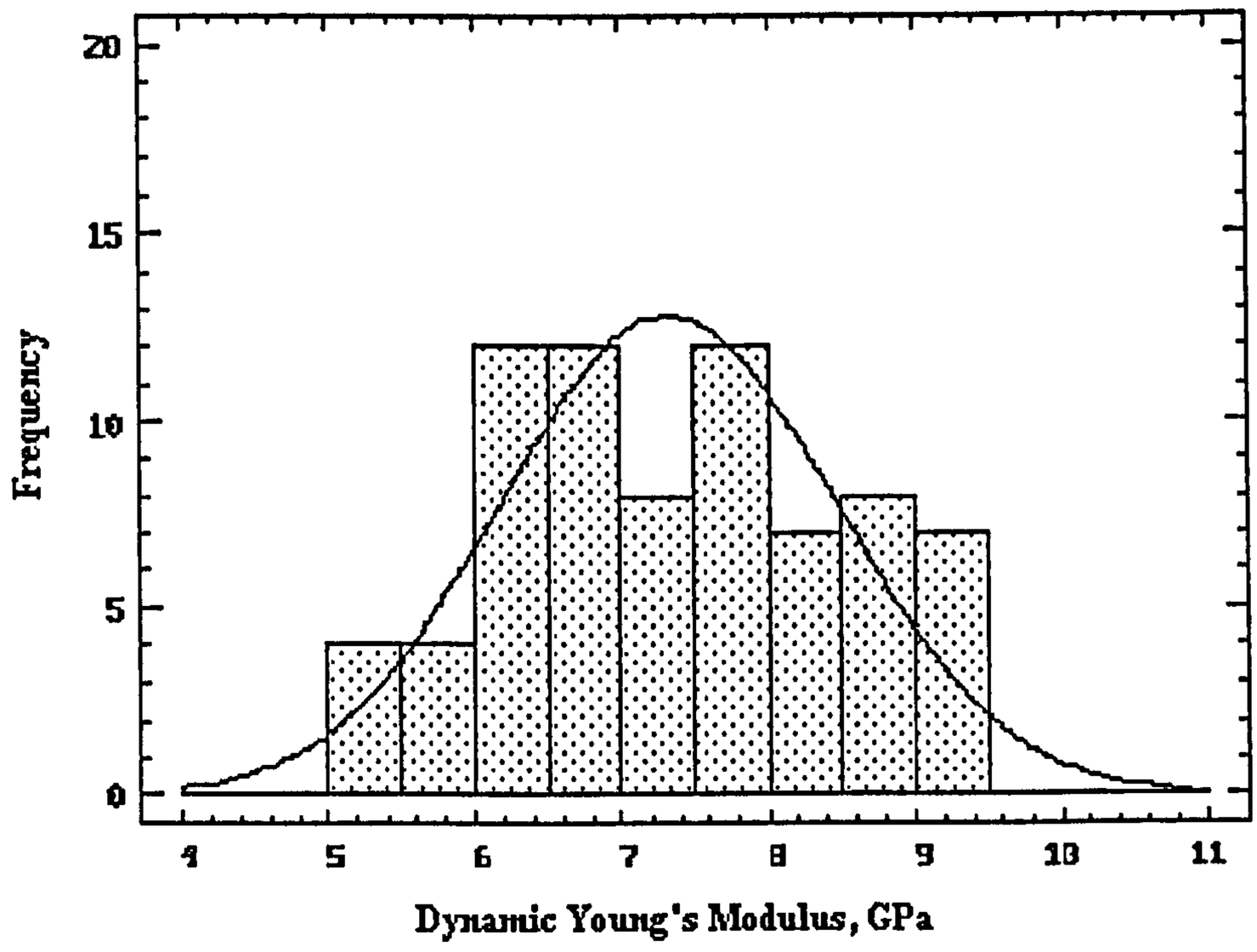

Figure 4.5 Normal distribution curve superimposed on frequency histogram for the directional dynamic Young's modulus $E_{d(x)}$ of the cubical specimens.

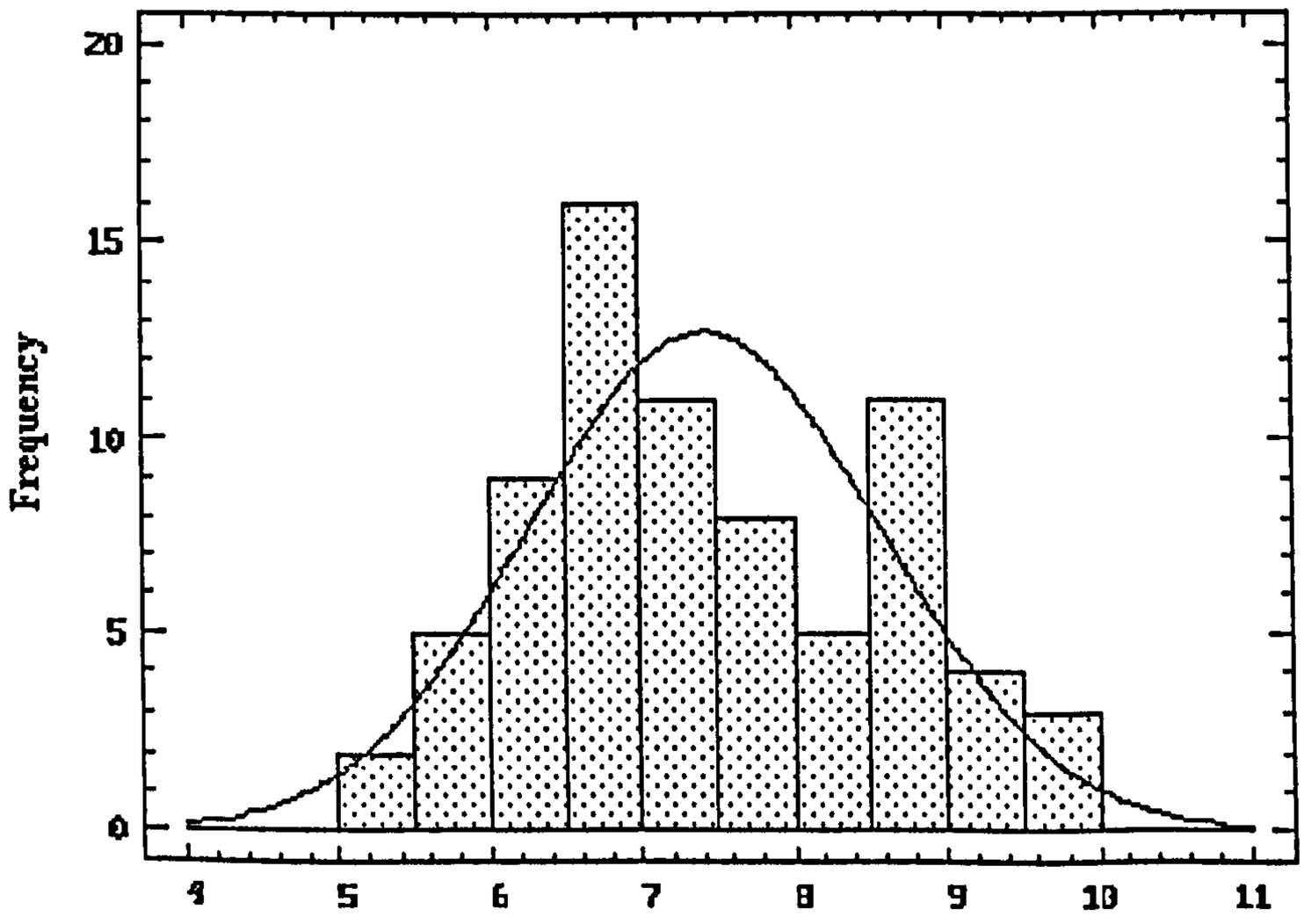

Figure 4.6 Normal distribution curve superimposed on frequency histogram for the directional dynamic Young's modulus $E_{d(y)}$ of the cubical specimens.

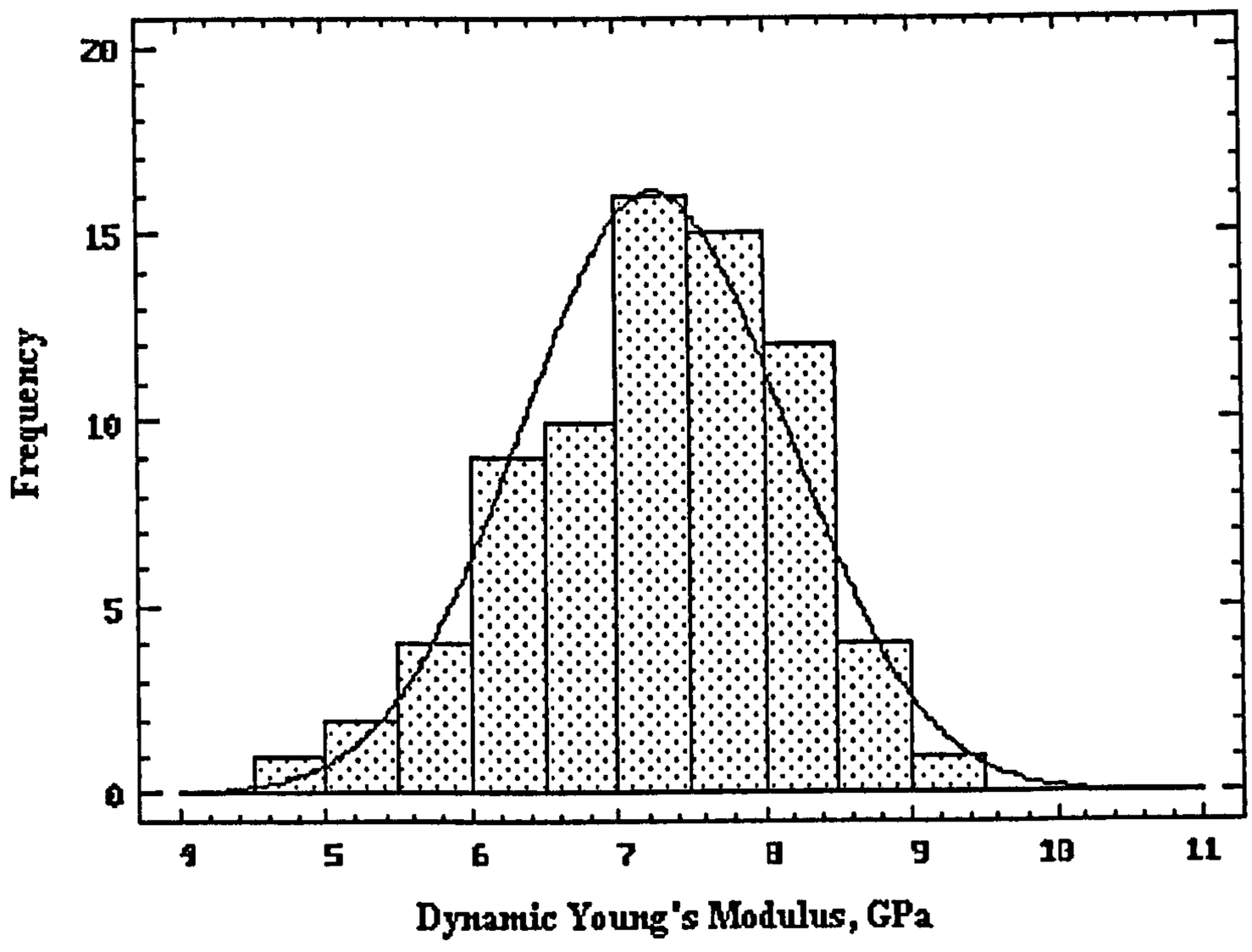

Figure 4.7 Normal distribution curve superimposed on frequency histogram for the directional dynamic Young's modulus $E_{d(z)}$ of the cubical specimens.

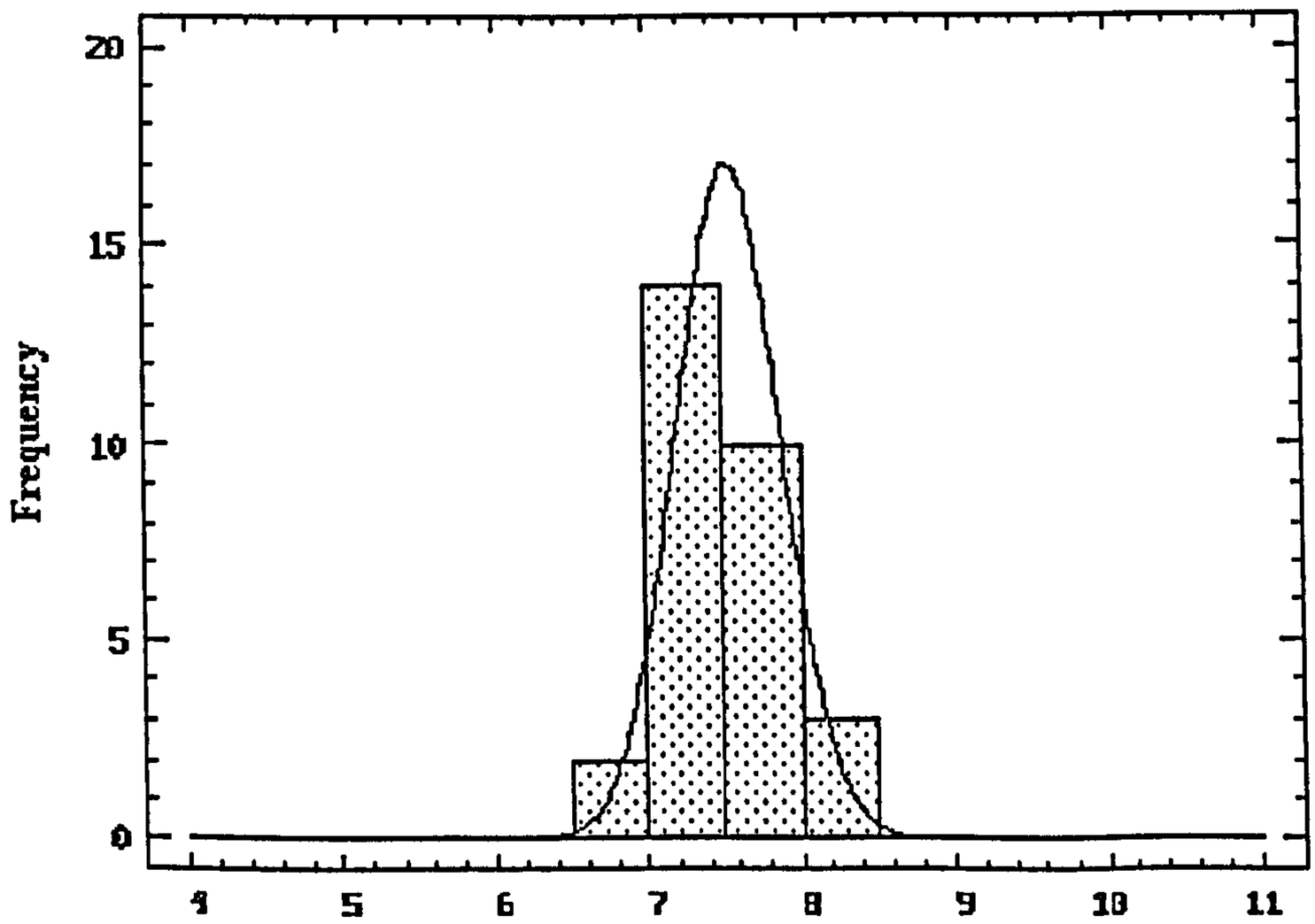

Figure 4.8 Normal distribution curve superimposed on frequency histogram for the directional dynamic Young's modulus $E_{d(z)}$ of the solid cylinders.

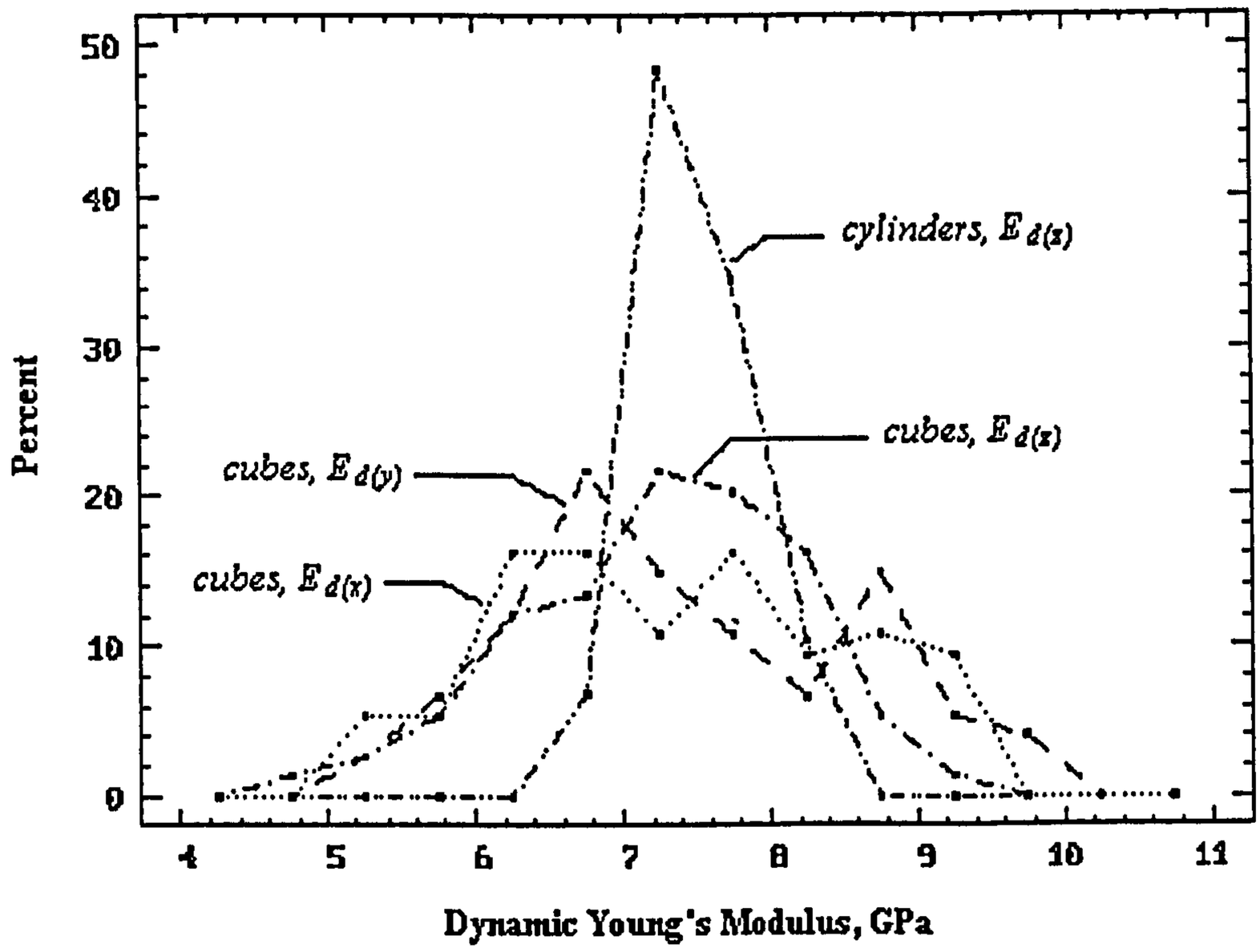

Figure 4.9 Relative frequency polygons for each of the directional dynamic Young's moduli $E_{d(x)}$, $E_{d(y)}$, $E_{d(z)}$.

4.5.7 Further Analysis for the Determination of the Overall Dynamic Young's Modulus of the Rock

In the light of the emerged evidence that the rock is isotropic, values of all moduli have been combined as one set of data and statistically analysed in order to ascertain the overall dynamic Young's modulus of the rock. Table 4.7 shows a summary of the statistics obtained. As might be expected, there is a good agreement between these results and those stated in Table 4.6 for the individual moduli. Figure 4.10 illustrates a fitted plot of the normal distribution curve superimposed on the frequency histogram, and Figure 4.11 illustrates a plot of the relative frequency polygon for the data. As can be seen from these figures, the data follow closely the normal distribution. A better picture of the distribution of the data compared to the normal distribution curve can be seen in Figure 4.12 in the form of hanging histobars. Figure 4.13 shows a normal probability plot for the data.

Table 4.7 Descriptive statistical measures for all values of $E_{d(x)}$, $E_{d(y)}$, $E_{d(z)}$ combined to determine the overall dynamic Young's modulus, E_d, of the rock.
Modulus value and related statistics are expressed in GPa.

Statistics	Value
Sample Size, No.	251
Average	7.354
Median	7.274
Mode	7.642
Geometric Mean	7.282
Variance	1.045
Standard Deviation	1.022
Standard Error	0.065
Variation Coefficient, %	13.90
Minimum	4.775
Maximum	9.954
Range	5.178
Lower Quartile	6.643
Upper Quartile	8.052
Interquartile Range	1.409
Skewness	0.084
Kurtosis	-0.333

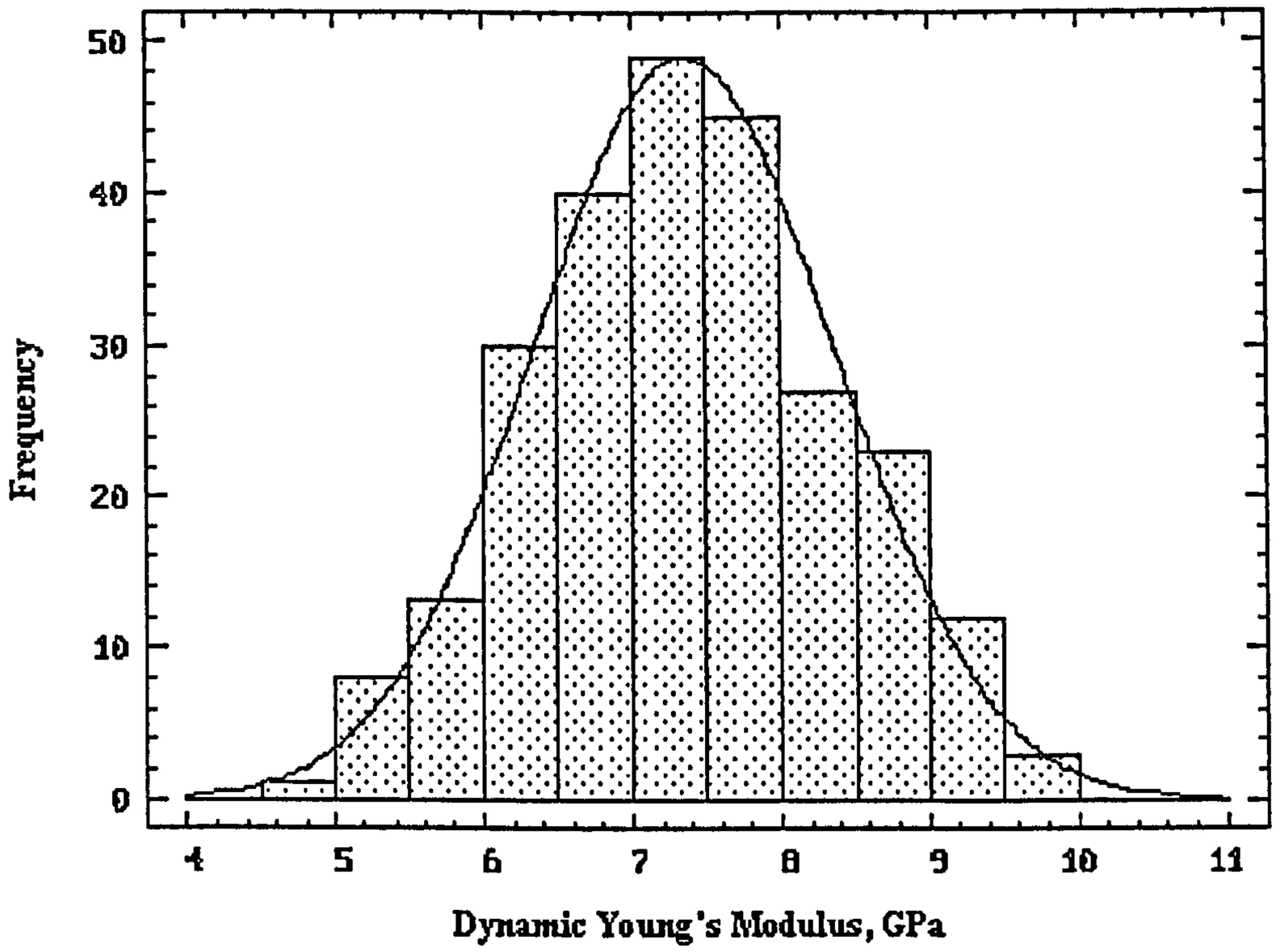

Figure 4.10 Normal distribution curve superimposed on frequency histogram for all measurements of the directional dynamic Young's moduli.

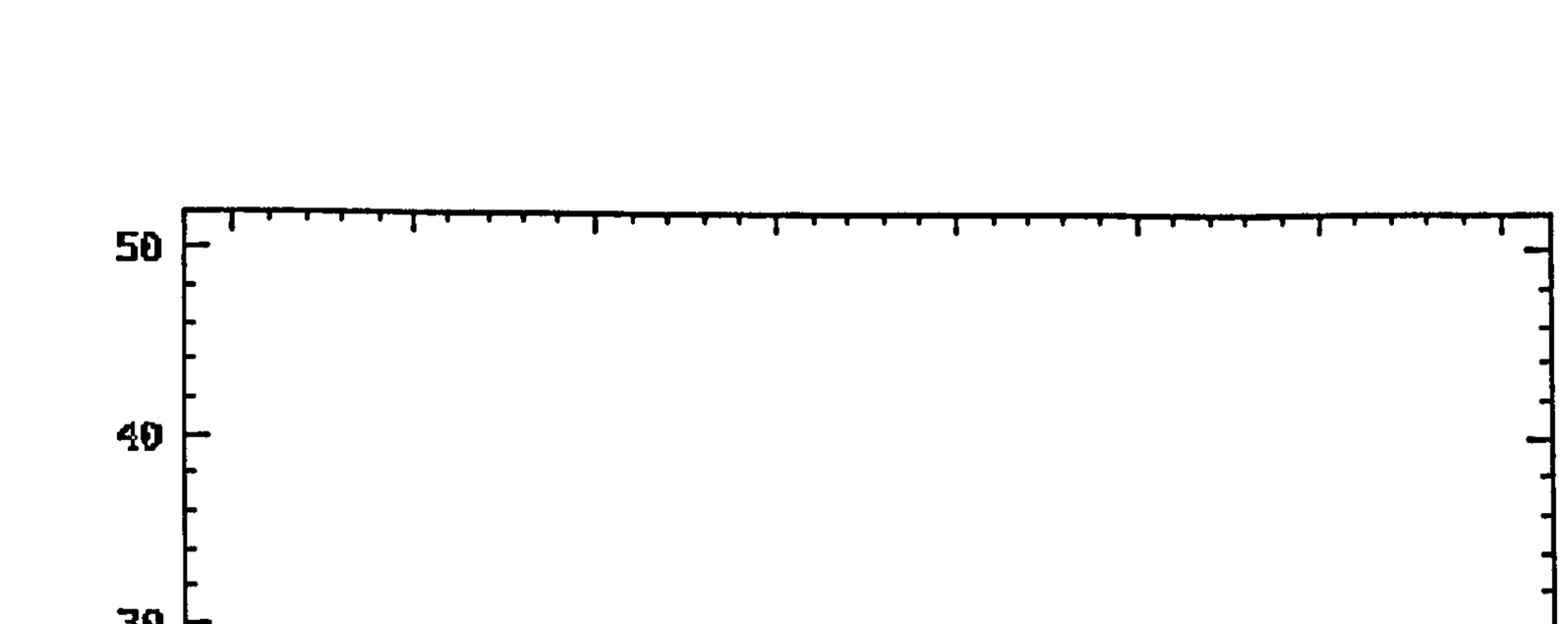

Figure 4.11 Relative frequency polygon for all measurements of the directional dynamic Young's moduli.

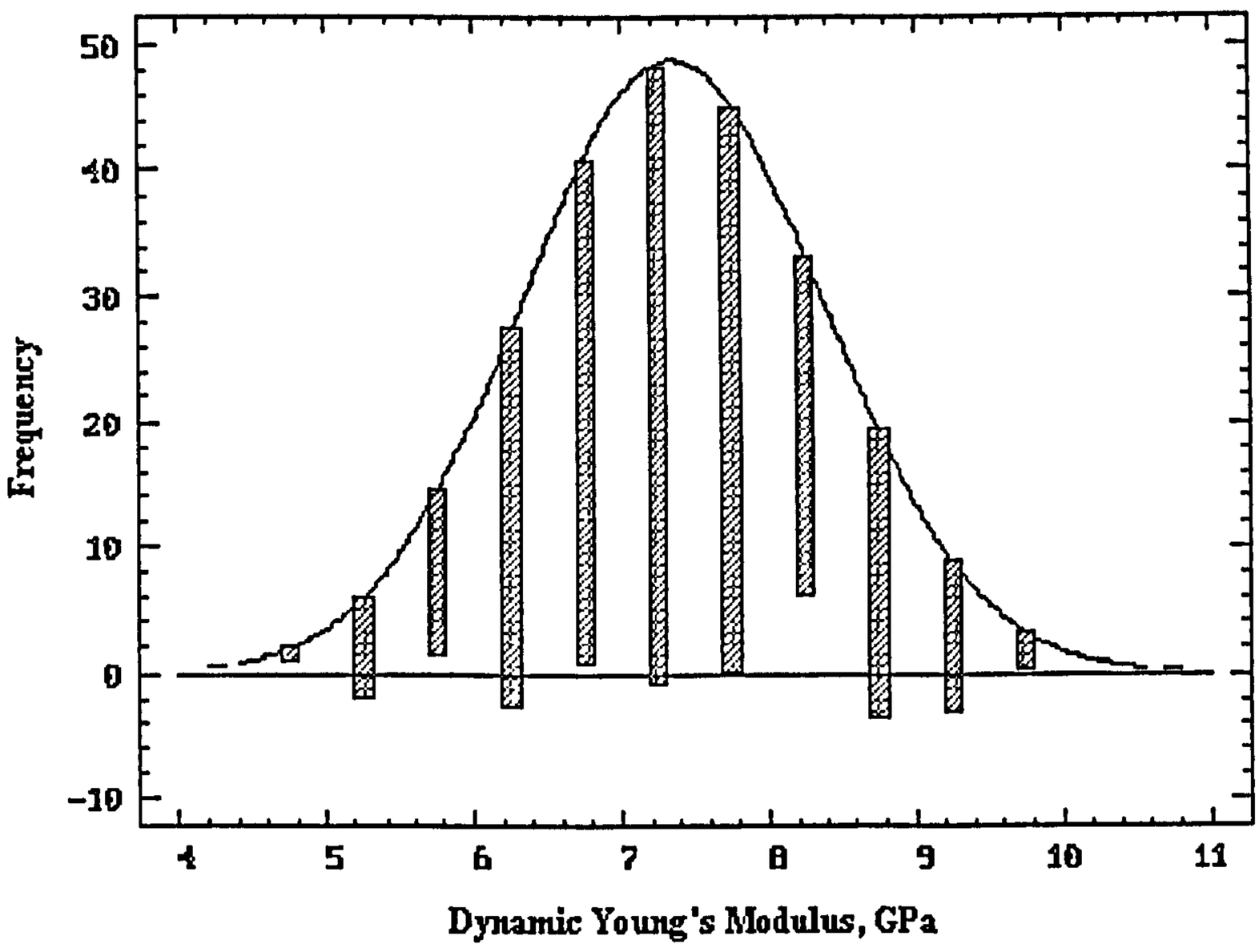

Figure 4.12 Hanging histobars and normal distribution curve for all measurements of the directional dynamic Young's moduli.

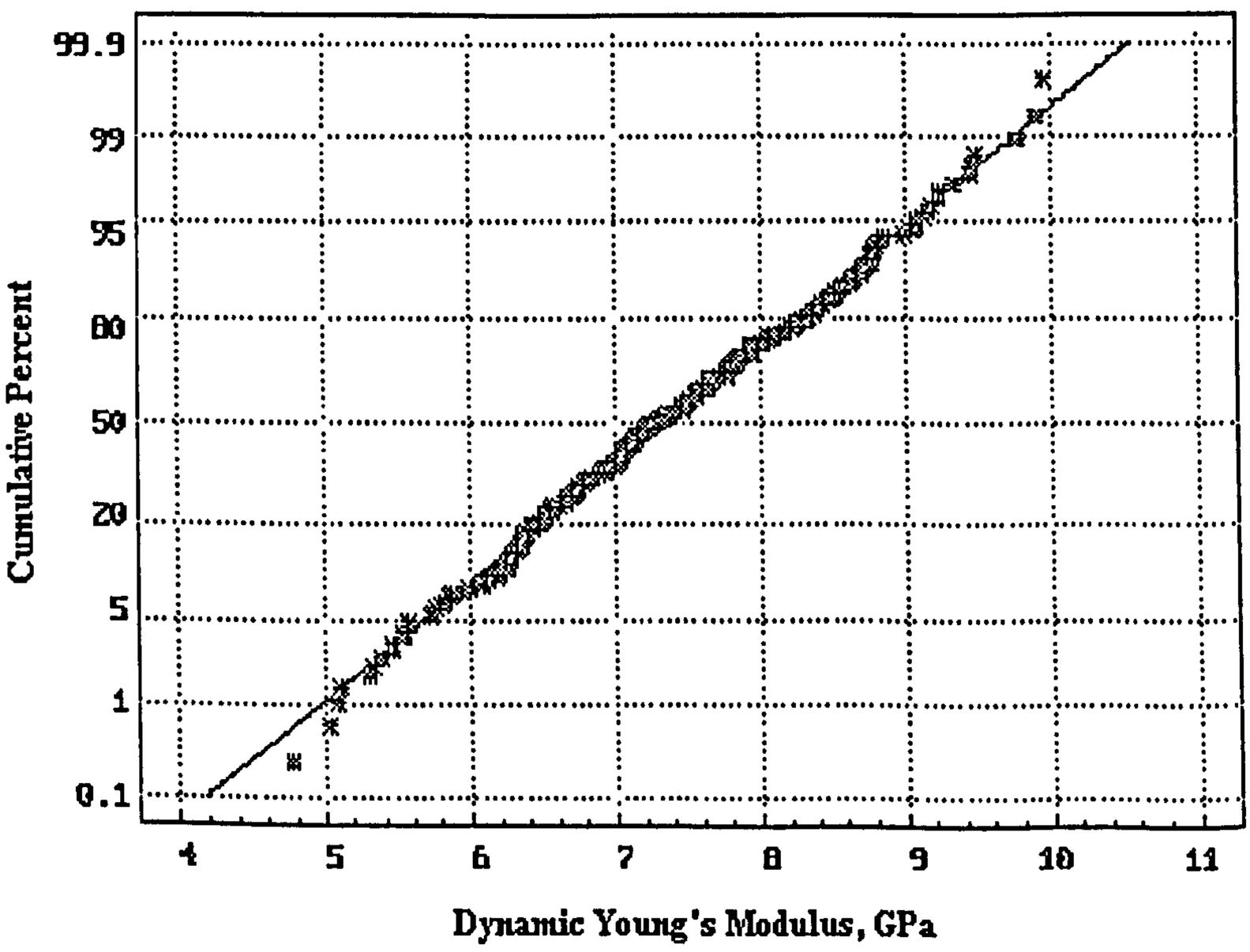

Figure 4.13 Normal probability curve for all measurements of the directional dynamic Young's moduli.

The nearly normal distribution of the values of all moduli combined as one set of data may be related to the increase in the sample size in comparison with that of the individual moduli. In fact many sets of experimental results in practice turn out to follow the normal distribution, Kennedy and Neville (1986), and a large sample is always expected to yield a more representative result. However, since the value of the dynamic Young's modulus of the Springwell sandstone is not exactly known, it is difficult to ascertain the credibility of the obtained results, and therefore, the present investigation can only give inference in terms of probability. In this respect, it may be more appropriate to evaluate the experimental results on the basis of the Students' *t* distribution.

The statistic *t* is defined as:

$$t = \frac{|\bar{x} - \mu|}{S_d / \sqrt{n}} \tag{4.7}$$

where $\bar{x}$ is the average or mean of the sample studied,

μ is the mean of the population,

S_d is the sample standard deviation, and

n is the sample size.

Like the normal distribution, the *t* distribution is symmetric, and *t* values measure either positive or negative deviations of the sample mean from that of the population in terms of relative frequencies or probabilities. Thus, from Equation (4.7), the population mean can be expressed as follows:

$$\mu = \bar{x} \pm t \left(S_d - \sqrt{n} \right) \tag{4.8}$$

The range within which the mean μ may lie is known as the confidence range, and the boundaries of this range are known as the confidence limits. The probability that μ will lie within the confidence range is referred to as the confidence level, $(1-\alpha)$, and the probability of error is referred to as the significance level, α.

Values of the statistic *t* are determined on the basis of the probability level chosen and the degrees of freedom used for the calculation of the variance or the standard deviation,

i.e. (n - 1). The appropriate t values can be obtained from statistical tables available in a number of relevant text books.

In the present analysis, since (n - 1) = 250, t values for ∞ degrees of freedom may be employed. If a significance level of $\alpha = 0.10$ is to be assumed, then the values of the statistic t are ±1.645. Thus, using Equation (4.8), with $\bar{x} = 7.354$ and $S_d = 1.022$ from Table 4.7, the confidence limits are:

$$7.354 \pm 1.645\ (1.022 / \sqrt{251}) = 7.354 \pm 0.106 \text{ GPa}$$

This suggests that the average value of the overall dynamic Young's modulus, E_d, of the Springwell sandstone can be expected, with 0.10 probability of error, to range from 7.248 to 7.460 GPa. Clearly, the deviation of the mean value of the experimental data from the suggested value of E_d is negligible. Such a close agreement between the two values may be ascribed to the large number of measurements involved in the analysis, i.e. the sample size, as well as the conformity of the data to the normal distribution. Although the t distribution is not normal, it approaches the normal distribution when n becomes large, and the two distributions become equivalent when n becomes infinite.

4.5.8 Comparison between the Static and Dynamic Young's Moduli of the Rock

As earlier determined from standard deformability tests, Table 4.3, the "static" Young's modulus, E_s or commonly denoted as E, of the Springwell sandstone has an average value of E_s = 7.527 GPa. If the results of the ultrasonic wave velocity tests obtained in this investigation are to be accepted as meaningful at all, and if the overall dynamic young's modulus is to be measured by the mean value suggested above, $E_d = 7.354 \pm 0.106$ GPa, then there is clearly a remarkable agreement between the dynamic and static Young's moduli of the rock.

It has often been advocated by researchers that for most rocks the dynamic and static moduli are likely to differ. Moreover, most of the results reported to date have indicated that the dynamic modulus is generally greater than the static modulus; amongst others

Rinehart *et al.* (1961), King (1970), Howarth (1985), Van Heerden (1987), and Eissa and Kazi (1988). The difference between the two moduli has commonly been attributed mainly to a greater influence on the static measurements by the presence of micro-cracks and pores.

The close agreement between the static and dynamic young's moduli in the present study is clearly an interesting finding. An ideally isotropic and homogeneous material may well be expected to have the same values of static and dynamic Young's moduli if determined under ideal conditions. However, it would be unrealistic to assume that such ideal conditions, with regard to both material and testing techniques, have in fact been met in the present investigation. On the other hand, it would equally be inadequate to suppose that the close agreement between the two moduli is just accidental and may be attributed to experimental errors. Undoubtedly, measurements of both moduli are likely to have been influenced by different errors inherent in all testing techniques. In this regard, the dynamic modulus may bear the influence of earlier described equipment and procedural errors which may have affected measurements of the ultrasonic wave travel time in the test specimens. Any suggestion to consider the possible effect of involving different specimens in the determination of the dynamic modulus is immediately refuted by the fact that the static modulus, determined from solid cylinders, is in complete agreement with the mean value of the dynamic modulus of the solid cylinders, Table 4.6. Nevertheless, it is possible that the dynamic modulus of the rock has been influenced by the use of the static Poisson's ratio, ν_s or ν, in Equation (4.6) to calculate the modulus values from the velocity of compressional wave. In contrast with the dynamic Young's modulus, the dynamic Poisson's ratio, ν_d, was reported by Van Heerden (1987) to be smaller than the static Poisson's ratio, ν_s. As can be deduced from Equation (4.6), a smaller value of Poisson's ratio would result in higher values of the dynamic modulus. However, the dynamic Poisson's ratio of the rock could not be determined in the present investigation because it involves measurements of the transversal or shear wave velocities in the test specimens. Such measurements could not be made due to technical limitations in the measuring device available. Therefore, the possible effect of the dynamic Poisson's ratio on the results can not be verified.

The common assumption that the dynamic Young's modulus of the rock is higher than the static modulus appears to be open to question . Eissa and Kazi (1988) pointed out that there are instances where the opposite is true. More importantly, King (1983) indicated that where the concentration of micro-cracks is low, the static elastic modulus for a dry rock approaches the dynamic value. Thus, considering the nature of the rock tested and the samples from which the test specimens were produced, the close agreement between the static and dynamic Young's moduli encountered in the present study may be a genuine one. On this basis, factors that seemed to have influenced the results may be held accountable mainly for the dispersion of the experimental data but did not significantly influence the overall average value of the dynamic Young's modulus of the rock.

Chapter 5

MULTIAXIAL COMPRESSION OF CUBICAL SPECIMENS

5.1 Introduction

The behaviour of intact rock under multiaxial compression has been investigated through a comprehensive testing programme carried out on cubical specimens of Springwell sandstone. A total of seventy-four cubes of the dimensions 74 × 74 × 74 mm have been subjected to different loading conditions involving the following stress fields:

- Polyaxial compression, $\sigma_1 > \sigma_2 > \sigma_3 > 0$
- Triaxial compression, $\sigma_1 > \sigma_2 = \sigma_3 > 0$
- Biaxial compression, $\sigma_1 > \sigma_2 > \sigma_3 = 0$
- Uniaxial compression, $\sigma_1 > \sigma_2 = \sigma_3 = 0$

In order to acquire more information from a single specimen, a number of polyaxial and triaxial tests have been extended to multiple failure states utilising the concept of the *Multiple Failure State Triaxial Test* introduced by Kovari and Tisa (1975).

The tests have been conducted using the multiaxial cubical test apparatus with the axial stress being always the major principal stress, σ_1, applied by the 5 MN servo-controlled testing machine. A special emphasis has been placed on the effect of friction between the test specimen and the loading platens, and PTFE sheets have been used to minimize this effect. All tests were axial strain controlled and involved direct measurements of the specimen deformations along the three principal directions. Prior to loading, each specimen underwent a non-destructive ultrasonic wave velocity test performed to examine the rock isotropy and assess the uniformity of the test specimens.

This chapter begins with a description of the general testing arrangement and procedure employed and then presents the experimental work. All tests of the same stress field are grouped together and introduced with an outline of their main features. Depending on the test objectives and emphasis, the polyaxial tests have been grouped into four series. Then, the test results are presented in various forms highlighting the most significant outcome of the tests. Finally, the results are specifically analysed and discussed. A general discussion and comparison of all cubical test results as well as results of other tests conducted in the present study has been reserved for Chapter 8.

5.2 General Testing Configuration and Procedure

The main testing facilities employed in multiaxial compression of cubical specimens, Figure 3.4, were described in some detail in Chapter 3, and may briefly be listed here as follows:

- A multiaxial cubical test apparatus, Figures 3.1 to 3.3, equipped with hydraulic rams, steel bearing platens, transducers and load cells.
- A servo-controlled loading system, Figure 3.13, capable of applying a maximum compressive force of 5 MN used for the application of the major principal stress, σ_1.
- A mobile hydraulic power pack of a maximum capacity of 70 MPa used in conjunction with a relief valve for the application of the intermediate principal stress, σ_2, via one of the two hydraulic rams of the cubical apparatus.
- A pressure intensifier system, Figure 3.14, of a maximum capacity of 70 MPa used for the application of the minor principal stress, σ_3, via the other hydraulic ram of the cubical apparatus.
- A data acquisition system with a personal computer, Figure 3.15, used for continual monitoring and recording of the experimental data obtained via the load cells and transducers of the test apparatus.
- An X-Y recorder connected to the servo-controlled loading system used to trace the output of the system load cell and LVDT, thus granting a direct plot of the axial load-axial displacement curve during the test.

The rock specimens were cubes of the dimensions 74 × 74 × 74 mm. As described in Chapter 4, each test specimen was weighed prior to loading and subjected to a non-destructive dynamic test in which measurements of the propagation velocity of the compressional wave, V_p, were determined along the three axes of the specimen. Although for most specimens V_p values along the three directions were very similar, implying isotropy, the decision was to annotate these directions in order of increasing magnitude of V_p for the application of the principal stresses σ_1, σ_2, σ_3 respectively. This approach was

implemented for all test specimens in order to diminish any possible discrepancy in the strength results.

In the light of the ISRM suggestions for the application of the axial load in triaxial compression testing, it was decided to carry out all tests under a constant axial strain rate of 0.25% / min. On this basis, the servo-controlled testing machine was set up to follow a prescribed loading sequence of a selected maximum ramp time of 2×10^3 s and a maximum output displacement level calculated as follows:

$$\text{output level} = \text{strain rate} \times \text{specimen height} \times \text{ramp time}$$

PTFE (Teflon) sheets of 0.32 mm thickness were used to eliminate the friction between the rock specimen and the surrounding steel bearing platens. Before introducing the test specimen into the cubical apparatus, the sheets were coated on one side with a very thin film of general purpose grease and then adhered to the bearing platens.

Upon adhering the PTFE sheets, the test specimen was placed on the seating platen and then hydrostatically confined among the bearing platens in the lateral directions by an initial seating compression of about 0.5 MPa. Spirit levels were used to ensure a correct setting of the specimen and the surrounding platens, Figure 5.1. Thereafter, the top bearing platen together with the axial load cells were mounted on the upper surface of the specimen and stabilised by an axial seating compression of 0.5 MPa applied manually by the testing machine. As described in Chapter 3, two load cells were incorporated in this direction: one was connected to the servo-controlled loading system and the other was connected to the data acquisition system.

On seating the test specimen, the two lateral transducers were mounted on the back of the hydraulic rams, and the axial transducer was mounted crosswise the LVDT of the servo-controlled loading system.

The foregoing process was followed by invoking the data acquisition program and initialising all input devices. It should be pointed out that by initialising the load cells, the applied seating compression of 0.5 MPa was regarded as the initial zero stress

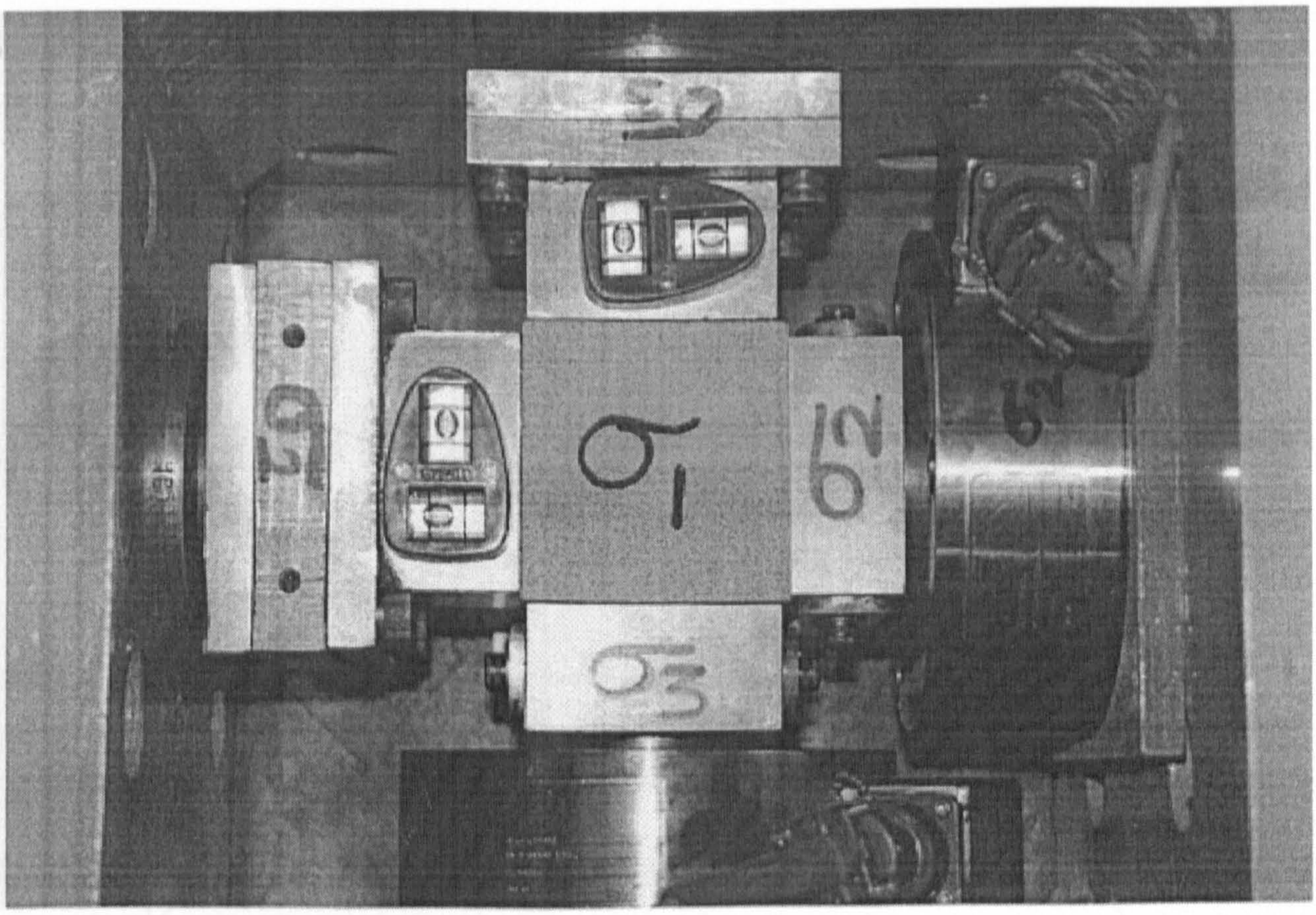

Figure 5.1 Setting up a specimen inside the cubical apparatus for a polyaxial compression test.

measurement in all directions. Furthermore, the data acquisition system was set up with regard to the specimen dimensions to directly convert the output measurements of the load cells and transducers to stress values in MPa and strain %, respectively. These measurements were to be continuously acquired at time intervals of 3 s, displayed on the PC monitor and stored in a data file. The X-Y plotter was prepared for direct plotting of the axial load-axial displacement curve .

At this stage, all the test equipment were on halt awaiting a key stroke, and the test was ready to run.

Polyaxial loading of the test specimen was performed in a manner similar to that suggested by ISRM for triaxial compression testing with the exception that there are two independent lateral stresses to be controlled. A diagrammatic illustration of the loading-unloading sequence employed is shown in Figure 5.2 in terms of stress versus time. The loading procedure may be described as follows:

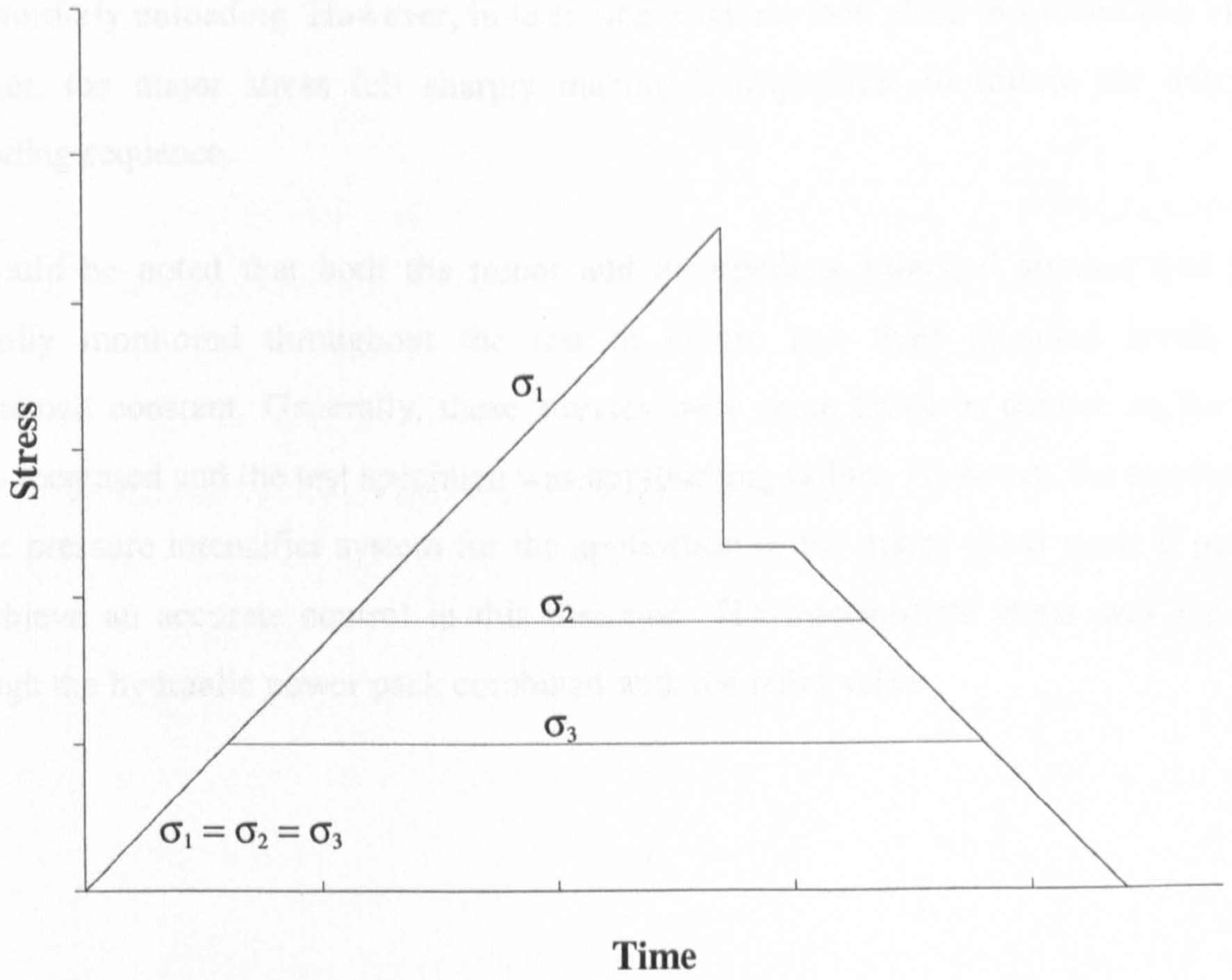

Figure 5.2 A diagrammatic illustration of general polyaxial loading-unloading sequence

At the commencement of the test, both the minor principal stress, σ_3, and the intermediate principal stress, σ_2, were manually increased simultaneously with the major principal stress, σ_1, applied axially by the testing machine at the predefined loading rate. Upon reaching its predetermined value, the minor stress was maintained constant while the increase of the intermediate and major stresses continued. Subsequently, the intermediate stress was maintained constant upon reaching its predetermined value and the application of the major stress was continued until the test specimen failed and the major stress dropped to its residual value.

Shortly after failure occurred, the loading machine was ramped down and the major stress was continuously reduced at the same preset loading rate. Following a similar sequence to that employed during loading, both the intermediate and minor stresses were successively reduced simultaneously with the major stress until the specimen was completely unloaded from all directions. Unloading the failed specimen in such a controlled manner was

intended to protect the failure mode from any possible disturbance that might be caused by disorderly unloading. However, in tests where failure took place in sudden and violent manner, the major stress fell sharply making it impossible to follow the described unloading sequence.

It should be noted that both the minor and intermediate principal stresses had to be carefully monitored throughout the test to ensure that their intended levels were maintained constant. Generally, these stresses were more liable to deviate as the axial stress increased and the test specimen was approaching failure. However, the employment of the pressure intensifier system for the application of the minor stress made it possible to achieve an accurate control in this direction. The intermediate stress was regulated through the hydraulic power pack combined with the relief valve.

5.3 Polyaxial Compression Tests - First Series

5.3.1 Outline of the Tests

Among the prime objectives of the first experimental series was to verify results from polyaxial tests on cubical specimens of Springwell sandstone conducted by Protopsaltis (1986). In these tests, the problem of friction at the specimen boundaries was dealt with by using PTFE sheets at σ_3 contacts, while σ_2 and σ_1 contacts were each covered by a set of five PTFE strips placed on the bearing platen with their longitudinal axis being normal to the direction of σ_3, Figure 5.6 and Figure 5.7c. This arrangement aimed at facilitating the expansion of the test specimen along the direction of the minor principal stress and overcoming any shear resistance that PTFE sheets might provide. Failure of the test specimens was reported to have occurred by clear tensile splitting parallel or nearly parallel to the σ_1-σ_2 plane.

In the course of this first experimental series, a total of thirteen cubes have been tested involving three distinct boundary conditions: PTFE strips arranged as described above and illustrated in Figure 5.7b, PTFE sheets, and direct specimen-platen contact without any friction reducer. The tests were carried out under different levels of minor and intermediate principal stresses. Some of the stress levels were cited from the previous study of Protopsaltis (1986) for comparison of the results. Details of the loading conditions for each individual test are shown in Table 5.1.

5.3.2 The Experimental Results

A typical plot of the loading sequence, stress versus time, is presented in Figure 5.3 for specimen CPI1. The unloading sequence is not shown for simplicity. Figure 5.4 shows a plot of the major principal stress, σ_1, versus the major, intermediate, and minor principal strains, ε_1, ε_2, ε_3, respectively, for the same specimen. Values of the principal stresses and strains recorded at failure for all the specimens tested in this series are given in Table 5.2.

Failure of the test specimens was marked by a clear fall in the value of the major principal stress often accompanied by audible cracking. Although the loading machine is servo-

Table 5.1 Boundary conditions and levels of applied minor and intermediate principal stresses, σ_3 and σ_2, respectively, for the first polyaxial test series on cubes.

Specimen No.	Boundary Conditions	σ_3, MPa	σ_2, MPa
CPI1	PTFE Strips	7.5	15.0
CPI2	=	9.0	43.5
CPI3	=	10.0	43.5
CPI4	=	10.0	20.0
CPI5	=	10.0	25.0
CPI6	=	15.0	30.0
CPI7	PTFE Sheets	9.0	43.5
CPI8	=	10.0	20.0
CPI9	=	10.0	20.0
CPI10	Direct Contact	2.8	27.5
CPI11	=	9.0	43.5
CPI12	=	9.0	43.5
CPI13	=	9.0	43.5

controlled, uncontrolled failure occurred in a few tests making it impossible to obtain a complete stress-strain curve. Regarding the failure mode, tensile splitting was not pure and signs of shear were evident in all tests. Generally, the test specimen failed along two or three major fracture planes lying in the direction of the intermediate principal stress and inclined to the direction of the major principal stress. In most tests, these fractures coalesced into wedge shapes in the σ_1- σ_3 plane. Typical failure patterns are shown in Figure 5.5.

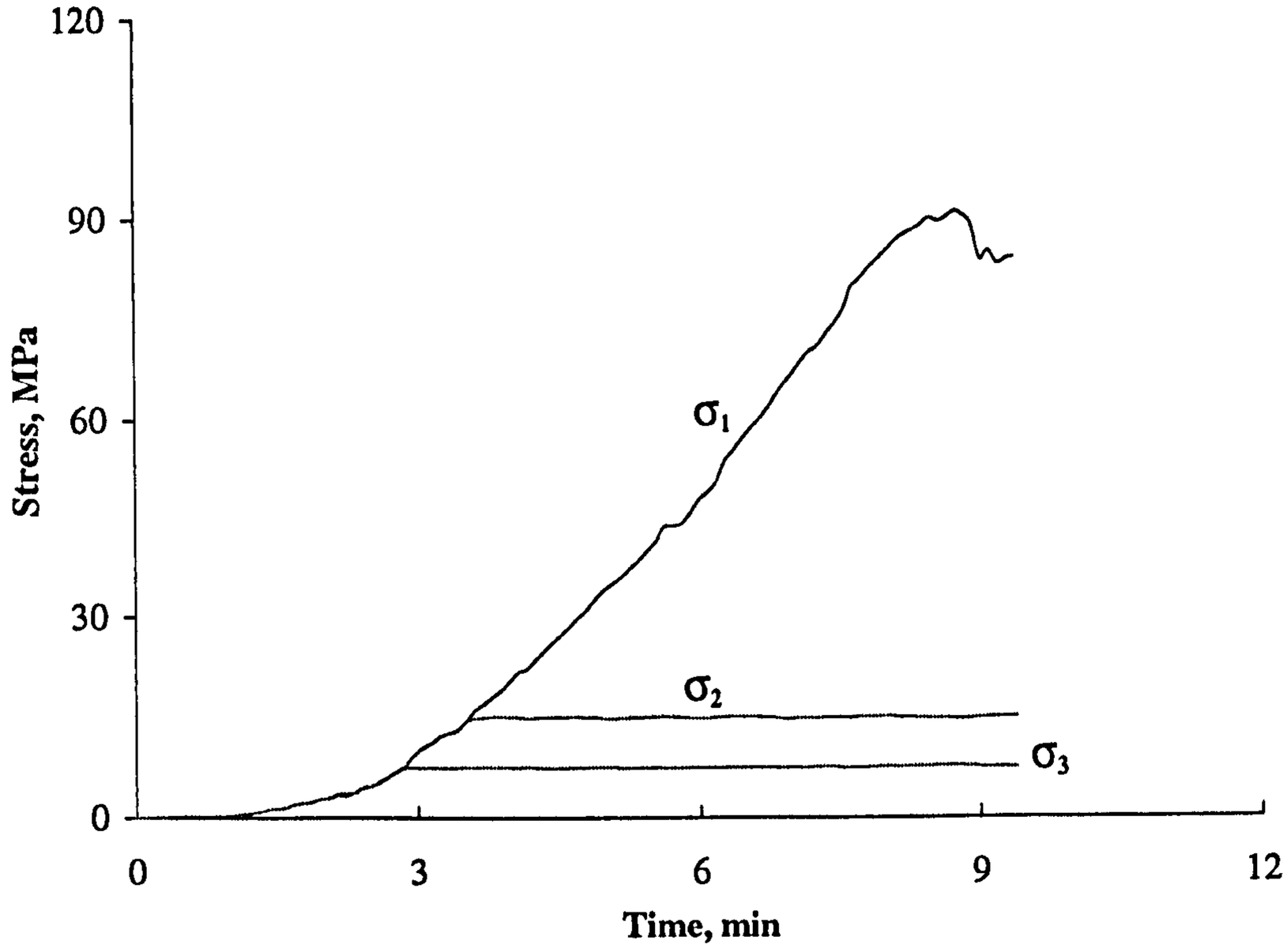

Figure 5.3 A typical loading sequence in polyaxial tests on cubical specimens.

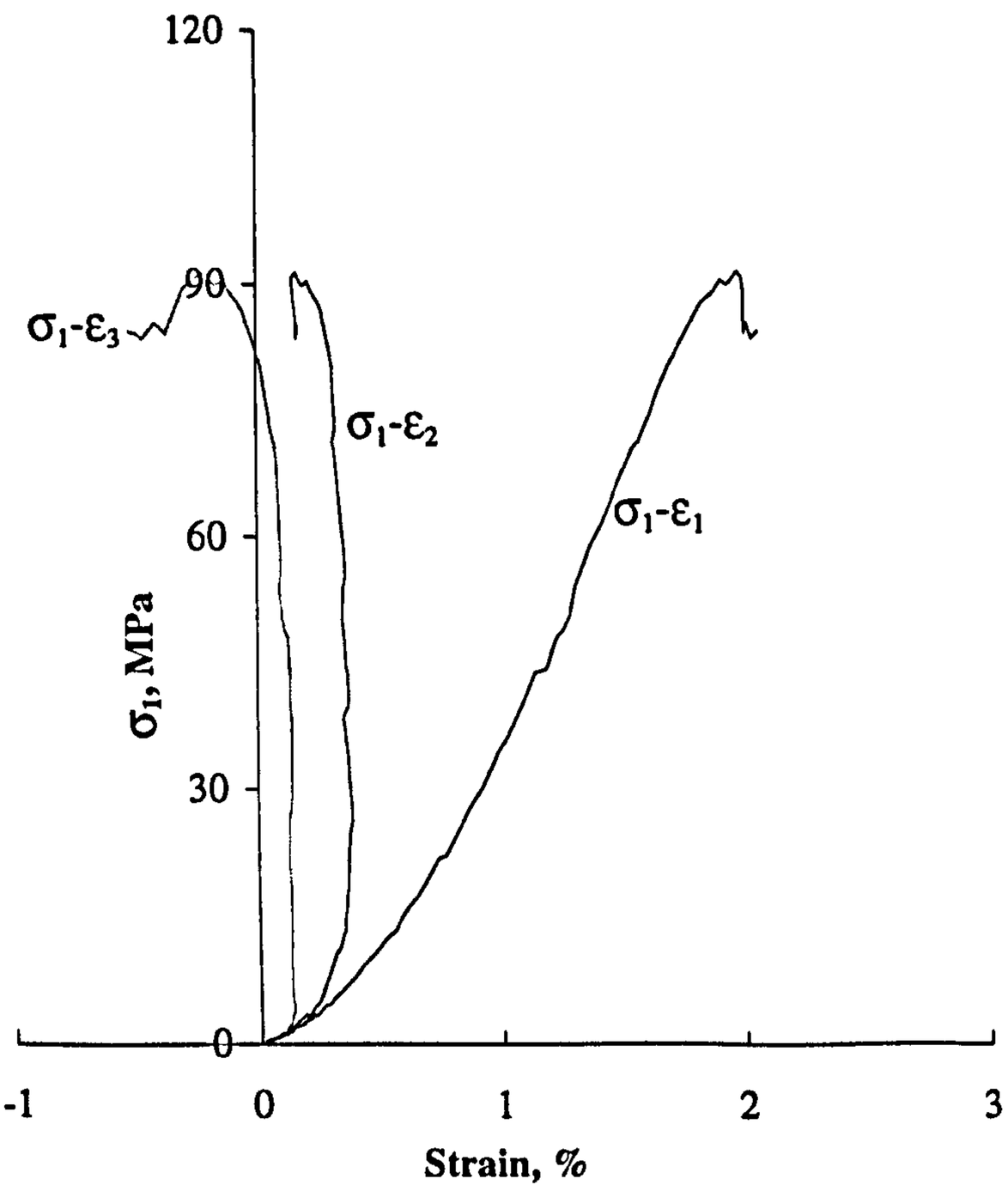

Figure 5.4 Typical curves of the major principal stress versus major, intermediate and minor principal strains from the first polyaxial test series on cubes of Springwell sandstone.

Table 5.2 Recorded values of principal stresses and strains at failure for the cubical specimens of the first polyaxial test series.

Specimen	Principal Stresses, MPa			Principal Strains, %		
No.	σ_3	σ_2	σ_1	ε_3	ε_2	ε_1
CPI1	7.753	14.746	91.348	-0.209	0.164	1.988
CPI2	9.170	43.419	85.106	0.093	0.963	1.493
CPI3	10.399	43.421	108.406	-0.081	0.946	2.296
CPI4	10.093	19.779	80.961	-0.242	0.494	1.675
CPI5	10.245	24.926	97.552	-0.102	0.417	1.921
CPI6	15.124	30.179	109.312	0.115	0.584	2.068
CPI7	9.039	43.695	84.383	-0.481	0.935	1.704
CPI8	10.227	19.890	88.451	-0.433	0.262	1.973
CPI9	10.373	19.975	91.086	-0.421	0.392	1.962
CPI10	2.828	27.355	92.425	-0.947	0.481	2.406
CPI11	9.153	43.751	131.732	-0.486	0.692	2.291
CPI12	9.331	43.459	137.690	-0.688	0.620	3.429
CPI13	9.022	43.679	118.937	-0.306	1.154	2.626

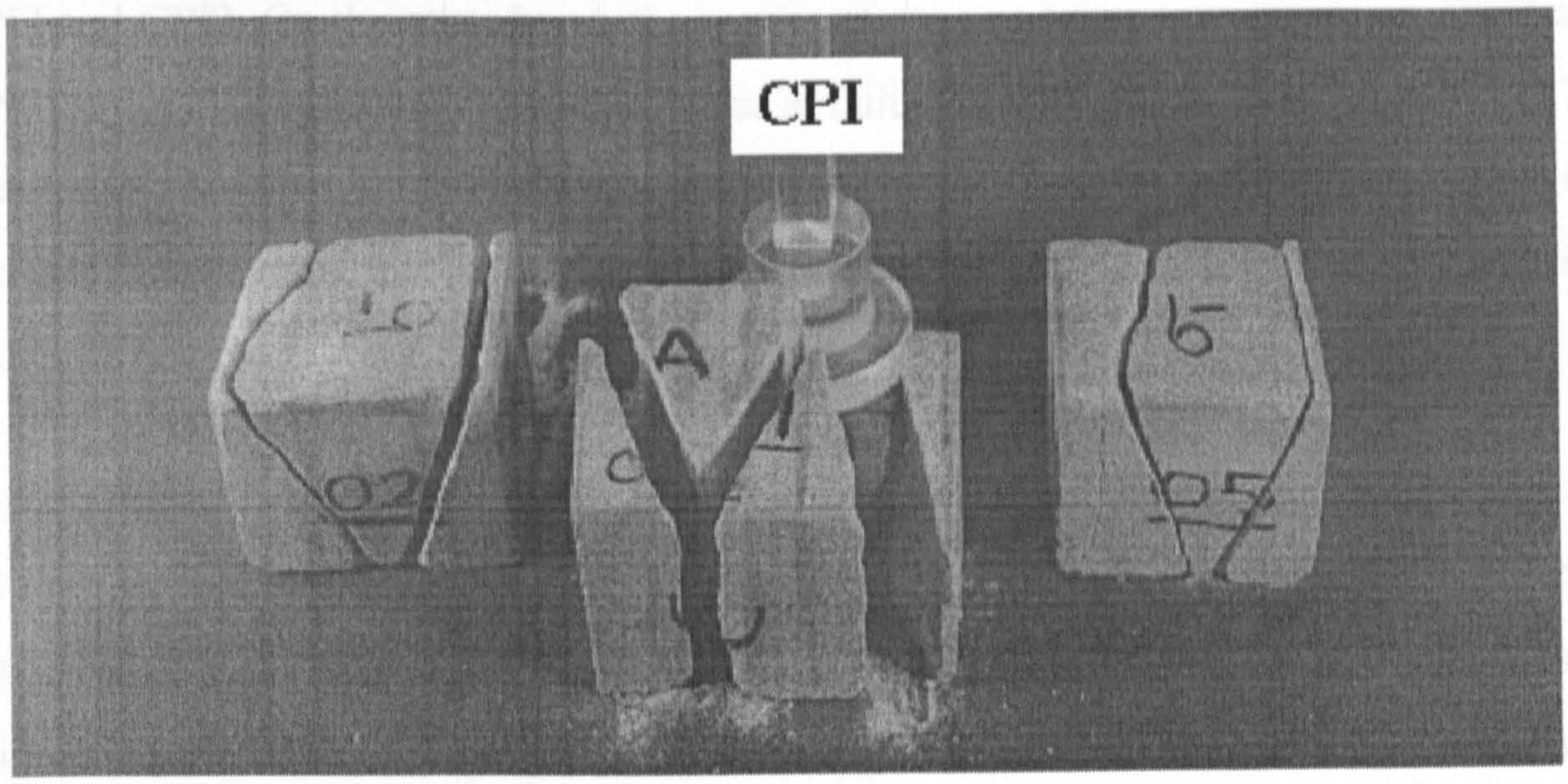

Figure 5.5 Typical failure patterns observed in the first polyaxial test series on cubes of Springwell sandstone

5.3.3 Discussion of the Results

As can be seen from Tables 5.1 and 5.2, there is generally a slight deviation in the values of the minor and intermediate principal stresses attained at failure from their prescribed values. Although the level of deviation is relatively insignificant, effort was made in forthcoming experimental series to achieve a better control over the applied stresses so that more accurate results are obtained. Clearly, one can only aim to minimise the level of deviation as exact values of the designated lateral stresses can hardly be attained. This is due to the fact that the applied stresses are monitored via highly sensitive load cells and acquired by a data logging system of high resolution compared to that of the loading devices.

An important outcome of this first experimental series appears to lie in the confirmation of the effect of the boundary conditions at the specimen-platen contacts on the apparent strength of the test specimen. Specimens CPI2, CPI7, CPI11, CPI12, and CPI13 were all tested under the same levels of minor and intermediate principal stresses but with different boundary conditions. Expectedly, those that were tested in direct contact with the loading platens, i.e. specimens CPI11, CPI12, and CPI13, appear to have sustained higher

levels of major principal stress at failure than specimens tested with friction reducer, i.e. CPI2 and CPI7. On the other hand, the results of the two latter specimens, i.e. CPI2 and CPI7, suggest that the major principal stress at failure is not influenced whether the PTFE material is used in the form of strips or sheets. This suggestion, however, may seem not strongly substantiated by the results of specimen CPI4 compared to the results of CPI8 and CPI9.

A comparison between the results of specimens CPI2 and CPI3 suggests that a slight increase in the level of the minor principal stress, σ_3, results in a remarkable increase in the value of the major principal stress, σ_1, at failure. An increase in σ_1 value is also evident when the intermediate principal stress, σ_2, is increased, as suggested by the results of specimens CPI4 and CPI5, or when both σ_3 and σ_2 are equally increased by the same amount, as can be seen from the results of specimens CPI5 and CPI6. The effect of increasing or decreasing both σ_3 and σ_2 by different amounts seems difficult to evaluate on the basis of these initial results. However, it is evident that any combination σ_3 and σ_2 appears to result in a different level of σ_1 at which the specimen fails. With the exception of specimen CPI13, reproducibility of the results is somehow satisfactory.

Unlike the stress results, the strain results are noticeably scattered and appear more difficult to assess. Nevertheless, it is worth noting in Figure 5.4 that under the initial stage of isotropic compression, $\sigma_1 = \sigma_2 = \sigma_3$, the test specimen appears to deform almost isotropically, $\varepsilon_1 = \varepsilon_2 = \varepsilon_3$, along the three principal directions. Near isotropic behaviour is also evident in the second stage of the test where $\sigma_1 = \sigma_2$ appears to result in almost $\varepsilon_1 = \varepsilon_2$. Following these stages, the specimen deformation along each principal direction appears to take a different course.

A notable phenomenon highlighted by these early tests and seen in Table 5.2 is the tensile nature of the minor principal strain, ε_3, at failure for most of the specimens tested. In fact, specimen extension along the direction of the minor principal stress was observed in all tests and appeared to grow as the specimen was approaching failure. This phenomenon can also be seen in Figure 5.4 which provides a characteristic example of the specimen deformability along the three principal directions.

While the results of these tests remain preliminary, they have provided a general picture of the specimen behaviour and highlighted a number of important issues related to this behaviour. However, the fact that failure did not occur by pure tensile splitting as described in previous work has been of prime concern and formed the basis for the next polyaxial test series.

5.4 Polyaxial Compression Tests - Second Series

5.4.1 Outline of the Tests

The second polyaxial test series was designed to primarily investigate the effect of the boundary conditions on the specimen failure. A total of sixteen cubes have been tested under different conditions of specimen-platen contacts. Various arrangements were explored including those used in the first experimental series. Particular attention has been directed towards the likely effect of overlapping the PTFE strips when adhered to the bearing platens. When PTFE strips were used in the first test series in an effort to diminish the effect of end restraint, they were carefully placed on the bearing platens insuring that the strips were adjacent but not overlapped, Figure 5.7b. Seemingly, this was not the case in the antecedent work of Protopsaltis (1986) in which the strips appear to have been overlapped, as can be seen in Figure 5.6. Thus, in order to ascertain whether

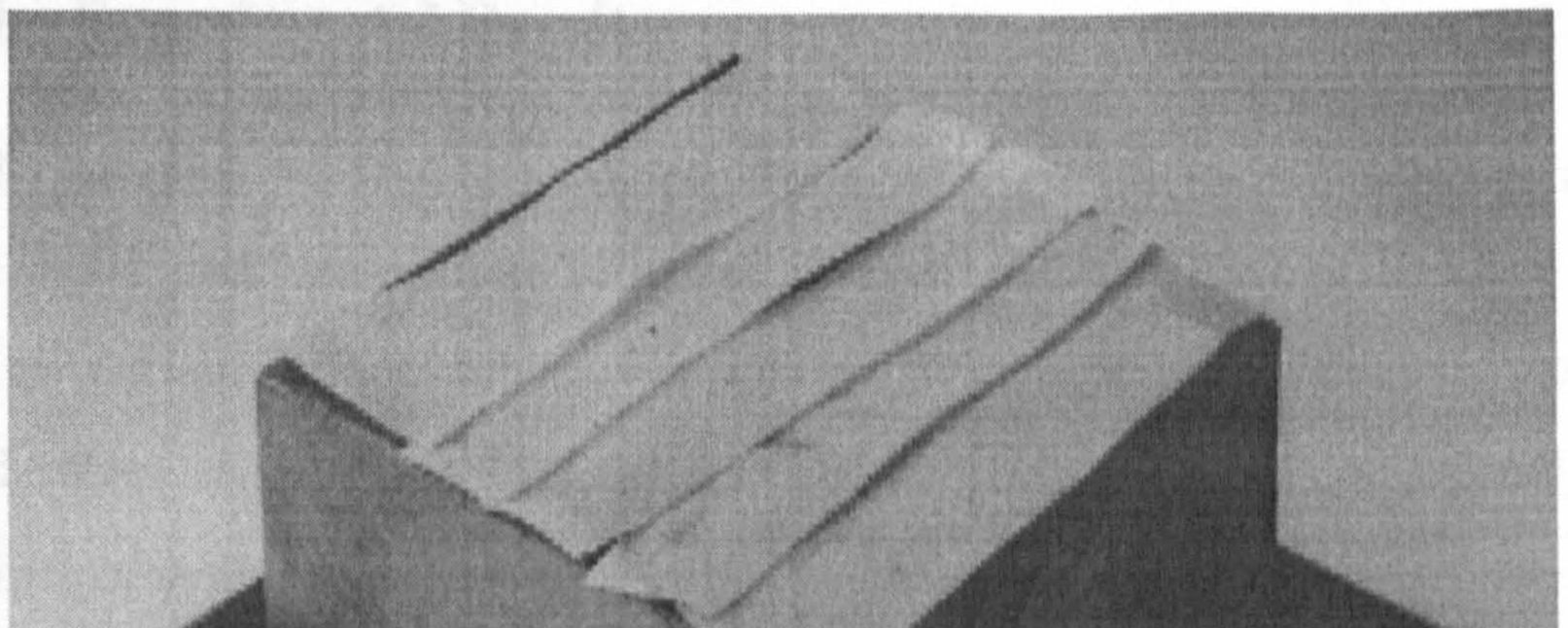

Figure 5.6 Loading platen with Teflon strips (after Protopsaltis, 1986)

this has any influence on the specimen failure, tests have been carried out with adjacent and overlapped PTFE strips oriented as described earlier in the first experimental series. As testing proceeded and the two arrangements appeared to yield different results, further tests were carried out with overlapped strips in various formats. Other tests were carried out with single PTFE sheets, double layers of PTFE sheets, and direct contact between the specimen and the bearing platens. Aiming for a more constructive comparison of the results, all tests have been conducted under the same levels of minor and intermediate principal stresses chosen as follows:

$$\text{Minor principal stress, } \sigma_3 = 5 \text{ MPa}$$

$$\text{Intermediate principal stress, } \sigma_2 = 30 \text{ MPa}$$

Details of the boundary conditions for each individual test conducted in this series are given in Table 5.3.

5.4.2 The Experimental Results

Expectedly, despite the fact that all specimens were loaded to failure under the same levels of minor and intermediate principal stresses, the tests have resulted in different strength results and failure modes depending on the specimen boundary conditions. Recorded values of the major principal stress, σ_1, at failure and the corresponding levels of the principal strains ε_1, ε_2, ε_3 for each individual specimen are listed in Table 5.4. The observed failure modes are described in Table 5.5. Typical failure patterns are shown in Figures 5.8 to 5.10.

Table 5.3 Boundary conditions for each individual test in the second polyaxial test series on cubes of Springwell sandstone.

Specimen No.	Boundary Conditions
CPJ1	A set of five adjacent PTFE strips arranged as described in 5.3.1 without overlapping, Figure 5.7b.
CPJ2	As above.
CPJ3	As above except that strips were overlapped, Figure 5.7c.
CPJ4	As above.
CPJ5	Two PTFE strips overlapped in the middle of the bearing platens, Figure 5.7d.
CPJ6	Two PTFE strips overlapped at 1/3 of platen length at one contact and 2/3 from the same edge at the opposite contact, Figure 5.7e.
CPJ7	As above.
CPJ8	Overlapped PTFE cuts forming a plane parallel to the direction of σ_1 and inclined to the direction of σ_2, as shown. in Figure 5.7f.
CPJ9	Similar arrangement to above but crossing from one σ_2-contact to a σ_3-contact, Figure 5.7g.
CPJ10	Overlapped PTFE cuts just at σ_1-contacts arranged as shown in Figure 5.7h. Uncut PTFE sheets were used at all other contacts.
CPJ11	Single PTFE sheets at all contacts.
CPJ12	As above.
CPJ13	A layer of two PTFE sheets at every contact.
CPJ14	As above.
CPJ15	Direct specimen-platen contacts.
CPJ16	As above.

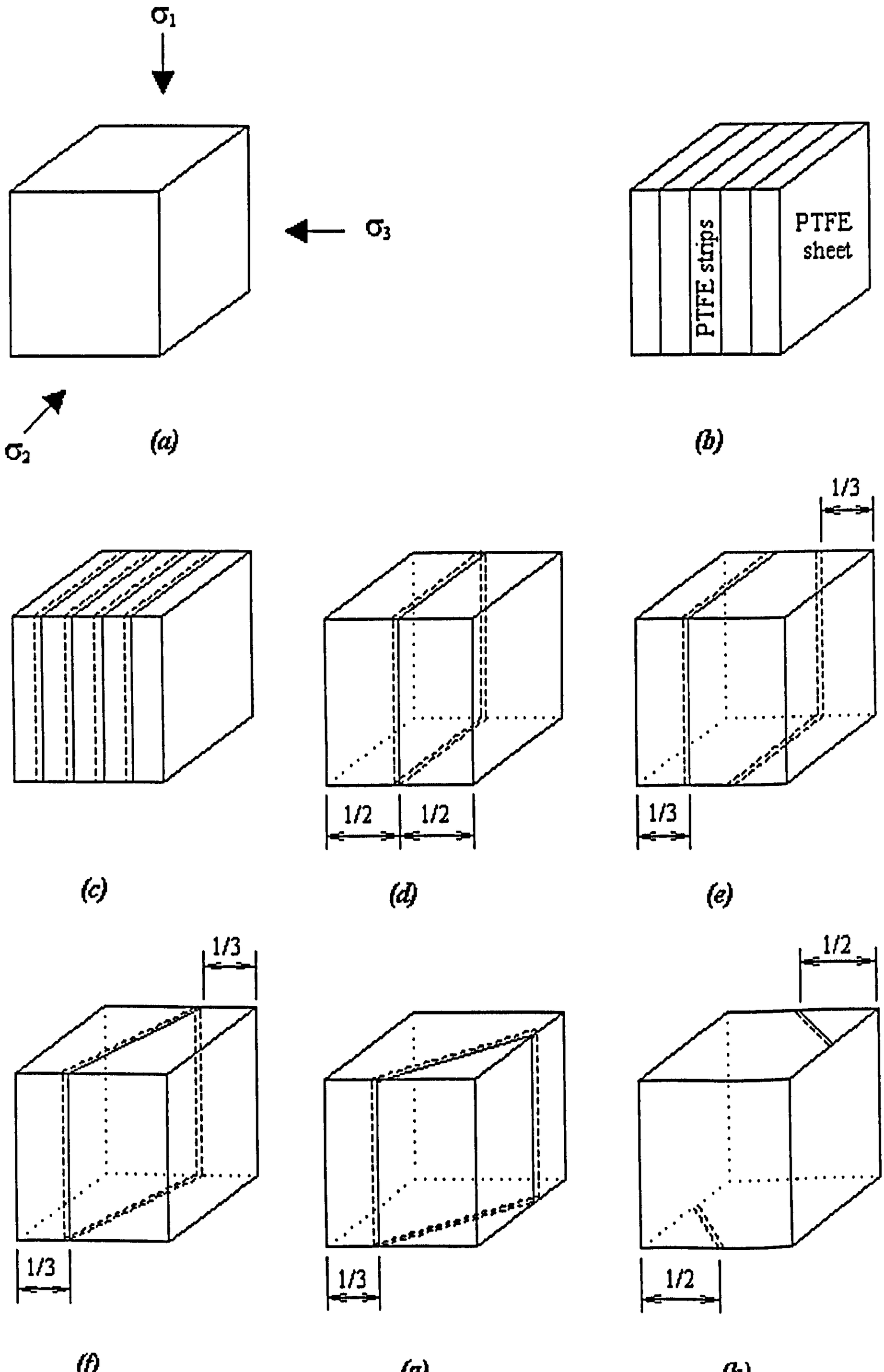

Figure 5.7 Illustrations of PTFE arrangements used at the specimen boundaries in the second polyaxial test series on cubes of Springwell sandstone

Table 5.4 Recorded values of the major principal stress, σ_1, and principal strains, ε_1, ε_2, ε_3, at failure for the cubical specimens of the second polyaxial test series. All tests were conducted under the same levels of intermediate and minor principal stresses of $\sigma_2 = 30$ MPa and $\sigma_3 = 5$ MPa, respectively.

Specimen No.	σ_1 MPa	ε_1 %	ε_2 %	ε_3 %
CPJ1	97.196	1.778	0.768	-0.153
CPJ2	98.893	1.808	0.617	-0.264
CPJ3	71.594	2.036	1.154	-0.278
CPJ4	63.664	1.624	1.161	-0.165
CPJ5	90.850	2.286	1.193	-0.460
CPJ6	76.626	1.875	1.024	-0.198
CPJ7	80.392	1.981	0.978	-0.485
CPJ8	92.607	1.931	1.006	-0.205
CPJ9	92.788	2.004	0.699	-0.078
CPJ10	95.121	1.881	0.659	-0.277
CPJ11	98.576	1.698	0.642	-0.262
CPJ12	102.262	1.752	0.612	-0.281
CPJ13	99.304	2.050	0.772	-0.312
CPJ14	98.835	2.044	0.726	-0.387
CPJ15	123.803	2.089	0.410	-0.591
CPJ16	111.701	2.091	0.638	-0.553

Table 5.5 Observed failure modes in the second polyaxial test series on cubes of Springwell sandstone.

Specimen No.	Failure Modes Observed
CPJ1	Three major fracture planes lying in σ_2 direction and inclined to σ_1 direction forming two opposite wedges in σ_1-σ_3 plane, Figure 5.8. The fracture surfaces exhibit signs of shear.
CPJ2	Similar to above.
CPJ3	Four major fracture planes almost perpendicular to σ_3 direction sliced the specimen along the lines where the PTFE strips were overlapped, Figure 5.9. Tensile splitting seems to have governed the specimen failure.
CPJ4	Similar to above.
CPJ5	The specimen split into halves by one major fracture plane perpendicular to σ_3 direction, Figure 5.9. A minor wedge is formed in one half by two fractures lying in σ_2 direction and inclined to σ_1 direction.
CPJ6	Two opposite wedges in σ_1-σ_3 plane formed by three major fracture planes, Figure 5.10. The vertices of these wedges coincide the lines where the PTFE strips were overlapped at σ_1 contacts.
CPJ7	Similar to above.
CPJ8	Two major fracture planes lying in σ_2 direction and inclined to σ_1 direction coalesced into a wedge shape in σ_1-σ_3 plane, Figure 5.8.
CPJ9	Two opposite wedges in σ_1-σ_3 plane formed by three major fractures, similar to CPJ1.
CPJ10	Similar to CPJ8.
CPJ11	Similar to CPJ1.
CPJ12	Similar to CPJ1.
CPJ13	Similar to CPJ8.
CPJ14	Similar to CPJ8.
CPJ15	Similar to CPJ8.
CPJ16	Similar to CPJ8 but fractures did not coalesce.

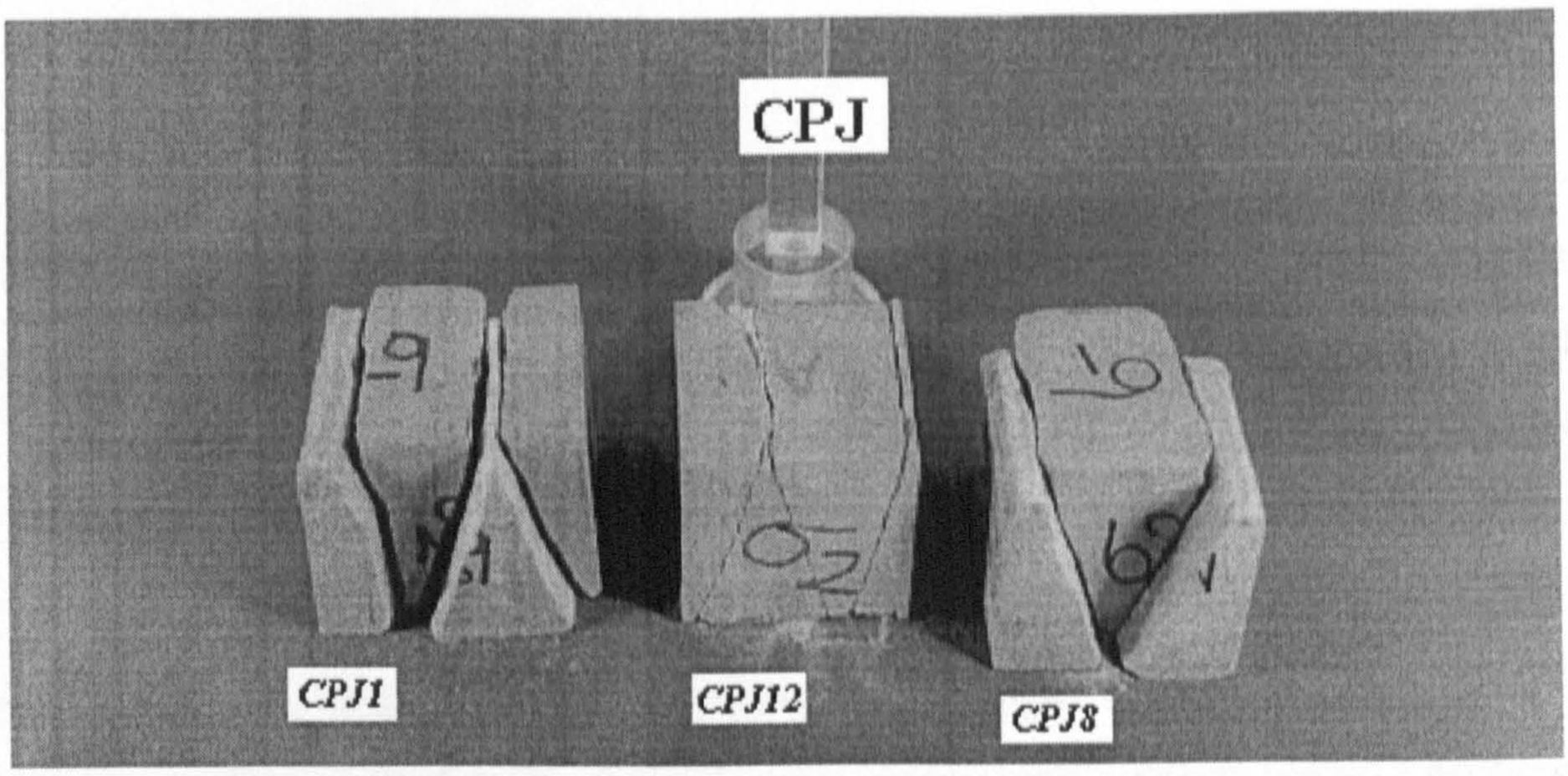

Figure 5.8 Typical fracture patterns observed in the second experimental series under different boundary conditions

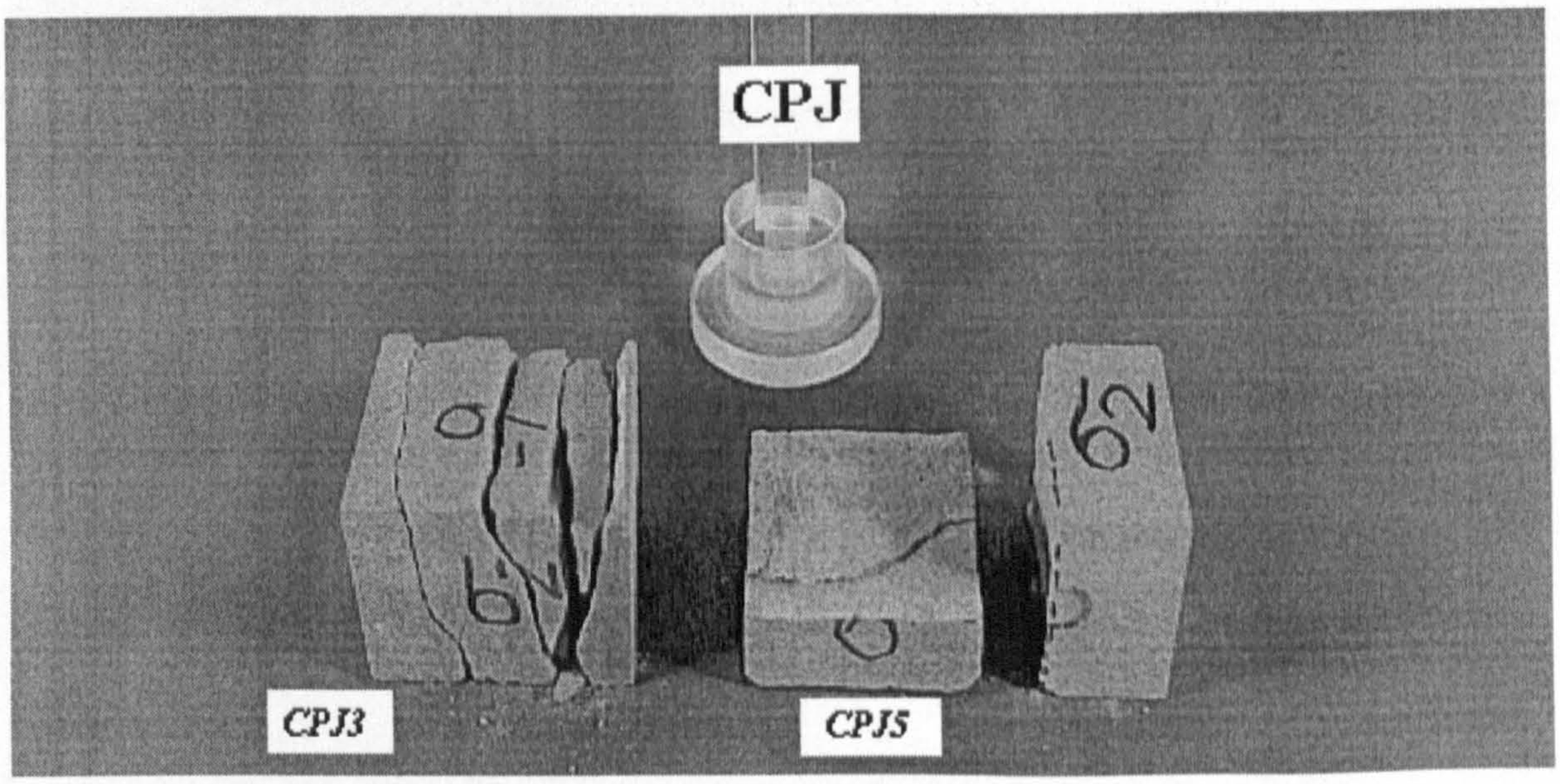

Figure 5.9 Fractures patterns resulted from overlapping PTFE strips at σ_1 and σ_2 contacts.

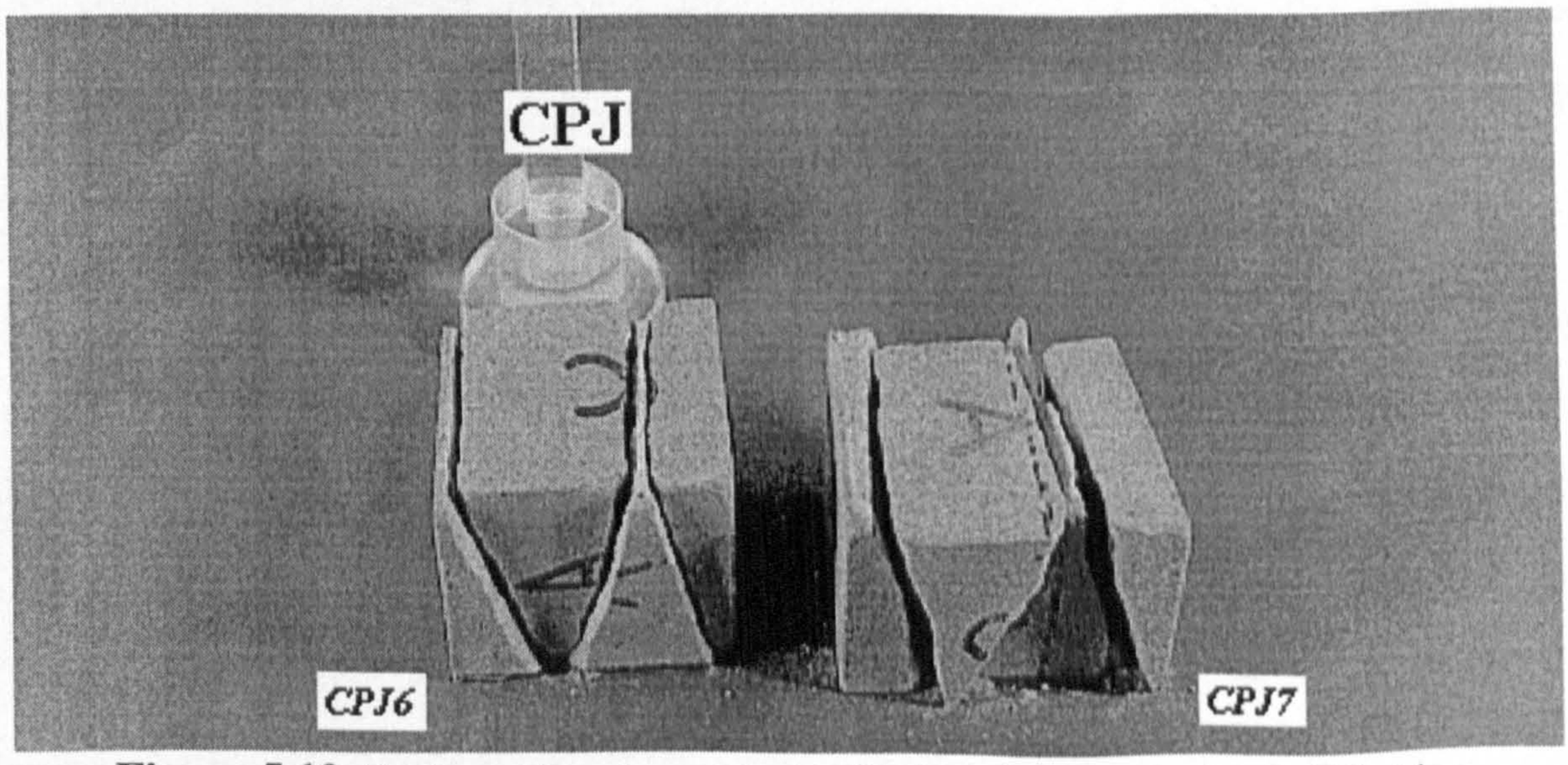

Figure 5.10 Vertices of wedges coincide the locations where the PTFE strips were overlapped at σ_1 contacts.

5.4.3 Discussion of the Results

One of the striking results revealed by this second experimental series is the remarkable effect that PTFE strips seem to have on the specimen failure when they are laid overlapped at the specimen boundaries. This effect appears to be more pronounced when the strips are overlapped at σ_1 and σ_2 contacts with their longitudinal axis being normal to σ_3 direction, as in the case of specimens CPJ3 and CPJ4. A comparison between the strength results of these two specimens and the results of specimens CPJ1 and CPJ2, which were surrounded by adjacent PTFE strips without overlapping, shows a decrease of about 30% in σ_1 level at failure when the strips are overlapped. Moreover, while specimens CPJ1 and CPJ2 failed along inclined fractures seemingly independent of the arrangement of the PTFE strips, specimens CPJ3 and CPJ4 split into slabs almost parallel to σ_1-σ_2 plane along the lines where the PTFE strips were overlapped. This mode of failure is confirmed by specimen CPJ5 which split into halves parallel to σ_1-σ_2 plane as a result of overlapping the PTFE strips along the middle of σ_1 and σ_2 contacts perpendicular to σ_3 direction. However, the less conspicuous decrease in the value of σ_1 at which this specimen failed may be attributed to the reduction in the number of strips overlapped in this case.

Both the values of σ_1 recorded at failure and the observed failure modes for specimens CPJ6 and CPJ7 appear also influenced by overlapping the PTFE strips in the arrangement made at their boundaries. Although other arrangements made at the boundaries of specimens CPJ8, CPJ9 and CPJ10 seem not to have influenced their failure modes, a slight decrease in the values of σ_1 at failure may be acknowledged.

The evident influence of overlapping the PTFE strips on the specimen failure may be ascribed to non-uniform stress distribution in the specimen caused by uneven specimen-platen contacts. Stress concentration is likely to develop along the lines where the strips are overlapped leading to a reduction in the apparent strength of the specimen and forcing it to split along these lines when they are perpendicular to the direction of the minor principal stress.

In agreement with the findings of the first experimental series, the results of specimens CPJ11 and CPJ12 seem to confirm that the behaviour of the test specimen is not influenced in any way whether the friction at the specimen boundaries is reduced by single PTFE sheets or adjacent strips. However, when the sheets are doubled, as in CPJ13 and CPJ14, a slight increase in the values of the principal strains appears to have taken place. This increase is likely to have been caused by the deformation of the additional PTFE sheets. Such consideration may as well explain the apparent increase in the values of the principal strains in tests where the PTFE strips were overlapped at the specimen contacts.

As found in the first experimental series, when the specimen is tested in direct contact with the bearing platens, as in CPJ15 and CPJ16, the effect of friction is more appreciable and the specimen fails under higher level of major principal stress than when PTFE sheets or adjacent strips are used. This leads to additional deformation in the direction of the major principal stress and seems also to cause further expansion or dilation in the test specimen along the direction of the minor principal stress. Although the effect on the specimen deformation in the direction of the intermediate principal stress may seem ambiguous, it is equally evident that a decrease in the deformation along this direction is likely to occur.

The general picture of the specimen deformational behaviour appears to resemble that already observed in the first test series. Irrespective of their boundary conditions, all specimens appear to have undergone dilation along the direction of the minor principal stress, σ_3. This is signified by the tensile nature of the minor principal strain, ε_3, recorded at failure, Table 5.4. An examination of the stress-strain curves for all specimens tested indicated that specimen dilation along σ_3 initiates at early stage of loading long before failure occurs. Evidence of this behaviour can be seen in Figure 5.11 which presents a plot of the major principal stress, σ_1, versus the principal strains, ε_1, ε_2, ε_3, for specimen CPJ11. To complete the picture, a plot of the specimen loading sequence is also presented in Figure 5.12. As these figures show, the specimen seems to initially contract almost isotropically under the hydrostatic state of stress, $\sigma_1 = \sigma_2 = \sigma_3$, imposed on the specimen

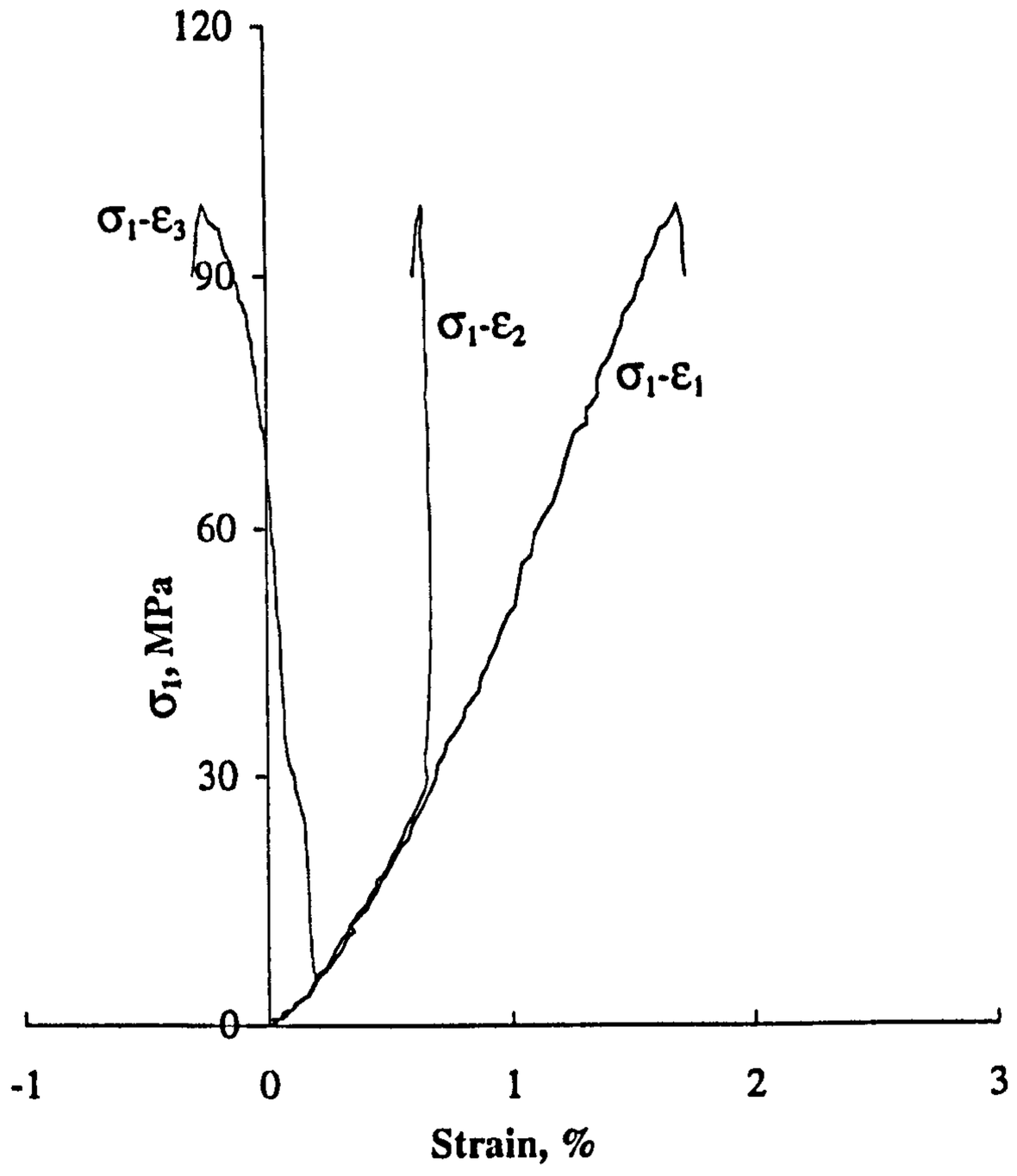

Figure 5.11 Typical curves of the major principal stress versus major, intermediate and minor principal strains from the second polyaxial test series on cubical specimens.

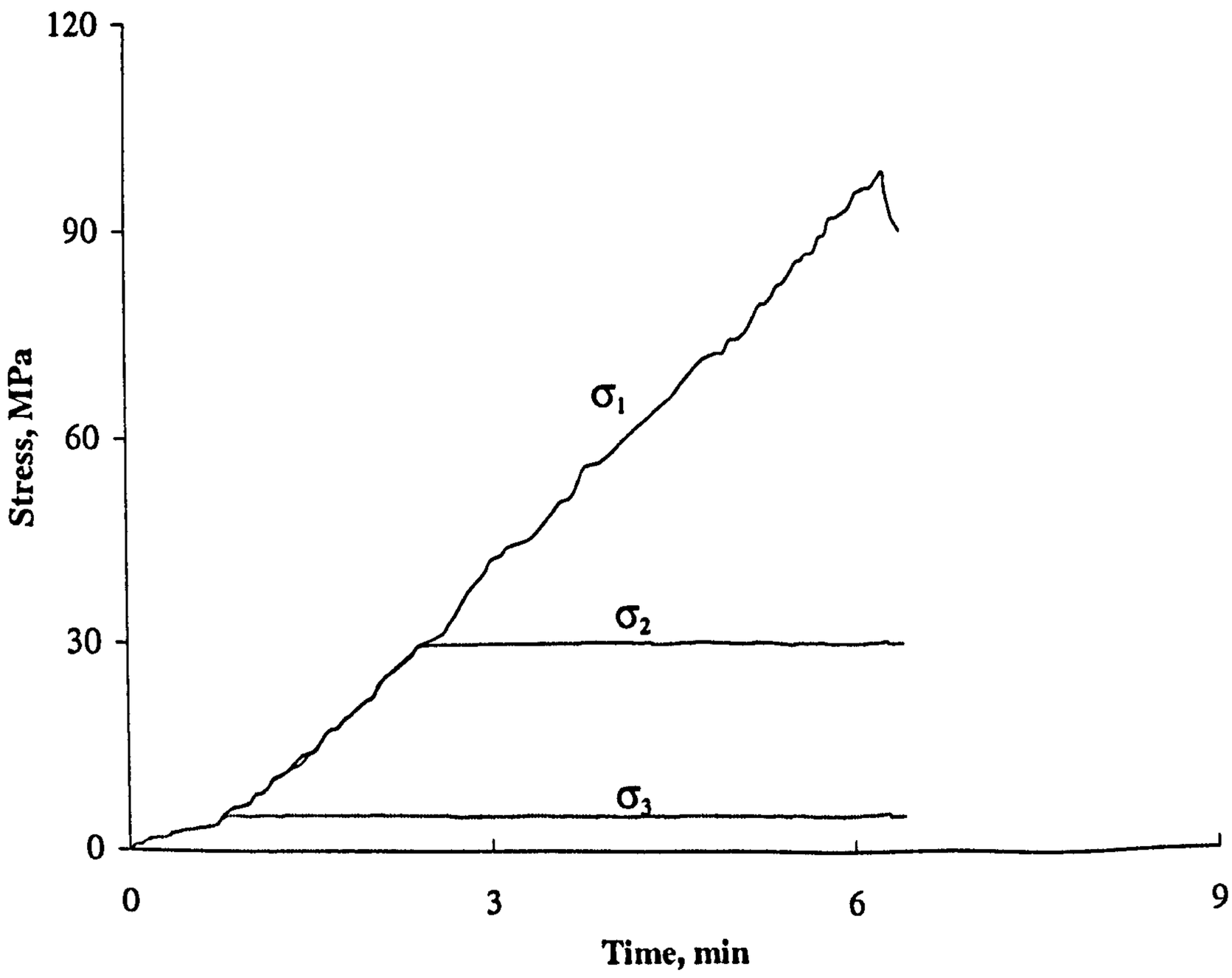

Figure 5.12 The corresponding polyaxial loading sequence for the above stress-strain curves.

from the beginning of the test up to reaching the designated level of σ_3. Upon maintaining σ_3 constant while keeping on increasing σ_1 and σ_2 simultaneously, the specimen starts to expand along σ_3 direction and continues to contract along the directions of σ_1 and σ_2. While specimen contraction along σ_2 seems almost to cease upon maintaining σ_2 constant when reaching its designated level, contraction along σ_1 and expansion along σ_3 progress with increasing σ_1 until the specimen fails.

It can be seen from σ_1-ε_3 curve in Figure 5.11 that specimen expansion along σ_3 direction at first counteracts its early contraction along this direction until complete recovery is attained where ε_3 decreases to zero. Thereafter, the specimen extends beyond its original length and ε_3 grows negative until failure occurs. There is also evidence that upon reaching σ_2 value, a change in the slope of σ_1-ε_3 curve takes place.

Clearly, the deformational behaviour of the test specimen demonstrates that failure was governed by progressive expansion along σ_3 direction. This seems to give credence to the suggestion that specimen failure under polyaxial compression is of the extension type rather than shear. In this respect, the fracture planes may be expected to ideally be first, normal to σ_3 direction and second, uninhabited by any symptoms of shear. In the present tests, all fracture planes were located in σ_2 direction and either inclined or almost parallel to σ_1 direction. While the parallel fractures appeared relatively not to exhibit pronounced signs of shear, such apparent signs in the form of grain contacts or surface rubbing were visible on almost all inclined fractures. However, as described in Table 5.5, parallel fractures were mainly obtained when the PTFE strips were overlapped at the specimen boundaries, and that the failure patterns have generally been typified by inclined fractures. This may hastily suggest that the general mode of failure is actually governed by shear. Yet, both the orientation of these inclined fractures and the stress-strain results indicate that failure of the test specimen has in fact propagated by extension along σ_3 direction.

Although realistically the specimen may not be expected to fail in an ideal manner or split into fractures of an ideal nature, it is believed that a number of factors are likely to have influenced the specimen failure. A leading factor may well lie in non-uniform expansion

of the test specimen attributed to intrinsic inhomogeneity in the rock material as well as the effect of friction at the specimen boundaries. Even though the Springwell sandstone is practically regarded as a homogeneous rock, the real fact is that inhomogeneity of some scale will always be present and in no circumstances will the rock material deform uniformly at all points. Similarly, never will the effect of friction at the specimen-platen contacts be completely eliminated, and that the PTFE material can only aid to reduce this effect. As a result of the non-uniform expansion of the test specimen, it is conceivable that the bearing platens in σ_3 direction are likely to concede some progressive tilting leading eventually to inclined fractures with traces of surface grain rubbing. These traces are bound to intensify upon failure and may appear in the form of surface sliding or shear if the level of the major principal stress, σ_1, drops sharply while σ_2 and particularly σ_3 are yet to be decreased. This suggests that if the test specimen would not be constrained in σ_3 direction, i.e. biaxial loading conditions, it would be able to expand more freely, and possibly more uniformly, and that the failure mode would likely to be more characteristic or at least less disturbed.

Finally, it is evident from the present findings that the results of the previous work by Protopsaltis (1986) were certainly influenced by overlapping the PTFE strips at the specimen boundaries. Moreover, it is clear that although the specimen failure appears to be caused by extension in the rock along σ_3 direction, pure splitting normal to this direction is unlikely to emerge. Such evidence appears to cast doubt on claim made in the previous work that "*tensile failure occurred in all the experiments*" and that the fracture surfaces showed "*no hint of rubbing or shear movement*". A comparison between fracture patterns observed in the present tests and patterns reported by Protopsaltis (1986) and shown in Figure 5.13 may give more credence to such doubt.

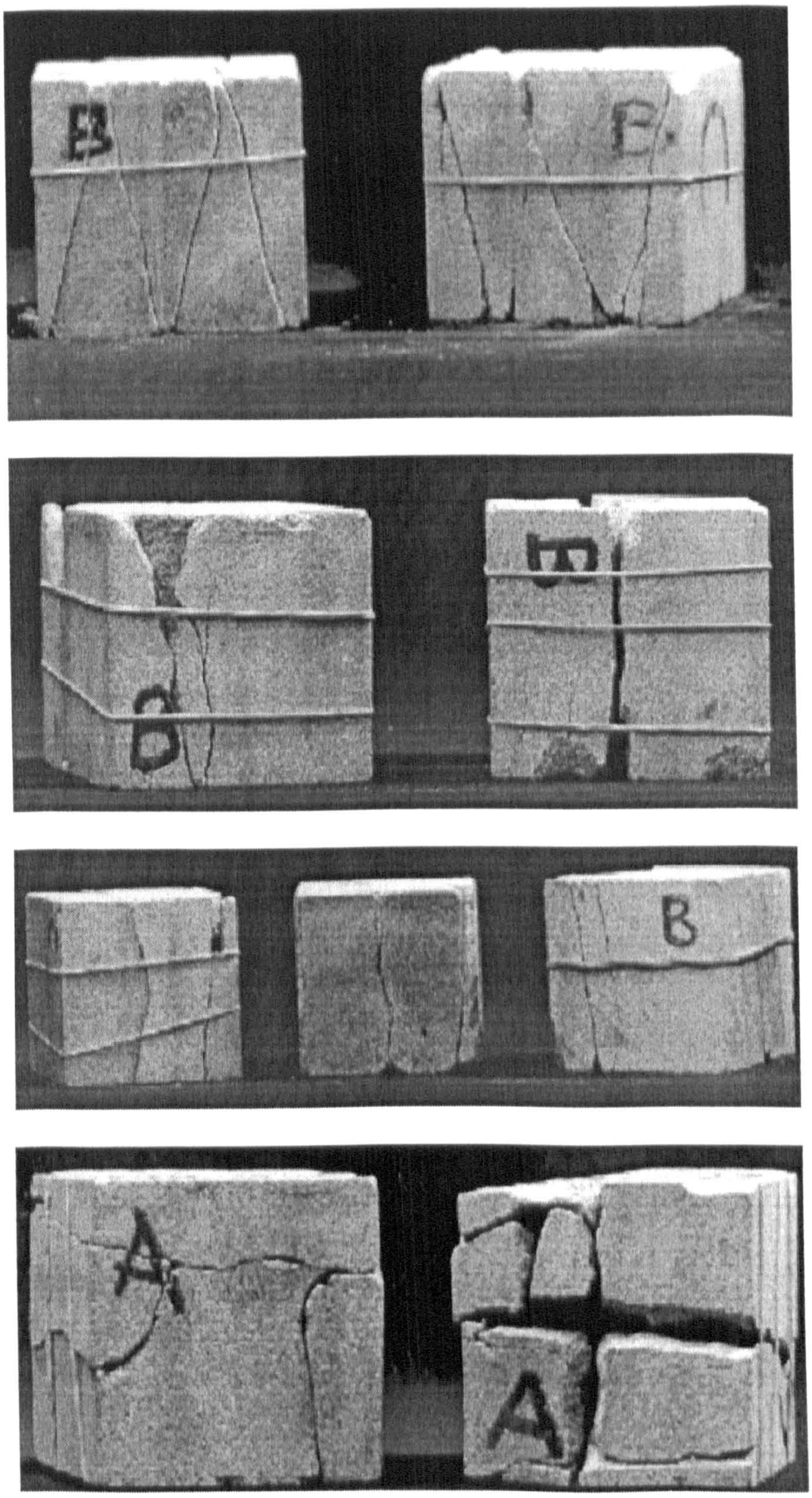

Figure 5.13 Failure patterns reported in previous study (after Protopsaltis, 1986)

5.5 Polyaxial Compression Tests - Third Series

5.5.1 Outline of the Tests

In the light of the results of the second experimental series, it was decided to use PTFE sheets at all specimen contacts. Subsequently, a total of fifteen cubes were tested involving different combinations of minor and intermediate principal stress levels selected to complement combinations already used in the first and second experimental series. The tests were intended to primarily verify the fundamental characteristics of the specimen behaviour under additional stress levels with uniform boundary conditions. Table 5.6 shows the selected levels of σ_3 and σ_2 for each individual test conducted in this third experimental series.

Table 5.6 Levels of applied minor and intermediate principal stresses, σ_3 and σ_2, respectively, for the third polyaxial test series on cubes of Springwell sandstone.

Specimen No.	σ_3, MPa	σ_2, MPa
CPK1	5	10
CPK2	5	10
CPK3	5	10
CPK4	5	10
CPK5	5	15
CPK6	5	15
CPK7	5	15
CPK8	5	15
CPK9	5	20
CPK10	5	20
CPK11	5	35
CPK12	10	15
CPK13	10	30
CPK14	10	30
CPK15	10	30

5.5.2 The Experimental Results

Different strength results have been obtained from the tests depending on the levels of σ_3 and σ_2 applied. Yet, all specimens failed in a similar manner resembling the general mode of failure observed in the foregoing tests under similar boundary conditions. Typical fracture patterns resulted from the tests are shown in Figure 5.14. The strength results have been grouped according to the levels of the minor or intermediate principal stresses and are presented in graphic forms. Figure 5.15 illustrates representative plots of the major principal stress, σ_1, versus the principal strains ε_1, ε_2, ε_3 for tests conducted under different levels of σ_2 with $\sigma_3 = 5$ MPa. Similar plots are illustrated in Figure 5.16 for tests in which $\sigma_3 = 10$ MPa. Plots for tests conducted under $\sigma_2 = 15$ MPa but different levels of σ_3 are illustrated in Figure 5.17.

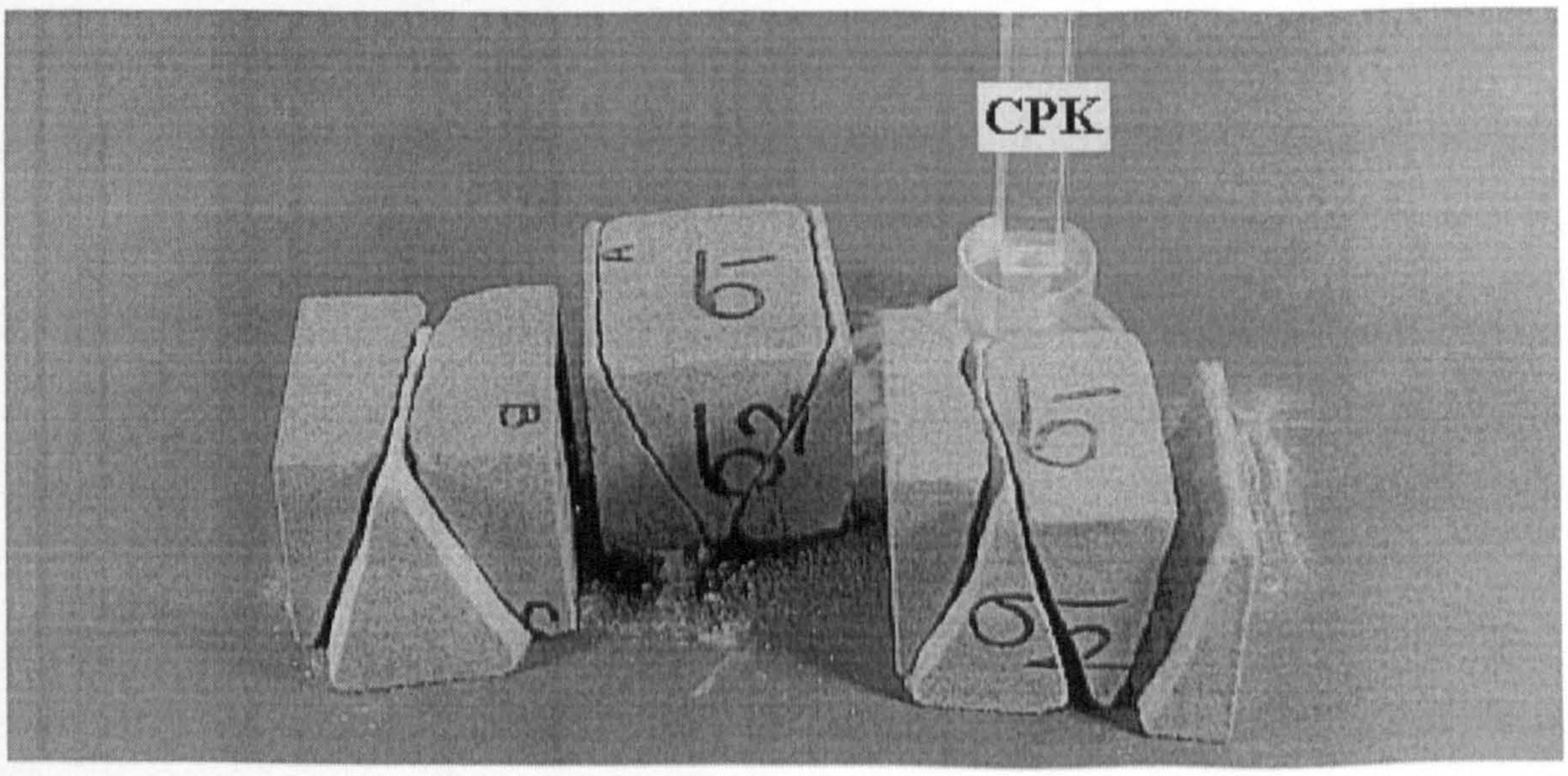

Figure 5.14 Typical failure patterns observed in the third polyaxial test series.

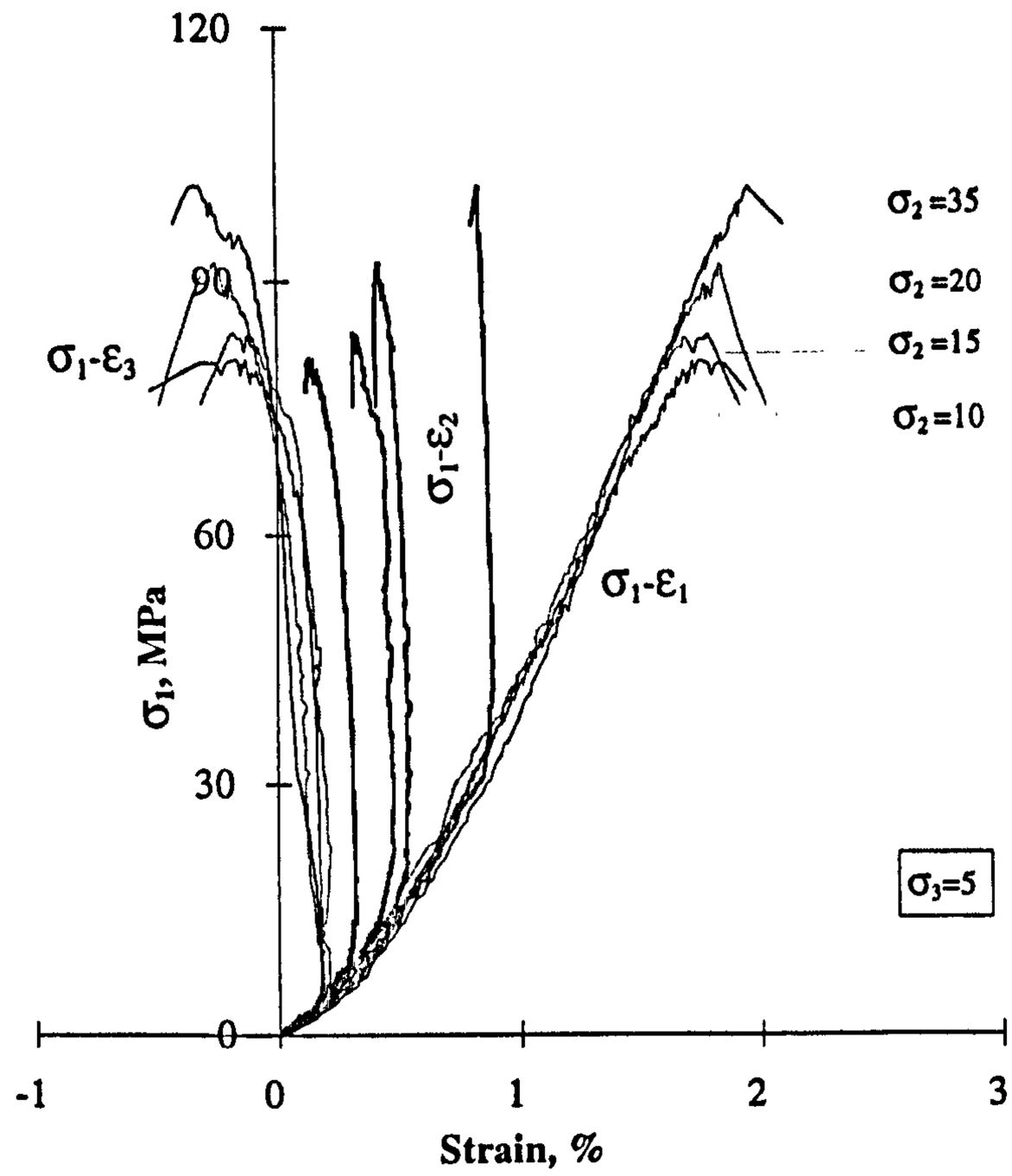

Figure 5.15 Typical curves of σ_1 versus ε_1, ε_2, ε_3 for different levels of σ_2 with σ_3 = 5 MPa

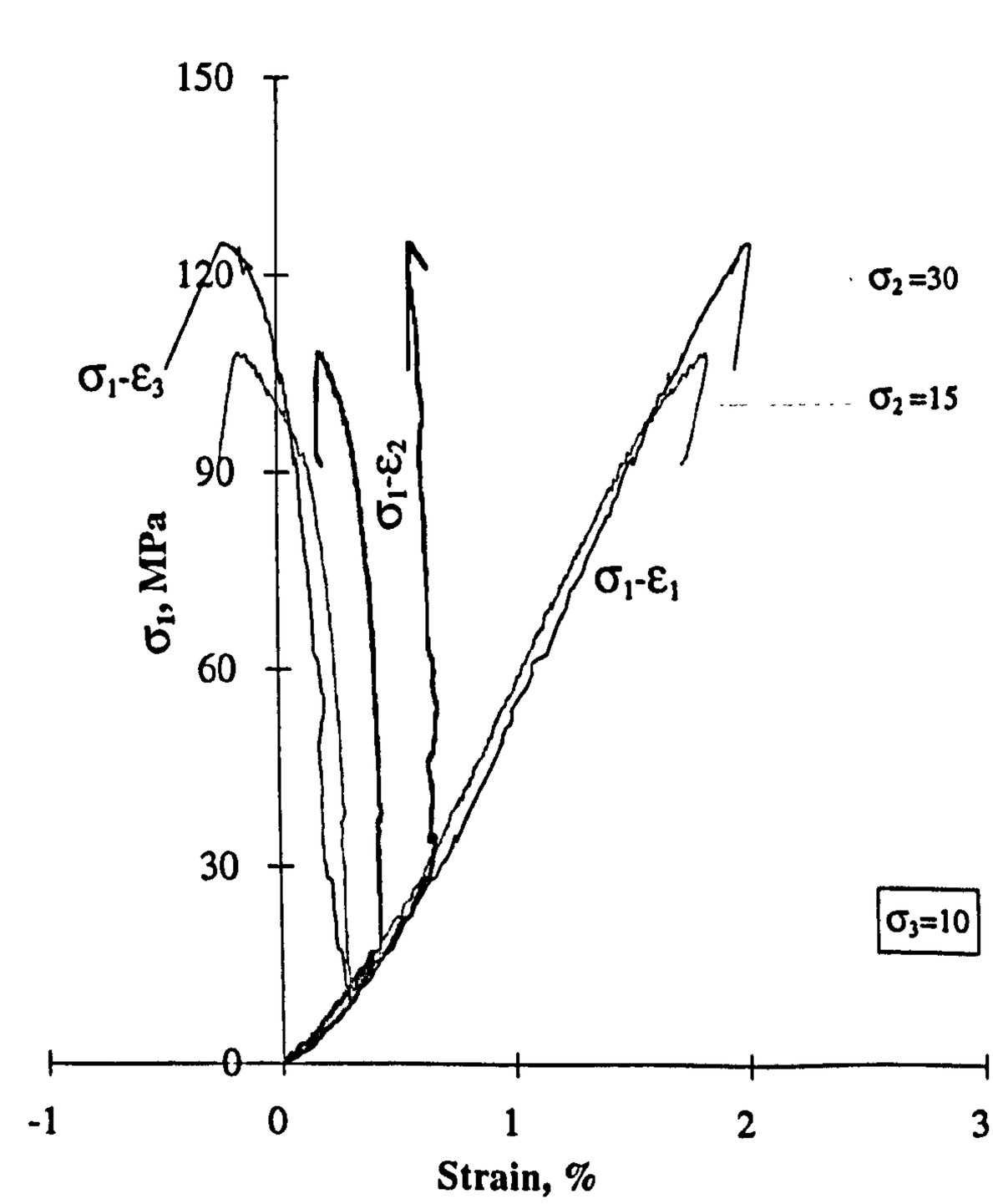

Figure 5.16 Typical curves of σ_1 versus ε_1, ε_2, ε_3 for different levels of σ_2 with σ_3 = 10 MPa

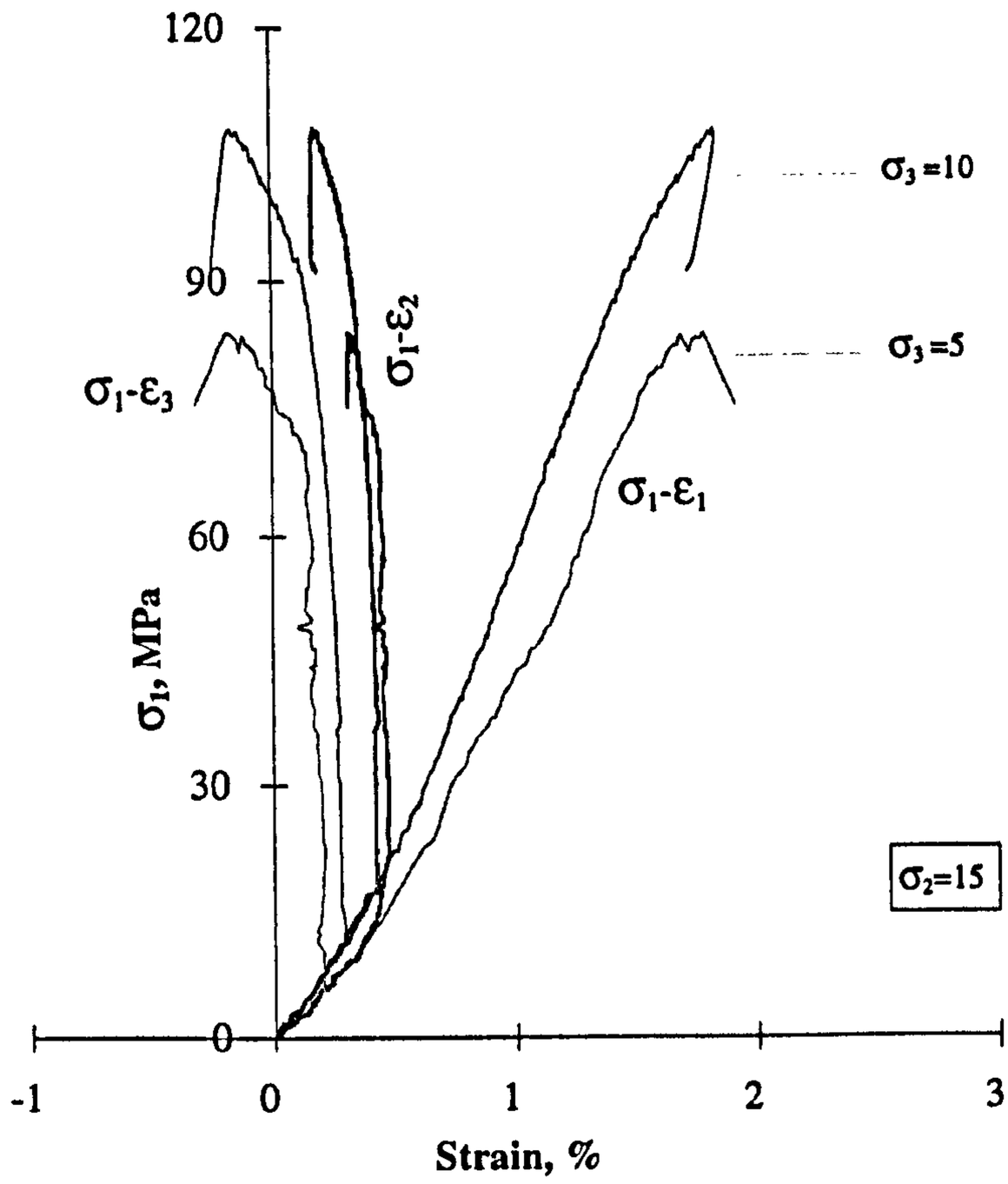

Figure 5.17 Typical curves of σ_1 versus ε_1, ε_2, ε_3 for different levels of σ_3 with σ_2 = 15 MPa

5.5.3 Discussion of the Results

Although the test specimens have been subjected to different combinations of minor and intermediate principal stress levels, a general observation of the stress-strain curves suggests that the deformational behaviour of the specimen in all tests remains fundamentally the same as observed in the previous experimental series. This behaviour is generally characterised by initial near isotropic contraction along the three principal directions up to the hydrostatic loading limit, $\sigma_1 = \sigma_2 = \sigma_3$, beyond which the specimen starts to expand along σ_3 direction and continues to contract along σ_1 direction until failure occurs. As for σ_2 direction, specimen contraction almost desists upon reaching the loading limit, $\sigma_1 = \sigma_2$, beyond which, and particularly on imminence of failure, the specimen may be susceptible to some expansion in this direction depending on the level of the lateral stress difference, $\sigma_2 - \sigma_3$.

Both Figures 5.15 and 5.16 confirm the effect that the intermediate principal stress, σ_2, has on the apparent strength of the test specimen. Under the same level of minor principal stress, σ_3, the specimen appears to sustain higher levels of major principal stress, σ_1, as the applied level of σ_2 increases. Similarly, Figure 5.17 demonstrates that under the same level of σ_2, the specimen fails at higher level of σ_1 with increasing the applied level of σ_3. These effects have already been endorsed by the results of the first experimental series. Regarding the specimen failure, the general mode remains to be typified by wedge shapes formed by two to three major fractures lying in σ_2 direction and inclined to σ_1 direction. Although the failure mechanism may be governed by progressive expansion along σ_3 direction, the fracture surfaces appear to show signs of shear.

5.6 Polyaxial Compression Tests - Fourth Series,

Multiple Failure State Polyaxial Tests

5.6.1 Outline of the Tests

As described in Chapter 7, the concept of the so called *Multiple Failure State Triaxial Test* introduced by Kovari and Tisa (1975) is of considerable benefit in triaxial testing of rock. Standard or conventional triaxial tests are carried out in such a way that only one point of the failure or peak strength envelope can be obtained from a single specimen. This point is defined by the applied confining pressure, $\sigma_2 = \sigma_3$, and the corresponding maximum axial stress, σ_1, sustained by the specimen. Thus, in order to determine the failure or strength envelope, several tests are usually conducted under different values of confining pressure. The multiple failure state triaxial test represents an extension of the standard triaxial test intended to produce the failure envelope and obtain more information about the mechanical properties of the rock from a single test. This is achieved by employing a stepwise procedure in which the confining pressure is increased by predetermined finite increments upon reaching maximum axial stress levels.

Based on the above concept, *Multiple Failure State Polyaxial tests* have been carried out in this investigation by increasing both σ_2 and σ_3 by equal amounts, maintaining the stress difference σ_2 - σ_3 constant, upon reaching maximum levels of σ_1. A typical loading sequence is illustrated in Figure 5.18. A total of four tests have been conducted resulting in sixteen failure points. In order to assess the credibility of the test results, some failure points were established under combinations of σ_2 and σ_3 levels used in the previous experimental series. Details of the applied levels of σ_2 and σ_3 at each failure state attained in each individual test are presented in Table 5.7.

5.6.2 The Experimental Results

A typical plot of the major principal stress, σ_1, versus the principal strains ε_1, ε_2, ε_3, is illustrated in Figure 5.19 for specimen CPM3 from which three failure points were established. The loading sequence of the same specimen is shown in Figure 5.18. Values of σ_1 and ε_1, ε_2, ε_3 recorded at each failure state attained in each individual test are presented in Table 5.7. The modes of failure were generally of similar characteristics to those observed in previous tests conducted under the same boundary conditions, and therefore are not presented.

Table 5.7 Results of multiple failure state polyaxial tests on cubes of Springwell sandstone.

Specimen No.	Failure State	Principal Stresses, MPa			Principal Strains, %		
		σ_3	σ_2	σ_1	ε_3	ε_2	ε_1
CPM1	F1	5	10	80.211	-0.159	0.147	1.565
	F2	10	15	103.626	-0.297	0.013	2.022
	F3	15	20	119.453	-0.381	0.050	2.350
CPM2	F1	5	10	84.961	-0.229	0.156	1.572
	F2	10	15	107.328	-0.220	0.177	1.906
	F3	15	20	117.932	-0.175	0.264	2.054
	F4	20	25	122.480	-0.203	0.302	2.151
CPM3	F1	5	15	85.838	-0.307	0.236	1.981
	F2	15	25	104.732	-0.484	0.336	2.512
	F3	25	35	127.274	-0.416	0.451	2.888
CPM4	F1	10	15	100.032	-0.116	0.145	1.995
	F2	15	20	113.023	-0.109	0.099	2.269
	F3	20	25	124.915	-0.143	0.064	2.603
	F4	25	30	132.945	-0.136	0.035	2.896
	F5	35	40	152.209	0.049	0.069	3.285
	F6	40	45	164.275	0.067	0.093	3.596

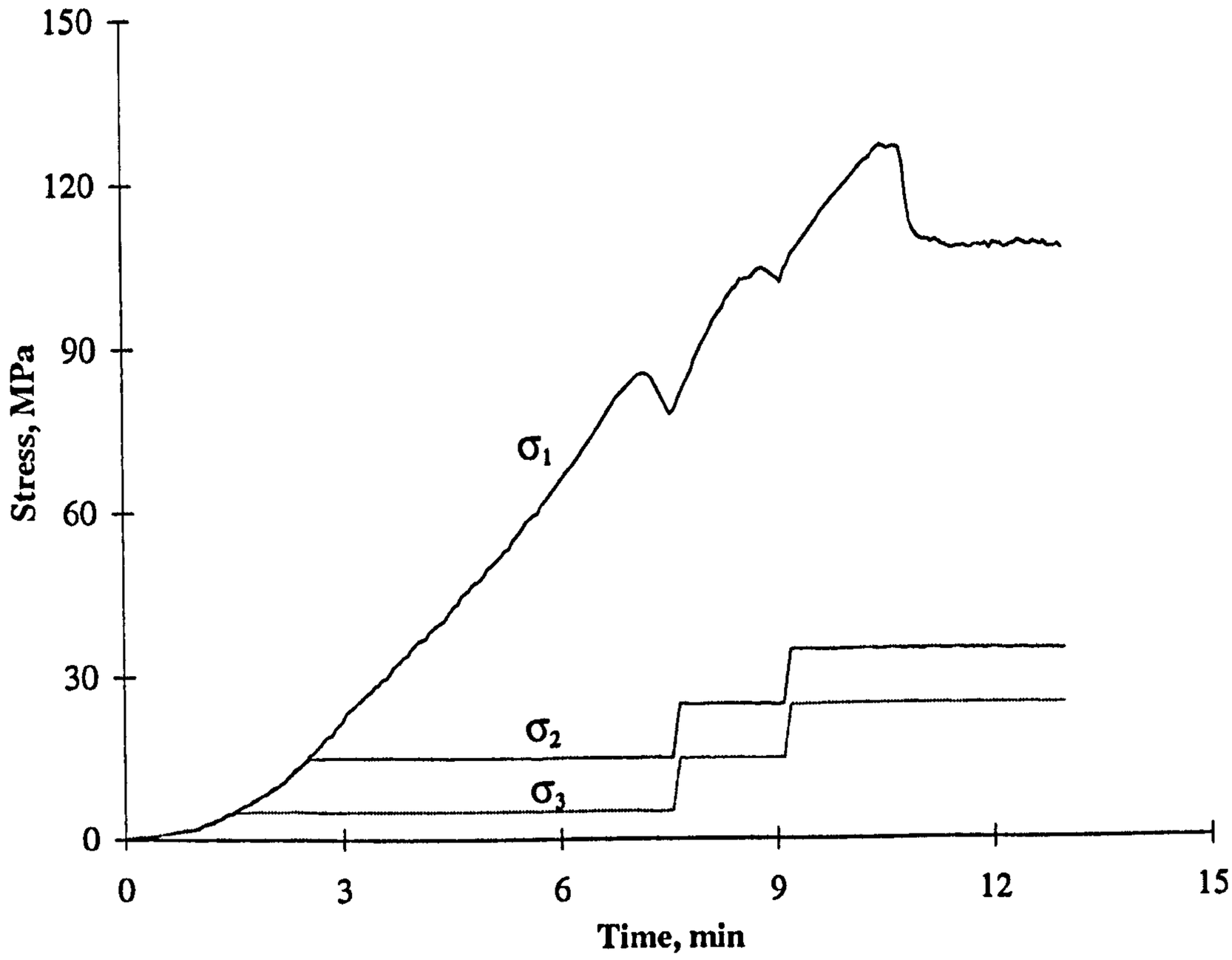

Figure 5.18 A typical loading sequence in a multiple failure state polyaxial test on cubes of Springwell sandstone.

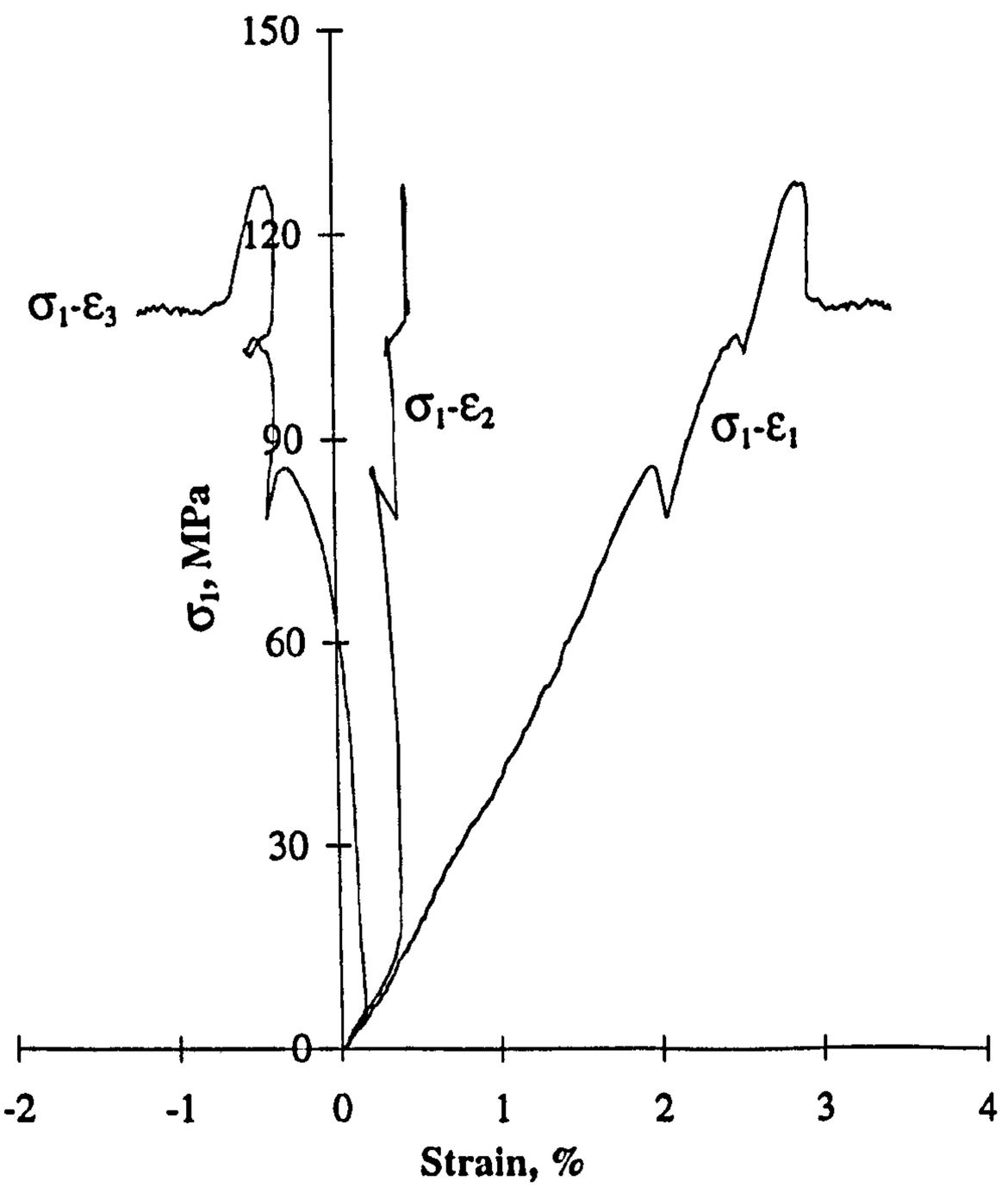

Figure 5.19 Typical curves of the major principal stress versus major, intermediate and minor principal strains from a multiple failure state polyaxial test.

5.6.3 Discussion of the Results

A comparative review of the results of various failure states attained under the same levels of minor and intermediate principal stresses shows that reproducibility of the results is overall satisfactory. Moreover, the results particularly with regard to the levels the major principal stress at failure are on the whole in good agreement with corresponding results obtained from single failure state tests conducted in the previous experimental series under the same loading conditions. This demonstrates the reliability of the test results and certifies the effectiveness of employing the concept of the multiple failure state test in polyaxial testing to produce more failure points from a single specimen. However, as far as the principal strains are concerned, mainly ε_1 and to a certain extent ε_2 values appear to be consistent throughout the various states of the test and also to virtually match corresponding values from single failure state tests. Evidently, this may not be the case for ε_3 values recorded beyond the first failure state. This phenomenon may be attributed to the effect of the specimen early expansion along σ_3 direction on its ability to gain complete recovery and deform uniformly when the stress level is increased. In a single failure state test and up to the first failure point in a multiple failure state test, the specimen deformation along each of the three principal directions is generally a consistent process induced by one state of stress imposed upon the originally intact specimen. On the other hand, when a maximum level of σ_1 is reached in a multiple failure state test, the specimen has already undergone considerable expansion along σ_3 direction and lost some of its cohesion. Upon increasing both σ_3 and σ_2, any extensile microcracks that have developed in the specimen are likely to experience some degree of closure depending on the level of the stress increase, but the rock will no longer be the continuum medium that characterised its original form. As can be seen from Figure 5.19, some recovery in the specimen early expansion occurs when σ_3 and σ_2 are increased. While this recovery is followed by initial contraction along σ_2 direction and somewhat proportional to σ_2 increase, very little deformation appears to emerge along σ_3 direction as σ_1 increases. Although the test specimen is bound to be hardened by σ_3 increase, it is equally conceivable that deformation is likely to take place within the fractured zone away from the specimen boundary where ε_3 is measured. Clearly, this picture of the specimen

deformation may vary from one test to another and also within the same test from one failure state to another depending on the levels of the stresses involved and the magnitude of expansion that may occur before σ_3 and σ_2 are increased. This may explain the apparent variations in ε_3 values recorded in the tests. Despite such a drawback, the concept of multiple failure state test appears to be of considerable benefit in polyaxial testing compared with the single failure state test.

5.7 Triaxial Compression Tests

5.7.1 Outline of the Tests

Following the polyaxial testing programme, a total of eight cubes were tested under conventional triaxial conditions in which $\sigma_1 > \sigma_2 = \sigma_3 > 0$. The testing set-up and procedure were the same as in the polyaxial tests with the exception that both σ_2 and σ_3 were maintained constant at equal levels. In order to obtain more experimental data, only three tests were terminated in the classic manner upon reaching a single failure state, while the other five tests were of multiple failure states as performed in the previous polyaxial test series. As a result, a total of eighteen failure points have been established. Details of the loading levels for each individual test are presented in Table 5.8.

5.7.2 The Experimental Results

A typical plot of the loading sequence in a multiple failure state triaxial test is presented in Figure 5.20 for specimen CTX5 which underwent four failure states attained under different levels of $\sigma_2 = \sigma_3$. The strength-deformability behaviour of the same specimen throughout the various stages of the test is illustrated in Figure 5.21 in the form of a plot of the major principal stress, σ_1, versus the principal strains ε_1, ε_2, ε_3. Figure 5.22 shows values of the peak strength, i.e. σ_1 at failure, for all specimens tested plotted versus the corresponding levels of $\sigma_2 = \sigma_3$. Similarly, recorded values of the principal strains ε_1, ε_2, ε_3 at failure for all specimens tested are plotted in Figures 5.23 and 5.24 against the corresponding levels of σ_1 and $\sigma_2 = \sigma_3$, respectively.

Failure of the test specimens resulted generally in two or three fracture planes inclined to the direction of σ_1 and lying in the direction of either σ_3 or σ_2. Several specimens fractured along both lateral directions with the fracture planes being more profound in one direction than the other. In both cases, the fracture surfaces were marked by symptoms of shear or surface rubbing more pronounced than those observed in the case of the polyaxial test specimens. Typical failure patterns observed are shown in Figure 5.25.

Table 5.8 Applied stress levels of $\sigma_2 = \sigma_3$ in single and multiple failure state triaxial tests on cubes of Springwell sandstone.

Specimen No.	Failure State	$\sigma_2 = \sigma_3$, MPa
CTX1	F1	5
CTX2	F1	10
CTX3	F1	10
CTX4	F1	5
	F2	10
	F3	15
CTX5	F1	5
	F2	10
	F3	15
	F4	25
CTX6	F1	15
	F2	25
	F3	35
CTX7	F1	20
	F2	30
	F3	40
CTX8	F1	30
	F2	40

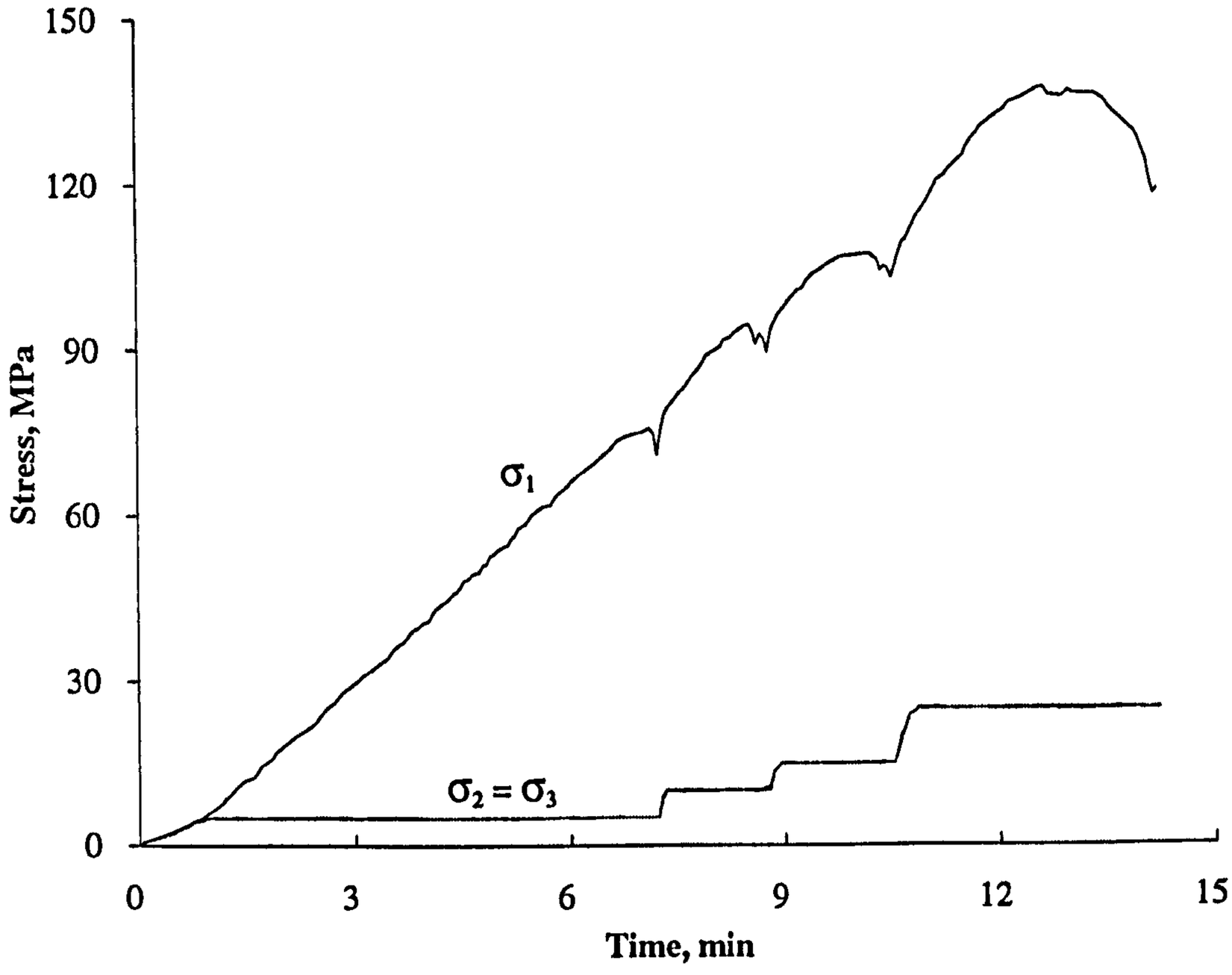

Figure 5.20 A typical loading sequence in a multiple failure state triaxial test on cubes of Springwell sandstone.

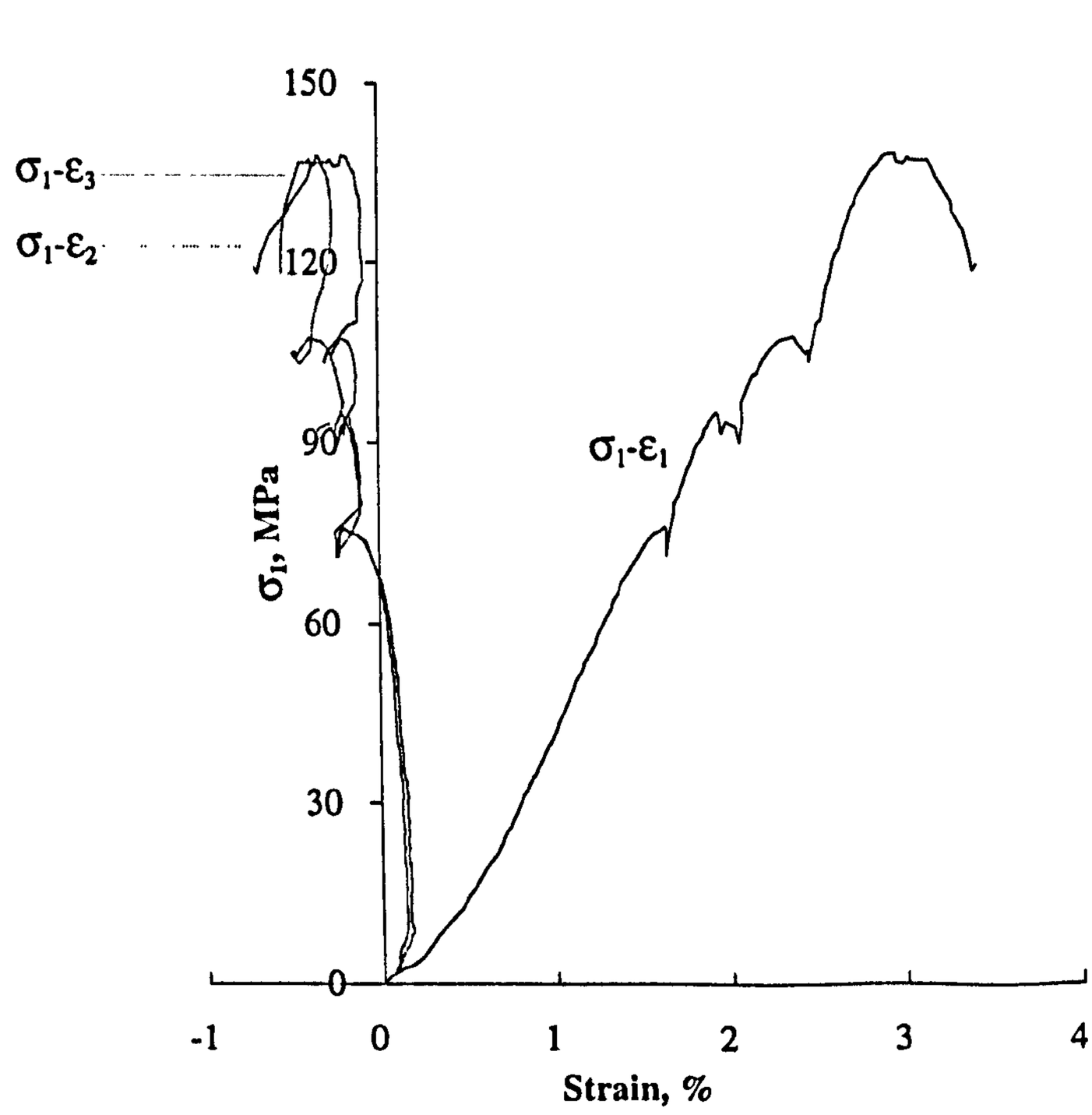

Figure 5.21 Typical curves of the major principal stress versus major, intermediate and minor principal strains from multiple failure state triaxial tests on cubes.

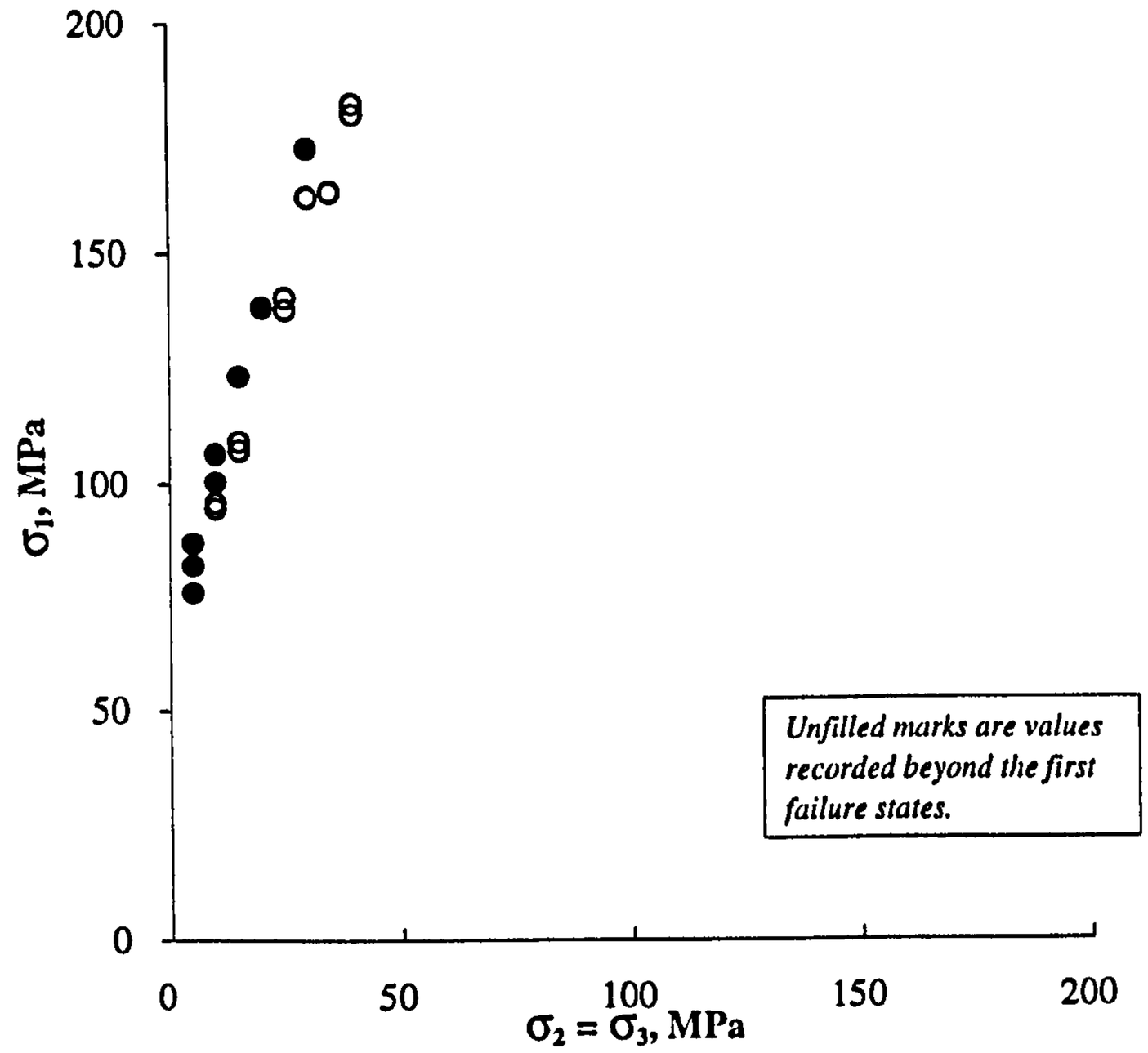

Figure 5.22 Variation of σ_1 at failure with $\sigma_2 = \sigma_3$ in single and multiple failure state triaxial tests on cubes of Springwell sandstone.

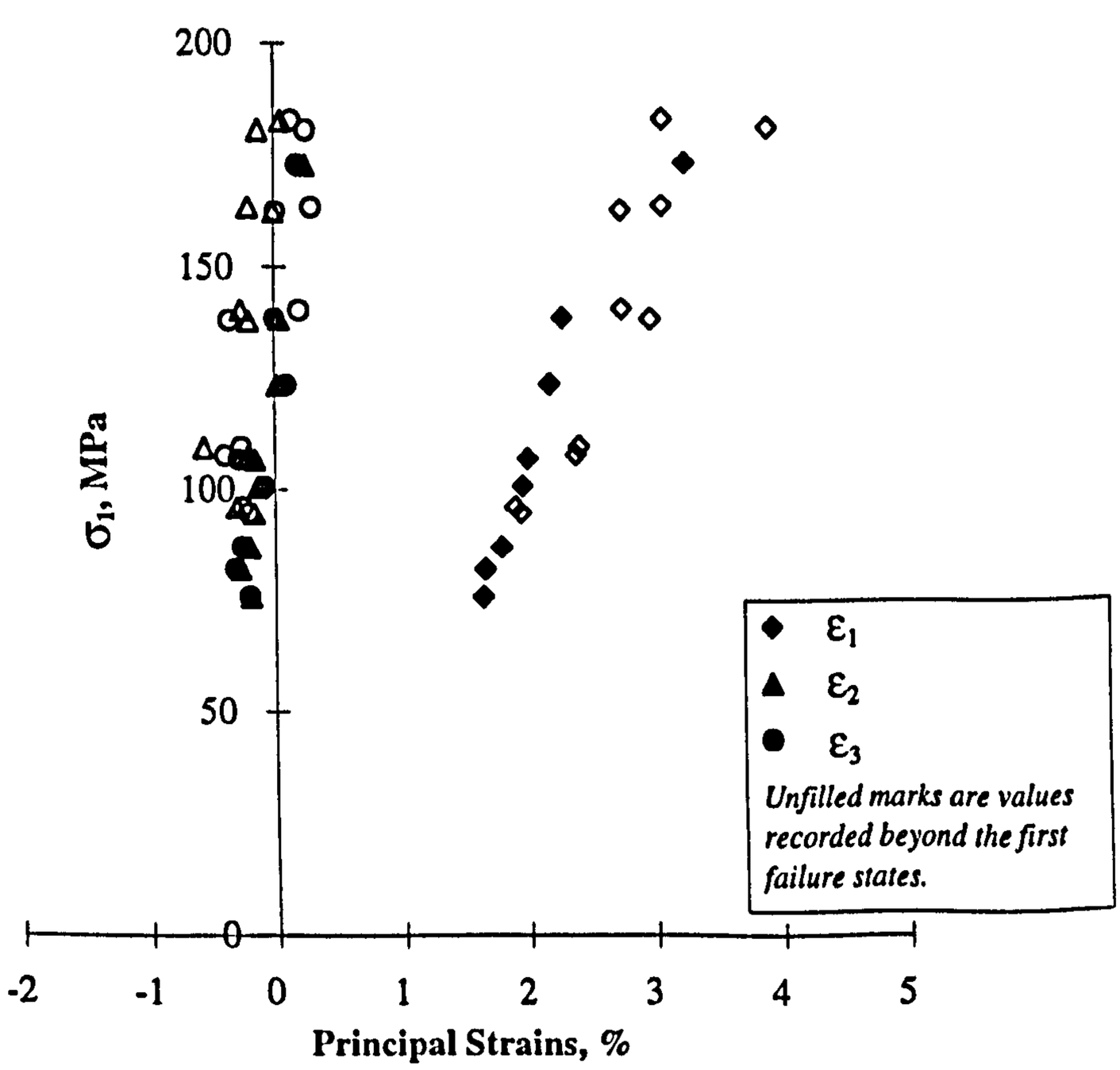

Figure 5.23 Major principal stress σ_1 at failure versus the principal strains ε_1, ε_2, ε_3 in single and multiple failure state triaxial tests on cubes of Springwell sandstone.

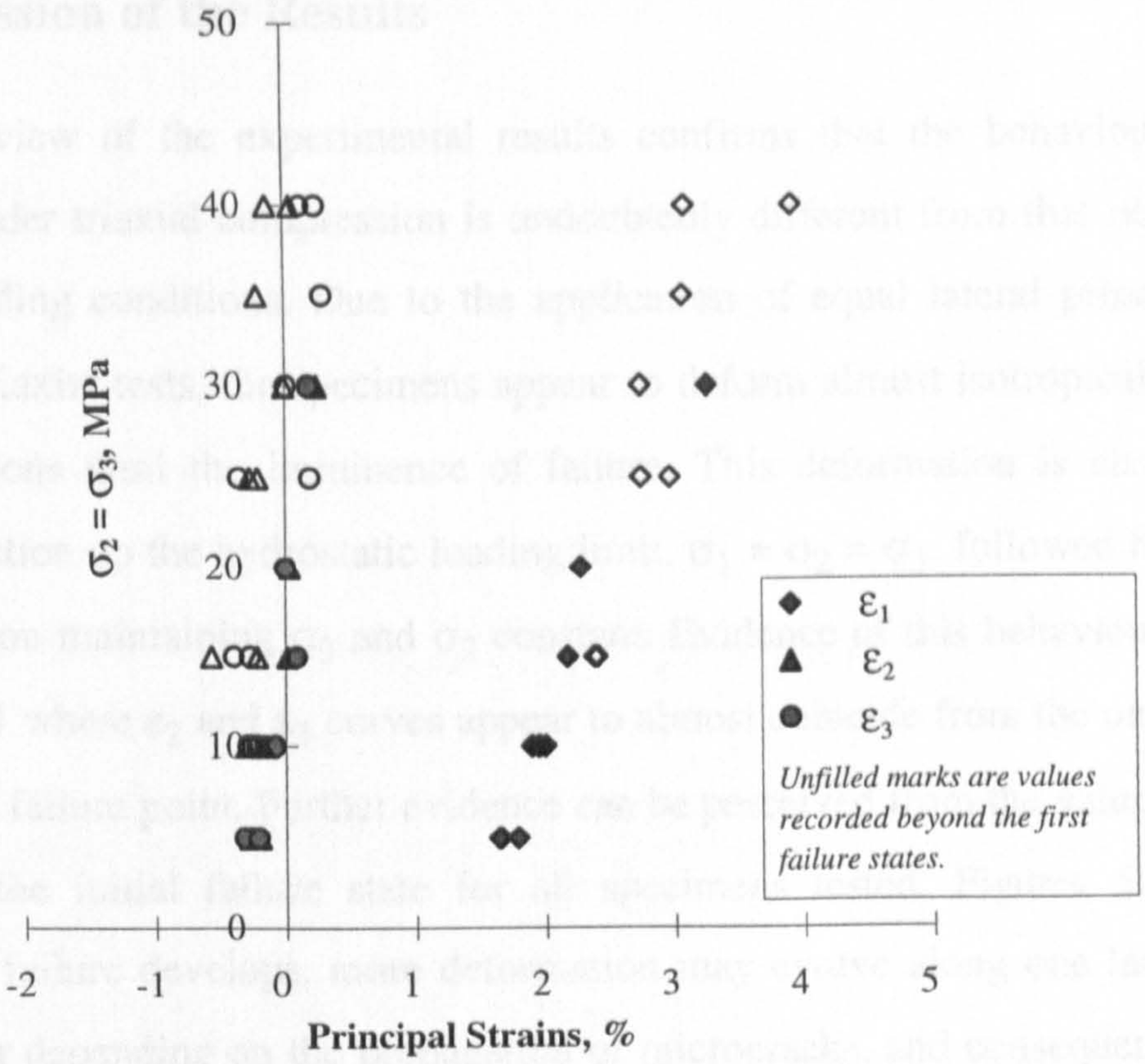

Figure 5.24 Variation of principal strains ε_1, ε_2, ε_3 at failure with $\sigma_2 = \sigma_3$ in single and multiple failure state triaxial tests on cubes of Springwell sandstone.

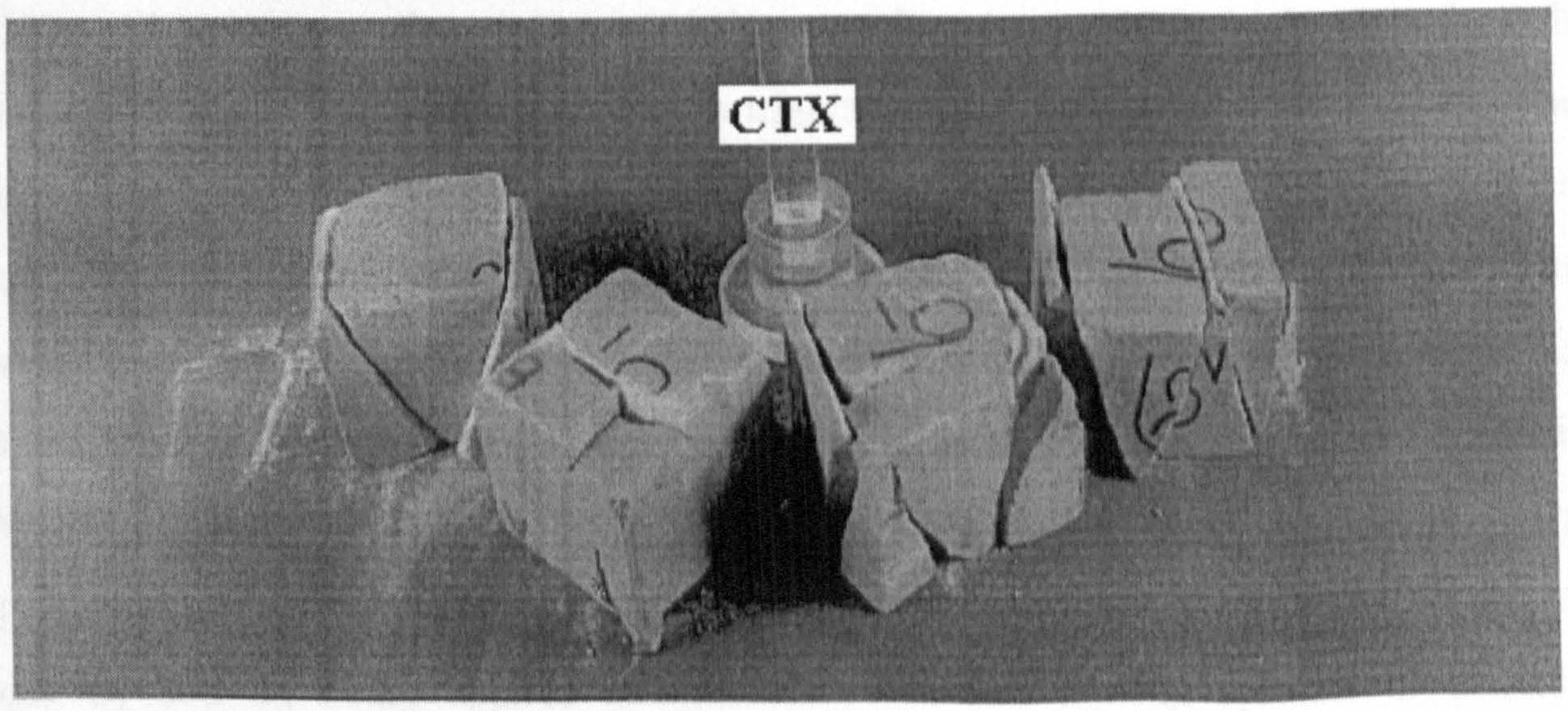

Figure 5.25 Typical failure patterns observed in triaxial compression tests on cubes of Springwell sandstone.

5.7.3 Discussion of the Results

A general review of the experimental results confirms that the behaviour of the test specimens under triaxial compression is undoubtedly different from that observed under polyaxial loading conditions. Due to the application of equal lateral principal stresses, $\sigma_2 = \sigma_3$, in triaxial tests, the specimens appear to deform almost isotropically along both lateral directions until the imminence of failure. This deformation is characterised by initial contraction up the hydrostatic loading limit, $\sigma_1 = \sigma_2 = \sigma_3$, followed by progressive expansion upon maintaining σ_3 and σ_2 constant. Evidence of this behaviour can be seen in Figure 5.21 where ε_2 and ε_3 curves appear to almost coincide from the onset of loading up to the first failure point. Further evidence can be perceived from the values of ε_2 and ε_3 recorded at the initial failure state for all specimens tested, Figures 5.23 and 5.24. However, as failure develops, more deformation may evolve along one lateral direction than the other depending on the propagation of microcracks, and consequently, ε_2 and ε_3 curves may notably diverge from each other. As Figure 5.21 shows, a greater divergence between the two curves is generally observed beyond the first failure state in multiple failure state tests leading to variations between ε_2 and ε_3 values at subsequent failure states, as demonstrated by Figures 5.23 and 5.24.

Unlike polyaxial tests where specimen failure was found to exclusively develop along the minor principal stress direction, failure in triaxial tests appears to take place along either lateral directions or both. However, with the test specimen being subjected to equal minor and intermediate principal stresses, $\sigma_2 = \sigma_3$, failure may be anticipated to ideally develop evenly along both lateral directions. The evidence that this has not been the general case in the present tests may primarily be attributed to the fact that the rock material intrinsically is never perfectly homogeneous nor isotropic. Although ε_2 and ε_3 curves appear sometimes to virtually coincide, their values are never absolutely equal. Moreover, with σ_2 and σ_3 being applied independently via two loading systems of different precision, it is rather impossible to achieve exact and equal levels of stresses in both lateral directions throughout the test. These factors are likely to have been combined with inherent variation in the level of friction at the specimen boundaries caused by the inability to practically ensure that all specimen surfaces are perfectly matched. In respect

of such factors, it is conceivable that failure would generally be inclined to progress more effectively along one lateral direction than the other, as emerged in the present tests.

Another conspicuous feature of the specimen failure in these triaxial tests has been the intensity of shear signs exhibited by the fracture surfaces in comparison with those observed in polyaxial tests. Although similar factors to those identified in the discussion of the polyaxial test results might have contributed to the development of such feature, it is equally believed in the light of the apparent picture of the specimen behaviour that failure would be liable to shear, a common characteristic of failure under conventional triaxial loading conditions.

On the whole, there appears to be fundamentally more agreement between the present test results and familiar results of conventional triaxial compression tests on solid cylinders than with results obtained from the foregoing polyaxial tests. Results of triaxial tests on solid cylinders of Springwell sandstone are presented in Chapter 7, and a comparison with the present results is presented in Chapter 8.

5.8 Biaxial Compression Tests

5.8.1 Outline of the Tests

A total of twelve cubes of Springwell sandstone have been loaded to failure under the special case of biaxial compression in which $\sigma_1 > \sigma_2 > \sigma_3 = 0$, a case of well recognised theoretical and practical importance. In order to free the test specimen along σ_3 direction from any degree of confinement and yet obtain measurements of ε_3, the bearing platens in this direction were removed from the cubical apparatus and an ε_3 transducer was mounted inside the apparatus with its armature resting against a small DEMAC disc glued to the centre of specimen face. As mentioned in Chapter 3, a special clamping platen has been designed to achieve this arrangement and enable proper mounting of the transducer, Figure 5.26. The rest of the testing configuration and procedure were the same as in the previous cubical tests with σ_2 being the only lateral stress applied. Table 5.9 shows the applied level of σ_2 for each individual test conducted.

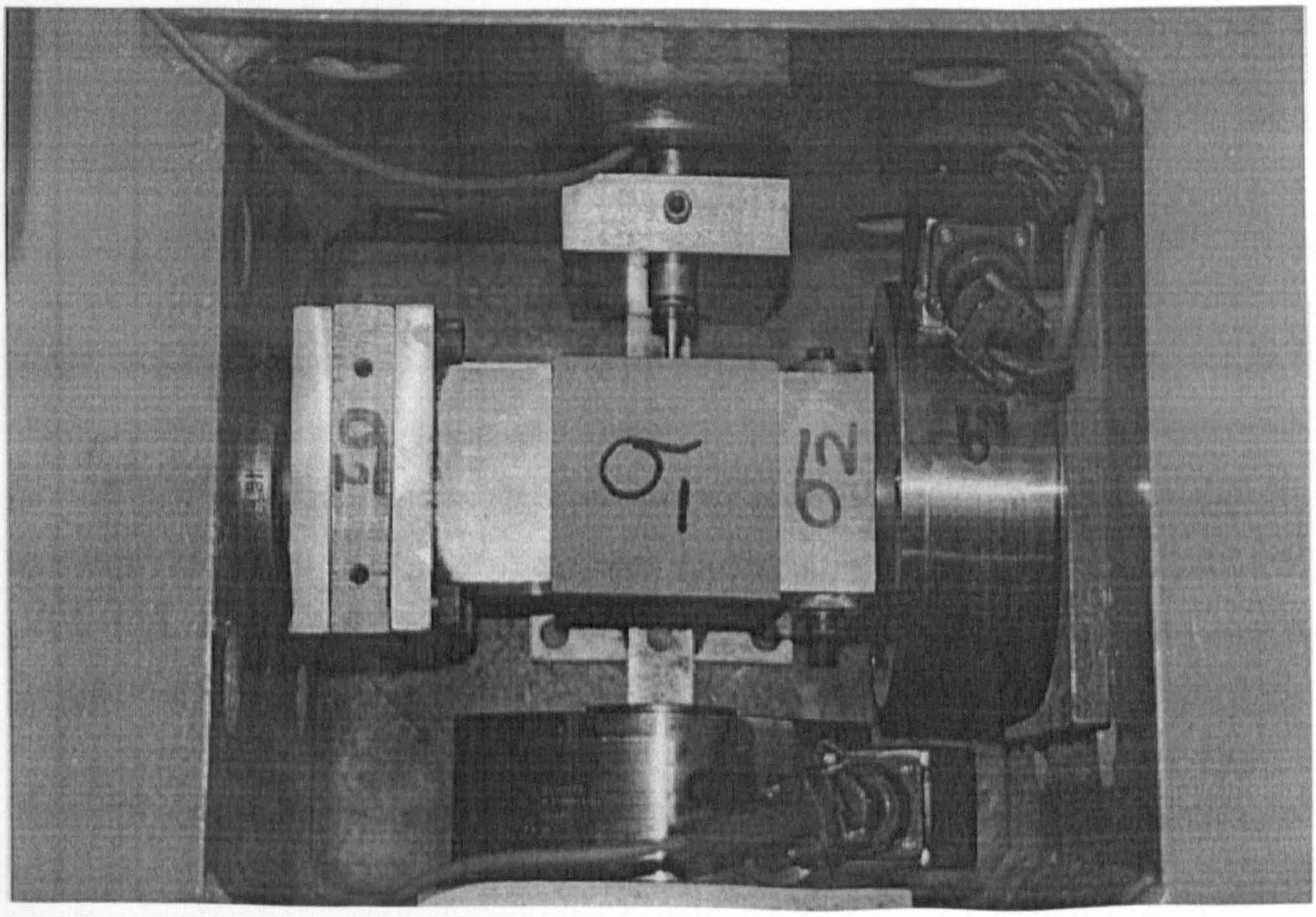

Figure 5.26 Setting up a specimen inside the cubical apparatus for a biaxial compression test.

Table 5.9 Applied levels of intermediate principal stress, σ_2, in biaxial compression tests on cubes of Springwell sandstone.

Specimen No.	σ_2, MPa
CBX1	5
CBX2	5
CBX3	10
CBX4	10
CBX5	20
CBX6	20
CBX7	30
CBX8	30
CBX9	30
CBX10	30
CBX11	40
CBX12	40

5.8.2 The Experimental Results

A characteristic picture of the deformational behaviour of a test specimen under biaxial compression is depicted up to the failure point in Figure 5.27 for specimen CBX4 in the form of a plot of the major principal stress, σ_1, versus the principal strains ε_1, ε_2, ε_3. Recorded values of ε_1, ε_2, ε_3 at failure for all specimens tested are plotted in Figures 5.28 and 5.29 against the corresponding levels of σ_1 and σ_2, respectively. Variation of σ_1 level at failure with the applied level of σ_2 is illustrated in Figure 5.30.

Generally, failure of the test specimen was marked by explosive fracturing accompanied by a sharp fall in the level of the major principal stress, σ_1. In most tests, the specimen disintegrated along multiple fracture planes most of which extended to the loading faces

of the specimen and formed almost parallel to the σ_1 - σ_2 plane and perpendicular to the direction of $\sigma_3 = 0$. Although in some cases the PTFE sheets particularly at σ_1 contacts appeared to have suffered some distortion or tear, most fracture planes were rough surfaces hardly exhibiting any signs of shear. In a few tests, the use of adjacent PTFE strips instead of sheets at the specimen boundaries proved once again not to have any apparent effect on the experimental results, and evidence of distortion in the PTFE strips could still be seen along the traces of the fracture bounds. Representative fracture patterns are shown in Figure 5.31.

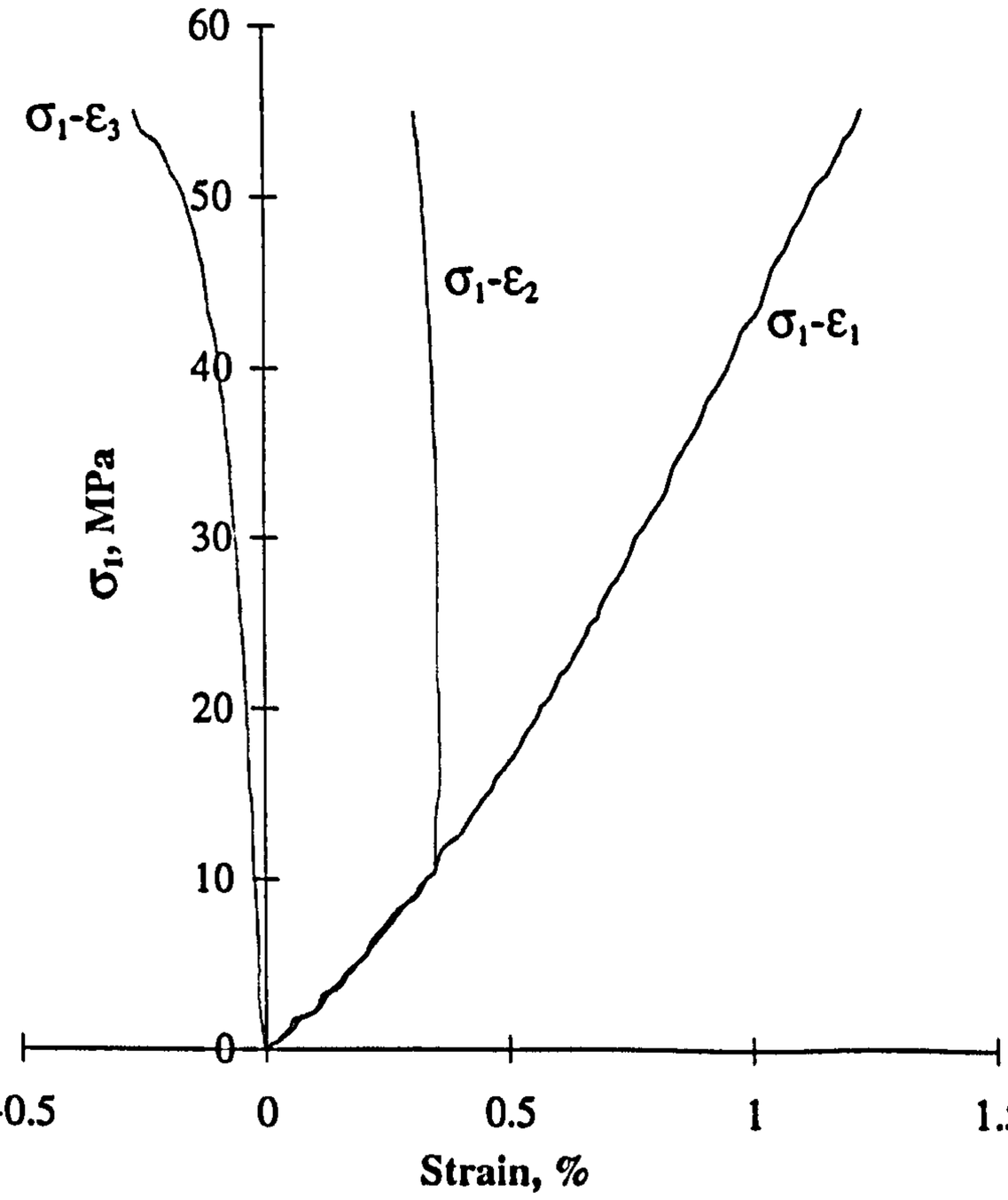

Figure 5.27 Typical curves of the major principal stress versus major, intermediate and minor principal strains from biaxial tests on cubes of Springwell sandstone.

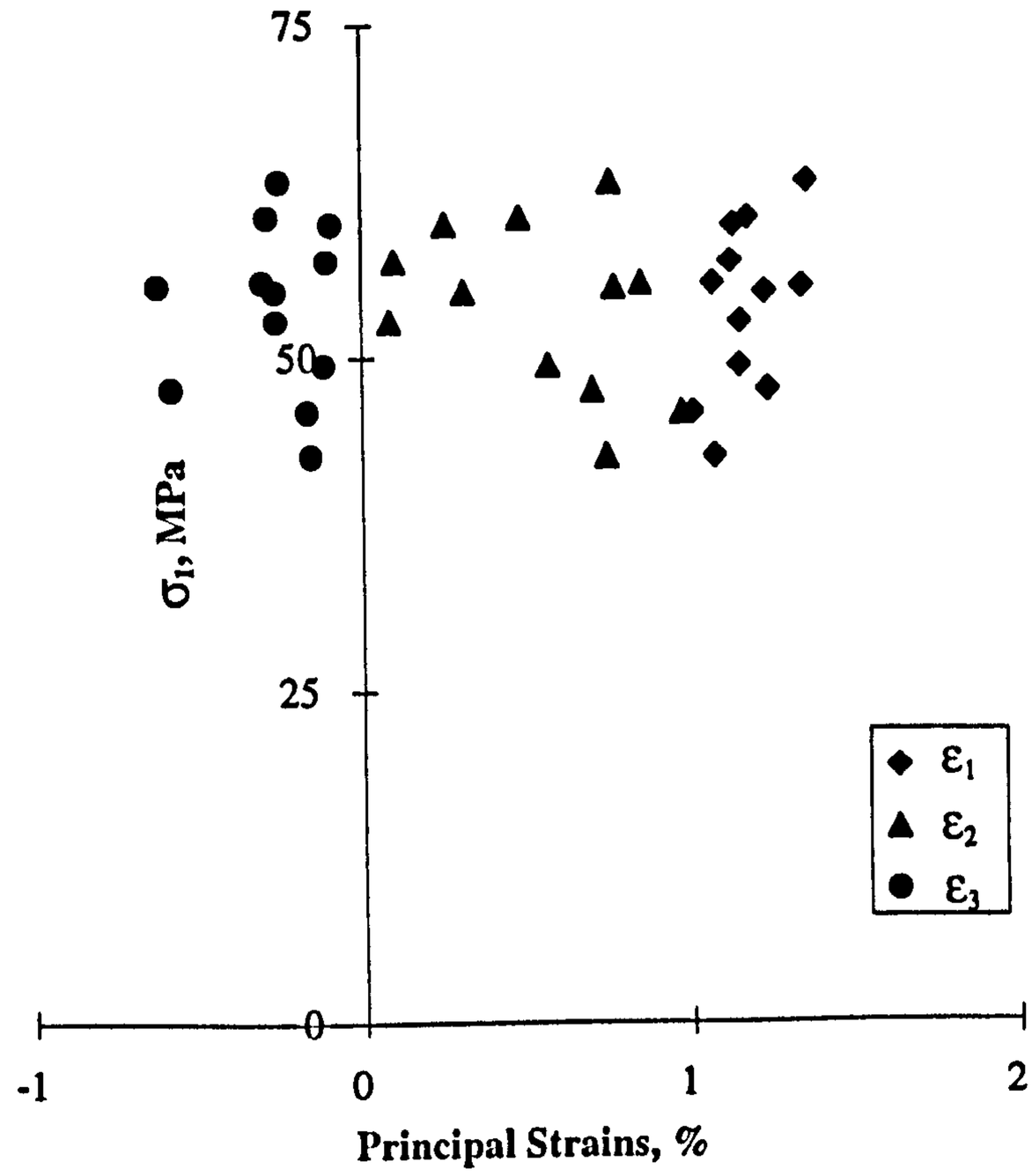

Figure 5.28 Major principal stress σ_1 at failure versus the principal strains ε_1, ε_2, ε_3 in biaxial compression tests on cubes of Springwell sandstone.

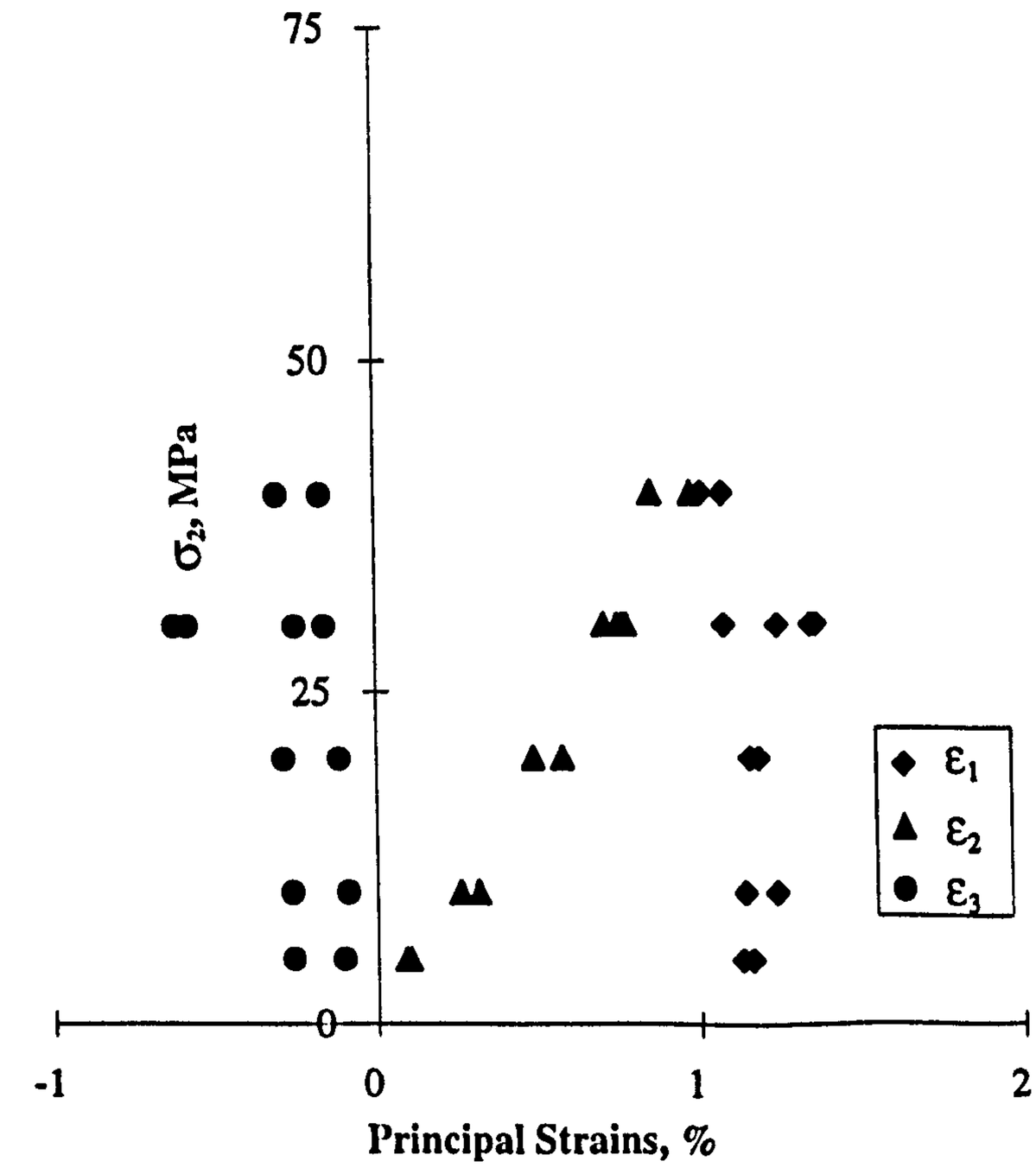

Figure 5.29 Variation of principal strains ε_1, ε_2, ε_3 at failure with σ_2 in biaxial compression tests on cubes of Springwell sandstone.

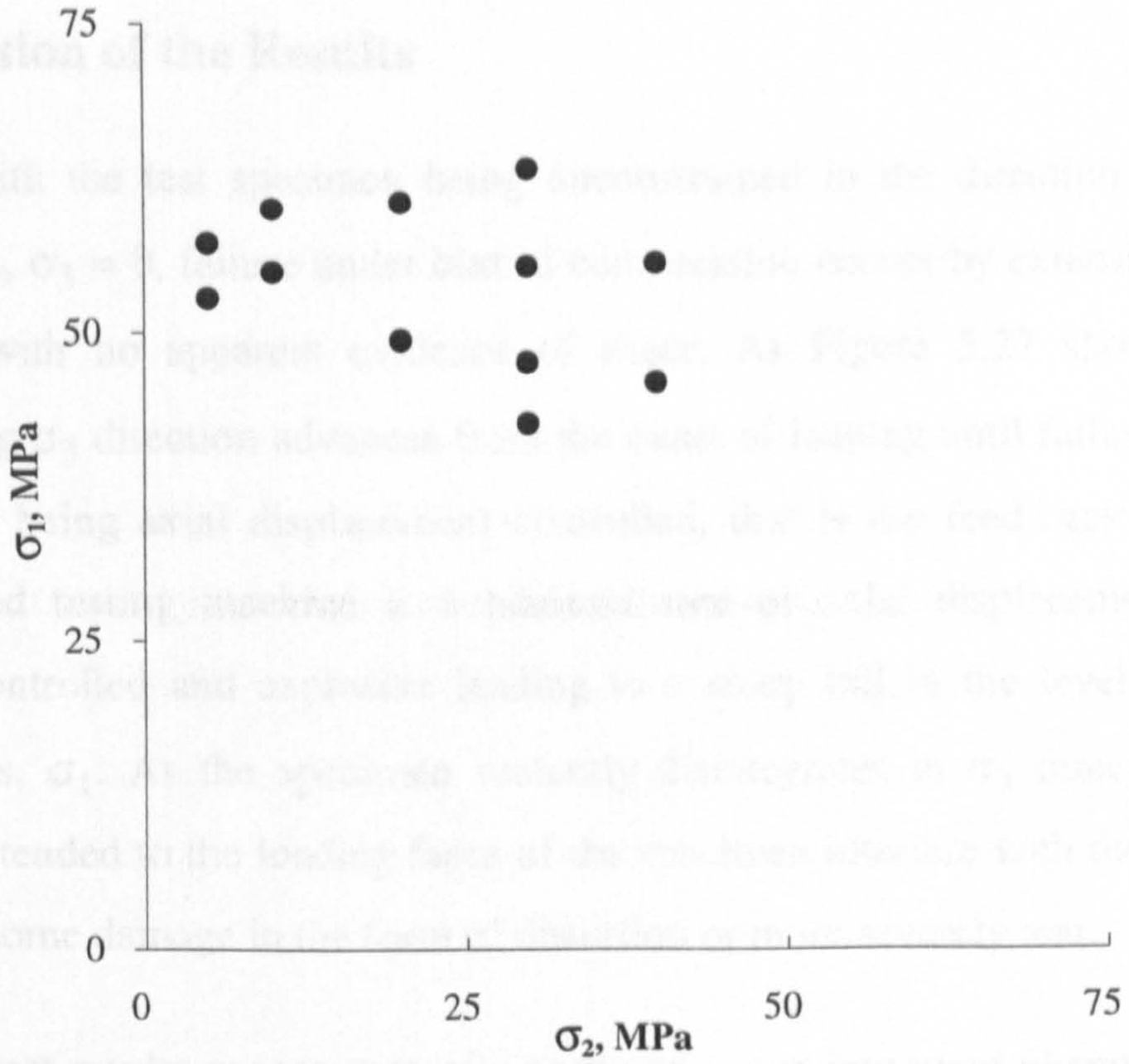

Figure 5.30 Variation of σ_1 at failure with σ_2 in biaxial compression tests on cubes of Springwell sandstone.

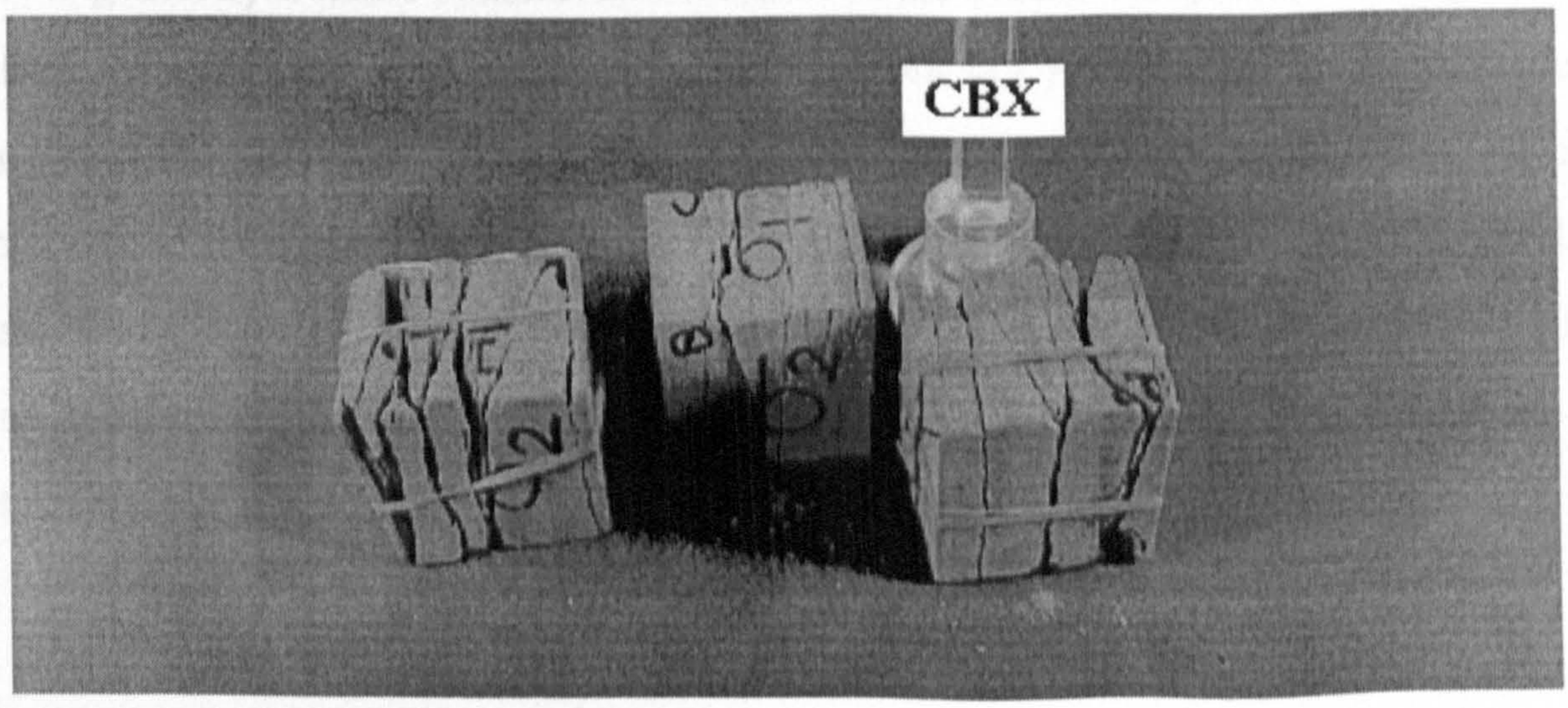

Figure 5.31 Typical failure patterns observed in biaxial compression tests on cubes of Springwell sandstone.

5.8.3 Discussion of the Results

Predictably, with the test specimen being unconstrained in the direction of the minor principal stress, $\sigma_3 = 0$, failure under biaxial compression occurs by extensile splitting in σ_3 direction with no apparent evidence of shear. As Figure 5.27 shows, specimen extension along σ_3 direction advances from the onset of loading until failure takes place. With the tests being axial displacement controlled, that is the feed-back signal of the servo-controlled testing machine is a constant rate of axial displacement, failure is generally uncontrolled and explosive leading to a sharp fall in the level of the major principal stress, σ_1. As the specimen violently disintegrates in σ_3 direction, fractures which have extended to the loading faces of the specimen interfere with the PTFE sheets causing them some damage in the form of distortion or more severely tear.

Although the test results appear generally scattered, some important phenomena can still be recognised. One such phenomenon is demonstrated by Figure 5.30 in which the biaxial compressive strength of the rock, i.e. maximum level of σ_1 at failure, seems to initially increase with increasing the applied level of the intermediate principal stress, σ_2, up to a point beyond which σ_1 starts to decrease. Furthermore, within the applied range of σ_2, there is generally a rather considerable increase in the biaxial compressive strength of the rock over its uniaxial compressive strength, $\sigma_u = 44.113$ MPa, determined in Chapter 4 from standard uniaxial tests on solid cylinders. With the average value of the biaxial compressive strength measured in all tests being equal to 53.811 MPa, the level of increase over σ_u value is 22%. Variation of the average level of increase with the applied level of σ_2 is illustrated in Figure 5.32. Clearly, this confirms that effect of the intermediate principal stress on the apparent strength of the rock.

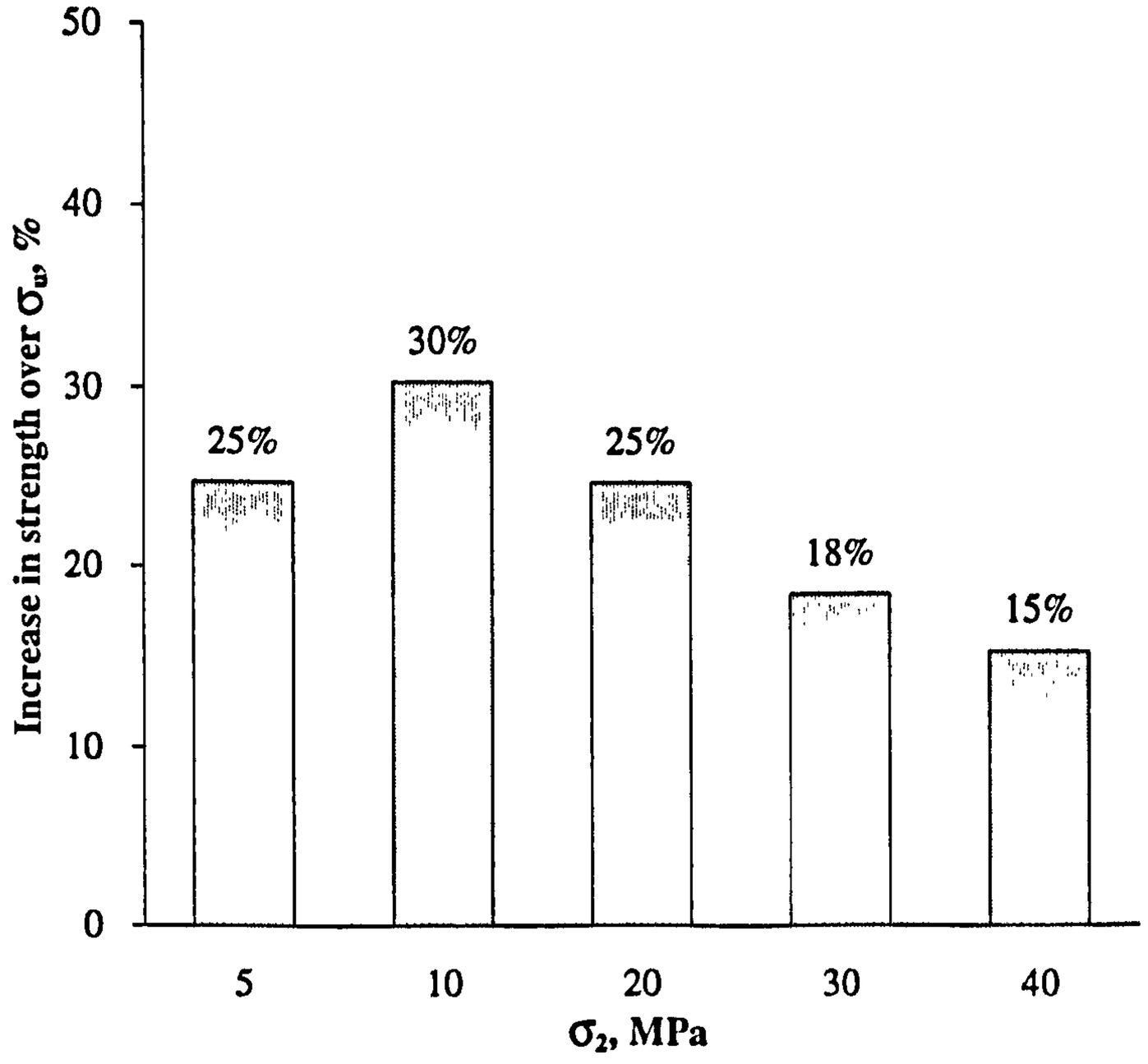

Figure 5.32 Average increase in σ_1 value at failure over the uniaxial compressive strength, σ_u, with increasing the level of the intermediate principal stress, σ_2, in biaxial tests on cubes.

5.9 Uniaxial Compression Tests

5.9.1 Outline of the Tests

The multiaxial testing programme on cubical specimens of Springwell sandstone has been concluded with six uniaxial compression tests, $\sigma_1 > \sigma_2 = \sigma_3 = 0$, involving two different boundary conditions. Three cubes were tested in line with the general testing procedure using PTFE sheets at the specimen boundaries, while the other three cubes were tested in direct contact with the loading platens for comparison with results of standard uniaxial compression tests on solid cylinders. In order to free the test specimen in both lateral directions and yet obtain measurements of ε_2 and ε_3, all lateral bearing platens were removed from the cubical test apparatus and two transducers were mounted on especially designed clamping platens to act directly against DEMAC discs located at the centre of specimen faces concerned, as arranged along $\sigma_3 = 0$ direction in the biaxial tests. A view of this arrangement is shown in Figure 5.33.

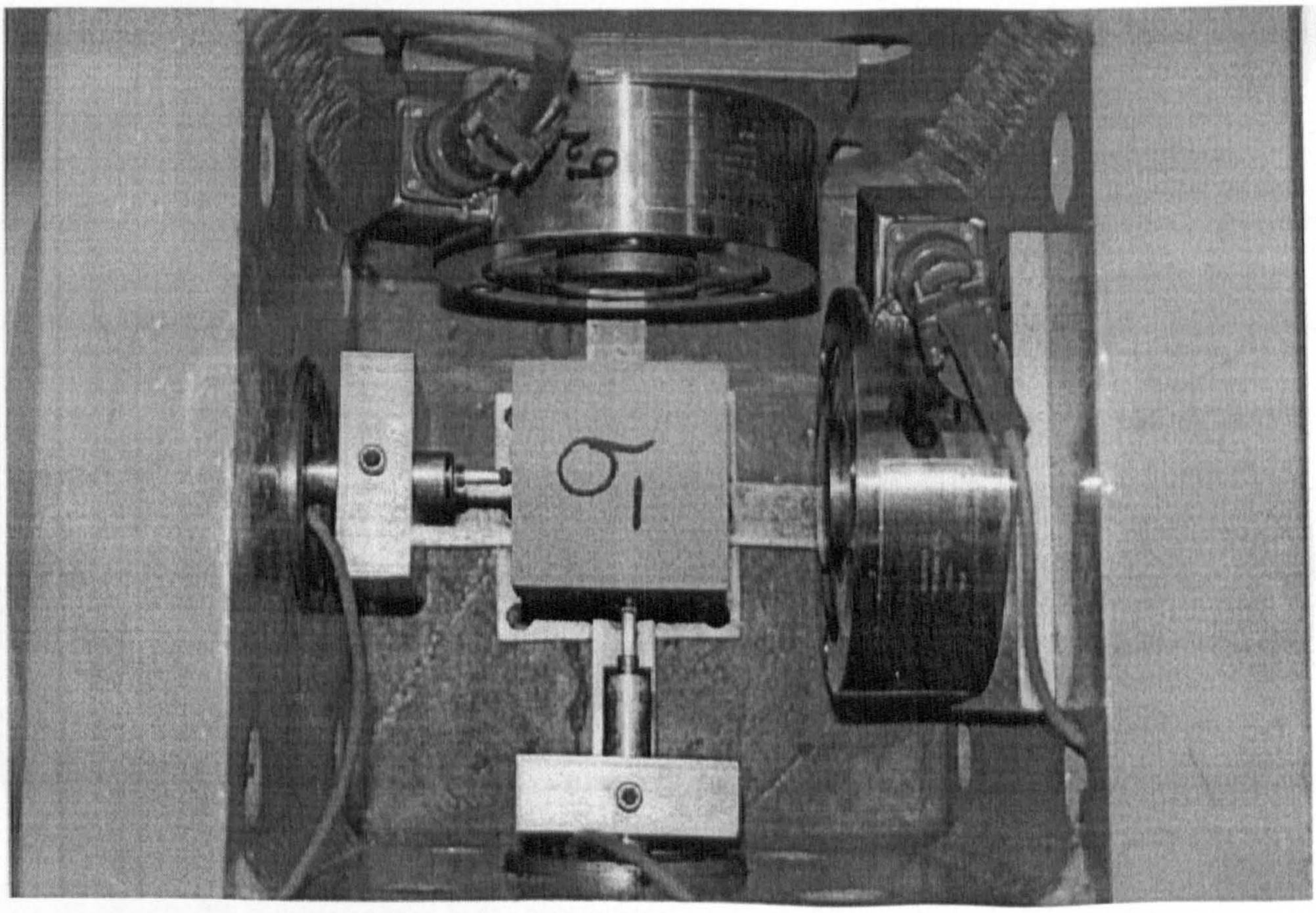

Figure 5.33 Setting up a specimen inside the cubical apparatus for a uniaxial compression test.

5.9.2 The Experimental Results

Figure 5.34 shows a typical plot of the axial compressive stress, σ_1, versus the principal strains ε_1, ε_2, ε_3 for a cubical uniaxial compression test conducted with PTFE sheets at the specimen loading boundaries. A similar plot is presented in Figure 5.35 for a specimen tested in direct contact with the loading platens. Values of the uniaxial compressive strength, i.e. maximum level of σ_1 at failure, for all specimens tested are presented in Table 5.10 together with the specimen-platen contact conditions.

Generally, the specimen failure appeared to be influenced by the conditions at the specimen loading boundaries. When PTFE sheets were used, the specimen failed relatively in a milder manner by extensile axial splitting towards both lateral directions. In contrast, with the specimen being in direct contact with the bearing platens, failure was more explosive and resulted in shear cones or wedge-shaped fractures. Pictures of the failure modes observed in both cases are presented in Figures 5.36 and 5.37, respectively.

Table 5.10 Results of uniaxial compression tests on cubes of Springwell sandstone.

Specimen No.	Boundary Conditions	Compressive Strength, MPa
CUX1	PTFE Sheets	43.157
CUX2	=	42.256
CUX3	=	46.746
CUX4	Direct Contact	58.606
CUX5	=	63.210
CUX6	=	59.692

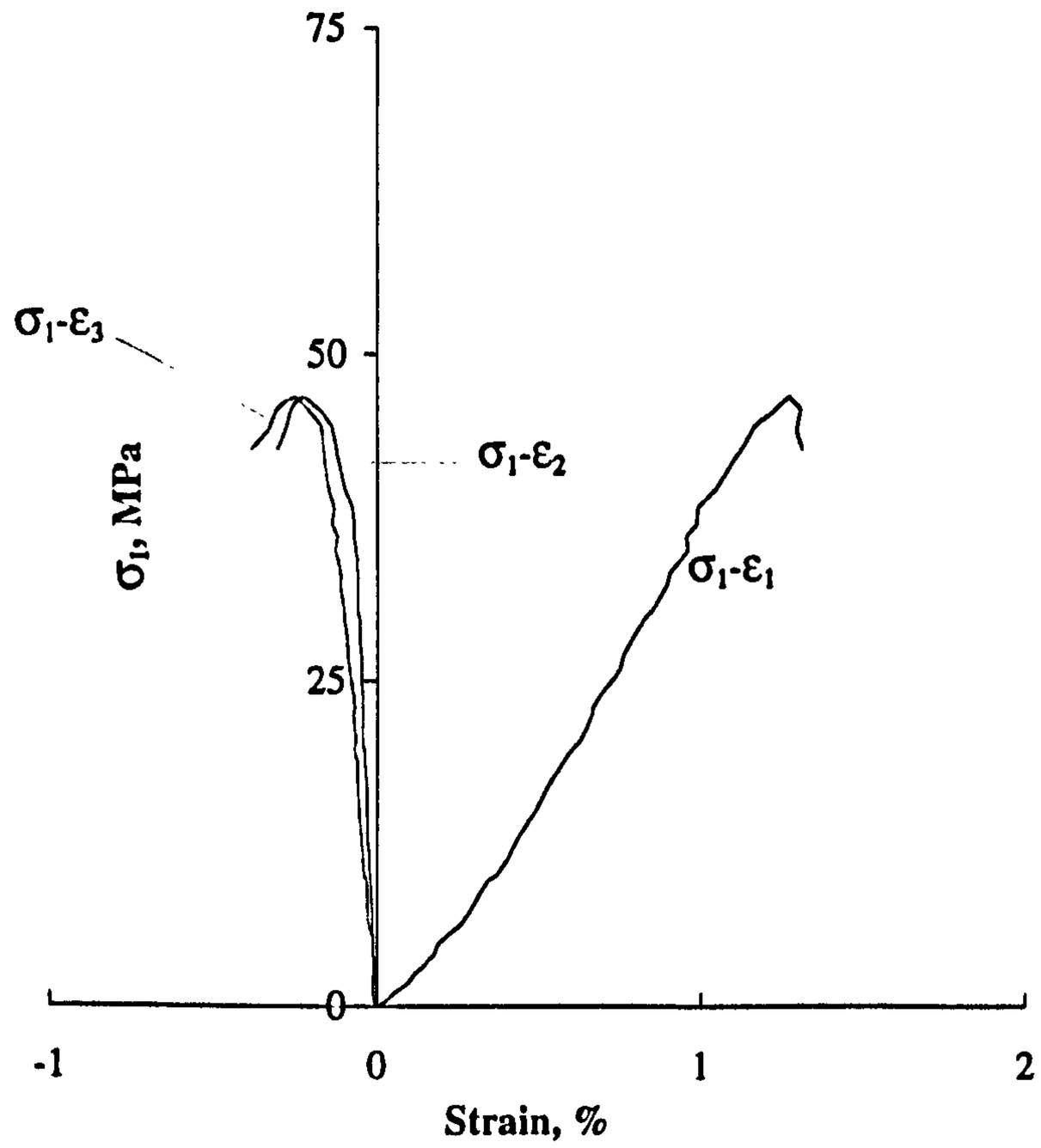

Figure 5.34 Typical curves of the axial stress versus principal strains from uniaxial tests on cubes loaded with PTFE sheets at their boundaries.

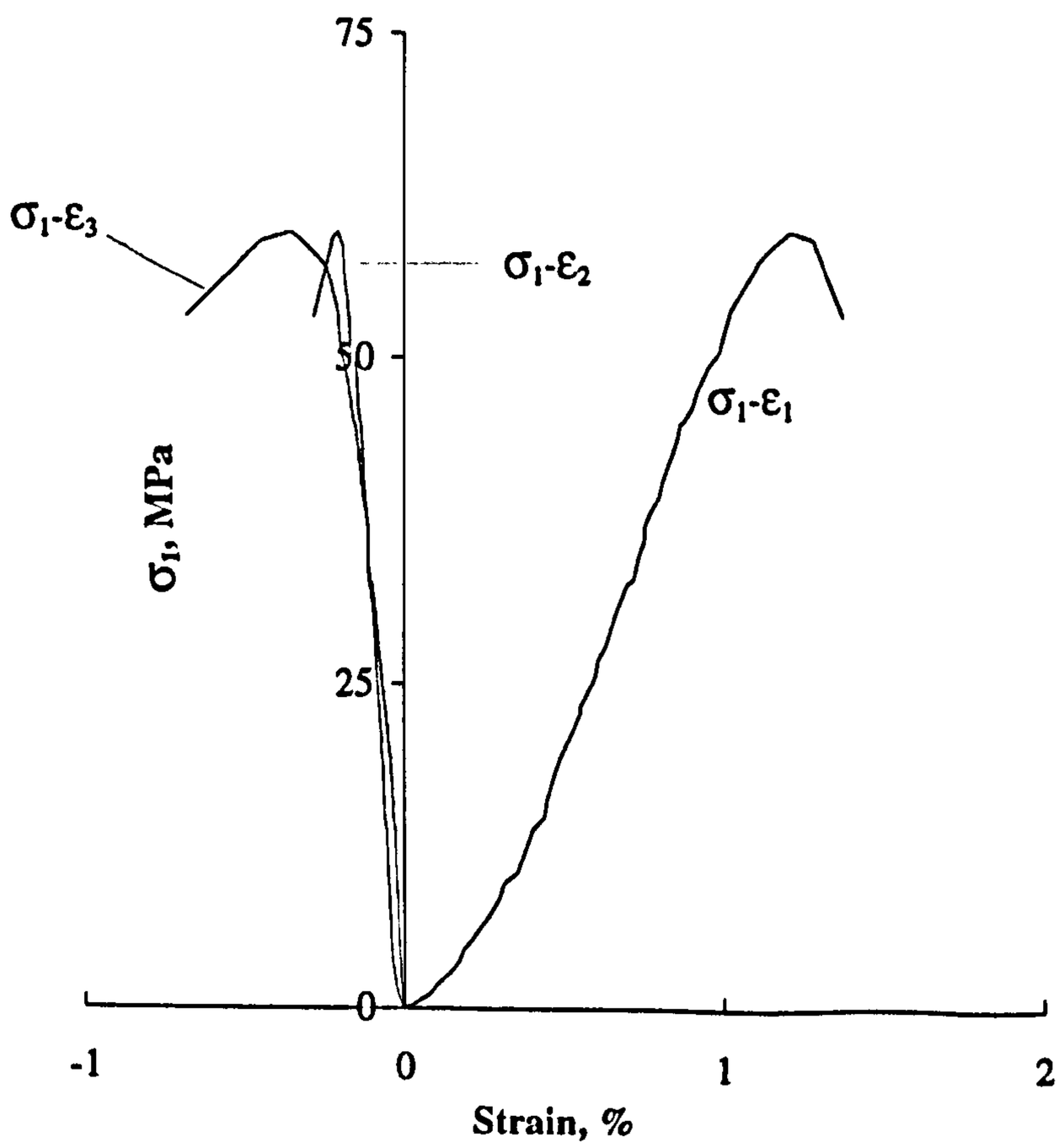

Figure 5.35 Typical curves of the axial stress versus principal strains from uniaxial tests on cubes loaded in direct contact with the bearing platens.

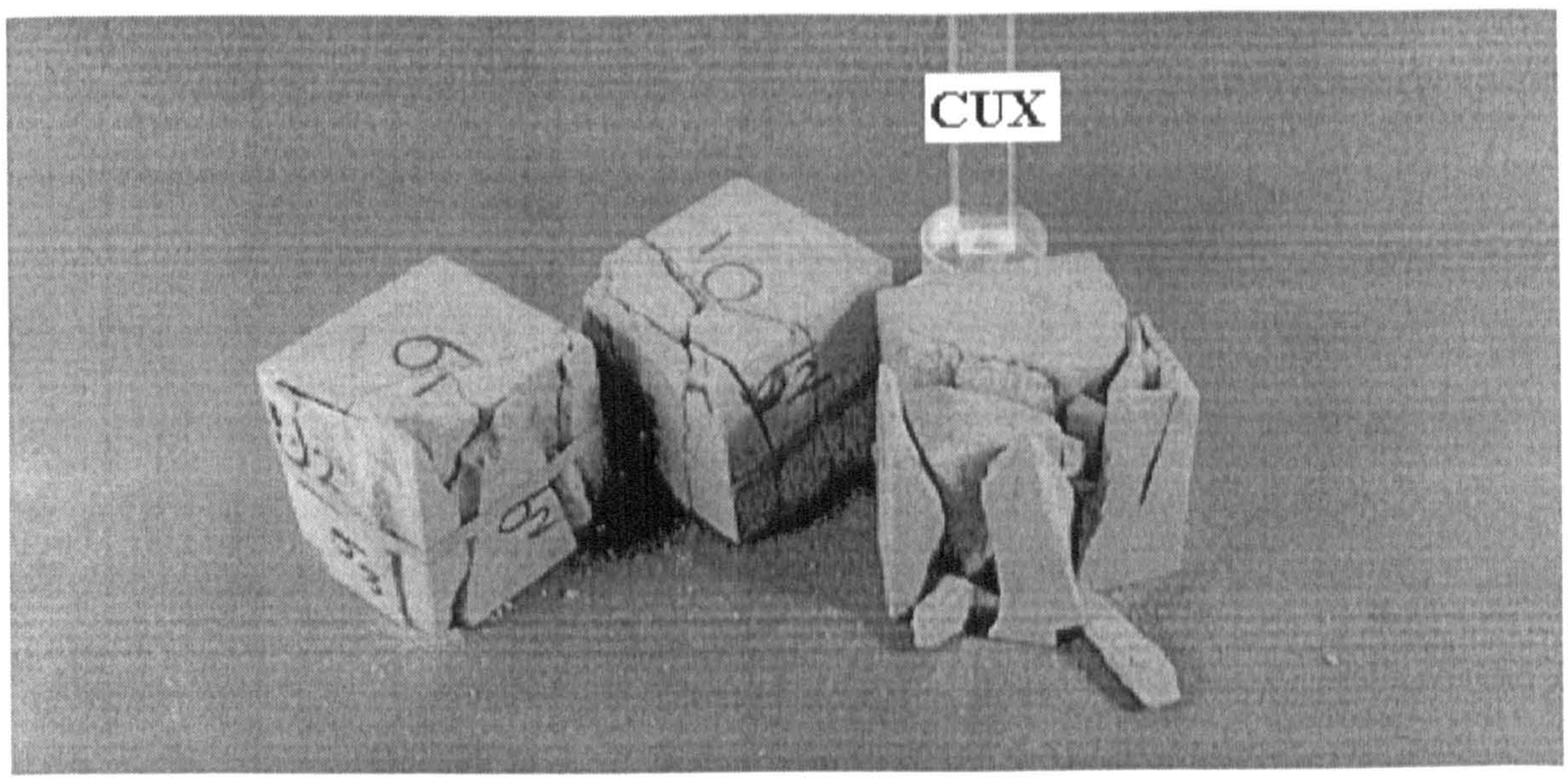

Figure 5.36 Failure modes under uniaxial compression for cubes tested with PTFE sheets at their loading boundaries.

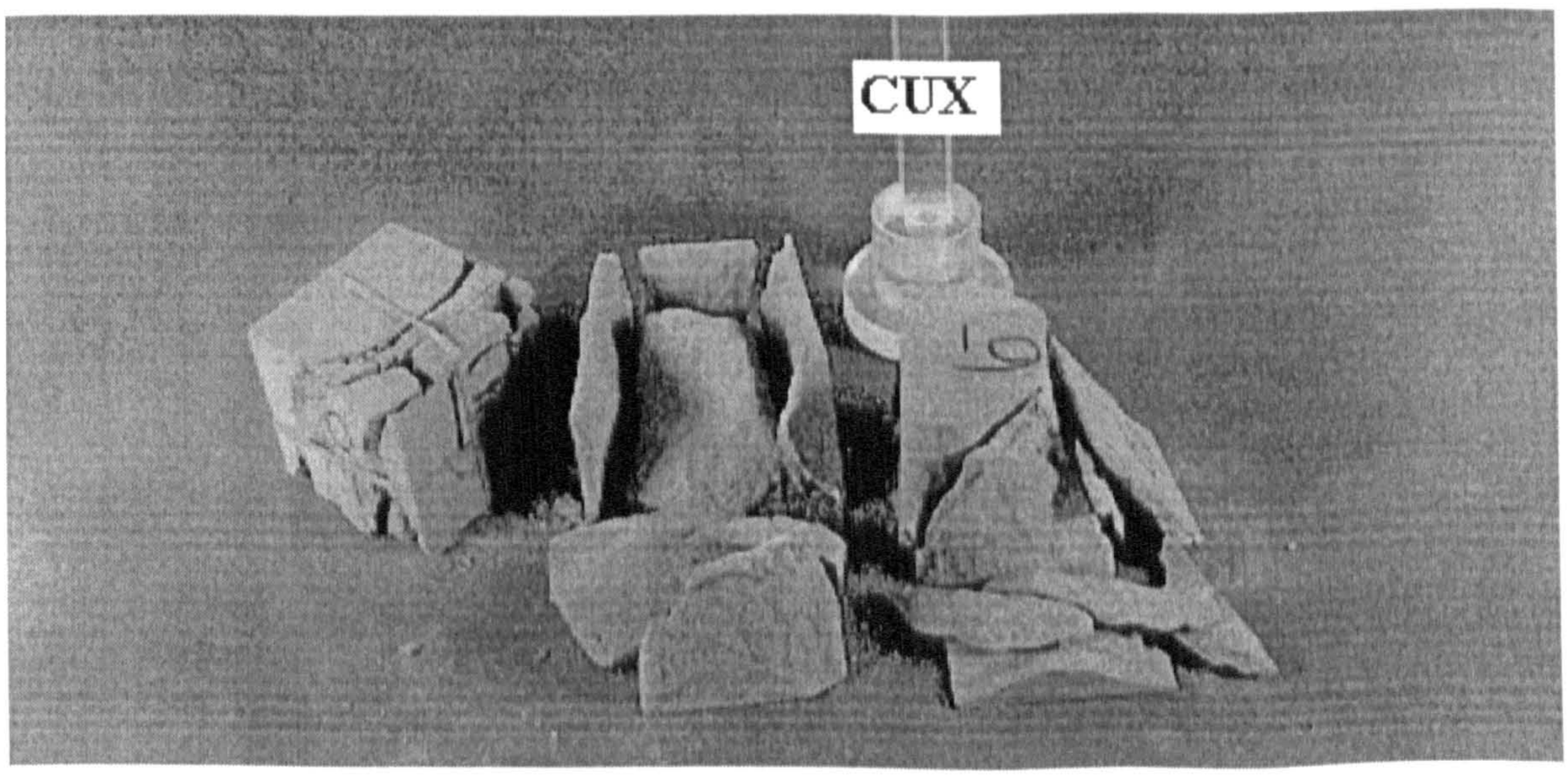

Figure 5.37 Failure modes under uniaxial compression for cubes tested in direct contact with the bearing platens.

5.9.3 Discussion of the Results

Once again, the behaviour of the test specimen appears to be highly influenced by the intensity of friction induced at its loading boundaries. When no attempt is made to reduce this effect and the specimen is loaded in direct contact with the bearing platens, the specimen failure occurs by shear at an average value of uniaxial compressive stress of 60.503 MPa. With the use of PTFE sheets between the specimen and the loading platens, the effect of friction at the specimen boundaries is substantially reduced leading to extensile failure at an average value of uniaxial compressive stress of 44.053 MPa. This suggests that there is a considerable increase of about 37% in the apparent uniaxial compressive strength of specimens tested in direct contact with the bearing platens over the strength of specimens tested with PTFE sheets at their loading boundaries.

As presented in Chapter 4, standard uniaxial compression tests on solid cylinders conducted in the conventional manner without any special treatment at the cylinder ends suggested that the uniaxial compressive strength of Springwell sandstone stands at an average value $\sigma_u = 44.113$ MPa. In comparison with the present test results, there appears to be a remarkable agreement between the value of σ_u and the strength of the cubical specimens tested with PTFE sheets. Clearly, this agreement sharply contrasts with an increase of about 37% over σ_u value in the apparent strength of cubes tested in direct contact with the bearing platens, as in the standard tests. Such a considerable difference may be attributed to a number of conceivable factors. One such factor which may be open to question is that although the cubical specimens have a side length of 74 mm, only an effective area of 70×70 mm^2 on which the bearing platen acts was considered when calculating the stress in the test specimens. However, if such a consideration would be proved inaccurate, it would account only for some increase in the strength and that the cubical specimens would remain to appear much stronger than the solid cylinders. In fact, taking the extreme case by assuming an effective area of 74×74 mm^2 would yield an average failure stress of 54.139 MPa, instead of 60.503 MPa, with an increase of about 23% over σ_u value. Obviously, a possible reason for this increase is the specimen shape. Cubical specimens have been reported to exhibit higher strength than cylindrical

specimens, Price (1960). This factor is likely to have been combined with two well recognised factors: the specimen size and height to width ratio, H/W. The cubical specimens are of a smaller size than the solid cylinders, and strength reported to increase as the specimen size decreases, Mogi (1962) and Lundborg (1967). The strength also reported by Hudson *et al.* (1971) to increase as the specimen height to width ratio decreases. With the cubical specimens being of H/W = 1/1, they may be expected to fail at a compressive stress higher than that of the solid cylinders whose H/W = 2/1.

Chapter 6

Multiaxial Compression of Thick-Walled Hollow Cylinders

6.1 Introduction

Following the assessment of the behaviour of Springwell sandstone through direct loading of cubical specimens, a similar multiaxial testing programme has been conducted on the same rock using specimens in the form of thick-walled hollow cylinders. A total of one hundred and sixty-one cylinders of 75 mm outer diameter, 27 mm inner diameter, and 150 mm height, have been subjected to different combinations of internal and external hydrostatic pressures as well as axial load. The levels of pressures applied were selected to induce at the specimen inner walls a range of predefined stress states calculated on the basis of the theory of elasticity. Using conventional cylindrical co-ordinates (r, θ, z) and denoting the principal stresses as radial, σ_r, tangential, σ_θ, and axial, σ_z, the series of experiments conducted and presented herein are typified by the following stress states:

- Polyaxial compression (1), $\sigma_z = \sigma_1 > \sigma_\theta = \sigma_2 > \sigma_r = \sigma_3 > 0$
- Polyaxial compression (2), $\sigma_z = \sigma_1 > \sigma_r = \sigma_2 > \sigma_\theta = \sigma_3 > 0$
- Triaxial compression, $\sigma_z = \sigma_1 > \sigma_r = \sigma_\theta = \sigma_2 = \sigma_3 > 0$
- Biaxial compression (1), $\sigma_z = \sigma_1 > \sigma_\theta = \sigma_2 > \sigma_r = \sigma_3 = 0$
- Biaxial compression (2), $\sigma_z = \sigma_1 > \sigma_r = \sigma_2 > \sigma_\theta = \sigma_3 = 0$
- Uniaxial compression (1), $\sigma_z = \sigma_1 > \sigma_\theta = \sigma_r = \sigma_2 = \sigma_3 = 0$
- Uniaxial compression (2), $\sigma_\theta = \sigma_1 > \sigma_z = \sigma_r = \sigma_2 = \sigma_3 = 0$
- Uniaxial indirect tension, $\sigma_r = \sigma_1 > \sigma_z = \sigma_2 > \sigma_\theta = \sigma_3 < 0$

The tests have been carried out using a thick-walled hollow cylinder test apparatus devised in the present study via a combination of a Hoek triaxial cell and a set of loading platens specifically designed for the application of internal hydrostatic pressure. The test apparatus was mounted in a 5 MN servo-controlled loading system by which the axial stress, σ_z, was exerted. A mobile hydraulic power pack was used to generate the required level of external pressure while a pressure intensifier system was employed for the application of internal pressure and the monitoring the volumetric change of the specimen hole. When σ_z acted as the major principal stress, $\sigma_z = \sigma_1$, the tests were axial strain controlled. Whereas the axial deformation of the test specimen was directly measured,

both radial and tangential deformations were calculated at the specimen inner surface from acquired measurements of the hole volumetric change.

This chapter begins with an overview of the theory of thick-walled hollow cylinder and the elastic solution for calculating the stresses and strains in the cylinder. Thereafter, in line with the cubical tests, the general testing configuration and procedure employed are described, and then the experimental series are presented. All tests of the same principal stress arrangement are grouped together and introduced with an outline of their main features. Then, the test results are presented in various forms highlighting the most significant aspects of the test outcome. Finally, the results are specifically analysed and discussed. A general discussion and comparison of all thick-walled hollow cylinder test results has been reserved for Chapter 8.

6.2 Fundamental Considerations

6.2.1 Stresses in a Hollow Cylinder

The stresses that may develop in a hollow cylinder of rock when acted upon by uniform internal and external hydrostatic pressures are usually analysed in two different manners depending on the thickness of the cylinder wall. In the case of a thin-walled hollow cylinder whose wall thickness is relatively much smaller than its inner diameter, the stresses are almost homogeneous and normally assumed to be uniformly distributed across the cylinder wall. Such an assumption does not hold well in the case of a thick-walled hollow cylinder whose wall thickness is near or larger than the inner diameter of the cylinder, and therefore, the problem must be dealt with taking into account that the stresses in the wall are not homogeneous. A full solution for the problem is provided by the theory of linear elasticity and can be obtained from a number of relevant text books, e.g. Nadai (1950), Obert and Duvall (1967), Jaeger and Cook (1979), Coates (1981). Therefore, only a summary of this solution is given herein.

Considering the general case illustrated in Figure 6.1 of a thick-walled hollow cylinder of an inner radius, R_i, an outer radius, R_o, and an axial length, L, subjected to uniform internal and external hydrostatic pressures, P_i and P_o, respectively, and an axial force, F. Using conventional cylindrical co-ordinates (r, θ, z) and denoting the principal stresses as radial, σ_r, tangential, σ_θ, and axial, σ_z, the following equations are used to calculate σ_r and σ_θ at any point of a radial distance r:

$$\sigma_r = \frac{P_o R_o^2 - P_i R_i^2}{R_o^2 - R_i^2} - \frac{(P_o - P_i) R_i^2 R_o^2}{r^2 (R_o^2 - R_i^2)} \tag{6.1}$$

$$\sigma_\theta = \frac{P_o R_o^2 - P_i R_i^2}{R_o^2 - R_i^2} + \frac{(P_o - P_i) R_i^2 R_o^2}{r^2 (R_o^2 - R_i^2)} \tag{6.2}$$

and for the present test configuration and apparatus used, the axial stress σ_z is given by:

$$\sigma_z = \frac{F}{\pi (R_o^2 - R_i^2)} - \frac{P_i R_i^2}{R_o^2 - R_i^2} \tag{6.3}$$

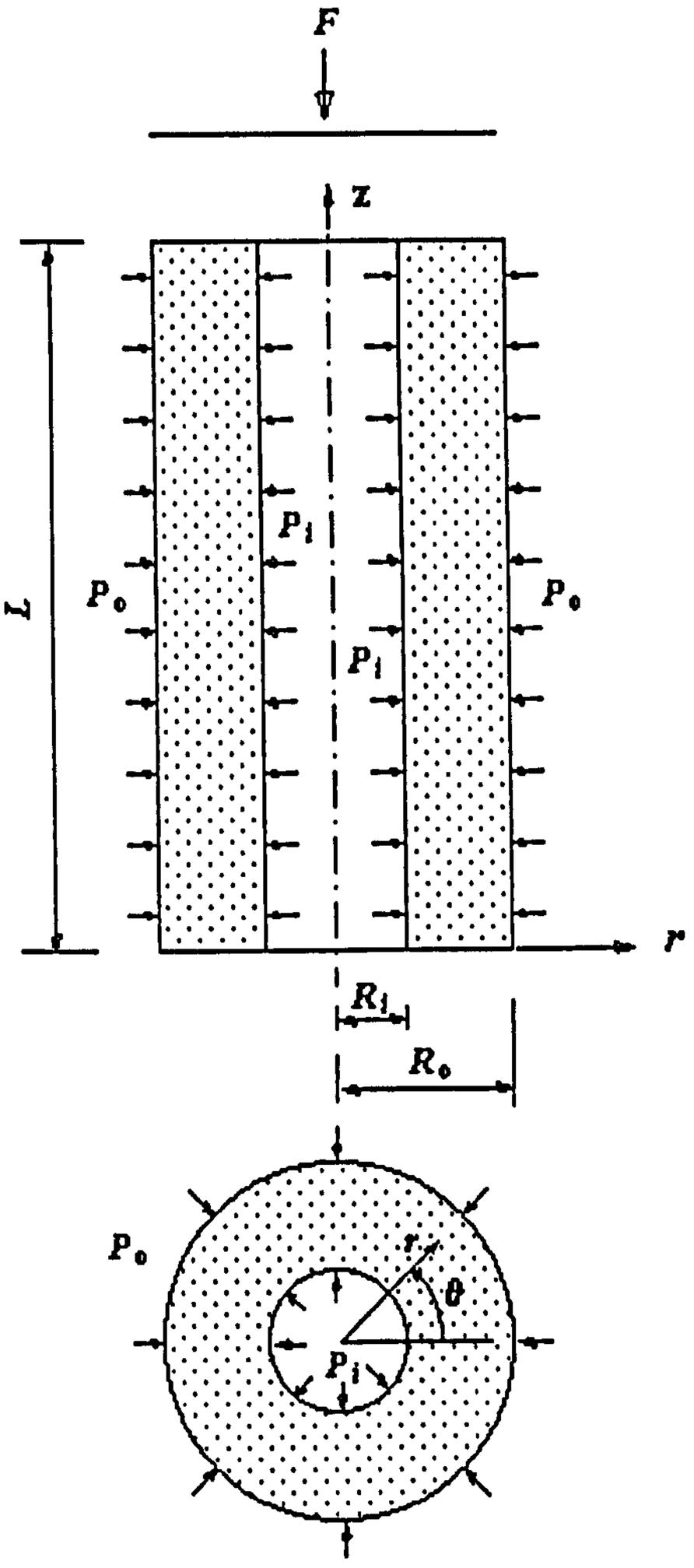

Figure 6.1 An illustration of a thick-walled hollow cylinder under internal pressure, external pressure and axial load, showing notation and co-ordinate system used.

While σ_z is usually assumed to be distributed uniformly over the surface of the cylinder ends, equations (6.1) and (6.2) show that both σ_r and σ_θ values vary across the cylinder walls with the radial distance r. An illustration of the distribution of σ_r and σ_θ through the walls of the present test cylinder is shown in Figures 6.2 and 6.3 for the limiting conditions $P_i = 0$ and $P_o = 0$, respectively. These figures demonstrate that the most critical combinations of σ_θ and σ_r values are found at the specimen inner wall where $r = R_i$.

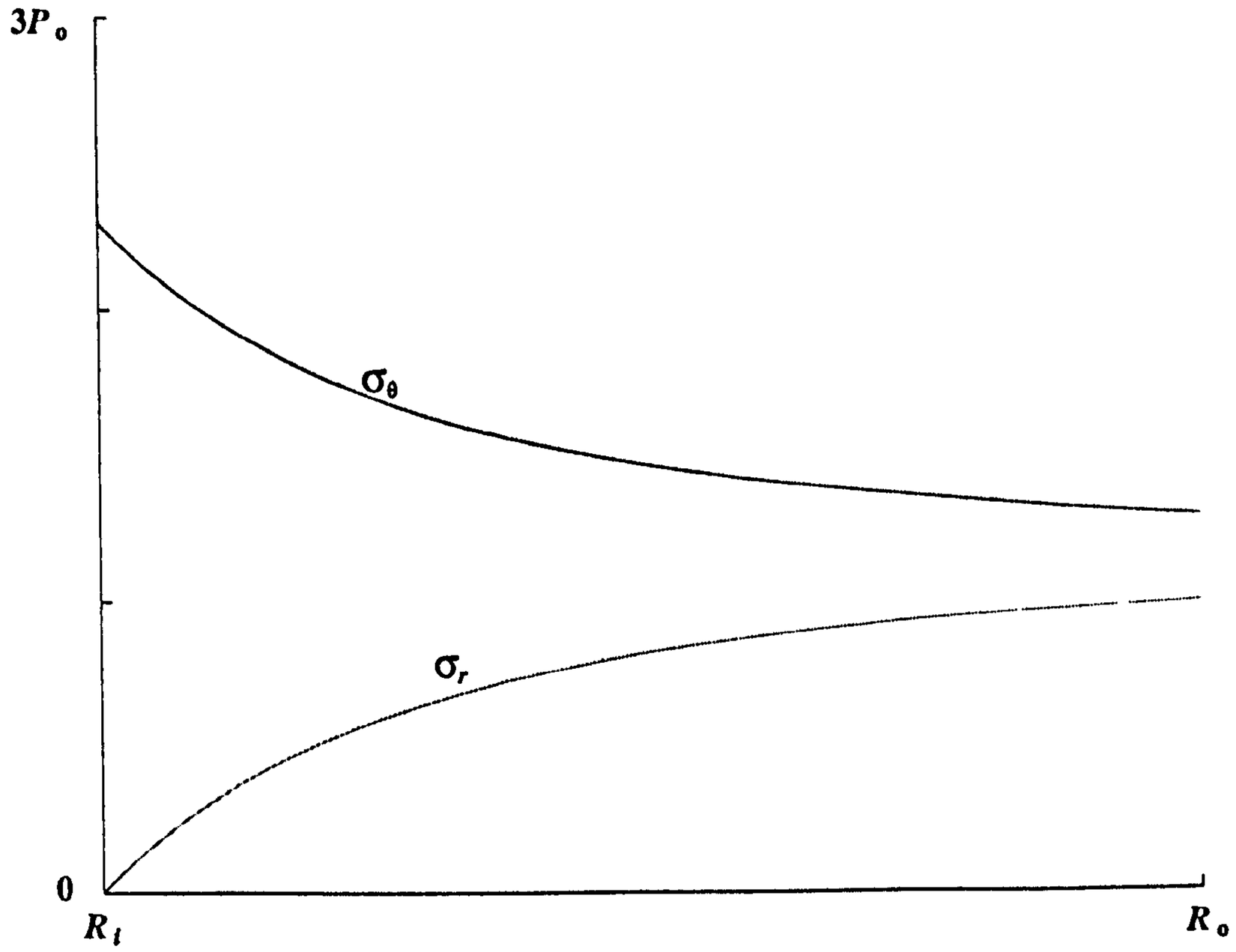

Figure 6.2 Distribution of σ_r and σ_θ through the walls of the test hollow cylinder for external pressure P_o only.

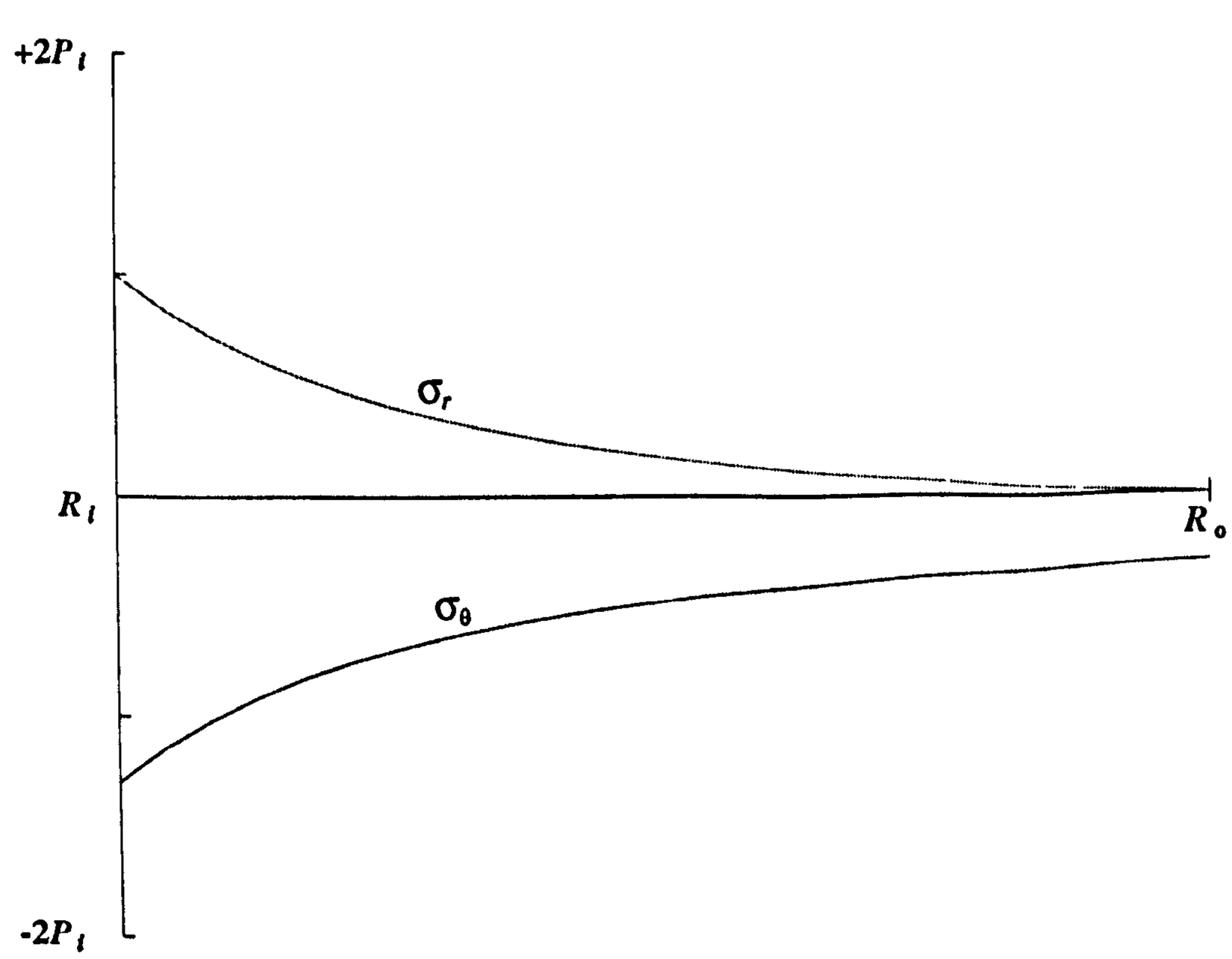

Figure 6.3 Distribution of σ_r and σ_θ through the walls of the test hollow cylinder for internal pressure P_i only.

6.2.2 Effect of Eccentricity

The solution presented in 6.2.1 for calculating the stresses in a thick-walled hollow cylinder is based on the assumption that the inner and outer surfaces of the cylinder are concentric. Jeffery (1921) treated the problem of a hollow cylinder whose cross-section is bounded by two non-concentric circles and is subjected to a uniform normal pressure over its internal surface and a different uniform normal pressure over its external surface. Using bipolar co-ordinates he gave, for plane strain, an exact solution for the stress distribution in the cylinder. However, for the simpler case when the cylinder is subjected to an external pressure P_o only, the tangential stress on the internal surface is:

$$\sigma_\theta = \frac{2P_o R_o^2 [(R_o^2 - e^2)^2 - R_i^2 (R_i + 2e\cos\beta)^2]}{(R_o^2 + R_i^2)[R_o^2 - (R_i - e)^2][R_o^2 - (R_i + e)^2]} \qquad (6.4)$$

and on the external surface:

$$\sigma_\theta = P_o + \frac{2P_o R_i^2 [R_o^2 (R_o - 2e\cos\beta)^2 - (R_i^2 - e^2)^2]}{(R_o^2 + R_i^2)[R_o^2 - (R_i - e)^2][R_o^2 - (R_i + e)^2]} \qquad (6.5)$$

Where e is the eccentricity defined as the distance between the centres of the inner and outer circles whose radii are R_i and R_o respectively.

β is one of the bipolar co-ordinates which is equal to π on the line of centres at the thinnest part of the cylinder and zero on the line of centres at the thickest part of the cylinder.

Jeffery stated that if the centre distance, e, is less than half the internal radius, R_i, the compressive stress in the inner surface decreases steadily from a maximum at the thinnest part of the cylinder to a minimum at the thickest part; otherwise there is a minimum at each of the points and maxima at the points corresponding to $\cos\beta = -R_i / 2e$. Similarly, if the centre distance, e, is less than half the external radius, R_o, the compressive stress in the outer surface decreases steadily from a maximum at the thinnest part of the cylinder to a minimum at the thickest part; if the centre distance exceeds this value the compression is a maximum at each of these points and minima at the points corresponding to $\cos\beta = R_i / 2e$.

6.2.3 Strains in the Cylinder

As in the case of stress relations, strain components in a thick-walled hollow cylinder can be calculated on the basis of the elastic theory and that a full solution may be obtained from a number of relevant text books, examples of which are given in 6.2.1. Using cylindrical polar (r, θ, z) co-ordinate system and denoting the principal strains as radial, ε_r, tangential, ε_θ, and axial, ε_z, a summary of the solution may be presented by the following equations:

$$\varepsilon_r = du_r / dr \tag{6.6}$$

$$\varepsilon_\theta = u_r / r \tag{6.7}$$

$$\varepsilon_z = du_z / dz \tag{6.8}$$

where u_r is the radial displacement component at any point of a radial distance r, and u_z is the displacement component in the axial z direction.

The volumetric strain, ε_v, is defined as the sum of the principal strain components:

$$\varepsilon_v = \Delta V / V = \varepsilon_r + \varepsilon_\theta + \varepsilon_z \tag{6.9}$$

6.2.4 Employed Procedure for Calculating the Principal Strains

In the tests conducted, direct measurements of the specimen axial displacement u_z were continuously acquired, and subsequently, the axial principal strain, ε_z, was calculated over the specimen entire length, L, as follows:

$$\varepsilon_z = u_z / L \tag{6.10}$$

Acquired measurements of the volumetric change of the specimen hole, ΔV_h, have been used to calculate the radial displacement at the specimen inner wall, u_{ri}, and subsequently, the corresponding tangential and radial strains, ε_θ and ε_r respectively, were calculated as follows:

Assuming V_{hi} is the initial volume of the specimen hole, and V_{hc} is the hole volume at ΔV_h volumetric change, the following equations can be written:

$$V_{hi} = \pi R_i^2 L \tag{6.11}$$

$$V_{hc} = \pi (R_i + u_{ri})^2 (L - u_z) \tag{6.12}$$

$$\Delta V_h = V_{hc} - V_{hi} \tag{6.13}$$

$$\varepsilon_{vh} = \Delta V_h / V_{hi} = \varepsilon_r + \varepsilon_\theta + \varepsilon_z \tag{6.14}$$

Substituting equation (6.12) in equation (6.13) and solving the latter for the only unknown variable u_{ri}, the following equation is obtained:

$$u_{ri} = - R_i + \sqrt{(V_{hi} + \Delta V_h) / \pi (L - u_z)} \tag{6.15}$$

This equation has been used to calculate the radial displacement of the specimen inner wall, u_{ri}, on the basis of the corresponding measurements of the hole volumetric change, ΔV_h, and the axial displacement, u_z.

With the consideration that u_{ri} is positive outwards from the centre of the hole, and that contractile strains are positive, the tangential strain, ε_θ, at the inner wall is calculated using equation (6.7) in the form:

$$\varepsilon_\theta = - u_{ri} / R_i \tag{6.16}$$

Subsequently, the radial strain, ε_r, is calculated from equation (6.14) as follows:

$$\varepsilon_r = \varepsilon_{vh} - (\varepsilon_z + \varepsilon_\theta) \tag{6.17}$$

6.3 General Testing Configuration and Procedure

The main testing facilities used in multiaxial loading of thick-walled hollow cylinders, Figure 3.12, were described in detail in Chapter 3, and may briefly be listed herein as follows:

- A hollow cylinder test apparatus, Figures 3.9 to 3.11, composed of a Hoek triaxial cell equipped with two sets of platens specially designed to enable the cell to be used for testing thick-walled hollow cylinders of rock under both external and internal hydrostatic pressures as well as axial load.

- A servo-controlled loading system, Figure 3.13, capable of applying a maximum compressive force of 5 MN used for the application of the axial load, F.

- A mobile hydraulic power pack of a maximum capacity of 70 MPa used in conjunction with a relief valve and a pressure transducer for applying and monitoring the external pressure, P_o.

- A pressure intensifier system, Figure 3.14, of a maximum capacity of 70 MPa used for the application of the internal pressure, P_i, and monitoring the volumetric change of the inner hole of the test specimen.

- A data acquisition system with a personal computer, Figure 3.15, used for continual monitoring and recording of the experimental data.

- An X-Y recorder connected to the servo-controlled loading system used to trace the output of system load cell and LVDT, thus granting a direct plot of the axial load-axial displacement curve during the test.

- A second X-Y recorder connected to both the servo-controlled loading system and the pressure intensifier for direct plotting of the axial displacement versus the volumetric change of the specimen hole.

The hollow cylinders of rock were of 150 mm height, 75 mm outer diameter and 27 mm inner diameter, retaining a wall thickness of 24 mm. Prior to testing, each cylinder was weighed and its bulk density was computed. As described in Chapter 4, the obtained results were then used to evaluate the overall bulk density of the Springwell sandstone.

Preparation for a hollow cylinder test involved a number of steps, and the procedure described herein is for the general case in which internal and external pressures together with axial load were applied. Figure 6.4 shows a test specimen with the hollow cylinder apparatus prior to being assembled for testing. The steps involved in the placement of the specimen in the apparatus are shown in Figures 6.5 to 6.12 and are outlined as follows:

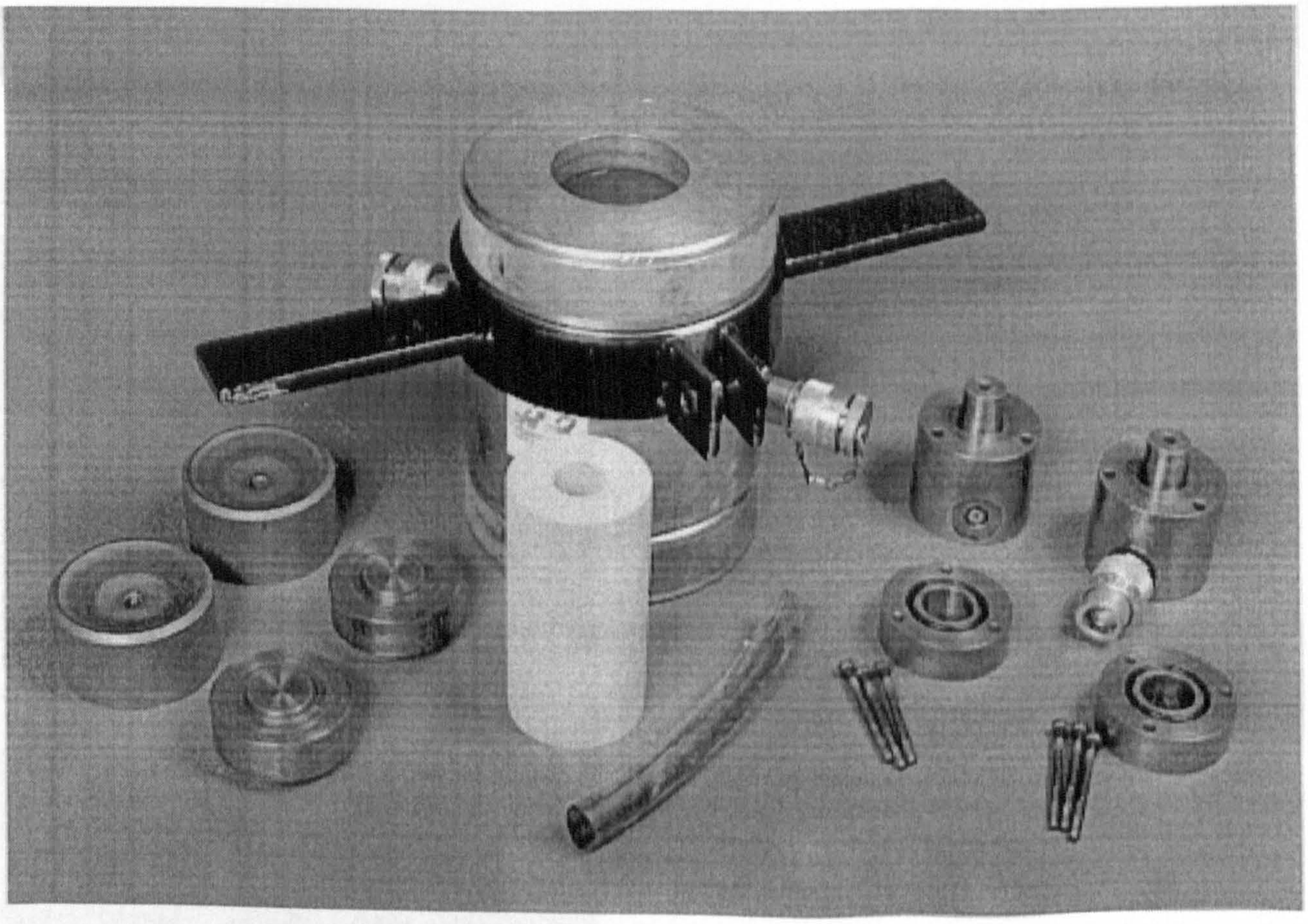

Figure 6.4 The hollow test cylinder apparatus with a specimen of Springwell sandstone before being assembled for testing.

Starting with the internal pressure arrangement, the rubber tube selected for sealing the specimen hole is first trimmed to appropriate length, taking into account the specimen height and the thickness of the hollow end platens, and then fitted to the spigot of the oil inlet platen.

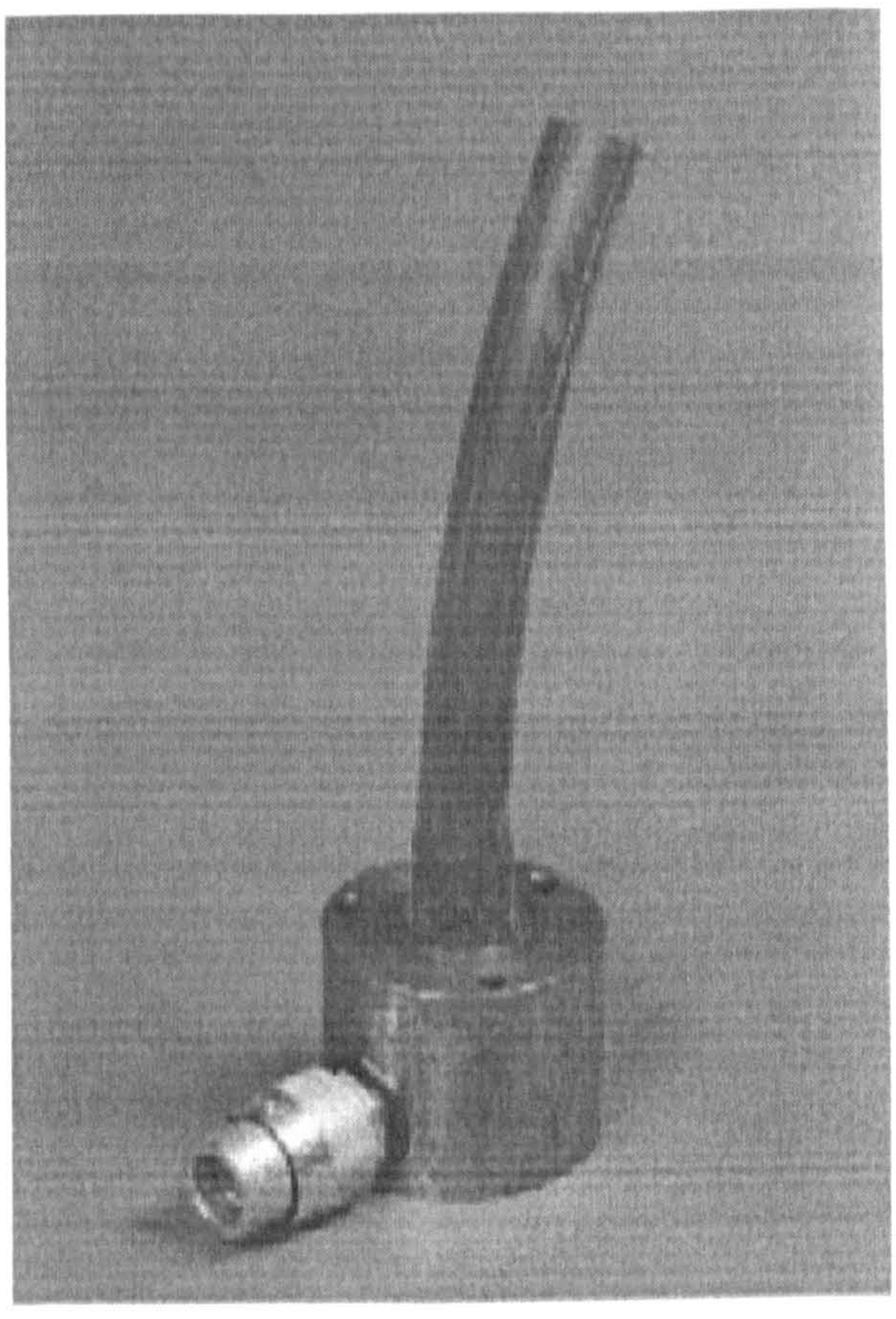

Figure 6.5

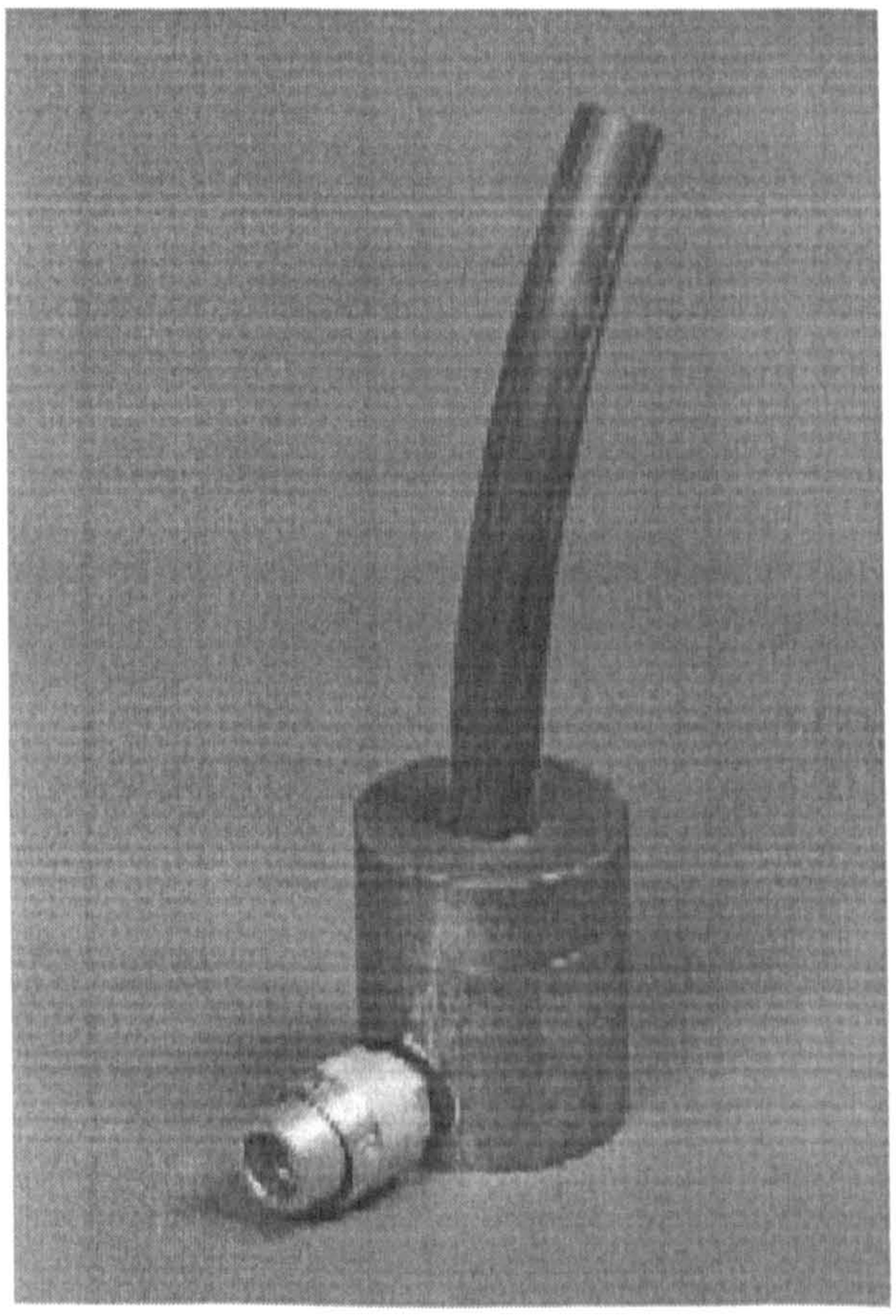

Figure 6.6

Then, the hollow end platen is inserted pinching the sleeve firmly between the platen inner surface and the spigot of the oil inlet platen. A perfect coupling and sealing between the two platens is achieved by bolting them together forcing the rubber O-ring on the end platen to actuate.

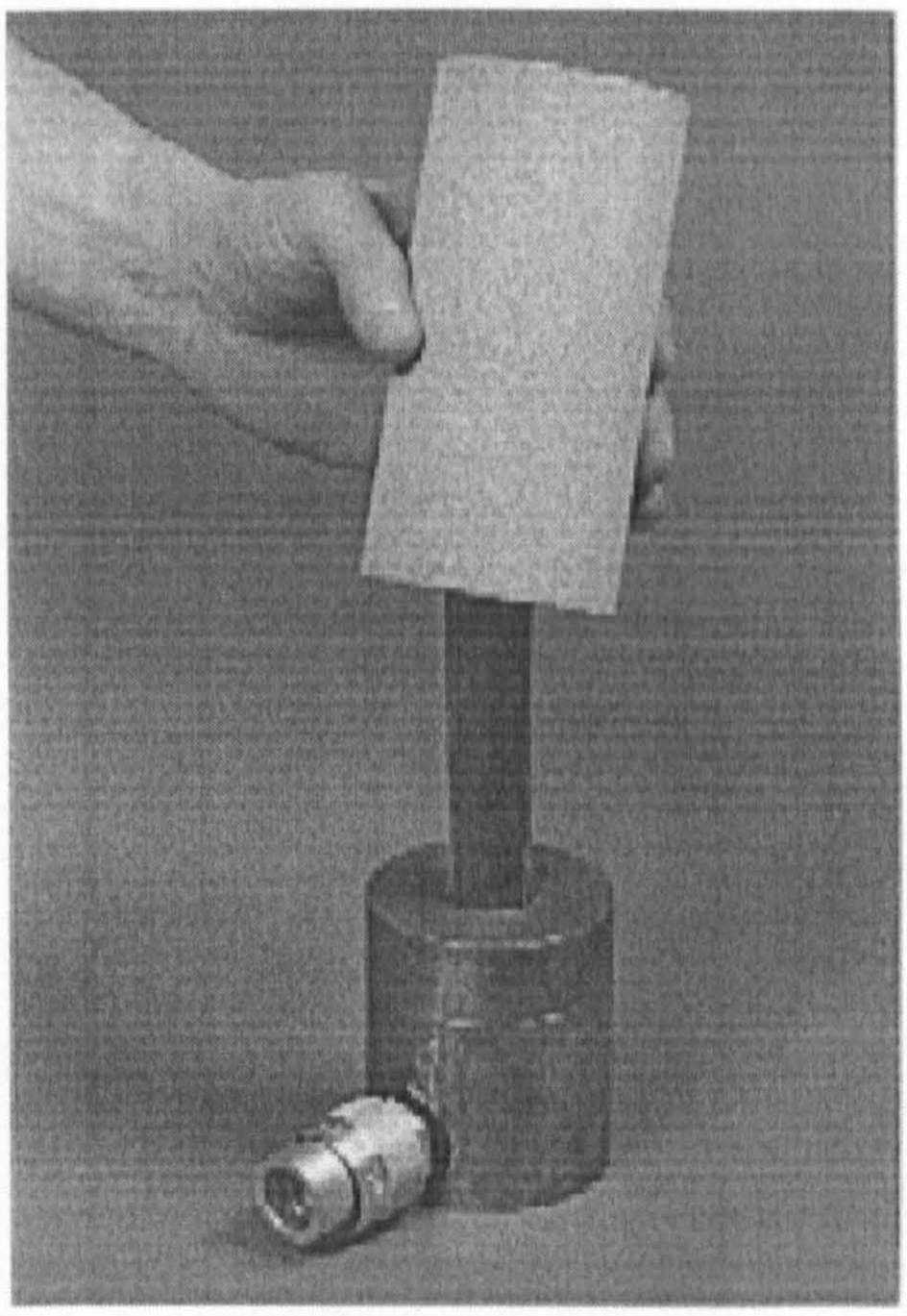

Figure 6.7

With the internal pressure arrangement being prepared from one end, the test specimen is placed in position passing the sleeve through the specimen hole.

Having positioned the test specimen, the top hollow end platen is laid with its sealing rubber O-ring located at the upper surface.

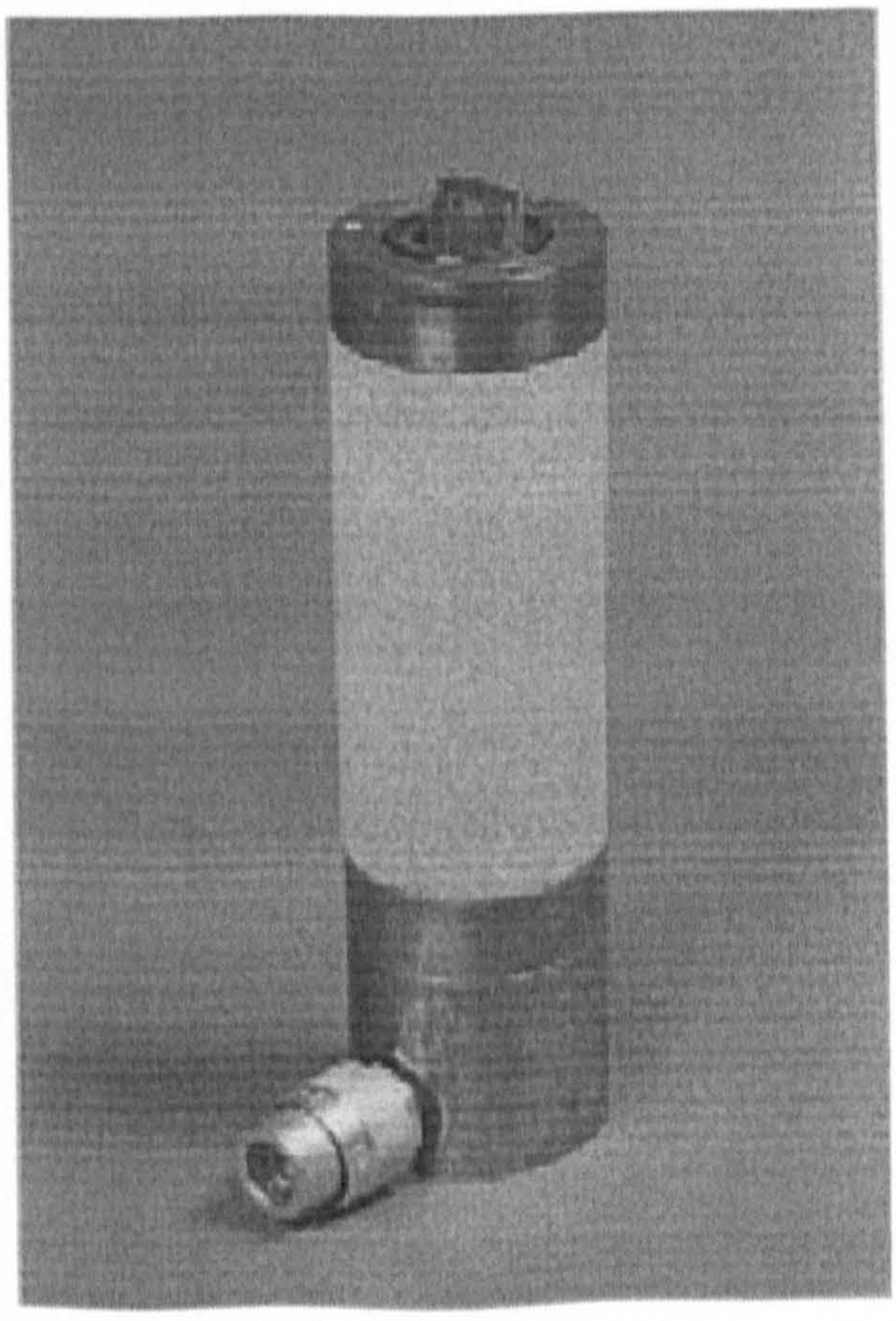

Figure 6.8

Subsequently, the inner cell is closed by fitting the other central platen, that contains the air bleed valve, propelling the spigot inside the rubber sleeve.

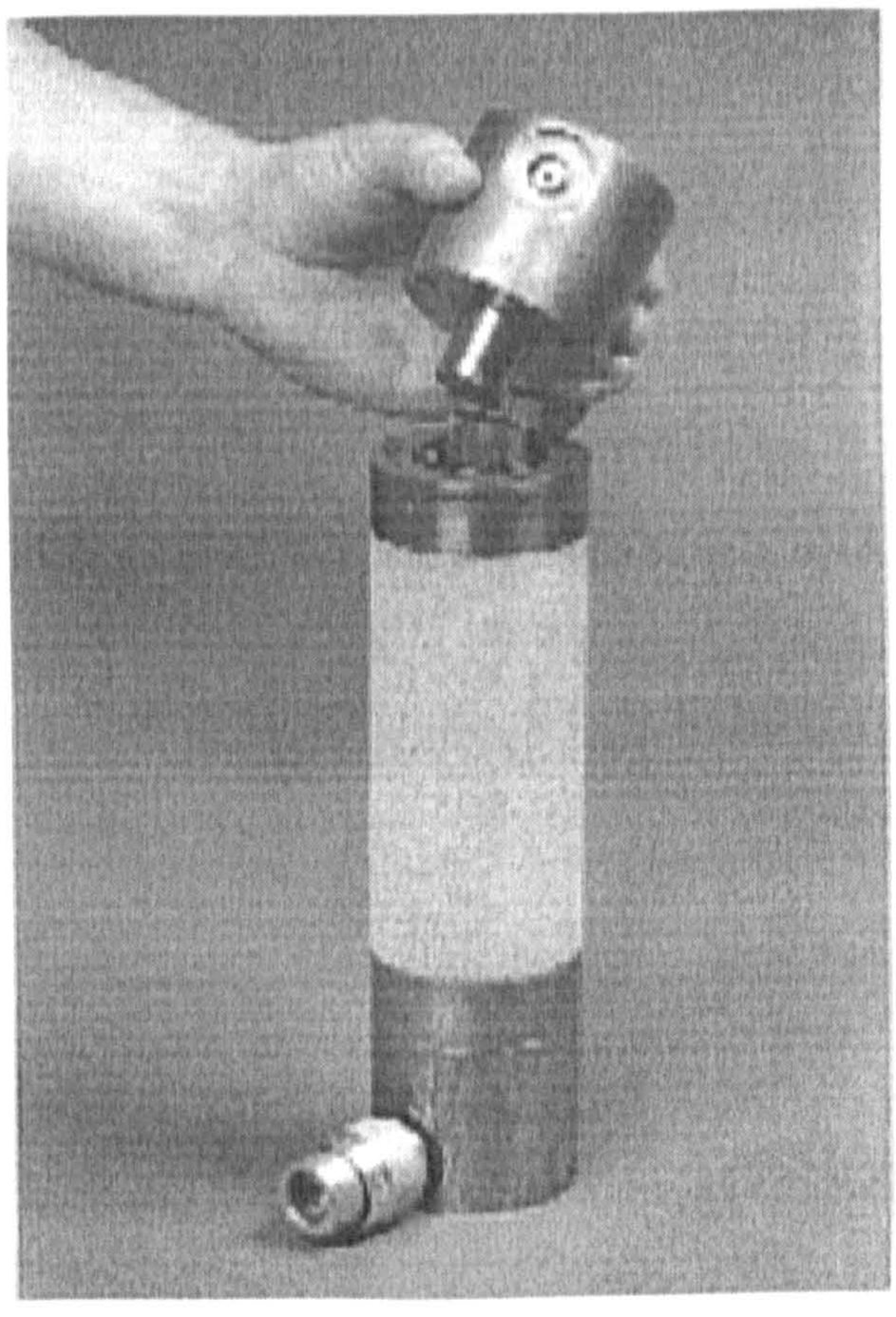

Figure 6.9

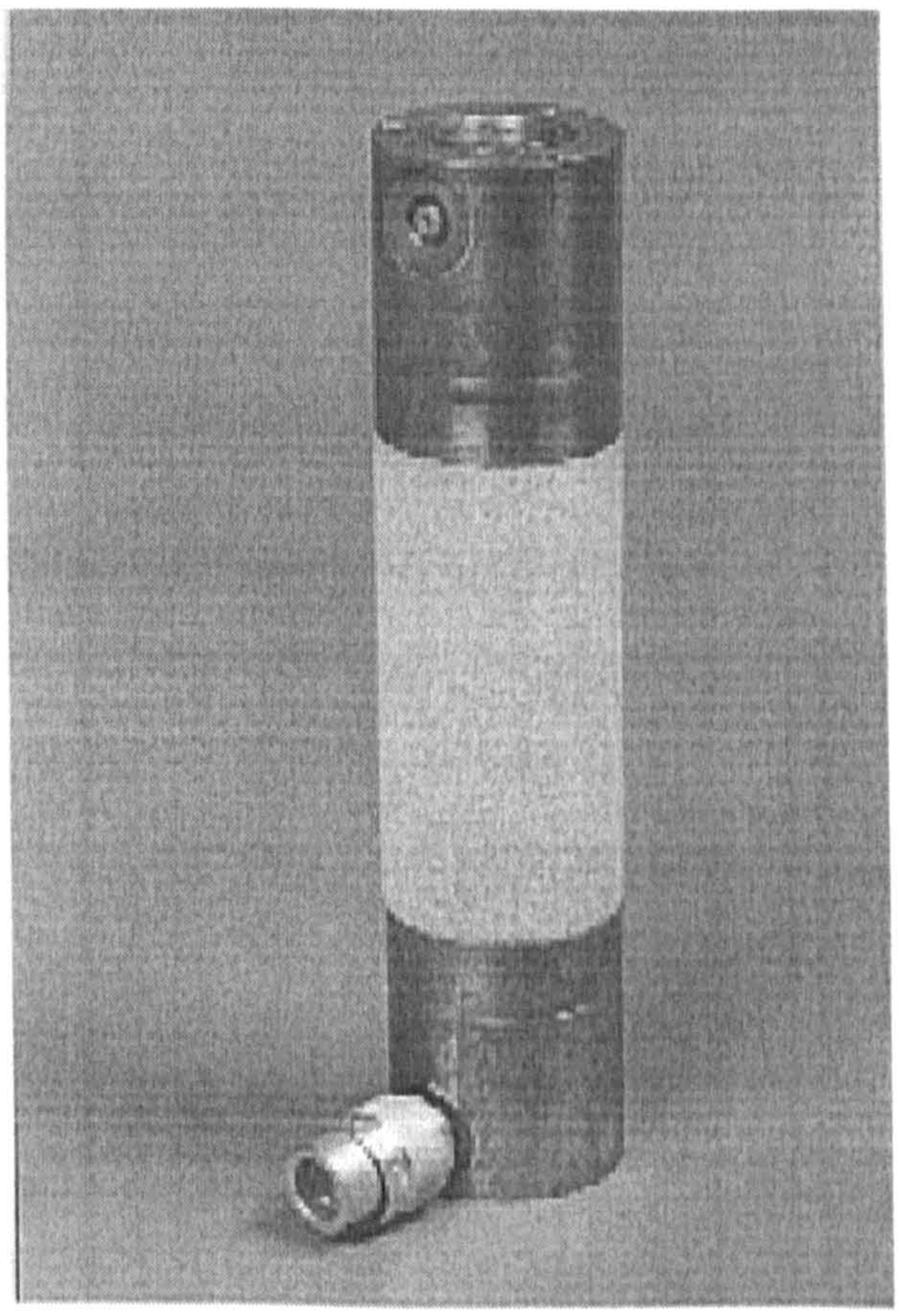

Figure 6.10

As in the case of the lower end, both the central platen and the hollow end one are bolted together actuating the rubber O-ring between them to ensure a positive sealing of the inner hole.

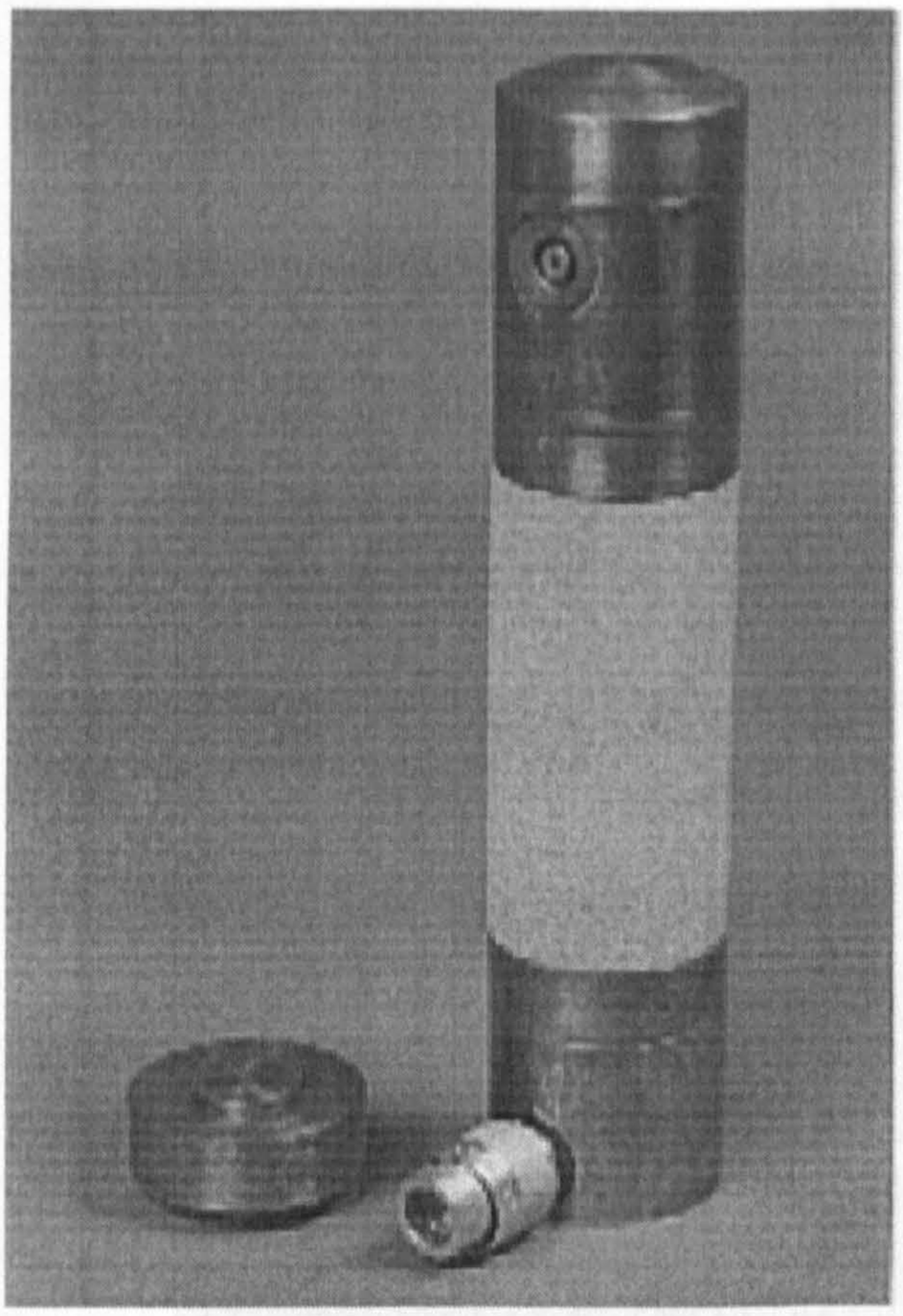

Figure 6.11

Upon assembling the specimen with the internal pressure configuration, the top spherical cap may be placed and the assembly is ready to be introduced into the Hoek cell.

Finally, the above assembly is carefully inserted in the Hoek cell and properly positioned ensuring that the specimen lies centrally in the cell. A sufficient level of external pressure is applied to hold the assembly in position while transferring the apparatus to the testing machine. Figure 6.13 summarises the foregoing steps, while Figure 6.14 shows the hollow cylinder apparatus mounted in the 5 MN testing machine.

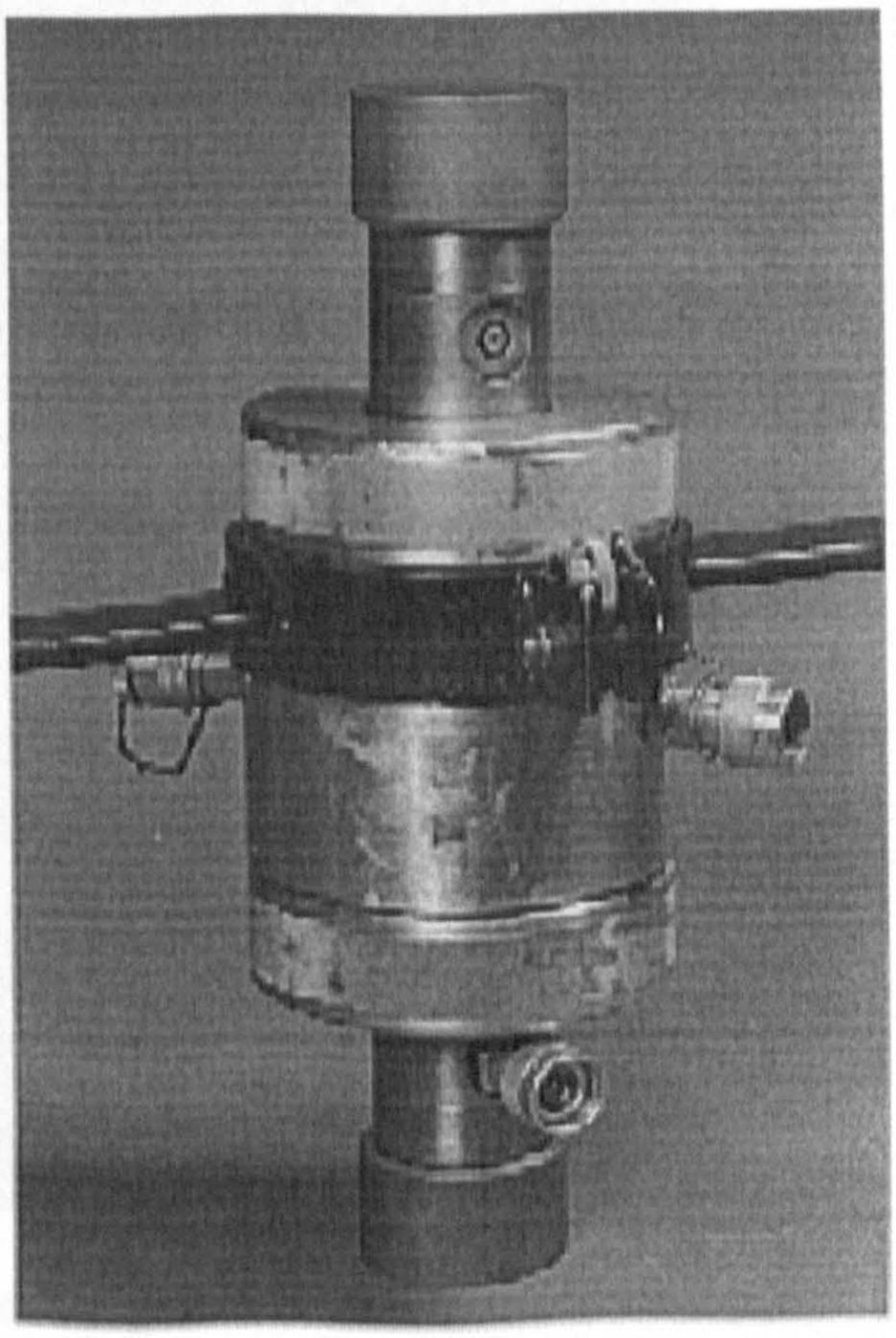

Figure 6.12

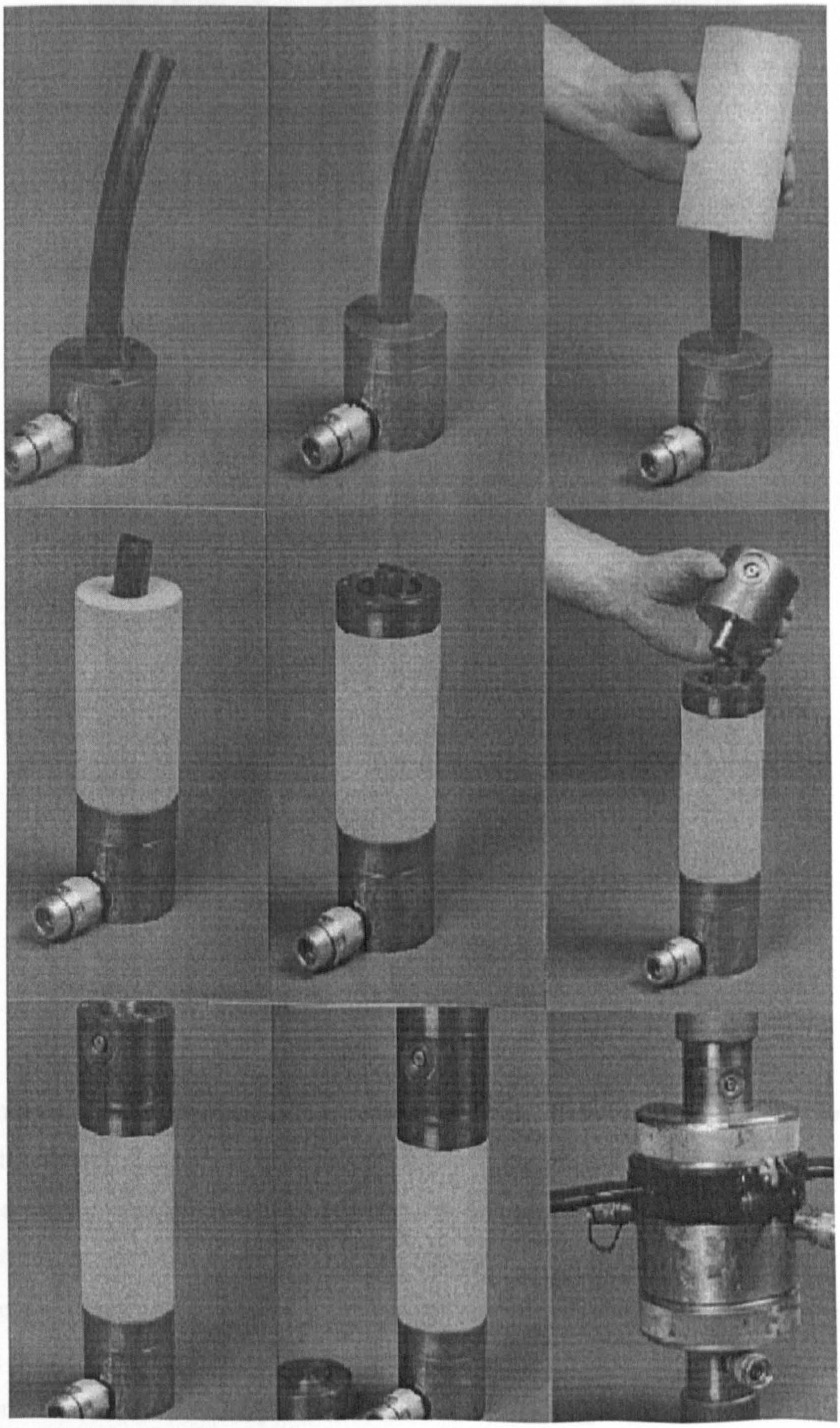

Figure 6.13 A summary of steps involved in assembling the test specimen with the hollow cylinder apparatus in preparation for testing.

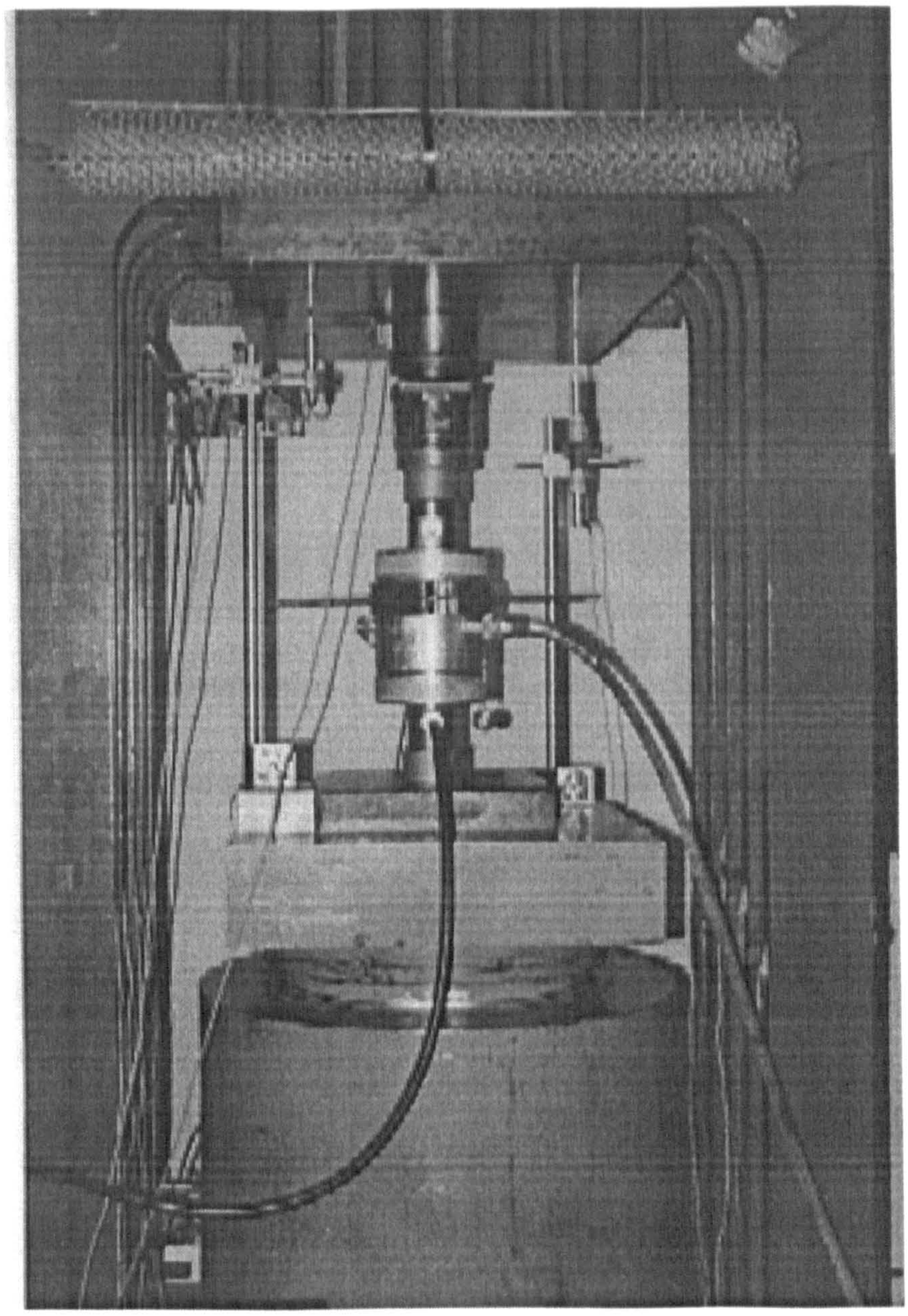

Figure 6.14 A view of the hollow cylinder test apparatus mounted in the 5 MN servo-controlled testing machine.

When mounting the cell in the testing machine, the spherical end cap was placed on top of the seating platen supplied with the Hoek cell and then the cell was positioned. Care was taken to ensure that the cell was properly levelled and centrally located on the bottom plate of the testing machine. Then, the top spherical cap was mated with the top seating platen of the Hoek cell. Two load cells of 1 MN capacity were incorporated on top of the seating platen: one was connected to the servo-controlled loading system and the other was connected to the data acquisition system for measuring the axial load. A transducer was mounted crosswise the LVDT of the loading system for measuring the axial deformation of the test specimen.

Prior to connecting to the pressure devices, the test apparatus was held stable by an axial seating compression of 0.5 MPa applied manually by the testing machine. Then, the external pressure power pack was connected and a pressure level of 0.5 MPa was applied after purging the confinement circuit of any trapped air. Following that, the pressure intensifier was connected to the internal pressure inlet and oil was pumped to fill the inner membrane allowing the air to escape through the bleeding valve. Upon completion, the bleeding valve was sealed and an internal pressure level of 0.5 MPa was retained. It is worth noting that these initial values of internal and external pressures together with the initial axial stress correspond to the initial compressive stress state imposed on the cubical specimens tested under polyaxial compression.

At this stage, the X-Y recorders were prepared, execution of the data acquisition commenced, all input devices were initialised and the test was ready to run. As in the cubical specimen tests, the data acquisition system was set up to directly convert load and deformation measurements to stress values in MPa and strain (%), respectively. Measurements were acquired at time intervals of 3 s, displayed on the PC monitor and stored in a data file.

Loading of the test specimen was based on subjecting it to increasing axial load and appropriate levels of internal and external pressures selected to induce at the specimen inner surface a predetermined principal stress field calculated from the theory of elasticity, 6.2.1. The loading-unloading procedure was quite similar to that described in Chapter 5 for the cubical specimen tests. Furthermore, in agreement with the cubical tests, all hollow cylinder compression tests were carried out under a constant axial strain rate of 0.25% / min, and the servo-controlled testing machine was regulated to follow a prescribed loading sequence of a selected maximum ramp time of 2×10^3 s and a maximum output displacement level calculated as follows:

$$\text{output level} = \text{strain rate} \times \text{specimen height} \times \text{ramp time}$$

6.4 Polyaxial Compression Tests - First Series

6.4.1 Outline of the Tests

The first experimental series on thick-walled hollow cylinders of Springwell sandstone involved a total of forty specimens loaded to failure under polyaxial compression. Different combinations of external and internal hydrostatic pressure levels were applied to induce at the specimen inner wall a predetermined principal stress field in which the axial stress is the major principal stress, $\sigma_z = \sigma_1$, the tangential stress is the intermediate principal stress, $\sigma_\theta = \sigma_2$, and the radial stress is the minor principal stress, $\sigma_r = \sigma_3$, corresponding to the arrangement:

$$\sigma_z = \sigma_1 > \sigma_\theta = \sigma_2 > \sigma_r = \sigma_3 > 0$$

Table 6.1 presents details of the applied levels of external and internal pressures in each test and the corresponding values of tangential and radial stresses calculated at the specimen inner wall on the basis of the theory of elasticity as described in 6.2.1.

6.4.2 The Experimental Results

A representative plot of a thick-walled hollow cylinder polyaxial loading sequence is shown in Figure 6.15 in which the applied internal pressure, P_i, external pressure, P_o, and axial stress, F / A, where F is the axial load and A is the cross-sectional area of the specimen, are plotted versus time. Figure 6.16 shows the same loading sequence in terms of the corresponding principal stresses, $\sigma_r = \sigma_3$, $\sigma_\theta = \sigma_2$, $\sigma_z = \sigma_1$, induced at the cylinder inner wall. Plots of the major principal stress, $\sigma_z = \sigma_1$, versus the major principal strain, $\varepsilon_z = \varepsilon_1$, are grouped according to the level of the minor principal stress, $\sigma_r = \sigma_3$, and presented in Figures 6.17 to 6.19. Similar plots are grouped according to the level of the intermediate principal stress, $\sigma_\theta = \sigma_2$, and presented in Figures 6.20 to 6.22.

Following the procedure described in 6.2.4, acquired values of the volumetric change of the specimen hole, ΔV_h, have been used to calculate the tangential strain, $\varepsilon_\theta = \varepsilon_2$, and

Table 6.1 Applied levels of external and internal pressures, P_o and P_i, and corresponding values of tangential and radial stresses, σ_θ and σ_r, at the specimen inner surface for the first polyaxial test series on thick-walled hollow cylinders of Springwell sandstone.

Specimen No.	P_o, MPa	P_i, MPa	$\sigma_\theta = \sigma_2$, MPa	$\sigma_r = \sigma_3$, MPa
HPG1	7.176	5	10	5
HPG2	7.176	5	10	5
HPG3	11.528	5	20	5
HPG4	11.528	5	20	5
HPG5	15.880	5	30	5
HPG6	15.880	5	30	5
HPG7	15.880	5	30	5
HPG8	20.232	5	40	5
HPG9	20.232	5	40	5
HPG10	24.584	5	50	5
HPG11	24.584	5	50	5
HPG12	12.176	10	15	10
HPG13	12.176	10	15	10
HPG14	14.352	10	20	10
HPG15	14.352	10	20	10
HPG16	18.704	10	30	10
HPG17	18.704	10	30	10
HPG18	18.704	10	30	10
HPG19	23.056	10	40	10
HPG20	23.056	10	40	10
HPG21	27.408	10	50	10
HPG22	27.408	10	50	10
HPG23	21.528	15	30	15
HPG24	21.528	15	30	15
HPG25	28.056	15	45	15
HPG26	28.056	15	45	15
HPG27	24.352	20	30	20
HPG28	24.352	20	30	20
HPG29	28.704	20	40	20
HPG30	28.704	20	40	20
HPG31	33.056	20	50	20
HPG32	33.056	20	50	20
HPG33	35.880	25	50	25
HPG34	35.880	25	50	25
HPG35	34.352	30	40	30
HPG36	34.352	30	40	30
HPG37	38.704	30	50	30
HPG38	38.704	30	50	30
HPG39	44.352	40	50	40
HPG40	44.352	40	50	40

radial strain, $\varepsilon_r = \varepsilon_3$, at the specimen inner walls. Figure 6.23 shows a typical plot of the measured values of the major principal strain, $\varepsilon_z = \varepsilon_1$, versus ε_θ, ε_r, and the volumetric strain of the hole, ε_{vh}, for specimen HPG10 which was subjected to an external pressure level of $P_o = 24.584$ MPa and an internal pressure level of $P_i = 5$ MPa, corresponding to intermediate principal stress level of $\sigma_\theta = \sigma_2 = 50$ MPa and minor principal stress level of $\sigma_r = \sigma_3 = 5$ MPa.

It should be noted that, at the beginning of the test and while the internal pressure was being applied simultaneously with both the external pressure and the axial load, it was not possible to monitor the volumetric change of the specimen hole. Therefore, as can be seen in Figure 6.23, the value $\varepsilon_{vh} = 0$ and related values of ε_θ and ε_r correspond to the point at which the prescribed level of P_i was reached and some axial displacement had taken place.

Specimen failure was generally marked by audible cracking accompanied by a pronounced fall in the level of the axial stress and a noticeable deviation in the volumetric change of the specimen hole. The nature of failure was predominantly shear resulting generally in a single fracture plane inclined at about 40° to the direction of the axial principal stress. Shear cones were also evident in a number of tests, and some specimens exhibited what appeared to be extensile fractures or specimen separation along the direction of the axial stress. Representative failure patterns are pictured in Figures 6.25 to 6.27, while the mode of failure observed in each individual test is described in Table 6.2.

In order to examine the initiation of failure, three tests were terminated as soon as the major principal stress reached its peak level. Subsequently, the test specimens were sawn into halves along their longitudinal axis and closely examined for any signs of early structural damage. There appeared to be evidence of minor spalling forming a minutely flaked circular region at about mid-height of the specimen inner wall. Furthermore, as Figure 6.28 shows, initial cracks could be observed laying diagonally at opposite sides of the hole and running across the specimen wall. These cracks appeared more visible at the inner surface of the specimen walls than at the outer surface.

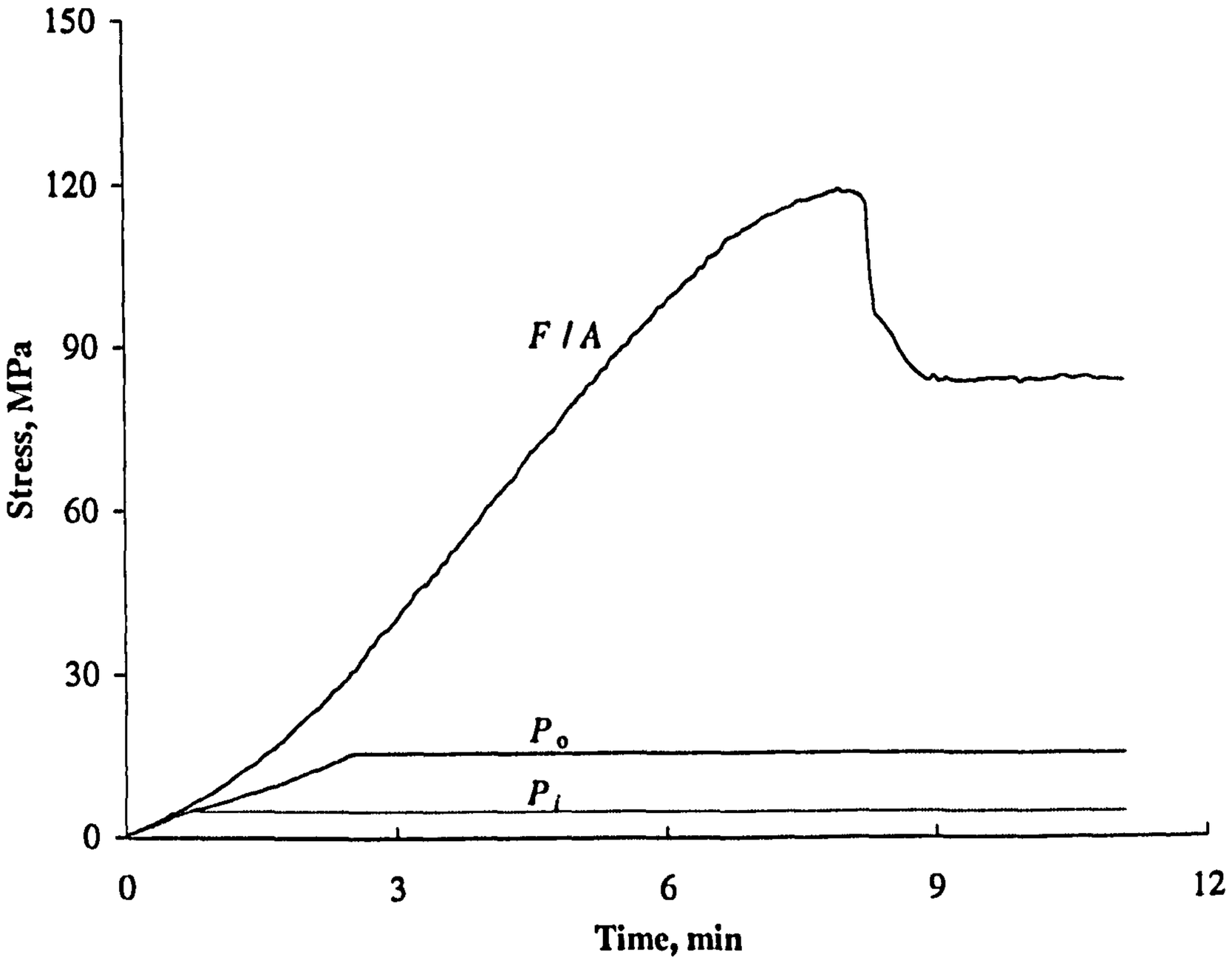

Figure 6.15 A typical loading sequence for the first polyaxial test series on hollow cylinders plotted in terms of applied internal pressure, P_i, external pressure, P_o, and axial stress, F / A, versus time.

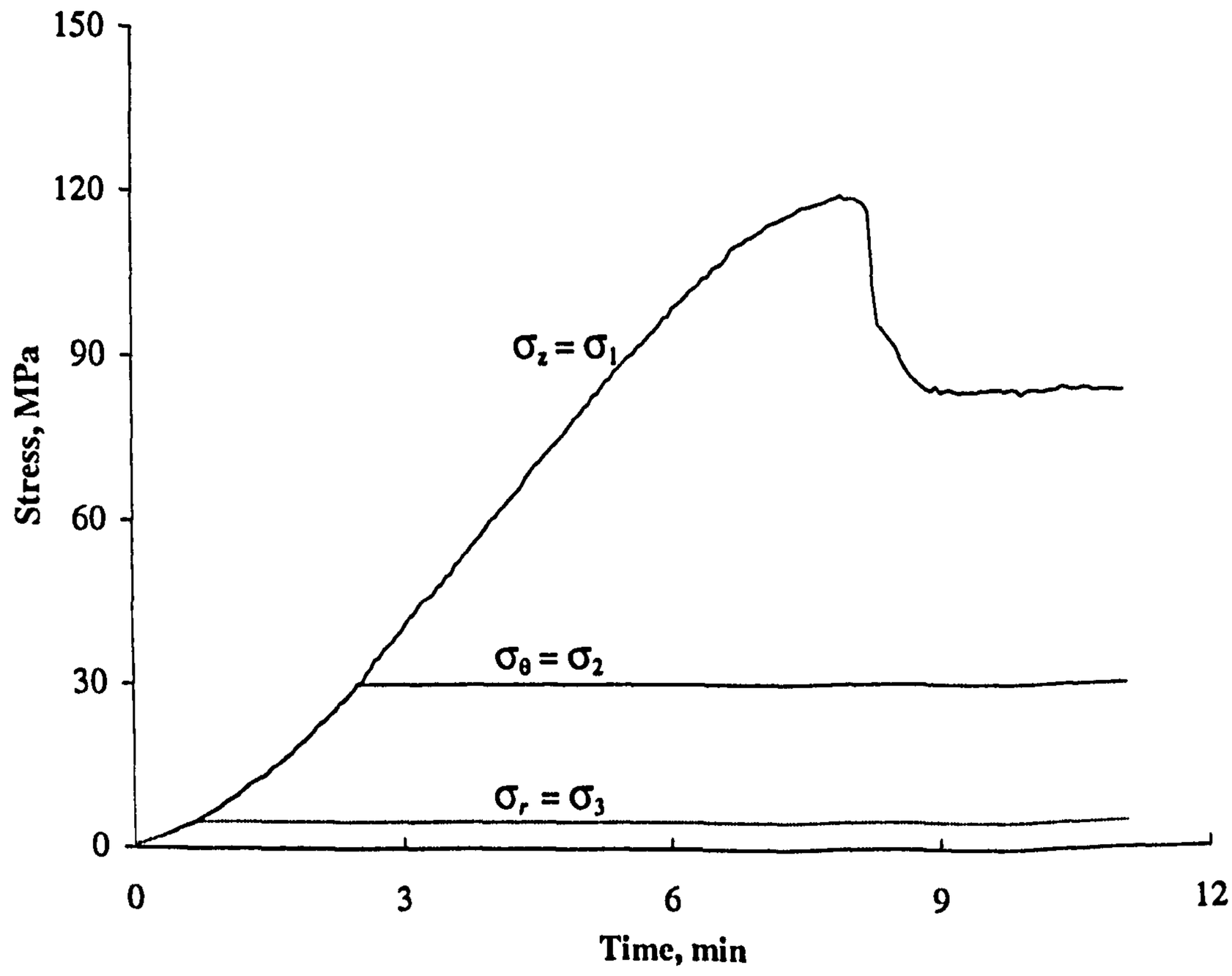

Figure 6.16 The above loading sequence in terms of the corresponding principal stresses, $\sigma_r = \sigma_3$, $\sigma_\theta = \sigma_2$, $\sigma_z = \sigma_1$, induced at the cylinder inner wall.

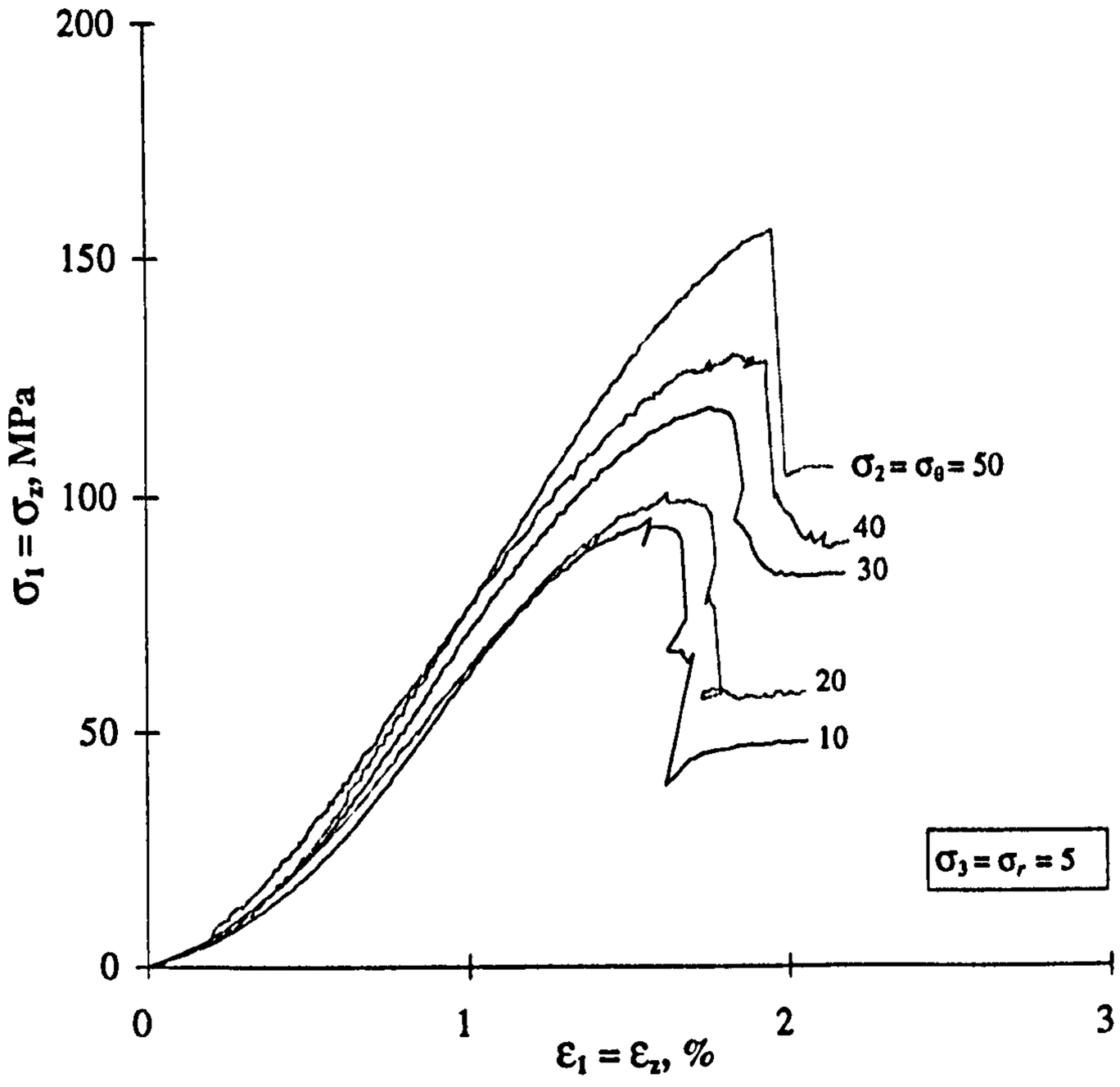

Figure 6.17 Major principal stress, $\sigma_1 = \sigma_z$, versus major principal strain, $\varepsilon_1 = \varepsilon_z$, for different levels of intermediate principal stress, $\sigma_2 = \sigma_\theta$, and minor principal stress level of $\sigma_3 = \sigma_r = 5$ MPa.

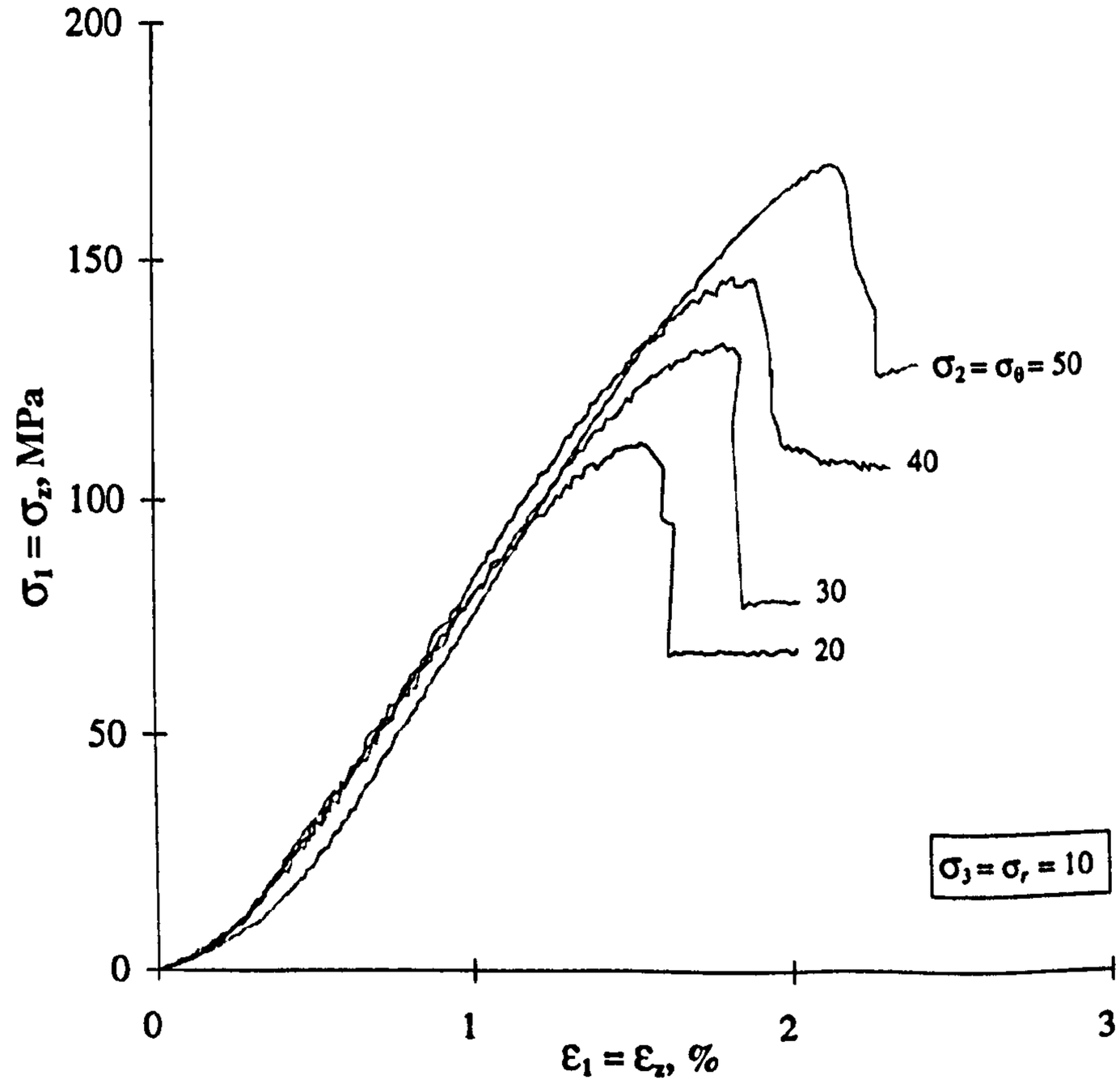

Figure 6.18 Major principal stress, $\sigma_1 = \sigma_z$, versus major principal strain, $\varepsilon_1 = \varepsilon_z$, for different levels of intermediate principal stress, $\sigma_2 = \sigma_\theta$, and minor principal stress level of $\sigma_3 = \sigma_r = 10$ MPa.

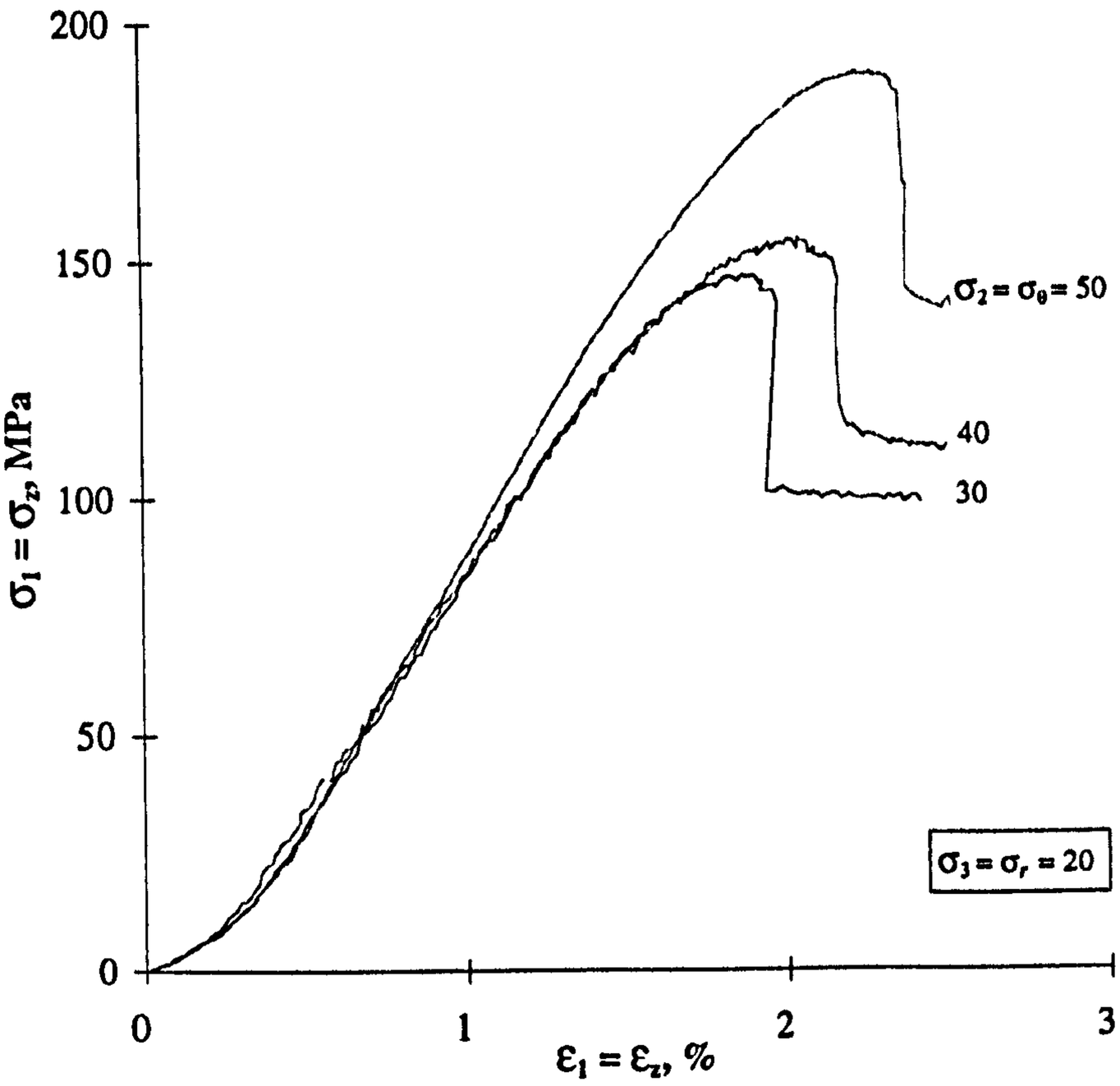

Figure 6.19 Major principal stress, $\sigma_1 = \sigma_z$, versus major principal strain, $\varepsilon_1 = \varepsilon_z$, for different levels of intermediate principal stress, $\sigma_2 = \sigma_\theta$, and minor principal stress level of $\sigma_3 = \sigma_r = 20$ MPa.

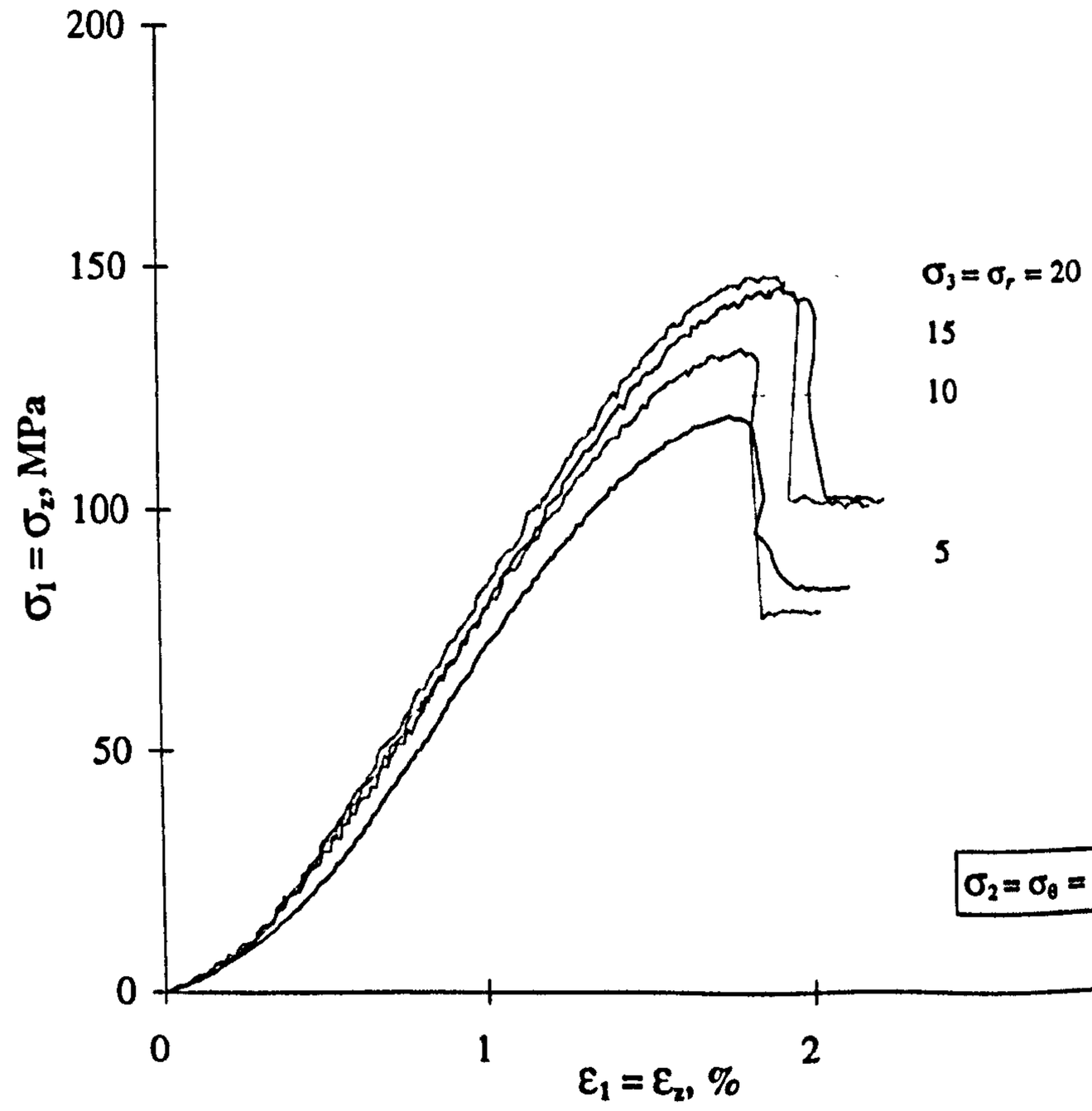

Figure 6.20 Major principal stress, $\sigma_1 = \sigma_z$, versus major principal strain, $\varepsilon_1 = \varepsilon_z$, for different levels of minor principal stress, $\sigma_3 = \sigma_r$, and intermediate principal stress level of $\sigma_2 = \sigma_\theta = 30$ MPa.

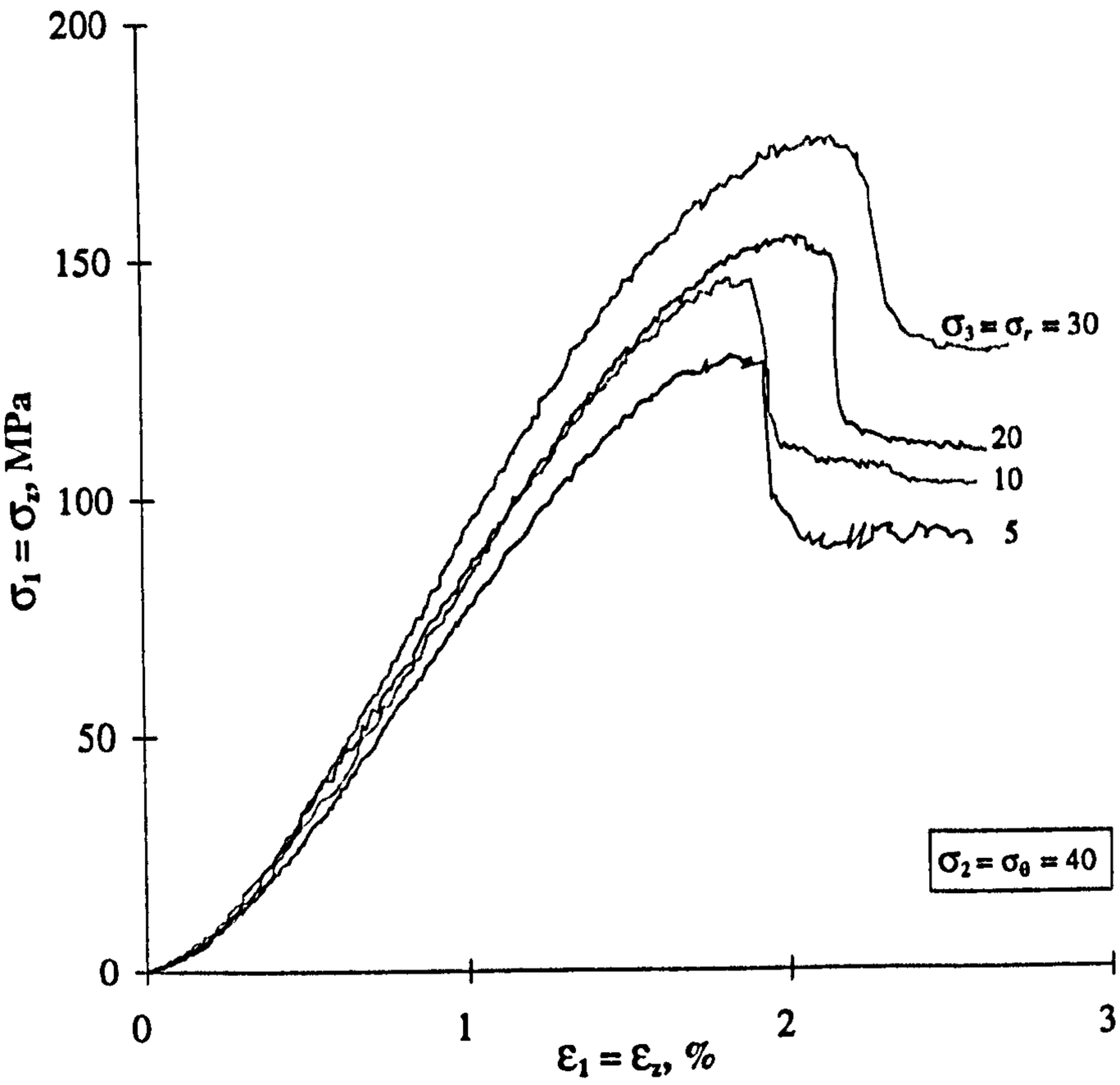

Figure 6.21 Major principal stress, $\sigma_1 = \sigma_z$, versus major principal strain, $\varepsilon_1 = \varepsilon_z$, for different levels of minor principal stress, $\sigma_3 = \sigma_r$, and intermediate principal stress level of $\sigma_2 = \sigma_\theta = 40$ MPa.

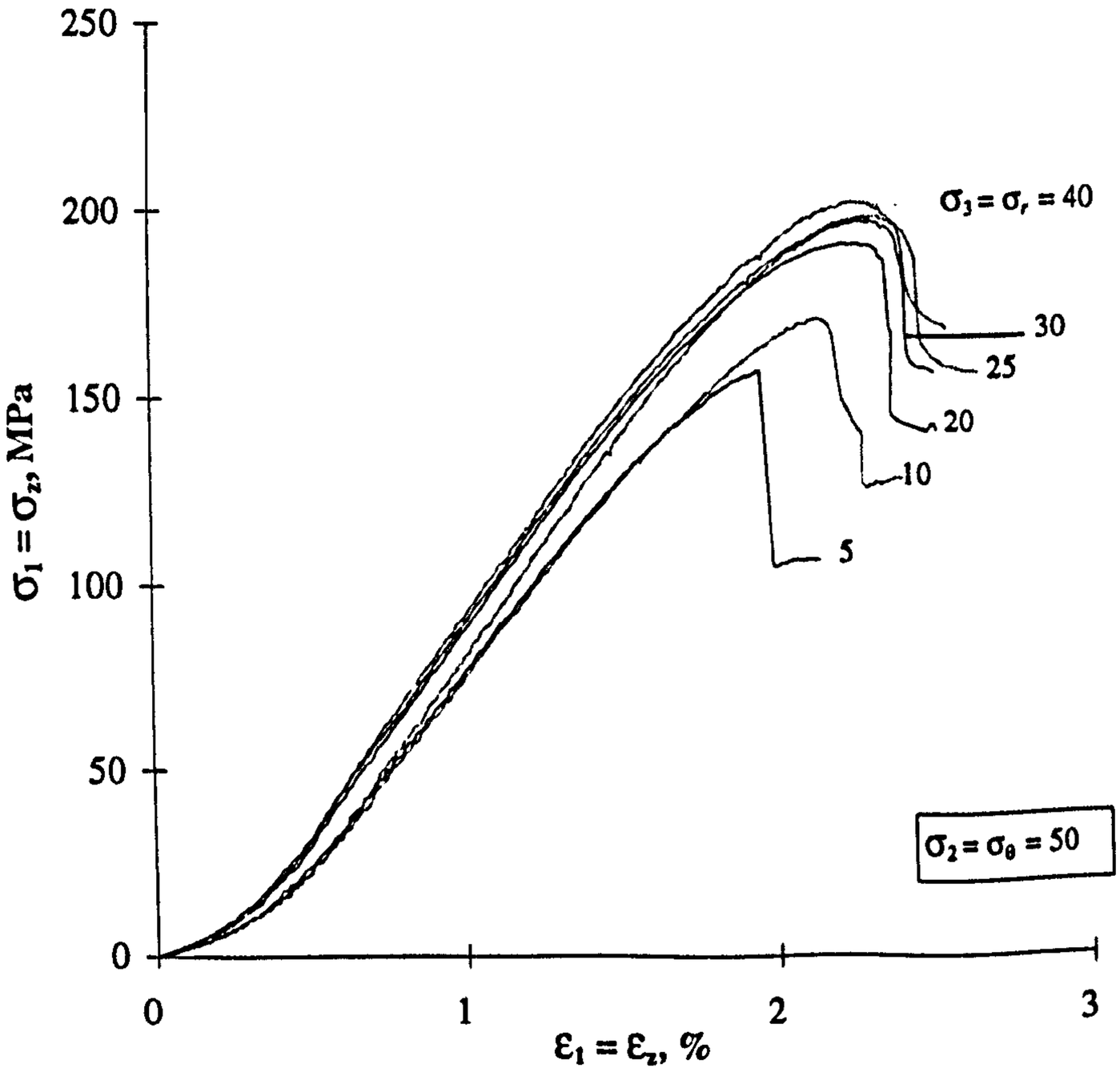

Figure 6.22 Major principal stress, $\sigma_1 = \sigma_z$, versus major principal strain, $\varepsilon_1 = \varepsilon_z$, for different levels of minor principal stress, $\sigma_3 = \sigma_r$, and intermediate principal stress level of $\sigma_2 = \sigma_\theta = 50$ MPa.

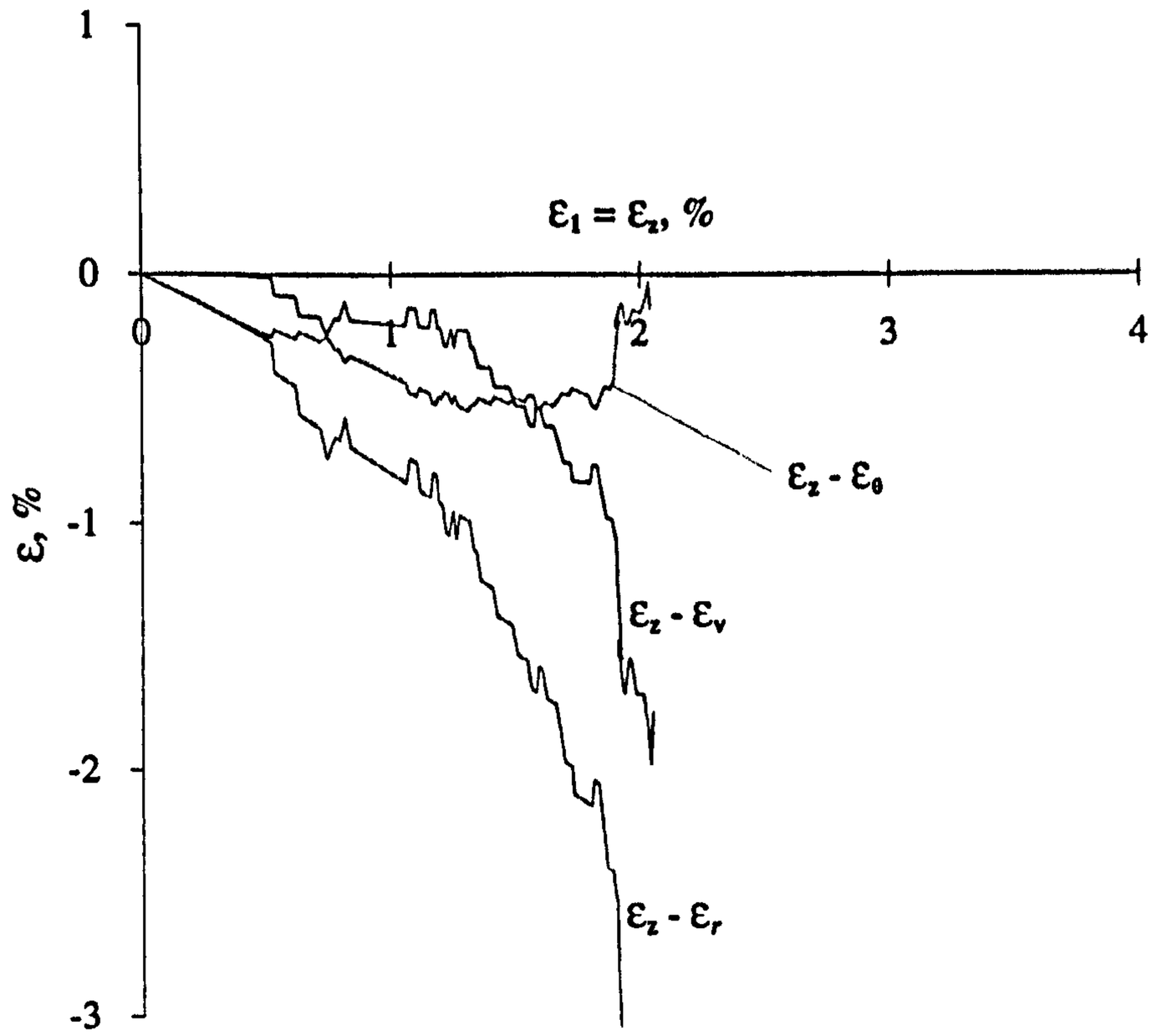

Figure 6.23 Typical curves of major principal strain, $\varepsilon_z = \varepsilon_1$, versus tangential strain, $\varepsilon_\theta = \varepsilon_2$, radial strain, $\varepsilon_r = \varepsilon_3$, and volumetric strain, ε_{vh}, at the specimen inner walls.

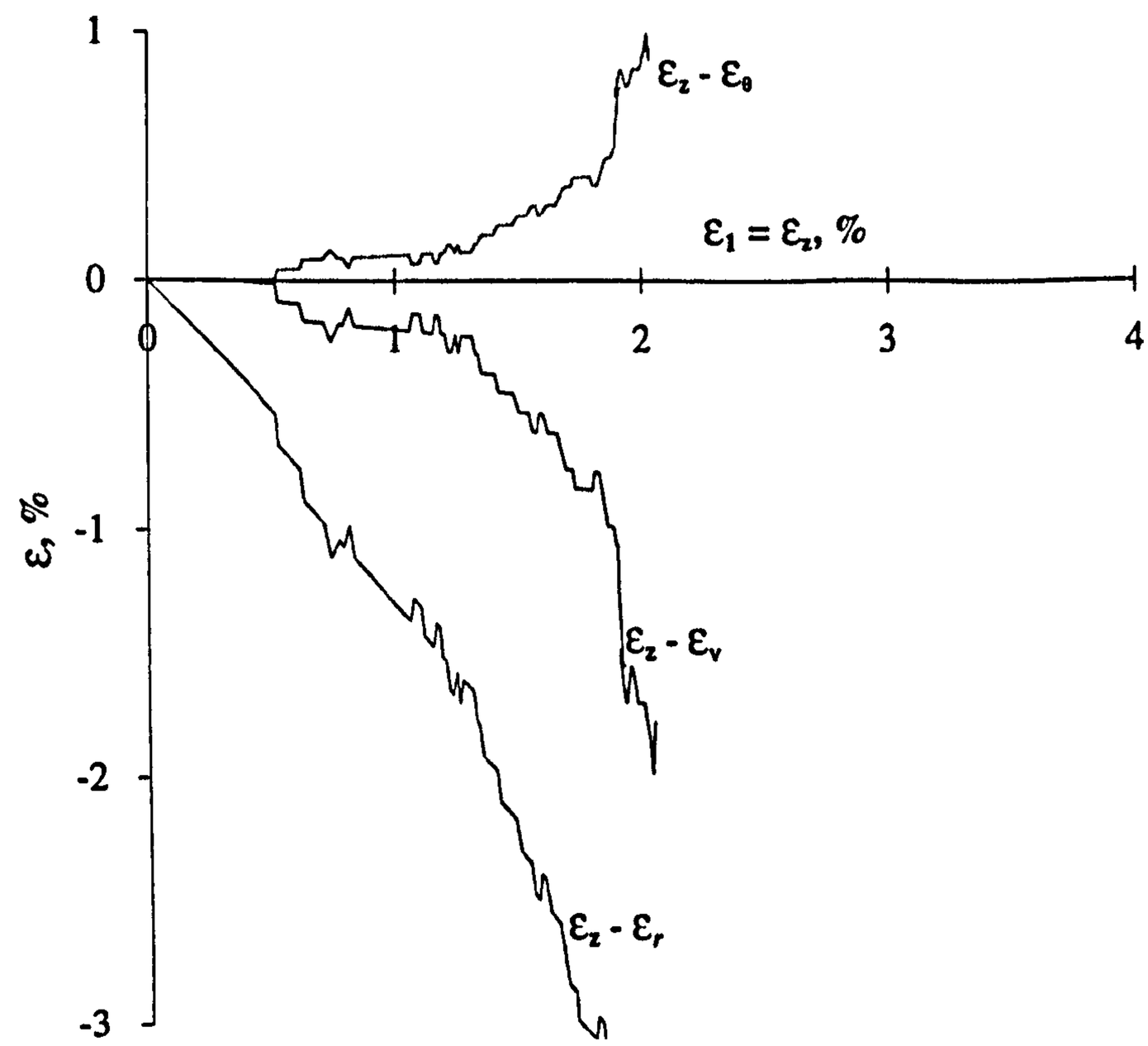

Figure 6.24 The same curves shown above reproduced ignoring the specimen axial deformation when calculating the radial deformation of the hole.

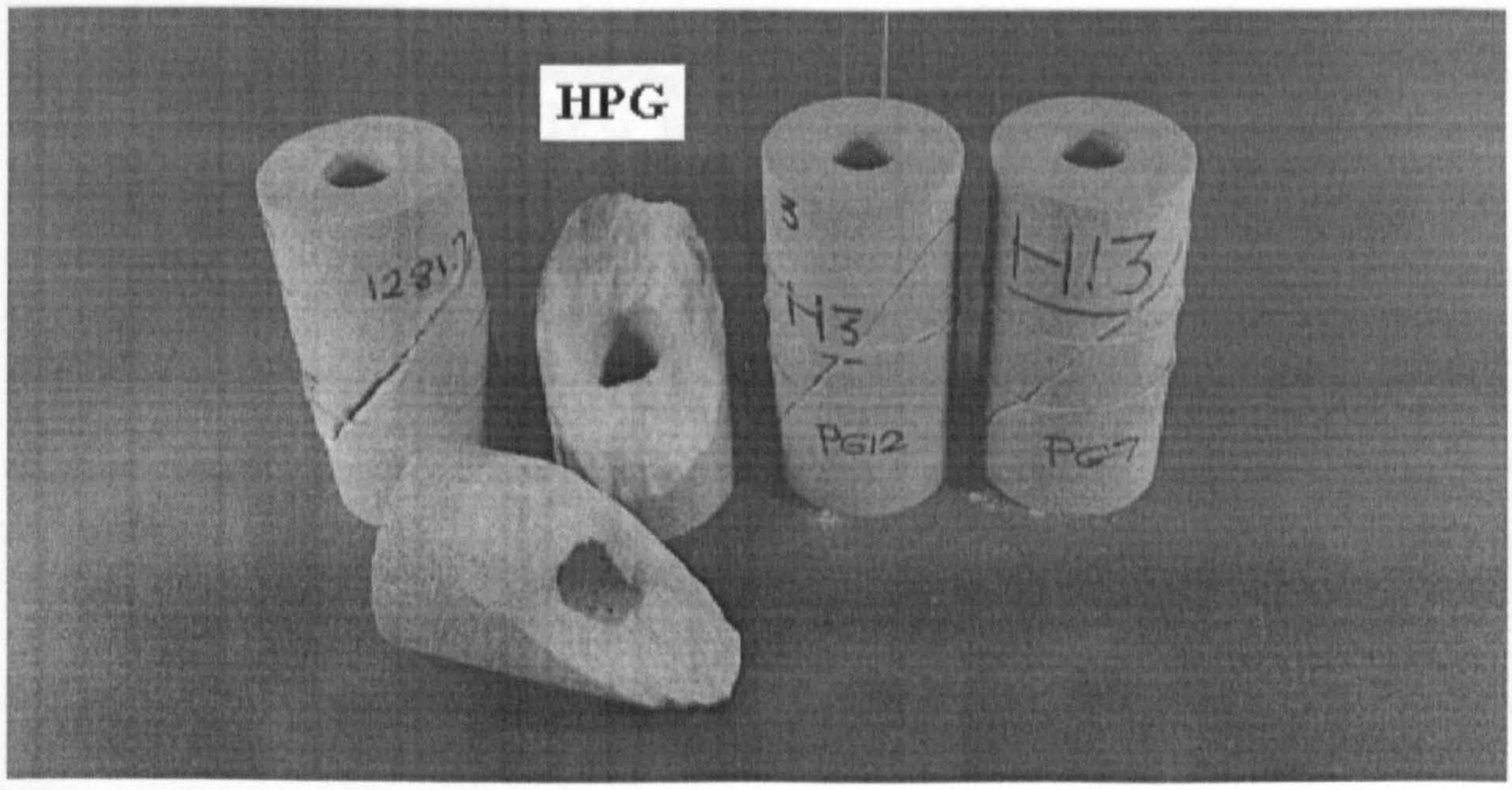

Figure 6.25 Failure of thick-walled hollow cylinders along single inclined shear fractures in polyaxial compression tests in which $\sigma_1 = \sigma_z > \sigma_2 = \sigma_\theta > \sigma_3 = \sigma_r > 0$.

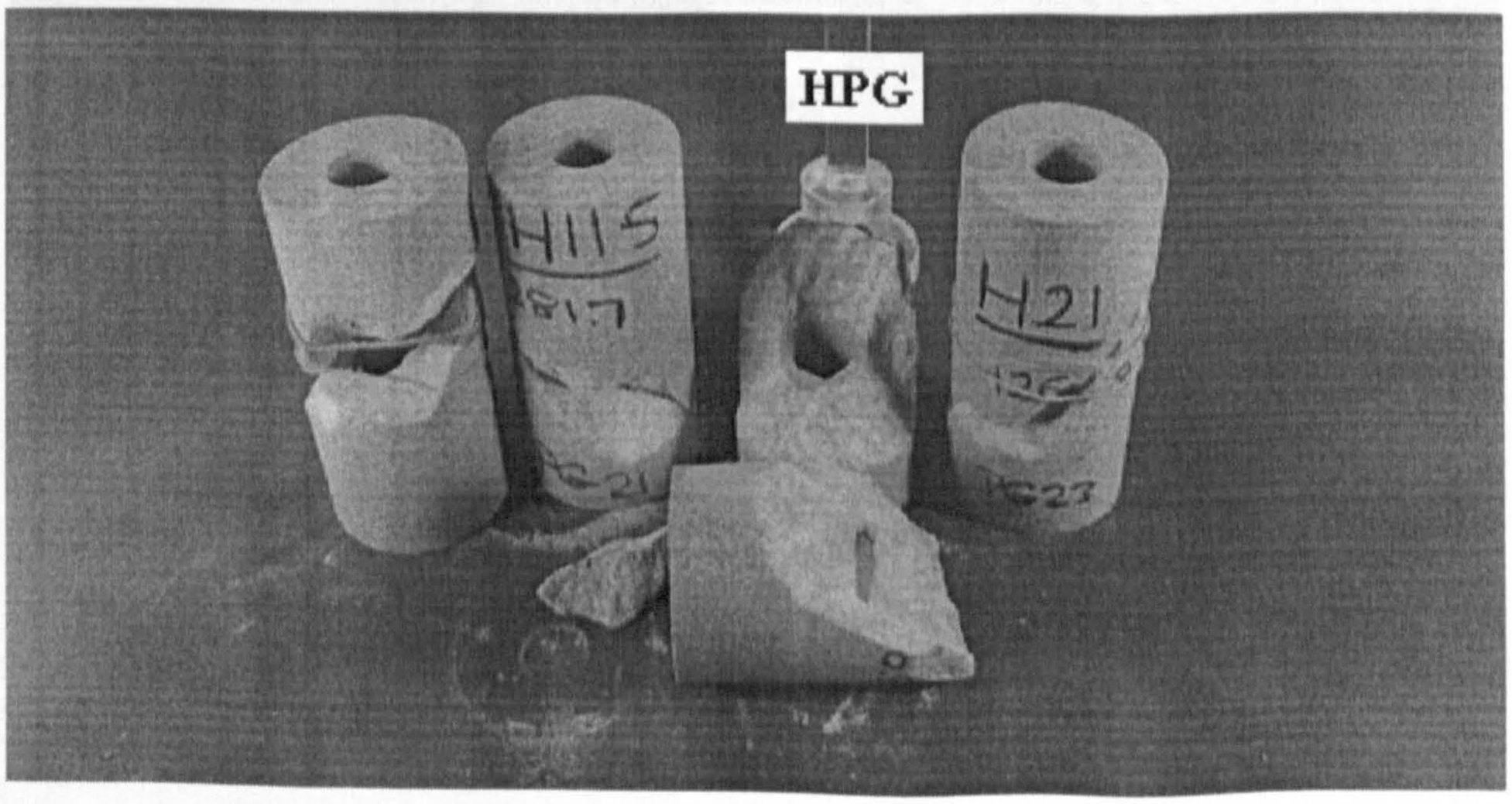

Figure 6.26 Typical failure modes dominated by shear cones

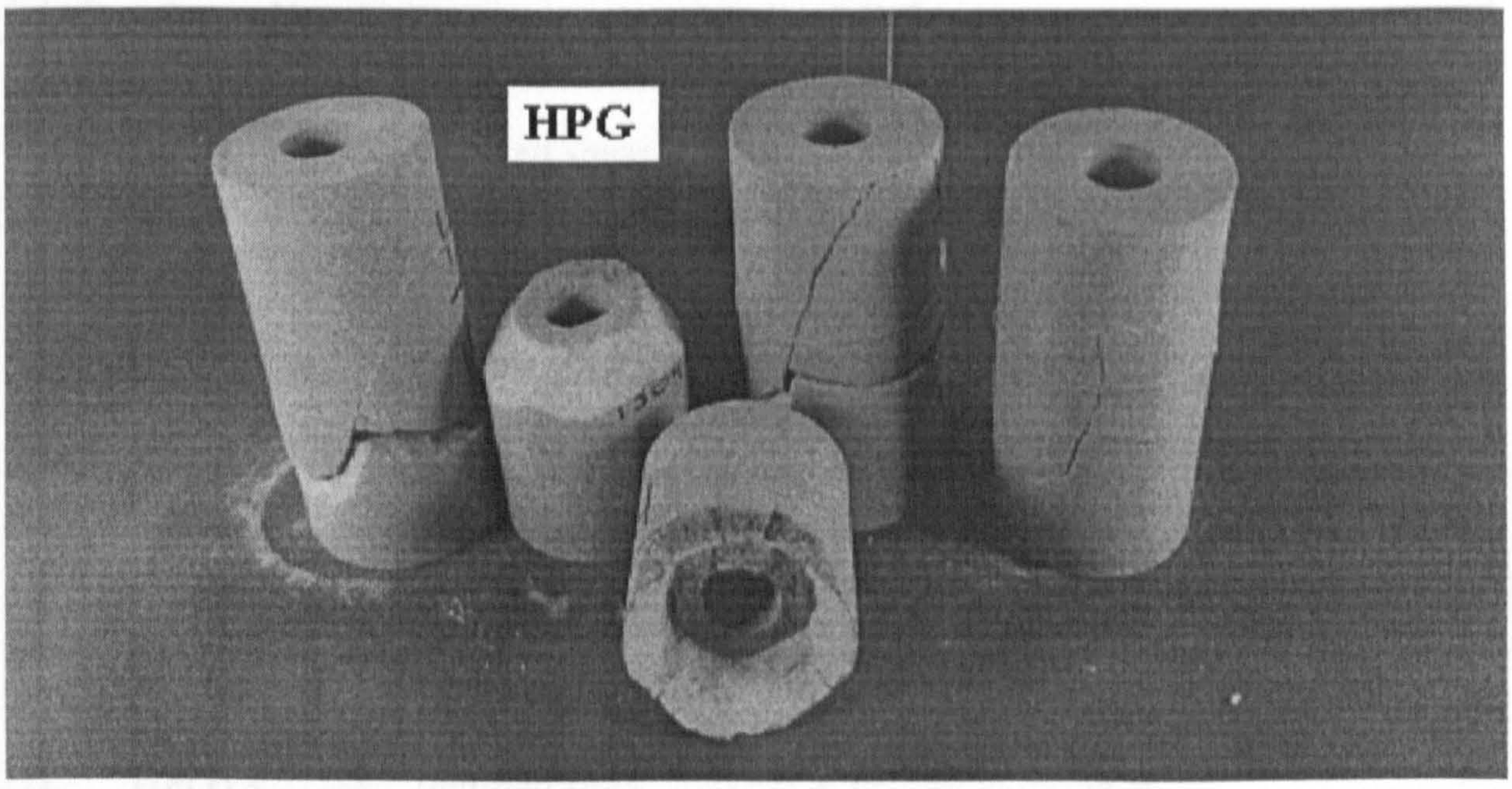

Figure 6.27 Multiple fractures with evidence of separation along the axial direction.

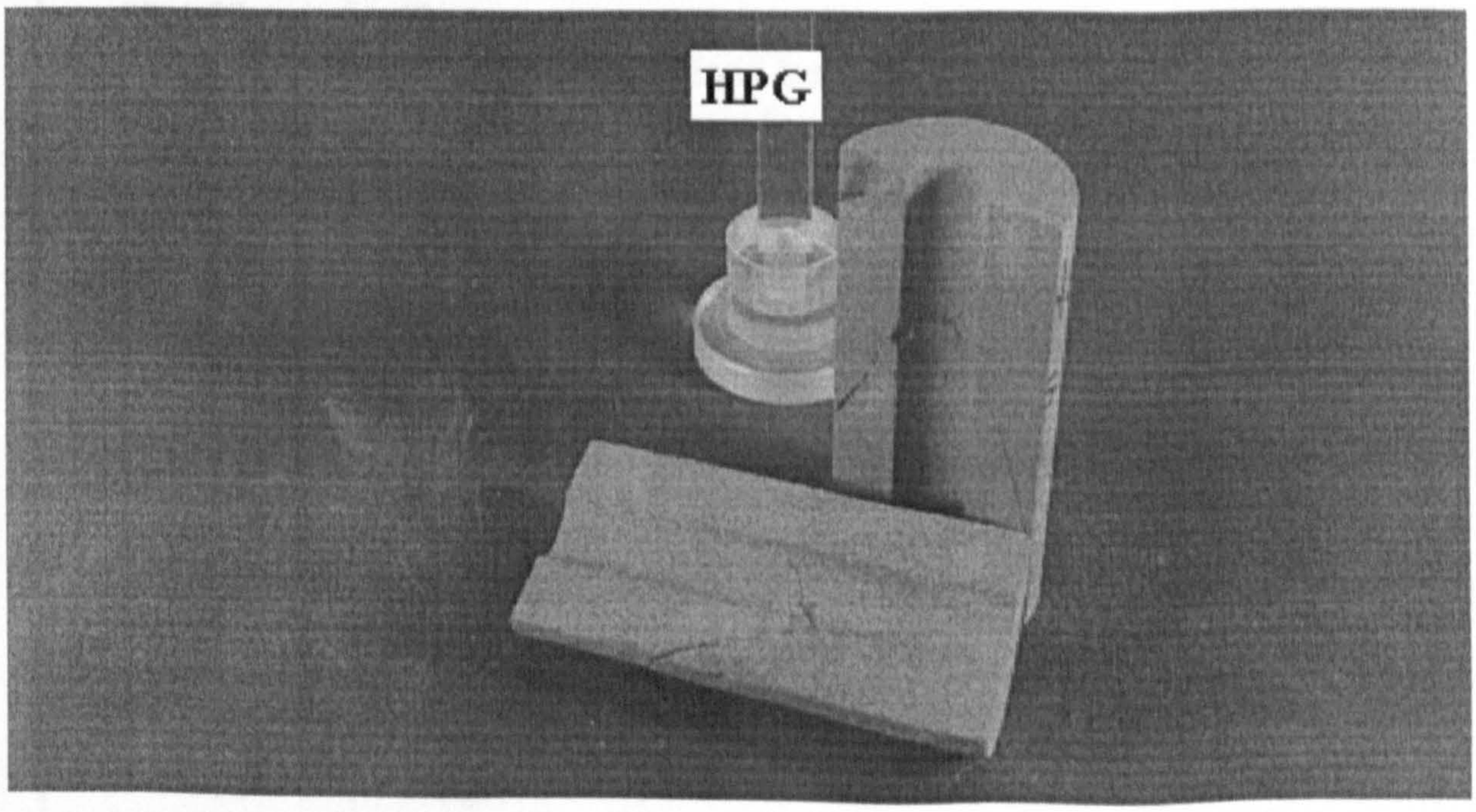

Figure 6.28 Initial cracks at maximum level of major principal stress.

Table 6.2 Observed failure modes in the first polyaxial test series on thick-walled hollow cylinders of Springwell sandstone.

Specimen No.	Mode of Failure
HPG1	Inclined shear fracture + extension along σ_1
HPG2	Test halted for inspecting the initiation of failure
HPG3	Single inclined shear fracture
HPG4	Inclined shear fracture + extension along σ_1
HPG5	Shear cone + extension along σ_1
HPG6	Inclined shear fracture + extension along σ_1
HPG7	Single inclined shear fracture
HPG8	Shear cone + extension along σ_1
HPG9	Shear cone + extension along σ_1
HPG10	Inclined shear fracture + some extension
HPG11	Test halted for inspecting the initiation of failure
HPG12	Single inclined shear fracture
HPG13	Inclined shear fracture + extension along σ_1
HPG14	Single inclined shear fracture
HPG15	Single inclined shear fracture
HPG16	Complete collapse
HPG17	Single inclined shear fracture
HPG18	Single inclined shear fracture
HPG19	Shear cone + extension along σ_1
HPG20	Single inclined shear fracture
HPG21	Shear cone
HPG22	Shear cone + extension along σ_1
HPG23	Shear cone + inclined fracture
HPG24	Single inclined shear fracture
HPG25	Test halted for inspecting the initiation of failure
HPG26	Shear cone + inclined fracture
HPG27	Single inclined shear fracture
HPG28	Single inclined shear fracture
HPG29	Single inclined shear fracture
HPG30	Single inclined shear fracture
HPG31	Inclined shear fracture
HPG32	Shear cone
HPG33	Single inclined shear fracture
HPG34	Shear fracture + some extension
HPG35	Single inclined shear fracture
HPG36	Shear cone
HPG37	Single inclined shear fracture
HPG38	Single inclined shear fracture
HPG39	Single inclined shear fracture
HPG40	Single inclined shear fracture

6.4.3 Discussion of the Results

A notable phenomenon that may be identified in the results of this first polyaxial test series on thick-walled hollow cylinders is the effect that the intermediate principal stress, σ_2, appears to have on the level of the major principal stress, σ_1, sustained by the test specimen. A review of Figures 6.17 to 6.22 confirms an increase in σ_1 level at failure with increasing the induced level of σ_2 at the specimen inner wall. Clearly, this confirmation is in an overall agreement with the corresponding results of the cubical tests presented in Chapter 5.

Turning to Figure 6.23, it appears that dilation occurs in the inner surface of the specimen under the imposed state of stress leading to a degree of closure in the specimen hole. This is evident by the decrease in the hole volume or the corresponding level of the volumetric strain, ε_{vh}, as the axial stress increases and the specimen contracts along its longitudinal axis. Dilation in the specimen inner wall is also reflected by the magnitude of the radial strain, $\varepsilon_r = \varepsilon_3$. Comparing the magnitudes of $\varepsilon_r = \varepsilon_3$ and $\varepsilon_\theta = \varepsilon_2$, there appears to be an agreement with the results of the cubical specimens with regard to the phenomenon that a prominent expansion in the rock takes place along the direction of the minor principal stress, σ_3. However, it is notable in Figure 6.23 that the amount of expansion along σ_3 is more extensive than levels of ε_3 recorded in the cubical tests, but it must be emphasised that this has not always been the case. In contrast with the cubical test results, the ε_θ curve shows that certain expansion also takes place along $\sigma_\theta = \sigma_2$ direction up to a point where the curve starts to change course. Moreover, in a number of tests more expansion appeared to occur along σ_θ up to near failure than along σ_r, suggesting expansion in the hole volume and / or compression in the rock at the inner surface of the specimen. In such cases, hole expansion was also evident by the volumetric change curve recorded during the test. Nevertheless, it has been observed that even when the volumetric change curve suggests hole closure or dilation in the rock at the inner wall, calculated values of ε_θ and ε_r may not conform to this suggestion.

Although it has been found that the presence of internal pressure does support the hole and reduces the rock dilation, it is believed that a number of factors are likely to have influenced measurements of the hole volumetric change in some tests, and consequently, calculated values of ε_{vh}, ε_θ, ε_r. A definite factor lies in the evidence that a perfect sealing of the inner pressure chamber was not always achieved. Signs of internal oil leakage often in a very small quantity were observed at the specimen ends in a number of tests, particularly when relatively high levels of internal pressure were involved. In order to maintain the applied internal pressure at a constant level, the pressure intensifier would naturally compensate any loss of oil resulting in overestimated measurements of the hole volume change. Clearly, these measurements do not reflect the actual deformation of the hole and may misleadingly suggest hole expansion.

Actual deformation of the hole might also have been influenced by what appeared to be a possible inherent malfunction in the pressure intensifier. It has been detected that even when the pressure intensifier is not connected to the test apparatus, and the pressure is raised to a certain level and then maintained constant, the volumetric change may gradually decrease. Generally, the rate of decrease is low and becomes lower when the filling pump is disconnected from the system. The observed irregularity was found to be highly inconsistent, making it very difficult to account for its effect on the test measurements.

It is conceivable that even when accurate measurements of the hole volumetric change are achieved, calculated values of ε_θ and ε_r may not represent the rock deformation as accurately as direct strain measurements made in the cubical tests. Interestingly enough, it has been found in a number of cases that ε_θ and ε_r may appear in a better agreement with the measurements of the hole volumetric change if a plane strain solution is assumed ignoring the specimen axial deformation when the radial deformation of the hole and the corresponding values of ε_θ and ε_r are calculated. Figure 6.24 shows a reproduction of Figure 6.23 based on such an assumption. As a result, the specimen hole appears to undergo more closure than indicated by Figure 6.23, and ε_θ no longer suggests extension along the direction of the intermediate principal stress. However, it is worth pointing out that a plane strain solution has been disregarded partly because it appeared to overestimate

the radial deformation of the hole, and mainly because it undermines the prime principle of polyaxial testing.

Even though calculated values of ε_θ and ε_r may not accurately correspond to the actual deformations of the hole, the general picture obtained indicates that failure of the test specimen is incited by successive hole closure resulting from rock dilation along the direction of the minor principal stress, $\sigma_3 = \sigma_r$. Early signs of failure observed in tests halted at maximum level of major principal stress suggest that the failure process initiates by rock spalling at the inner surface and progresses across the wall until the specimen collapses. Although failure may lead to different types of fractures, Table 6.2, the failure mode is predominantly shear. An unusual phenomenon observed in some tests has been the presence of an apparent extensile fracture lying perpendicular to the direction of the axial or major principal stress. A noteworthy feature of these fractures was that they appeared to generally develop around mid-height of the test specimen, a zone already weakened by the effect of spalling. However, despite the presence of such fractures, it was evident that specimen failure was still dominated by shear. This may suggest that the extensile fractures are likely to have been secondary or post-failure ones developed when a rapid uncontrolled drop in the level of the major principal stress occurred. Similar fractures were reported by Hoskins (1969) to be what Borg and Handin (1966) termed as release fractures which are thought to develop as a result of differential expansion during release of differential stress and / or confining pressure.

6.5 Polyaxial Compression Tests - Second Series

6.5.1 Outline of the Tests

The second polyaxial test series on thick-walled hollow cylinders of Springwell sandstone was designed to primarily assess the validity of using the theory of elasticity to calculate the stresses assumed to develop in the cylinder when subjected to external and internal pressures. A total of thirty-six specimens were loaded to failure under different combinations of external and internal pressures in addition to axial load. The main criteria in choosing the pressure levels applied was to induce at the specimen inner wall predetermined polyaxial principal stress states identical to stress states involved in the first test series with the exception that the radial stress in this case is the intermediate principal stress, $\sigma_r = \sigma_2$, while the tangential stress is the minor principal stress, $\sigma_\theta = \sigma_3$, and the axial stress remains the major principal stress, $\sigma_z = \sigma_1$, corresponding to the arrangement:

$$\sigma_z = \sigma_1 > \sigma_r = \sigma_2 > \sigma_\theta = \sigma_3 > 0$$

According to the elasticity theory, such an arrangement of principal stresses requires the internal pressure to be of higher level than the external pressure, and this could easily lead to the development of tensile tangential stresses if the applied pressures are not accurately balanced. Therefore, every care was taken in all tests to prevent such development and ensure that the specimen failure is governed by polyaxial compression rather than tensile stresses. Table 6.3 presents the levels of external and internal pressures applied in each test together with the corresponding values of tangential and radial stresses at the specimen inner walls.

6.5.2 The Experimental Results

Figure 6.29 shows a typical plot of a test specimen loading sequence in terms of the external pressure, P_o, internal pressure, P_i, and axial stress, F / A, plotted versus time. A plot of the same loading sequence is shown in Figure 6.30 in terms of the corresponding

Table 6.3 Applied levels of external and internal pressures, P_o and P_i, and corresponding values of tangential and radial stresses, σ_θ and σ_r, at the specimen inner surface for the second polyaxial test series on thick-walled hollow cylinders of Springwell sandstone.

Specimen No.	P_o, MPa	P_i, MPa	$\sigma_\theta = \sigma_3$, MPa	$\sigma_r = \sigma_2$, MPa
HPR1	7.824	10	5	10
HPR2	7.824	10	5	10
HPR3	13.472	20	5	20
HPR4	13.472	20	5	20
HPR5	19.120	30	5	30
HPR6	19.120	30	5	30
HPR7	24.768	40	5	40
HPR8	24.768	40	5	40
HPR9	30.416	50	5	50
HPR10	30.416	50	5	50
HPR11	15.648	20	10	20
HPR12	15.648	20	10	20
HPR13	21.296	30	10	30
HPR14	21.296	30	10	30
HPR15	26.944	40	10	40
HPR16	26.944	40	10	40
HPR17	32.592	50	10	50
HPR18	32.592	50	10	50
HPR19	23.472	30	15	30
HPR20	23.472	30	15	30
HPR21	31.944	45	15	45
HPR22	31.944	45	15	45
HPR23	25.648	30	20	30
HPR24	25.648	30	20	30
HPR25	31.296	40	20	40
HPR26	31.296	40	20	40
HPR27	36.944	50	20	50
HPR28	36.944	50	20	50
HPR29	39.120	50	25	50
HPR30	39.120	50	25	50
HPR31	35.648	40	30	40
HPR32	35.648	40	30	40
HPR33	41.296	50	30	50
HPR34	41.296	50	30	50
HPR35	45.648	50	40	50
HPR36	45.648	50	40	50

principal stresses, $\sigma_\theta = \sigma_3$, $\sigma_r = \sigma_2$, $\sigma_z = \sigma_1$, calculated at the cylinder inner wall. A representative plot of the major principal stress, $\sigma_z = \sigma_1$, versus the major principal strain, $\varepsilon_z = \varepsilon_1$, is presented in Figure 6.31 for specimen HPR4 which was subjected to an external pressure level of $P_o = 13.472$ MPa and an internal pressure level of $P_i = 20$ MPa, corresponding to minor principal stress of $\sigma_\theta = \sigma_3 = 5$ MPa and intermediate principal stress of $\sigma_r = \sigma_2 = 20$ MPa.

Following the procedure outlined in 6.2.4, acquired values of the volumetric change of the specimen hole, ΔV_h, have been used to calculate the tangential strain, $\varepsilon_\theta = \varepsilon_3$, and radial strain, $\varepsilon_r = \varepsilon_2$, at the specimen inner wall. Figure 6.32 shows a plot of the recorded values of the major principal strain, $\varepsilon_z = \varepsilon_1$, versus the calculated values of ε_θ, ε_r, and the volumetric strain of the hole, ε_{Vh}, for specimen HPR4.

In order to compare the test results with the results of the previous experimental series, recorded values of the major principal stress, $\sigma_z = \sigma_1$, at failure from both test series have been grouped according to σ_3 or σ_2 levels and plotted versus the corresponding levels of σ_2 or σ_3, respectively. Similar plots have been produced in terms of $\sigma_z = \sigma_1$ versus the corresponding values of $\varepsilon_z = \varepsilon_1$ recorded at failure. The obtained plots are presented in Figures 6.33 to 6.44.

As observed in the previous tests, the specimen failure was generally marked by loud cracking often accompanied by a sharp fall in the level of the axial stress and a noticeable deviation in the curve of the hole volumetric change. The nature of failure appeared to be governed by pure shear generally across a major single fracture forming a plane inclined to the direction of the axial principal stress at an average angle of about 30°, less than the one emerged in the previous tests. Only three specimens were found sheared across two parallel planes, and unlike the previous tests, neither shear cones nor extensile fractures were observed. Moreover, although traces of undeveloped cracks were frequently noted at the specimen inner wall, signs of spalling or slabbing could hardly be observed. Typical failure patterns are pictured in Figures 6.45 and 6.46.

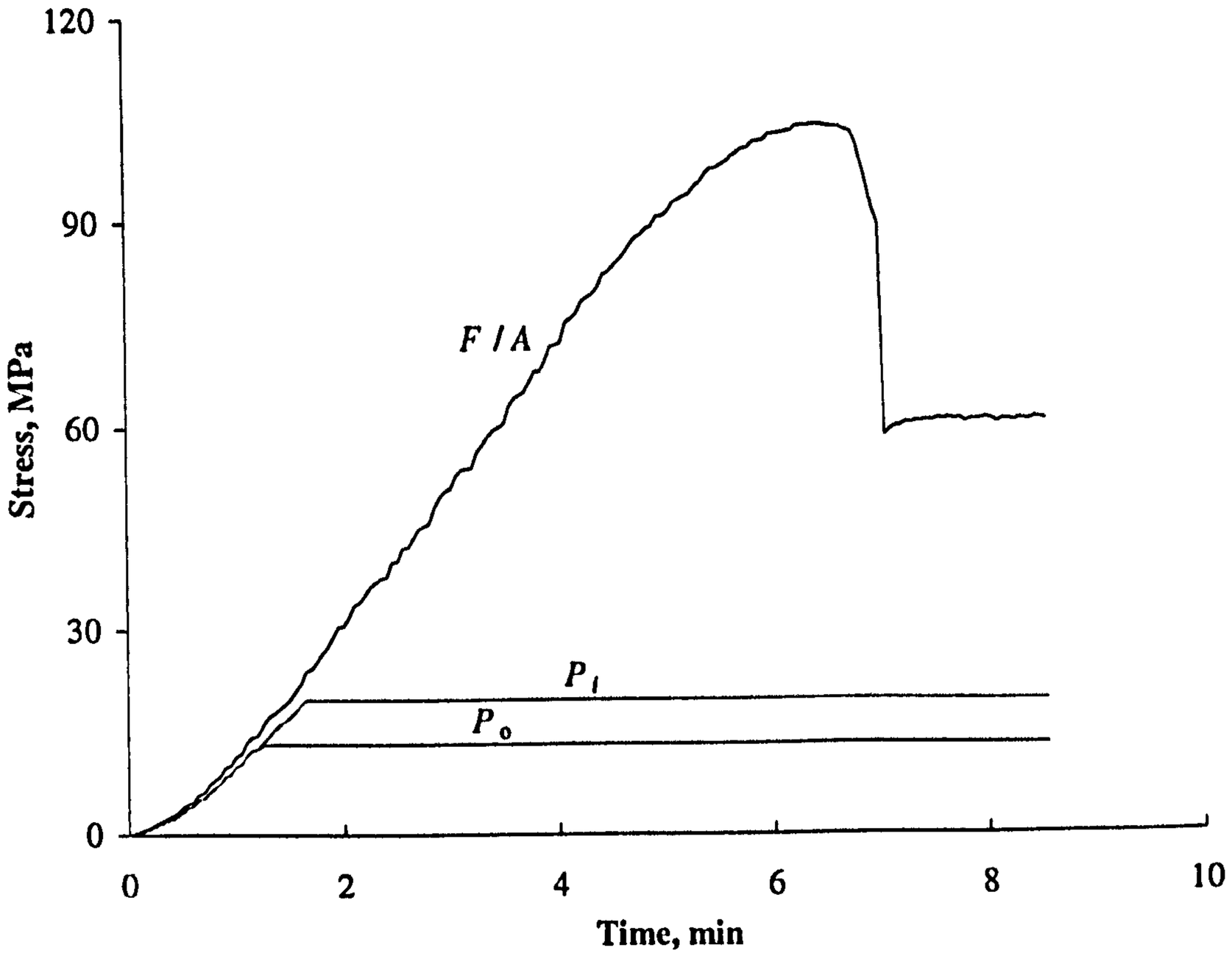

Figure 6.29 A typical loading sequence for the second polyaxial test series on hollow cylinders plotted in terms of applied external pressure, P_o, internal pressure, P_i, and axial stress, F / A, versus time.

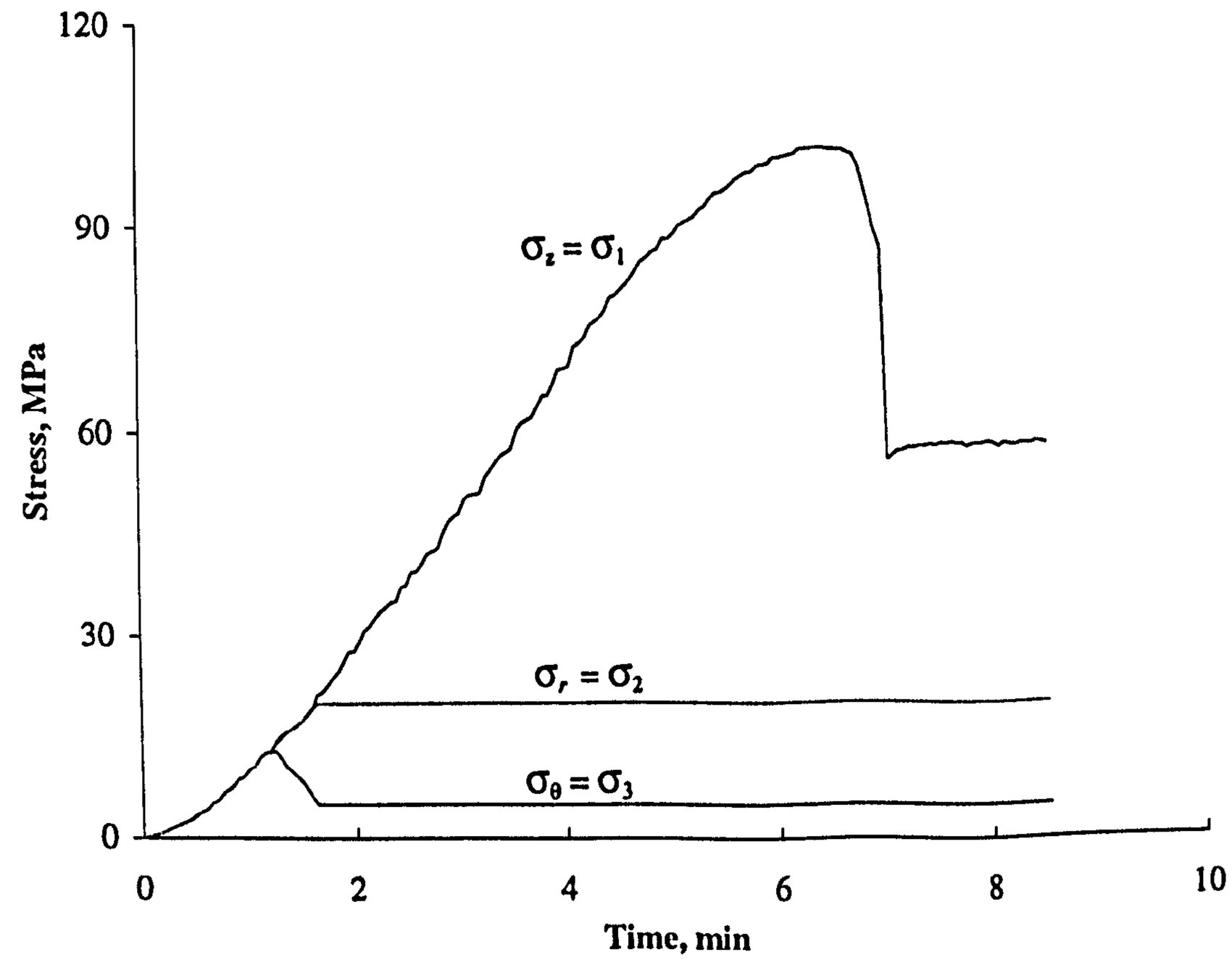

Figure 6.30 The above loading sequence in terms of the corresponding principal stresses, $\sigma_\theta = \sigma_3$, $\sigma_r = \sigma_2$, $\sigma_z = \sigma_1$, induced at the cylinder inner wall.

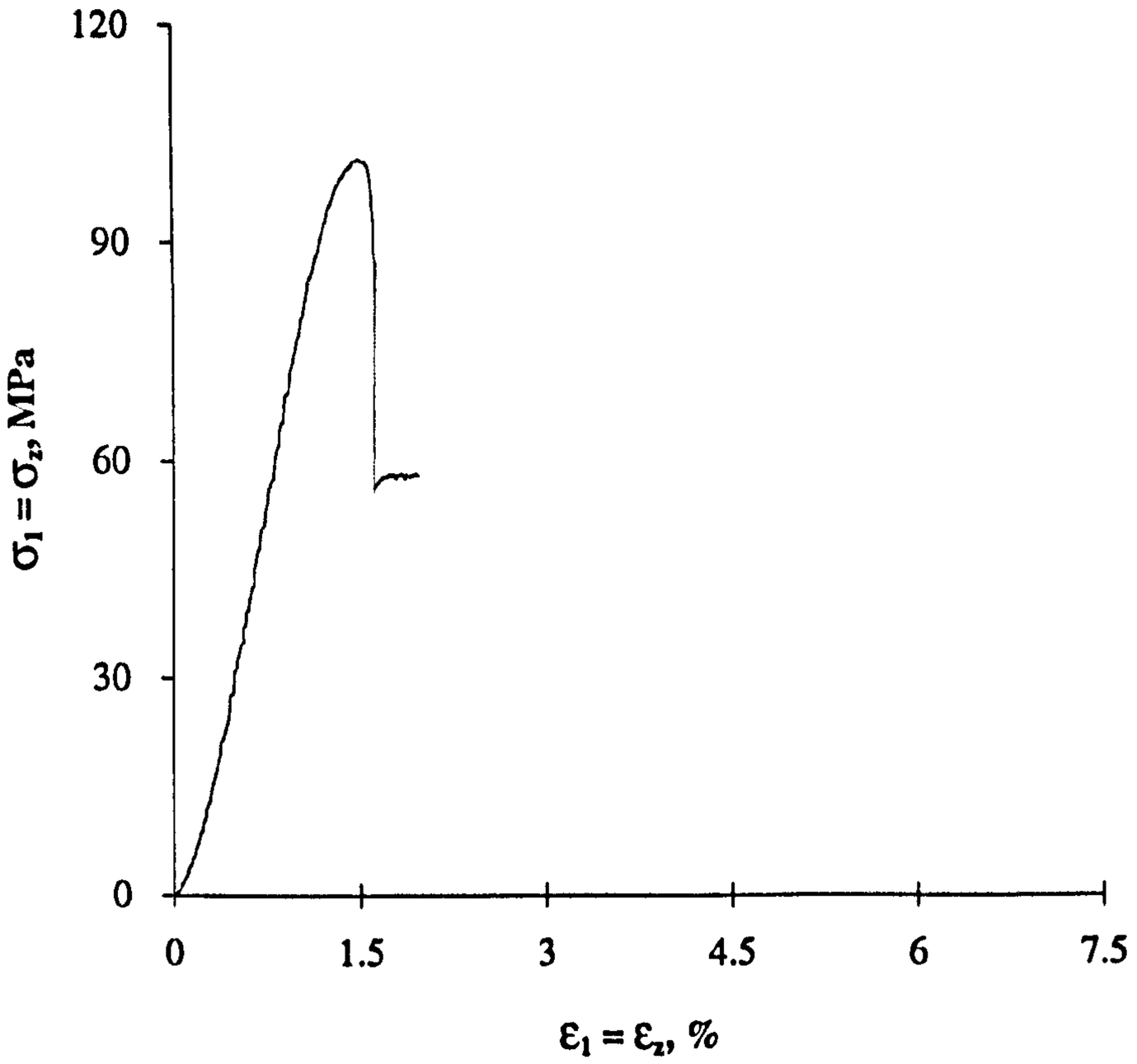

Figure 6.31 Major principal stress, $\sigma_1 = \sigma_z$, versus major principal strain, $\varepsilon_1 = \varepsilon_z$, for a hollow cylinder polyaxial test in which $\sigma_2 = \sigma_r = 20$ MPa and $\sigma_3 = \sigma_\theta = 5$ MPa.

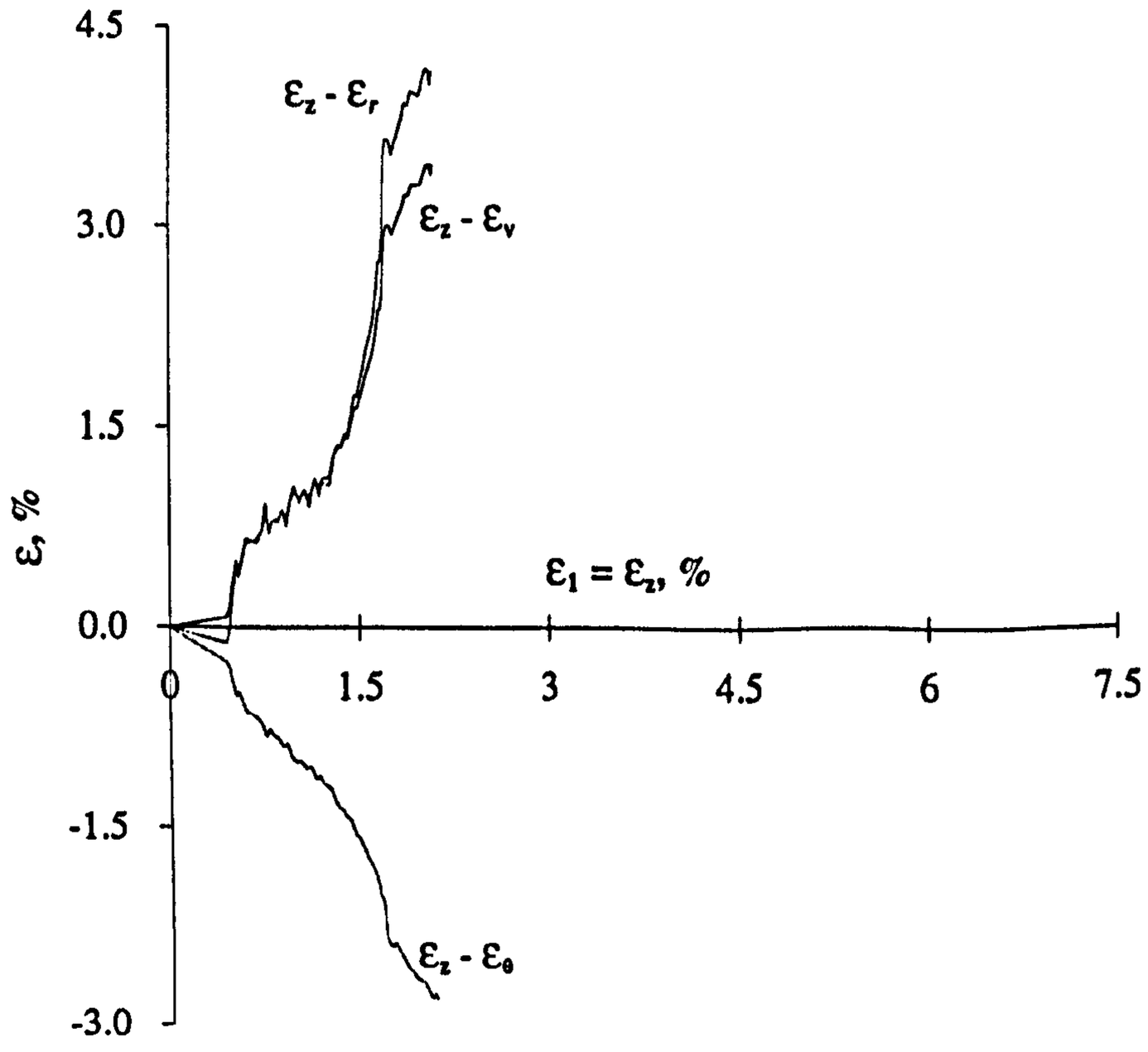

Figure 6.32 Major principal strain, $\varepsilon_z = \varepsilon_1$, versus radial strain, $\varepsilon_r = \varepsilon_2$, tangential strain, $\varepsilon_\theta = \varepsilon_3$, and volumetric strain, ε_{vh}, at the specimen inner walls.

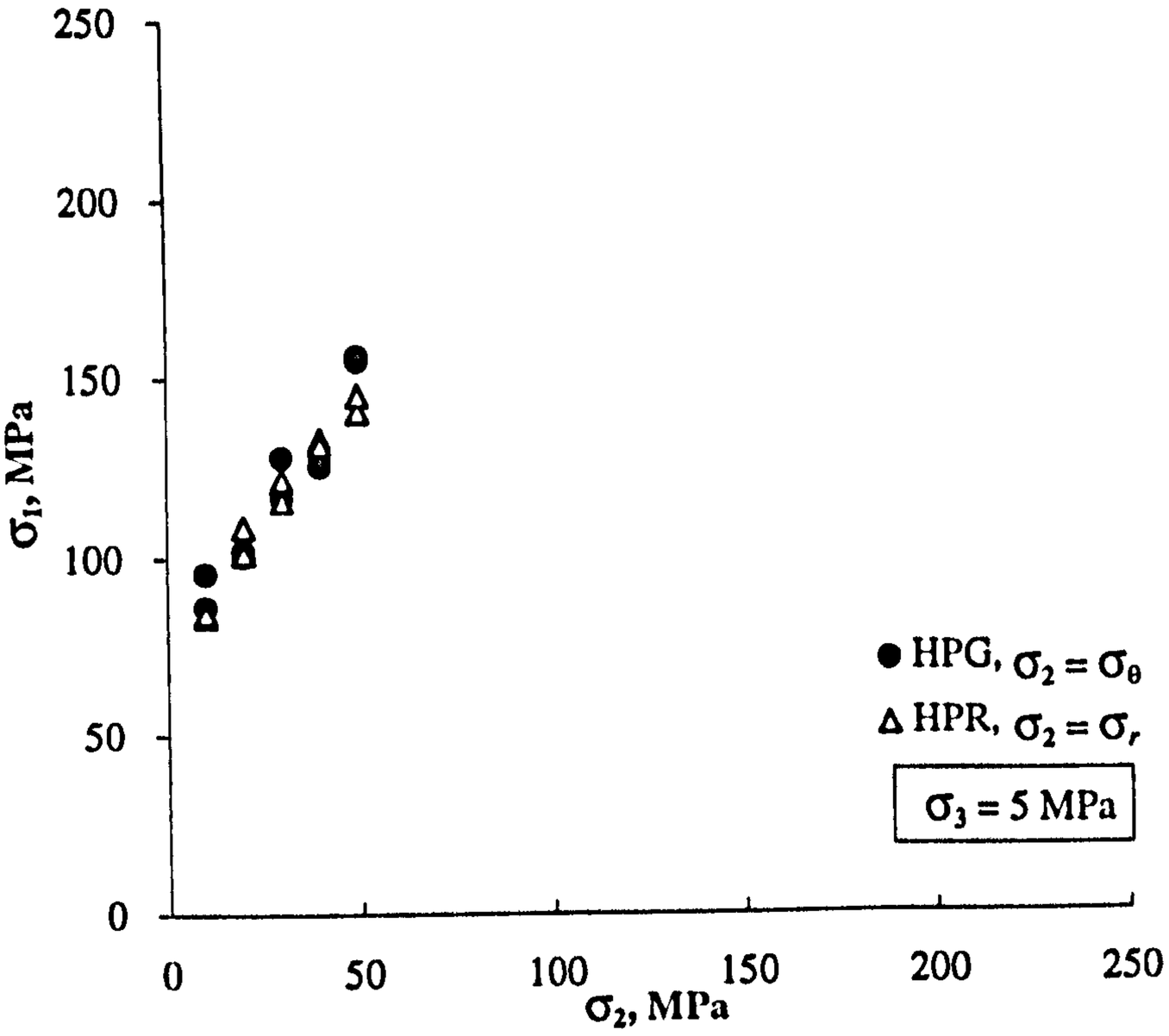

Figure 6.33 Variation of $\sigma_1 = \sigma_z$ at failure with σ_2 in polyaxial tests on thick-walled hollow cylinders conducted under σ_3 = 5 MPa.

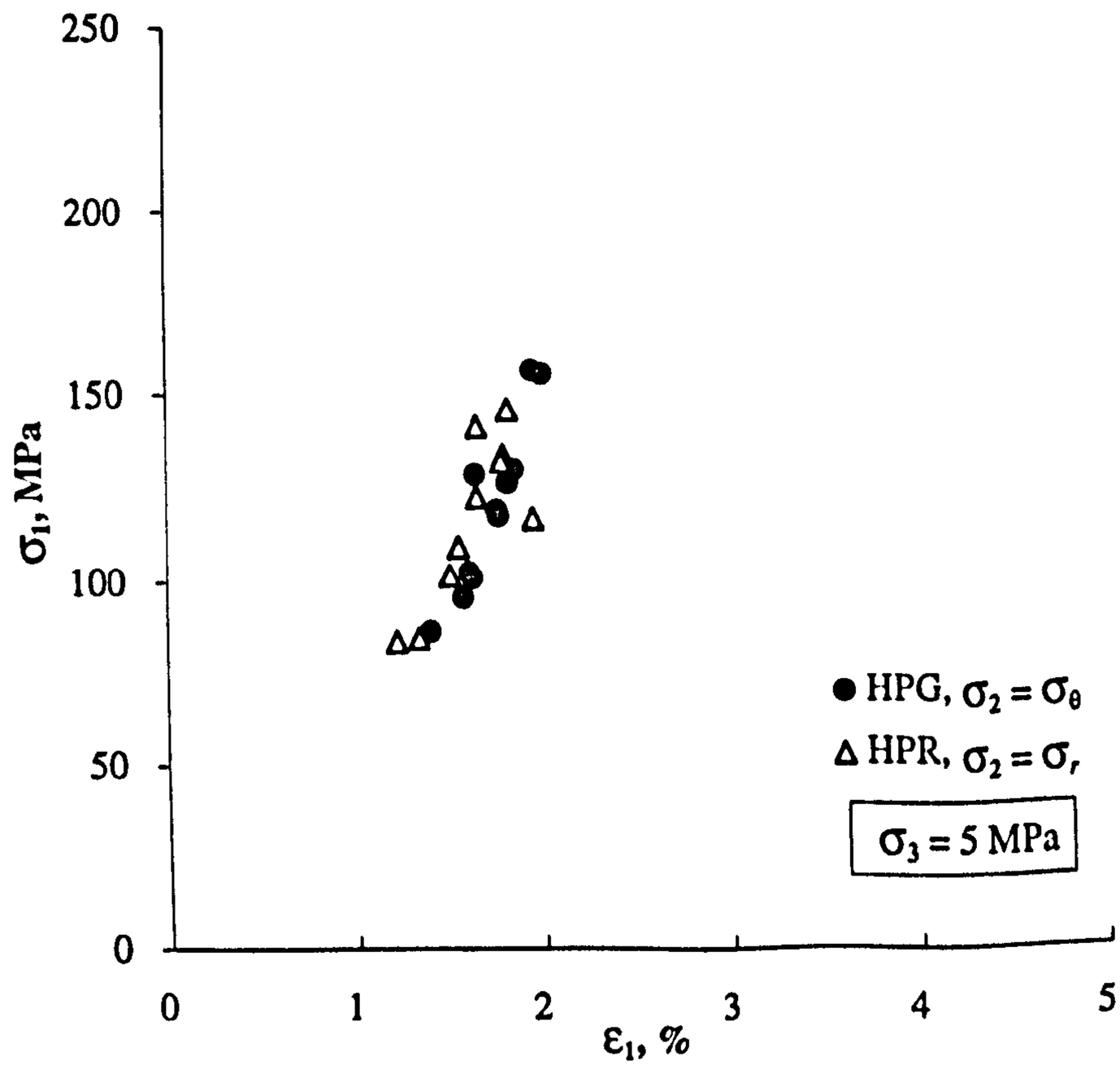

Figure 6.34 Major principal stress, $\sigma_1 = \sigma_z$, at failure versus major principal strain, $\varepsilon_1 = \varepsilon_z$, for the above tests.

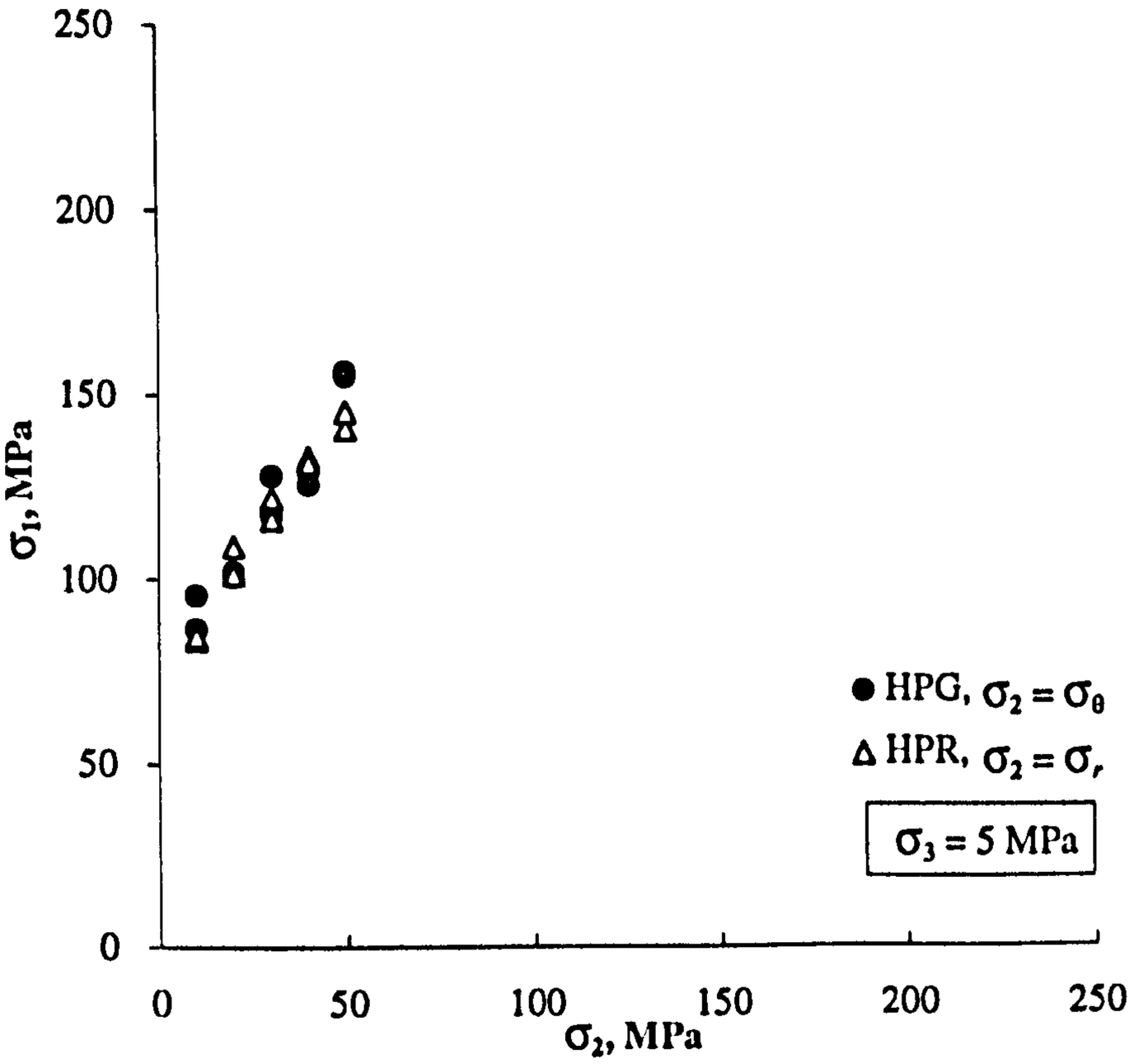

Figure 6.35 Variation of $\sigma_1 = \sigma_z$ at failure with σ_2 in polyaxial tests on thick-walled hollow cylinders conducted under σ_3 = 10 MPa.

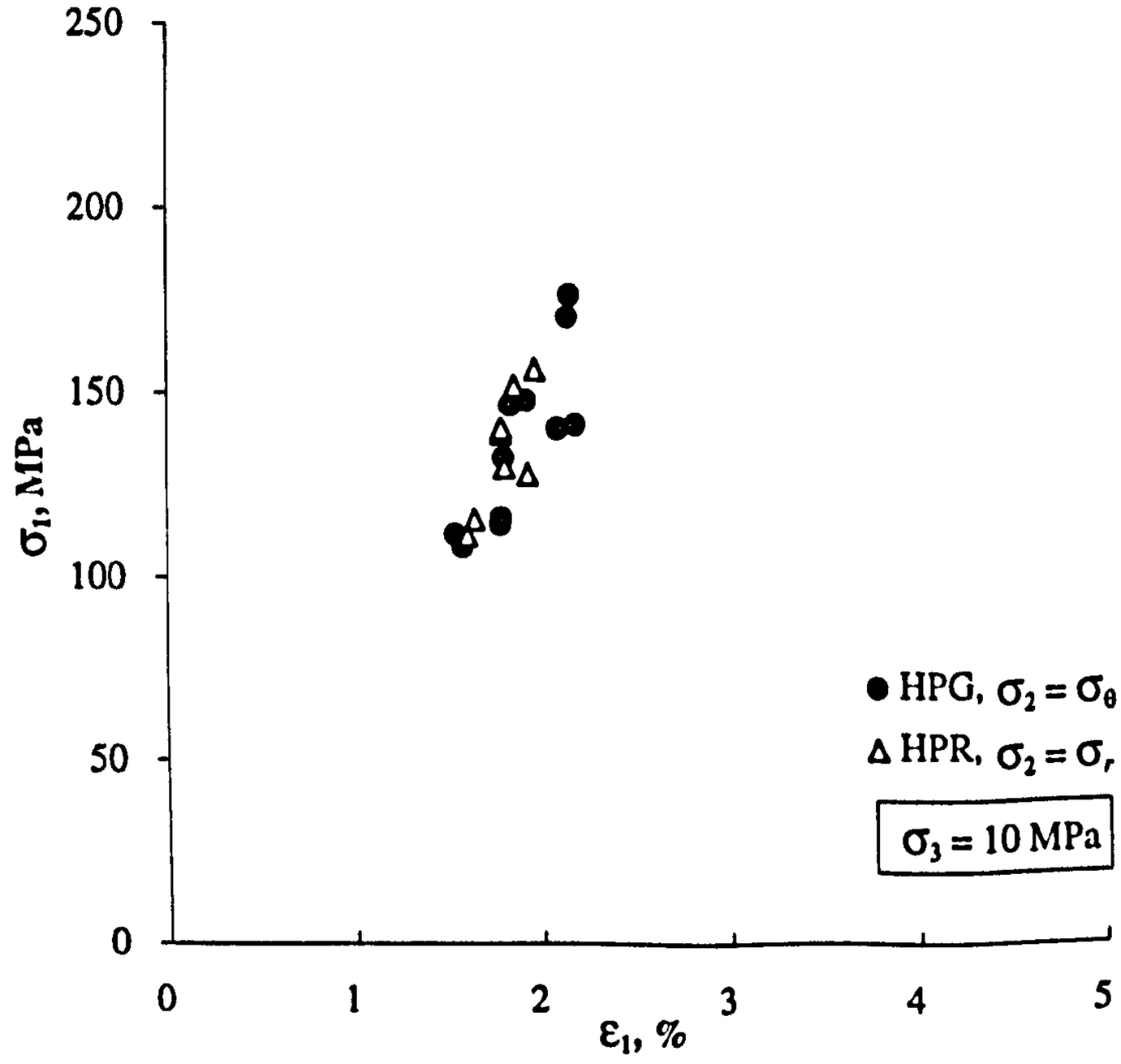

Figure 6.36 Major principal stress, $\sigma_1 = \sigma_z$, at failure versus major principal strain, $\varepsilon_1 = \varepsilon_z$, for the above tests.

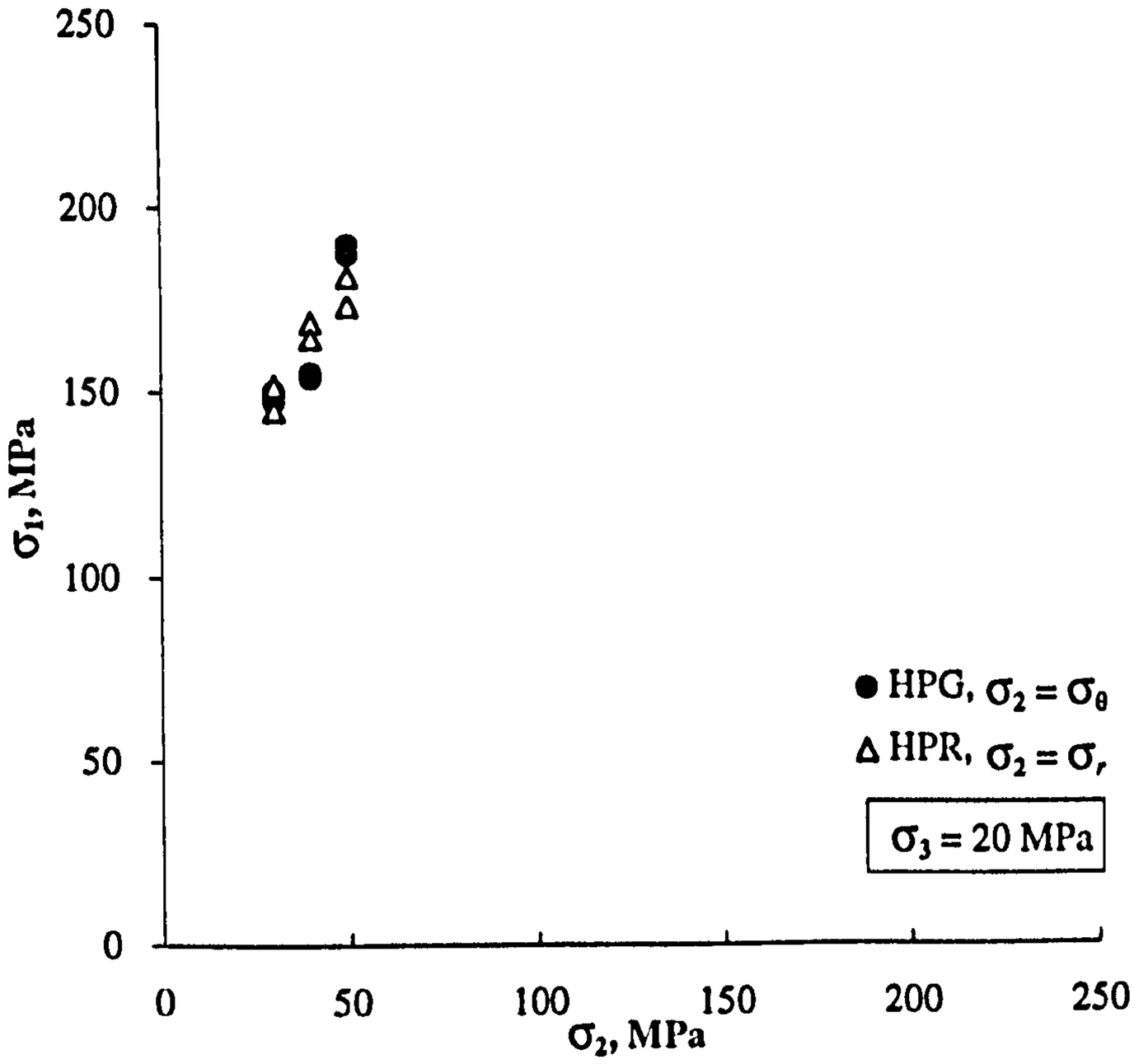

Figure 6.37 Variation of $\sigma_1 = \sigma_z$ at failure with σ_2 in polyaxial tests on thick-walled hollow cylinders conducted under $\sigma_3 = 20$ MPa.

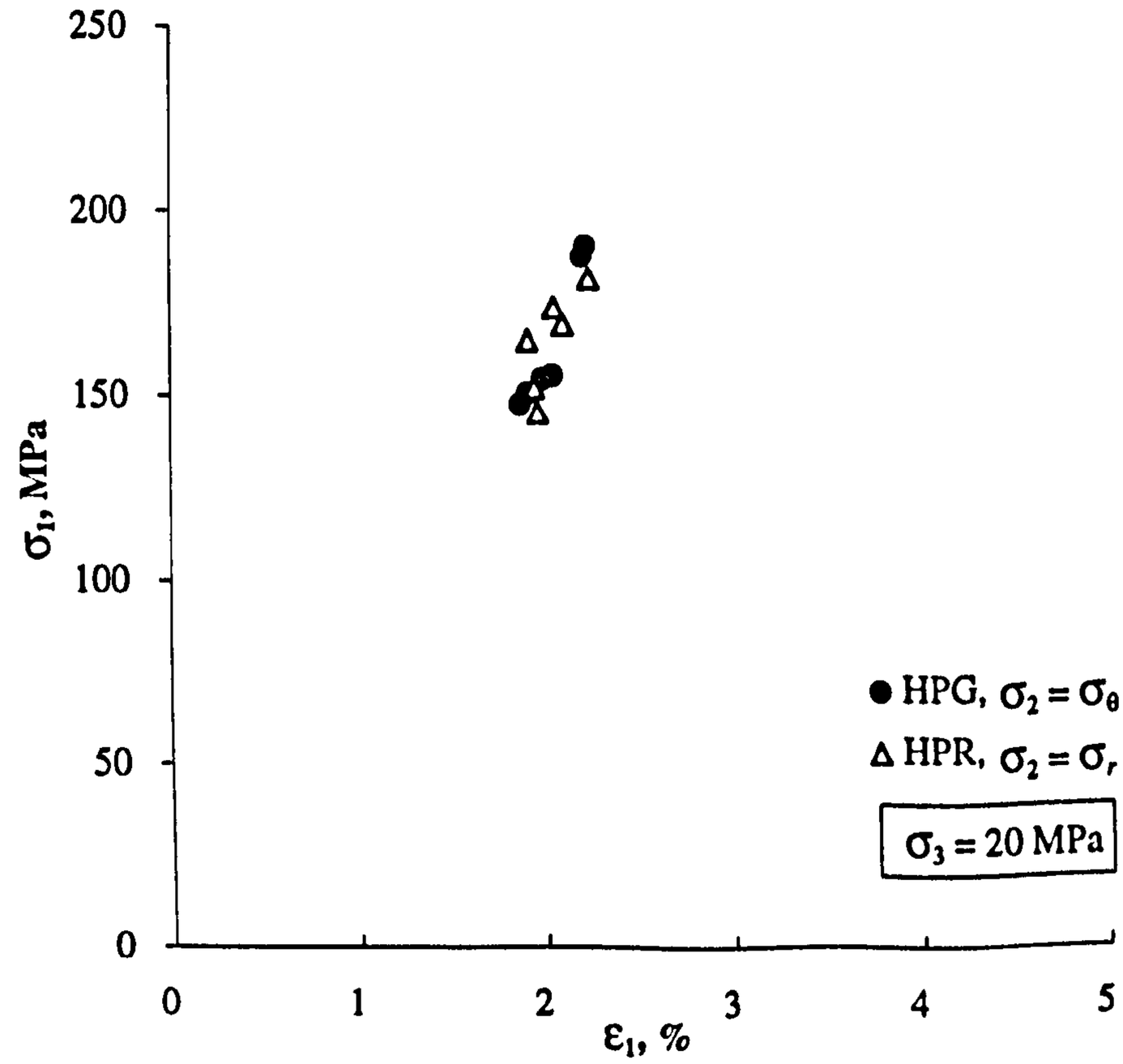

Figure 6.38 Major principal stress, $\sigma_1 = \sigma_z$, at failure versus major principal strain, $\varepsilon_1 = \varepsilon_z$, for the above tests.

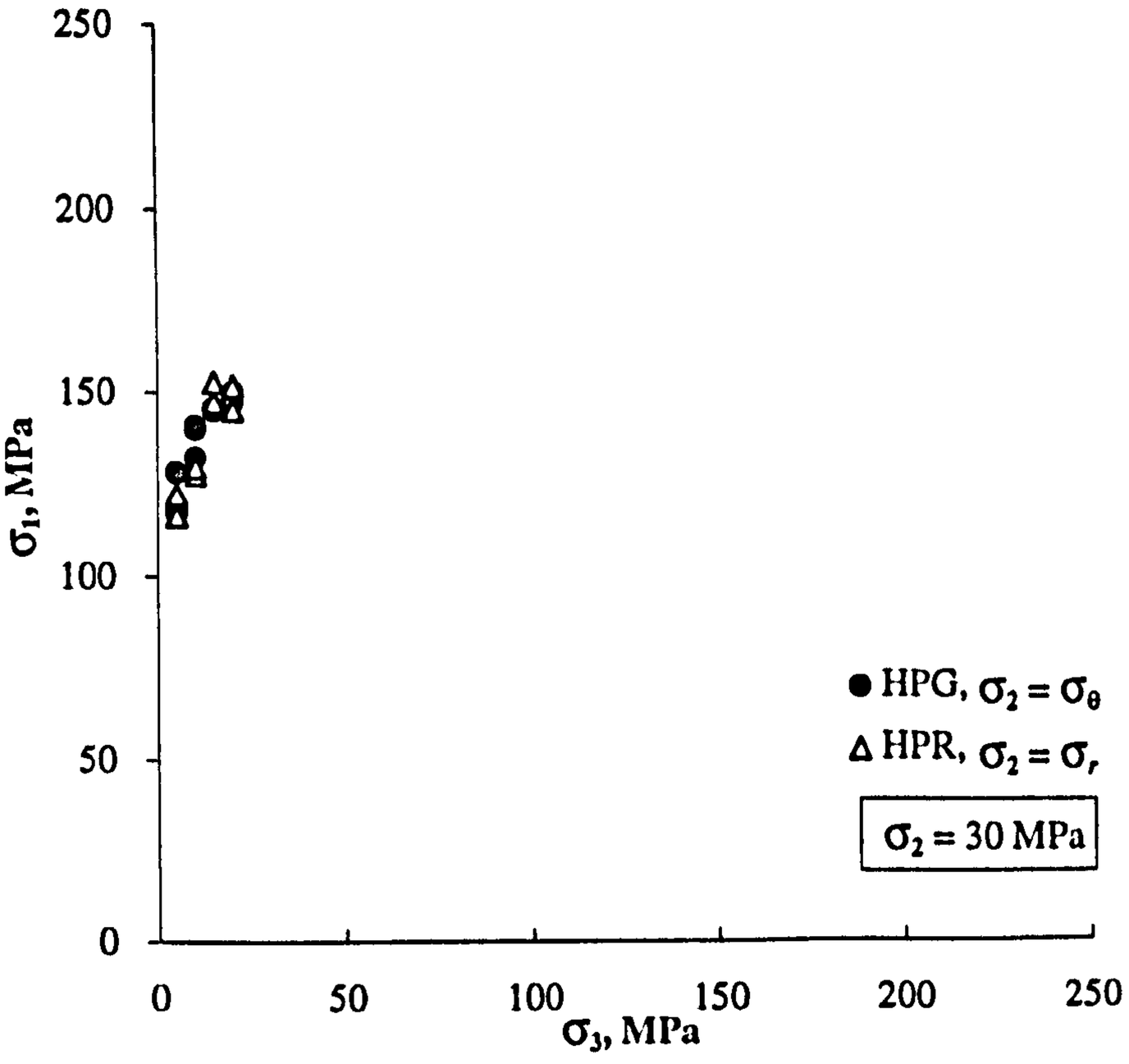

Figure 6.39 Variation of $\sigma_1 = \sigma_z$ at failure with σ_3 in polyaxial tests on thick-walled hollow cylinders conducted under σ_2 = 30 MPa.

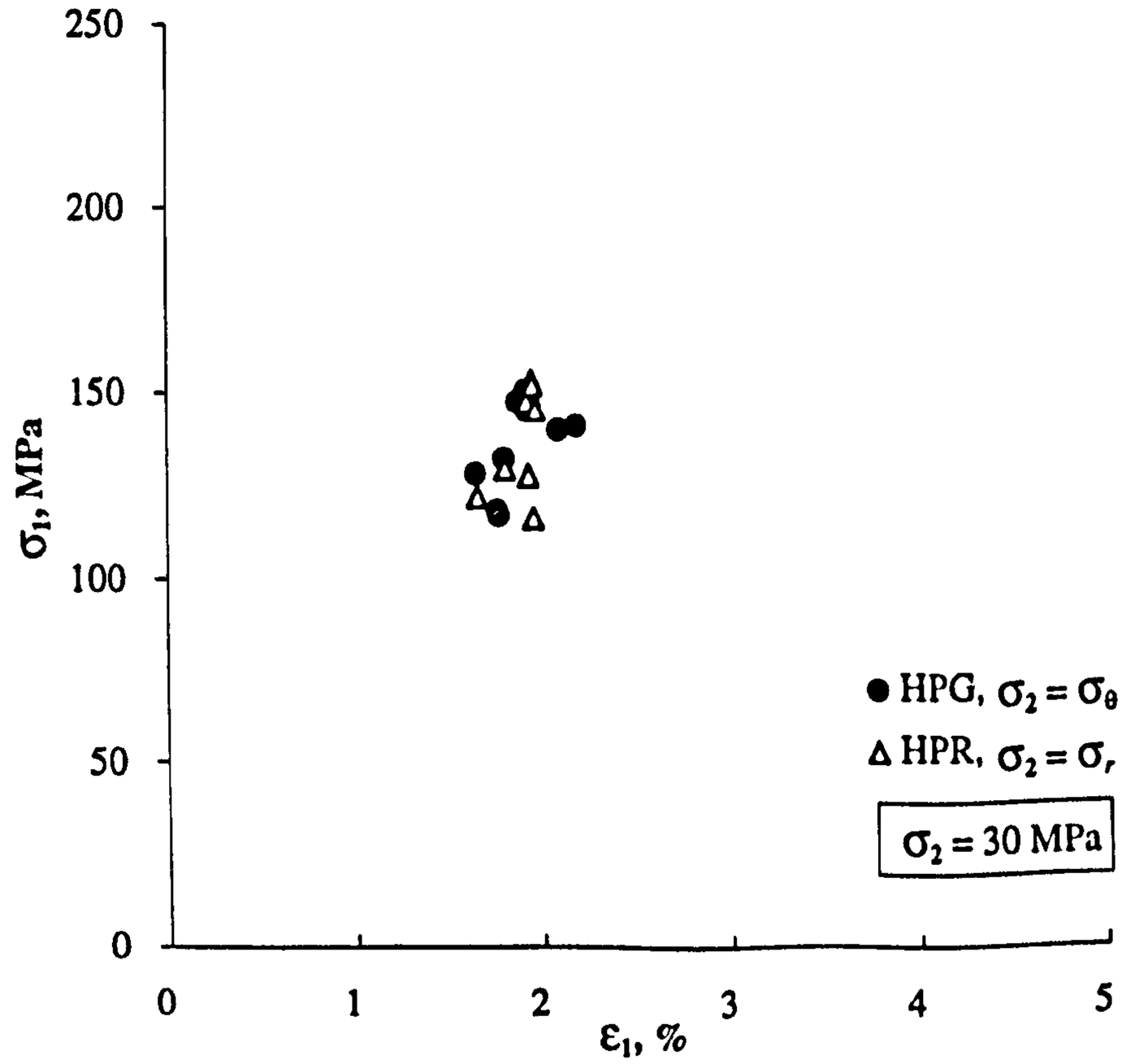

Figure 6.40 Major principal stress, $\sigma_1 = \sigma_z$, at failure versus major principal strain, $\varepsilon_1 = \varepsilon_z$, for the above tests.

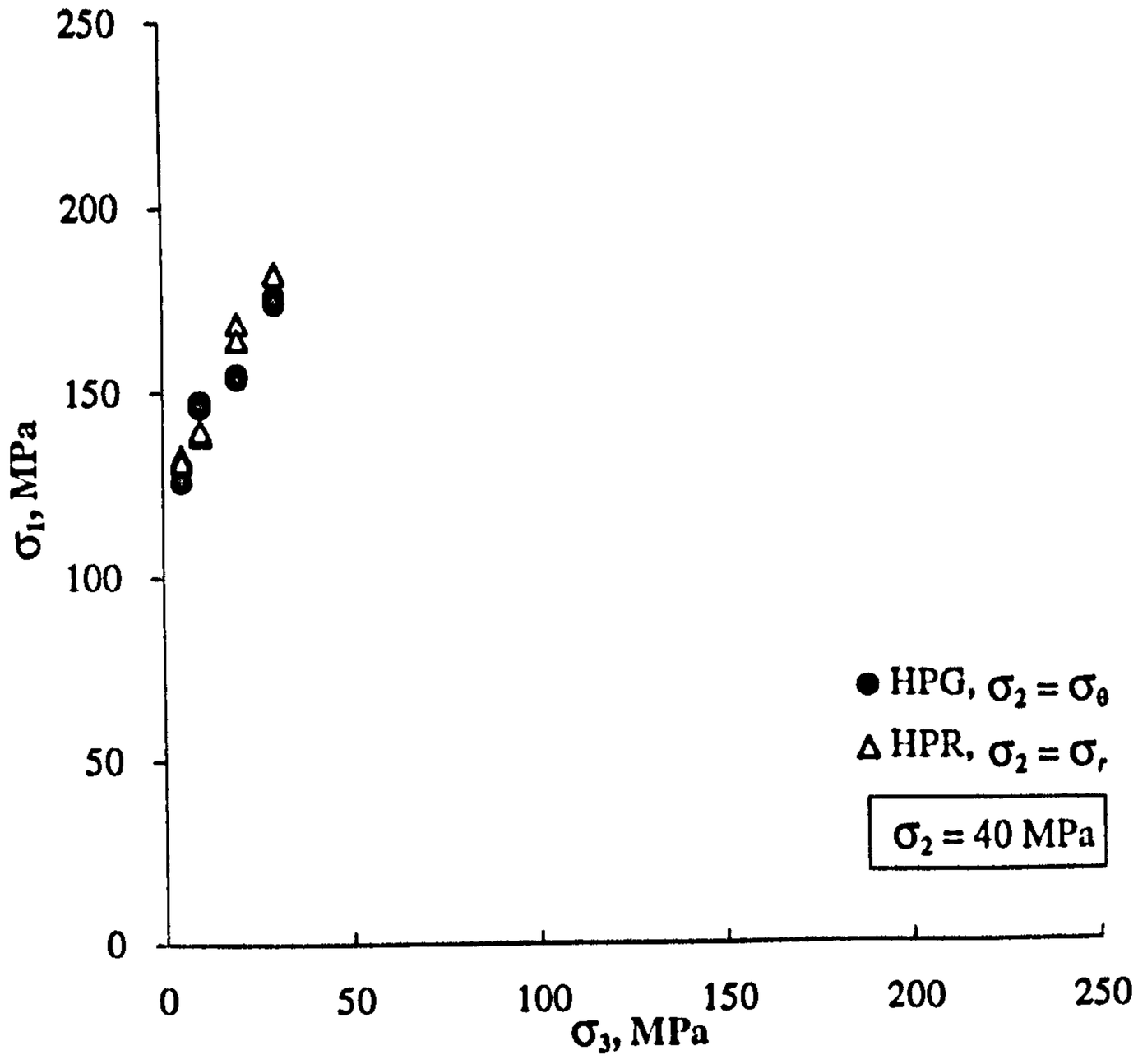

Figure 6.41 Variation of $\sigma_1 = \sigma_z$ at failure with σ_3 in polyaxial tests on thick-walled hollow cylinders conducted under $\sigma_2 = 40$ MPa.

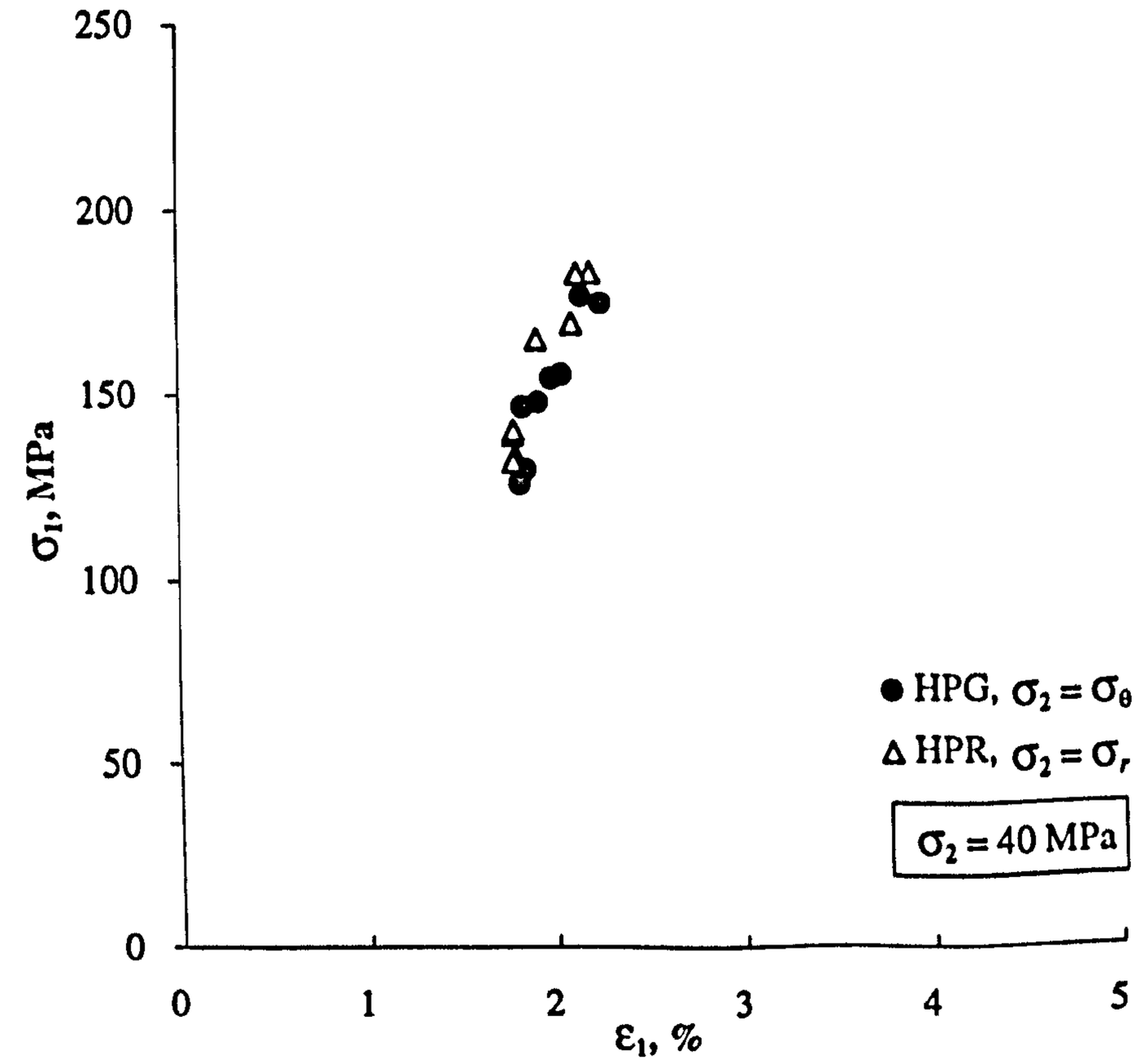

Figure 6.42 Major principal stress, $\sigma_1 = \sigma_z$, at failure versus major principal strain, $\varepsilon_1 = \varepsilon_z$, for the above tests.

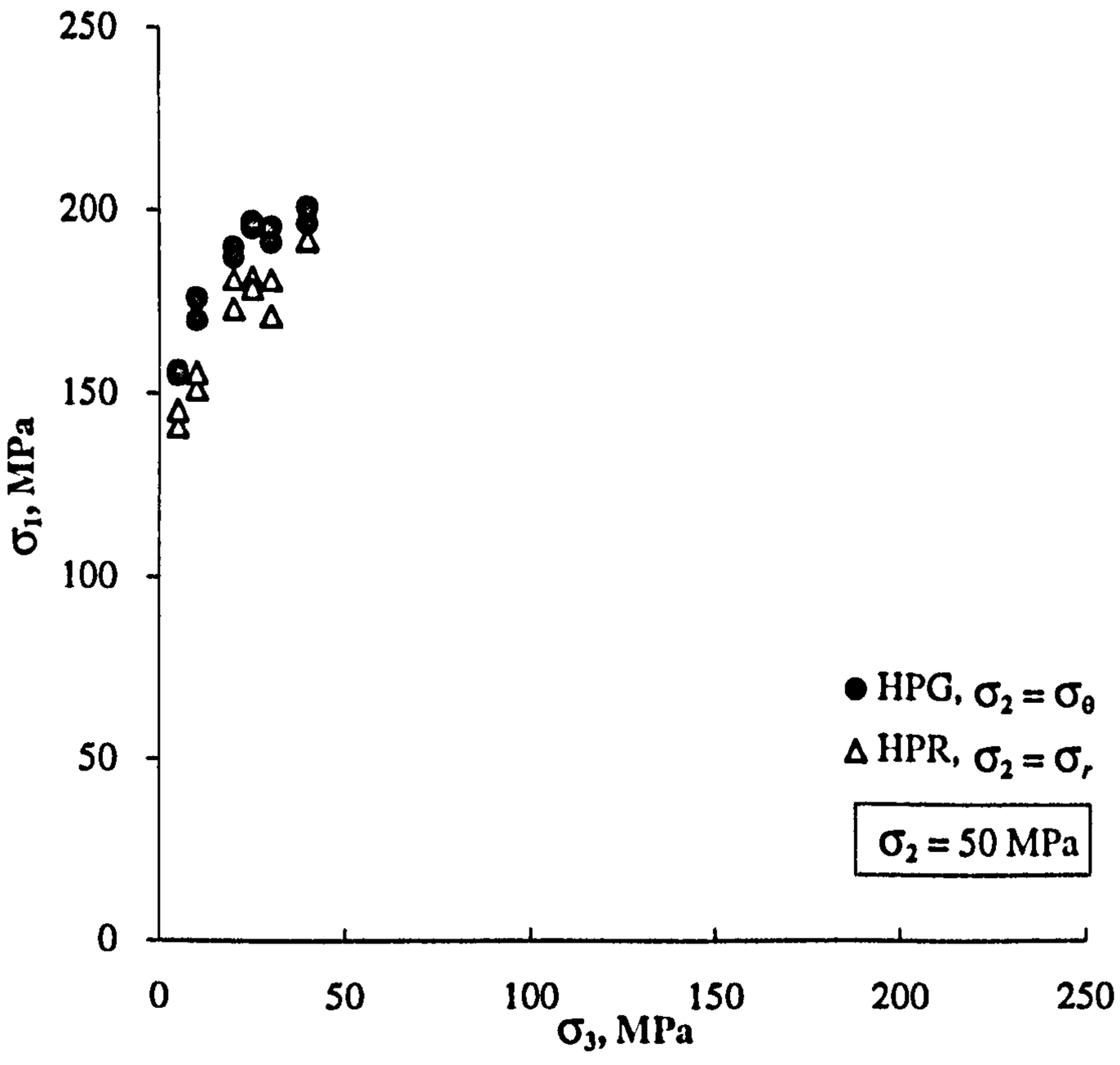

Figure 6.43 Variation of $\sigma_1 = \sigma_z$ at failure with σ_3 in polyaxial tests on thick-walled hollow cylinders conducted under σ_2 = 50 MPa.

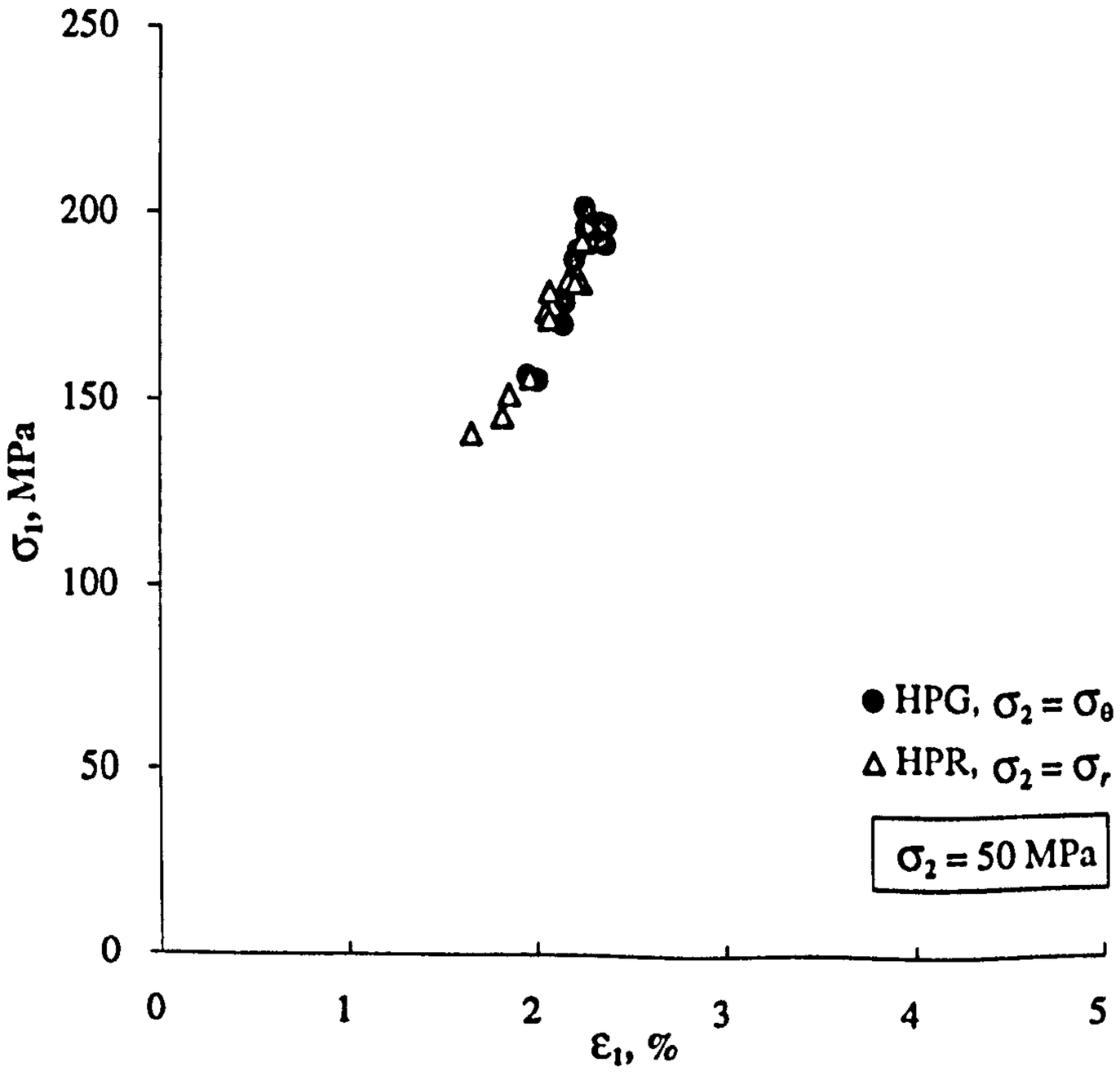

Figure 6.44 Major principal stress, $\sigma_1 = \sigma_z$, at failure versus major principal strain, $\varepsilon_1 = \varepsilon_z$, for the above tests.

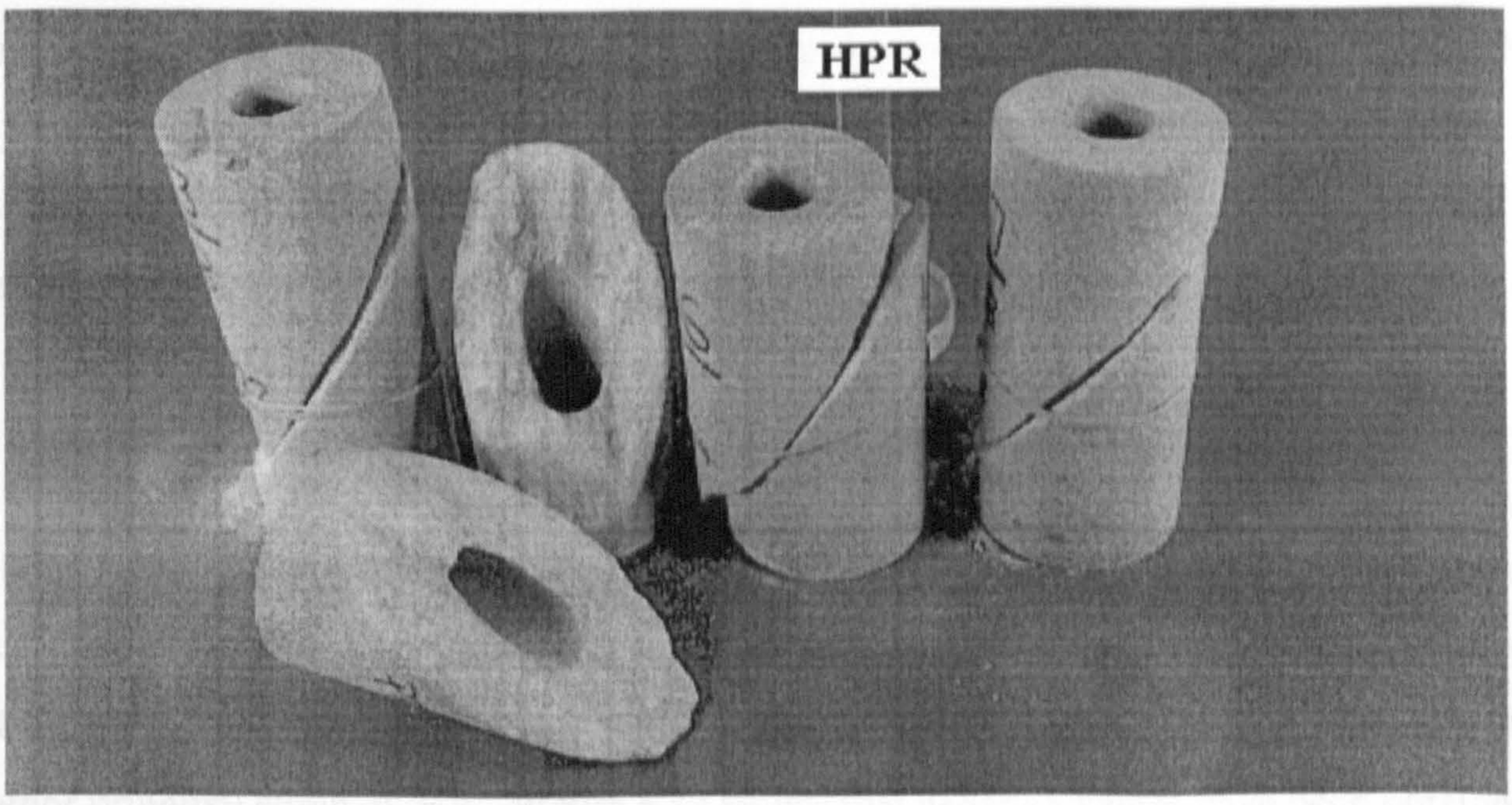

Figure 6.45 Failure of thick-walled hollow cylinders along single inclined shear fractures in polyaxial compression tests in which $\sigma_1 = \sigma_z > \sigma_2 = \sigma_r > \sigma_3 = \sigma_\theta > 0$.

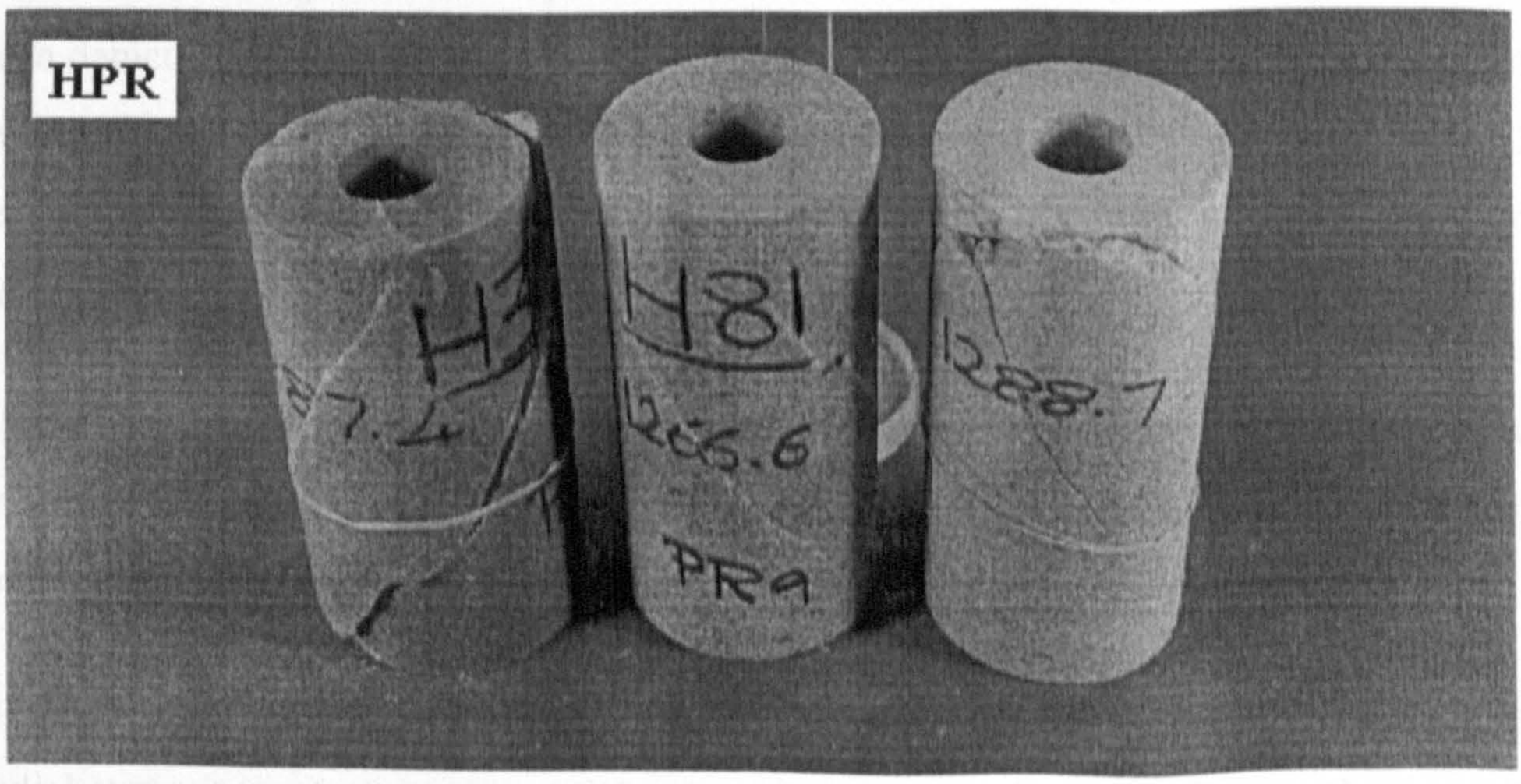

Figure 6.46 Only three specimens were found sheared across two parallel planes.

6.5.3 Discussion of the Results

In examining Figures 6.33 to 6.44, obviously there are some variations between the strength results of the present tests and those conducted in the previous series. However, it is clear that the level of variation is not substantial and appears to be typified by scatter rather than trend. Furthermore, close agreement between both test results is also evident in a number of instances.

Regarding the deformation of the specimen hole, Figure 6.32 shows that with the radial stress being the intermediate principal stress, the rock at the inner wall undergoes compression leading to expansion of the hole. This is evident by the increase in the level of both the radial strain, $\varepsilon_r = \varepsilon_2$, and the volumetric strain of the hole, ε_{vh}. As for the minor principal strain, $\varepsilon_\theta = \varepsilon_3$, Figure 6.32 shows that negative values have been obtained, indicating that the strain vector is of opposite direction to that of the minor principal stress, $\sigma_\theta = \sigma_3$. This suggests dilation in the rock along the minor principal direction, a feature generally observed in all tests series.

It is worth pointing out that the picture of the hole deformation given by Figure 6.32 has been depicted by the results of all tests conducted in this series. However, results of some tests appeared to have been influenced by similar factors to those discussed in 6.4.3, leading to discrepancies in the results as well as exaggerated levels of the hole deformations.

The specimen failure appears to be governed by shear regularly resulting in inclined shear fractures. No other modes of failure seem to evolve. In addition, with the rock at the inner wall undergoing compression, spalling or slabbing is unlikely to take place.

It is clear from the above observations that with the intermediate principal stress being the radial stress instead of the tangential stress, the most pronounced difference between the results of the two types of tests lies in the nature of the hole deformation. Apart from that, specimens that may be tested under either conditions are likely to sustain similar levels of major principal stress and fail by shear generally across single inclined fractures.

6.6 Triaxial Compression Tests

6.6.1 Outline of the Tests

Following the polyaxial test series, a total of sixteen thick-walled hollow cylinders were tested under standard triaxial loading conditions in which $\sigma_2 = \sigma_3$. The testing set-up and procedure were the same as in the polyaxial tests with the exception that both internal and external pressures were maintained constant at equal levels, thus inducing at the specimen inner wall a state of stress in which:

$$\sigma_z = \sigma_1 > P_i = P_o = \sigma_r = \sigma_\theta = \sigma_2 = \sigma_3 > 0$$

As in previous tests, the concept of the multiple failure state test was utilised. Half of the tests were limited to a single failure state while the other half were of two or three failure states, producing a total of twenty-eight failure points. Details of the loading levels for each individual test are presented in Table 6.4.

6.6.2 The Experimental Results

Figure 6.47 shows a typical plot of a triaxial compression loading sequence of a thick-walled hollow cylinder subjected to three consecutive failure states. The resultant axial stress, $\sigma_z = \sigma_1$, versus axial strain, $\varepsilon_z = \varepsilon_1$, curve is presented in Figure 6.48. Calculated values of the hole volumetric strain, ε_{vh}, together with the tangential and radial strains at the specimen inner wall, ε_θ and ε_r, respectively, are plotted in Figure 6.49 versus the major principal strain, $\varepsilon_z = \varepsilon_1$, for the same specimen. Recorded values of the major principal stress at failure, $\sigma_z = \sigma_1$, for all specimens tested are presented in both Figures 6.50 and 6.51 versus the corresponding levels of $\sigma_r = \sigma_\theta$ and $\varepsilon_z = \varepsilon_1$, respectively.

Failure of the test specimens appeared to be of the shear type resulting in fractures similar to those observed in both polyaxial test series. Typical failure modes are pictured in Figure 6.52.

Table 6.4 Applied loading levels in single and multiple failure state triaxial compression tests on thick-walled hollow cylinders of Springwell sandstone. Note that stresses are calculated at the specimen inner walls and that $P_i = P_o = \sigma_r = \sigma_\theta = \sigma_2 = \sigma_3$.

Specimen No.	Failure State	$\sigma_2 = \sigma_3$, MPa
HTX1	F1	10
HTX2	F1	15
HTX3	F1	25
HTX4	F1	25
HTX5	F1	30
HTX6	F1	40
HTX7	F1	50
HTX8	F1	50
HTX9	F1	5
	F2	10
HTX10	F1	5
	F2	10
	F3	15
HTX11	F1	10
	F2	20
HTX12	F1	15
	F2	30
	F3	40
HTX13	F1	20
	F2	30
	F3	40
HTX14	F1	20
	F2	30
	F3	40
HTX15	F1	30
	F2	40
HTX16	F1	40
	F2	50

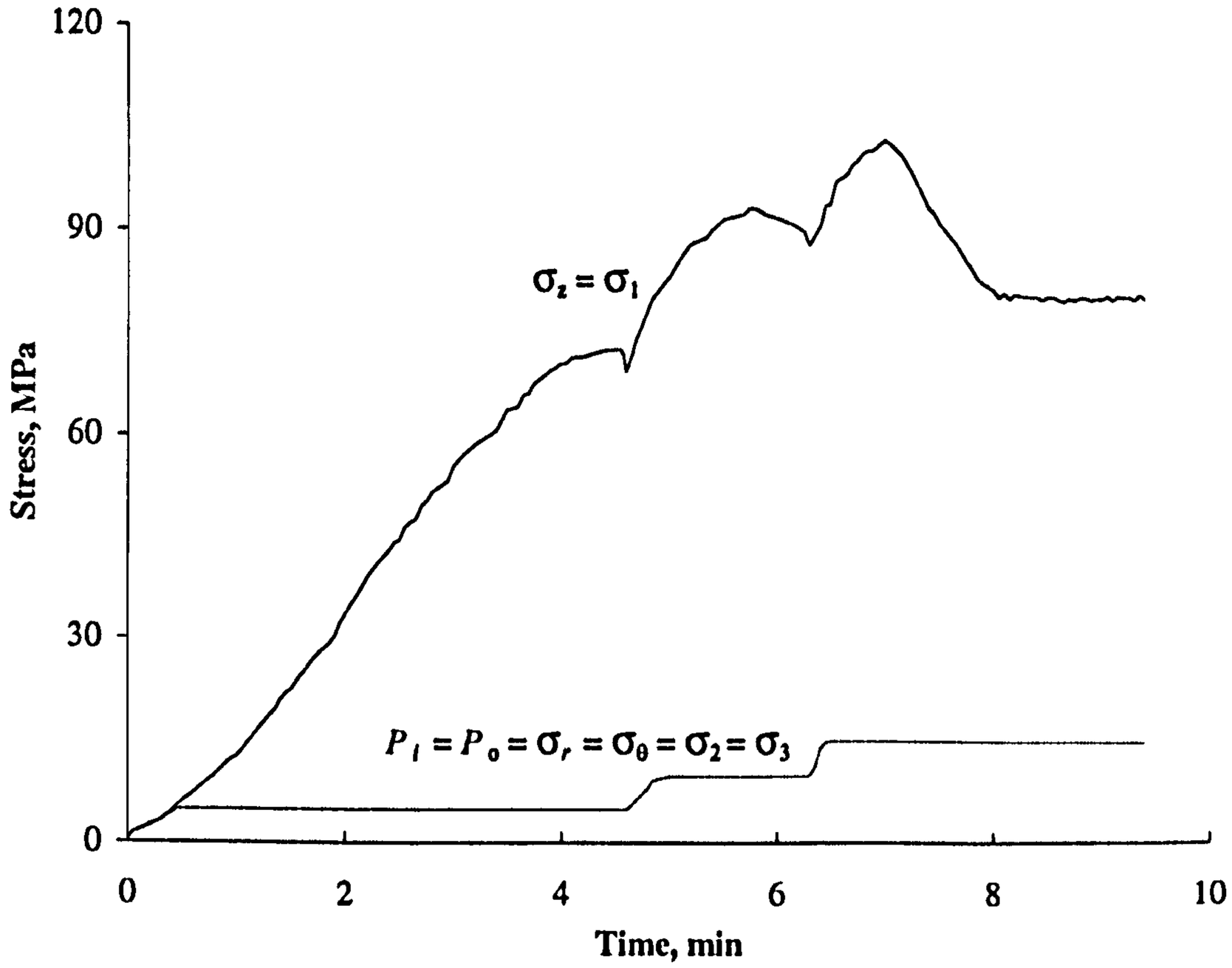

Figure 6.47 A typical loading sequence in terms of stress versus time for multiple failure state triaxial tests on hollow cylinders in which $\sigma_1 = \sigma_z > P_i = P_o = \sigma_r = \sigma_\theta = \sigma_2 = \sigma_3 > 0$.

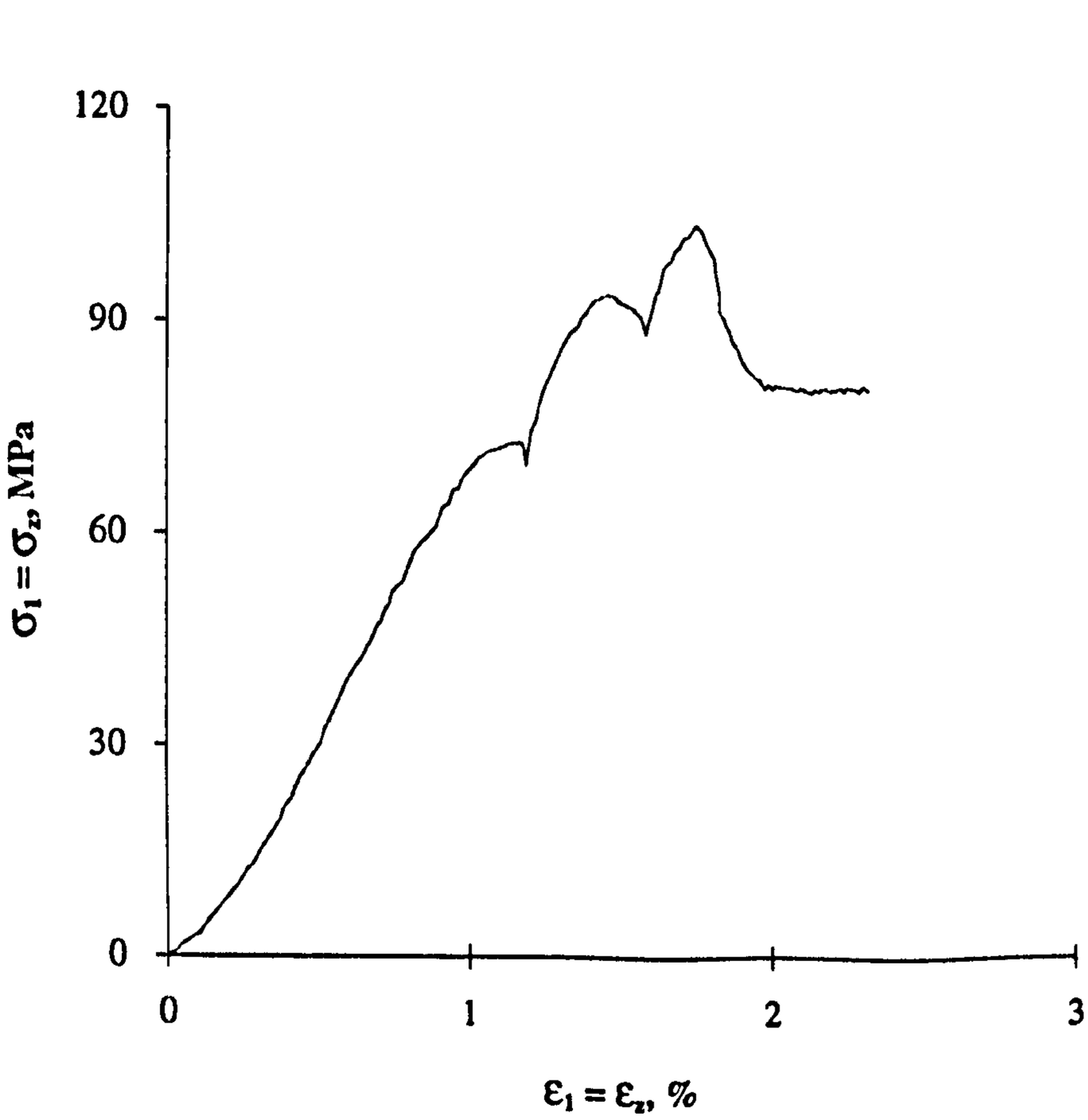

Figure 6.48 Major principal stress, $\sigma_1 = \sigma_z$, versus major principal strain, $\varepsilon_1 = \varepsilon_z$, for the above multiple failure state triaxial test on a hollow cylinder of Springwell sandstone.

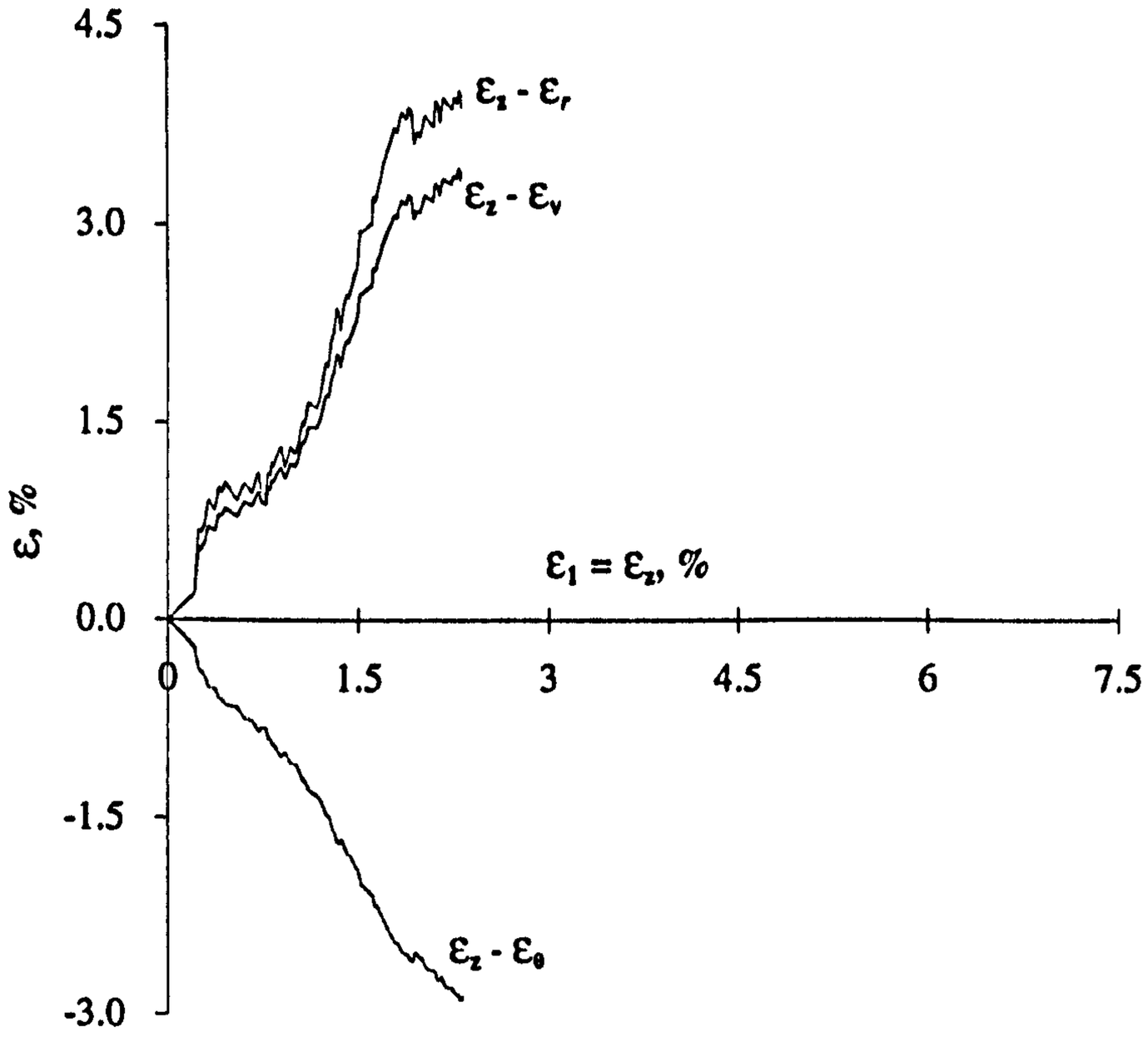

Figure 6.49 Major principal strain, $\varepsilon_z = \varepsilon_1$, versus radial strain, ε_r, tangential strain, ε_θ, and volumetric strain, ε_{vh}, at the specimen inner walls.

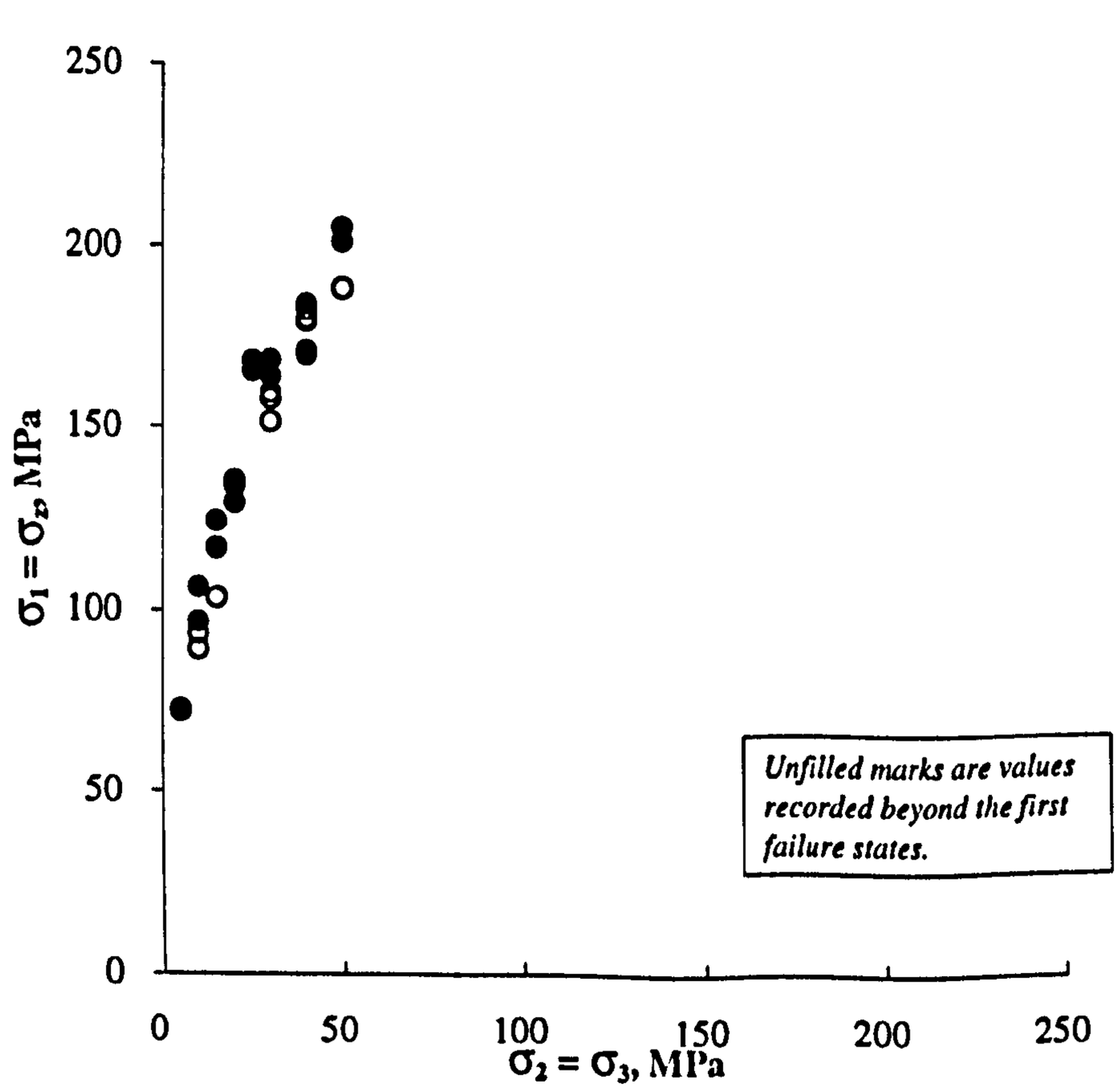

Figure 6.50 Variation of $\sigma_1 = \sigma_z$ at failure with $\sigma_2 = \sigma_3$ in single and multiple failure state triaxial tests on thick-walled hollow cylinders of Springwell sandstone.

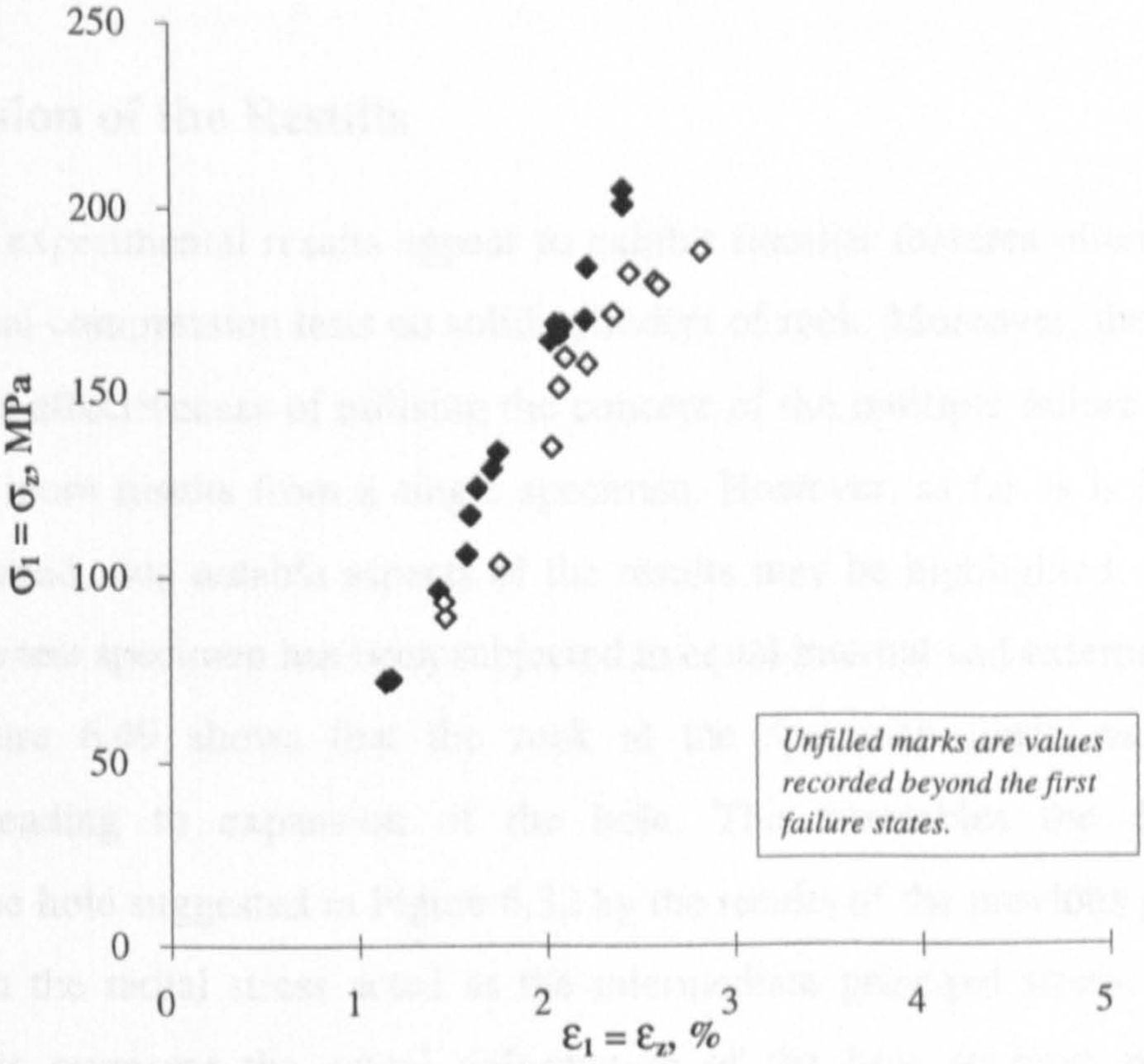

Figure 6.51 Major principal stress, $\sigma_1 = \sigma_z$, at failure versus major principal strain, $\varepsilon_1 = \varepsilon_z$, for single and multiple failure state triaxial tests on thick-walled hollow cylinders.

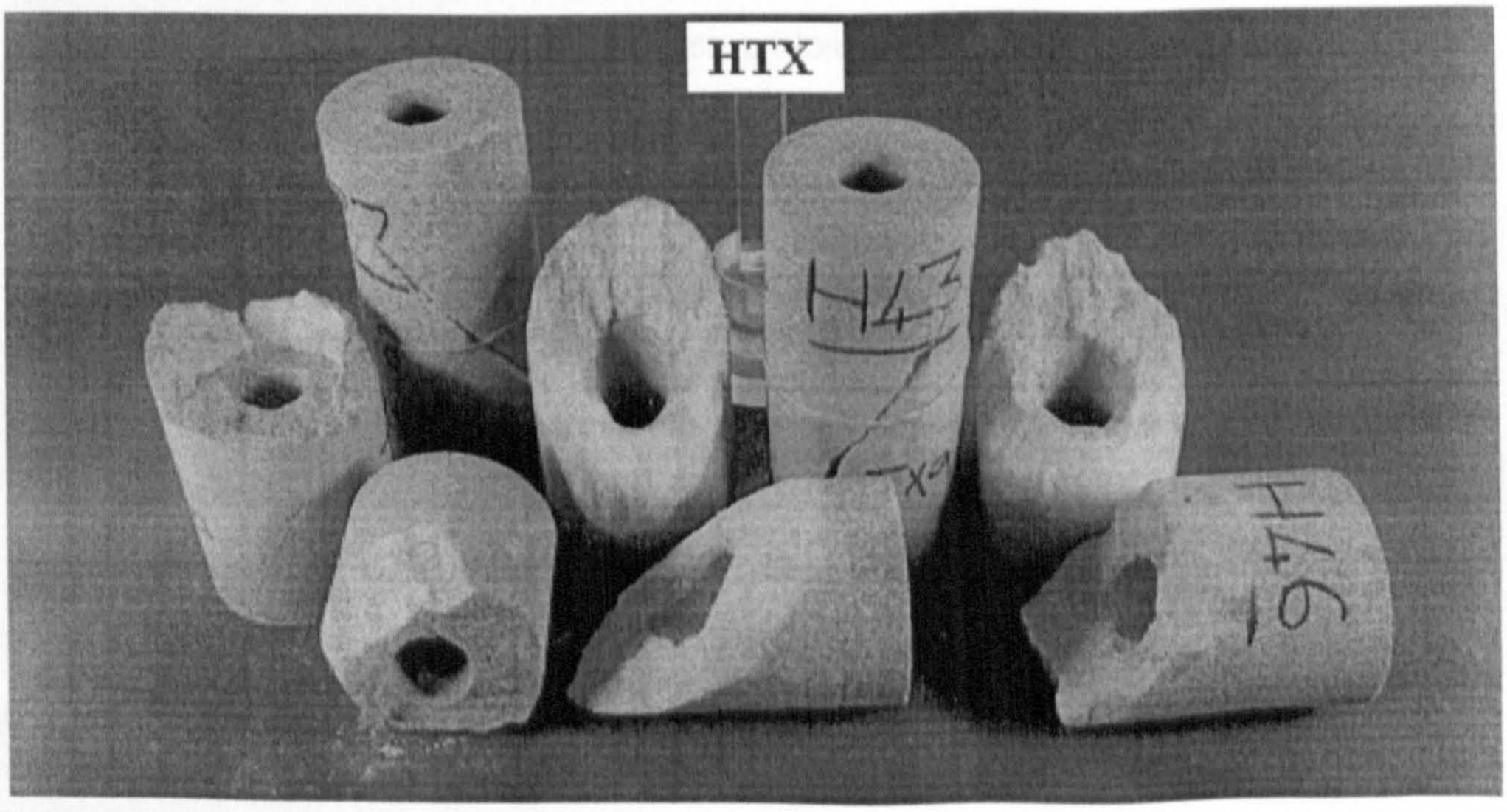

Figure 6.52 Failure of thick-walled hollow cylinders of Springwell sandstone in triaxial compression tests in which $\sigma_1 = \sigma_z > P_i = P_o = \sigma_r = \sigma_\theta = \sigma_2 = \sigma_3 > 0$.

6.6.3 Discussion of the Results

In general, the experimental results appear to exhibit familiar features often observed in results of triaxial compression tests on solid cylinders of rock. Moreover, they once again demonstrate the effectiveness of utilising the concept of the multiple failure state triaxial test to acquire more results from a single specimen. However, as far as hollow cylinder tests are concerned, two notable aspects of the results may be highlighted. First, despite the fact that the test specimen has been subjected to equal internal and external hydrostatic pressures, Figure 6.49 shows that the rock at the specimen inner wall undergoes compression leading to expansion of the hole. This resembles the deformational behaviour of the hole suggested in Figure 6.32 by the results of the previous polyaxial test series in which the radial stress acted as the intermediate principal stress. Whether the obtained results represent the actual deformation of the hole or have possibly been influenced by factors discussed earlier in 6.4.3 is a matter of interpretation.

The other notable outcome of the present tests lies in the specimen failure. In agreement with results commonly obtained from triaxial compression tests, the specimen failure appears to be governed by shear. However, a close resemblance has been found between failure patterns resulted from the present tests and those developed under polyaxial loading conditions. Clearly, any variations in the balance of the internal and external pressures during triaxial tests are likely to influence the specimen failure, and such variations are bound to occur as exact pressure levels can hardly be maintained. In addition, as observed in triaxial compression tests on cubes, failure is unlikely to propagate evenly along both lateral principal directions. Therefore, similarity between triaxial test results and results of polyaxial tests may emerge.

6.7 Biaxial Compression Tests - First Series

6.7.1 Outline of the Tests

In line with the cubical test programme, biaxial compression tests have been carried out on thick-walled hollow cylinders of Springwell sandstone. A total of thirty-two specimens of the same size to those used in the foregoing polyaxial and triaxial hollow cylinder tests have been involved in this first biaxial test series. Biaxial compression has been achieved by subjecting the test specimen to axial load and external hydrostatic pressure, P_o, only. Different levels of P_o were applied to induce at the specimen inner walls predetermined biaxial stress states in which:

$$\sigma_z = \sigma_1 > \sigma_\theta = \sigma_2 > \sigma_r = \sigma_3 = 0$$

While the basic principle of the tests was to maintain the specimen inner hole vacant, half of the test specimens were subjected to a nominal internal pressure, P_i, of no more than 0.5 MPa, so that measurements of hole volumetric change could be made. The loading conditions for each individual test conducted in this series are presented in Table 6.5.

6.7.2 The Experimental Results

A representative plot of a biaxial loading sequence of a thick-walled hollow cylinder is illustrated in Figure 6.53 in terms of the applied external pressure, P_o, and the axial stress, F / A, plotted versus time. The same loading sequence is shown in Figure 6.54 in terms of the corresponding principal stresses, $\sigma_\theta = \sigma_2$ and $\sigma_z = \sigma_1$ calculated at the cylinder inner wall. Figure 6.55 shows a typical plot of the major principal stress, $\sigma_z = \sigma_1$, versus the major principal strain, $\varepsilon_z = \varepsilon_1$. An illustration of the hole deformation is presented in Figure 6.56 in which recorded values of the axial strain, $\varepsilon_z = \varepsilon_1$, are plotted versus the tangential strain, $\varepsilon_\theta = \varepsilon_2$, radial strain, $\varepsilon_r = \varepsilon_3$, and volumetric strain ε_{vh}. These values have been calculated at the specimen inner wall on the basis of the obtained measurements of the hole volumetric change, ΔV_h, following the same method employed in the foregoing hollow cylinder tests and outlined in 6.2.4. Recorded levels of $\sigma_z = \sigma_1$ at

Table 6.5 Applied levels of external pressure, P_o, and corresponding values of tangential stress, σ_θ, at the specimen inner surface for the first biaxial test series on thick-walled hollow cylinders. Also shown maximum level of internal pressure, P_i, applied.

Specimen No.	P_o, MPa	$\sigma_\theta = \sigma_2$, MPa	Max. P_i, MPa
HBG1	2.176	5	0
HBG2	2.176	5	0
HBG3	2.176	5	0.5
HBG4	2.176	5	0.5
HBG5	4.352	10	0
HBG6	4.352	10	0
HBG7	4.352	10	0.5
HBG8	4.352	10	0.5
HBG9	6.528	15	0
HBG10	6.528	15	0
HBG11	6.528	15	0.5
HBG12	6.528	15	0.5
HBG13	8.704	20	0
HBG14	8.704	20	0
HBG15	8.704	20	0.5
HBG16	8.704	20	0.5
HBG17	10.880	25	0
HBG18	10.880	25	0
HBG19	10.880	25	0.5
HBG20	10.880	25	0.5
HBG21	13.056	30	0
HBG22	13.056	30	0
HBG23	13.056	30	0.5
HBG24	13.056	30	0.5
HBG25	17.408	40	0
HBG26	17.408	40	0
HBG27	17.408	40	0.5
HBG28	17.408	40	0.5
HBG29	21.760	50	0
HBG30	21.760	50	0
HBG31	21.760	50	0.5
HBG32	21.760	50	0.5

failure for all specimens tested are plotted in Figure 6.57 and Figure 6.58 versus the corresponding values of $\sigma_\theta = \sigma_2$ and $\varepsilon_z = \varepsilon_1$, respectively. Different markers have been used in these figures to distinguish between results of tests conducted with zero internal pressure, $P_i = 0$, and those in which a minimum level of P_i was applied.

As generally observed under previous loading conditions, the specimen failure in these biaxial tests was often marked by audible fracturing accompanied by a marked fall in the level of the major principal stress. Moreover, failure appeared to be of the shear type often resulting in a major inclined fracture. However, unlike the previous polyaxial and triaxial tests, most fracture surfaces did not exhibit intense signs of rubbing or sliding. Shear cones were also visible in a number of tests. Most specimens, particularly those tested without internal pressure and subjected to relatively high levels of external pressure, showed conspicuous evidence of spalling from their inner walls. Representative failure patterns are pictured in Figure 6.59.

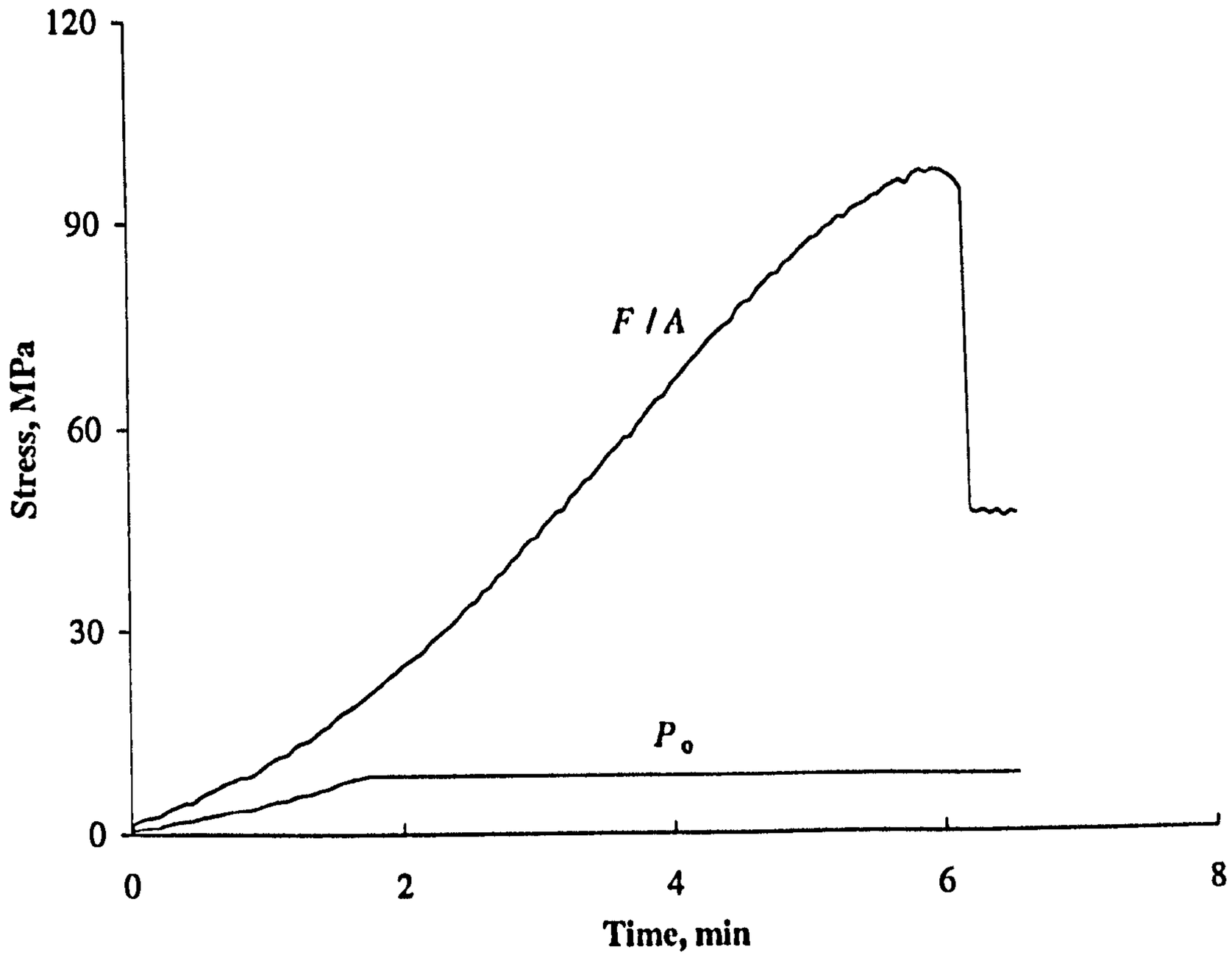

Figure 6.53 A typical loading sequence for the first biaxial test series on hollow cylinders plotted in terms of applied external pressure, P_o, and axial stress, F / A, versus time.

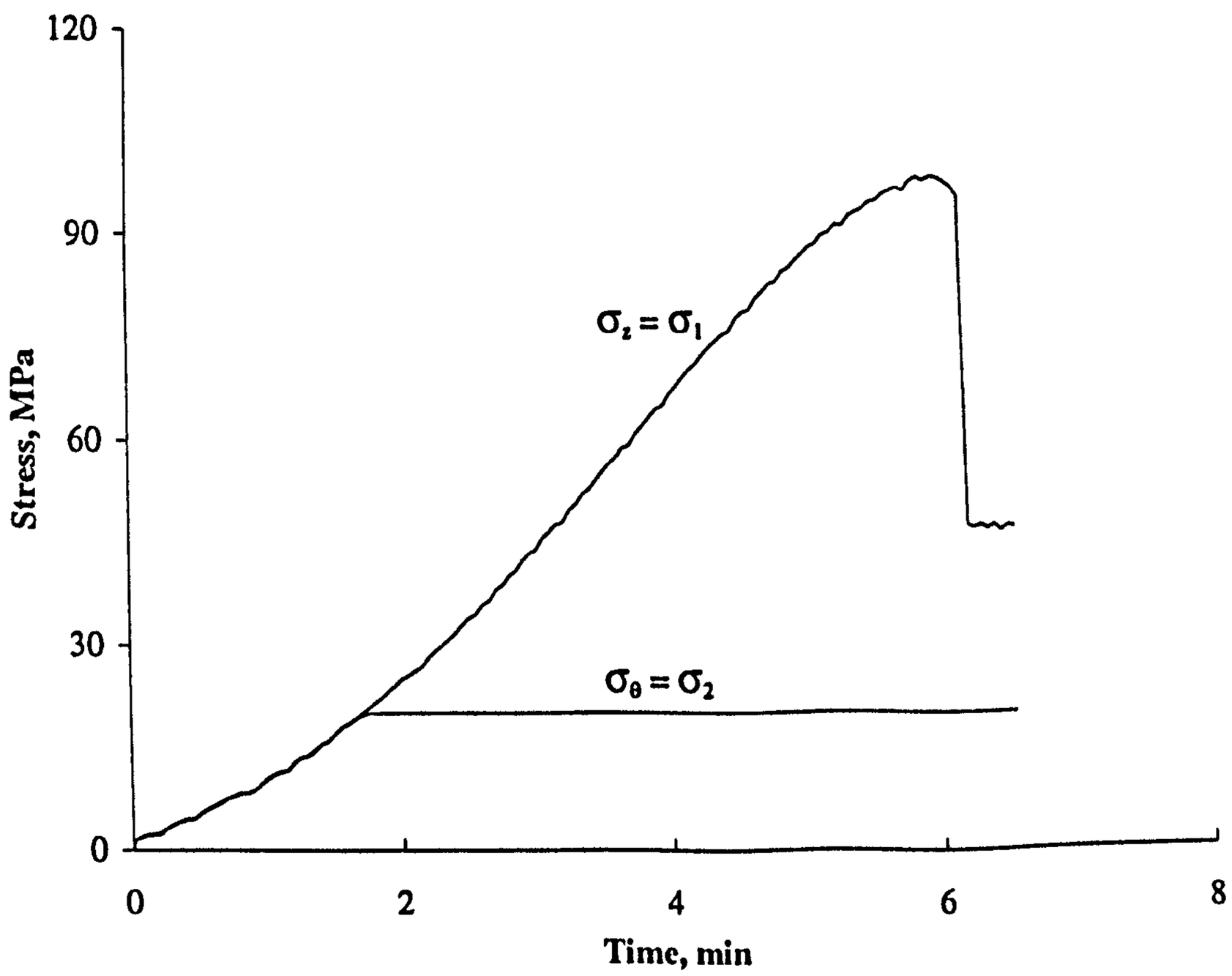

Figure 6.54 The above loading sequence in terms of the corresponding principal stresses $\sigma_\theta = \sigma_2$ and $\sigma_z = \sigma_1$ induced at the cylinder inner wall.

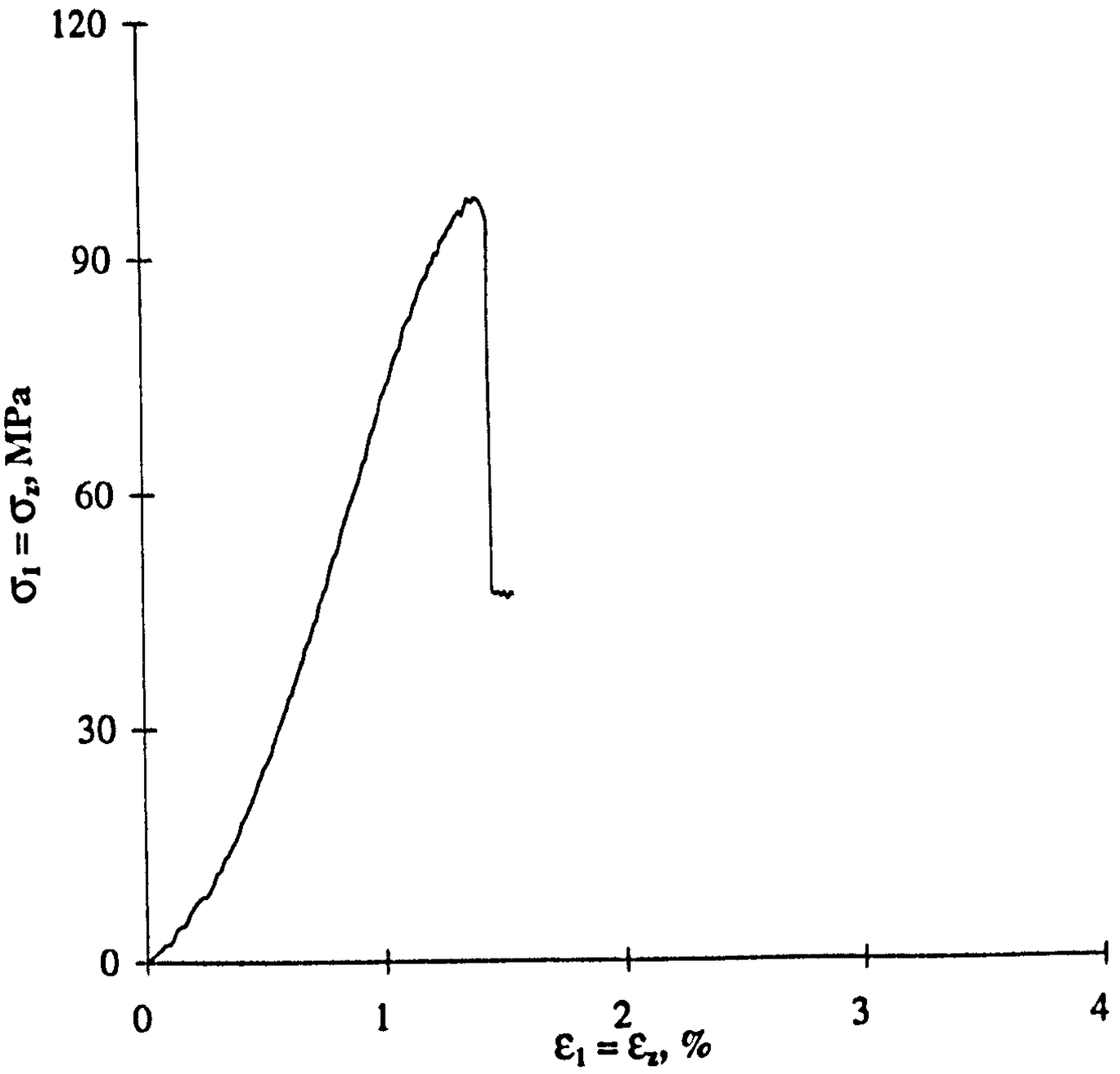

Figure 6.55 Major principal stress, $\sigma_1 = \sigma_z$, versus major principal strain, $\varepsilon_1 = \varepsilon_z$, for a hollow cylinder biaxial compression test in which $\sigma_2 = \sigma_\theta = 20$ MPa.

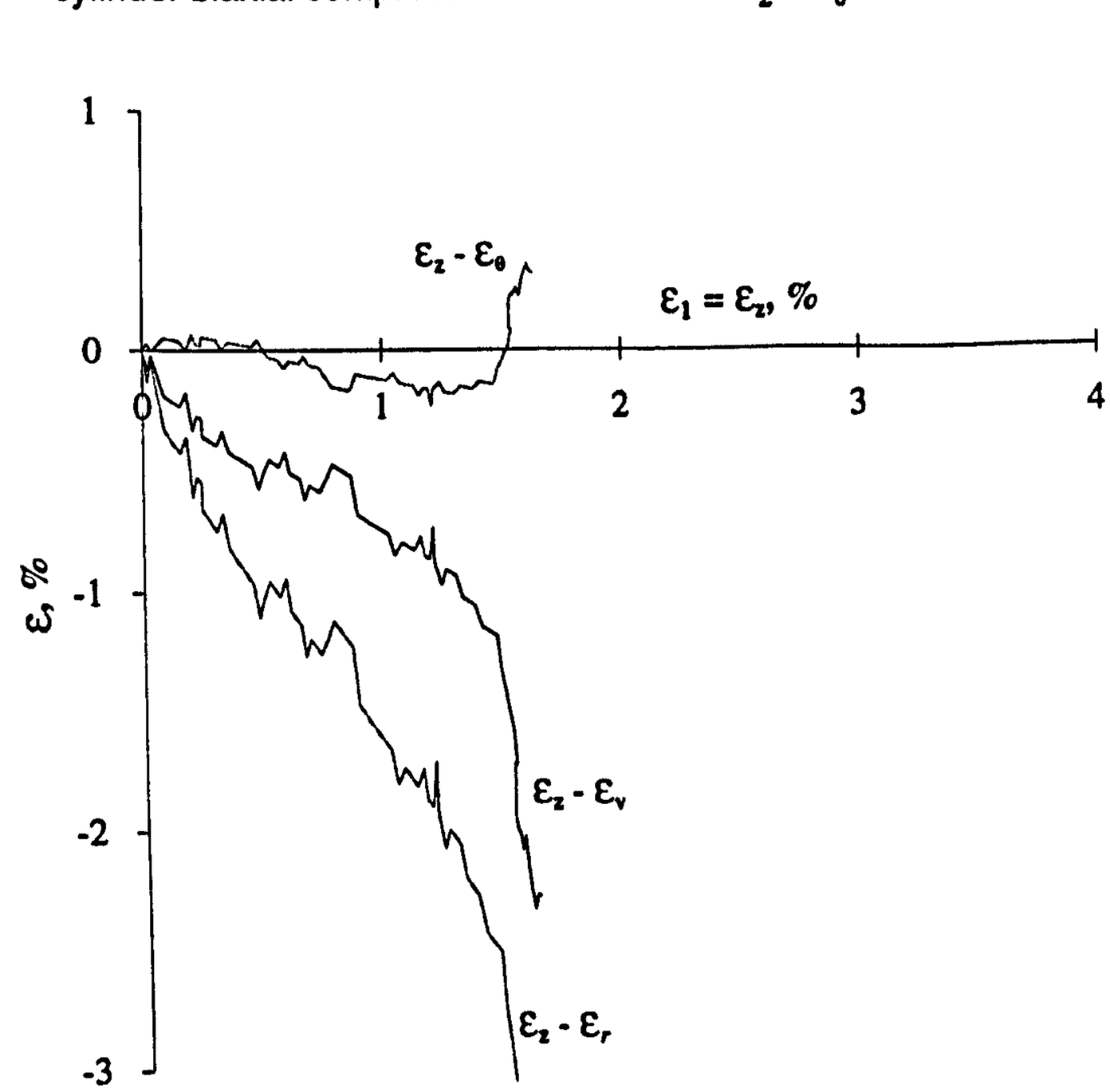

Figure 6.56 Major principal strain, $\varepsilon_z = \varepsilon_1$, versus tangential strain, $\varepsilon_\theta = \varepsilon_2$, radial strain, $\varepsilon_r = \varepsilon_3$, and volumetric strain, $\varepsilon_{v/h}$, at the specimen inner walls.

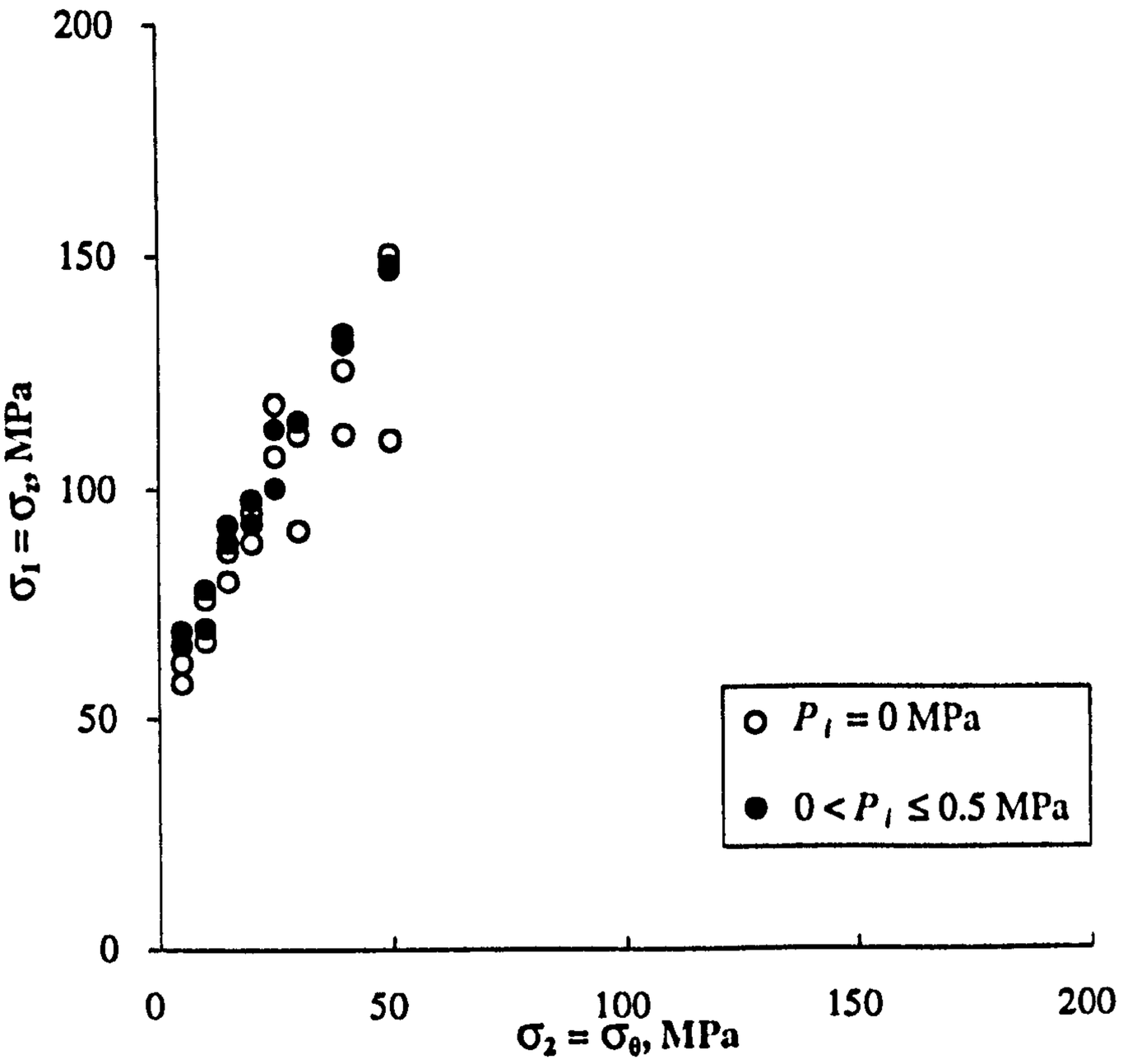

Figure 6.57 Variation of $\sigma_1 = \sigma_z$ at failure with $\sigma_2 = \sigma_\theta$ in biaxial compression tests on thick-walled hollow cylinders in which $\sigma_1 = \sigma_z > \sigma_2 = \sigma_\theta > \sigma_r = \sigma_3 = 0$.

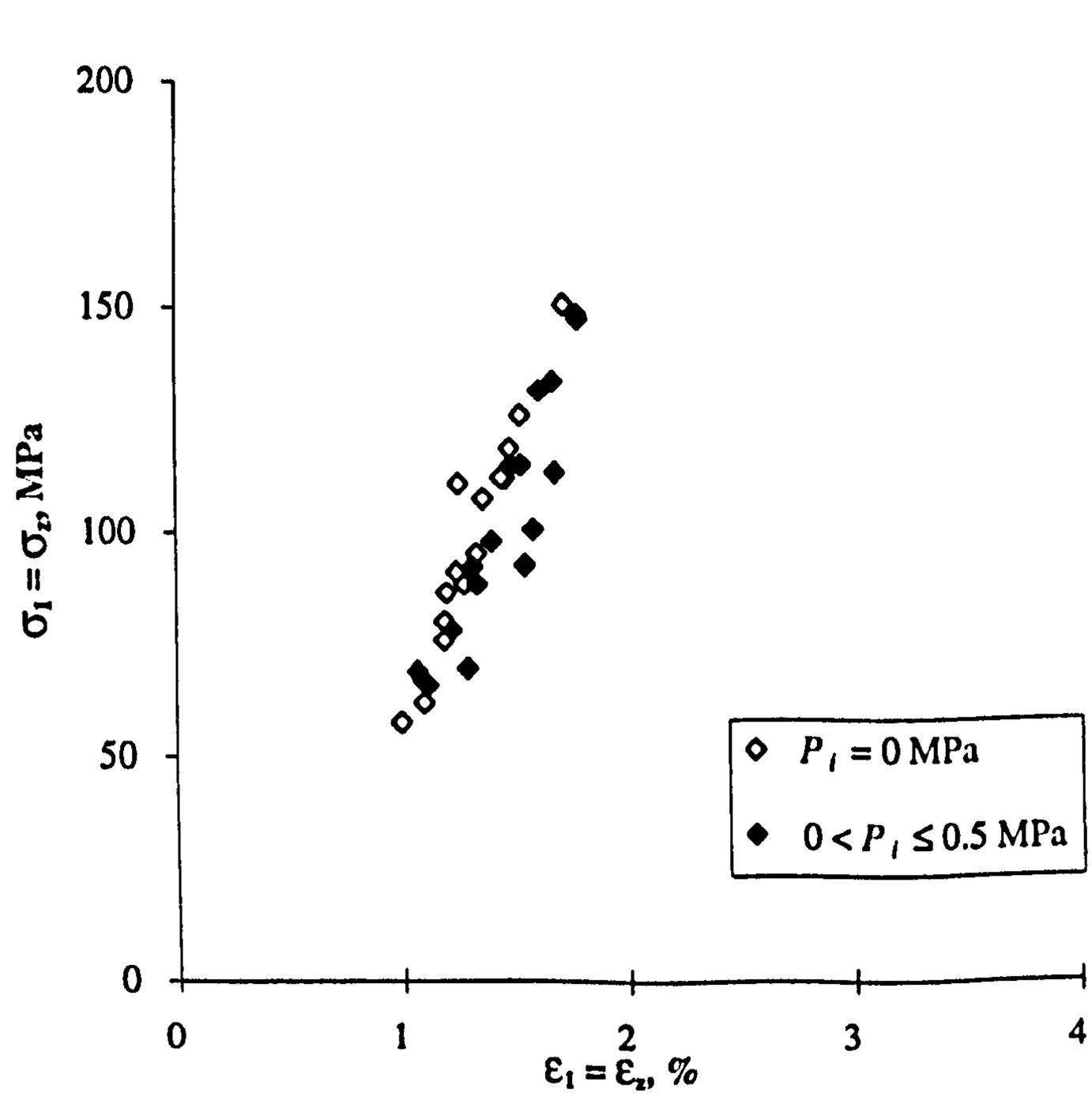

Figure 6.58 Major principal stress, $\sigma_1 = \sigma_z$, at failure versus major principal strain, $\varepsilon_1 = \varepsilon_z$, for the above biaxial tests on hollow cylinders of Springwell sandstone.

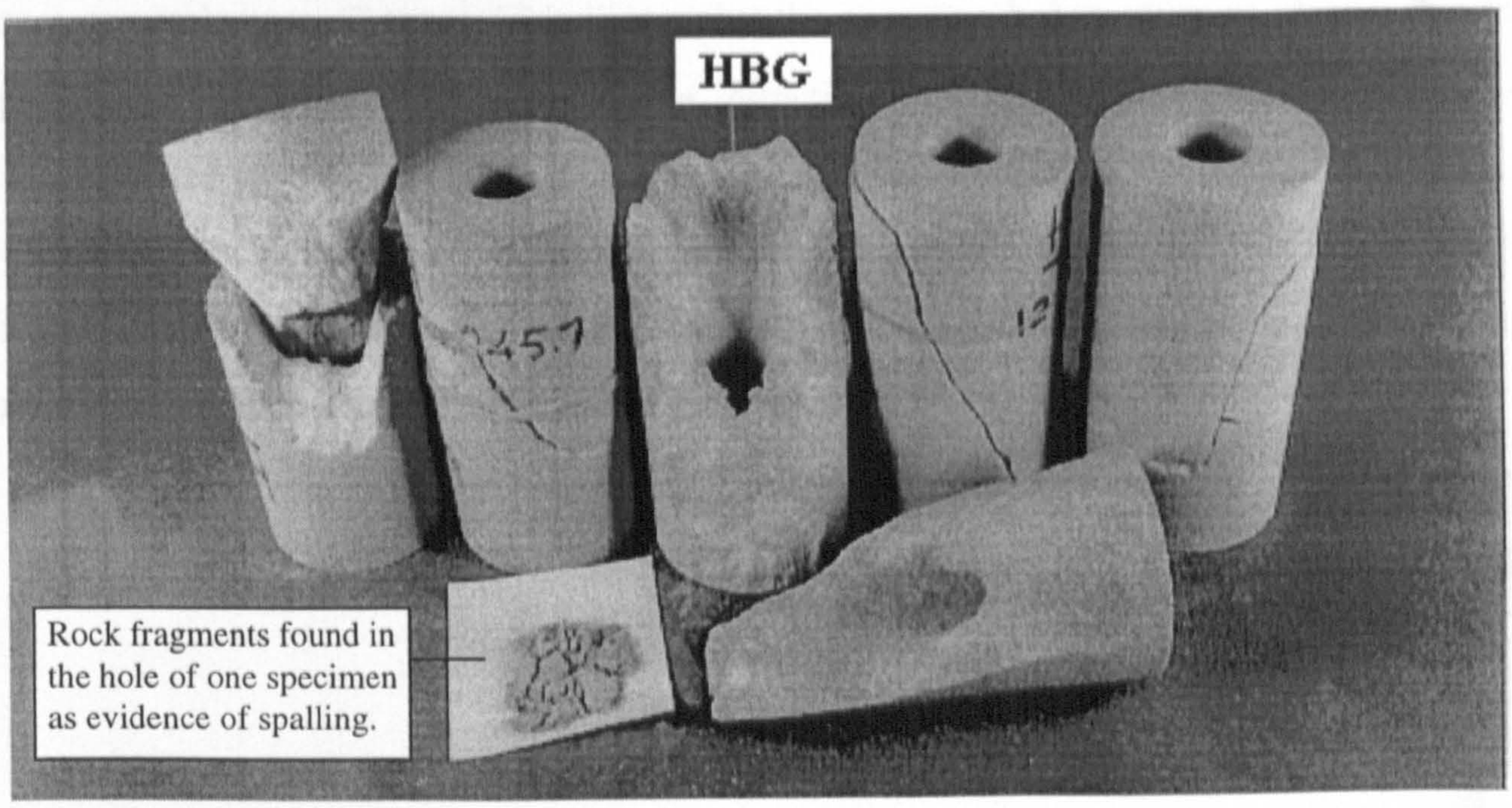

Figure 6.59 Typical failure patterns observed in the first biaxial test series on hollow cylinders of Springwell sandstone in which $\sigma_1 = \sigma_z > \sigma_2 = \sigma_\theta > \sigma_r = \sigma_3 = 0$.

6.7.3 Discussion of the Results

Although the application of a nominal internal pressure in some tests was necessary to enable measurements of the hole volumetric change to be made, it was of concern whether this would have any influence on the test results. As earlier pointed out, evidence of spalling in the specimen hole was found to be more pronounced in tests conducted without internal pressure. However, as far as the specimen strength is concerned, both Figures 6.57 and 6.58 do not exhibit any notable phenomenon that may be attributed to the presence of internal pressure.

As Figure 6.57 shows, there appears to be a considerable increase in the magnitude of the major principal stress, $\sigma_1 = \sigma_z$, at failure with increasing the magnitude of the intermediate principal stress, $\sigma_2 = \sigma_\theta$. In comparison with the cubical biaxial tests, the level of increase is clearly much more pronounced. Moreover, although the increase in σ_1 level in some tests conducted with $P_i = 0$ appears to cease or fall at relatively higher levels of σ_2, most tests show that σ_1 continues to increase as σ_2 level increases.

Predictably, with the minor principal stress, $\sigma_3 = \sigma_r$, at the specimen inner walls being zero or nearly zero, Figure 6.56 indicates that the specimen hole undergoes closure due to progressive rock expansion along the direction of σ_3. The process is evidently accompanied by brittle spalling of small rock fragments from the specimen inner walls. Consequently, shear fractures appear to develop leading eventually to the specimen failure. Due to the absence of support pressure in the hole, failure is likely to propagate more freely leaving the fracture surfaces less liable to intense shear.

6.8 Biaxial Compression Tests - Second Series

6.8.1 Outline of the Tests

As carried out under polyaxial loading conditions, a second biaxial test series on thick-walled hollow cylinders of Springwell sandstone has been conducted with the radial stress, σ_r, at the specimen inner walls being in this case the intermediate principal stress, σ_2, while the tangential stress is the minor principal stress, $\sigma_\theta = \sigma_3 = 0$, and the axial stress remains the major principal stress, $\sigma_z = \sigma_1$, as expressed by the following equation:

$$\sigma_z = \sigma_1 > \sigma_r = \sigma_2 > \sigma_\theta = \sigma_3 = 0$$

According to the theory of elasticity, such a stress field is achieved by subjecting the test cylinders to axial load and both internal and external pressures with the internal pressure being of higher level than that of the external pressure. As pointed out in the second polyaxial test series, such a loading arrangement can easily result in the development of tensile tangential stresses if the applied pressures are not accurately balanced. Therefore, every care was taken to prevent such development and ensure that the specimen failure is induced by biaxial compression rather than tensile stresses.

A total of sixteen cylinders were tested in this series under predetermined levels of σ_2 identical to those used in the first biaxial test series. Table 6.6 presents the levels of external and internal pressures applied in each test, and the corresponding values of tangential and radial stresses induced at the specimen inner walls.

6.8.2 The Experimental Results

Figure 6.60 shows a typical plot of a loading sequence for the present type of biaxial compression tests on thick-walled hollow cylinders. The plot is presented in terms of the applied external pressure, P_o, internal pressure, P_i, and axial stress, F / A, versus time. The same loading sequence is illustrated in Figure 6.61 in terms of the corresponding principal stresses, $\sigma_\theta = \sigma_3$, $\sigma_r = \sigma_2$, $\sigma_z = \sigma_1$, calculated at the specimen inner wall. A

Table 6.6 Applied levels of external and internal pressures, P_o and P_i, and corresponding values of tangential and radial stresses, σ_θ and σ_r, at the specimen inner surface for the second biaxial test series on thick-walled hollow cylinders of Springwell sandstone.

Specimen No.	P_o, MPa	P_i, MPa	$\sigma_\theta = \sigma_3$, MPa	$\sigma_r = \sigma_2$, MPa
HBR1	2.824	5	0	5
HBR2	2.824	5	0	5
HBR3	5.648	10	0	10
HBR4	5.648	10	0	10
HBR5	8.472	15	0	15
HBR6	8.472	15	0	15
HBR7	11.296	20	0	20
HBR8	11.296	20	0	20
HBR9	14.120	25	0	25
HBR10	14.120	25	0	25
HBR11	16.944	30	0	30
HBR12	16.944	30	0	30
HBR13	22.592	40	0	40
HBR14	22.592	40	0	40
HBR15	28.240	50	0	50
HBR16	28.240	50	0	50

representative plot of the major principal stress, $\sigma_z = \sigma_1$, versus the major principal strain, $\varepsilon_z = \varepsilon_1$, is illustrated in Figure 6.62. Plots of $\varepsilon_z = \varepsilon_1$ versus the calculated values of the tangential strain, $\varepsilon_\theta = \varepsilon_3$, radial strain, $\varepsilon_r = \varepsilon_2$, and volumetric strain, $\varepsilon_{v/h}$, of the specimen hole are presented in Figure 6.63. Maximum values of the major principal stress, $\sigma_z = \sigma_1$, recorded at failure for all specimens tested are plotted in Figure 6.64 and Figure 6.65 versus the corresponding values of $\sigma_r = \sigma_2$ and $\varepsilon_z = \varepsilon_1$, respectively. In order to compare the strength results of the present tests with those of the previous biaxial tests, recorded values of $\sigma_z = \sigma_1$ at failure from both test series are plotted together in Figure 6.66 versus the corresponding levels of the intermediate principal stress, σ_2. A similar plot is presented in Figure 6.67 in terms of $\sigma_z = \sigma_1$ at failure versus the corresponding values of $\varepsilon_z = \varepsilon_1$.

The specimen failure appeared in most respects to resemble that of the second polyaxial test series generally resulting in a single inclined fracture but with the fracture surfaces showing less profound symptoms of rubbing or sliding. In contrast with the previous biaxial tests, neither shear cones nor extensile cracks were formed. Moreover, evidence of spalling in the specimen hole could hardly be observed. Only three specimens departed from the general failure mode and failed along multiple fractures forming a wedge shaped patterns. Figure 6.68 pictures representative failure modes obtained.

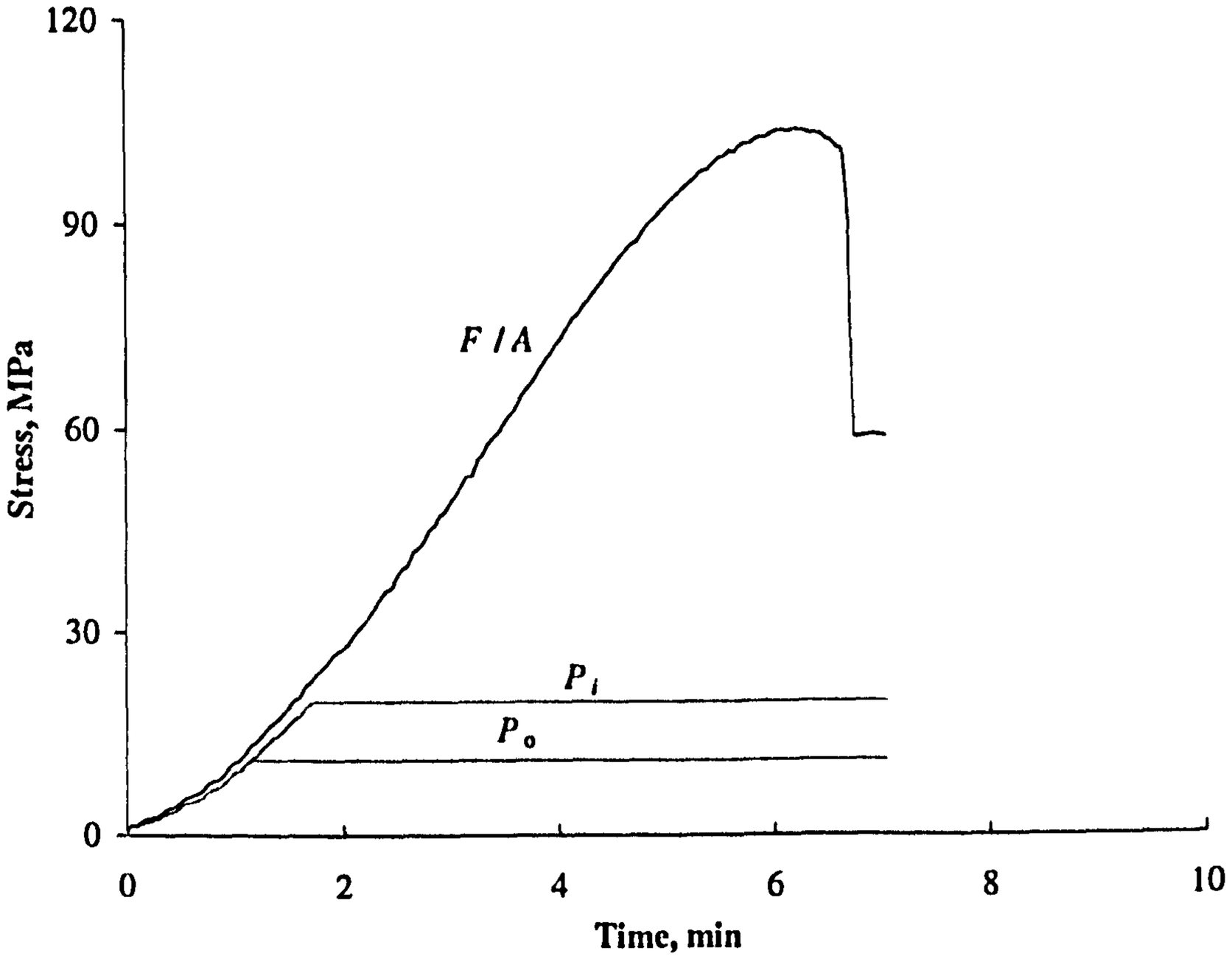

Figure 6.60 A typical loading sequence for the second biaxial test series on hollow cylinders plotted in terms of applied external pressure, P_o, internal pressure, P_i, and axial stress, F / A, versus time.

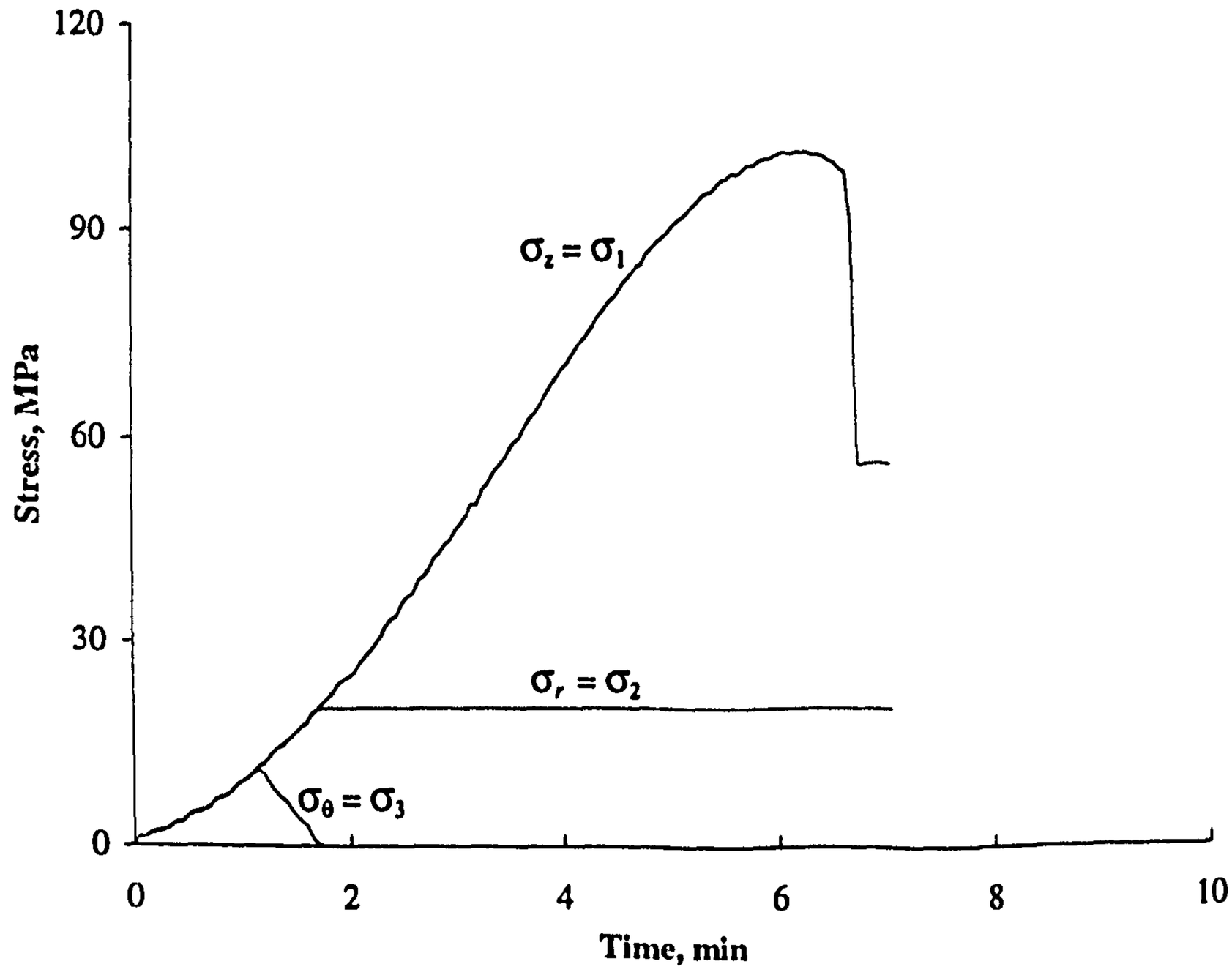

Figure 6.61 The above loading sequence in terms of the corresponding principal stresses induced at the cylinder inner wall where $\sigma_1 = \sigma_z > \sigma_2 = \sigma_r > \sigma_\theta = \sigma_3 = 0$.

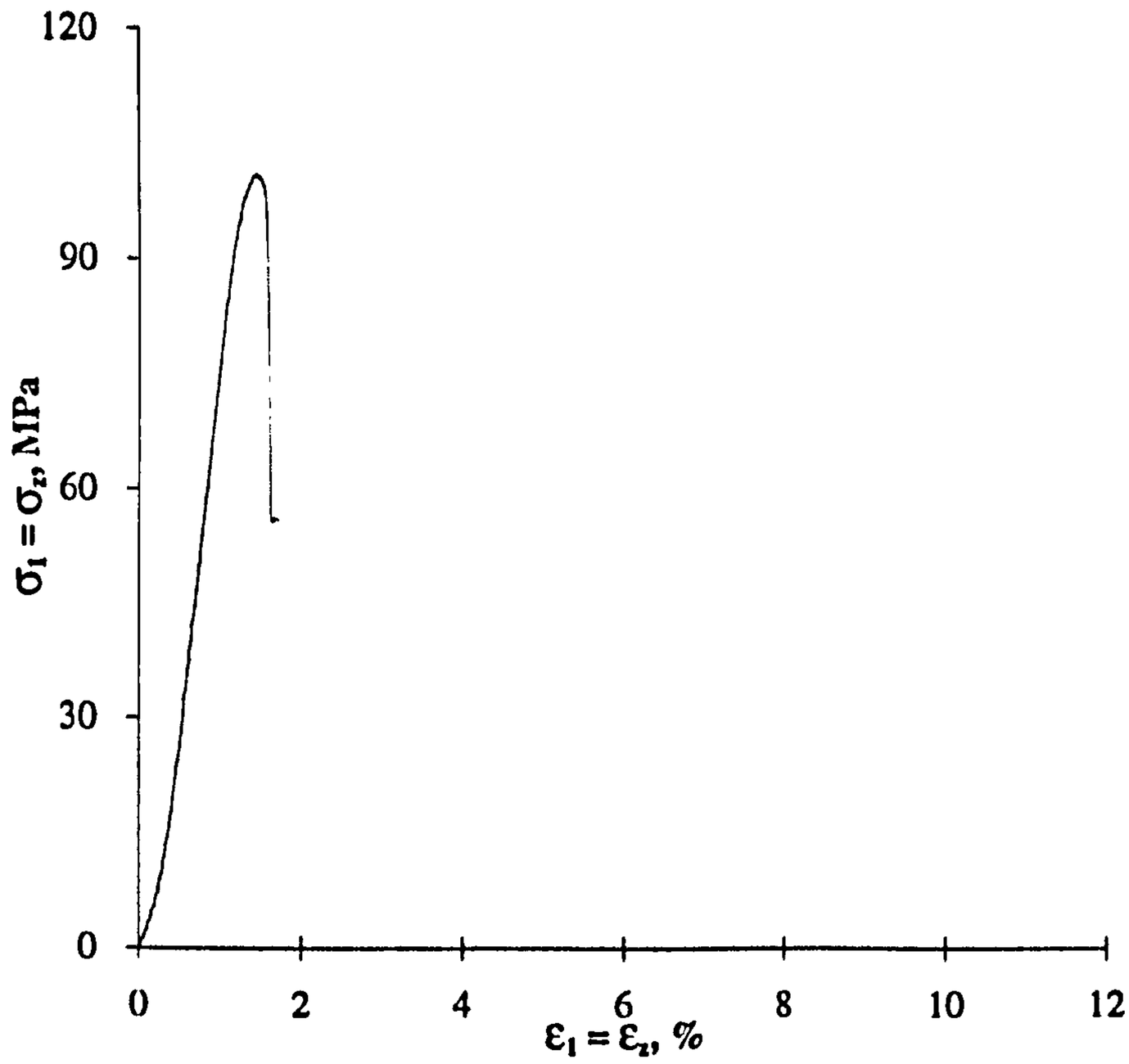

Figure 6.62 Major principal stress, $\sigma_1 = \sigma_z$, versus major principal strain, $\varepsilon_1 = \varepsilon_z$, for a hollow cylinder biaxial compression test in which $\sigma_2 = \sigma_r = 20$ MPa.

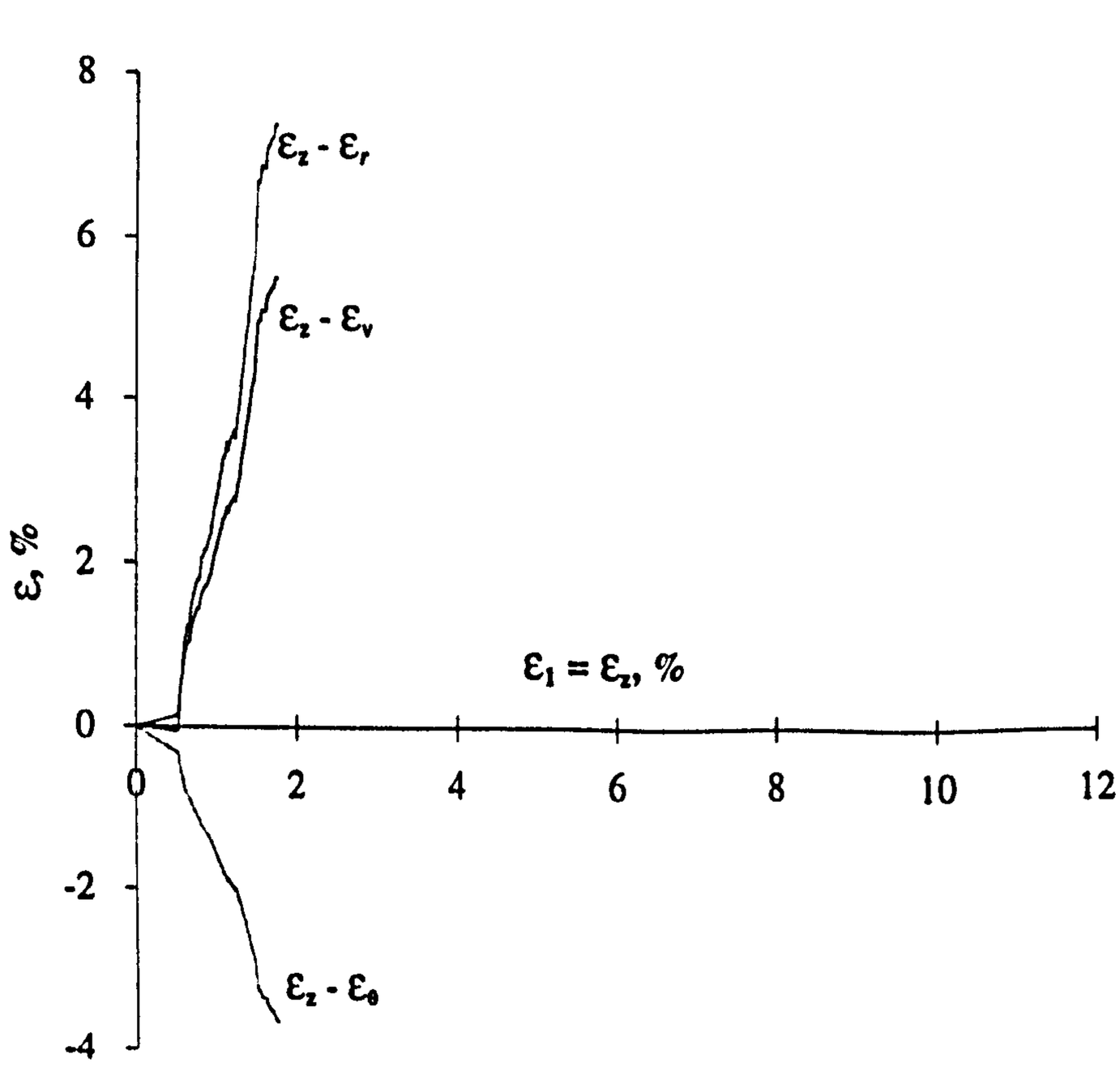

Figure 6.63 Major principal strain, $\varepsilon_z = \varepsilon_1$, versus radial strain, $\varepsilon_r = \varepsilon_2$, tangential strain, $\varepsilon_\theta = \varepsilon_3$, and volumetric strain, ε_{vh}, at the specimen inner wall.

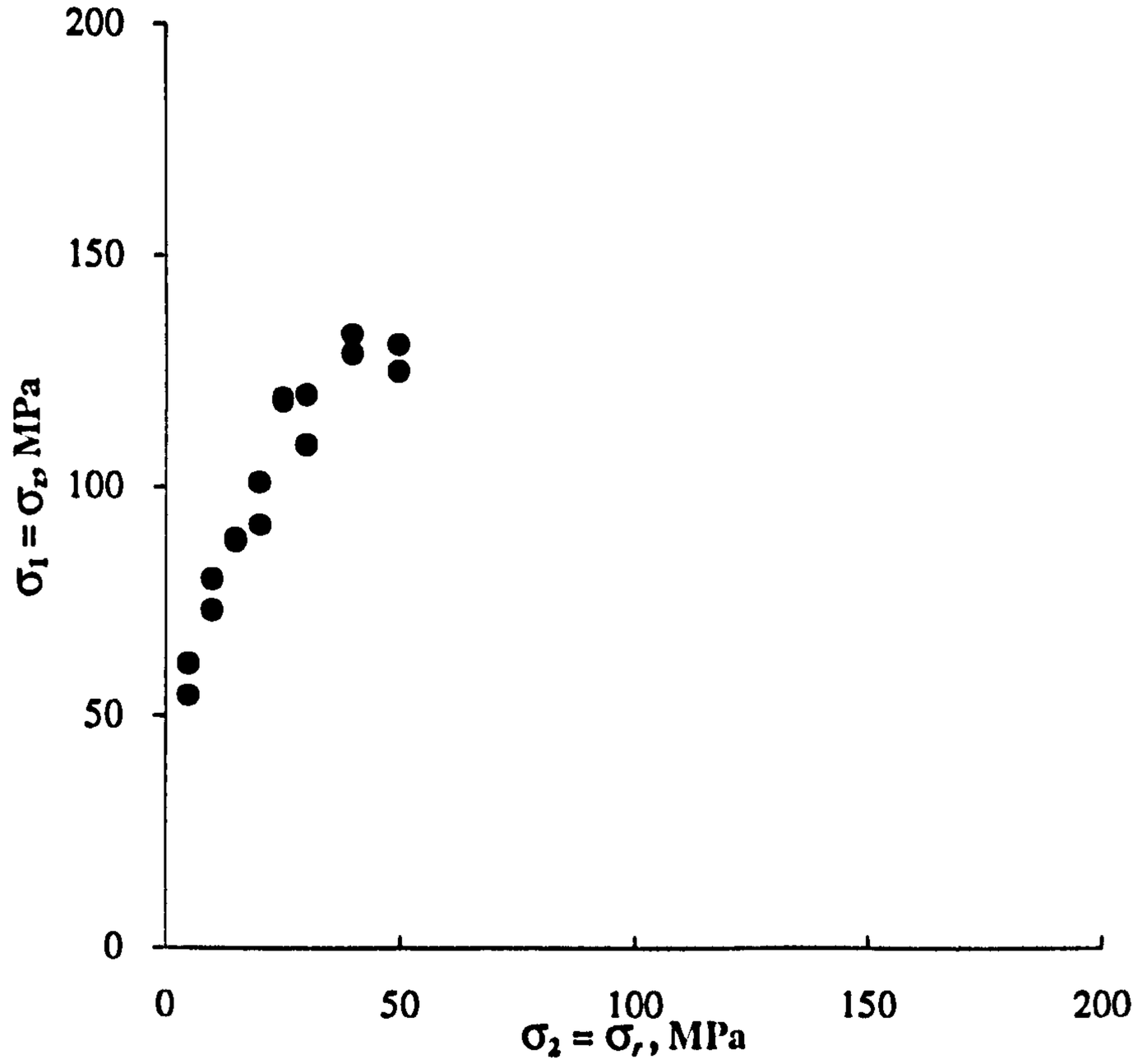

Figure 6.64 Variation of $\sigma_1 = \sigma_z$ at failure with $\sigma_2 = \sigma_r$ in biaxial compression tests on thick-walled hollow cylinders in which $\sigma_1 = \sigma_z > \sigma_2 = \sigma_r > \sigma_\theta = \sigma_3 = 0$.

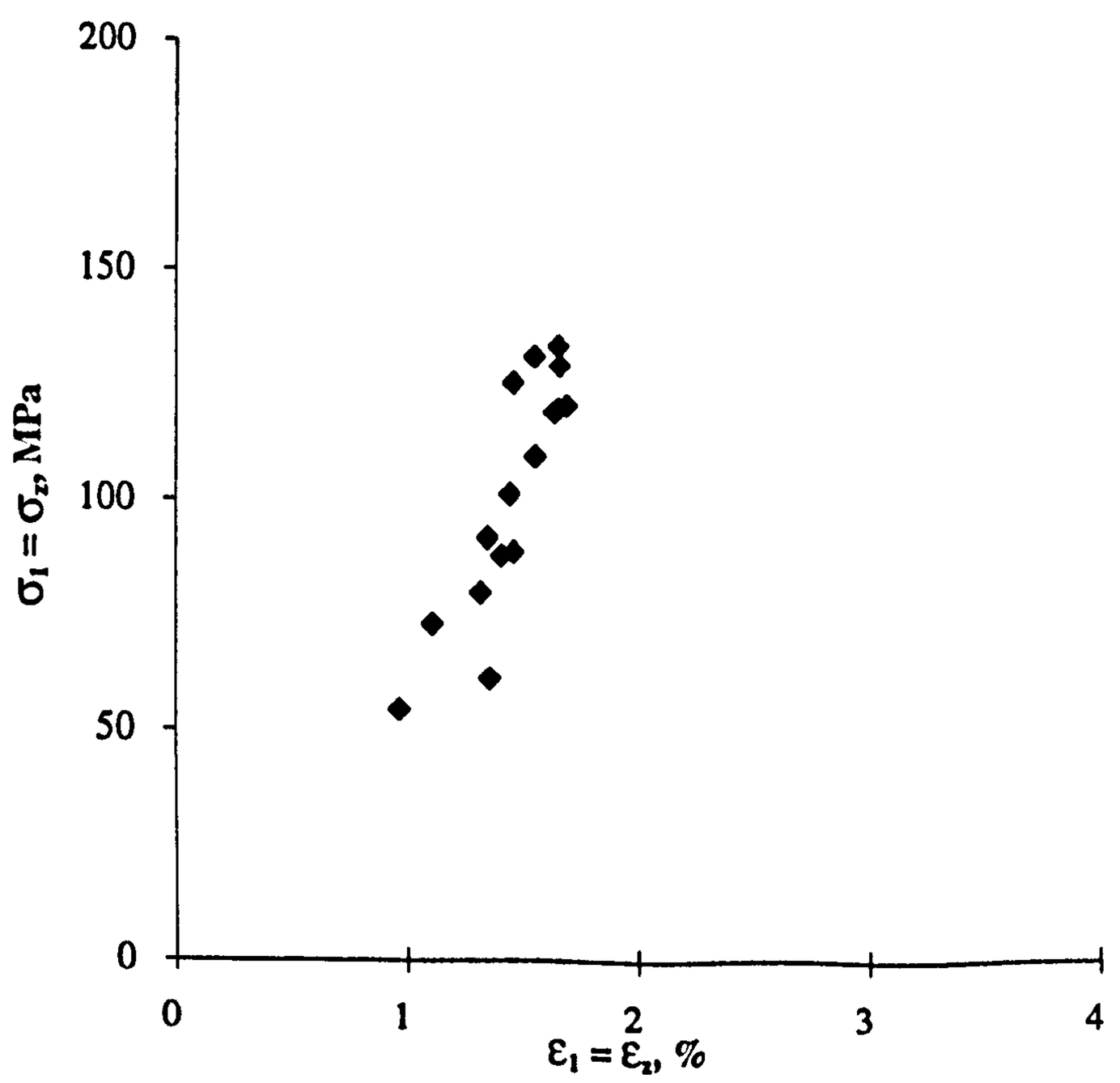

Figure 6.65 Major principal stress, $\sigma_1 = \sigma_z$, at failure versus major principal strain, $\varepsilon_1 = \varepsilon_z$, for the above biaxial tests on hollow cylinders of Springwell sandstone.

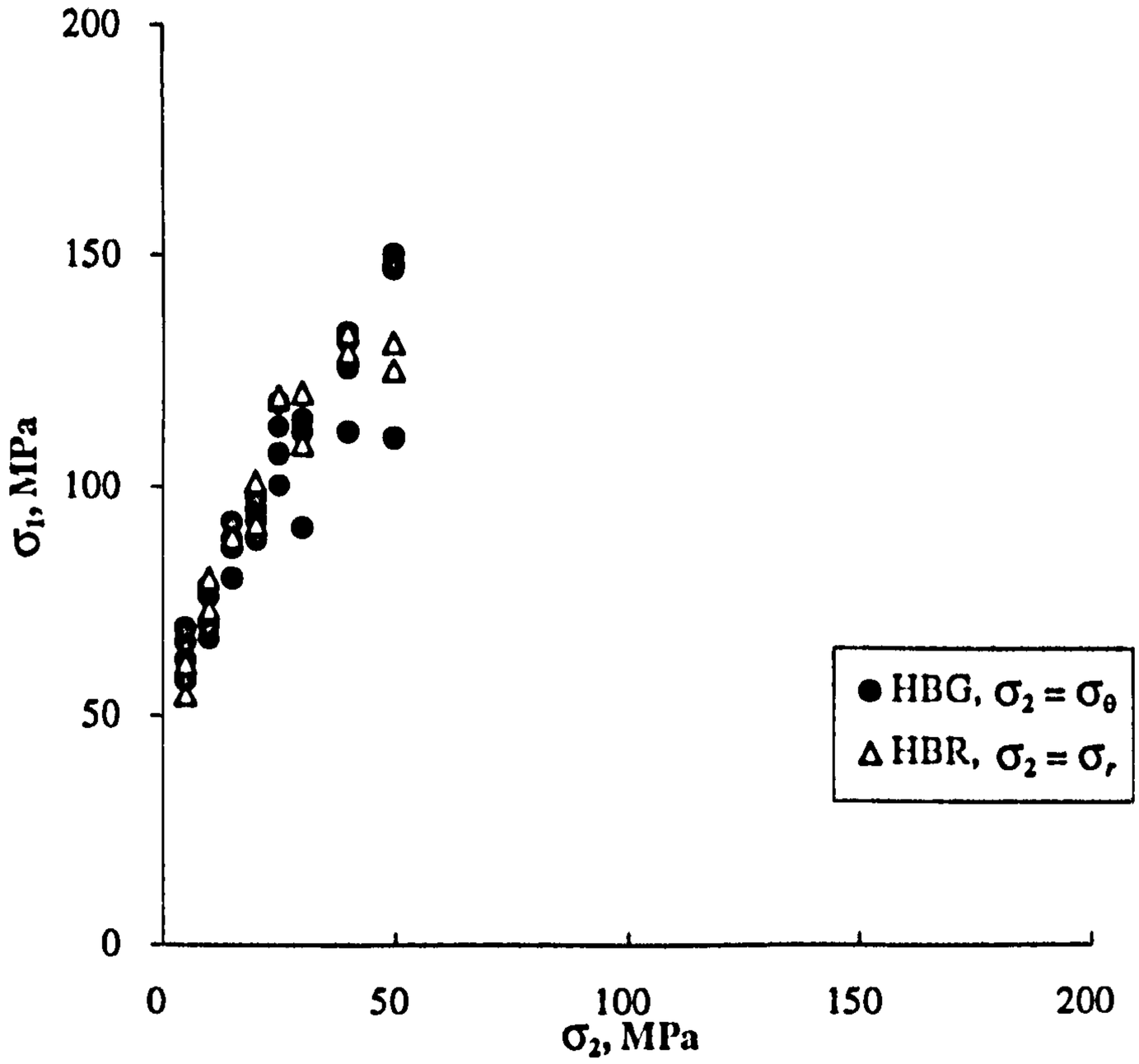

Figure 6.66 Variation of $\sigma_1 = \sigma_z$ at failure with σ_2 in biaxial tests on thick-walled hollow cylinders conducted under different loading conditions.

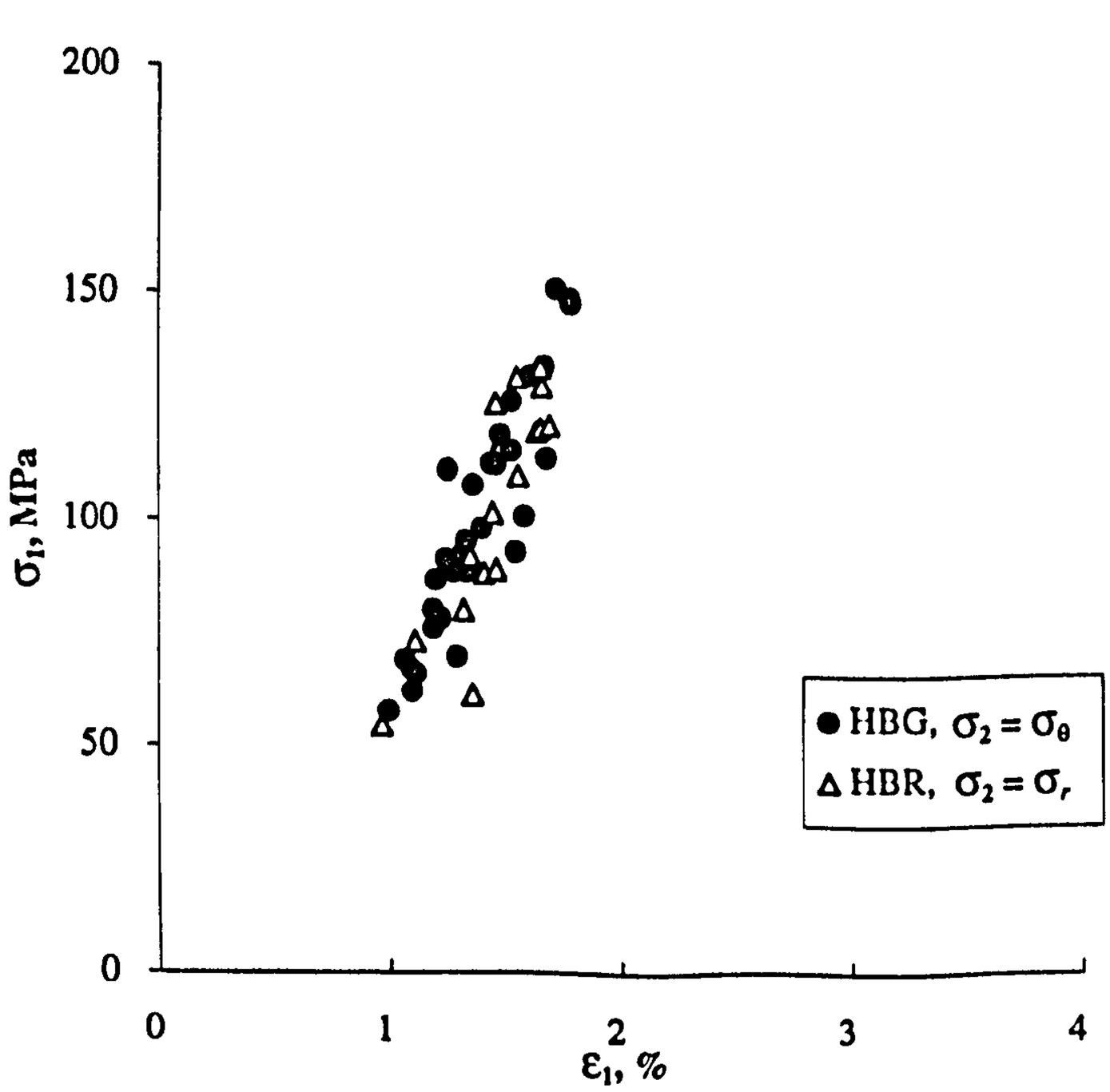

Figure 6.67 Major principal stress, $\sigma_1 = \sigma_z$, at failure versus major principal strain, $\varepsilon_1 = \varepsilon_z$, for the above biaxial tests on hollow cylinders of Springwell sandstone.

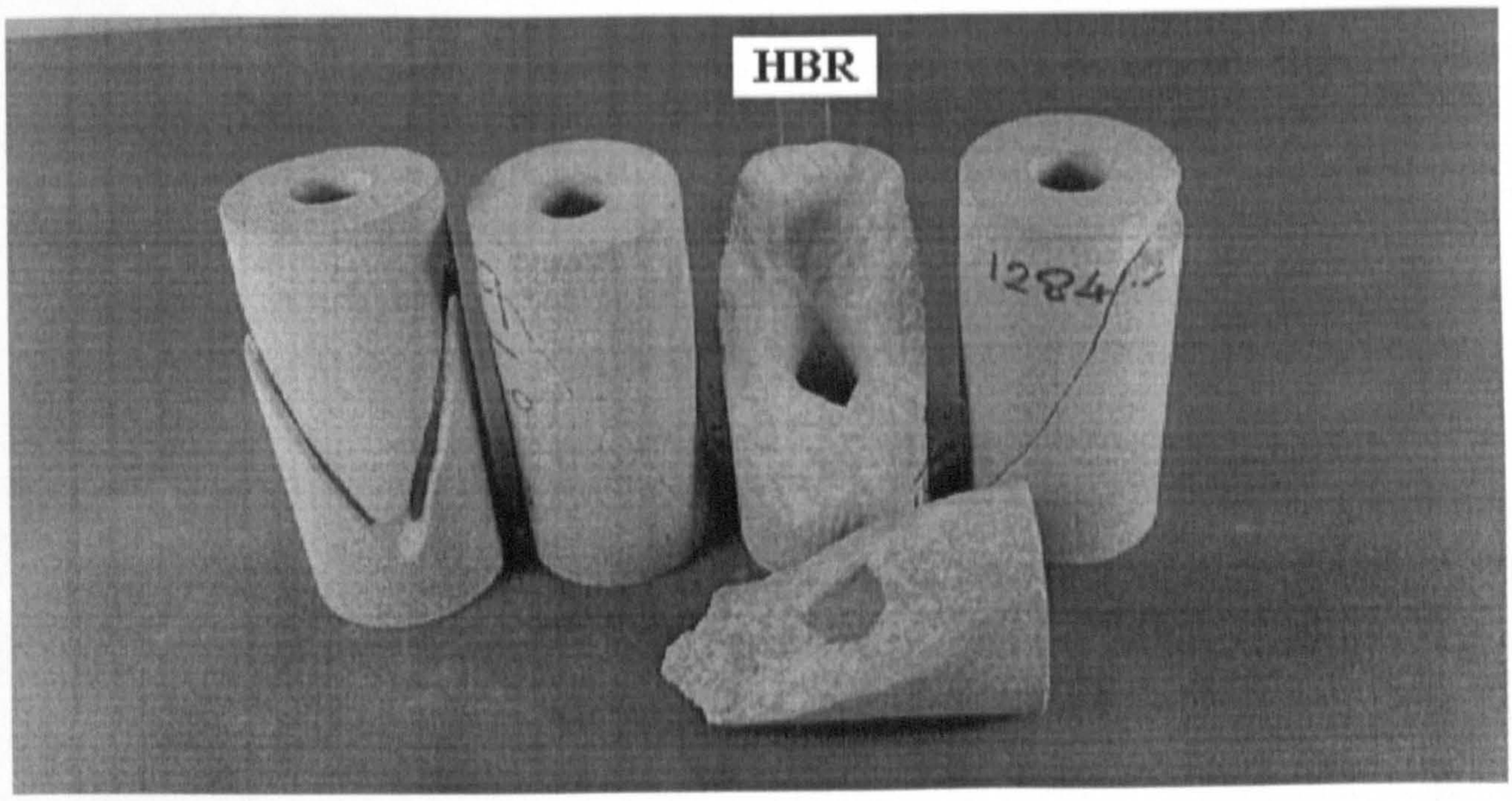

Figure 6.68 Typical failure patterns observed in the second biaxial test series on hollow cylinders of Springwell sandstone in which $\sigma_1 = \sigma_z > \sigma_2 = \sigma_r > \sigma_\theta = \sigma_3 = 0$.

6.8.3 Discussion of the Results

A general review of the experimental results shows considerable similarity with the results of the first biaxial test series. The most distinguished difference between the outcome of both types of tests appears to lie in the deformational behaviour of the specimen hole. As noted in the second polyaxial test series, with the intermediate principal stress being the radial stress, $\sigma_2 = \sigma_r$, Figure 6.63 demonstrates that the rock at the specimen inner walls undergoes progressive compression resulting in expansion of the hole.

Both Figures 6.66 and 6.67 show a good agreement between strength results recorded in the present tests and corresponding results obtained from the first biaxial test series. However, some discrepancy between the results can be seen in the levels of the major principal stress, $\sigma_z = \sigma_1$, recorded at failure under relatively high levels of the intermediate principal stress, σ_2. In addition, clearer indications are given by the present

tests that the increase in σ_1 with increasing of σ_2 level ceases at some point beyond which σ_1 starts to decrease.

Once again, with the internal pressure being higher than the external pressure, rock spalling at the specimen inner surface does not occur. Failure of the test specimen is evidently similar to that observed in the second polyaxial test series. However, with the rock being under biaxial compression, the fracture surfaces appear not to exhibit intense signs of shear.

6.9 Biaxial Compression Tests - Effect of Eccentricity

6.9.1 Outline of the Tests

When the test hollow cylinders were prepared, every effort was made to ensure that their inner and outer surfaces were perfectly concentric. Nevertheless, it was of concern whether and to what extent eccentricity can influence the experimental results. Although an antecedent investigation by the author, Alsayed (1988), suggested that the effect of eccentricity is negligible even for relatively considerable errors of centring, it was decided to re-assess this effect on the basis of the specimen size and rock type used in the present study. Five cylinders were prepared with arbitrary degrees of eccentricity and subjected to different levels of external pressure and axial load, thus inducing at the cylinder inner surface a biaxial compressive stress field in which:

$$\sigma_z = \sigma_1 > \sigma_\theta = \sigma_2 > \sigma_r = \sigma_3 = 0$$

All specimen holes were kept vacant and therefore measurements of the hole volumetric change could not be made. Table 6.7 presents the level of eccentricity, e, and external pressure , P_o, applied in each individual test. It is worth noting that e is defined as the distance measured between the centres of the inner and outer circular boundaries of the hollow cylinder.

6.9.2 The Experimental Results

Using Equation (6.4), induced levels of the tangential stress, $\sigma_{\theta e}$, have been calculated at the specimen inner surface on the basis of the centre distance e. The obtained values are compared with σ_θ levels calculated in the usual way using Equation (6.2) with the assumption that $e = 0$. The results are presented in Table (6.7). A further comparison is made in Figures 6.69 and 6.70 in which the levels of the major principal stress at failure, $\sigma_1 = \sigma_z$, recorded in the present tests are plotted versus $\sigma_\theta = \sigma_2$ and $\varepsilon_z = \varepsilon_1$, respectively, and compared with corresponding results from the first biaxial test series.

The failure patterns observed were similar to those of the first biaxial test series, and therefore, are not presented.

Table 6.7 Details of biaxial tests on thick-walled hollow cylinders of Springwell sandstone conducted to investigate the effect of eccentricity, *e*, on the experimental results.

Specimen No.	*e*, mm	P_o, MPa	σ_θ, MPa	$\sigma_{\theta e}$, MPa	$\sigma_{\theta e} / \sigma_\theta$
HBE1	4.6	2.176	5	5.067	1.013
HBE2	5.4	4.352	10	10.161	1.016
HBE3	3.7	13.056	30	30.314	1.010
HBE4	2.1	17.408	40	40.226	1.006
HBE5	4.3	21.760	50	50.619	1.012

6.9.3 Discussion of the Results

A simple inspection of the results presented in Table 6.7 confirms the marginal effect of eccentricity on the calculated values of the tangential stress, as suggested by Hobbs (1962) and Alsayed (1988). More confirmation is evident in Figure 6.69 in which recorded levels of the major principal stress at failure, $\sigma_1 = \sigma_z$, for the present tests appear to fall within the range of corresponding values from the first biaxial test series. Agreement between the results of both test series can also be found in Figure 6.70 in terms of the major principal stress at failure and the corresponding levels of the major principal strain.

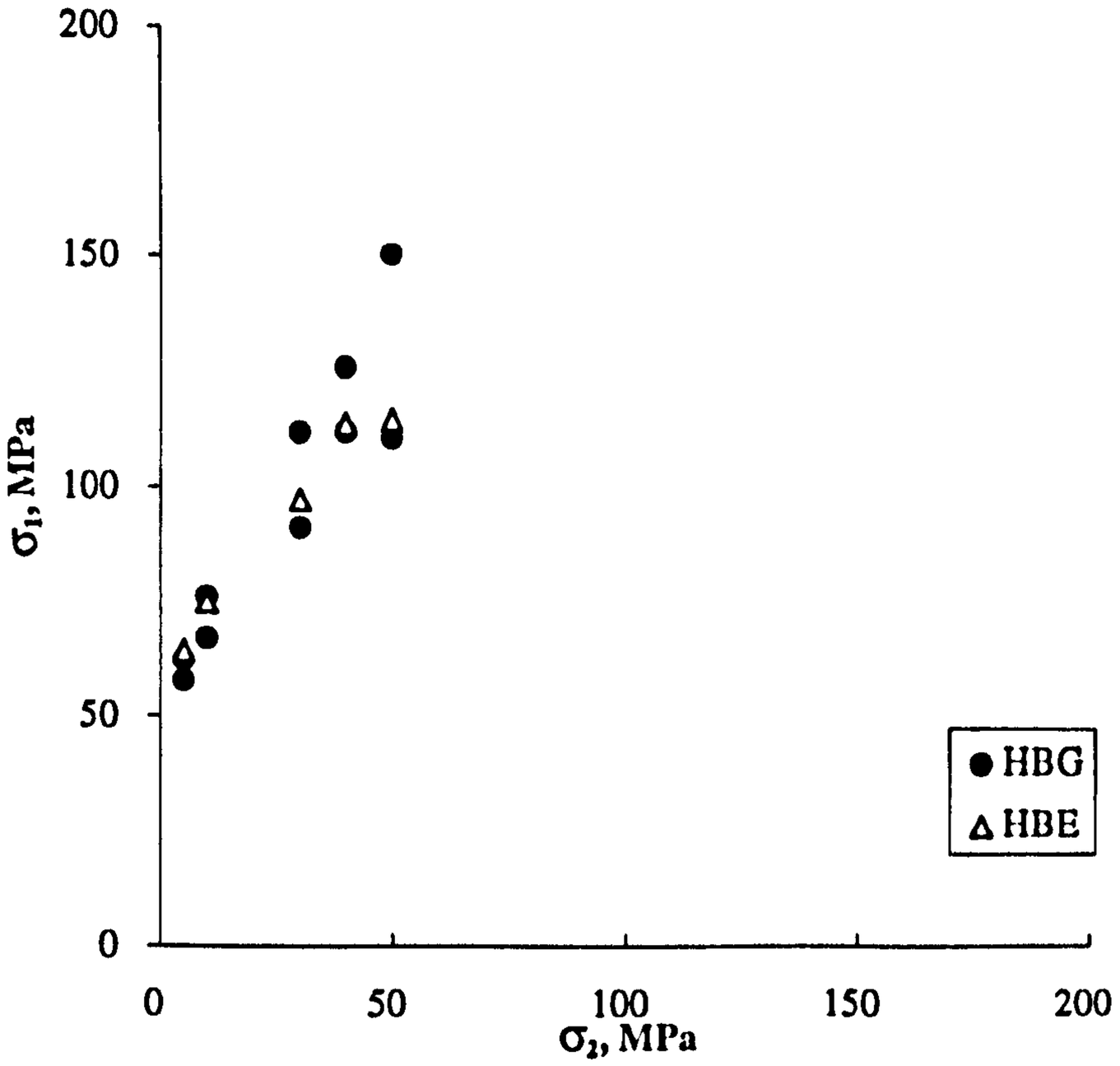

Figure 6.69 Variation of $\sigma_1 = \sigma_z$ at failure with $\sigma_2 = \sigma_\theta$ in biaxial tests on non-concentric hollow cylinders, HBE, and corresponding results from the first biaxial test series, HBG.

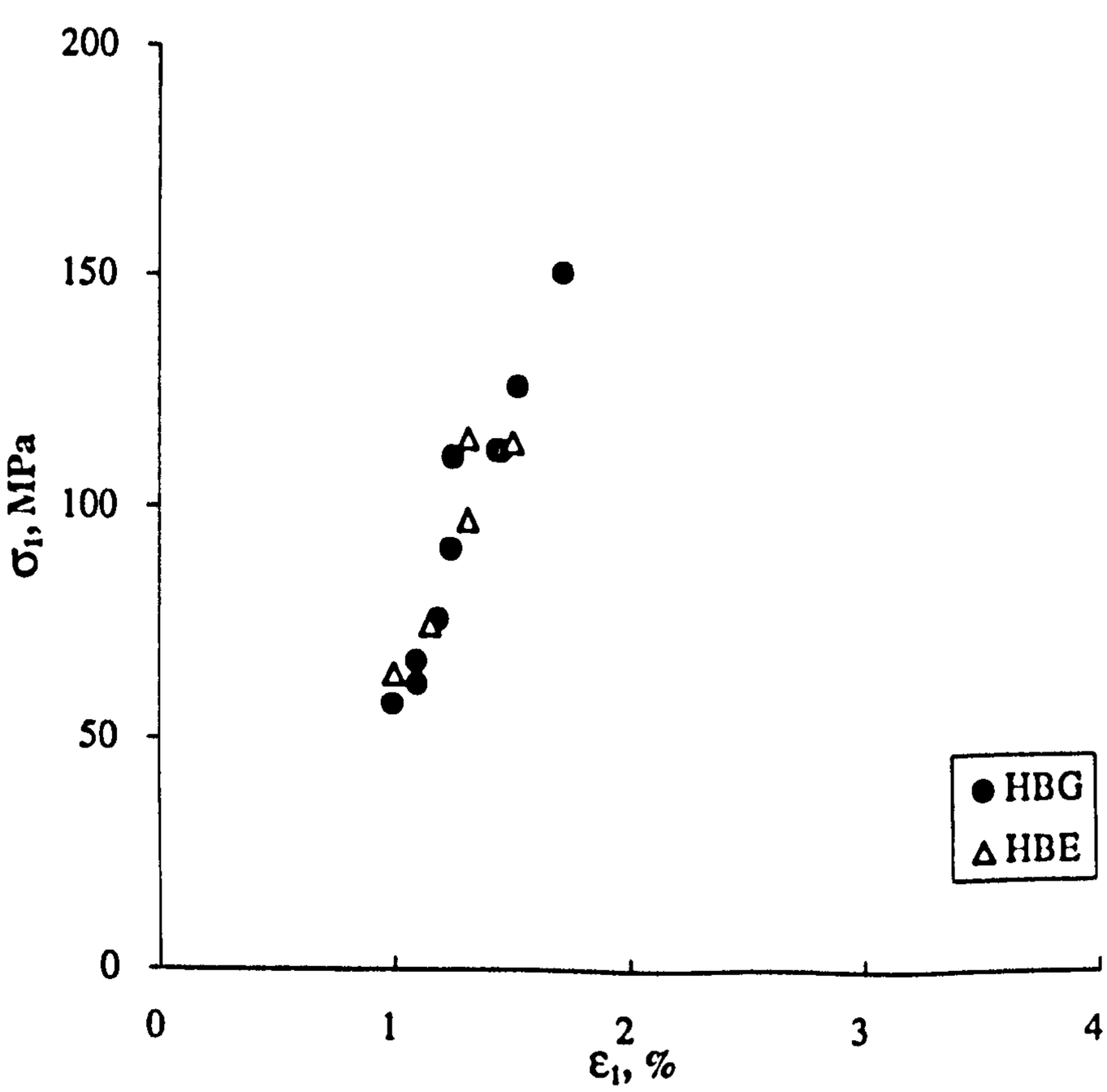

Figure 6.70 Major principal stress, $\sigma_1 = \sigma_z$, at failure versus major principal strain, $\varepsilon_1 = \varepsilon_z$, for the above biaxial tests on hollow cylinders of Springwell sandstone.

6.10 Uniaxial Compression Tests - First Series

6.10.1 Outline of the Tests

In line with the cubical testing programme, thick-walled hollow cylinders of Springwell sandstone have been loaded to failure under uniaxial compression conforming to the following arrangement of principal stresses:

$$\sigma_z = \sigma_1 > \sigma_\theta = \sigma_r = \sigma_2 = \sigma_3 = 0$$

A total of eight specimens were tested involving two different loading configurations. In order to acquire measurements of the hole volumetric change, ΔV_h, four specimens were loaded inside the hollow cylinder test apparatus with a seating external pressure, P_o, level of about 0.5 MPa. The same level of internal pressure, P_i, was applied so that measurements of ΔV_h can be made. The other four specimens were loaded outside the apparatus free from any form of lateral confinement. In all tests, the axial load was applied via the 5 MN servo-controlled loading machine. The loading conditions for each individual test are presented in Table 6.8.

6.10.2 The Experimental Results

Figure 6.71 illustrates a typical plot of the major principal stress, $\sigma_z = \sigma_1$, versus major principal strain, $\varepsilon_z = \varepsilon_1$, for a thick-walled hollow cylinder loaded under uniaxial compression. Maximum levels of $\sigma_1 = \sigma_z$ recorded at failure for all specimens tested are presented in Table 6.8. As in previous tests, acquired measurements of the volumetric change of the specimen hole, ΔV_h, have been used to calculate the tangential strain, ε_θ, radial strains, ε_r, and volumetric strain, $\varepsilon_{v/h}$, at the specimen inner walls. Figure 6.72 shows a typical plot of ε_θ, ε_r, and $\varepsilon_{v/h}$ versus the axial strain, $\varepsilon_z = \varepsilon_1$.

Failure of the test specimens resulted generally in a major inclined shear fracture accompanied by minor near axial cracks. Most fracture surfaces appeared not to exhibit pronounced evidence of rubbing or sliding. Representative modes of failure are pictured in Figure 6.73.

Table 6.8 Loading conditions and levels of major principal stress, $\sigma_1 = \sigma_z$, at failure for the first uniaxial compression test series on hollow cylinders of Springwell sandstone.

Specimen No.	Max. P_o & P_i, MPa	$\sigma_1 = \sigma_z$, MPa
HUX1	0	38.644
HUX2	=	35.033
HUX3	=	36.781
HUX4	=	41.968
HUX5	0.5	46.501
HUX6	=	37.300
HUX7	=	45.214
HUX8	=	52.669

6.10.3 Discussion of the Results

Regarding the levels of axial stress, $\sigma_1 = \sigma_z$, recorded at failure and listed Table 6.8, there generally appears to be an increase in the uniaxial compressive strength of specimens tested with minimum levels of external and internal pressures. Specimens that were loaded without any form of lateral confinement, HUX1 to HUX4, appear to have failed at an average axial stress level of σ_1 = 38.107 MPa, while those subjected to minimum levels of external and internal pressures, HUX5 to HUX8, sustained an average level of σ_1 = 45.421 MPa. This suggests an increase of about 19% in the apparent uniaxial compressive strength.

In comparison with results of uniaxial compression tests on cubes and solid cylinders, the unconfined hollow cylinders appear the weakest. However, there appears to be a good

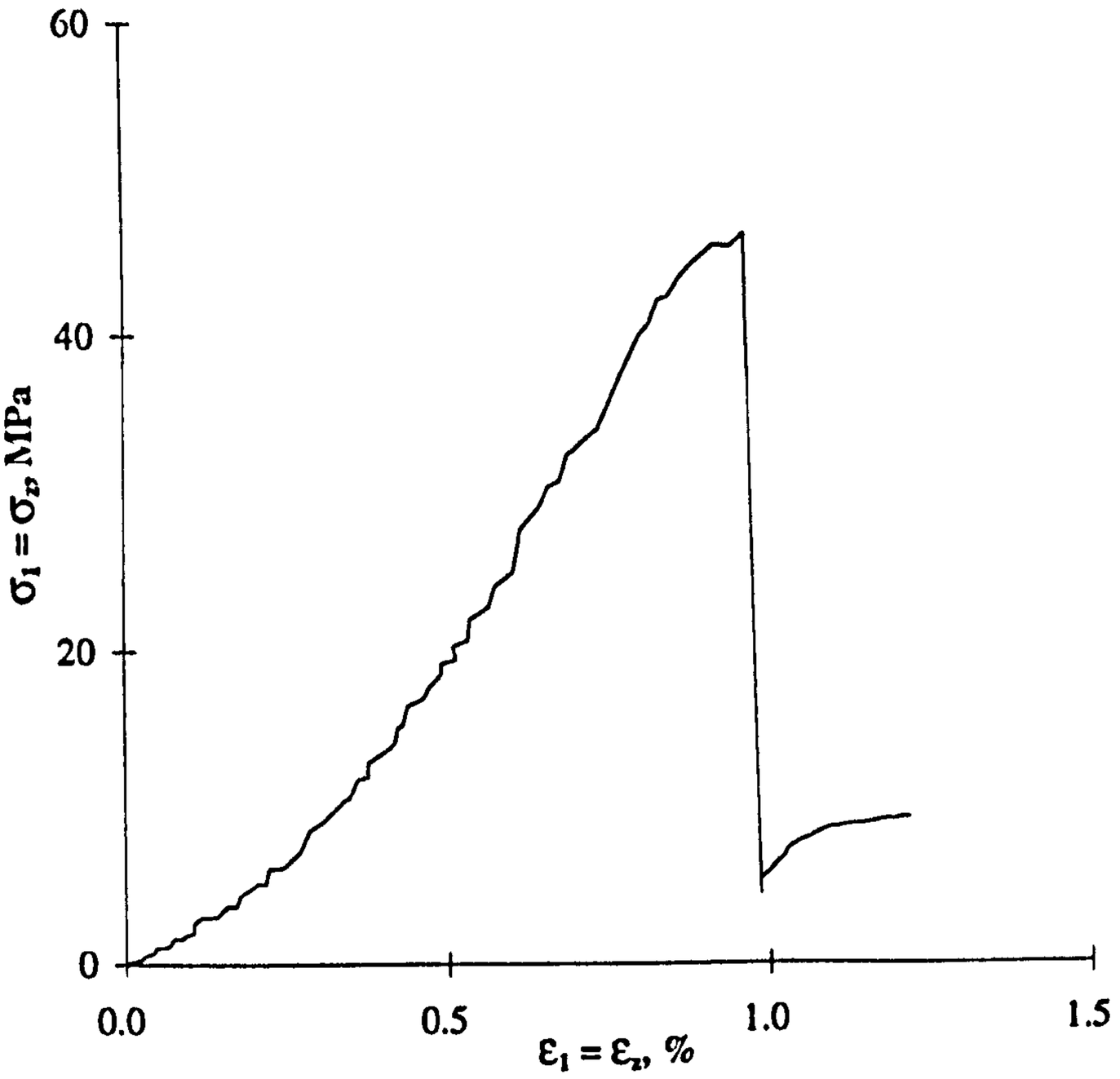

Figure 6.71 Major principal stress, $\sigma_1 = \sigma_z$, versus major principal strain, $\varepsilon_1 = \varepsilon_z$, for a thick-walled hollow cylinder tested under uniaxial compression.

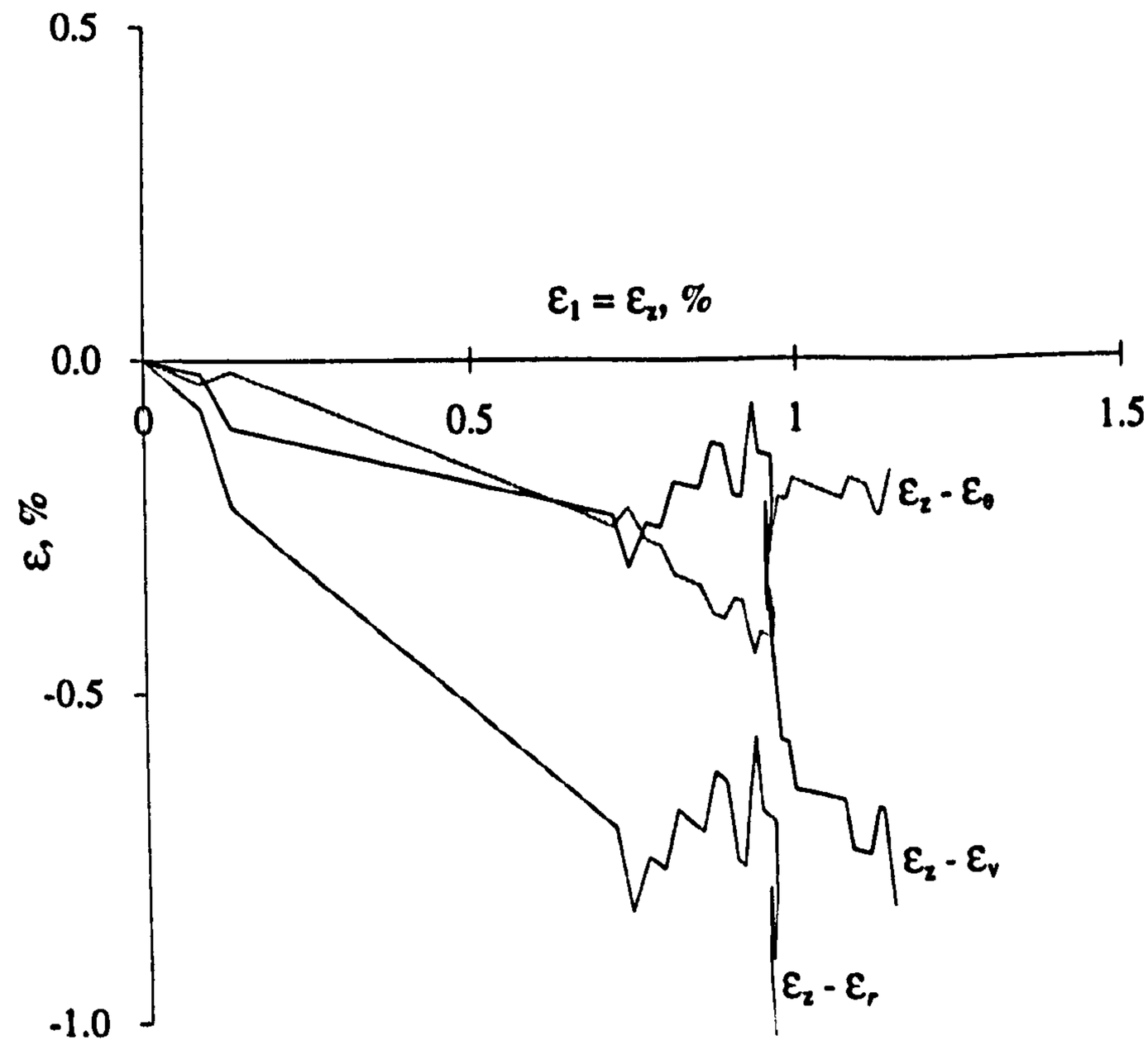

Figure 6.72 Major principal strain, $\varepsilon_z = \varepsilon_1$, versus radial strain, ε_r, tangential strain, ε_θ, and volumetric strain, ε_{vh}, at the specimen inner wall.

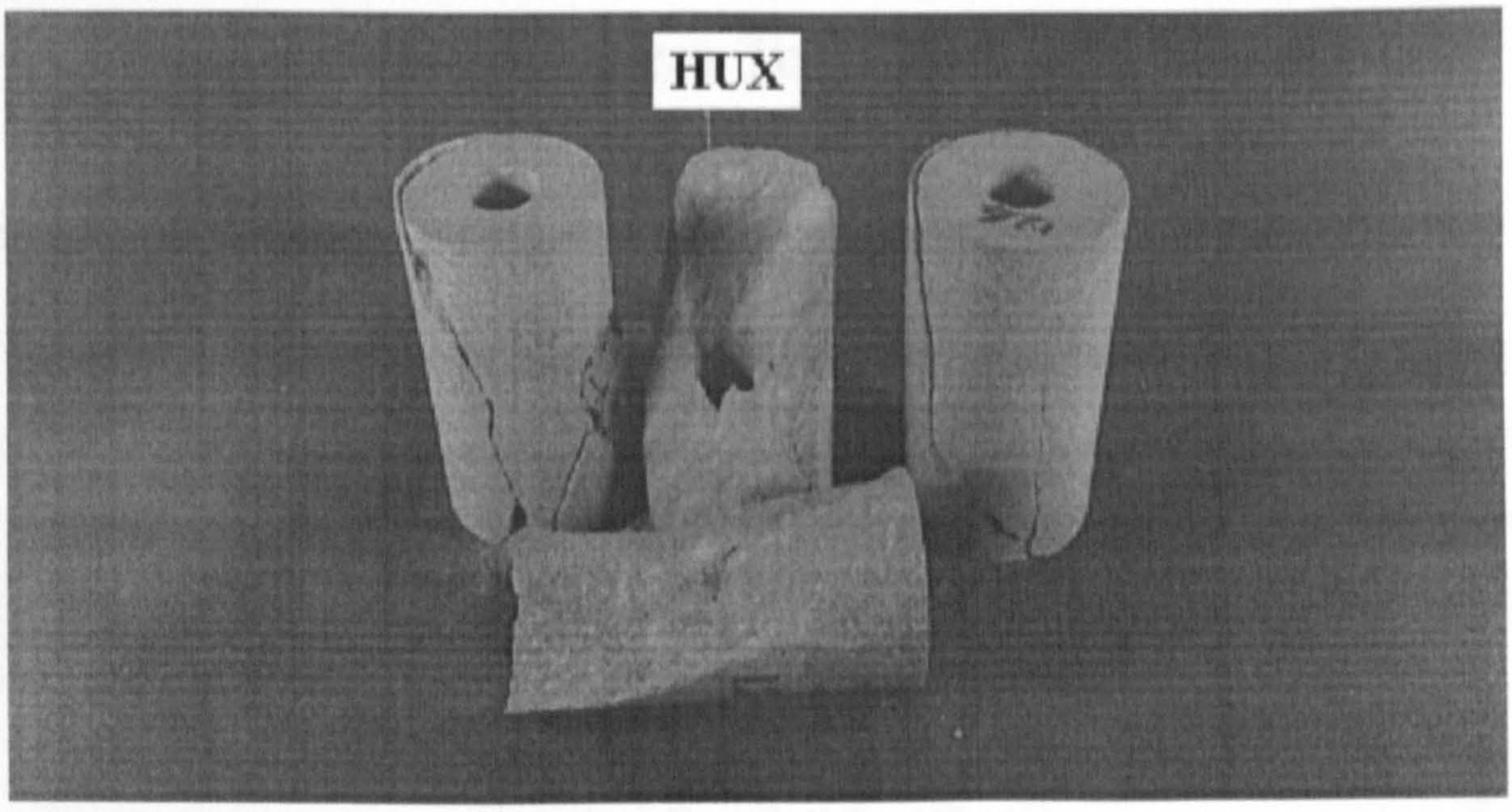

Figure 6.73 Typical failure patterns observed in uniaxial compression tests on hollow cylinders of Springwell sandstone in which $\sigma_1 = \sigma_z$.

agreement between the uniaxial strength of the confined hollow cylinders and that of the solid cylinders. A similar agreement can also be seen with the uniaxial strength of cubical specimens tested with PTFE sheets at their loading surfaces.

Figure 6.72 shows a decrease in the volume of the specimen hole, suggesting rock dilation at the specimen inner surface. More evidence of this behaviour is revealed by the calculated values of the radial strain, ε_r. Dilation seems also to take place along the tangential strain direction as indicated by the obtained values of ε_θ. The phenomenon that both ε_r and ε_θ suggest dilation in the rock appear to fundamentally agree with results of uniaxial compression tests on cubes as well as standard uniaxial compression tests on solid cylinders. Nonetheless, unlike those tests where generally near isotropic lateral dilation appeared to develop, Figure 6.72 shows that ε_r and ε_θ are far from being equal and that more dilation seems to occur along the radial strain direction.

In the light of the observed fractures, the specimen failure appears not to be influenced by the minimum level of confinement applied in some tests. Inclined shear fractures remain the main outcome of failure with some evidence of axial splitting.

6.11 Uniaxial Compression Tests - Second Series

6.11.1 Outline of the Tests

Following the foregoing uniaxial compression tests, five more thick-walled hollow cylinders were subjected to a similar stress field but with the tangential stress being in this case the major principal stress. Only hydrostatic external pressure, P_o, was applied increasingly with time to induce at the specimen inner surface a state of uniaxial compression in which:

$$\sigma_\theta = \sigma_1 > \sigma_z = \sigma_r = \sigma_2 = \sigma_3 = 0$$

While the specimen hole was kept free from any internal pressure, $P_i = 0$, an axial stress of about $\sigma_z = 0.5$ MPa was applied in order to retain the specimen properly positioned inside the test apparatus. However, as the external pressure was increased, a gradual build up in σ_z level occurred. The problem was not dealt with in the first three tests in order to study the specimen behaviour under such loading conditions. In the remaining two tests, σ_z was manually regulated and maintained reasonably constant.

Due to limitations appeared to lie in the available testing facilities, all tests were prematurely terminated before failure occurred. A major problem encountered was the lack of a hydraulic power system capable of generating external pressure level high enough to fracture the test specimen. Although the hydraulic power pack used is supposed to provide a maximum operating pressure of 70 MPa, it failed to operate when the external pressure level reached about 60 MPa. However, any efforts that could have been made to overcome this problem were halted by the inability of the external pressure sleeve to withstand higher levels of pressure, particularly when the axial stress was kept at a minimum level. Except in the first two tests, the external sleeve burst at a pressure level lower than what the hydraulic power pack can generate. Table 6.9 presents details of the loading conditions for all tests conducted and problems encountered.

Table 6.9 Second uniaxial compression test series on thick-walled hollow cylinders of Springwell sandstone in which $\sigma_1 = \sigma_\theta$.

Specimen No.	P_o, MPa	σ_z, MPa	ε_z, %	$\sigma_1 = \sigma_\theta$, MPa	Problems Occurred
HUG1	57.104	10.603	0.008	131.214	Max P_o reached
HUG2	57.856	10.142	0.020	132.942	=
HUG3	54.479	9.777	0.016	125.181	Sleeve burst
HUG4	33.266	0.672	-0.749	76.439	=
HUG5	40.058	0.749	-0.284	92.044	=

6.11.2 The Experimental Results

A typical plot of the loading sequence in terms of external pressure versus time is presented in Figure 6.74 for a test in which the axial stress, σ_z, was allowed to build up. A similar plot is presented in Figure 6.75 in terms of the induced tangential stress, $\sigma_\theta = \sigma_1$. Clearly, due to the build up in σ_z level, Figure 6.76 shows that hardly any axial deformation took place. In contrast, in tests where σ_z was maintained constant at its minimum level, the specimen appeared to undergo extension along σ_Z direction as demonstrated by Figure 6.77. Table 6.9 lists some experimental results recorded at maximum levels of external pressure applied.

As earlier pointed out, none of the test specimens collapsed under the levels of external pressure attained. Yet, all specimens were carefully inspected for any signs of failure initiation. Only specimens HUG1 and HUG2 appeared to exhibit clear evidence of rock spalling from their inner walls. Such evidence can be seen in Figure 6.78 in which the test specimen is presented sawn axially in halves.

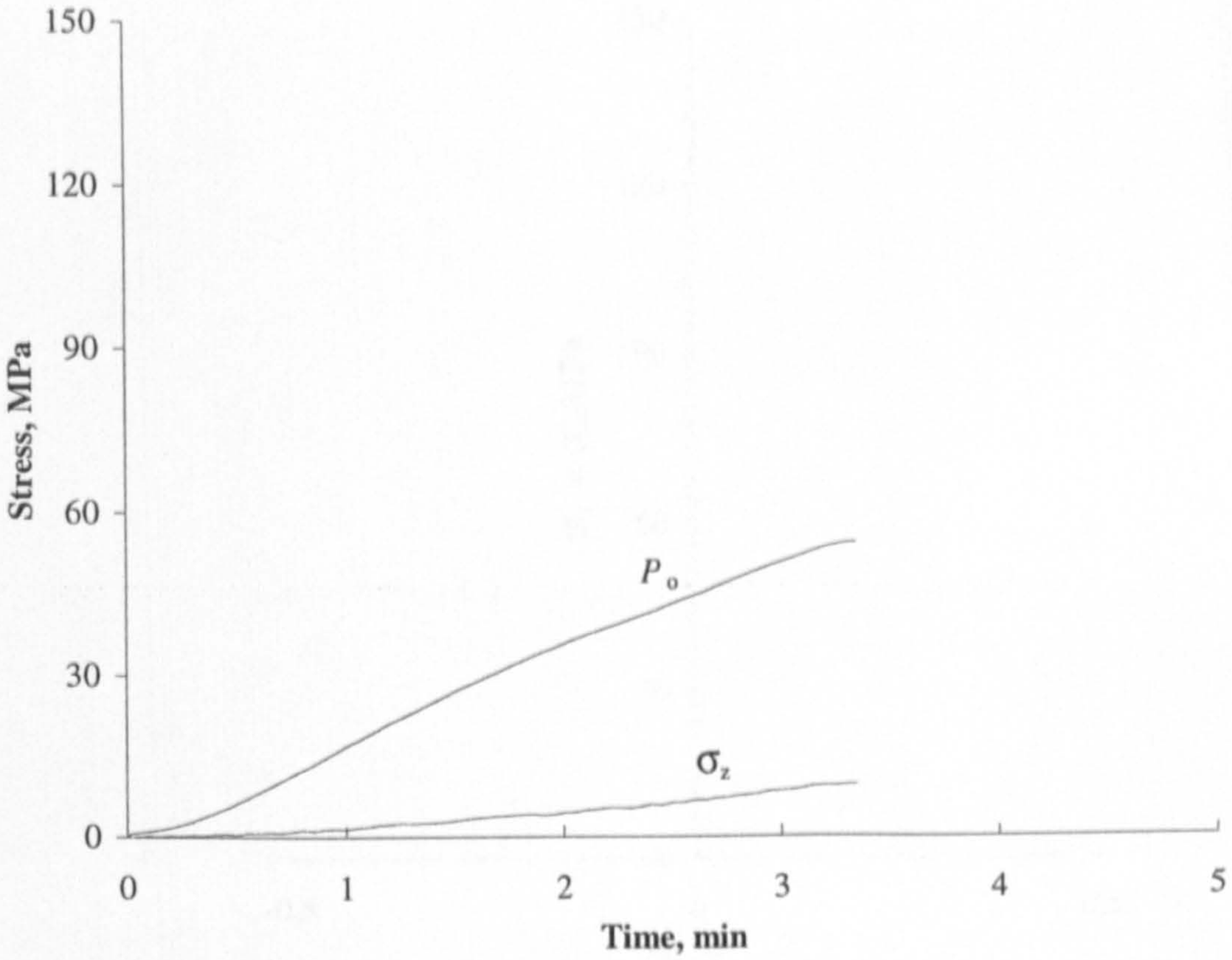

Figure 6.74 A loading sequence for a hollow cylinder uniaxial compression test conducted under external pressure, P_o, only with the axial stress, σ_z, being allowed to build up.

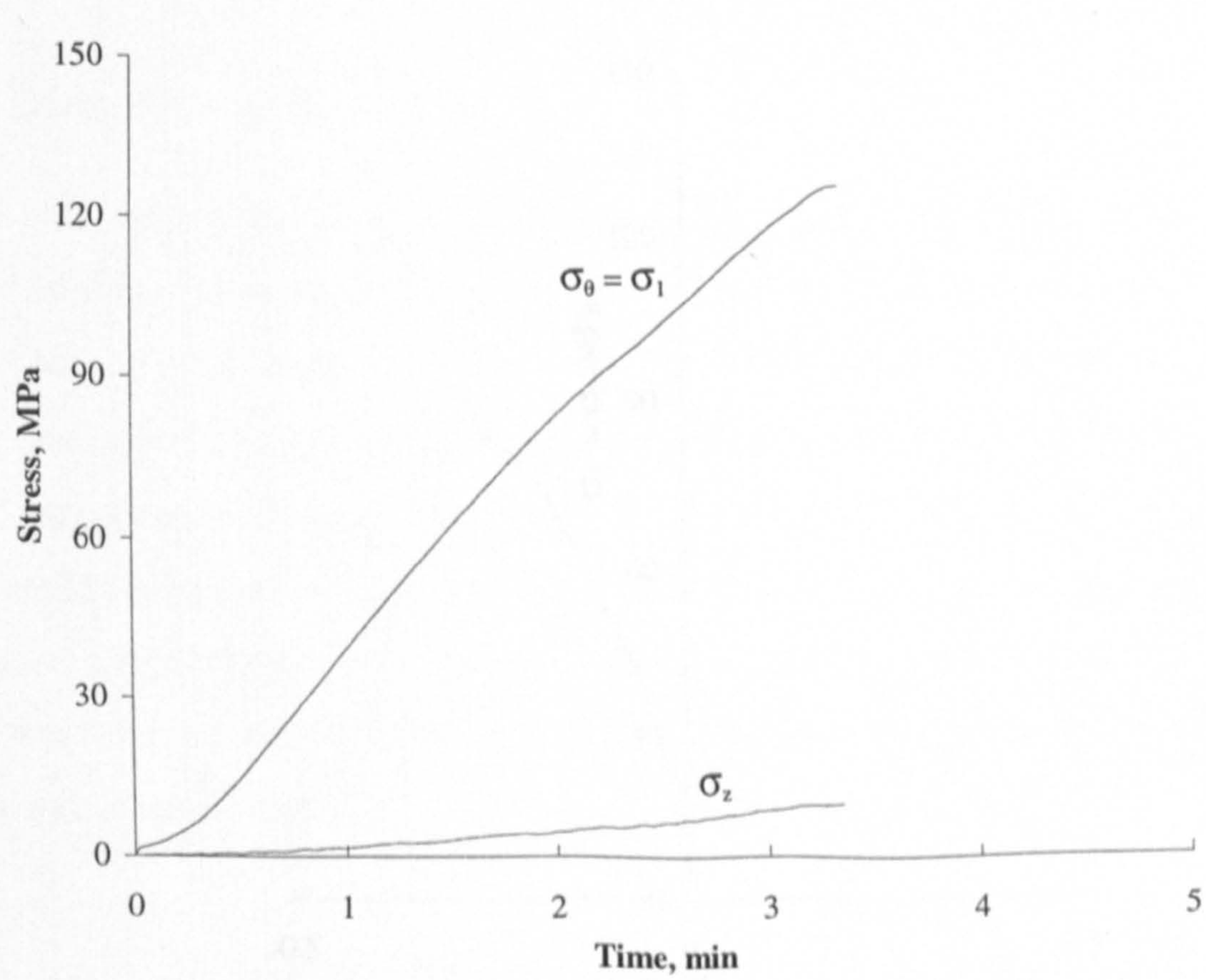

Figure 6.75 The above loading sequence in terms of the corresponding tangential stress, $\sigma_\theta = \sigma_1$, induced at the cylinder inner wall and the axial stress, σ_z.

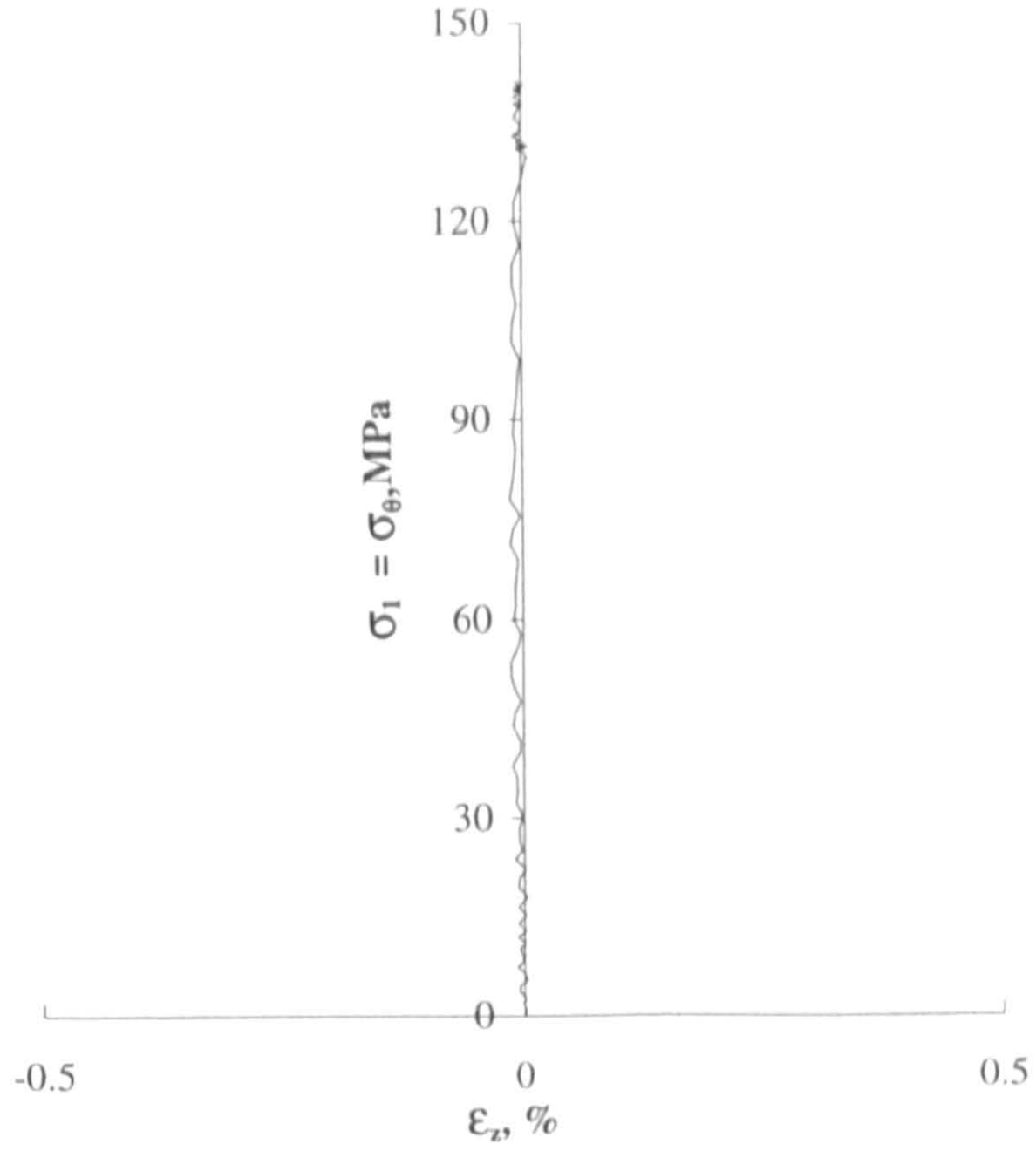

Figure 6.76 Major principal stress, $\sigma_1 = \sigma_\theta$, versus axial strain, ε_z, for a hollow cylinder uniaxial compression test in which the axial stress, σ_z, was allowed to build up.

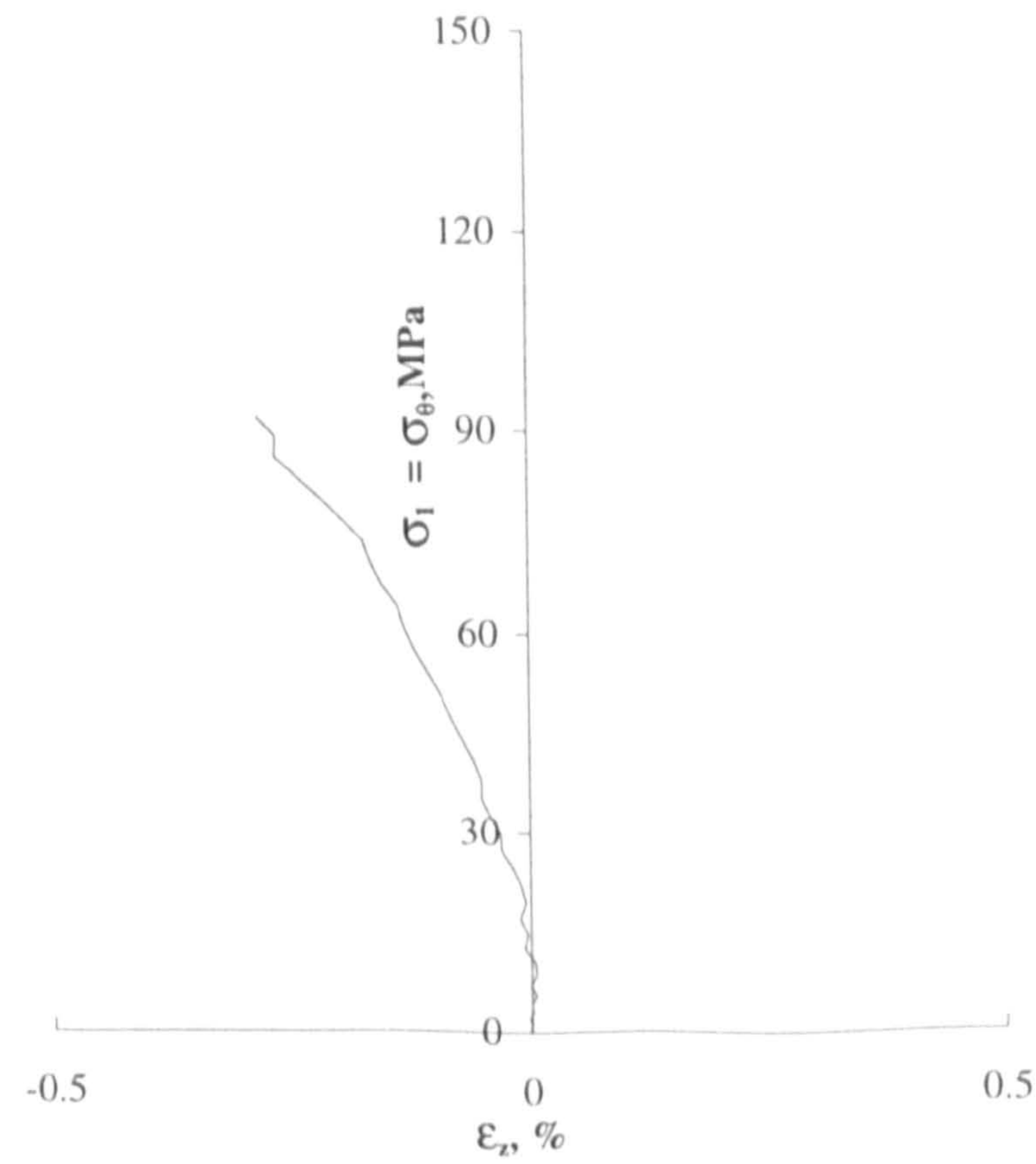

Figure 6.77 Major principal stress, $\sigma_1 = \sigma_\theta$, versus axial strain, ε_z, for a hollow cylinder uniaxial compression test in which the axial stress, σ_z, was maintained constant at a minimum level.

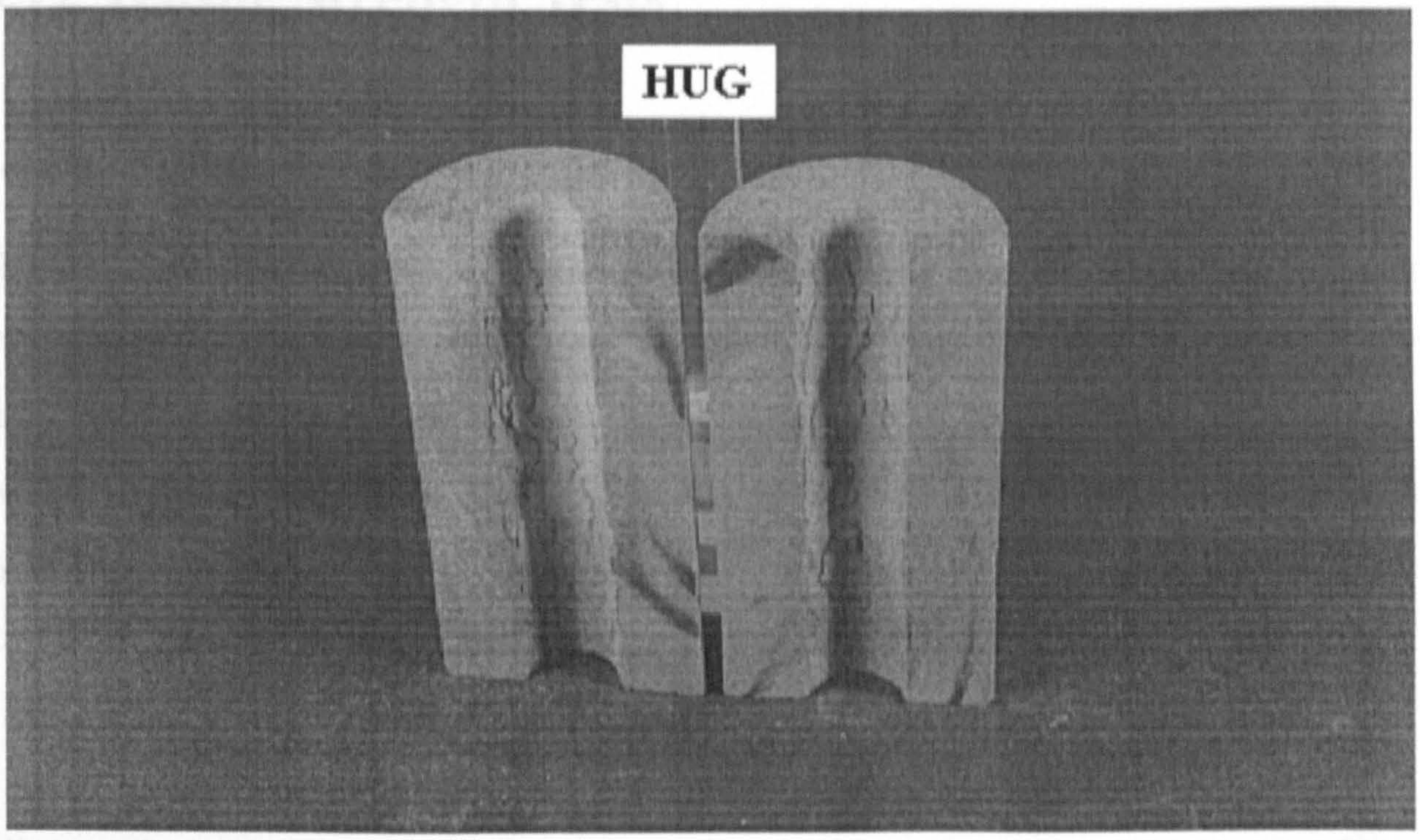

Figure 6.78 Evidence of spalling at the inner walls of a thick-walled hollow cylinder of Springwell sandstone loaded uniaxially under external hydrostatic pressure.

6.11.3 Discussion of the Results

Clearly, with the test specimen being subjected to some axial compression, the state of stress is no longer pure uniaxial one. As a result, the specimen appears to sustain high levels of tangential or major principal stress, $\sigma_\theta = \sigma_1$, particularly when the axial stress, σ_z, is permitted to build up. Although complete failure could not be attained, the levels of $\sigma_\theta = \sigma_1$ sustained remain much higher than the specimen could bear in the previous tests under axial compression, and equally, much higher than the uniaxial compressive strength of the rock determined from standard tests on solid cylinders. The evidence of spalling observed at the inner walls of cylinders HUG1 and HUG2 confirms that failure initiates at the specimen inner surface.

6.12 Tensile Strength Tests

6.12.1 Outline of the Tests

The last experimental series on thick-walled hollow cylinders of Springwell sandstone was intended to examine the rock tensile strength and compare it with results established in Chapter 4 from the commonly used Brazilian disc tests. Three cylinders were loaded to failure under increasing internal hydrostatic pressure, P_i, only, thus inducing at the cylinder inner walls a state of stress in which the tangential stress, σ_θ, is tensile. Such a state of stress corresponds to the following arrangement of principal stresses:

$$\sigma_r = \sigma_1 > \sigma_z = \sigma_2 > \sigma_\theta = \sigma_3 < 0$$

Whereas the test specimen was not subjected to any form of external confinement, $P_o = 0$, some axial compression had to be imposed in order to constrain the loading platens while the internal pressure, P_i, was applied. Generally, the level of the axial compression imposed did not exceed 0.75 MPa, and this was sufficient to counteract the effect of P_i in the axial direction and maintain σ_z compressive. Table 6.10 shows the levels of P_i and σ_z sustained by each cylinder tested.

6.12.2 The Experimental Results

Figure 6.79 shows a typical plot of the specimen loading sequence in terms of internal pressure, P_i, and axial stress, F / A, versus time. A similar plot is presented in Figure 6.80 in terms of the induced principal stresses σ_r, σ_z, σ_θ calculated at the specimen inner wall. The stress levels at which the test specimens failed are presented in Table 6.10. All three specimens failed by axial splitting in halves along one major plane as pictured in Figure 6.81.

Table 6.10 Tensile strength tests on thick-walled hollow cylinders of Springwell sandstone.

Specimen No.	$P_i = \sigma_r = \sigma_1$, MPa	$\sigma_z = \sigma_2$, MPa	$\sigma_3 = \sigma_\theta$, MPa
HSG1	4.342	0.053	-5.635
HSG2	4.317	0.106	-5.602
HSG3	4.625	0.061	-6.002

6.12.3 Discussion of the Results

The concept of loading thick-walled hollow cylinders of rock under internal hydrostatic pressure only appears to present a simple indirect tensile strength test marked by highly reproducible results. All three specimens tested have failed in the same manner and sustained similar levels of internal pressure. With the development of tensile tangential stress, $\sigma_\theta = \sigma_3$, at the specimen inner surface, failure appears to occur at an average value of $\sigma_\theta = -5.746$ MPa by axial splitting or extensile separation across a plane perpendicular to the direction of σ_θ as shown in Figure 6.81.

Brazilian disc tests conducted in Chapter 4 showed that the tensile strength of Springwell sandstone stands at an average value of $\sigma_t = -3.725$ MPa. In comparison with the present test results, the rock in the form of hollow cylinders appear to sustain a tensile stress of about 1.5 times greater than its tensile strength suggested by the classical Brazilian test. Clearly, variations in the results of the two types of tests are likely to emerge and may be attributed to a number of conceivable factors. Among such factors is the obvious fact that hollow cylinder and Brazilian disc tests differ in the specimen shape as well as the stress

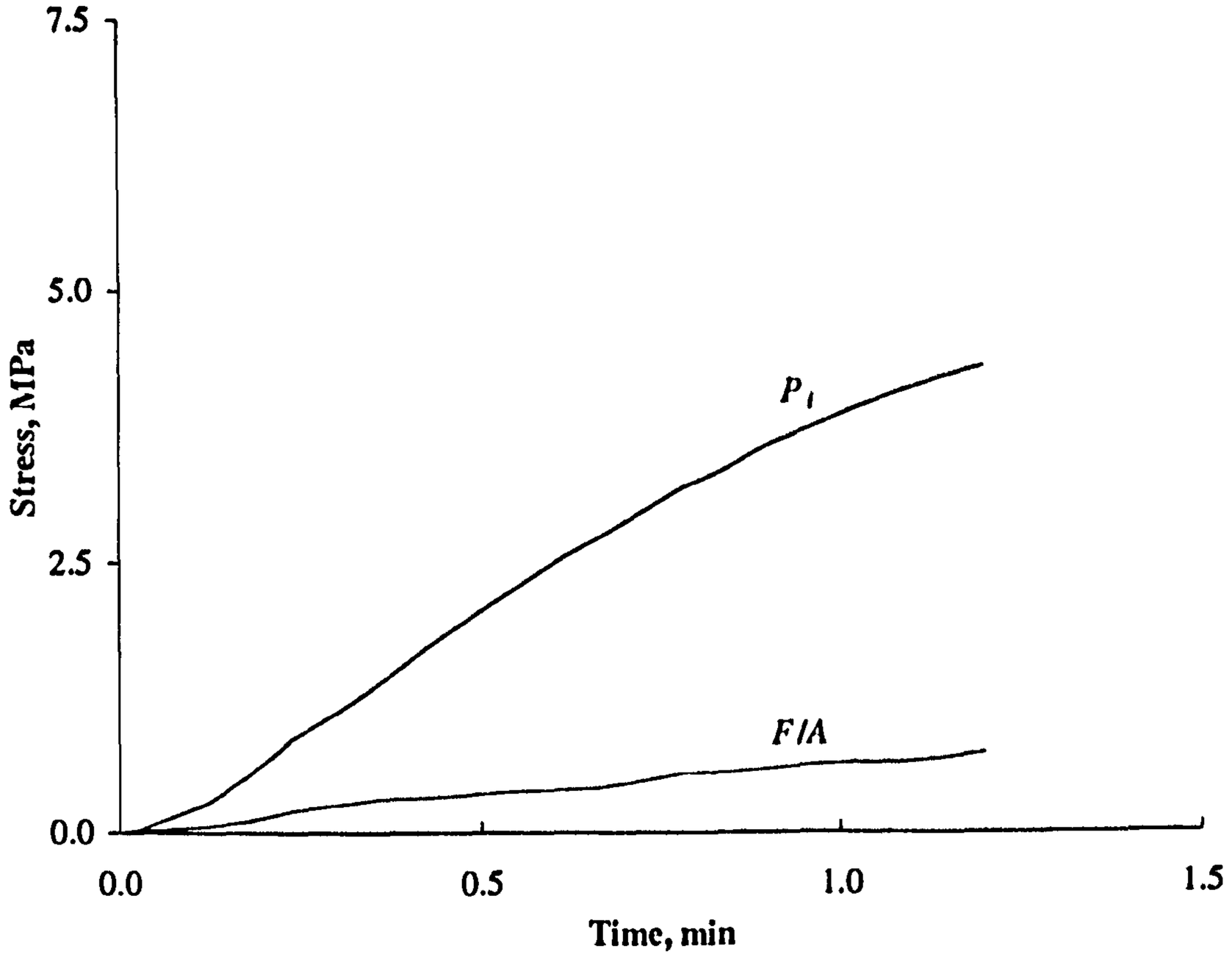

Figure 6.79 A typical loading sequence in tensile strength tests on hollow cylinders plotted in terms of applied internal pressure, P_i, and axial stress, F/A, versus time.

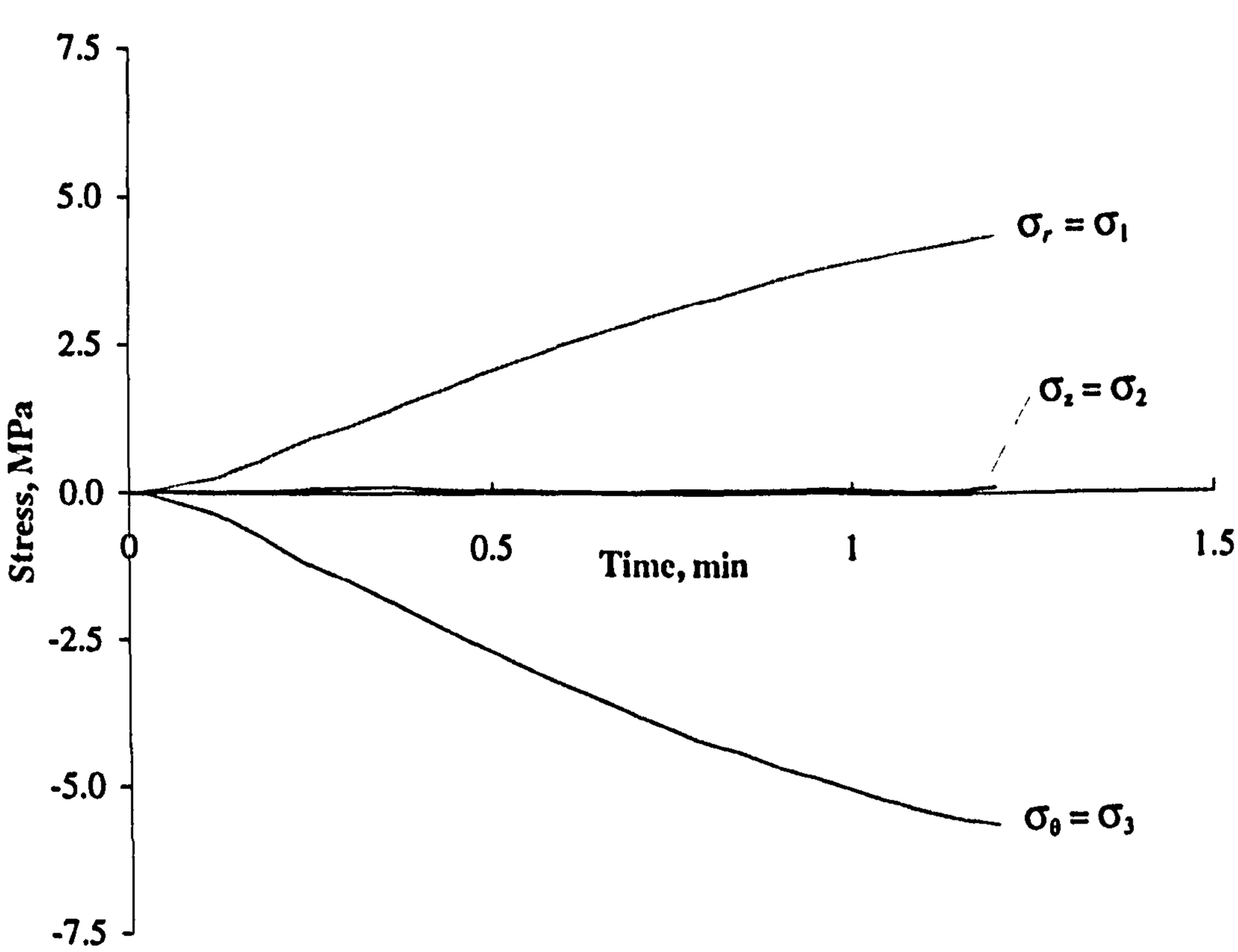

Figure 6.80 The above loading sequence in terms of the corresponding principal stresses σ_r, σ_z, σ_θ induced at the cylinder inner wall.

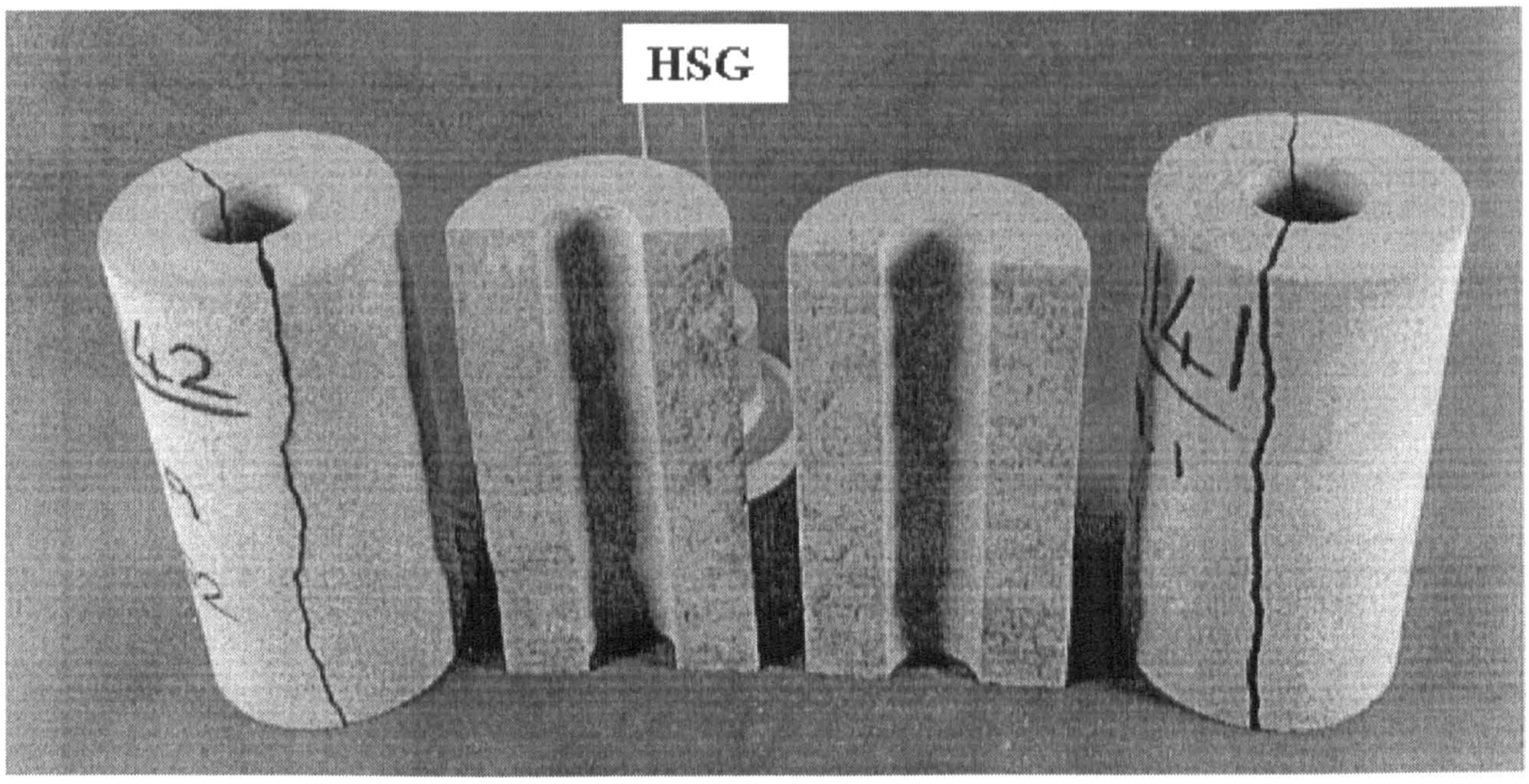

Figure 6.81 Failure of thick-walled hollow cylinders of Springwell sandstone in tensile strength tests conducted under internal hydrostatic pressure only.

distribution within the specimen. Furthermore, although the intermediate principal stress, $\sigma_2 = \sigma_z$, in the hollow cylinder tests was kept at minimum level, it may still have influenced the test results and led to an increase in the hollow cylinder apparent tensile strength. Such influence is not present in the case of the Brazilian test in which $\sigma_2 = 0$.

Chapter 7

TRIAXIAL COMPRESSION OF SOLID CYLINDERS

7.1 Introduction

Upon investigating the behaviour of rock in the form of cubes and thick-walled hollow cylinders under various loading conditions, the experimental work has been concluded by a series of tests representing the most conventional method used in the study of the mechanical properties of rock, namely triaxial compression of solid cylinders in which $\sigma_1 > \sigma_2 = \sigma_3$. Although results of such tests are well documented in a number of previous studies, it was aimed to produce original results under conditions similar to those of the cubical and hollow cylinder tests, thus eliminating any unknown factors that often makes test results incomparable. Consequently, a total of nineteen solid cylinders of Springwell sandstone measuring 150 mm in height and 75 mm in diameter were loaded axially to failure under different levels of lateral hydrostatic confinement. In order to obtain more information from a single test, all specimens were to experience multiple failure by employing the concept of the so called *Multiple Failure State Triaxial Test* introduced by Kovari and Tisa (1975). As a result, a total of fifty-seven points of the peak strength or failure envelope were established.

The tests have been conducted using similar set-up to that used in the hollow cylinder tests with the main exception that no internal pressure was involved in the present tests. As in the cubical and hollow cylinder tests, all experiments were axial strain controlled. During the test, direct measurements of the specimen axial stress and axial deformation were continuously acquired. The hydrostatic confining pressure was generated using a pressure intensifier system which provided and maintained an accurate control over the pressure level applied, and enabled measurements of the specimen volumetric change to be made. These measurements were then used to calculate the volumetric strain, and subsequently, the lateral deformation of the test specimen.

Prior to triaxial loading, all cylinders underwent a simple non-destructive ultrasonic wave velocity test intended to examine the uniformity of the test specimens as well as the isotropy of the rock used, as described in Chapter 4.

This chapter first describes the testing configuration and procedure employed. Then, the experimental series is outlined and the tests results are thereafter presented and specifically discussed. A comparison of the results of these solid cylinder triaxial compression tests with results obtained from corresponding tests on cubes and hollow cylinders is presented in Chapter 8.

7.2 Testing Configuration and Procedure

The testing facilities employed in triaxial compression of solid cylinders are part of the facilities used in the hollow cylinder tests and are described in detail in Chapter 3. Nevertheless, they can briefly be listed herein as follows:

- A Hoek triaxial cell, Figures 3.6 to 3.9, designed for testing solid cylinders of rock measuring 75 mm in diameter and 150 mm in height.

- A servo-controlled loading system, Figure 3.13, capable of applying a maximum compressive force of 5 MN used for the application of the axial major principal stress, σ_1.

- A pressure intensifier system, Figure 3.14, of a maximum capacity of 70 MPa used for the application of the hydrostatic confining pressure, $\sigma_2 = \sigma_3$, and monitoring the volumetric change of the test specimen, ΔV.

- A data acquisition system with a personal computer, Figure 3.15, used for continual monitoring and recording of the experimental data.

- An X-Y recorder connected to the servo-controlled loading system used to record the output of the system load cell and LVDT, thus granting a direct plot of the axial load-axial displacement curve during the test.

- A second X-Y recorder connected to both the loading system and the pressure intensifier used for direct plotting of the axial displacement versus the volumetric change of the test specimen.

The rock cylinders were of 150 mm height and 75 mm diameter. Prior to testing, each cylinder was weighed for its bulk density and then subjected to a non-destructive ultrasonic wave velocity test in which the travel time of the compressional wave along the

cylinder longitudinal axis was measured. As described in Chapter 4, these measurements were used to examine the rock isotropy as well as the uniformity of the test specimens.

Preparation for triaxial loading was a familiar procedure. First, the rock cylinder was inserted in the Hoek triaxial cell and enclosed from both ends by a pair of spherical end platens. Then, holding both platens, a proper contact with the specimen was insured and the specimen was carefully positioned so that it lies centrally in the cell. A sufficient level of confining pressure was pumped up to hold the assembly firm in position.

When mounting the cell in the testing machine, the spherical end platens were mated with a pair of seating platens and the assembly was properly positioned ensuring that the cell was levelled and centrally located in the loading frame. Two load cells of 1 MN capacity were incorporated on top of the seating platen: one was connected to the servo-controlled loading system and the other was connected to the data acquisition system for measuring the axial load. An axial seating compression of about 0.5 MPa was manually applied to hold the complete assembly firm. Then, the pressure intensifier was connected and a pressure level of about 0.5 MPa was applied after purging the confinement circuit of any trapped air. It is worth noting that these initial values of axial stress and confining pressure correspond to the initial compressive seating stresses applied in both the cubical and hollow cylinder tests.

At this stage, a transducer was properly mounted crosswise the LVDT of the loading system for measuring the axial deformation of the test specimen. Subsequently, the X-Y recorders were prepared and the data acquisition program was initiated. All input devices were initialised and the test was ready to run. As in all previous tests, the data acquisition system was set up to directly convert load and deformation measurements to stress values in MPa and strain %, respectively. Measurements were acquired at time intervals of 3 s, displayed on the PC monitor and stored in a data file.

As in the cubical and hollow cylinder tests, all triaxial compression tests were axial strain controlled carried out under a constant axial strain rate of 0.25% / min. Accordingly, the servo-controlled loading system was programmed to follow a prescribed loading sequence

of a selected maximum ramp time of 2×10^3 s and a maximum output displacement level calculated as follows:

$$\text{output level} = \text{strain rate} \times \text{specimen height} \times \text{ramp time}$$

Loading of the test specimen was based on subjecting it to multiple failure states attained under increasing axial load and predetermined levels of confining pressure. The procedure followed was similar to that suggested by ISRM (1983) for multiple failure state triaxial compression testing. Illustrated diagrammatically in Figure 7.1, the loading procedure may be described as follows:

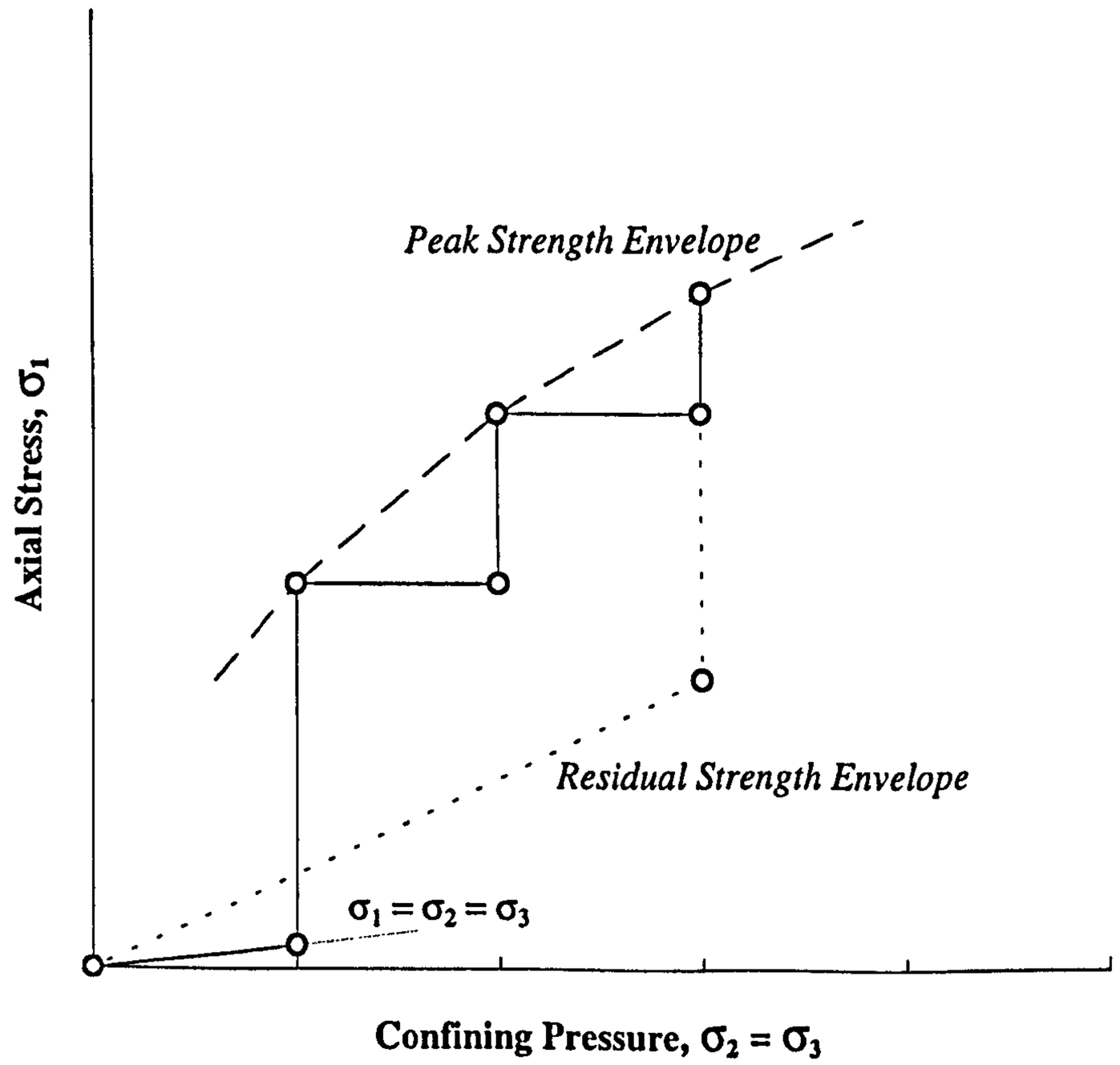

Figure 7.1 Loading procedure in a multiple failure state triaxial test.

At the start of the test, the confining pressure, $\sigma_2 = \sigma_3$, is manually increased simultaneously with the major principal stress, σ_1, applied axially by the testing machine at the constant preset loading rate. Upon reaching its first predetermined value, the confining pressure is maintained constant while the axial stress is continued until the

corresponding peak strength is observed in the axial stress-axial strain curve plotted by the X-Y recorder. At this point, the confining pressure is increased in one step to its predetermined value for the second stage of the test and then maintained constant while the axial stress continues to increase until a second peak strength point is observed. This stepwise procedure is continued until the last prescribed failure state is reached and the axial stress drops to its residual value.

Shortly after failure occurs, the loading machine is ramped down and the axial stress is continuously reduced at the same preset loading rate. Following a similar sequence to that employed during loading, the confining pressure is simultaneously reduced with the axial stress until the specimen is completely unloaded.

7.3 Outline of the Tests

As earlier mentioned, a total of nineteen solid cylinders of Springwell sandstone have been subjected to triaxial compression under a range of confining pressure of 0-50 MPa. Such a range of confining pressure has been chosen to match loading levels applied in the triaxial compression tests on cubes and hollow cylinders. Utilising the concept of the multiple failure state triaxial test, a minimum of two points of the failure envelope were established from each test, totalling fifty-seven points overall. Details of the applied levels of confining pressure, $\sigma_2 = \sigma_3$, at each failure state attained in the tests are presented in Table 7.1.

Table 7.1 Applied levels of confining pressure, $\sigma_2 = \sigma_3$, in multiple failure state triaxial compression tests on solid cylinders of Springwell sandstone.

Specimen No.	Failure State	$\sigma_2 = \sigma_3$, MPa
STX1	F1	0
	F2	5
STX2	F1	0
	F2	5
	F3	10
STX3	F1	0
	F2	5
	F3	15
STX4	F1	0
	F2	5
	F3	10
	F4	15
STX5	F1	0
	F2	5
	F3	10
	F4	15
STX6	F1	0
	F2	10
	F3	15
	F4	20
STX7	F1	5
	F2	10
	F3	15
STX8	F1	5
	F2	10
	F3	15
	F4	20
	F5	25
STX9	F1	5
	F2	20
	F3	25

Continued..

Continued from Table 7.1

Specimen No.	Failure State	$\sigma_2 = \sigma_3$, MPa
STX10	F1	10
	F2	20
	F3	25
STX11	F1	10
	F2	20
	F3	25
STX12	F1	15
	F2	25
	F3	50
STX13	F1	20
	F2	25
STX14	F1	20
	F2	30
STX15	F1	25
	F2	40
	F3	50
STX16	F1	30
	F2	40
	F3	50
STX17	F1	30
	F2	40
	F3	50
STX18	F1	40
	F2	50
STX19	F1	40
	F2	50

7.4 The Experimental Results

Figure 7.2 shows a typical plot of the loading sequence in a multiple failure state triaxial test in terms of axial stress versus confining pressure. The plot is for specimen STX8 which was subjected to five loading states. The resultant axial stress - axial strain curve for same specimen is presented in Figure 7.3. Recorded peak values of the axial stress, σ_1, in all tests conducted are plotted in Figure 7.4 against the corresponding levels of the applied confining pressure, $\sigma_2 = \sigma_3$. The same peak values of the axial stress are plotted in Figure 7.5 versus the corresponding levels of the axial strain, ε_1.

Measurements of the volumetric change, ΔV, have been used to compute the volumetric strain of the test specimen, $\varepsilon_v = \Delta V / V$, where V is the original volume of the specimen, and subsequently the lateral strain, $\varepsilon_2 = \varepsilon_3$, was calculated using the relations:

$$\varepsilon_v = \Delta V / V = \varepsilon_1 + \varepsilon_2 + \varepsilon_3 \qquad (7.1)$$

$$\varepsilon_2 = \varepsilon_3 = \tfrac{1}{2} \ (\varepsilon_v - \varepsilon_1) \qquad (7.2)$$

Figure 7.6 shows a typical plot of the measured values of ε_1 versus the calculated values of ε_v and $\varepsilon_2 = \varepsilon_3$ for specimen STX8. Recorded values of ε_1 at peak levels of axial stress for all specimens tested are plotted in Figure 7.7 versus the corresponding values of both ε_v and $\varepsilon_2 = \varepsilon_3$.

The specimen failure appeared to be a brittle one marked by a fall in the axial stress level to its residual value. All specimens failed by shear, characterised generally by a single major fracture inclined at about 30-40° to the specimen longitudinal axis. Representative fractured specimens are shown in Figure 7.8.

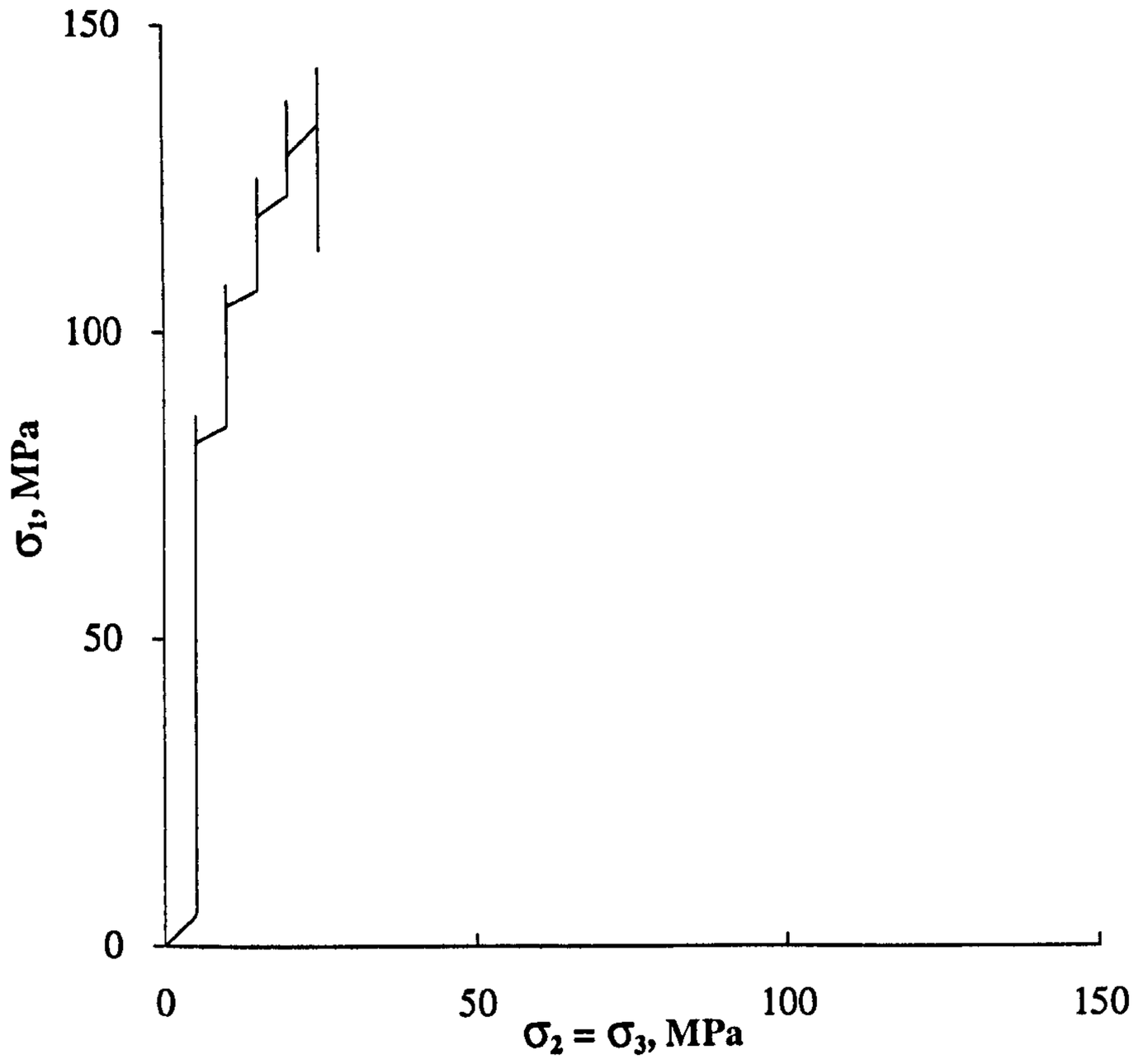

Figure 7.2 Axial stress, σ_1, versus confining pressure, $\sigma_2 = \sigma_3$, in a multiple failure state triaxial compression test on a solid cylinder of Springwell sandstone.

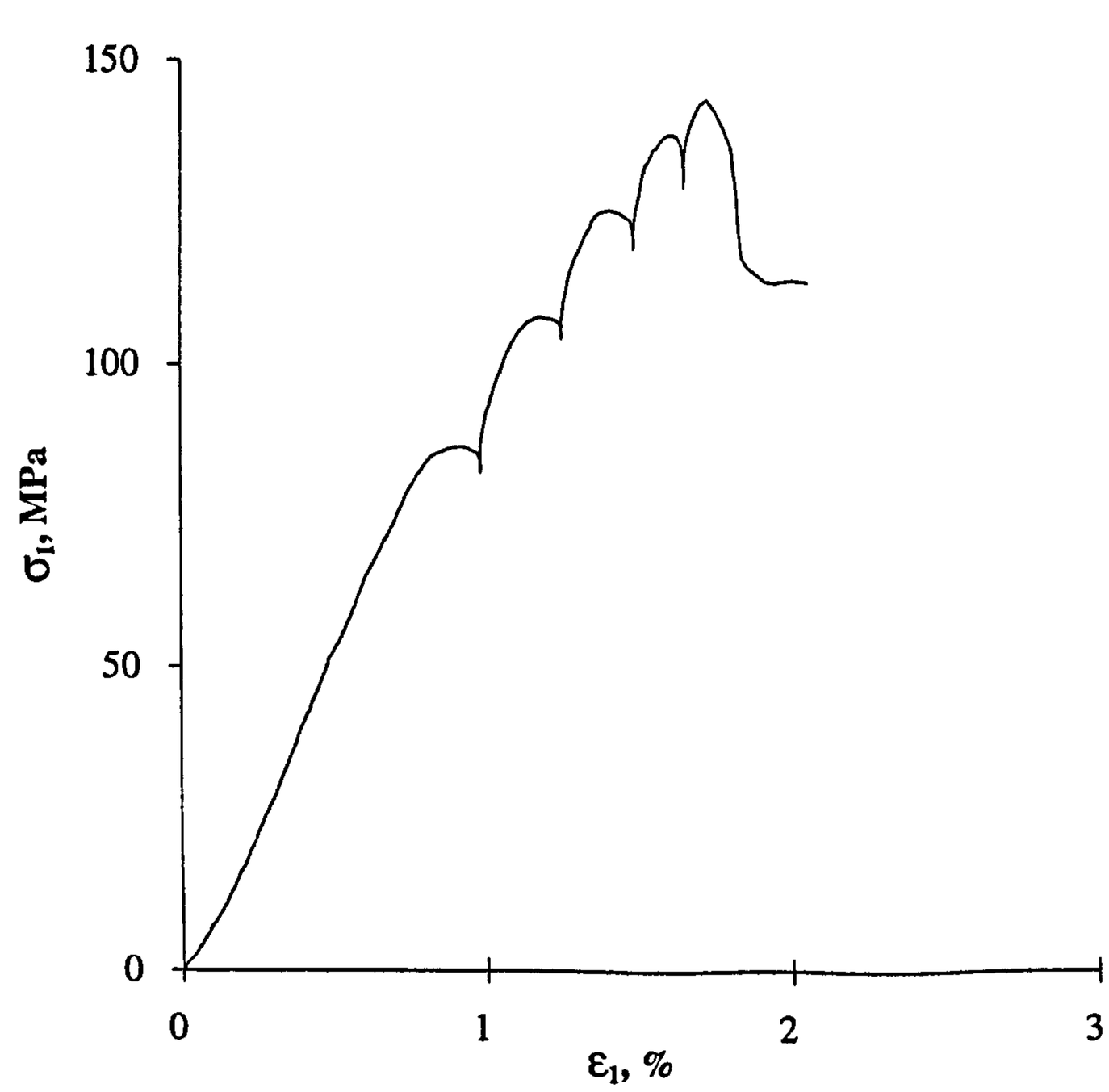

Figure 7.3 Axial stress, σ_1, versus axial strain, ε_1, for the above multiple failure state triaxial compression test on a solid cylinder of Springwell sandstone.

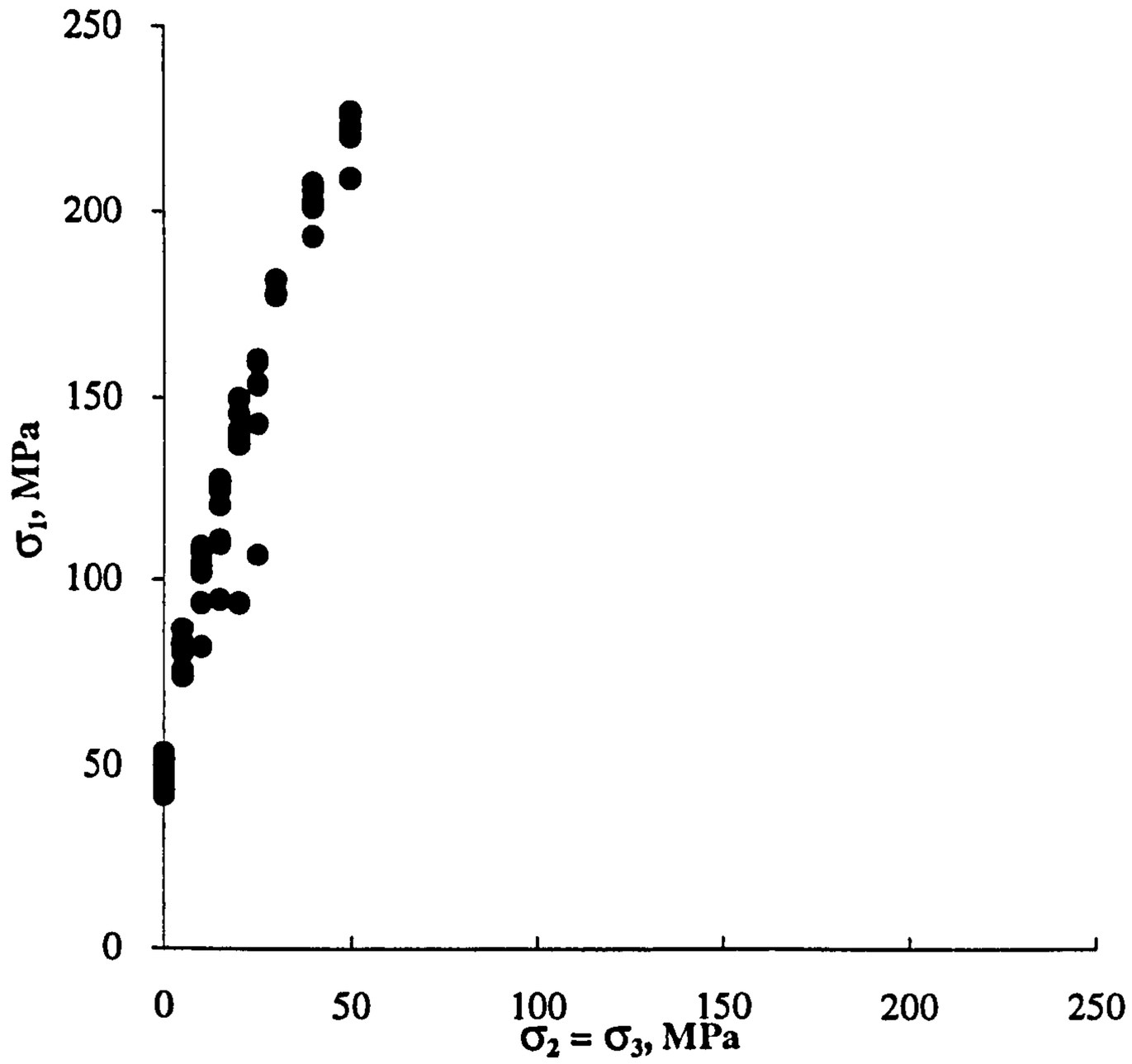

Figure 7.4 Axial stress, σ_1, at failure versus confining pressure, $\sigma_2 = \sigma_3$, in multiple failure state triaxial compression tests on solid cylinders of Springwell sandstone.

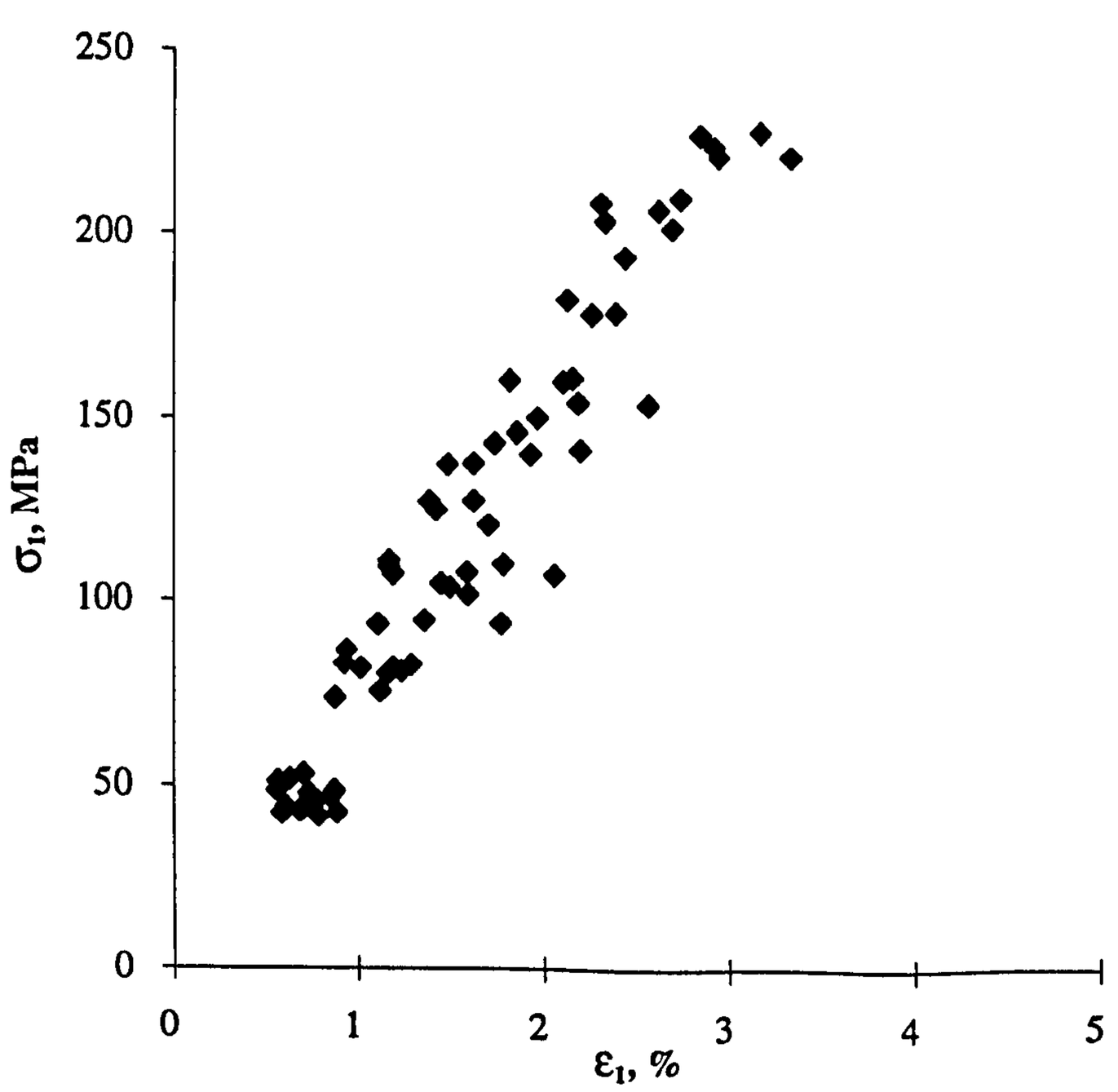

Figure 7.5 Axial stress, σ_1, at failure versus axial strain, ε_1, in multiple failure state triaxial compression tests on solid cylinders of Springwell sandstone.

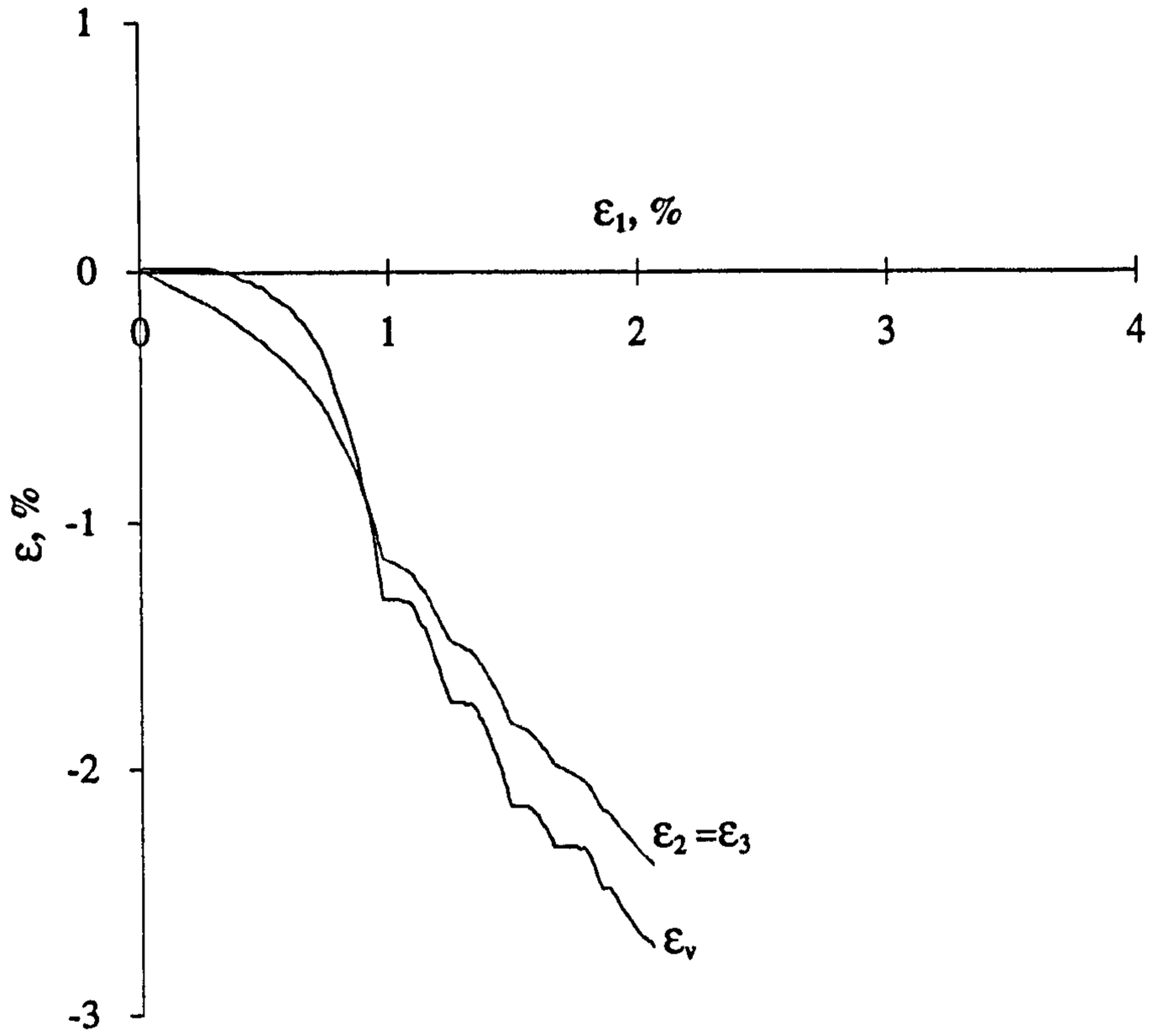

Figure 7.6 Axial strain, ε_1, versus radial strain, $\varepsilon_2 = \varepsilon_3$, and volumetric strain, ε_v, in a multiple failure state triaxial compression test on a solid cylinder of Springwell sandstone.

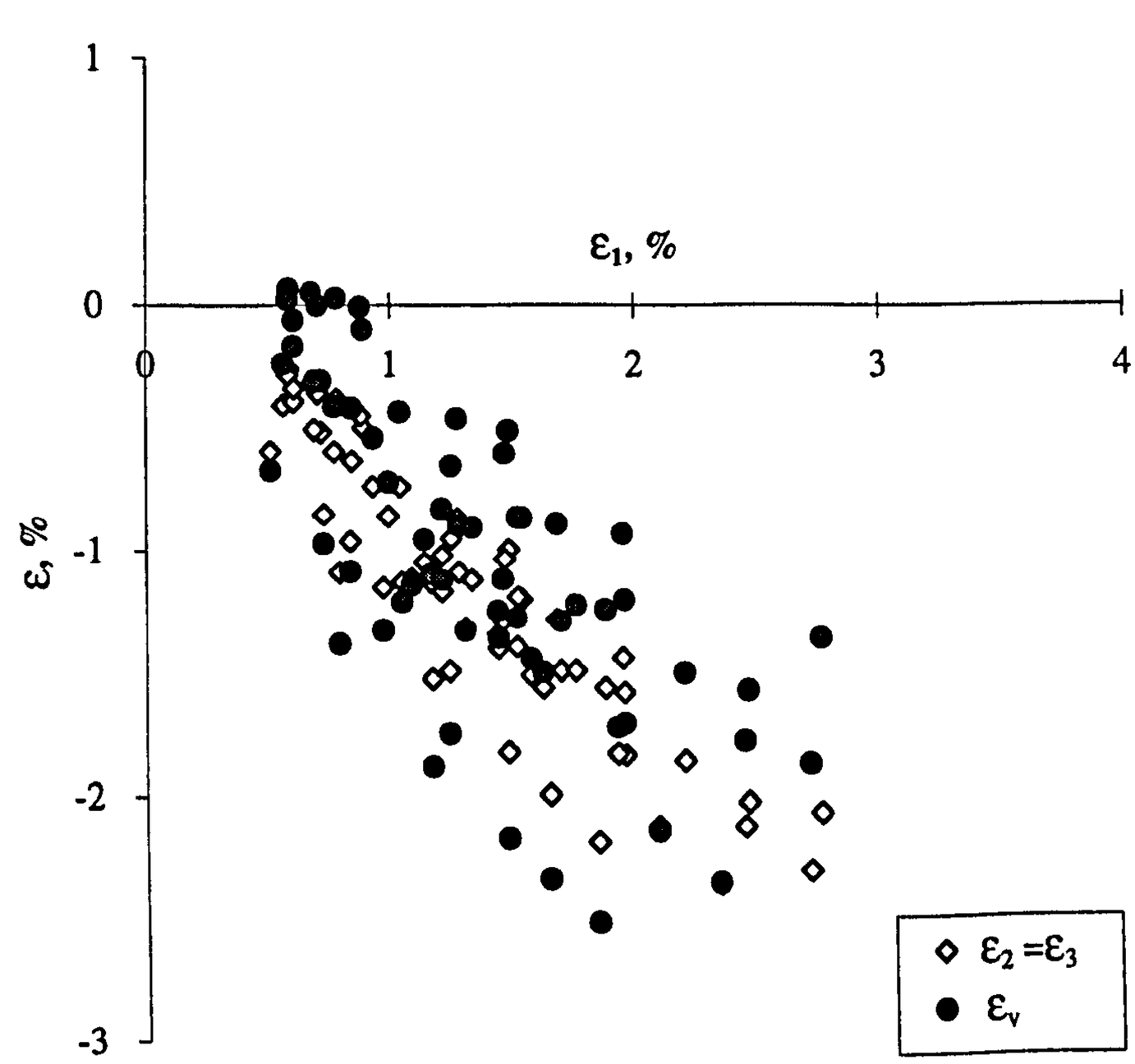

Figure 7.7 Axial strain, ε_1, at failure versus radial strain, $\varepsilon_2 = \varepsilon_3$, and volumetric strain, ε_v, in multiple failure state triaxial compression tests on solid cylinders of Springwell sandstone.

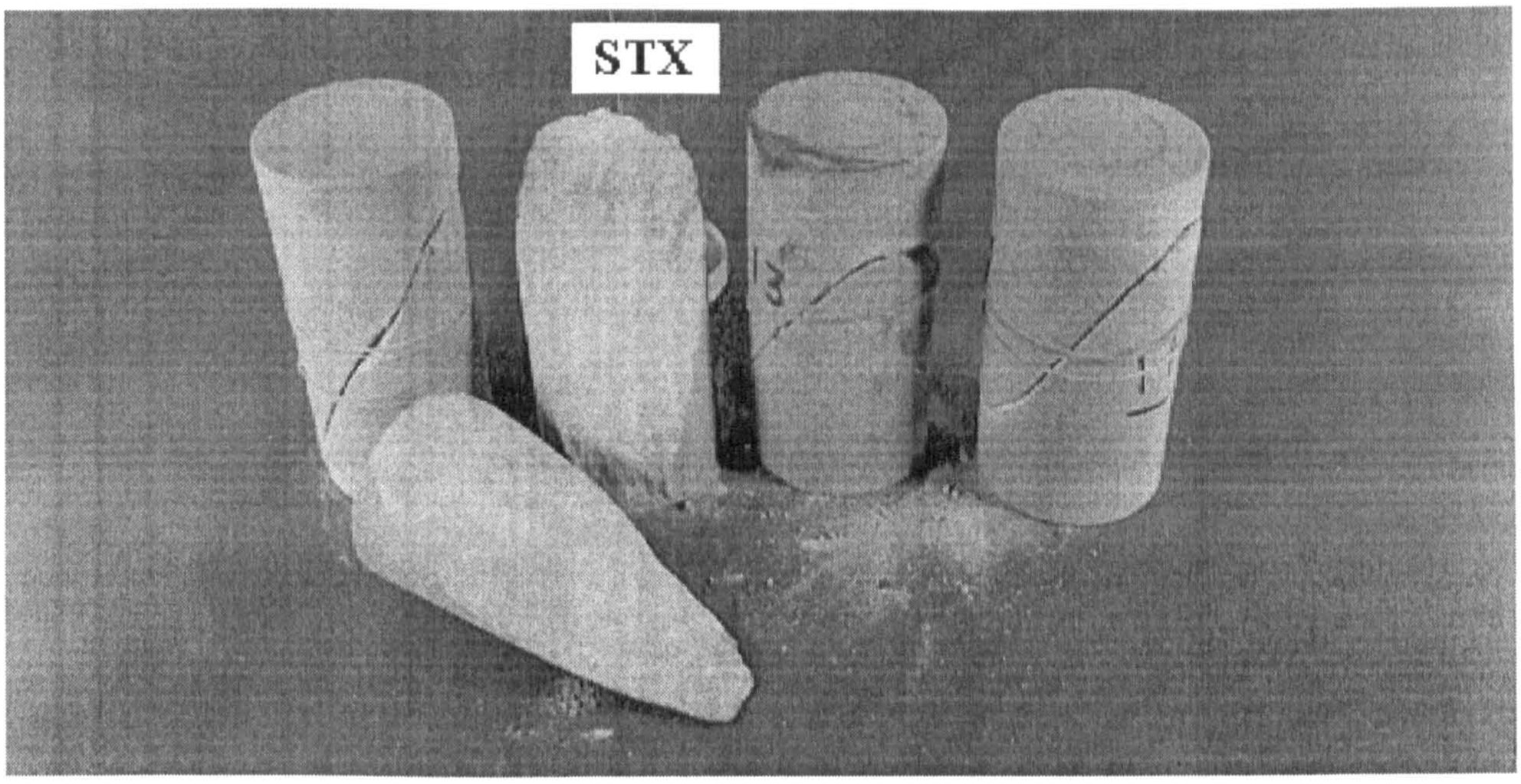

Figure 7.8 Failure of solid cylinders of Springwell sandstone in triaxial compression tests.

7.5 Discussion of the Results

On the whole, the test results are quite familiar and appear to echo features commonly exhibited by results of standard triaxial compression tests. They also present a sound confirmation of the productivity and effectiveness of the multiple failure state triaxial test in acquiring more results from a single specimen. Evidence of this confirmation can be seen in both Figures 7.2 and 7.3 which demonstrate how one specimen has been utilised to produce what would have required five specimens in standard single failure state triaxial tests.

Turning back to Figures 7.2 and 7.4, there is a clear increase in the sustained level of axial stress, σ_1, with increasing the applied level of confining pressure, $\sigma_2 = \sigma_3$. This increase appears largely regular and ceaseless within the range of confining pressure used. As the axial stress increases, both Figures 7.3 and 7.5 show a corresponding increase in the level of the specimen axial strain, ε_1. Although recorded peak levels of σ_1-ε_1 appear somewhat scattered, Figure 7.5, the general trend remains rather consistent.

Expectedly, the progressive contraction in the specimen length with increasing σ_1 appears in Figure 7.6 to result in lateral expansion represented by $\varepsilon_2 = \varepsilon_3$ values. While the computed values of the volumetric strain at failure appear widely scattered in Figure 7.7, the corresponding values of $\varepsilon_2 = \varepsilon_3$ exhibit a better and more regular relation with ε_1 values. The scattering of the results may be attributed to some of the factors thought to have influenced measurements of hole volumetric change in the hollow cylinder tests. In addition, as observed in the cubical tests, deformation measurements beyond the first failure point in multiple failure state tests are likely to vary, and this may also be the case for measurements of the specimen volumetric change.

Failure of the test specimens appears to conform to a classical mode generally recognised in triaxial compression tests under intermediate levels of confining pressure. This mode is characterised by brittle shear failure along a single inclined plane, as observed in the present tests.

Chapter

8

General Discussion and Comparison of the Results

8.1 Introduction

Rock behaviour under multiaxial compression has thoroughly been examined in the present study involving different loading arrangements and specimen forms. Cubes and thick-walled hollow cylinders of Springwell sandstone have been subjected to a range of comparable stress fields corresponding to uniaxial, biaxial, triaxial and polyaxial compression. In addition, solid cylinders of the same rock have been used in standard uniaxial and triaxial compression tests. This chapter is devoted to primarily comparing results obtained from all these tests and assessing the effect of both the stress conditions and test configuration on the apparent behaviour of rock.

The results of different multiaxial compression tests are regrouped in this chapter according to the types of stress fields under which they have been obtained. Within each group, the test results are compared placing particular emphasis on three main aspects: the specimen deformation, apparent strength and failure characteristics. The results are also evaluated in the light of findings reported in previous studies, and whenever possible, comparisons are drawn with corresponding test results.

Upon comparing the experimental results, the chapter is concluded with a discussion of the applicability of the most commonly used failure criteria. Over the years, numerous theories have been proposed on the basis of various concepts and considerations, but none of them appears to explain the diversity of the results obtained in this study.

It is worth noting that further discussions and analyses specific to all multiaxial test results reviewed herein, as well as results obtained from various investigations conducted in this study, can be found in preceding chapters where the results have initially been presented.

8.2 Results of Polyaxial Compression

Presented in Chapters 5 and 6, results of polyaxial compression in which $\sigma_1 > \sigma_2 > \sigma_3 > 0$ have been obtained from tests on specimens of Springwell sandstone in the form of cubes and thick-walled hollow cylinders, respectively. A general review of the results shows that qualitatively the rock specimen undergoes a similar deformation process in both types of tests. This process is generally characterised by contraction in the rock along the major principal stress, σ_1, and expansion along the minor principal stress, σ_3. As for the direction of the intermediate principal stress, σ_2, the specimen deformation in both types of tests appears to depend on the level of the principal stress difference (σ_2 - σ_3), with further dependence on the orientation of σ_2 and σ_3 in the hollow cylinder tests.

As pointed out in 6.4.2, technical limitations in the hollow cylinder experiments prevented the acquisition of measurements of the hole volumetric change during the initial hydrostatic loading stage in which $\sigma_1 = \sigma_2 = \sigma_3$. Consequently, only measurements of the major principal strain, ε_1, are available and that neither ε_2 nor ε_3 could be evaluated during this initial stage. However, direct measurements of the specimen deformations acquired throughout the cubical tests, Figures 5.4, 5.11, 5.15 to 5.17, 5.19, showed that near isotropic contraction in the rock occurs along the three principal directions from the onset of loading up to the hydrostatic loading limit. Upon maintaining σ_3 constant at its prescribed level, the specimen starts to expand along σ_3 direction and continues to contract along the directions of σ_1 and σ_2 as these stresses are increased. While specimen contraction along σ_2 generally ceases upon maintaining σ_2 constant, contraction along σ_1 and expansion along σ_3 progress with increasing σ_1 until the specimen fails.

Polyaxial compression of thick-walled hollow cylinders involved two distinct loading configurations, 6.4.1 and 6.5.1, corresponding to different orientations of the minor and intermediate principal stresses. Strain results obtained in both cases at the cylinder inner walls show that, qualitatively, while the rock deformations along σ_1 and σ_3 directions appear to conform to the same process as in the cubical tests, the deformation along σ_2 direction follows a different course depending on the principal stress arrangement. In tests where the tangential stress acted as intermediate principal stress, $\sigma_\theta = \sigma_2$, the results

showed that, Figures 6.23, the rock at the specimen inner wall undergoes some expansion along $\sigma_\theta = \sigma_2$ direction up to a point beyond which contraction begins to take place. In contrast, with the radial stress being the intermediate principal stress, $\sigma_r = \sigma_2$, the rock at the inner wall appears to undergo progressive compression leading to expansion of the hole, Figure 6.32.

Although qualitative agreement is generally evident between the deformational behaviour of a cubical specimen and that of a thick-walled hollow cylinder, corresponding values of principal strains obtained from the two types of tests appear to quantitatively differ, particularly along the intermediate and minor principal stress directions. In most hollow cylinder tests, both ε_2 and ε_3 values have been found considerably higher than corresponding values obtained from cubical tests.

Despite the fact that both the cubes and hollow cylinders have been subjected to the same stress field, variations between the results are likely to emerge due to fundamental differences between the test configurations. However, as far as the specimen deformation is concerned, disagreement between the test results may primarily be attributed to the use of different measuring techniques. While all principal strains ε_1, ε_2, ε_3 were directly and independently measured in the cubical tests, both ε_2 and ε_3 in the hollow cylinder tests were calculated from acquired measurements of the volumetric change of the cylinder hole, ΔV_h. As discussed in 6.4.3, measurements of ΔV_h have been found liable to the influence of various factors that are likely to lead to an overestimation in the levels of ε_2 and ε_3. In addition, with both ε_2 and ε_3 being correlated to ΔV_h measurements, cessation of deformation along σ_2 direction at the inner wall of a hollow cylinder is unlikely to occur as long as a change in hole volume is taking place. This may explain the apparent difference between the deformation process along σ_2 direction in the hollow cylinder tests and that observed in the cube tests.

It is clear from above that the measurements of rock deformations along the intermediate and minor principal stress directions in a hollow cylinder test may not be expected to quantitatively compare well with corresponding measurements obtained from a cube test under the same levels of principal stresses. Furthermore, since ε_2 and ε_3 are directly and

independently measured in the cube tests, they may be regarded to reflect the actual deformations of the rock more accurately than values suggested by the hollow cylinder tests.

Direct and independent measurements have been acquired in the hollow cylinder tests for the major principal stress, σ_1, and major principal strain, ε_1, and these measurements may be compared with corresponding ones obtained from similar tests on cubes. Figures 8.1 to 8.6 provide such comparisons in terms of σ_1 values recorded at failure in both types of tests, grouped according to σ_3 or σ_2 levels, and plotted versus the corresponding levels of σ_2 or σ_3, respectively. Similar plots have been produced in terms of σ_1 versus ε_1 values at failure. Going through these figures, both test results appear marked by some degree of scattering, a common feature of experimental outcome. Nevertheless, as already noted in Chapters 5 and 6, a general increase in the level of the major principal stress, σ_1, at failure is evident in both types of tests with increasing the applied level of the intermediate principal stress, σ_2. This provides a confirmation of the ever debated effect of σ_2 on the apparent strength of rock reported in numerous studies, e.g. Mogi (1967), Hojem and Cook (1968), Hoskins (1969), Michelis (1985), Wang *et al.* (1987). However, regarding the levels of σ_1 at which failure occurs, it is evident from Figures 8.1 to 8.6 that under to the same levels of intermediate and minor principal stresses, σ_2 and σ_3, respectively, higher levels of σ_1 are generally sustained by the hollow cylinders than the cubes. Yet, less discrepancies are seen between corresponding measurements of the major principal strain, ε_1, recorded in both types of tests.

The apparent evidence in these polyaxial tests that hollow cylinders are stronger than cubes may be attributed to a combination of various factors. An obvious factor is that while σ_2 and σ_3 are independently and directly applied in the cube tests, both stresses are calculated at the inner walls of the hollow cylinders from the applied internal and external pressures on the basis of the theory of linear elasticity. Results of characterisation tests presented in Chapter 4, as well as uniaxial compression test results discussed subsequently in 8.5, have confirmed that the Springwell sandstone may be regarded as linear elastic. Furthermore, hollow cylinder tests presented in Chapter 6 and involved different arrangements of principal stresses have indicated that the elastic theory does

provide an adequate solution for the stress distribution in the cylinders. Nevertheless, this solution remains far from being exact particularly when microcracking initiates and deviation from linear behaviour occurs before the peak stress is reached. As a result, calculated values of σ_2 and σ_3 in the hollow cylinder tests may not be as accurate as corresponding values applied directly and independently in the cube tests.

Variations between the 'polyaxial' strength, i.e. greatest level of σ_1 at failure under certain levels of σ_2 and σ_3, of hollow cylinders and cubes may also be related to the stress distribution in the test specimens. In the case of the cubes, the stresses are fairly distributed throughout the body of the specimen, and therefore, failure may initiate at any weakness point when a maximum stress level is reached. In contrast, the stresses in a hollow cylinder are not homogeneous; stress gradients exist and stress concentration is induced at the cylinder inner surface, making it less likely for a weakness point and a maximum stress level to coincide. A similar interpretation was conceived by Pomeroy and Hobbs (1962) when hollow cylinders of coal appeared stronger than cubes in biaxial compression tests.

Another reason for hollow cylinders to appear stronger than cubes may lie in the effect of the specimen geometry on the development of failure. Results of both types of tests have demonstrated that failure of the test specimen is governed by progressive expansion in the rock along the direction of the minor principal stress, σ_3. With the cubical specimen boundaries being well defined with regard to the principal stresses, expansion along σ_3 may be expected to progress more effectively than in the hollow cylinders.

One more factor that is likely to have caused a reduction in the apparent strength of the cubes is the use of PTFE sheets at the specimen-platen contacts in an effort to minimise the effect of friction. No such an effort was made in the hollow cylinder tests and that all cylinders were loaded with their ends being in direct contact with the bearing platens. An increase in the apparent strength of the test specimen due to friction between the specimen and the end platens has long been recognised, Föppl (1900), Mogi (1967), Brown (1974), Demiris (1987). On the other hand, it is widely acknowledged that any soft material inserted between the specimen and the platens to diminish the effect of friction can induce tangential tensile stresses across the specimen ends, Brady (1971), Jaeger and Cook

(1979), Brady and Brown (1993), and such stresses are likely to have a weakening effect on the test specimen. The influence of the end conditions on the apparent strength of the test specimen has also been confirmed in the present study. Cubes that were loaded in direct contact with the bearing platens appeared in 5.3 and 5.4 to sustain higher levels of major principal stress, σ_1, at failure than cubes tested with PTFE sheets at their ends. Moreover, less discrepancies can be found between σ_1 values recorded at failure in hollow cylinder tests and values obtained from corresponding tests on cubes loaded in direct contact with the bearing platens.

Regarding the specimen failure, both types of specimens failed in a brittle manner marked by a notable fall in the level of the major principal stress from its peak to a residual level. Generally, the types of fractures observed are similar to those described by other researchers in corresponding polyaxial studies reported in Chapter 2. In the case of the cubical specimens, failure has generally occurred along two to three major fracture planes lying in the direction of the intermediate principal stress, σ_2, and inclined to the direction of the major principal stress, σ_1, Figures 5.5, 5.8, 5.14. These fractures often converged at σ_1 contacts forming wedge shapes in σ_1- σ_3 plane. Signs of grain contacts or surface rubbing were visible on the fracture surfaces, suggesting that failure may be of the shear type. However, in respect of the deformational behaviour of the test specimen, failure may be anticipated to be governed by progressive expansion in the rock along the direction of the minor principal stress, σ_3, suggesting that failure is actually of the extension type rather than shear. The fact that the observed fractures may not substantiate this suggestion has been attributed to various factors discussed in 5.4.3 and conceived to have influenced the failure process.

A number of previous polyaxial studies on specimens in the form of cubes or prisms have reported similar fracture patterns to those observed in the present tests. e.g. Hojem and Cook (1968), Akai and Mori (1970), Demiris (1987). However, more relevantly, in an antecedent polyaxial study conducted at the University of Newcastle upon Tyne on cubes of Springwell sandstone, Protopsaltis (1986) reported that "*tensile failure occurred in all the experiments*" and that the fracture surfaces showed "*no hint of rubbing or shear movement*". An investigation carried out in 5.4 into such findings appeared to cast doubt

on their credibility and revealed that the failure mechanism in these experiments was highly influenced by overlapping strips of PTFE at the specimen-platen interface.

In comparison with the cubical specimens, failure of the hollow cylinders appeared to be dominated by shear resulting generally in a single fracture plane inclined to the direction of the major principal stress, $\sigma_z = \sigma_1$, Figures 6.25 and 6.45. In addition, in some tests where $\sigma_z = \sigma_1 > \sigma_\theta = \sigma_2 > \sigma_r = \sigma_3 > 0$, shear conical fractures developed, Figure 6.26, and a number of specimens exhibited what appeared to be extension fractures splitting the specimen across a surface perpendicular to the direction of the major principal stress, Figure 6.27. However, as discussed in 6.4.3, similar extension fractures were reported by Hoskins (1969) and are believed to be secondary or post-failure fractures developed when a rapid uncontrolled drop in the level of the major principal stress occurred.

On the whole, there appears to be a good agreement between the failure characteristics in these polyaxial hollow cylinder tests and findings reported by Hoskins (1969) from corresponding polyaxial tests on hollow cylinders of various rocks. In tests where $\sigma_z = \sigma_1 > \sigma_\theta = \sigma_2 > \sigma_r = \sigma_3 > 0$, signs of minor spalling were generally present in the hole in the form of minute rock fragments or small flakes ejected from the specimen inner walls. In addition, an investigation into the onset of failure in these tests confirmed that, Figure 6.28, the failure process initiates at the specimen inner surface and progresses across the wall till the specimen collapses.

Clearly, the signs of spalling at the cylinder inner walls provide further evidence of rock expansion along the direction of the minor principal stress, $\sigma_r = \sigma_3$ in this case, as already indicated by the strain results. Although this appears to endorse the cubical test suggestion that failure may be of the extension type, inclined shear fractures or shear cones are likely to develop in hollow cylinder tests as a result of the effect of the specimen geometry and end restraint. If so, then this may give credence to the suggestion by Kotsovos (1983) that the slope of the shear plane is not an intrinsic material property but rather a direct result of the boundary shear between the loading platen and the specimen.

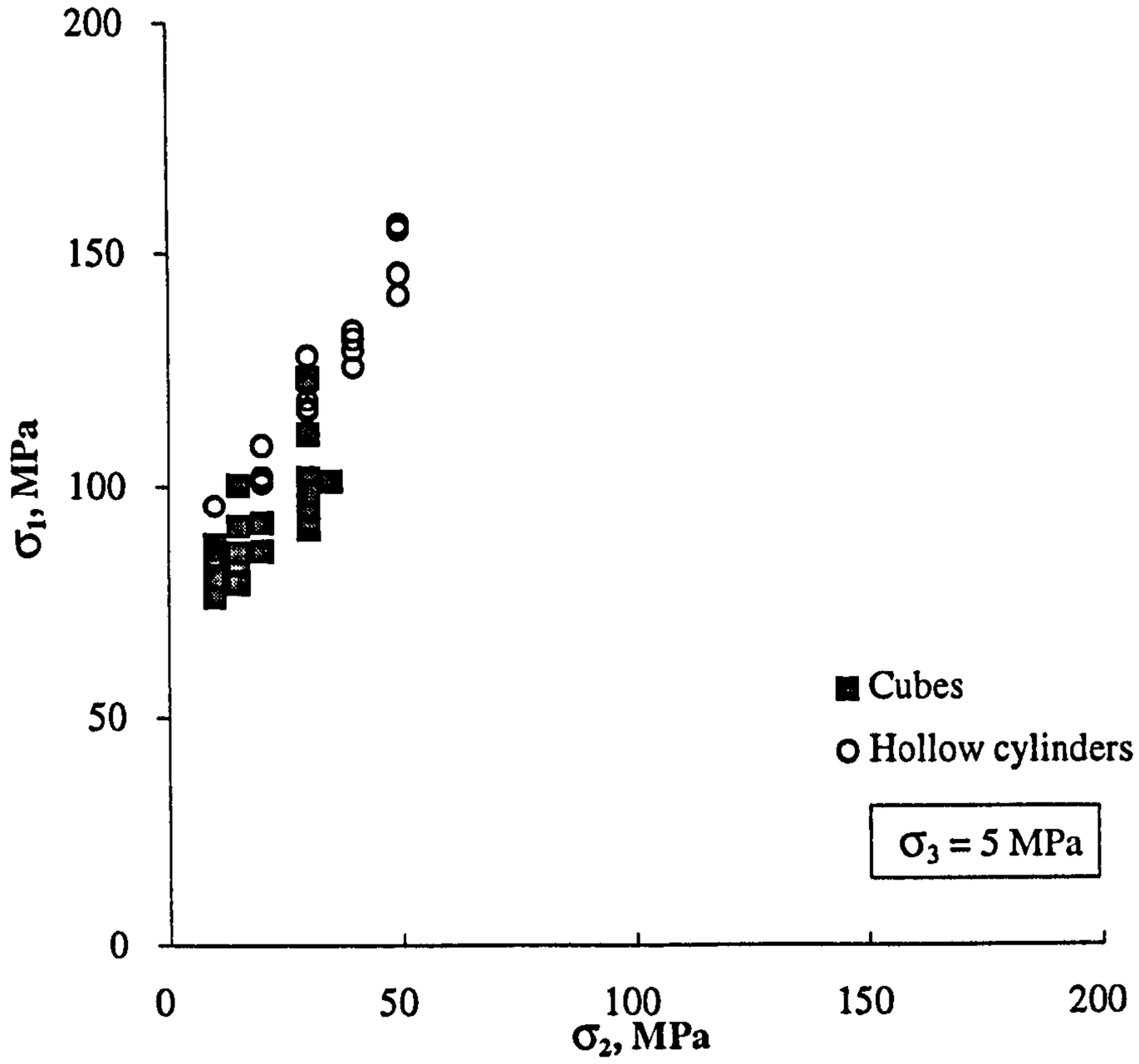

Figure 8.1 Variation of σ_1 at failure with σ_2 in polyaxial tests on cubes and thick-walled hollow cylinders of Springwell sandstone conducted under σ_3 = 5 MPa.

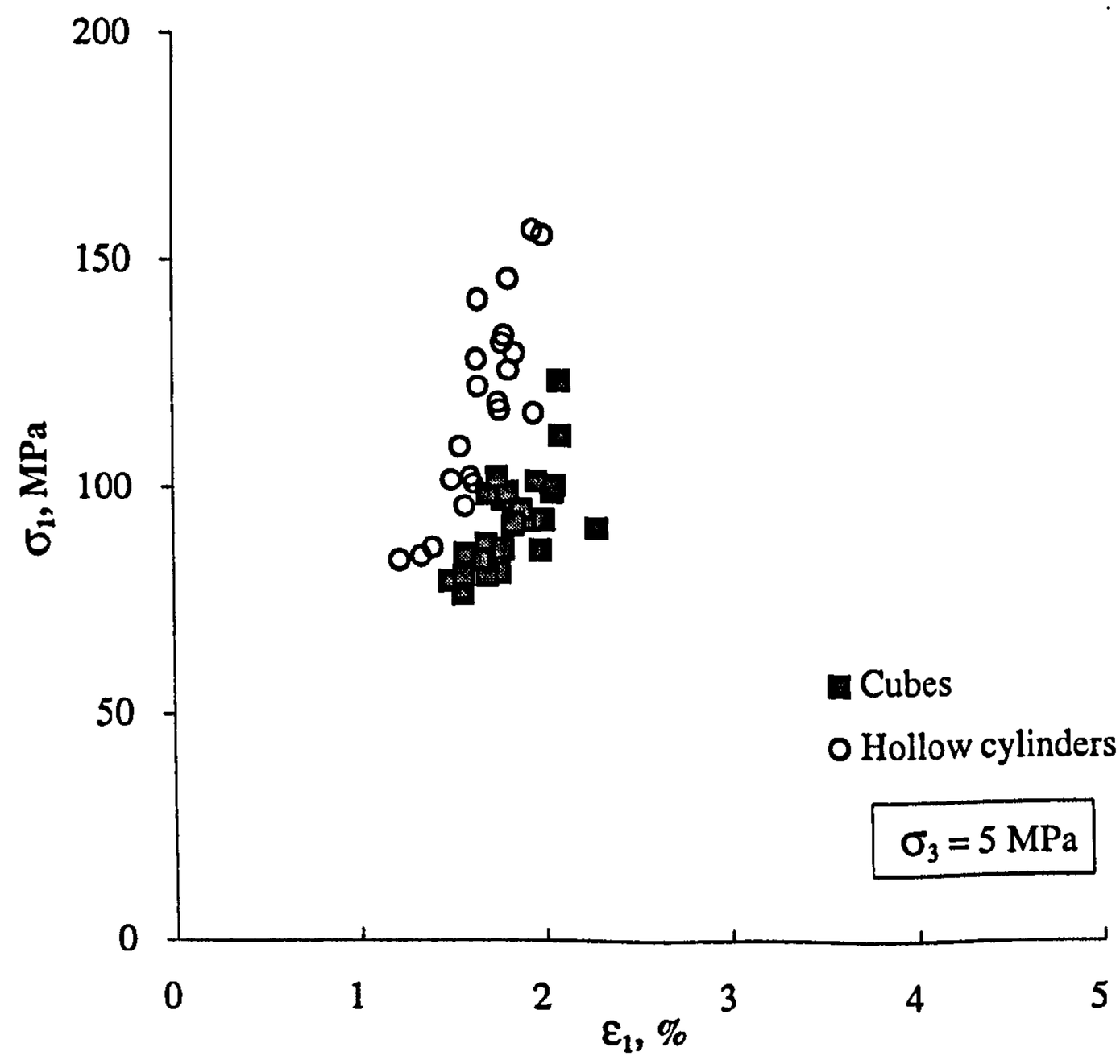

Figure 8.2 Major principal stress, σ_1, at failure versus major principal strain, ε_1, for the above polyaxial compression tests.

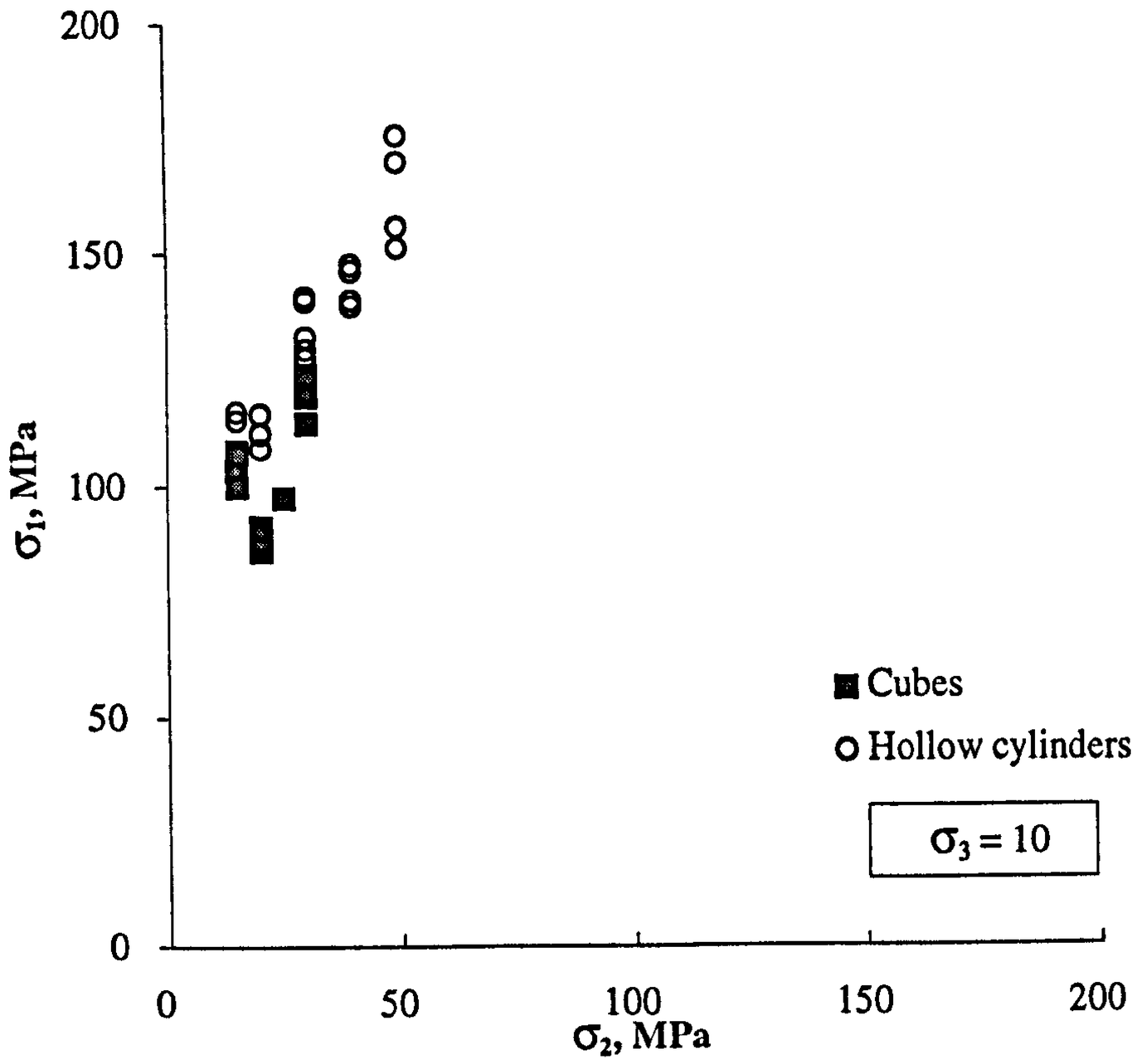

Figure 8.3 Variation of σ_1 at failure with σ_2 in polyaxial tests on cubes and thick-walled hollow cylinders of Springwell sandstone conducted under σ_3 = 10 MPa.

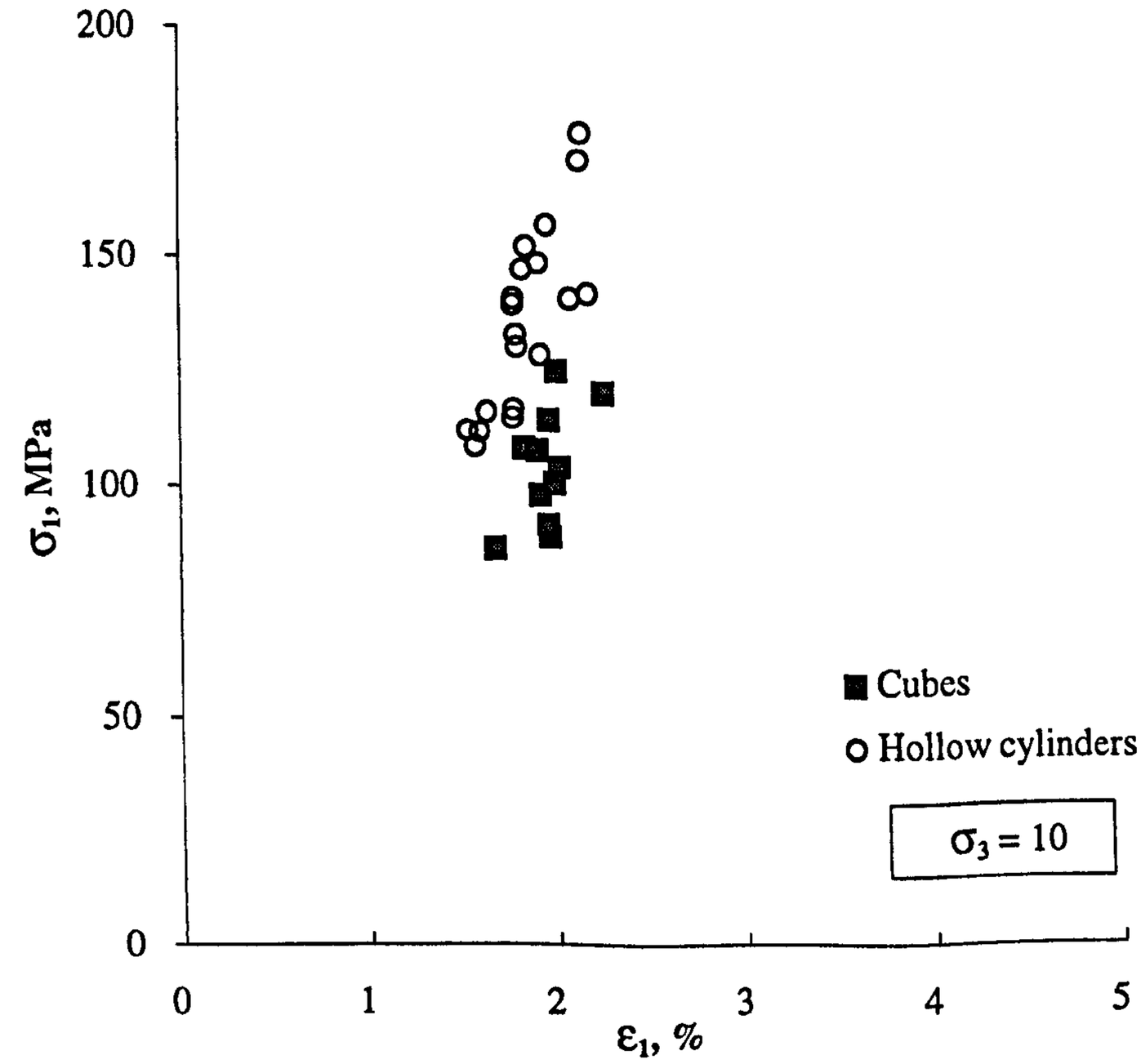

Figure 8.4 Major principal stress, σ_1, at failure versus major principal strain, ε_1, for the above polyaxial compression tests.

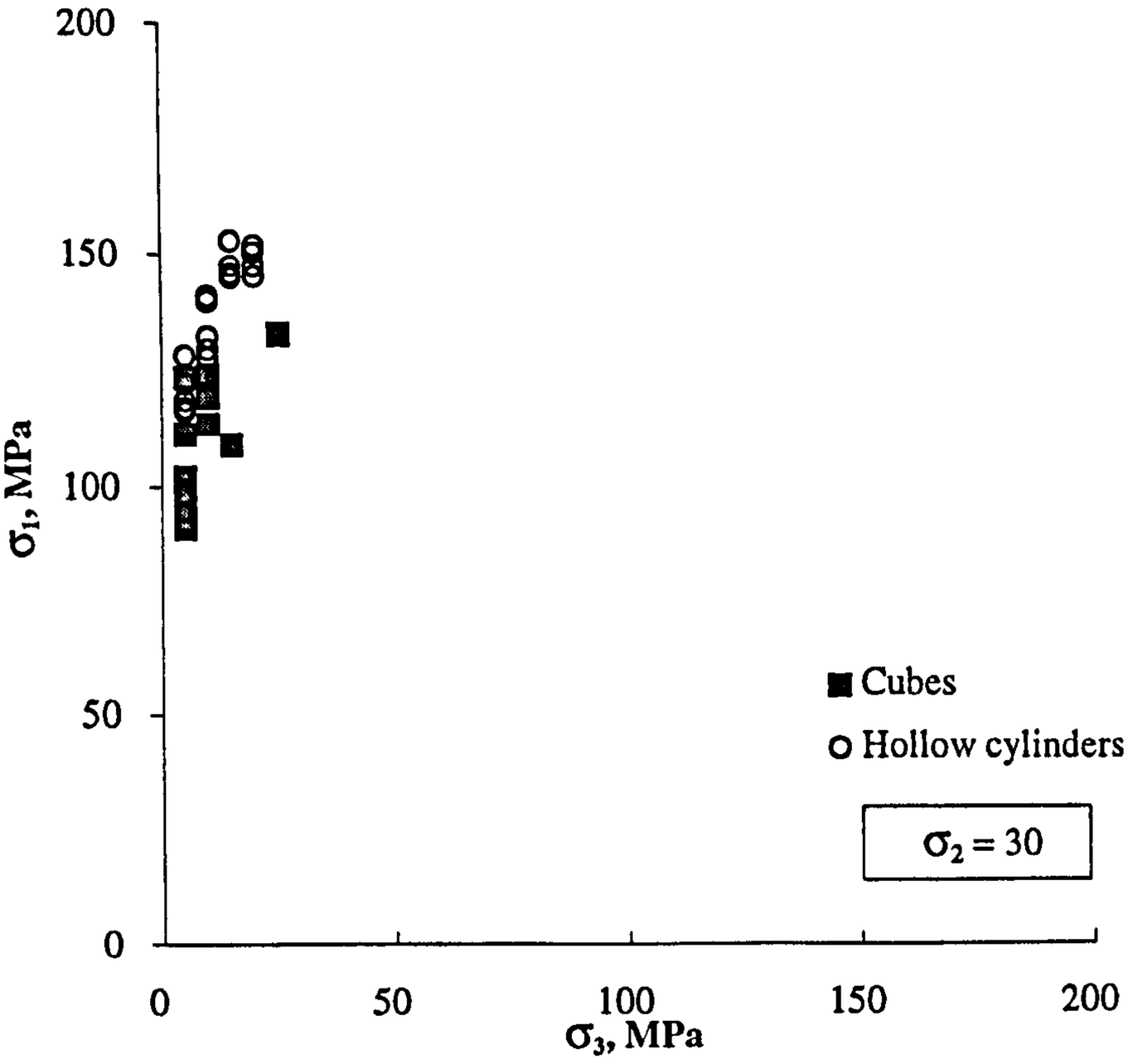

Figure 8.5 Variation of σ_1 at failure with σ_3 in polyaxial tests on cubes and thick-walled hollow cylinders of Springwell sandstone conducted under $\sigma_2 = 30$ MPa.

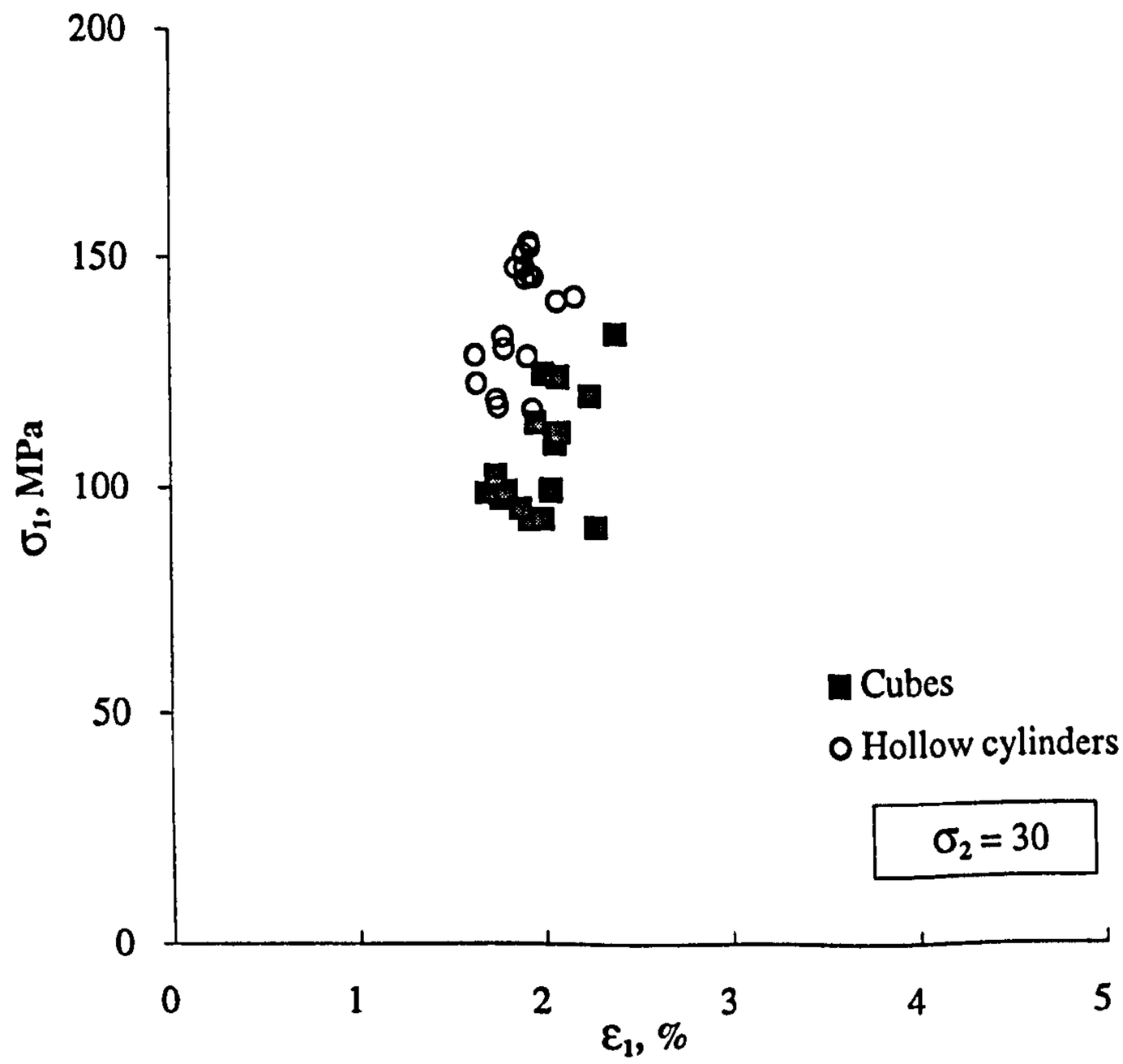

Figure 8.6 Major principal stress, σ_1, at failure versus major principal strain, ε_1, for the above polyaxial compression tests.

8.3 Results of Triaxial Compression

Results of triaxial compression in which $\sigma_1 > \sigma_2 = \sigma_3$ have been obtained from cubical specimen tests presented in Chapter 5, hollow cylinder tests presented in Chapter 6, and conventional solid cylinder tests presented in Chapter 7. The concept of the *Multiple Failure State Triaxial Test* introduced by Kovari and Tisa (1975) has been utilised in most of these tests enabling a minimum of two points of the failure envelope to be established from a single specimen. In comparison with the standard triaxial test which is limited to one failure point, the multiple failure state test has generally proved to be effective and useful particularly with regard to measurements of the major principal stress and strain. However, as the first failure state is reached, the rock specimen is likely to become less homogeneous and may no longer be expected thereafter to deform as isotropically as an intact specimen may do. As a result, measurements of the specimen lateral deformations and corresponding values of the principal strains ε_2 and ε_3 obtained beyond the first failure state may show more discrepancies than in a single failure state test.

Irrespective of the specimen geometry, the three types of triaxial tests have exhibited fundamental similarities concerning the specimen behaviour and failure mechanism. Nevertheless, some differences are also found notably among measurements of the specimen lateral deformations and the corresponding levels of the intermediate and minor principal strains, ε_2 and ε_3, respectively.

In the case of the standard solid cylinder triaxial tests where both σ_2 and σ_3 are equally represented by the confining pressure, the values of ε_2 and ε_3 are likewise assumed equal. As explained in 7.4, these values were calculated from acquired measurements of the specimen volume change and major principal strain, ε_1. The obtained results, Figures 7.6 and 7.7, have shown that while the test specimen undergoes contraction in the direction of the major principal stress, σ_1, progressive lateral expansion occurs with increasing σ_1 until the specimen fails.

Both σ_2 and σ_3 and corresponding values of ε_2 and ε_3 in the cubical triaxial tests were measured directly and independently. The test results which are presented in 5.7.2 have indicated that the deformation process initiates by near isotropic contraction along the

three principal stress directions up to the hydrostatic loading limit in which $\sigma_1 = \sigma_2 = \sigma_3$. Upon maintaining σ_2 and σ_3 constant at equal levels, contraction continues in σ_1 direction while near isotropic expansion develops along σ_2 and σ_3 directions and progresses until failure occurs.

Triaxial compression of thick-walled hollow cylinders has been achieved by subjecting the cylinders to equal levels of internal and external pressures in addition to axial load, thus inducing a state of a stress in which $\sigma_z = \sigma_1 > P_i = P_o = \sigma_r = \sigma_\theta = \sigma_2 = \sigma_3 > 0$. Following the procedure described in 6.2.4, both the tangential strain, ε_θ, and radial strain, ε_r, at the specimen inner walls were calculated from acquired measurements of the volumetric change of the specimen hole and the major principal strain, $\varepsilon_z = \varepsilon_1$. As discussed in 6.6.3, the test results have suggested that the rock at the specimen inner walls undergoes compression leading to expansion of the hole.

While ε_2 and ε_3 are assumed equal in the solid cylinder tests, and have been found to almost coincide in the cube tests, they appear in the hollow cylinder tests to differ in terms of both sign and magnitude as can be seen in Figure 6.49. Moreover, different magnitudes of ε_2 and ε_3 have been obtained from each type of tests under the same levels of $\sigma_2 = \sigma_3$. Clearly, with the cubical test measurements being acquired directly and independently, they are likely to be more reliable than results obtained from hollow and solid cylinder tests. As earlier pointed out, ε_2 and ε_3 values in these tests were calculated from measurements of the volumetric change on the basis of various assumptions, and as discussed in 6.4.3, these measurements are liable to the influence of a number of factors. In addition, unlike in the cube tests where measurements of the specimen deformations along all principal directions were recorded from the onset of loading till the test was terminated, measurements of the volumetric change in both the solid and hollow cylinder tests could not be made during the initial isotropic loading stage in which $\sigma_1 = \sigma_2 = \sigma_3$, and this is bound to affect the overall picture of the specimen lateral deformation.

As in the case of the polyaxial test results, a more appropriate comparison between the triaxial test results may be made in terms of the major principal stress and strain, σ_1 and ε_1, whose values were directly and independently measured in all tests. Such a

comparison is illustrated in Figures 8.7 and 8.8 in which recorded levels of σ_1 at failure are plotted versus the corresponding levels of $\sigma_2 = \sigma_3$ and ε_1, respectively. A common phenomenon exhibited in these figures by all test results is the increase in σ_1 level with increasing the level of $\sigma_2 = \sigma_3$. This a typical phenomenon generally observed in results of triaxial compression tests, Vutukuri *et al.* (1974), Jaeger and Cook (1979), Brady and Brown (1993). More importantly, unlike under polyaxial compression where the hollow cylinders were found generally stronger than the cubes, a better agreement can be seen under triaxial compression as all specimens appear to sustain similar levels of σ_1 at failure. Although the solid cylinders may appear somewhat stronger than both the cubes and hollow cylinders at relatively higher levels of $\sigma_2 = \sigma_3$, the lack of enough experimental data in this region makes such evidence rather inconclusive. Mazanti and Sowers (1966) found a close agreement between strength results of solid cylinder triaxial compression tests and results of hollow cylinder tests conducted under the same triaxial stress field.

The evident agreement between the 'triaxial' compressive strength, i.e. maximum level of σ_1 at failure under certain level of $\sigma_2 = \sigma_3$, of hollow cylinders and that of cubes and solid cylinders may be ascribed to a fairer stress distribution in this case than under polyaxial loading conditions. With the internal and external pressures being equal in triaxial compression of hollow cylinders, stress gradients no longer exist and, as in the case of the cubes and solid cylinders, the stresses may be regarded homogeneous and uniformly distributed throughout the body of the test specimen. In addition, the stresses are no longer calculated from the theory of elasticity and $\sigma_2 = \sigma_3$ values are those of the internal and external pressures applied.

In the light of the above evidence, it appears that strength results of triaxial compression tests are less susceptible to a number of factors found to influence other test results. Byerlee (1967) conducted triaxial compression tests on granite specimens of two different configurations and found no appreciable effect on the level of σ_1 at failure.

While all types of specimens appear to fail under similar levels of major principal stress, σ_1, corresponding levels of ε_1 recorded in Figure 8.8 suggest that generally more

deformation along σ_1 direction occurs in the cube tests than in the hollow and solid cylinder tests. This may be attributed to the presence of PTFE sheets at the cube boundaries and the additional deformation that these sheets are likely to introduce to the overall deformation measurements.

Failure of the test specimen under triaxial compression appears in all tests to be a brittle one dominated by shear. The observed fracture patterns suggest that the outcome of failure is highly influenced by the specimen geometry. In the case of the solid cylinders, Figure 7.8, failure occurred in a familiar manner across a major fracture plane inclined at about 30-40° to the specimen longitudinal axis. This corresponds to failure patterns commonly observed in standard triaxial compression tests under moderate levels of confining pressure and conforms to the widely accepted classification of failure presented by Jaeger an Cook (1979).

In the case of the hollow cylinders, similar fractures to those emerged under polyaxial loading conditions were also observed in the hollow cylinder triaxial tests, Figure 6.52. However, the general mode of failure appeared to be dominated by inclined shear fractures as in the solid cylinder tests. A close resemblance between failure modes of hollow and solid cylinders under conventional triaxial loading conditions has also been reported by Mazanti and Sowers (1966).

In contrast with the solid and hollow cylinders, failure of the cubes resulted generally in two to three fracture planes inclined to the direction of σ_1. Unlike under polyaxial loading conditions, these fractures were lying in the direction of either σ_2 or σ_3. Moreover, a number of cubes fractured along both lateral directions with the fracture planes being more profound in one direction than the other.

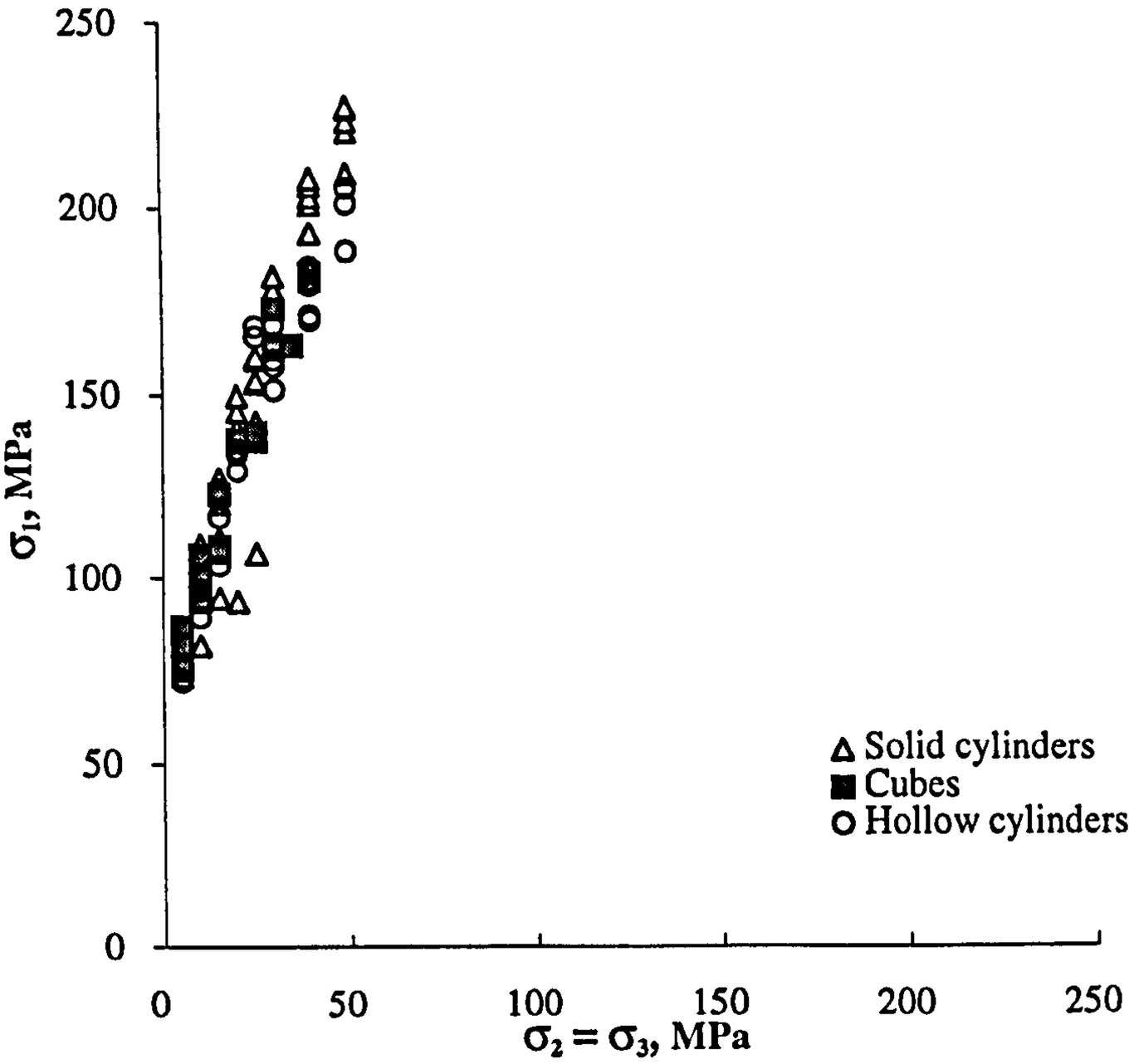

Figure 8.7 Variation of σ_1 at failure with $\sigma_2 = \sigma_3$ in triaxial tests on solid cylinders, cubes and thick-walled hollow cylinders of Springwell sandstone.

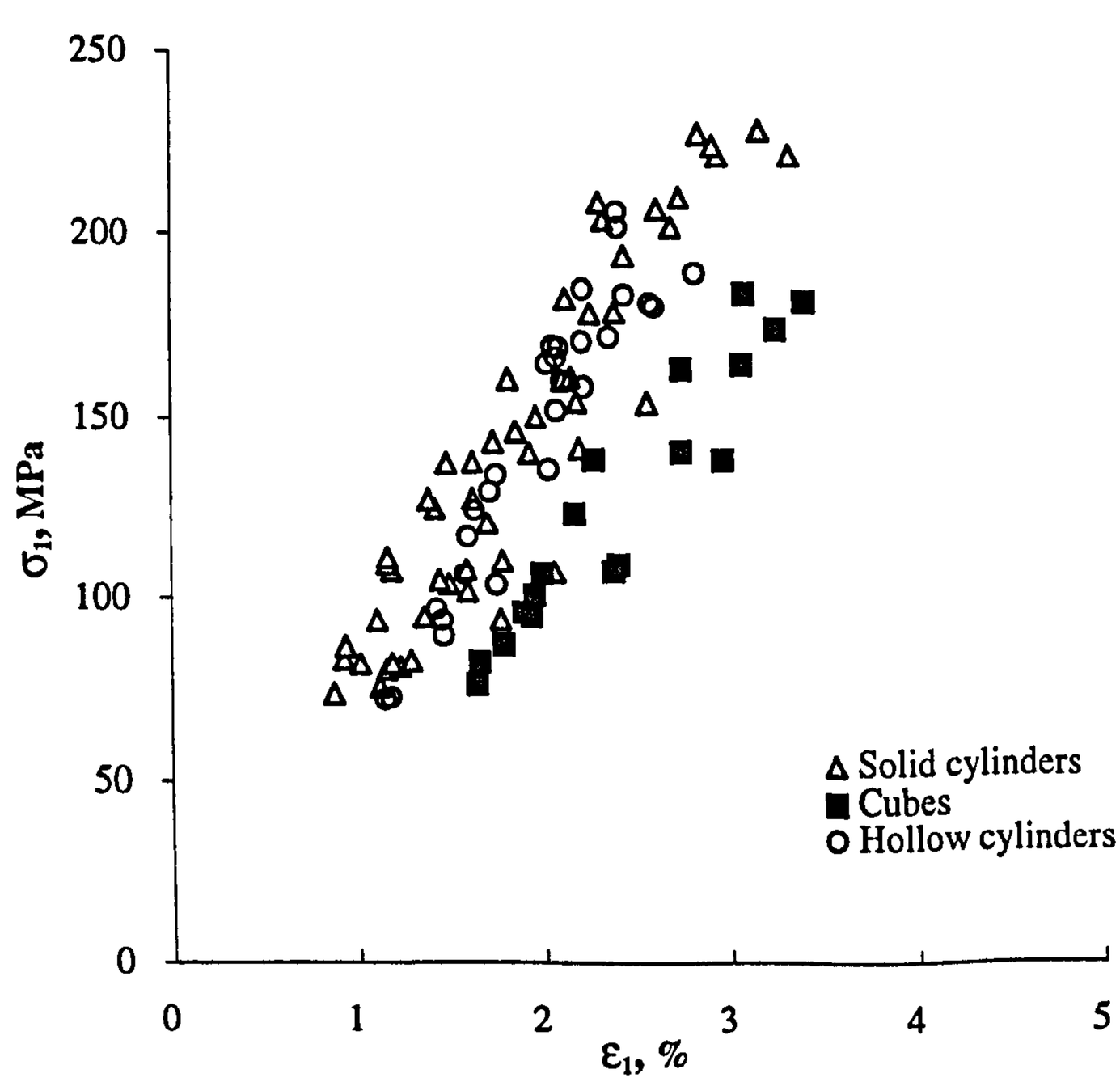

Figure 8.8 Major principal stress, σ_1, at failure versus major principal strain, ε_1, for the above triaxial compression tests.

8.4 Results of Biaxial Compression

Under the special case of biaxial compression in which $\sigma_1 > \sigma_2 > \sigma_3 = 0$, experimental results have been obtained from tests on cubes and thick-walled hollow cylinders and are presented in Chapters 5 and 6, respectively. As already ascertained under polyaxial and triaxial loading conditions, qualitative agreement along with quantitative differences are generally found between the results of both types of tests. In addition, differences are also present between the biaxial test results and those obtained from polyaxial or triaxial tests.

Biaxial compression tests on cubes have confirmed that the specimen failure is governed by rock extension along the direction of the minor principal stress, $\sigma_3 = 0$. As Figure 5.27 indicates, while the specimen deformations along σ_1 and σ_2 directions follow the same process as in polyaxial compression tests, extension along σ_3 direction progresses from the onset of loading till the specimen fails. In contrast with the polyaxial and triaxial tests in which failure occurred across inclined fractures with evidence of shear, extensile splitting in σ_3 direction dominated the failure mode under biaxial compression. Generally, the specimen disintegrated across multiple fracture planes nearly perpendicular to σ_3 direction and parallel to the σ_1-σ_2 plane, Figure 5.31. Most of the fracture planes were rough surfaces hardly exhibiting any traces of shear.

The above observations appear to be consistent with those reported in numerous biaxial studies reviewed in Chapter 2 and involved test specimens in the form of cubes, prisms or plates. Akai and Mori (1970) reported failure by axial splitting or slicing in biaxial compression tests on cubes of sandstone. Brown (1974) tested plates of Wombeyan marble and concluded that failure in biaxial compression would generally occur by extension in the direction of the minor principal stress, $\sigma_3 = 0$. Maso and Lerau (1980) conducted biaxial compression tests on prisms of Darney sandstone and observed tensile failure with the main fracture surface being almost perpendicular to the direction of σ_3. Amadei *et al.* (1984) tested cubes of Indiana limestone and noted that failure was of the extension type rather than shear.

In the case of the hollow cylinders, biaxial compression has been achieved through two different loading arrangements, 6.7 and 6.8. The test specimens appeared to qualitatively

undergo a similar deformation process as in polyaxial hollow cylinder tests conducted under corresponding loading arrangement. Moreover, similar fractures to those developed in the polyaxial tests were observed, Figures 6.59 and 6.68, with the exception that the fracture surfaces were noticeably less inhabited by symptoms of grain rubbing or surface sliding. Although the fracture patterns may suggest that failure is of the shear type, it is equally evident that the development of failure is primarily governed by rock extension in the direction of the minor principal stress, σ_3. In tests conducted without any internal pressure, $\sigma_z = \sigma_1 > \sigma_\theta = \sigma_2 > \sigma_r = \sigma_3 = 0$, rock extension along σ_3 direction resulted in a considerable amount of spalling from the specimen inner surface, Figure 6.59. Yet, the specimen geometry seems to have a leading effect on the failure mode.

Biaxial compression of hollow cylinders has generally been achieved in other studies via a combination of external pressure and axial load. Similar fractures to those emerged in the present study under similar loading conditions were reported by Hoskins (1969) and Alsayed (1988), and evidence of spalling at the cylinder inner surface has commonly been observed, Adams (1912), Mazanti and Sowers (1966), Périé and Goodman (1988).

Although fundamental agreements may be found between the deformational behaviour of a hollow cylinder and that of a cube subjected to the same biaxial stress field, variations are naturally present. These variations appear in most aspects similar to those found in 8.2 between results of polyaxial tests on both types of specimens, and equally, similar factors to those conceived in 8.2 may be held accountable for these variations.

As far as the biaxial compressive strength of the rock is concerned, i.e. maximum level of σ_1 at failure under certain level of σ_2 with $\sigma_3 = 0$, considerable differences are found between the results of the cube tests and those obtained from corresponding tests on hollow cylinders. A comparison between the results is illustrated in Figures 8.9 and 8.10 in which σ_1 values at failure in both types of tests are plotted versus the relative levels of σ_2 and ε_1, respectively. Although the results of both tests appear scattered, the general trend remains rather unmistakable.

Both the hollow cylinders and the cubes appear in Figure 8.9 to initially sustain higher levels of the major principal stress, σ_1, at failure with increasing the applied level of the

intermediate principal stress, σ_2. Such a phenomenon confirms the effect of σ_2 on the apparent strength of the rock as repeatedly advocated in numerous biaxial studies reviewed in Chapter 2, e.g. Hobbs (1962), Pomeroy and Hobbs (1962), Mazanti and Sowers (1966), Mogi (1967), Brown (1974), Maso and Lerau (1980), Stavropoulou (1982), Amadei *et al.* (1984), Alsayed (1988). However, in agreement with a number of these studies, and with some exceptions particularly in the case of the hollow cylinder tests, it is evident from the results that the increase in σ_1 level ceases at a certain point beyond which σ_1 begins to decrease as σ_2 increases. This point appears to correspond to a higher level of σ_2 in the hollow cylinder tests than in the cube tests.

Turning again to Figure 8.9, it is clear that the hollow cylinders are much stronger than the cubes and that the increase in σ_1 level with increasing σ_2 is more pronounced in the hollow cylinder tests than in the cube tests. This agrees with results obtained by Pomeroy and Hobbs (1962) from biaxial compression tests on cubes and hollow cylinders of coal. It is also consistent with the polyaxial test findings and may as well be attributed to similar factors to those conceived in 8.2 in the light of these findings. In addition, as the failure mode may suggest, the effect of the specimen geometry is likely to be more profound under biaxial compression and the cubes may be expected to expand in σ_3 direction much more effectively and disintegrate more rapidly than the hollow cylinders.

In comparison with the uniaxial compressive strength of the rock, σ_u, determined in 4.3.2 from standard tests on solid cylinders, failure under biaxial compression appears to occur at σ_1 levels higher than σ_u depending on the specimen shape and the level of σ_2 applied. In the case of the cubical specimens, the average level of σ_1 at failure within the applied range of σ_2 was found in 5.8.3 to vary from about $1.15\sigma_u$ to $1.3\sigma_u$ with an overall average of $1.22\sigma_u$. Much higher levels of σ_1 at failure were recorded in the hollow cylinder tests ranging from an average of $1.41\sigma_u$ to about $3\sigma_u$ with an overall average of $2.26\sigma_u$.

The above evidence that the strength of rock in biaxial compression is higher than in uniaxial compression appears to agree, at least qualitatively, with similar evidence reported in a number of the earlier mentioned biaxial studies, e.g. Brown (1974) and Amadei *et al.* (1984).

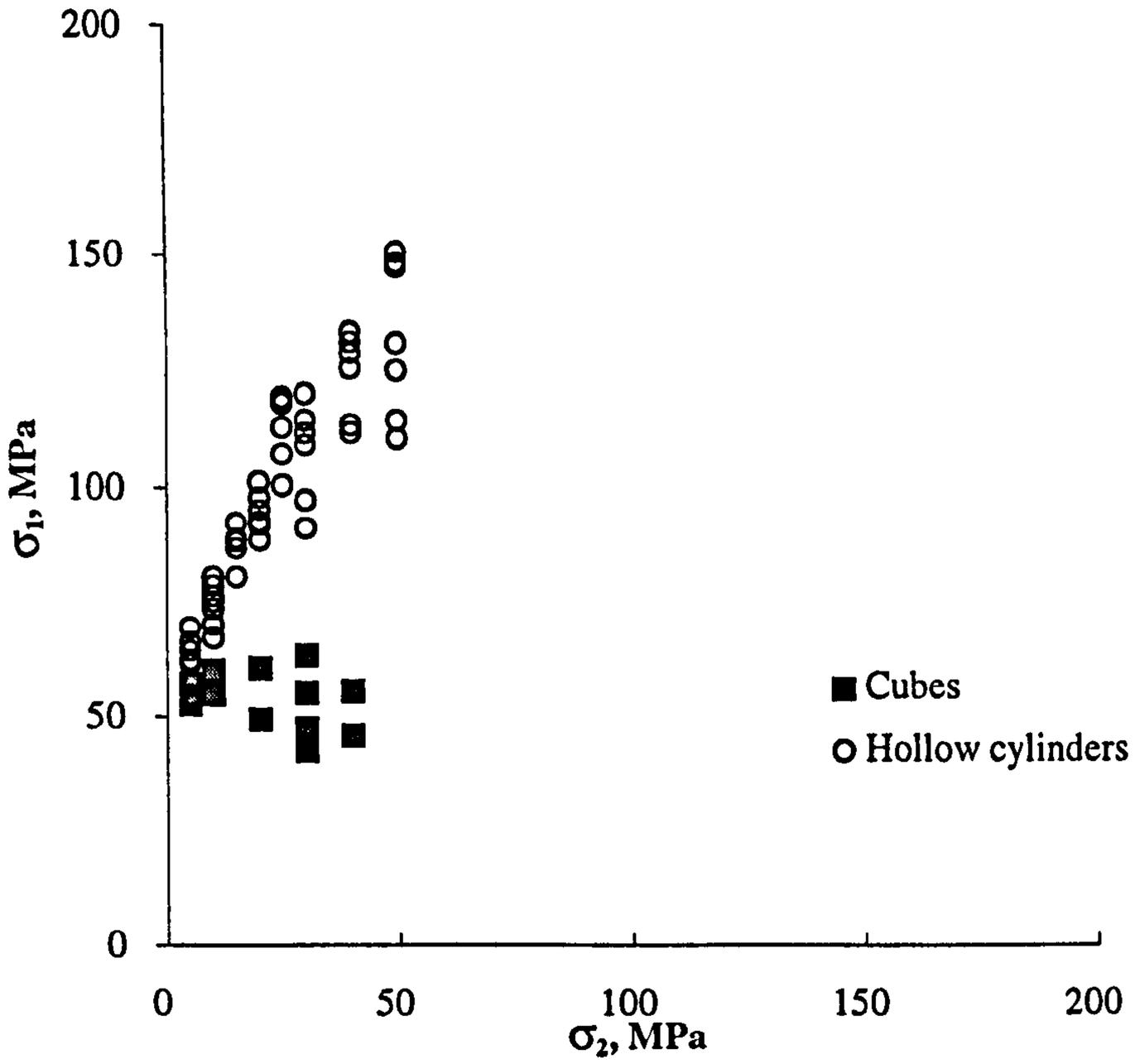

Figure 8.9 Variation of σ_1 at failure with σ_2 in biaxial compression tests on cubes and thick-walled hollow cylinders of Springwell sandstone.

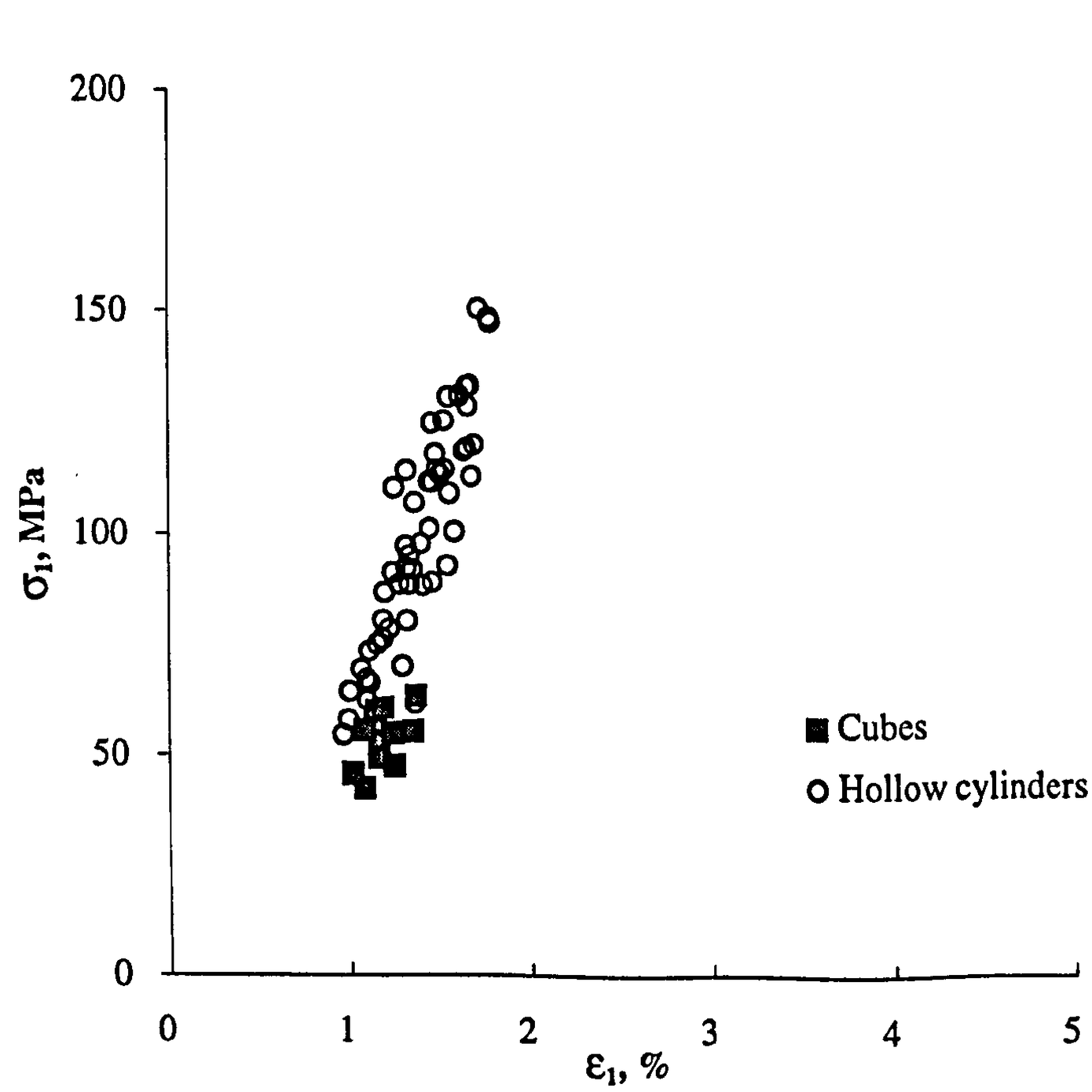

Figure 8.10 Major principal stress, σ_1, at failure versus major principal strain, ε_1, for the above biaxial compression tests.

8.5 Results of Uniaxial Compression

Under uniaxial compression in which $\sigma_1 > \sigma_2 = \sigma_3 = 0$ results have been obtained from standard tests on solid cylinders presented in Chapter 4, cube tests presented in Chapter 5 and hollow cylinder tests presented in Chapter 6. One of the most important outcome of these tests lies in the confirmation of the influence of the test configuration on the apparent uniaxial compressive strength of the rock, σ_u. Following the conventional procedure suggested by ISRM, Brown (1981), an average value of $\sigma_u = 44.113$ MPa was obtained in 4.3.2 from standard uniaxial compression tests on solid cylinders. Different values have been suggested by the cubical and hollow cylinder tests depending on the loading conditions.

In the case of the cubical tests, the results appeared to be highly influenced by the effect of friction at the specimen-platen contacts. When PTFE sheets were used in an effort to minimise this effect, a close agreement was found with the results of the solid cylinder tests and the cubes failed at an average uniaxial compressive stress of 44.053 MPa. However, with the cubes being in direct contact with the bearing platens as in the solid cylinder tests, failure occurred at an average uniaxial compressive stress of 60.503 MPa, suggesting an increase of about 37% over σ_u value.

Uniaxial compression tests on thick-walled hollow cylinders involved different loading arrangements, and consequently, different results have been obtained. In 6.10 and under the loading conditions $\sigma_z = \sigma_1 > \sigma_\theta = \sigma_r = \sigma_2 = \sigma_3 = 0$ conforming to uniaxial compression along the cylinder longitudinal axis without any form of confinement, failure occurred at an average uniaxial stress of 38.107 MPa, about 14% less than σ_u value suggested by the standard tests. However, when the cylinders were subjected to a minimum level of internal and external confinement of about 0.5 MPa in order to measure the hole deformation, an increase in the apparent strength was recorded and failure occurred at an average uniaxial compressive stress of 45.421 MPa, which is clearly close to σ_u value.

Another uniaxial loading arrangement attempted in 6.11 on hollow cylinders involved subjecting the cylinders to external hydrostatic pressure only, thus inducing at the cylinder

inner wall a state of uniaxial compressive stress in which $\sigma_\theta = \sigma_1 > \sigma_z = \sigma_r = \sigma_2 = \sigma_3 = 0$. However, an axial stress level of about $\sigma_z = 0.5$ MPa was applied in these tests in order to achieve the intended loading arrangement. While in some tests the specimen was allowed to deform in the axial direction by maintaining σ_z constant at its minimum level, axial deformation was prevented in other tests and a gradual built up in σ_z level was permitted with increasing the external pressure. Due to limitations in the loading facilities available, all tests in this series were halted before complete failure occurred. Nevertheless, signs of failure initiation in the form of spalling at the specimen inner walls were observed in tests where σ_z was allowed to develop. More importantly, although complete failure did not occur, the level of $\sigma_\theta = \sigma_1$ attained was in all tests much higher than the uniaxial compressive strength of the rock, σ_u, determined from solid cylinder tests. In tests where the axial stress level was maintained constant at about $\sigma_z = 0.5$ MPa, a maximum $\sigma_\theta = \sigma_1$ level of about $2\sigma_u$ was attained. This level increased to about $3\sigma_u$ in tests where a gradual increase in the axial stress took place reaching a maximum level of about $\sigma_z = 10$ MPa. Clearly, such loading conditions do not correspond to true uniaxial compression but rather biaxial compression in which $\sigma_\theta = \sigma_1 > \sigma_z = \sigma_2 > \sigma_r = \sigma_3 = 0$. As reported in 8.4, hollow cylinders tested under biaxial compression appeared to sustain levels of the major principal stress, σ_1, considerably higher than σ_u value. In addition, σ_1 level at failure was also found to initially increase with increasing the level of the intermediate principal stress, σ_2. Therefore, it is hardly surprising in these tests that a build up in σ_z level is accompanied by higher levels of σ_1. Moreover, even when σ_z is kept constant at a minimum level, it is likely to have a strengthening effect.

The above results appear to be in quantitive agreement with results of similar tests reported by a number of other researchers and reviewed in Chapter 2. Ewy *et al.* (1988) subjected thick-walled hollow cylinders of Berea sandstone to external hydrostatic pressure and prevented them from any axial deformation. The 'unconfined' strength of the hole wall was found to be 2 to 3 times higher than the uniaxial compressive strength of the rock. This high strength was attributed to a combination of size effect, the presence of an intermediate (axial) principal stress, stress gradients, and restriction of dilation due to the concave hole geometry. Similar results were confirmed by Ewy and Cook (1990a) using hollow cylinders of Berea sandstone and Indiana limestone. Tests with zero axial

stress were conducted by Santarelli and Brown (1989) on hollow cylinders of various rocks. The major principal stress at failure, $\sigma_\theta = \sigma_1$, was found to be between 2 to 2.8 times higher than the uniaxial compressive strength measured in standard tests.

Evidently, the 'indirect' uniaxial compressive strength of the rock measured at the inner wall of a thick-walled hollow cylinder is much higher than strength measurements obtained via direct axial compression of rock specimens in the form of solid cylinders as in standard tests, hollow cylinders and cubes. Direct measurements appear also to differ but relatively to a lesser degree depending on the loading conditions. Considering direct measurements obtained under similar loading conditions as in standard solid cylinder tests, i.e. without a friction reducer in the cube tests and without any form of confinement in the hollow cylinder tests, the cubes appear the strongest and the hollow cylinders are the weakest with the solid cylinders being in between. This may be attributed to a number of factors. Both the solid and hollow cylinders are of the same shape and size, and clearly, the presence of the hole reduces the effective cross section of the hollow cylinders and weakens their structure. Robertson (1955) reported in Figure 2.8 an increase in the level of external hydrostatic pressure at failure of hollow cylinders with increasing a ratio of outer radius to inner radius. Equally, Haimson and Herrick (1989) reported a decrease in the ratio of tangential stress at failure to uniaxial compressive strength with increasing the hole size. Thus, with the absence of the hole altogether in the case of the solid cylinders, they are likely to sustain higher levels of uniaxial stress. However, a minimum level of confinement appears to compensate for the presence of the hole and bring the strength of the hollow cylinders closer to that of the solid cylinders.

With regard to the cube results, a comparison with the uniaxial compressive strength of the solid cylinders was made in 5.9.3 and a number of factors were deemed accountable for the increase in the apparent strength of cubes tested in direct contact with the bearing platens. A common factor in all cubical tests is that only the area acted upon by the bearing platen was considered effective when calculating the stress in the test specimen. Since this area is smaller than the actual cross section of the specimen, such a 'debatable' assumption may have resulted in stress levels that are overestimated. Indeed, using the actual cross sectional area of the specimen reduces the stress level by about 10%, thus

narrowing the increase over σ_u to about 23%. As discussed in 5.9.3, this remaining increase may be attributed to a combination of the effects of shape, size and height to width ratio. Unit cubes were reported by Price (1960) to have greater strength than unit cylinders, although Grosvenor (1963) reported to the contrary and Alekseev *et al* (1970) found that the specimen shape has no effect on its strength. More definitely, the cubical specimens are of a smaller size than the solid cylinders, and the strength has been found to increase as the specimen size decreases, Mogi (1962), Lundborg (1967), Hoek and Brown (1980a), Brady and Brown (1993). An increase in strength has also been reported as the specimen height to width ratio decreases, Hudson *et al.* (1971), Vutukuri *et al.* (1974), Brady and Brown (1993), and this ratio is lower in the cubical specimens than in the solid cylinders. However, when PTFE sheets are used at the cubical specimen ends, the effect of friction is reduced and the apparent strength of the cubes drops to a value remarkably close to that of the solid cylinders.

Despite the variation of the apparent uniaxial compressive strength of the rock with the test configuration, qualitative as well as quantitative agreements are found among the deformation results. Evidence of this can be seen in Figure 8.11 which presents typical curves of the axial stress, σ_1, versus the principal strains ε_1, ε_2, ε_3 obtained from uniaxial compression tests on cubes, solid and hollow cylinders loaded under similar conditions. No measurements of the lateral deformation of the hollow cylinder were made in this case, and therefore, only σ_1-ε_1 curve is illustrated. In the case of the solid cylinders, measurements of the specimen deformations were acquired in both axial and lateral directions. Isotropy was assumed in the lateral directions and the lateral strain, $\varepsilon_2 = \varepsilon_3$, was calculated from the average of three displacement measurements made at the specimen mid-height with 120° circumferential spacing. As a result, two curves are illustrated in Figure 8.11 representing σ_1-ε_1 and σ_1-(ε_2=ε_3). In the cube tests, independent deformation measurements were acquired along the three principal directions maintaining the same notations used under other loading conditions, thus three curves are illustrated in Figure 8.11 representing σ_1-ε_1, σ_1-ε_2 and σ_1-ε_3.

Regardless of their shapes, all specimens appear to qualitatively undergo the same deformation process from the onset of loading till failure occurs. This process is

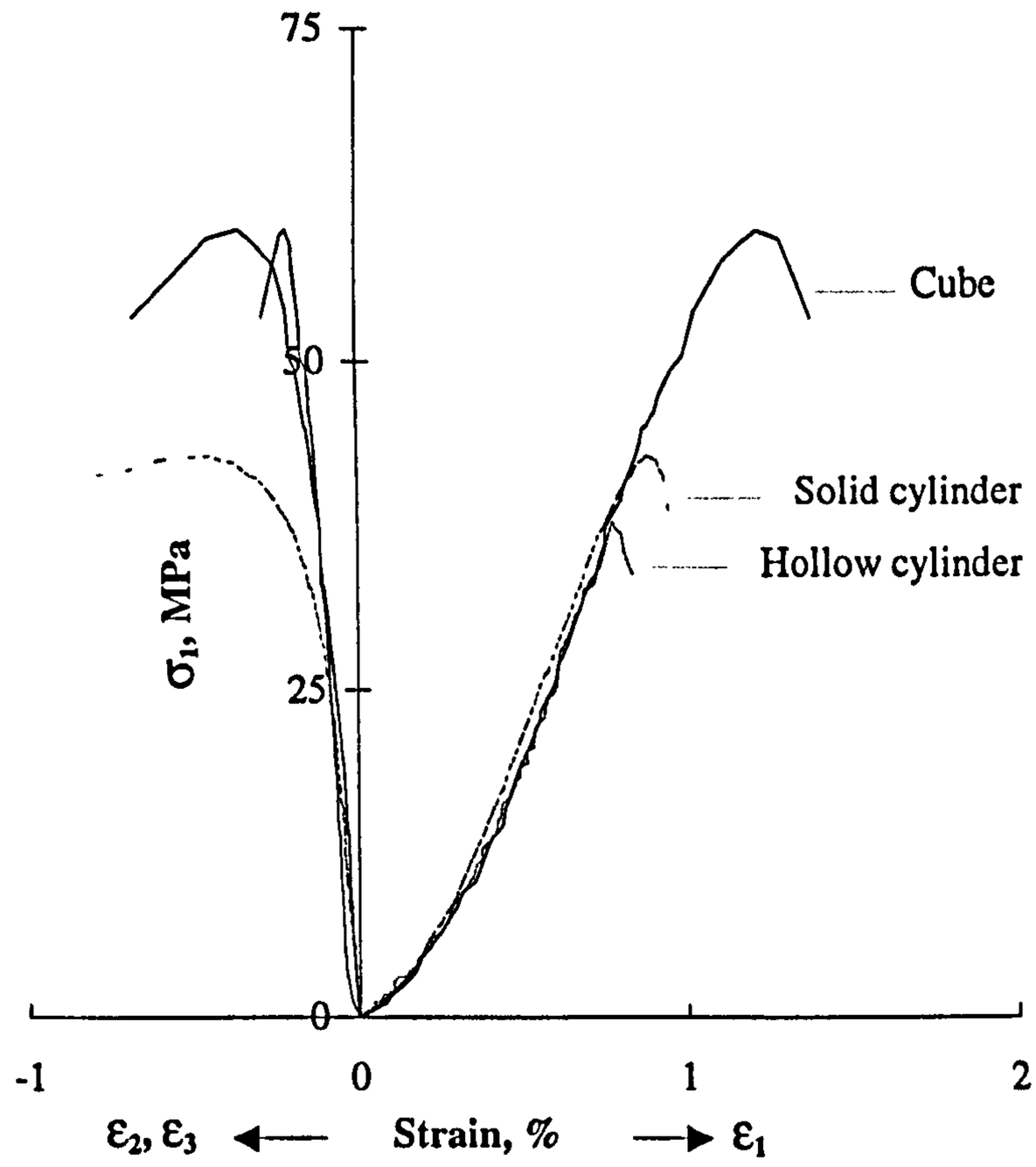

Figure 8.11 Typical curves of axial stress versus principal strains from uniaxial tests on cubes, solid and hollow cylinders. Only σ_1-ε_1 curve is shown for the hollow cylinder test.

characterised by contraction in the axial direction and expansion in the lateral directions. Although no evidence of the hollow cylinder lateral deformation is present in Figure 8.11, cylinders that were loaded axially with minimum level of internal and external pressures appeared in 6.10.3 to conform to the same behaviour.

Quantitatively, the deformational behaviour of the Springwell sandstone under uniaxial compression is closely depicted in Figure 8.11 by the results of all tests. A remarkable agreement is found in the axial direction where the axial stress-axial strain curves for all specimens appear to coincide over the entire stress range they share. A similar agreement is also evident among the axial stress-lateral strain curves for the cubes and solid cylinders up to a point where the curves begin to diverge. Depending on the level of stress sustained in each test, this point appears to generally coincide with the limit of the linear range of the curve. As defined in 4.3.2, the rock elastic constants, namely Young's modulus and Poisson's ratio, are usually determined from the slope of the linear portions of the axial

and lateral stress-strain curves. On this basis, the harmony among the stress-strain curves in the linear range implies that the rock elastic constants remain the same in all tests.

If the variations in the uniaxial compressive strength of the rock are accepted to have primarily been brought about by the earlier mentioned geometric factors, then some of the commonly assumed fundamental properties of the Springwell sandstone appear to be well substantiated by the results of these uniaxial tests. One such a property is the rock homogeneity. As described in 4.4, preparation of the various types of specimens was carried out over a period of time involving different blocks of rock which in turn were obtained from different locations at the Springwell Quarry. The fact that corresponding stress-strain curves obtained from different tests appear nonetheless to coincide is in itself a clear indication of the homogeneity of the Springwell sandstone. Furthermore, the evident agreement between strain results obtained along different lateral directions in the cube tests, and also the agreement of these results with corresponding results from solid cylinder tests, appear to give credence to the conclusion in 4.5.6 that the Springwell sandstone may for all practical purposes be regarded as isotropic.

Turning back to Figure 8.11, it is obvious that nearly elastic behaviour occurs in most part of all tests along both axial and lateral directions. This appear to suggest that the Springwell sandstone may in effect be described as linearly elastic, and consequently, justify the application of the elasticity theory to the test results. All curves exhibit an initial slightly convex upwards portion and then mostly a very nearly linear region followed by a concave downwards part just before reaching a peak ordinate. The initial non-linearity of the curves may be ascribed to the closure of pre-existing microcracks or pore space oriented at suitable angles to the applied stress, Farmer (1983), and the deviation from linearity before the peak stress is reached indicates that the deformation is no longer homogeneous but rather localised, Hadley (1975). It is in this late stage of the tests where microcracking initiates and the axial stress-lateral strain curves diverge as the microcracks propagate until failure occurs.

Failure in all tests conducted under increasing axial stress occurred in a brittle manner. In the standard uniaxial compression tests on solid cylinders, different fracture patterns emerged ranging from axial splitting to inclined shear fractures and developing shear

cones, Figure 4.3. Unlike in triaxial compression, the fracture surfaces were rough with little signs of grain rubbing or surface sliding. Generally, failure in uniaxial compression and at very low confining pressures is reported to occur by axial splitting, Jaeger and Cook (1979). Nevertheless, different patterns, though not necessarily as in the present tests, were observed by Santarelli and Brown (1989) in uniaxial compression tests on different types of rock. Fairhurst and Cook (1966) observed both longitudinal splitting and shear fractures in tests on quartzite.

In the case of the hollow cylinders, rough inclined fractures with longitudinal cracks as in the standard tests have also emerged under increasing axial compressive stress, Figure 6.73. The presence of minimum level of confinement in some of these tests appeared not to have any influence on the failure mode. However, as earlier pointed out, tests on hollow cylinders conducted under increasing external pressure only were terminated before complete failure occurred. Yet, signs of spalling or particle ejection from the specimen inner wall were observed in tests where the axial stress was allowed to build up, Figure 6.78, and such signs were regarded as evidence of failure development. A number of studies, e.g. Bridgman (1918), Daemen and Fairhurst (1970), Ewy *et al.* (1988), have shown that failure in these tests is one of progressive spalling and slabbing.

The use of PTFE sheets at the specimen-platen interface in some cube tests appears to confirm the effect of friction on the failure mode. Failure of cubes loaded in direct contact with the bearing platens was generally explosive and resulted in shear cones or wedge-shaped fractures, Figure 5.37. On the other hand, when PTFE sheets were used, failure occurred in a relatively milder manner by extensile axial splitting towards both lateral directions, Figure 5.36.

Jaeger and Cook (1979) ascribed the development of shear fractures and conical or wedge-shaped fragments in uniaxial compression to end-effects. They also pointed out that when these effects were eliminated, longitudinal splitting was observed. However, any form of a friction reducer between the specimen and the bearing platens is likely to induce lateral tensile stresses across the specimen ends, Brady (1971), Jaeger and Cook (1979), Brady and Brown (1993), and these stresses may also affect the apparent failure mode of the test specimen.

8.6 Applicability of Available Failure Criteria

A material is regarded to have failed if it has lost its strength permanently. This may be signified by loss of cohesion or fracturing if the material is brittle, or by irrecoverable deformation or plastic yielding if the material is ductile. A failure criterion may simply be defined as a quantitive relation expressed in terms of stresses, strains or other parameters which may be used to predict failure under different conditions.

Numerous failure criteria have been proposed over the years and some of the most commonly recognised ones have been reviewed by various authors, e.g. Nadai (1950), Robertson (1955), Jaeger (1965, 1966 & 1969), Trollope (1978), Jaeger and Cook (1979), Brady and Brown (1993). Although a number of these criteria have widely been applied to experimental results, they all seem to suffer from different disadvantages and that none has proved to successfully predict failure under all practicable loading conditions.

Most classical failure criteria, such as those of Coulomb (1773) or Coulomb-Navier as it is sometimes called, Tresca (1868), Mohr (1900), suffer from two major disadvantages: first, they are based on maximum shear stress considerations, and second, they neglect the effect of the intermediate principal stress, σ_2, on the development of failure. As found in the present study, and reported in biaxial tests by Brown (1974), Maso and Lerau (1980), Amadei *et al.* (1984), failure can be of the extension type rather than shear. Moreover, the present experimental results confirm the effect of σ_2 on failure, and many of the studies reviewed in Chapter 2 appear to discredit any failure criterion that does not account for this effect, e.g. Hobbs (1962), Pomeroy and Hobbs (1962), Mogi (1967), Hoskins (1969), Brown (1974), Amadei *et al.* (1984), Alsayed (1988).

Griffith (1921) postulated that failure by fracturing is initiated by tensile stress concentrations at the tips of minute *Griffith* cracks, and this was developed into what is known as Griffith two dimensional failure criterion. Besides ignoring the effect of the intermediate principal stress, this criterion is undermined by the fact that it neglects the influence of friction on the cracks when they close under high compressive stresses.

Griffith original failure criterion was subsequently modified by Brace (1960) and McClintock and Walsh (1962) to account for the influence of friction on the cracks, and was also extended by Murrell (1963) to three dimensions, thus recognising the effect of the intermediate principal stress on failure. Nevertheless, none of these versions has been found to fit different experimental results particularly well, Jaeger and Cook (1979). In addition, Brady and Brown (1993) pointed out that the use of Griffith's essentially microscopic theory to predict the macroscopic behaviour of rock material under a variety of boundary conditions, requires the introduction of a set of Griffith crack size, shape and orientation distribution functions which have not yet been defined.

A number of failure criteria have been based on strain energy considerations or octahedral shear stress. The von Mises-Hencky constant elastic strain energy of distortion criterion, derived from von Mises (1913) and Hencky (1924), acknowledges the effect of the intermediate principal stress and has been found applicable to the yielding of ductile metals. However, the disadvantage of this criterion is that it predicts the same strength in tension and compression. This makes it inapplicable to brittle rocks whose strength is much lower in tension than in compression.

The evidence that failure can be of the extension type is substantiated by failure theories based on maximum tensile stress, Taylor *et al.* (1972), Trollope (1968), or maximum extensional strain, Baker (1970), Tasuji *et al.* (1978). These theories have particularly been favoured by biaxial studies such as those of Brown (1974), Maso and Lerau (1980), Amadei *et al.* (1984).

With most conventional strength theories being inadequate, various failure criteria have been developed on the basis of empirical considerations and numerical modelling. Among such criteria are those of Bieniawski (1974), Hoek and Brown (1980b), Kim and Lade (1984), Sheorey *et al.* (1989). Generally, these criteria involve a number of material parameters, and therefore, the accuracy of their prediction depend on determining the appropriate values of these parameters. In addition, most of these criteria account only for a limited range of rock types and loading conditions, and with the exception of Kim and Lade criterion, none of them is σ_2 dependant.

A variety of other failure criteria have been proposed employing different concepts and considerations, but an account of these criteria seems to be of little benefit. As with more established theories, all these criteria appear to suffer from various limitations and none of them is able to predict failure under general loading conditions.

In the light of the above review, it is clear that an ideal failure criterion, which would predict failure for all materials under all practicable loading conditions, remains far from being found. All available criteria bear some advantages and disadvantages, but none of them appears to explain the diversity of the experimental results obtained in this study. It is therefore believed that a better approach towards failure criteria is to seek out a specific criterion for specific conditions rather than searching for a universal criterion that does not exist and may never do.

Chapter

9

Conclusions and Recommendations

9.1 Introduction

Experimental studies of the behaviour of rock and other engineering materials generally utilise conventional axisymmetric tests in which specimens in the form of solid cylinders are subjected to a state of uniaxial compression, $\sigma_1 > \sigma_2 = \sigma_3 = 0$, or more frequently triaxial compression, $\sigma_1 > \sigma_2 = \sigma_3 > 0$. Since rock in nature and around engineering structures can in many situations be under biaxial compression, $\sigma_1 > \sigma_2 > \sigma_3 = 0$, or under the general case of polyaxial compression, $\sigma_1 > \sigma_2 > \sigma_3 > 0$, conventional tests have long been realised as being inadequate to assess such stress fields.

In preference to conventional tests, two main types of experimental techniques are used to simulate multiaxial stress conditions. One in which predetermined principal stresses are directly applied to the opposite faces of prisms or cubes, and the other in which predetermined principal stresses are indirectly induced in hollow cylinders via a combination of internal and external pressures in addition to axial load. Both techniques are versatile, and have advantages and disadvantages over each other. Nevertheless, researchers have generally been biased in favour of one technique or the other.

It has been the prime aim of this study to utilise both types of multiaxial testing techniques as well as conventional methods to thoroughly examine the behaviour of rock under a wide range of compressive stress fields and assess the effect of the test configuration on the experimental results. Such a comprehensive task has first involved designing and constructing new hollow cylinder test apparatus, modifying existing multiaxial cubical test apparatus, and equipping these apparatuses with efficient loading and monitoring facilities. Subsequently, well over three hundred specimens of Springwell sandstone of various shapes and sizes have been employed in a series of experimental investigations ranging from characterisation tests to uniaxial, biaxial, triaxial and polyaxial compression tests.

This chapter recapitulates on the main aspects of this study, summarises major findings and conclusions reached and provides recommendations for further research.

9.2 Previous Multiaxial Studies

A thorough review of literature has shown that standard tests such as uniaxial and triaxial compression of solid cylinders are widely recognised as being inadequate to assess other in-situ conditions in which the rock is under biaxial or polyaxial compression. Numerous studies have therefore utilised more versatile testing methods to simulate these conditions and investigate various issues related to engineering concepts and design criteria. These studies have generally involved either direct loading of cubes or indirect loading of hollow cylinders. Despite their contribution towards a better understanding of the behaviour of rock, most previous studies may be criticised for being biased in favour of the testing method they used. It is to the best of the author's knowledge that no study has ever attempted to simultaneously involve cubes, hollow and solid cylinders in comparable multiaxial compression tests in order to assess the effect of the test configuration on the apparent behaviour of rock.

9.3 Testing Facilities, Design and Developments

A significant contribution of this study has been the development of a hollow cylinder test apparatus capable of accommodating internal and external pressures in addition to axial load, thus enabling any combination of principal stresses to be attained. The apparatus has been developed using a Hoek triaxial cell and two sets of platens especially designed for the application of internal pressure. Such a practical approach appears to have real potential for being widely utilised to have a standard triaxial and hollow cylinder test apparatus by simply extending the versatility of Hoek cell which is commonly used and readily available. This potential will be explored.

Another area of development has involved an existing multiaxial cubical test apparatus which was suffering from various problems and has therefore undergone major modifications. These modifications have included equipping the apparatus with new load cells and transducers, repositioning the seating platen and rectifying considerable levels of eccentricity along the three principal loading directions. Moreover, new bearing platens of

the same cross-section as that of other surrounding platens have been accommodated between the specimen and the load cells, thus unifying the loading boundaries of the test specimen. For the case of biaxial or uniaxial compression tests where one or two faces of the specimen are kept free from any contact, special platens have been constructed to mount the transducers inside the apparatus so that measurements of the specimen lateral deformations can be made.

An important addition to the testing facilities has been made by the acquisition of a pressure intensifier system which has been employed to provide and maintain an accurate control over the confining pressure as well as to monitor the volume change of the test specimen. In addition, an existing data acquisition system has been enhanced by an up-to-date personal computer, and the operating program has been modified to secure all test data and ensure compatibility with new hardware and software used.

9.4 Testing Configurations and Procedures

Both the cubical and hollow cylinder test apparatuses have been used in conjunction with similar testing facilities. In order to overcome the effect of the machine stiffness on the failure process, the axial stress, generally the major principal stress, σ_1, has been applied by a servo-controlled loading system. The lateral stresses, generally the intermediate and minor principal stresses, σ_2 and σ_3, have been generated using a mobile hydraulic power pack and a pressure intensifier system. However, any future polyaxial study will considerably benefit if another pressure intensifier system is made available so that both σ_2 and σ_3 can be controlled more effectively.

The pressure intensifier system has also been utilised in both standard triaxial and hollow cylinder tests to acquire measurements of the volume change, and these measurements have been used with direct measurements of the major principal strain, ε_1, to calculate the intermediate and minor principal strains, ε_2 and ε_3. Although this technique remains helpful, obtained values of ε_2 and ε_3 may not be as accurate as corresponding values directly measured in the cube tests. This may be verified in future work by exploring the possibility of using strain gauges in all tests in order to obtain more comparable results.

In the light of the ISRM suggestions for triaxial compression testing, all tests have been carried out under a constant axial strain rate of 0.25% / min. However, with the evidence that failure of the test specimen may be governed by lateral extension along σ_3 direction, it may be of interest to attempt tests, mainly on cubes, under minor principal strain rate.

While all hollow and solid cylinders have been tested in direct contact with the end platens, PTFE (Teflon) sheets have been used in cube tests to minimise the effect of friction between the specimen and the bearing platens. Perhaps a better approach would be to conduct all tests under the same boundary conditions.

The loading procedure in all tests has basically been quite similar to that suggested by ISRM for triaxial compression testing. Regarding the general case of polyaxial loading, the three principal stresses were initially increased simultaneously at the predefined axial strain rate. Then, upon reaching their designated levels successively, both σ_3 and σ_2 were held constant while σ_1 was continued till the specimen failed. Clearly, such a stress path is not necessarily what an element of rock may experience in real life, and therefore, other stress paths may be followed in future studies.

The concept of the so called multiple failure state triaxial test introduced by Kovari and Tisa (1975) has successfully been utilised in triaxial tests on cubes, solid and hollow cylinders. In addition, the concept has been extended to conduct multiple failure state polyaxial tests on cubes. Despite the effectiveness of this concept in establishing more failure points from a single specimen, measurements of the specimen lateral deformations obtained beyond the first failure state may exhibit more discrepancies than in a single failure state test.

9.5 Rock Characterisation

The rock selected for the present study is known as Springwell sandstone which belongs to the Middle Coal Measures, Upper Carboniferous-Westphalian C. It is available from a local quarry and has been used in a number of previous experimental investigations. In order to obtain results specific to the samples used in this study, most of the fundamental

characteristics of the rock have been re-assessed in accordance with the ISRM suggested methods. These results have confirmed that the Springwell sandstone may be described as uniformly fine-grained, well sorted, medium strong, linear elastic, homogeneous and isotropic.

Statistical analysis of results of non-destructive ultrasonic wave velocity tests performed on all cubes and solid cylinders have revealed a very close agreement between the rock dynamic Young's modulus determined from these tests and the 'static' Young's modulus determined from standard deformability tests. However, technical limitations in the apparatus used have prevented the determination of the rock dynamic Poisson's ratio, and consequently, the 'static' ratio has been used when calculating the dynamic Young's modulus. Therefore, an effort may be made to determine the dynamic Poisson's ratio of the rock and verify the outcome of this investigation.

Hollow cylinders have been found to provide an alternative test for measuring the rock indirect tensile strength by subjecting the cylinder to increasing internal hydrostatic pressure only. However, this strength is likely to be higher than measurements obtained by classical methods such as the Brazilian disc test.

9.6 Rock Strength in Multiaxial Compression

Cubes and thick-walled hollow cylinders of Springwell sandstone have been loaded to failure under comparable stress fields corresponding to uniaxial, biaxial, triaxial and polyaxial compression. In addition, solid cylinders have been tested under standard uniaxial and triaxial compression.

Whereas all principal stresses have been directly and independently applied to the cubes, they have been induced in the hollow cylinders by a combination of axial load, internal and external pressures on the basis of the theory of elasticity. In the case of solid cylinder triaxial tests, σ_1 has been directly imposed on the cylinders and both σ_2 and σ_3 have been assumed equal to the confining pressure applied.

The validity of using the theory of elasticity to calculate the stresses in the hollow cylinders has been investigated under both polyaxial and biaxial compression by rotating the directions of σ_2 and σ_3 with respect to the tangential and radial stresses. While this has influenced the nature of the hole deformation, no appreciable effect has been found on the level of σ_1 at failure or the general failure mode. However, the elastic solution remains far from being exact particularly when microcracking initiates and deviation from linear behaviour occurs before the peak stress is reached. It is therefore suggested to further investigate this problem and assess whether the actual stress at failure is the peak stress or rather that at some point in the nonlinear range.

An assessment of the effect of eccentricity on the strength results of hollow cylinders has proved that such an effect is negligible even for relatively considerable errors of centring between the inner and outer surfaces of the cylinder.

An investigation into the effect of the boundary conditions in cube tests has confirmed that the apparent strength of rock is influenced by friction between the specimen and the loading platens. Cubes that were tested in direct contact with the loading platens have been found to fail at higher levels of σ_1 than when PTFE (Teflon) sheets were inserted between the specimen and the loading platens. However, there appears to be a common belief that any soft material between the specimen and the platens can induce lateral tensile stresses across the specimen ends, and this is likely to have a weakening effect on the test specimen.

The maximum level of the major principal stress, σ_1, at which the rock fails has been found in this study to be remarkably influenced by both the stress field applied and the test configuration used.

Under polyaxial compression, $\sigma_1 > \sigma_2 > \sigma_3 > 0$, hollow cylinders have been found to sustain higher levels of σ_1 at failure than cubes loaded under the same levels of intermediate and minor principal stresses, σ_2 and σ_3, respectively. This phenomenon has been attributed to a combination of the following factors: possible discrepancies between calculated stresses in the hollow cylinders and directly applied ones to the cubes, the presence of non-homogenous stresses in the hollow cylinders and the relative effect of

stress gradients, the effect of the specimen geometry on the development of failure, and the use of PTFE sheets to minimise the effect of friction in the cube tests.

Obtained measurements of σ_1 at failure in polyaxial tests on both cubes and hollow cylinders have confirmed the effect of the intermediate principal stress, σ_2, on the apparent strength of rock. Under the same level of minor principal stress, σ_3, an increase in σ_1 level at failure has generally been observed with increasing the level of σ_2.

Under triaxial compression, $\sigma_1 > \sigma_2 = \sigma_3 > 0$, cubes, hollow and solid cylinders have remarkably been found to fail at similar levels of σ_1 and sustain higher levels of this stress with increasing the level of $\sigma_2 = \sigma_3$. None of the factors that are regarded to influence other test results appears to have any appreciable effect on the results of triaxial compression tests. Most notably, the stresses in the hollow cylinders are in this case homogenous; stress gradients do not exist and the stresses are no longer calculated from the theory of elasticity, as $\sigma_2 = \sigma_3$ values are those of the equal internal and external pressures applied.

Under biaxial compression, $\sigma_1 > \sigma_2 > \sigma_3 = 0$, strength results obtained from tests on both cubes and hollow cylinders have been found to qualitatively agree with results of corresponding polyaxial tests. Obtained measurements of σ_1 at failure have suggested that hollow cylinders are much stronger than cubes. In addition, both types of specimens have been found to sustain higher levels of σ_1 with increasing the level of the intermediate principal stress, σ_2, up to a point beyond which σ_1 decreases as σ_2 is increased. However, it has been observed that the increase in σ_1 level is much more pronounced in hollow cylinder tests and that the cessation of this increase occurs at higher level of σ_2 than in cube tests.

The strength of rock in biaxial compression has been found in all tests higher than its uniaxial compressive strength, σ_u, determined from standard solid cylinder tests. Within the applied levels of σ_2, failure of the cubes has occurred at σ_1 levels ranging from about $1.15\sigma_u$ to $1.3\sigma_u$ with an overall average of $1.22\sigma_u$. Much higher levels of σ_1 have been

sustained by the hollow cylinders ranging from about $1.41\sigma_u$ to $3\sigma_u$ with an overall average of $2.26\sigma_u$.

Under the same loading conditions of uniaxial compression, $\sigma_1 > \sigma_2 = \sigma_3 = 0$, solid cylinders have been found stronger by about 14% than hollow cylinders but weaker by about 37% than cubes. The weakness of the hollow cylinders has primarily been attributed to the presence of the hole, while the high strength of the cubes has been related to the likely effects of specimen shape, size, height to width ratio, and the fact that only the area acted upon by the bearing platens has been considered when calculating the stresses in the cubes. However, when the cubes were loaded with PTFE sheets at their ends, and the hollow cylinders were subjected to a minimum level of internal and external pressures of no more than 0.5 MPa, both types of specimens have been found to fail at similar levels of axial stress as that of the rock uniaxial compressive strength suggested by the solid cylinder tests.

An attempt to measure the 'indirect' uniaxial compressive strength of the rock at the inner surface of hollow cylinders has suggested that this strength is likely to be 2 to 3 times higher than the uniaxial compressive strength measured in direct axial compression tests.

9.7 Rock Deformability

Evaluating the rock deformation under different stress fields is an area where cubical tests appear to have an advantage over both hollow and solid cylinder tests by providing direct and independent measurements of all three principal strains. Only the axial or major principal strain, ε_1, has been measured directly in the hollow cylinder tests, and this has been used with acquired measurements of the hole volume change to calculate both the intermediate and minor principal strains, ε_2 and ε_3, at the cylinder inner surface. A similar technique has also been used in standard triaxial compression tests on solid cylinders where ε_2 and ε_3 have been assumed equal and calculated using ε_1 values and acquired measurements of the specimen volume change. In addition to its inaccuracy in comparison with direct strain measurements, this technique is associated with the disadvantage that the volume change can not be measured while the confining pressure is being applied,

thus preventing the assessment of both ε_2 and ε_3 during the initial hydrostatic loading stage in which $\sigma_1 = \sigma_2 = \sigma_3$. Therefore, in all hollow cylinder tests and solid cylinder triaxial tests, obtained levels of ε_2 and ε_3 may not be expected to reflect the actual deformation of the rock. Nevertheless, qualitative agreements are generally found between the results of these tests and results obtained from corresponding tests on cubes. As earlier pointed out, future studies may attempt to use strain gauges in all tests in order to obtain more comparable results.

Under the general case of polyaxial compression, strain measurements obtained from cubical tests have shown that near isotropic contraction in the rock occurs along the three principal directions from the onset of loading up to the hydrostatic loading limit. Upon maintaining σ_3 constant, the specimen begins to expand along σ_3 direction but continues to contract along both σ_1 and σ_2 directions as these stresses are increased. While contraction along σ_2 direction generally ceases upon maintaining σ_2 constant, contraction along σ_1 and expansion along σ_3 progress with increasing σ_1 until the specimen fails.

Specimen expansion along σ_3 has been observed to first counteract its early contraction in this direction until complete recovery where ε_3 decreases to zero. Thereafter, the specimen extends beyond its original length and ε_3 grows negative until failure occurs. In addition, depending on the level of the stress difference σ_2-σ_3, cessation of contraction along σ_2 direction may also be followed by some expansion particularly on imminence of failure.

Contraction in the rock along σ_1 and expansion along σ_3 have also been exhibited by strain results of hollow cylinder polyaxial tests. As for σ_2 direction, the deformation process seems to depend on the stress difference σ_2-σ_3 as well as on the orientation of σ_2 and σ_3 with regard to the tangential and radial stresses.

Under triaxial compression, results from cube tests have indicated that the deformation process initiates as in polyaxial tests by near isotropic contraction along the three principal stress directions up to the hydrostatic loading limit. Upon maintaining σ_2 and σ_3 constant at equal levels, contraction continues in σ_1 direction while near isotropic

expansion develops along both σ_2 and σ_3 directions. However, as microcracking initiates at a late stage of the test, the deformation becomes localised and consequently more deformation may evolve along one lateral direction than the other. Such a phenomenon is obscured in standard triaxial compression tests on solid cylinders in which both ε_2 and ε_3 are assumed equal, but the deformation process remains basically similar to that of the cubes. However, in the hollow cylinder triaxial tests, obtained values of ε_2 and ε_3 have been found to differ in terms of both sign and magnitude

With $\sigma_3 = 0$ in biaxial compression, results obtained from cube tests have shown that while the specimen deformations along σ_1 and σ_2 directions follow the same process as in polyaxial compression tests, extension along σ_3 direction progresses from the onset of loading till the specimen fails. In the case of the hollow cylinders, the test specimen has been found to qualitatively undergo a similar deformation process as in polyaxial hollow cylinder tests conducted under corresponding loading arrangement.

Under the simple case of uniaxial compression, the deformational behaviour of all types of specimens is characterised by contraction in the axial direction and expansion in the lateral directions from the onset of loading until failure occurs. In the case of the cube tests, near isotropic expansion develops along both lateral directions up to the initiation of microcracking where the deformation becomes no longer homogenous but rather localised, and consequently, the axial stress - lateral strain curves begin to diverge. This is usually obscured in results of standard uniaxial compression tests on solid cylinders by averaging measurements of the specimen lateral deformations on the basis of the assumption that both ε_2 and ε_3 are equal. In the case of the hollow cylinders, more deformation has been found to occur along the radial direction than along the tangential direction.

All specimens have exhibited nearly elastic behaviour in most part of the tests along both axial and lateral directions. The obtained stress-strain curves have been marked by an initial slightly convex upwards portion and then mostly a very nearly linear region followed by a concave downwards part just before reaching a peak ordinate. Although the three types of specimens appeared to sustain different levels of uniaxial compressive stress, their axial stress - axial strain curves have been found to generally coincide over

the entire stress range they share. A similar agreement has also found between the axial stress - lateral strain curves for the cubes and solid cylinders up to the onset of microcracking or localisation where the curves diverged. These agreements appeared to suggest that the rock elastic constants, namely Young's modulus and Poisson's ratio, remain the same in all tests and that the Springwell sandstone may well be regarded as linear elastic, homogenous and isotropic.

9.8 Rock Failure Characteristics

Failure in all tests has been of the brittle type often marked by audible cracking and a notable fall in the level of the major principal stress from its peak to a residual level. However, different failure modes have been observed depending on the stress conditions and test configuration.

Under polyaxial compression, cubical specimens have generally failed across two to three major fracture planes lying in the direction of the intermediate principal stress, σ_2, and inclined to the direction of the major principal stress, σ_1. These fractures have often converged at σ_1 contacts forming wedge shapes in σ_1- σ_3 plane. Signs of grain rubbing or surface sliding have been visible on the fracture surfaces, suggesting that failure is of the shear type. Although the deformational behaviour of the specimen appears to suggest that failure is governed by progressive extension in the rock along the direction of the minor principal stress, σ_3, a number of factors are likely to prevent failure in polyaxial compression from ideally being by extensile splitting or slabbing perpendicularly to σ_3 direction.

An investigation into the influence of the boundary conditions on the failure of cubes has shown that single PTFE sheets may be used to minimise the effect of friction between the specimen and the loading platens. The use of adjacent PTFE strips instead of sheets has been found not to have any notable effect on the mechanism of failure. However, if the edges of the strips are overlapped, as apparently used in a previous polyaxial study, failure is likely to occur along these edges and the results may therefore be misleading.

Failure of hollow cylinders under polyaxial compression has appeared to be dominated by shear resulting generally in a single fracture plane inclined to the direction of the major principal stress, $\sigma_z = \sigma_1$. In addition, in tests where the tangential stress is the intermediate principal stress, $\sigma_z = \sigma_1 > \sigma_\theta = \sigma_2 > \sigma_r = \sigma_3 > 0$, shear conical fractures may also develop, and secondary or post-failure extension fractures splitting the specimen across a surface perpendicular to $\sigma_z = \sigma_1$ direction may accompany the inclined or conical fractures. Signs of minor spalling have generally been observed in these tests in the form of minute rock fragments or small flakes ejected from the specimen inner walls. Furthermore, an investigation into the onset of failure has confirmed that the failure process initiates at the cylinder inner surface and progresses across the wall till the specimen collapses.

The signs of spalling at the inner walls of hollow cylinders have been perceived as evidence of rock expansion along the direction of the minor principal stress, $\sigma_r = \sigma_3$ in this case, as indicated by the strain results. Although this appears to endorse the cubical test suggestion that failure may be of the extension type, it is believed that inclined shear fractures or shear cones are likely to develop in hollow cylinder tests as a result of the effect of the specimen geometry and end restraint.

Under triaxial compression, failure of cubes, hollow and solid cylinders has been found to be dominated by shear. Yet, the specimen geometry appears to have a leading influence on the outcome of failure. In the case of the solid cylinders, failure has generally occurred across a major fracture plane inclined at about 30-40° to the cylinder longitudinal axis. Failure of the hollow cylinders has resulted in similar fractures to those observed in polyaxial tests with the general failure mode being also dominated by inclined shear fractures as in the case of the solid cylinders. On the other hand, failure of the cubes has generally occurred across two to three fracture planes inclined to the direction of σ_1 and lying in one lateral direction or the other, unlike in polyaxial tests where all fractures have been found lying in the direction of σ_2. Moreover, a number of cubes have fractured along both lateral directions but with the fracture planes being often more profound in one direction than the other.

Under biaxial compression, failure of the cubes has appeared to be of the extension type characterised by extensile splitting in the direction of the minor principal stress, $\sigma_3 = 0$. Generally, the specimen has disintegrated across multiple fracture planes nearly perpendicular to σ_3 direction and parallel to the σ_1-σ_2 plane. Most of the fracture planes were rough surfaces with hardly any traces of shear. However, in the case of the hollow cylinders, failure has once again resulted in similar fractures to those observed in polyaxial tests with the exception that the fracture surfaces were noticeably less inhabited by symptoms of grain rubbing or surface sliding. Although the fracture patterns may suggest that failure is of the shear type, the deformational behaviour of the specimen has indicated, as in the cube tests, that failure is governed by progressive extension in the rock along σ_3 direction. In tests conducted without any internal pressure, a considerable amount of spalling has occurred at the specimen inner surface. Nevertheless, the specimen geometry seems, as in all tests, to govern the apparent failure mode.

Under uniaxial compression, failure of solid cylinders has resulted in different fractures ranging from axial splitting to inclined shear fractures and developing shear cones. Unlike in triaxial compression, the fracture surfaces were rough with little signs of grain rubbing or surface sliding. In the case of the hollow cylinders, the failure mode has generally been characterised by rough inclined fractures often accompanied by longitudinal cracks. As for the cubes, the specimen failure has once again been found influenced by the end conditions. Failure of cubes loaded in direct contact with the bearing platens has generally been explosive and resulted in shear cones or wedge-shaped fractures, while when PTFE sheets were used at the specimen ends, failure has occurred in a relatively milder manner by extensile axial splitting towards both lateral directions.

When hollow cylinders have been subjected to uniaxial compression under increasing external pressure only, failure has been found to initiate by spalling at the cylinder inner surface. However, complete failure could not be achieved in these tests, and therefore, the failure mode has not been ascertained.

Under indirect tension induced by internal pressure only, hollow cylinders have been found to fail by axial splitting in halves along one major plane.

9.9 Failure Criteria

Numerous failure criteria have been proposed over the years on the basis of various concepts and considerations but an ideal criterion, which would predict failure for all materials under all practicable loading conditions, remains far from being found. All available criteria have some advantages and disadvantages, but none of them appears to explain the diversity of the results obtained in this study. It is therefore suggested that a better approach towards failure criteria is to seek out a specific criterion for specific conditions rather than searching for a universal criterion that does not exist and may never do.

9.10 Suggestions for Further Research

Since only Springwell sandstone has been used in this study, it may be necessary to carry out comparable tests on other types of rock. However, an effort may first be made to explore the possibility of using strain gauges in multiaxial tests on cubes, hollow and solid cylinders of Springwell sandstone in order to verify strain results obtained in this study via diverse means. In addition, the behaviour of rock may further be examined involving other stress paths that are of direct relevance to loading conditions encountered around rock structures or during excavation. In this regard, both cubes and hollow cylinders are versatile and may equally be used to fully map the rock failure surface in the stress space.

A variety of stress path tests may be carried out by imposing an initial state of stress such as isotropic compression and then examining the consequence of following a series of linear stress paths. A special case, in which solid cylinders may also be involved, is that of the so called triaxial extension test where all principal stresses are initially increased simultaneously up to a point beyond which two of the stresses, $\sigma_1 = \sigma_2$, are held constant or increased while the other stress, σ_3, is decreased or held constant, respectively.

Hollow cylinders in particular may be utilised to perform a series of combined multiaxial compression - tension tests in order to study the behaviour of rock when one of the principal stresses is tensile. Such tests can be achieved by various combinations of axial

stress, external pressure and a level of internal pressure high enough to induce a tensile tangential stress at the cylinder inner surface.

A much wider range of stress paths can be investigated if torsion is incorporated in the loading configuration of hollow cylinders. This would enable the principal stresses to have different angles with the cylinder axis and rotate either continuously or intermittently during the test. Such a technique can be utilised to study the behaviour of anisotropic rocks.

The validity of using the theory of linear elasticity to calculate the stresses in hollow cylinders requires further investigation to assess whether the actual stress at failure is the peak stress or rather that at some point in the nonlinear range.

Although the available testing facilities may still be utilised for most of the tests proposed herein, there is a general need for more capable pressure devices in order to attain higher levels of minor and intermediate principal stresses. More importantly, an additional pressure intensifier system is needed to achieve a better control over these stresses in polyaxial tests. However, in a longer term, a real effort is required to develop computer-controlled multiaxial loading systems and testing procedures.

Finally, while further experimental investigations may be carried out in the light of the preceding proposals, the results of this study can be used to guide the formulation of constitutive models for the behaviour of rock under multiaxial compression.

REFERENCES

ADAMS, F. D. (1912). An experimental contribution to the question of the depth of the zone of flow in the earth's crust. *J. Geol.*, Vol. 20, pp. 97-118.

AKAI, K. and MORI, H. (1970). Ein Versuch über Bruchmechnismus von Sandstein unter mehrachsigem Spannungszustand. *Proc. 2nd Congress, ISRM*, Vol. 2, Belgrade, pp. 207-213.

ALEKSEEV, A. D., ZHURAVLEV, V. I., YAROVAYA, L. I. and MOLCHANENKO, V. S. (1970). Effect of geometry and fracturing of rock specimens on their strength. *Sov. Min. Sci.*, No. 3, pp. 281-285.

ALSAYED, M. I. (1988). Laboratory testing of thick-walled hollow cylinders of rock. MSc dissertation, University of Newcastle upon Tyne.

AMADEI, B., JANOO, V., ROBISON, M. and KUBERAN, R. (1984). Strength of Indiana limestone in true biaxial loading conditions. In *Rock Mechanics in Productivity and Protection*, Eds. C. H. Dowding and M. M. Singh, *Proc. 25th U.S. Symp. Rock Mech.*, Northwestern University, Evanston, Illinois, pp. 338-348.

AMADEI, B. and ROBISON, M. J. (1986). Strength of rock in multiaxial loading conditions. In *Rock Mechanics: Key to Energy Production*, Ed. H. L. Hartman, *Proc. 27th U.S. Symp. Rock Mech.*, University of Alabama, Tuscaloosa, Alabama, pp. 47-55.

ANGELI RADOVANI, B. (1986). Deformational behaviour of concrete under triaxial compressive stress state. *Proc. 9th Congress on Material Testing*, pp. 344-345.

ANGELI RADOVANI, B. (1990). Grain size of adopted aggregate influence on strain-softening of concrete. *Engineering Fracture Mechanics*, Vol. 35, No. 4/5, pp. 709-718.

BAKER, A. L. L. (1970). A criterion of concrete failure. *Proceedings, ICE*, Vol. 45, pp. 269-278.

BANDIS, S. C., LINDMAN, J. and BARTON, N. (1987). Three-dimensional stress state and fracturing around cavities in overstressed weak rock. *Proc. 6th Int. Congress on Rock Mech.*, Montréal, Vol. 2, pp. 769-775.

BAŽANT, Z. P. (1983). Comment on orthotropic models for concrete and geomaterials. *J. Engng. Mech.*, Vol. 109, No. 3, ASCE, pp. 849-865.

BEYER, W. H. (1981). *Standard Mathematical Tables*. 26th edn, CRC Press, Florida.

BIENIAWSKI, Z. T. (1974). Estimating the strength of rock materials. *J. S. Afr. Inst. Min. Metall.*, Vol. 74, pp. 312-320.

BORG, I. and HANDIN, J. (1966). Experimental deformation of crystalline rocks. *Tectonophysics* 5, pp. 251-267.

BRACE, W. F. (1960). An extension of Griffith theory of fracture to rocks. *J. Geophys. Res.*, Vol. 65, pp. 3477-3480.

BRADY, B.T. (1971). Effects of inserts on the elastic behaviour of cylindrical materials loaded between rough end-platens. *Int. J. Rock Mech. Min. Sci.*, Vol. 8, No. 4, pp. 357-369.

BRADY, B. H. G. and BROWN, E. T. (1993). *Rock Mechanics for Underground Mining*. 2nd edn, Chapman and Hall, London.

BRIDGMAN, P. W. (1918). The failure of cavities in crystals and rocks under pressure. *Am. J. Sci.*, Vol. 45, Ser. 4, No. 268, pp. 243-268.

BROWN, E. T. (1974). Fracture of rock under uniform biaxial compression. In *Advances in Rock Mechanics, Proc. 3rd Congress, ISRM*, Denver, Colorado, Vol. 2, Part A, pp. 111-117.

BROWN, E. T. (1981). *Rock Characterization, Testing and Monitoring. ISRM Suggested Methods*. Pergamon press, Oxford.

BYERLEE, J. D. (1967). Frictional characteristics of granite under high confining pressure. *J. Geophys. Res.*, Vol. 72, No. 14, pp. 3639-3648.

CANLI, T. (1983). Rock mechanics investigations into the failure of rocks under uniaxial and polyaxial loading conditions. MSc dissertation, University of Newcastle upon Tyne.

COATES, D. F. (1981). *Rock Mechanics Principles*. CANMET, Energy, Mines and Resources Canada.

COOK, N. G. W. (1965). The failure of rock. *Int. J. Rock Mech. Min. Sci.*, Vol. 2, pp. 389-403.

COULOMB, C. A. (1773). Sur une application des règles de maximis et minimis à quelques problèmes de statique relatifs à l'architecture. *L'Académie Royale des Sciences Memoires de Mathématique et de Physique*, Vol. 7, pp. 343-382.

DAEMEN, J. J. K. and FAIRHURST, C. (1971). Influence of failed rock properties on tunnel stability. In *Dynamic Rock Mechanics*, Ed. G. B. Clark, *Proc. 12th Symp. Rock Mech.*, Rolla, Missouri, pp. 855-875.

DEMIRIS, C. A. (1987). Investigation of boundary friction effects in polyaxial tests. *Geotech. Testing J.*, GTJODJ, Vol. 10, No. 2, pp. 86-90.

EISSA, E. A. and KAZI, A. (1988). Relation between static and dynamic Young's moduli of rocks. *Int. J. Rock Mech. Min. Sci. & Geomech. Abstr.*, Vol. 25, No. 6, pp. 479-482.

EWY, R. T., COOK, N. G. W. and MYER, L. R. (1988). Hollow cylinder tests for studying fracture around underground openings. In *Key Questions in Rock Mechanics*, Eds. Cundall *et. al.*, *Proc. 29th U.S. Symp. on Rock Mech.*, Balkema, Rotterdam, pp. 67-74.

EWY, R. T. and COOK, N. G. W. (1990a). Deformation and fracture around cylindrical openings in rock - I. Observations and analysis of deformations. *Int. J. Rock Mech. Min. Sci. & Geomech. Abstr.*, Vol. 27, No. 5, pp. 387- 407.

EWY, R. T. and COOK, N. G. W. (1990b). Deformation and fracture around cylindrical openings in rock - II. Initiation, growth and interaction of fractures. *Int. J. Rock Mech. Min. Sci. & Geomech. Abstr.*, Vol. 27, No. 5, pp. 409- 427.

FAIRHURST, C. and COOK, N. G. W. (1966). The phenomenon of rock splitting parallel to a free surface under compressive stress. *Proc. 1st Congress ISRM*, Lisbon, Vol. 1, pp. 687-692.

FARMER, I. W. (1983). *Engineering Behaviour of Rocks*, 2nd edn, Chapman and Hall, London.

FÖPPL, A. (1900). Die abhangigkeit der Bruchgefahr von der Art des Spannungszustandes, *Mitt. Mech. - Tech. Lab., Technische Hochschule*, Munchen, Vol. 27.

GAU, Q., CHENG, H. and ZHUO, D. (1983). The strength deformation and rupture characteristics of red sandstone under polyaxial compression. *Proc. 5th Congress, ISRM*, Vol. 1, A, Melbourne, pp. 157-160.

GAY, N. C. (1973). Fracture growth around openings in thick-walled cylinders of rock subjected to hydrostatic compression. *Int. J. Rock Mech. Min. Sci. & Geomech. Abstr.*, Vol. 10, pp. 209- 233.

GAY, N. C. (1976). Fracture growth around openings in large blocks of rock subjected to uniaxial and biaxial compression. *Int. J. Rock Mech. Min. Sci. & Geomech. Abstr.*, Vol. 13, pp. 231- 243.

GERSTLE, K. H., ASCHL, H., BELLOTTI, R. *et al.* (1980). Behaviour of concrete under multiaxial stress states. *J. Engng. Mech. Div.*, ASCE, Vol. 106, No. EM6, pp. 1383-1403.

GRIFFITH, A. A. (1921). The phenomena of rupture and flow in solids. *Phil. Trans. Roy. Soc.*, London, Series A, Vol. 221, pp. 163-198.

GROSVENOR, N. E. (1963). Specimen proportion - Key to better compressive strength tests. *Min. Eng.*, Vol. 15, No. 1, pp. 31-33.

GUANGZHI, Y., HE, L. and XUEFU X. (1988). The effect of the stress path on strength of rock. In *Key Questions in Rock Mechanics*, Eds. Cundall *et. al.*, *Proc. 29th U.S. Symp. on Rock Mech.*, Balkema, Rotterdam, pp. 95-101.

HADLEY, K. (1975). Azimuthal variation of dilatancy. *J. Geophys. Res.*, Vol. 80, pp. 4845-4850.

HAIMSON, B. C. and HERRICK, C. G. (1989). Borehole breakouts and in situ stress. *Proc. 12th Annual Energy-Sources Technology Conf. and Exhibition, Drilling Symp.*, pp. 17-22. ASME, New York.

HANDIN, J., HEARD, H. C. and MAGOUIRK, J. N. (967). Effects of the intermediate principal stress on the failure of limestone, dolomite, and glass at different temperatures and strain rates. *J. Geophys. Res.*, Vol. 72, No. 2, pp. 611-640.

HENCKY, H. (1924). Zur Theorie plastischer Deformationen und der hierdurch im Material hervorgerufenen Nebenspannungen. *Proc. 1st Int. Congr. Appl. Mech.*, Delft, pp. 312-317.

HILSDORF, H. K. (1965). Die Bestimmung der zweiachsigen Festigkeit von Beton. *Proc. Deutsher Ausschuss fur Stahlbeton*, Vol. 173.

HOBBS, D. W. (1962). The strength of coal under biaxial compression. *Colliery Engng.*, Vol. 39, pp. 285- 290.

HOEK, E. and BROWN, E. T. (1980a). *Underground Excavation in Rock.* Institute of Mining and Metallurgy. London.

HOEK, E. and BROWN, E. T. (1980b). Empirical strength criterion for rock masses. *J. Geotech. Engng. Div.*, Vol. 106, No. GT9, ASCE, pp. 1013-1035.

HOEK, E. and FRANKLIN, J. A. (1968). Simple triaxial cell for field or laboratory testing of rock. *Trans. Inst. Min. Metall.*, Vol. 77, Sec. A, pp. A22-26.

HOJEM, J. P. M. and COOK, N. G. W. (1968). The design and construction of a triaxial and polyaxial cell for testing rock specimens. *S. Afr. Mech. Eng.*, Vol. 18, No. 2, pp. 57-61.

HOSKINS, E. R. (1969). The failure of thick-walled hollow cylinders of isotropic rock. *Int. J. Rock Mech. Min. Sci.*, Vol. 6, No.1, pp. 99-125.

HOWARTH, D. F. (1985). Development and evaluation of ultrasonic piezoelectric transducers for the determination of dynamic Young's modulus of triaxially loaded rock cores. *Geotech. Testing J.*, GTJODJ, Vol. 8, No. 2, pp. 59-65.

HUDSON, J. A., FAIRHURST, C. and BROWN, E. T. (1971). Shape of the complete stress-strain curve for rock. *Proc. 13th Symp. Rock Mech.*, Urbane, Illinois, pp. 773-795.

HUNSCHE, U. and ALBRECHT, H. (1990). Results of true triaxial strength tests on rock salt. *Engineering Fracture Mechanics*, Vol. 35, No. 4/5, pp. 867-877.

ISRM (1983). International Society for Rock Mechanics Commission on Standardization of Laboratory and Field Tests. Suggested methods for determining the strength of rock materials in triaxial compression: revised version. *Int. J. Rock Mech. Min. Sci. & Geomech. Abstr.*, Vol. 20, No. 6, pp. 283-290.

JAEGER, J. C. (1965). Fracture of rocks. *Tewksbury symposium on fracture*, Faculty of Engineering, University of Melbourne, pp. 268-283.

JAEGER, J. C. (1966). Brittle fracture of rocks. In *Failure and Breakage of Rock*, Ed. C. Fairhurst, *Proc. 8th Symp. on Rock Mechanics*, University of Minnesota, pp. 3-58.

JAEGER, J. C. (1969). *Elasticity, Fracture and Flow*. 3rd edn, Methuen & Co. Ltd.

JAEGER, J. C. and COOK, N. G. W. (1979). *Fundamentals of Rock Mechanics*. 3rd edn, Chapman and Hall, London.

JEFFERY, G. B. (1921). Plane stress and plane strain in bipolar co-ordinates. *Phil. Trans. Roy. Soc.*, Ser. A, Vol. 221, pp. 265-293.

KAWAMOTO, T., TOMITA, K. and AKIMOTO, M. (1970). Characteristics of deformation of rock-like materials under triaxial compression. *Proc. 2nd Congress, ISRM*, Belgrade, Vol. 1, pp. 287-293.

KENNEDY, J. B. and NEVILLE, A. M. (1986). *Basic Statistical Methods for Engineering and Scientists*. 3rd edn, Harper & Row, New York.

KIM, M. K. and LADE, P. V. (1984). Modelling rock strength in three dimensions. *Int. J. Rock Mech. Min. Sci. & Geomech. Abstr.*, Vol. 21, No. 1, pp. 21-33.

KING, L. V. (1912). On the limiting strength of rocks under conditions of stress existing in the earth's interior. *J. Geol.*, Vol. 20, pp. 119-138.

KING, M. S. (1970). Static and dynamic elastic moduli of rocks under pressure. *Proc. 11th U.S. Symp. on Rock Mechanics*, Berkeley, pp. 329-351.

KING, M. S. (1983). Static and dynamic elastic properties of rocks from the Canadian shield. *Int. J. Rock Mech. Min. Sci. & Geomech. Abstr.*, Vol. 20, No. 5, pp. 237-241.

KOTSOVOS, M. D. (1983). Effect of testing techniques on the post-ultimate behaviour of concrete in compression. *Materials and Structures*, RILEM, Vol. 16, No. 91, pp. 3-12.

KOVARI, K. and TISA, A. (1975). Multiple failure state and strain controlled triaxial tests. *Rock Mechanics* 7, pp. 17-33.

LADERIAN, A. (1987). Rock failure characteristics under polyaxial loading conditions. MSc dissertation, University of Newcastle upon Tyne.

LEEMING, J. J. (1969). *Statistical Methods for Engineers*. Blackie, London & Glasgow.

LUNDBORG, N. (1967). The strength-size relation of granite. *Int. J. Rock Mech. Min. Sci.*, Vol. 4, No. 3, pp. 269-272.

MASO, J. -C. and LERAU, J. (1980). Mechanical behaviour of Darney sandstone in biaxial compression. *Int. J. Rock Mech. Min. Sci. & Geomech. Abstr.*, Vol. 17, pp. 109-115.

MAZANTI, B. B. and SOWERS, G. F. (1966). Laboratory testing of rock strength. *Testing Techniques for Rock Mech. ASTM STP402*, Am. Soc. Testing Mats., pp. 207-227.

McCLINTOCK, F. A. and WALSH, J. B. (1962). Friction on Griffith cracks under pressure. *Proc. 4th U.S. Nat. Cong. of Appl. Mech.*, Berkeley, California, Vol. 2, pp. 1015-1021.

MICHELIS, P. (1985). Polyaxial yielding of granular rock. *J. Engng. Mech.*, Vol. 111, No. 8, ASCE, pp. 1049-1066.

MOGI. K. (1962). The influence of the dimensions of specimens on the fracture strength of rocks. *Bull. Earthquake Res. Inst.*, Tokyo Univ., Vol. 40, pp. 175-185.

MOGI, K. (1967). Effect of the intermediate principal stress on rock failure. *J. Geophys. Res.*, Vol. 72, No. 20, pp. 5117-5131.

MOHR, O. (1900). Welche Umstände bedingen die Elastizitätsgrenze und den Bruch eines Materials? *Z. Ver. dt. Ing.*, Vol. 44, pp. 1524-1530 & 1572-1577.

MURRELL S. A. F. (1963). A criterion for brittle fracture of rocks and concrete under triaxial stress and the effect of pore pressure on the criterion. *Proc. 5th Rock Mech. Symp.*, University of Minnesota, In *Rock Mechanics*, Ed. C. Fairhurst, Pergamon Press, Oxford, pp. 563-577.

NADAI, A. (1950). *Theory of Flow and Fracture of Solids*. Vol. 1, 2nd edn, McGraw-Hill Book Company, Inc., USA.

OBER,T. L. and STEPHENSON, D. E. (1965). Stress conditions under which core discing occurs. *Soc. Min. Engrs.*, Trans., 232, pp. 227-234.

OBER,T. L. and DUVALL, W. I. (1967). *Rock Mechanics and the Design of Structures in Rock.* John Wiley & sons, Inc., USA.

PATERSON, M. S. (1978). *Experimental Rock Deformation-The Brittle Field.* Springer-Verlag, Berlin.

PÉRIÉ, P. -J. and GOODMAN R. E. (1988). Evidence of new failure patterns in a thick-walled cylinder experiment. *12th Ann. Energy Sources Technology*, Vol. 22, pp. 23-27.

POMEROY, C. D. and HOBBS, D. W. (1962). The fracture of coal specimens subjected to complex stresses, *Steel & Coal*, pp. 1124-1133.

PRICE, N. J. (1960). The compressive strength of coal measure rocks. *Coll. Eng.*, Vol. 37, pp. 283-292.

PRICE, A. M. (1980). The servo-controlled testing facilities, an introduction and operating manual. University of Newcastle upon Tyne.

PROTOPSALTIS, P. K. (1982). The effect of the intermediate principal stress on the failure of rock under polyaxial loading conditions using solid platens. MSc dissertation, University of Newcastle upon Tyne.

PROTOPSALTIS, P. K. (1986). Rock failure characteristics under polyaxial loading conditions. PhD thesis, University of Newcastle upon Tyne.

RINEHART, J. S., FORTIN, J. P. and BURGIN, L. (1961). Propagation velocity of longitudinal waves in rock. Effect of state of stress, stress level of the wave, water content, porosity, temperature, stratification and texture. *3rd technical session, Min. Eng. Ser.*, pp. 119-135.

ROBERTSON E. C. (1955). Experimental study of the strength of rocks. *Bull. Geo. Soc. Am.*, Vol. 66, pp. 1275-1314.

SANTARELLI, F. J. and BROWN, E. T. (1989). Failure of three sedimentary rocks in triaxial and hollow cylinder compression tests. *Int. J. Rock Mech. Min. Sci. & Geomech. Abstr.*, Vol. 26, No. 5, pp. 401- 413.

SARGAND, S. M., HAZEN, G. A. and MILLER, K. M. (1987). Multiaxial testing of compacted shales. *Proc. Int. Symp. on Prediction and Performance in Geotechnical Engineering*, Calgary, pp.377-383.

SENSENY, P. E., MELLEGARD, K. D. and WAGNER, L. A. (1989). Hollow cylinder tests on natural rock salt. *Geotech. Testing J.*, GTJODJ, Vol. 12, No. 2, pp. 157-162.

SHEOREY, P. R., BISWAS, A. K. and CHOUBEY, V. D. (1989). An empirical criterion for rocks and jointed rock masses. *Engineering Geology*, 26, pp. 141-159.

STAVROPOULOU, V. G. (1982). Behaviour of brittle sandstone in plane-strain loading conditions. In *Issues in Rock Mechanics*, Eds. R. E. Goodman and F. E. Heuze, *Proc. 23rd U.S. Symp. Rock Mech.*, Berkeley, California, pp. 351-358.

TASUJI, E., SLATE, F. O. and WILSON, A. M. (1978). Stress-strain response and fracture of concrete in biaxial loading. *J. American Concrete Institute*, Vol. 75, pp. 306-312.

TAYLOR, M. A., JAIN, A. K. and RAMEY, M. R. (1972). Path-dependent biaxial compressive testing of an all lightweight aggregate concrete. *J. American Concrete Institute*, Vol. 69, pp. 758-764.

TOUNTAS, A. A. (1991). The effect of axial loading on the cutting characteristics of sandstone. MSc dissertation, University of Newcastle upon Tyne.

TRESCA, H. (1868). Mémoire sur l'ecoulement des corps solides. *Mém. prés. div. Sav. Acad. Sci., Inst. Fr.*, Vol. 18, pp. 733-799.

TROLLOP, D. H. (1978). Failure criteria for brittle rock. In *An Introduction to Rock Mechanics*, Ed. H. Bock, Dept. Civil and Systems Engng. James Cook University of North Queensland, Australia, pp.109-130.

TROLLOPE, D. M. (1968). The mechanics of discontinua or clastic mechanics in rock problems. In *Rock Mechanics in Engineering Practice*, Eds. K. G. Stagg and O. C. Zienkiewicz, John Wiley, London, pp. 275-320.

VUTUKURI, V. S., LAMA, R. D. and SALUJA, S. S. (1974). *Handbook on Mechanical Properties of Rocks*. Vol.1, 1st edn, Trans Tech publications, Clausthal, Germany.

VAN HEERDEN, W. L. (1987). Determination of deformational characteristics of rock using wave velocity methods. *Proc. 6th Int. Congress on Rock Mech.*, Montréal, Vol. 2, pp. 1295-1298.

VAN MIER, J. G. M. (1987). Fracture propagation in concrete under complex stress. *SEM / RILEM Int. Conf. on fracture of concrete and rock*, Houston, Texas, Eds. S. P. Shah and S. E. Swartz, pp. 597-610.

VOLK, W. (1980). *Applied Statistics for Engineering*, 2nd edn, McGraw-Hill, New York.

VON MISES, R. (1913). Mechanik der festen Körper im plastich deformablen Zustand. *Nachr. Ges. Wiss. Göttingen, Mathematisch-physikalische Klasse*, pp. 582-592.

WANG, C., GUO, Z. and ZHANG, X. (1987). Experimental investigation of biaxial and triaxial compressive concrete strength. *ACI Materials J.*, Vol. 84, No. 2, pp. 92-100.

WHITNEY, C. S. (1943). Discussion on paper by V. P. Jensen, *J. Am. Concr. Inst.*, Vol. 39, pp. 584-586.

WICHTER, L. (1979). On the Geotechnical properties of a Jurassic clay shale. *Proc. 4th Int. Congress on Rock Mech.*, ISRM, Montreux, Vol. 1, pp. 319-326.

ZAITSEV, Y. V. (1985). Inelastic properties of solids with random cracks. In *Mechanics of Geomaterials: Rocks, Concrete and Soils*, Ed. Z. P. Bažant, pp. 89-128, Wiley, New York.